

Engineering Materials

Ram K. Gupta *Editor*

NanoCarbon: A Wonder Material for Energy Applications

Volume 1: Basics to Advanced
Applications for Energy Production

 Springer

Engineering Materials

This series provides topical information on innovative, structural and functional materials and composites with applications in optical, electrical, mechanical, civil, aeronautical, medical, bio- and nano-engineering. The individual volumes are complete, comprehensive monographs covering the structure, properties, manufacturing process and applications of these materials. This multidisciplinary series is devoted to professionals, students and all those interested in the latest developments in the Materials Science field, that look for a carefully selected collection of high quality review articles on their respective field of expertise.

Indexed at Compendex (2021) and Scopus (2022)


Ram K. Gupta
Editor

NanoCarbon: A Wonder Material for Energy Applications

Volume 1: Basics to Advanced Applications
for Energy Production

 Springer

Editor

Ram K. Gupta 

Department of Chemistry

Pittsburg State University

Pittsburg, KS, USA

ISSN 1612-1317

ISSN 1868-1212 (electronic)

Engineering Materials

ISBN 978-981-99-9934-7

ISBN 978-981-99-9935-4 (eBook)

<https://doi.org/10.1007/978-981-99-9935-4>

© The Editor(s) (if applicable) and The Author(s), under exclusive license to Springer Nature Singapore Pte Ltd. 2024

This work is subject to copyright. All rights are solely and exclusively licensed by the Publisher, whether the whole or part of the material is concerned, specifically the rights of translation, reprinting, reuse of illustrations, recitation, broadcasting, reproduction on microfilms or in any other physical way, and transmission or information storage and retrieval, electronic adaptation, computer software, or by similar or dissimilar methodology now known or hereafter developed.

The use of general descriptive names, registered names, trademarks, service marks, etc. in this publication does not imply, even in the absence of a specific statement, that such names are exempt from the relevant protective laws and regulations and therefore free for general use.

The publisher, the authors, and the editors are safe to assume that the advice and information in this book are believed to be true and accurate at the date of publication. Neither the publisher nor the authors or the editors give a warranty, expressed or implied, with respect to the material contained herein or for any errors or omissions that may have been made. The publisher remains neutral with regard to jurisdictional claims in published maps and institutional affiliations.

This Springer imprint is published by the registered company Springer Nature Singapore Pte Ltd.

The registered company address is: 152 Beach Road, #21-01/04 Gateway East, Singapore 189721, Singapore

Paper in this product is recyclable.

Preface

Carbon is one of the unique materials that exist in different forms such as fullerenes, carbon nanotubes, graphene, etc. Nanocarbons are attracting considerable research interest in electrochemical energy production and storage due to their tuneable electrochemical behavior, electronic structure, and porosity. Currently, there is no book covering unique aspects of nanocarbon including types, synthesis, characteristics, and emerging applications in the energy area. There are many opportunities in nanocarbons for energy applications as their properties can be tuned in many ways. For example, heteroatom doping, functionalization, and making composites with other materials can significantly improve their energy production and storage capacity.

The main purpose of this book is to provide current, state-of-the-art knowledge, fundamentals of electrochemistry, design strategies, and future challenges in carbon-based materials for electrochemical energy storage devices. The key goals for nanocarbon-based electrochemical devices are to provide safe operation, sustainability, high energy and power density, long working life, and reduced cost. In this book, the fundamentals and working principles of nanocarbon for electrochemical energy applications are explored. Volume 1 covers fundamentals and advancement in nanocarbon for energy storage applications. This book covers new approaches to the synthesis of nanocarbons for energy applications. The future of electrochemical devices and challenges for commercial applications are also explored. All the chapters are covered by experts in these areas, making this a suitable textbook for students and providing new directions to researchers and scientists working in science and technology areas.

Ram K. Gupta
Professor of Polymer Chemistry
Department of Chemistry
National Institute for Materials
Advancement
Pittsburg State University
Pittsburg, KS, USA

Contents

| | |
|---|-----|
| Introduction to Nanocarbon | 1 |
| Shivaraj Dhanushree and Chandrasekaran Nithya | |
| Synthesis and Characterizations of Nanocarbon | 17 |
| Diego R. Lobato-Peralta, Alejandro Ayala-Cortés, Estefanía Duque-Brito, and Patrick U. Okoye | |
| Electrochemical Properties of Nanocarbon | 35 |
| Shilpa Pande, Bidhan Pandit, Shoyebmohamad F. Shaikh, and Mohd Ubaidullah | |
| Tunability of Electrochemical Properties of Nanocarbon for Sustainable Energy | 57 |
| Kavitha Mulackampilly Joseph, Maliha Marzana, Ayush Raut, and Vesselin Shanov | |
| One-Dimensional Carbon for Electrocatalytic Activities | 81 |
| Niharika Maley, Pratik Patel, Felipe M. de Souza, and Ram K. Gupta | |
| Graphene as a Metal-Free Catalyst—Recent Case Studies | 99 |
| T. Stach, A. Seif, and U. Burghaus | |
| 3D Graphene: A Nanocarbon Innovation in Electrochemical Sensor Technology | 119 |
| Sahar Foroughirad, Behnaz Ranjbar, and Zahra Ranjbar | |
| Nanocomposites of Carbon for Dye-Sensitized Solar Cell Applications | 139 |
| Kulandai Velu Ramanathan, Vishnu Vardhana Chary, Shantikumar V. Nair, and Dhamodaran Santhanagopalan | |
| Nanocarbon for Electrocatalysis | 159 |
| Yingna Chang, Tian Zhang, and Guoxin Zhang | |

| | |
|--|-----|
| Graphene-Based Electrocatalysts | 179 |
| Touba Rezaee Adriani and Ali A. Ensafi | |
| Electrocatalytic Properties of Fullerene-Based Materials | 199 |
| Emilia Grądzka | |
| Nanocomposites of Carbon as Electrocatalyst | 219 |
| Veena Mounasamy and Ponpandian Nagamony | |
| Graphene-Based Fuel Cells | 237 |
| Suba Lakshmi Madaswamy, N. Veni Keertheeswari, and Ragupathy Dhanusuraman | |
| Nanocomposites of Carbon for Fuel Cells | 257 |
| James F. Amaku and Raymond Taziwa | |
| Carbon Nanomaterials as One of the Options for Hydrogen Storage | 275 |
| B. Viswanathan | |
| Nanocarbon as Catalyst Support for Fuel Hydrogen Generation by Hydrolysis of Sodium Borohydride | 293 |
| Iterlandes M. Junior, Gabriel H. Sperandio, Renata P. L. Moreira, and Tiago A. Silva | |
| Exploiting the Potential of Carbon Nanotubes and Nanofluids to Boost Efficiency in Solar Applications | 309 |
| Amir M. Alinia and M. Sheikholeslami | |
| Recent Advancements in Conducting Polymers for Biomedical Sensors | 325 |
| Aniruddh Mehra, Mayankkumar Chaudhary, Filipe De Souza, and Ram K. Gupta | |

Introduction to Nanocarbon



Shivaraj Dhanushree and Chandrasekaran Nithya

Abstract The field of nanomaterials has received much attention in recent years for its cutting-edge applications in areas such as energy, environmental, and life sciences. Owing to their distinct physio-chemical characteristics, nanocarbon with various dimensions such as 0D fullerenes and carbon-dots, 1D graphene nanoribbons and carbon nanotubes, 2D graphene oxides and graphene, and 3D nanodiamonds have gained a great deal of interest for applications in photovoltaics, optoelectronics, and electronics and as well as bio-imaging, sensing, and therapeutics. More interestingly graphene and CNTs offer unique structural properties like flexibility, mechanical stability, and electrical and thermal stability which create a revolution in the field of energy storage and sensing applications. This chapter systematically summarizes the synthesis of nanocarbons with distinct morphology and discusses how the synthesis methods influence the structural properties of nanocarbons. Further, the challenges in the synthesis methods and future perspectives of nanocarbons also discussed.

Keywords Nanocarbon · 2D graphene · Graphene oxides · Carbon nanotubes · Hard/soft carbon · Nanodiamonds

1 Introduction

By means of coupled hybridizing and assembly in a 1D, 2D, or 3D network, carbon bids an astonishing range of opportunities for the formation of various nanostructures [1]. The phrase “nanocarbon” refers to a large class of carbon materials, and it is believed that quantum dimensions at the nanoscale stages have a significant influence in determining performances [2]. It includes many kinds of carbon materials, from the more well-known ones, such as single or multiwalled CNTs, CNFs, fullerenes, and graphene, to the less well-known ones, such as CNHs, nano coils, nanodiamonds, CNDs, onions, and various hybrid forms, graphdiyne, etc.

S. Dhanushree · C. Nithya (✉)

Department of Chemistry, PSGR Krishnammal College for Women, Coimbatore 641004, Tamil Nadu, India

e-mail: nithyajcs@gmail.com

Due to three different carbon hybridizations (sp^3 , sp^2 , and sp^1) giving rise to a distinct group of nanomaterials in the absence of an analogue in another group of materials, there are a variety of different types of nanocarbons [3]. Other carbon compounds, such as glassy carbon, soft carbon, carbon black, hard carbon, and carbon foams, among others, exhibit a smaller amount of organized structure, as do other amorphous carbon and active carbon materials. Nanocarbons are being used to create better materials in several cutting-edge sectors of application, like storage of energy and conversion, catalytic activity, and others [4]. The following are some of the various industries that improved with carbon materials: solar panels, batteries, supercapacitors, fuel cells, electrolyzers, and photo electrocatalytic systems [5]. Particularly, manufactured nanocarbon substances including fullerenes, CNTs, CNHs, and graphene have been demonstrated to be particularly advantageous in several biology-related applications, including medicine transport, biolabeling, and nanomedicine. Nakamura et al., for instance, recently discussed the use of functionalized fullerenes to deliver the gene encoding the protein that glows green both in-vivo and in-vitro; elevated expression of genes was seen in both the spleen and the liver. The present study raises the possibility of using fullerenes as innovative gene therapy agents. Both carbon nanotubes and carbon nano horns have been demonstrated to serve as promising candidates for the delivery of drugs and controlled discharge due to their high drug-loading capacities and protracted blood circulation times. Nanodiamonds are a new platform for drug administration, imaging, and sensors that has recently gained attention. These substances have higher biocompatibility, photostable fluorescence, and increased therapeutic efficacy. A comparatively recent part of the nanocarbon family of materials, graphene, also exhibits potential for use in biomedical procedures including drug delivery and regenerative medicine. Numerous publications have already been written about the properties and potential applications of nanotubes of carbon, graphene, as well as amorphous nanoparticles of carbon in biomedicine [6].

Laser evaporation, plasma therapy, molecular beam epitaxy, deposition of chemical vapor, microwave-assisted technologies, micromechanical splitting, chemical removal, and arc discharge are only a few of the methods used to create carbon nanomaterials. High temperatures for the reaction are required for these traditional methods, which also have the shortcomings of complexity, high expenses, and protracted growth cycles, which restrict their practical use. The advantages of these traditional methods include high-purity products, effective composition management, uniform particle dispersion, source of carbon variability, and access to a wide range of morphologies. To produce crystalline substances at comparatively low critical temperatures, control reaction parameters to enhance product purity reduce agglomeration, and produce carbons with outstanding configuration specificity and distinctive physical characteristics, solvothermal processes methods are used to produce the majority of synthetic and doped carbon [7].

2 Synthesis of Various Types of Nanocarbon

2.1 Synthesis of Graphene

A variety of various precursors were used to create monolayer graphene using a general direct solid-state pyrolytic conversion process. Now, let's use its transformation from sodium gluconate as an illustration. Sodium gluconate (10.907 g) and Na_2CO_3 powder (105.99 g) were typically thoroughly crushed in an agate mortar and pestle at a 1:20 molar ratio. Using a corundum tube and boat, the product was transferred into a corundum tube placed in a typical horizontal tube furnace (55 cm length, 5 cm diameter). After being flushed with a flow of Ar for 30 min, the reactor heated up to 950 °C at a rate of 3 °C/min and kept there for 10 min. After that, the apparatus was put in an Ar flow and allowed to naturally cool to room temperature. Treatment with weak hydrochloric acid was done to get rid of any last remnants of the Na_2CO_3 salt. The pyrolysis products were then cleaned using vacuum filtration while being cleaned with distilled H_2O and 100% ethanol until the filtrate's pH was neutral. The pure powder of monolayer graphene (7.37 g, 51.4%) was obtained after a further 12 h of drying at 80 °C. When monolayer graphene was produced, its crystalline structure and phase purity were determined using X-ray diffractometry (XRD; Bruker D8, CuK source, $\lambda = 1.54178$). Transmission electron microscopy (TEM, JSM-2100F, 200 kV) images shown in Fig. 1 [8] and field emission scanning electron microscopy (FESEM, Hitachi S-4800) were used to examine the product's morphology and microstructure. On an FEI Tecnai G2 F20 microscope, high-resolution TEM and high-angle annular dark field scanning transmission electron microscopy (HAADF-STEM) were carried out at a 200 kV accelerating voltage [9].

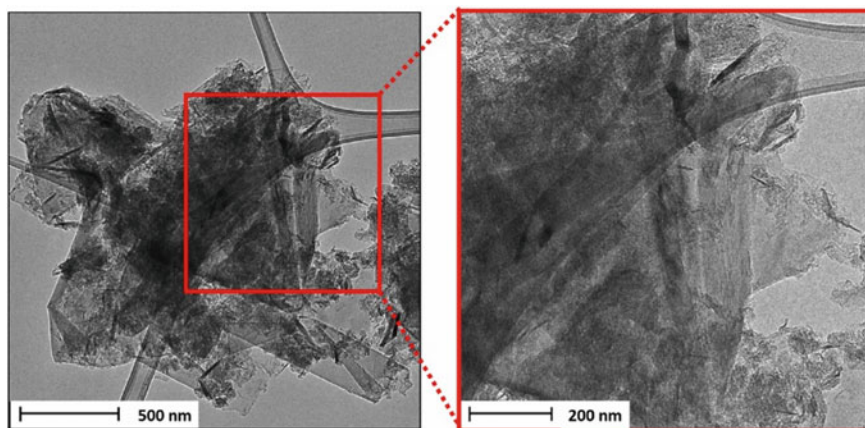


Fig. 1 TEM micrographs of graphene. Adapted with permission [8]. Copyright (2023) Elsevier

In 2004, Geim and Novoselov performed ground-breaking research on two-dimensional graphene utilizing the scotch tape approach. To produce graphene, both top-down and bottom-up methods are accessible. For instance, in the top-down process of mechanical cleavage, graphite is converted into graphene, but in the bottom-up approach of chemical vapor deposition, silicon carbide is transformed into graphene.

2.1.1 Mechanical Exfoliation

As discussed earlier, weak van der Waals forces keep the sheets of graphene together. High-purity graphene can be produced if these forces are dismantled. The weak connections are broken, and the individual sheets are separated using mechanical energy in the mechanical exfoliation procedure. Exfoliation typically involves regularly peeling graphite to obtain layers of graphene. Highly oriented pyrolytic graphite (HOPG) was used as a precursor when Geim and Novoselov first invented this process. In this procedure, HOPG sheet with a thickness of 1 mm is utilized to dry etch with oxygen plasma to produce several 5 m-deep mesas (an isolated surface with a flat top). The mesas were then covered with these using photo resistance and baking. The graphene layers on the graphite were then peeled off with scotch tape. The acetone was then used to liberate these tiny flakes, which were subsequently placed on a Si substrate. So, on a Si substrate, pure graphene flakes are created. This method's drawback is that it is impossible to scale up huge industrial output.

2.1.2 Liquid Phase Exfoliation

One of the most widespread procedures for producing graphene is liquid phase exfoliation (LPE), which was first described in 2008. Through the exfoliation of graphite, a firm dispersion of a monolayer or a few layers of graphene is created using this top-down approach. Graphite dispersion in an appropriate solvent, exfoliation, and purification of the finished products are some of the main phases in LPE. By defeating the van der Waals forces, graphene layers are separated via this method of exfoliation. As a result, choosing the right solvent is crucial. Surface energy, Hildebrand solubility, Hansen solubility parameters, and surface tension are a few of the characteristics that have been considered when choosing a solvent. Surface energies (for solids) or surface tensions (for liquids) within 40–50 mJ/m² or 70–80 mJ/m² were discovered to be favourable for the formation of graphene, according to research. Sonification is a crucial element to consider throughout this synthesis technique in addition to the solvent. The ends and basal planes may be impacted by sonification, despite the LPE approach being a successful way for producing graphene. By maximizing the sonification time, temperature, and intensity, this can be fixed. The yield of this technology, which is insufficient for industrial applications at macroscopic size, is one of its main drawbacks. Solvents' high cost, toxicity, and shrinkage of the

nanosheets' size are other drawbacks. Future research should be done to increase the effectiveness and viability of this strategy economically [10].

2.2 *Synthesis of Graphite*

The apparatus required for treating iron carbide with Cl under barometric pressure has been extensively defined. Iron carbide was inserted into a long horizontal quartz tube reactor and then positioned inside of it. Once the reaction temperature was reached, argon gas was used to cleanse the reactor. The sample was later subjected to running ^{12}C gas for three hours before being purged with argon once more throughout the cooling process. The stable temperature of the reaction and the flow rate of gases were kept during the course of a single experimental run. At temperatures between 400 and 1200 °C, the reaction between iron carbide and chlorine was studied; all other variables remained constant. When necessary, the carbon extracted from the quartz boat was refined by eliminating any lingering impurity with 10% HCl, then using de-ionized water three times in a row, followed by meticulously drying at a temperature of between 100 and 1500 °C.

The environmental field-emission (FE) SEM from Philips, model XL-30, was used to examine the chlorinated samples. EDS analysis was always performed in addition to SEM examination to confirm that the substance under study was carbon. To construct the TEM samples, the synthesized products were distributed in propane-2-ol across a TEM grid covered in a lacey carbon sheet. The examination was performed using a JEOL JEM-2010F electron microscope. The carbon regions and impurities were located using a GIF and EELS. Using Raman microspectroscopy with an excitation wavelength of 514.5 nm (Ar ion laser), a range of 800–2000 cm^{-1} , and an exposure time of 10 s, the level of carbon ordering was investigated. Each sample's spectra were gathered using a 2-mm spot size at a minimum of five separate places. To prevent the sample from being damaged or heated, a low laser power was used. Peak fitting and deconvolution were performed using GRAMMES 32 v5.2 spectral analysis software. It is demonstrated that the ID/IG ratio—a measure of the relationship between the D band at (1350 cm^{-1}) and the G band at 1580 cm^{-1}) and the in-plane crystallite size of graphite, L_a . According to Tuinstra and Koenig's work [15] for 2.5 nm v , it can be estimated as: $L_a = 4.4 (\text{ID/IG})^{-1}$ (nm) [11].

2.3 *Synthesis of CNTs*

CNTs were created by catalysing the breakdown of ethyne over a Fe catalyst. Studies were done on two acetylene/nitrogen ($\text{C}_2\text{H}_2/\text{N}_2$) compositions of gases, 2.5% and 10%, respectively. The ethyne/ N_2 mixture of gases was initiated into the chamber at a rate of 110 cm^3/min with an excess pressure of 180 Torr once the catalyst had been lowered. The temperature immediately climbed, rising to 690 °C after 10 min,

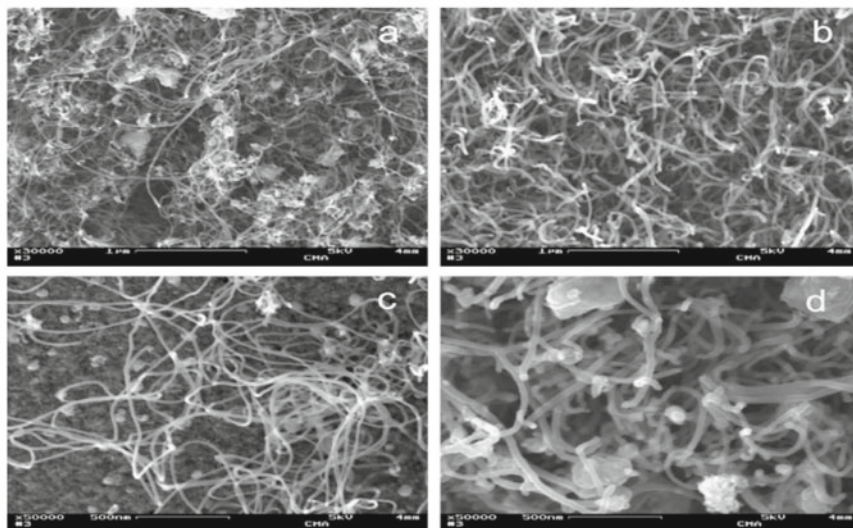


Fig. 2 SEM images of MWCNTs synthesized with (a) and (c) 2.5% C₂H₂/N₂; (b) and (d) 10% C₂H₂/N₂. Adapted with permission [12]. Copyright (2007) Elsevier

where it stayed for 5 min. The temperature controller was ultimately set for 3 h at 6000 °C. Following the development of the CNTs, nitrogen gas was utilized to bring the furnace's temperature to room temperature. SEM images of synthesized MWCNTs shown in Fig. 2. HR-TEM Philips CM200 and FEG-SEM Zeiss LEO 982 GEMINI were used to study the form, diameter, and wall structure of synthetic CNTs. Shimadzu TGA-51 and Shimadzu DTA-50 were achieved with air flowing at 50 cm³ min⁻¹ and samples weighing 15 mg. The samples of the nanotube were separated from the catalyst when necessary, using ultrasonic dispersal in C₂H₅OH [12].

2.4 Synthesis of Hard Carbon

We used two distinct methods to create hard carbon from the argan shell: the conventional method and the HCl-washing method. To remove any soluble organics, the raw argan shell was first cleaned in acetone before being dried at room temperature and smashed. It was subsequently warmed up in a furnace of horizontal tube at a 5 °C/min heating rate, kept at 800, 1000, 1200, and 1300 °C for an hour, and then sprayed with argon. The following abbreviations for the goods are Ar-800, Ar-1000, Ar-1200, and Ar-1300, correspondingly. Alkali metals and transition metals are two examples of the inorganic components that will be further eliminated during the HCl-washing procedure. Acetone was used to clean the argan shell before it was powdered and concerned with 2.0 mol/dm³ aqueous HCl. For the procedure, the hydrochloric acid

was mixed with the powdered crushed argan shell and aged for 20 h at 60 °C. Filtration was used to separate the powder, and it was then rinsed with deionized water to eliminate any remaining HCl at a pH of 6.5–7.0. The resulting powder was dried in an argon environment for one hour at 110 °C. The following carbonization/pyrolysis settings mirror those of the typical procedure depicted. Since cellulose and lignin make up the majority of an argan shell, we also created hard carbons by carbonizing the two substances, as illustrated. We've fixed the carbonization temperature for this method at 800 °C. Like the above samples, these hard carbons are designated as Cellulose-800, Lignin-800, Cellulose-800W, and Lignin-800W. Since cellulose, lignin, and hemicelluloses make up most of the shell of argan, a HTT approach was used to manufacture the argan carbon material from it. After being cleaned with acetone, the raw material powder turns brown, which should be caused by the presence of lignin. After HTT, the powder became black carbon powder. By measuring XRD patterns, the crystallinity of carbon compounds made from argan shells was examined. Ar800, Ar-1000, Ar-1200, and Ar-1300 XRD patterns are shown, and physical parameters inferred from the XRD data are listed. The fact that two large peaks at 22.2°–22.9° and 43° in 2θ are given to the graphite 002 and 100/101 diffraction lines, correspondingly, demonstrates that the black particles formed are made of non-graphitizable carbon. Small graphene domains are the cause of the extensive and minor peaks for argan carbon seen for diffraction lines 100/101.

XRD and Raman spectrometers are used to describe the structure of hard carbons. Surface characterization techniques such as SEM and TEM were used to investigate the morphology. SEM images of synthesized hard carbon is shown in the Fig. 3 [13]. Additionally, we checked for the presence of metallic components in Ar-carbon products using an ED XRF spectrometer prepared through 3-D polarisation optics. Raw materials were subjected to thermogravimetric analysis (DTG-60/60, Shimadzu) at a warming rate of 5 °C min⁻¹ from 30 to 600 °C. The N₂ adsorption/desorption isotherms at 77 K were used to evaluate the morphological features of the substances with BET theory and BELSORP-mini II. Previous to analysis, the samples were out-gassed in a vacuum for three hours at 200 °C. The specific surface area of BET was calculated by means of a relative pressure (P/P₀) range of 0.08–0.3 [14].

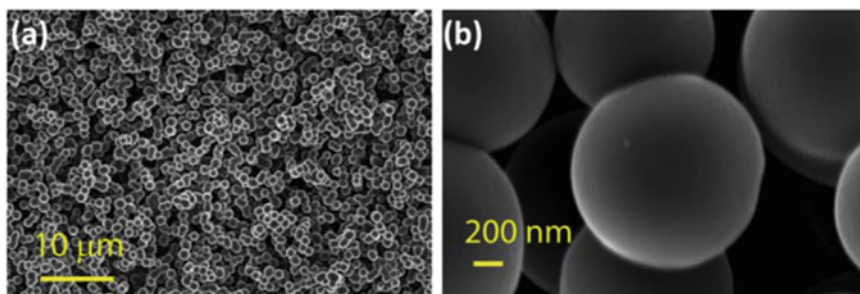


Fig. 3 The SEM images in (a) and (b) taken at different magnifications show the typical spherical morphology of the hard carbon. Adapted with permission [13]. Copyright (2020) Elsevier

2.5 *Synthesis of Soft Carbon*

Petroleum coke was mixed with 4 weight percent of phosphoric acid for an hour at room temperature in a homogenizer. After that, the combination underwent a two-hour heating process at 1100 °C with an Ar flow at a warming rate of 5 K/min. The completed product was permitted to naturally cool at ambient temperature before being sieved through a 250-mesh screen. A soft carbon sample that had just been synthesised was examined using powder XRD, EDX, HR-TEM microscopy, and FESE microscopy. The Raman spectra are captured using a confocal Roman microscope (DXR, ThermoFisher Scientific, 532 nm excitation) [15].

2.6 *Synthesis of Fullerene*

David Jones in 1966 first proposed the idea of producing a hollow and spherical C-molecule. It would be made of “a sheet-polymer like graphite, whose elementary molecule is a sheet of flat carbon atoms bonded hexagonally, somewhat similar to chicken wire,” according to what he wrote. After a few years, this idea was ignored until Osawa in 1970 theorised the potential for polyhedral C-clusters. The molecule C₆₀, which has 60 carbon atoms organized in a truncated icosahedron, was invented before he knew it existed. No one was able to experimentally validate or disprove these predictions for a very long period. When a solid sample of graphite in 1985 was exposed to laser light, Kroto et al. analyzed the resulting mass spectra and discovered lines that they later identified as belonging to the C₆₀ and C₇₀ molecules. Numerous scholarly publications about novel techniques for synthesizing fullerenes and the impact of different factors on their synthesis were published during the start of the 1990s. In general, temperatures of 1200 °C or more are required for the synthesis of fullerenes to efficiently form molecules from the carbon source and transition it into the gas phase. Several procedures, such as plasmatron, electron irradiation, high-temperature treatment, shock waves, electric arc, etc., were projected to attain the need for high temperature. The heat of combustion experiments estimates the strain energy of C₆₀ to be an additional of 600 kcal/mol. Laser ablation is the method used the most frequently to create fullerenes. The effectiveness of this method was initially demonstrated by Smalley and colleagues. In essence, the long quartz tube was used by the team that was housed within the T-C tube furnace. The researcher was able to regulate the gas flow and pressure by connecting this quartz tube at the front to an aluminium input block. Usually, the back end was attached to a vacuum pump. At pressures a few 100 Torr and 1200 °C temperatures, noble gas was used to create fullerene. Shortly et al. identified the presence of endohedral LaCl₃ by detecting signal of LaC₆₀ in the mass spectrum. For indicating the metal encapsulation in fullerenes, they adopted sign “@”. Graphite and BN were combined, and when that mixture was evaporated using a laser, fullerenes, and boron-containing analogs like

$C_{59}B$ and $C_{54}B$ were created. By synthesizing fullerenes using the arc discharge technique, Krätschmer and Huffman et al. invented the technique of direct current. One technique for creating fullerenes in grams is the arc discharge approach. In the method of arc discharge, a temperature of around $103\text{ }^{\circ}\text{C}$ was used to warm up the resistant graphite electrodes in a passive atmosphere of 100–200 Torr using either He or Ar gas. The carbon in graphite is transformed into higher-density gas flow by an absorbed pulsed laser. The yield of fullerenes has also been increased by adding transition metals or catalysts of metal oxide. The arc discharge furnace was given N_2 gas during the authors' tests, and this occasionally resulted in $Sc_3N@C_{80}$ formation. Later, NH_3 , SO_2 , O_2 , and countless more chemical and inorganic compounds were introduced in a variety of papers that used the same methodology. $ErSc_2N@C_{80}$, $Sc_3N@C_{84}$, $Sc_3C_2@C_{80}$, $Sc_4C_2@C_{80}$, $Sc_4O_2@C_{80}$, $YCN@C_{82}$, $H_2@C_{60}$, $Er_xSc_{3-x}N@C_{80}$ ($x = 1-3$), and $TiM_2N@C_{80}$ ($M = Sc, Y$) are a few of them that lead to the production of filled fullerenes. Multi-shell fullerenes with a cage-in-a-cage concentric structure were made using the arc discharge technique. Examples include the double-shell $C_{60}@C_{240}$ and triple-shell $C_{60}@C_{240}@C_{560}$. Fullerene development without metals is still up for debate.

Another method for creating fullerenes is the direct vaporization of carbon under concentrated sunlight. Uniquely, large-scale solar furnaces can produce fullerenes in large quantities using renewable energy. Methods based on the vaporization of graphite and the burning of hydrocarbons in a fuel-rich flame have received a lot of attention. A range of combined combustible substances have been identified through research as having different fullerene produced in low-pressure premixed laminar flames under varied conditions. A significant yield of fullerene species was obtained when benzene and oxygen were combined at a 1:1 ratio in a laminar flow. Substantial growth has been achieved in the fullerene preparation as well as in our comprehension of how they are produced. The most successful of these processes is the fullerene synthesis using hydrocarbon combustion. Fullerenes can be produced using this method in large quantities each year. However, it is still unclear how fullerene is produced in flames. To comprehend the creation of fullerenes, the theories and methodologies have been created. According to the universal theory, the C supply is initially split down to its smaller components, such as C-atoms and maybe C-dimers, within a specific pressure and temperature range, and these constituents then undertake a sequence of actions earlier recombining to form fullerenes. Additional experimental data, however, did not back up this method. Another theory to clarify the creation of fullerenes was the icospiral particle nucleation scheme. This model predicts that the corannulene-like Carbon 20 molecule, with five hexagons surrounding a pentagon, initiates the icospiral nucleation process. This structure with high reactivity grows and has a predisposition to yield open spiral shells by collecting particles of C that break on adsorption over the outermost layer of such shells. The sequential preparation of fullerenes is described by the sporadic statistical closing of a structure with the proper arrangement of pentagons. Another technique for creating fullerenes is by annealing carbon clusters. With between 34 and 60 atoms, these C complexes might be in 2- or 3-cycles, chains, or rings that cling to one another and later anneal. Further, it was proposed that the hidden phase (or intermediate phase) at

the nanoscale is where fullerenes first formed. The formation of groups in this intermediate stage is commanded by non-equilibrium circumstances, known as kvataron. According to the “the shrinking hot giant road to fullerene formation” theory put forth by Irlle and colleagues, by the shrinking of gigantic fullerenes, the formation of fullerenes takes place. Based on the outcomes of studies of the dynamics of self-assembling in a heated carbon vapor that is beyond thermodynamic equilibrium, quantum chemical molecular dynamics, this mechanism was developed [16].

3 Properties of Various Types of Nanocarbon

3.1 Properties of Graphene

Graphene owns many outstanding properties such as electronic conduction, thermal conduction, mechanical strength, and optical transparency [17].

The phrase “the mother of all carbon graphitic forms” refers to the 1-sheet of C-atoms known as graphene, which binds via an interlocking framework of sp^2 hybrid bonds. The remarkable features of graphene are due to the 2p orbitals, resulting in the delocalization of state bands across the carbon sheet that constitutes it. Since it has no effective mass, is gas-tight, has excellent carrying mobility, and is optically transparent, graphene is also very stiff, has a very high heat conductivity, and is without effective mass. About comparable materials that have been employed in various applications, graphene has an edge thanks to all these characteristics [18].

The planar density of graphene is 0.77 mg/m^2 and is called a superlight material. A hexagonal carbon ring having a surface area of 0.052 nm^2 makes up a single unit of graphene. There are just 2 carbon atoms in this hexagonal carbon ring, and each one at the vertex has been shared by the other three-unit rings. The structure of graphene, which has a sheet of C-atoms 1-atom thick, gives it a special quality that makes it an extremely light and thin material. Owing to the 1-atom thick sheet of C-atom in graphene it is a highly transparent material of 97.7% and it absorbs only 2.3% of visible light. This difference is the same between a single layer and a double layer as well as a substrate and single layer of graphene. This is particularly important since it shows the graphene layer’s effective numbers, which are further supported by numerous simulation studies utilizing the non-interacting Dirac Fermion theory.

The mechanical strength and thermal conductivity of graphene is also very high and considered the hardest crystal-structured material among all the known materials. Graphene has a strength limit of 42 N/m with tensile strengths and elastic moduli of 125 GPa and 1.1 TPa, correspondingly. One square meter of graphene is capable of supporting 4 kg of weight, which is nearly 100 times more powerful than steel. This special attribute is considered for 2D augmentation in composite substances and has a wide range of uses.

At ambient temperature, graphene has a thermal conductivity of approximately $53,103 \text{ W m}^{-1} \text{ K}$, which is ten times more than the thermal conductivity of 401 W

m^{-1} K of copper. It is discovered that graphene has a particular surface area of $2630 \text{ m}^2 \text{ g}^{-1}$. By analyzing the drastic variations in resistance caused by the adsorption and desorption behavior of gas molecules, is utilized to detect gas molecules in micro detectors. Additionally, simulations show that the porous mixture of graphene and lithium has a great capacity to hold hydrogen [17].

3.2 Properties of Graphite

A semimetal crystalline allotropic form of carbon is called graphite. The unit cell of a crystal in a semimetal has an even number of valence electrons, and the presence of free carriers at T50K results from the overlap of the conduction and valence bands [19]. Extremely hydrophobic particles of commercially available microcrystalline graphite form thin films when they encounter a solvent. Graphite oxide is created when treated in highly oxidizing acidic conditions. The structural makeup of $\text{C}_8\text{O}_2(\text{OH})_2$ an epoxidized variation of the sp^2 -bonded C system with acid functional groups at the ends and electron acceptor interposed in the inter arcuate space provides a method for quick de-intercalation of oxidants, which allows for the exfoliation of graphite. To develop uses for graphite oxide, different oxidative routes have been researched. The thinnest graphitic film thickness was 1.4 nm, and the components created unstable dispersions [20].

Graphite nanoparticles offer another feature of carbon-based nanoparticles with conjugated π -electron systems. The edges that wrap the graphite particles appear whenever a graphite crystal is broken into nanoparticles. A nanoparticle of graphite is made up of stacked nanoscale graphene sheets, each of which has dangling bonds along its edges. In real life, however, oxygen and hydrogen react with these hanging bonds to produce completed bonds [21].

The smallest energy state of graphite is represented by elemental carbon at standard pressure and temperature. The term “graphene layer” or “graphene sheet” refers to a mono-carbon layer in the graphite lattice of a crystalline honeycomb. The crystal lattice of graphite is composed of tons of parallel two-dimensional graphene sheets with closely connected sp^2 hybridized C-atoms. Because the 2p_z orbitals of the C-atoms might coincide most efficiently if their positions are parallel, when the graphene sheet is fully flat, it has the least energy. The anisotropic nature of graphite is because of the contrast between the carbon atoms’ in-plane and out-of-plane bonding. Diamond and graphite are stronger in the plane because the elastic modulus of graphite is more parallel to the plane than it is perpendicular to the plane. The graphene sheet is made thermally and electrically conductive by the orbital, which is dispersed across the entire material. Graphite’s layered structure demonstrates three-dimensional (3D) order [22].

3.3 Properties of Carbon Nanotubes

Currently, there is a lot of attention on CNTs across the world. Given that the potential of CNTs have exhibited unique physical properties that could have an impact on many areas of science and business, from nanoelectronics to exceptionally strong composites, this interest in them is not surprising. According to recent experimental tests, carbon nanotubes are the stiffest material known to mankind. When subjected to strong bending or compressive forces, they buckle elastically rather than breaking. These mechanical properties unequivocally show that nanotubes have great promise for cutting-edge composites [23].

The structure and inherent complexity of the nanotube result from the helicity in the configuration of the C-atoms in hexagonal groupings on their surface honeycomb lattices, which gives its uniqueness. Due to the considerable changes of states in the electronic density brought about by helicity (local symmetry) and diameter, nanotubes have a distinct electronic character. These innovative electronic properties give rise to a vast range of exciting electronic device applications; Another crucial element that defines the distinctiveness in physical attributes is topology, or a closed system of every single nanotube shell. A portion of the anisotropic characteristics of graphite are lost when layers are closed on themselves, causing the structure to stand out from graphite. Nanotubes have significant mechanical properties due to their combination of size, structure, and topography, as well as unique surface properties (such as selectivity, and surface chemistry) [24].

3.4 Properties of Soft Carbon

Low porosity, comparatively high hydrogen, and low oxygen content materials are the sources of soft carbons, which also have low porosity. Soft carbons can be converted into graphitic carbon via the graphitization process. During the carbonization process, most soft carbons go through a fluid (plastic) stage. Mesophase is formed in the liquid phase while the system is fluid. Planar aromatic molecules are essentially layered on top of one another in the mesophase's tiny anisotropic spheres. Mesophase development is a requirement for the material to continue growing into an ordered structure. Complete graphitization of soft carbons is achievable with thermal treatment alone, meaning that time and temperature play a role in the graphitization process. The soft carbons include pitches, pitch coke, petroleum coke, and polynuclear aromatic complexes.

3.5 *Properties of Hard Carbon*

Hard carbons undergo pyrolysis rather than fusion. This is because of the heat treatment procedure maintaining a crosslinked structure of molecules. Even after prolonged extreme pressure and temperature conditions can hard carbides be fully graphitized. Wood (cellulose), non-fusing coals, and glassy (vitreous) carbons are all examples of hard carbons. Small and flawed aromatic layers result in spaces of microporosity between the crystallites as well as erratic stacking patterns [25].

Hard carbons typically have a disordered structure made up of holes, different types of faults, and are randomly concerned with and lightly stacked nanosheets of graphite. To demonstrate the link between the Na^+ storage mechanisms and the structure of hard carbon, Steven and Dahn presented the distinctive structure of hard carbons. They achieved this by using the “House of Cards” model. According to the model, hard carbons have two different sorts of areas with two different microstructures, leading to two different mechanisms of Na^+ storage. Multiple layers of parallel graphene, also known as graphitic nanodomains, are one sort of region that is contained inside the domains of disorder. The additional form of the area is the vacant space (porosity) within nanodomains of graphite, which is caused by the haphazard adaption of layers or domains in relation to one another and the various types of defects. A mixture of 2 different mechanisms, including (a) intercalation/insertion between graphitic nanodomains of parallel graphene layer and (b) surface-active sites absorption like deficiency and nanopore stuffing, has been proposed as the mechanism by which sodium is stored in hard carbons [26].

3.6 *Properties of Fullerene*

The discovery of Buckminster fullerenes occurred in 1985. The n vertices of fullerenes F_n are organized in 12 pentagons and hexagons. They are closed hollow polyhedrons. On the cage surface, each sp^2 hybridized carbon atom is linked to its three carbon neighbors by three carbon bonds ($n/2$ carbon bonds). All even $n \geq 20$ and $n \equiv 2 \pmod{2}$ have the condition that F_n exists. Due to its availability, great symmetry, and inexpensive cost, C_{60} is the fullerene that is most investigated. Major synthesis pathways include the burning of hydrocarbons, inductively linked RF evaporation, laser ablation, and graphite arc vaporization. The processability and solubility of the fullerene molecule are both improved by functionalization. Their commercial applications have thousands of patents. Electrical conductivity, catalysts for hydrocarbon upgrading, artificial photosynthesis, organic photovoltaics, cosmetics, nonlinear optics surface coatings, pharmaceuticals, and nonlinear optics are the main applications (but they are still too expensive) [27].

4 Conclusion and Future Perspectives

Materials of nanocarbon, including CNTs, graphene (graphene oxide), CNHs, and carbon blacks, have set up a special class for the applications of nanomaterial such as solar panels, batteries, supercapacitors, fuel cells, electrolyzers, and photo electrocatalytic systems. Most of the synthetic and doped carbon is produced by solvothermal methods, which have the advantage of being able to crystallize substances at extremely low critical temperatures, control the parameters of the reaction to improve product purity and decrease agglomeration, and develop carbons with outstanding configuration specificity and different physical properties. The extraordinary qualities of graphene continue to make it a special substance with potential for useful applications. The orbital, which is spread over the complete material, renders the sheet of graphene electrically and thermally conductive. Nanotubes have a distinctive electrical character as an outcome of the significant changes in the states of electronic density brought about by helicity and diameter. The future perspective is to utilize these nanocarbon materials for the electrochemical reaction during battery operation. Nanocarbon catalysts are predicted to be used in bulk applications as more effects become apparent. We review some recent initiatives that may be seen as the nexus of energy and environmental sustainability and that sought to address urgent demands in metal-free catalytic applications. A wide range of research has been conducted with a wealth of fruitful findings thanks to the improved science surrounding the underlying mechanisms of doped/defective nanocarbons and the significance of these characteristics in their catalytic performances. In a more general way, the $C_5H_6O_2$ - (Conc. $HNO_3 + NO_2$) system could be the starting point for a future conversation about “carbon from rocket fuel,” mainly considering the abundance of bipropellants of rockets currently available on the market and the field’s ongoing advancement with new hypergolic fuels.

Acknowledgements The author C. Nithya wishes to thank the DST-Science and Engineering Research board, Government of India for SERB-POWER Grant (SPG/2021/004543).

References

1. Perathoner, S., Centi, G.: Advanced nanocarbon materials for future energy applications. In: *Emerging Materials for Energy Conversion and Storage*, pp. 305–325. Elsevier (2018)
2. Su, D.S., Perathoner, S., Centi, G.: Nanocarbons for the development of advanced catalysts. *Chem. Rev.* **113**, 5782–5816 (2013)
3. Itami, K., Maekawa, T.: Molecular nanocarbon science: present and future. *Nano Lett.* **20**, 4718–4720 (2020)
4. Dai, L., Chang, D., Baek, J.B., Lu, W.: Carbon nanomaterials for advanced energy conversion and storage. *Small* **8**, 1130–1166 (2012)
5. Su, D.S., Centi, G.: A perspective on carbon materials for future energy application. *J. Energy Chem.* **22**, 151–173 (2013)
6. Wang, J., Hu, Z., Xu, J., Zhao, Y.: Therapeutic applications of low-toxicity spherical nanocarbon materials. *NPG Asia Mater.* **6**, 84–84 (2014)

7. Lai, J., Niu, W., Luque, R., Xu, G.: Solvothermal synthesis of metal nanocrystals and their applications. *Nano Today* **10**, 240–267 (2015)
8. Storti, E., Lojka, M., Lencová, S., Hubálková, J., Jankovský, O., Aneziris, C.G.: Synthesis and characterization of graphene nanoplatelets-containing fibers by electrospinning. *Open Ceram.* **15**, 100395–100404 (2023)
9. Youqi, Z., Tai, C., Chuanbao, C., Xilan, M., Xingyan, X., Yadong, L.: A general synthetic strategy to monolayer graphene. *Nano Res.* **11**, 3088–3095 (2018)
10. Santhiran, A., Iyngaran, P., Abiman, P., Kuganathan, N.: Graphene synthesis and its recent advances in applications—a review. *C* **7**, 76–89 (2021)
11. Dimovski, S., Nikitin, A., Ye, H., Gogotsi, Y.: Synthesis of graphite by chlorination of iron carbide at moderate temperatures. *J. Mater. Chem.* **14**, 238–243 (2004)
12. Escobar, M., Moreno, M., Candal, R.J., Marchi, M.C., Caso, A., Polosecki, P.I., Goyanes, S.: Synthesis of carbon nanotubes by CVD: effect of acetylene pressure on nanotubes characteristics. *Appl. Surf. Sci.* **254**, 251–256 (2007)
13. Asfaw, H.D., Tai, C.W., Valvo, M., Younesi, R.: Facile synthesis of hard carbon microspheres from polyphenols for sodium-ion batteries: insight into local structure and interfacial kinetics. *Mater. Today Energy* **18**, 100505 (2020)
14. Dahbi, M., Kiso, M., Kubota, K., Horiba, T., Chafik, T., Hida, K., Komaba, S.: Synthesis of hard carbon from argan shells for Na-ion batteries. *J. Mater. Chem. A* **5**, 9917–9928 (2017)
15. Wang, H., Yu, Q., Qu, J.: Synthesis of phosphorus-doped soft carbon as anode materials for lithium and sodium ion batteries. *Russ. J. Phys. Chem. A* **91**, 1152–1155 (2017)
16. Paukov, M., Kramberger, C., Begichev, I., Kharlamova, M., Burdanova, M.: Functionalized fullerenes and their applications in electrochemistry, solar cells, and nanoelectronics. *Materials* **16**, 1276–1297 (2023)
17. Zhen, Z., Zhu, H.: Structure and properties of graphene. In: *Graphene*, pp. 1–12. Academic Press (2018)
18. Papageorgiou, D.G., Kinloch, I.A., Young, R.J.: Mechanical properties of graphene and graphene-based nanocomposites. *Prog. Mater. Sci.* **90**, 75–127 (2017)
19. Djurišić, A.B., Li, E.H.: Optical properties of graphite. *J. Appl. Phys.* **85**, 404–7410 (1999)
20. Niyogi, S., Bekyarova, E., Itkis, M.E., McWilliams, J.L., Hamon, M.A., Haddon, R.C.: Solution properties of graphite and graphene. *J. Am. Chem. Soc.* **128**, 7720–7721 (2006)
21. Tanaka, K., Yamashita, S., Yamabe, H., Yamabe, T.: Electronic properties of one-dimensional graphite family. *Synth. Met.* **17**, 143–148 (1987)
22. Sengupta, R., Bhattacharya, M., Bandyopadhyay, S., Bhowmick, A.K.: A review on the mechanical and electrical properties of graphite and modified graphite reinforced polymer composites. *Prog. Polym. Sci.* **36**, 638–670 (2011)
23. Odom, T.W., Huang, J.L., Kim, P., Lieber, C.M.: Structure and electronic properties of carbon nanotubes. *J. Phys. Chem. B* **104**, 2794–2809 (2000)
24. Ajayan, P.M., Zhou, O.Z.: Applications of carbon nanotubes. *Carbon nanotubes: synthesis, structure, properties, and applications.* **80**, 391–425 (2001)
25. Mishra, R., Panigrahy, S., Barman, S.: Single-source-derived nitrogen-doped soft carbons for application as anode for sodium-ion storage. *Energy Fuels* **36**, 6483–6491 (2022)
26. Mittal, U., Djuandhi, L., Sharma, N., Andersen, H.L.: Structure and function of hard carbon negative electrodes for sodium-ion batteries. *J. Phys. Energy* **4**, 042001–042026 (2022)
27. Greil, P.: Perspectives of nano-carbon based engineering materials. *Adv. Funct. Mater.* **17**, 124–137 (2015)

Synthesis and Characterizations of Nanocarbon



Diego R. Lobato-Peralta, Alejandro Ayala-Cortés, Estefanía Duque-Brito,
and Patrick U. Okoye

Abstract Nanocarbons have become increasingly relevant in the field of energy storage due to their diverse properties, which make them suitable for use in a variety of devices such as batteries, supercapacitors, and fuel cells. The properties of carbon-based materials are heavily influenced by the choice of precursor, process conditions, and reactor type used in their synthesis. Thus, understanding the interplay between these factors is crucial for designing carbon-based energy storage materials with tailored performance characteristics. This chapter provides an overview of the latest and traditional technologies used to obtain nanocarbon materials, including innovative approaches like reactors that use concentrated solar energy and traditional methods like tubular furnaces. We also outline the common methodologies used to synthesize diverse nanocarbon materials, such as carbon nanotubes, graphene, and nanoporous carbons. Furthermore, this chapter discusses the techniques commonly used to characterize nanocarbon materials and evaluate their properties. These techniques include surface area measurement, determination of chemical composition, evaluation of the degree of order/disorder, identification of functional groups on the surface, and electrochemical characterization for energy storage applications, among others.

Keywords Activated carbon · Solar reactors · Sustainable precursors · Biomass · Green chemistry · Carbon characterization

D. R. Lobato-Peralta (✉) · E. Duque-Brito · P. U. Okoye
Department of Bioenergy, Instituto de Energías Renovables-Universidad Nacional Autónoma de México, Privada Xochicalco S/N, 62580 Temixco, Morelos, Mexico
e-mail: drlp@ier.unam.mx

D. R. Lobato-Peralta · A. Ayala-Cortés
Department of Energy and Environment, Instituto de Carboquímica – CSIC, Miguel Luesma Castán 4, 50018 Zaragoza, Aragón, Spain

1 Sustainable Precursor for Nanocarbon Materials

Nanocarbons are highly significant materials with diverse applications, notably with a focus in energy storage. It is widely recognized that nanocarbons can be derived from various precursors, each with varying environmental and social implications. For instance, it may be considered inappropriate to utilize an edible precursor that could potentially jeopardize food security. In this sense, it is extremely important to continuously search for sustainable alternatives to be used as carbon precursors. Among these alternatives, abundant materials should be considered. Additionally, it is important to utilize materials that lack commercial value and have no other use, in other words, wastes that are not relevant to industry and do not compromise other human needs [1]. Lignocellulosic waste can be considered an excellent sustainable alternative for carbon production, in this sense, biomass represents approximately 545 gigatons of carbon (Gt C) and lignocellulosic biomass accounts for 450 Gt C [2]. Due to its abundance and versatility in being transformed into a wide variety of products, lignocellulosic biomass is a promising candidate for valuable applications [3]. A wide variety of lignocellulosic precursors that have no other applications have been tested as precursors, such as residue lignin, durian husk, tea waste, jute fiber, bamboo, rice husk, and date seed, among many others [4]. Using biomass to produce carbon nanomaterials presents an appealing, environmentally friendly alternative within the circular economy. The carbon materials that can be derived from renewable sources include nanoparticles, graphene, carbon nanofibers, biochars, nanocellulose, porous carbon, and carbon quantum dots, among others. Furthermore, biomass is widespread globally and exhibits variability in composition due to differences in climate and soil properties across regions. As a result, certain minor elements (such as Ca, Mg, K, Ti, Si, Al, and Na) can play a decisive role in the properties of carbon nanomaterials, while others (such as Cu, Fe, Mn, Mo, and Zn) may have catalytic effects [5]. Similarly, precursors from other sources are also suitable for the production of carbon materials. To mention some examples, it is possible to include wasp hives that are abandoned by wasps after a short period of time [6] or disposable diapers, which are extremely abundant residues, that can be a breeding site for new pathogens and infectious diseases [7].

Carbon materials derived from wastes can be utilized for various purposes. However, the central theme of this chapter is carbons for energy storage, including their production and characterization techniques, as explained in greater detail in the following sections.

2 Process Conditions: Temperature, Heating Rate, Activation

To transform a precursor into a carbon material, a thermochemical process must be conducted, altering its chemical composition and structure. The properties of the resulting carbon materials primarily rely on the precursor and the production conditions, with temperature, heating rate, and activation being the key factors. Hence, carbon materials generated under identical conditions but derived from distinct precursors exhibit distinct physicochemical properties.

Temperature emerges as the paramount factor influencing the properties of the resulting carbon material. It directly impacts the presence of heteroatoms on the carbon surface, thereby influencing the abundance of functional groups and the degree of structural order/disorder. These aspects, in turn, influence hydrophilic properties and the distribution of porosity, along with other pertinent characteristics. Typically, the elevation of the activation temperature promotes the development of textural properties in carbonaceous materials, including pore size, pore volume, and specific surface area, up to a certain optimal point [8]. Practically, it is suggested that the increase in temperature is limited and varies depending on other experimental factors, such as the activated agent and precursor involved in the carbon conversion process. Moreover, the temperature factor not only influences the chemical and physical properties of the carbon but also affects the quantity of carbon yield resulting from the conversion process [9].

On the other hand, the heating rate has an important impact on the performance of the resulting carbon material. Specifically, an increase in the heating rate promotes the presence of light volatile compounds that originate from the cracking of the precursor. This leads to a shorter residence time and, in some cases, a reduction in the yield of carbon produced [10]. Conversely, a lower heating rate necessitates a longer residence time, which, in turn, can trigger secondary reactions. As a result, a lower heating rate can yield approximately 30–35% of carbonaceous material [11]. Additionally, it has been observed that the heating rate influences the development of porosity and, consequently, the surface area, although not to the same extent as the temperature factor [12, 13].

The aforementioned factors heavily depend on the selected activation method for converting the precursor into activated carbon (Fig. 1), in other words, carbons with a high surface area due to an abundance of pores. Chemical and physical activation methods are widely employed to obtain this type of material, whereas physicochemical is less common. Chemical activation is characterized by simultaneous carbonization and activation stages, although it has recently been conducted in two steps. This method typically requires temperatures of up to 900 °C. Similarly, chemicals such as K_2CO_3 , NaOH, KOH, $ZnCl_2$, and H_3PO_4 are widely utilized as activating agents, promoting the development of the resulting carbon's textural properties.

In contrast, physical activation requires separate stages for carbonization and activation. The first stage occurs at temperatures ranging from 400 to 700 °C, while the second stage takes place at temperatures of 800–1100 °C. This results in a significant

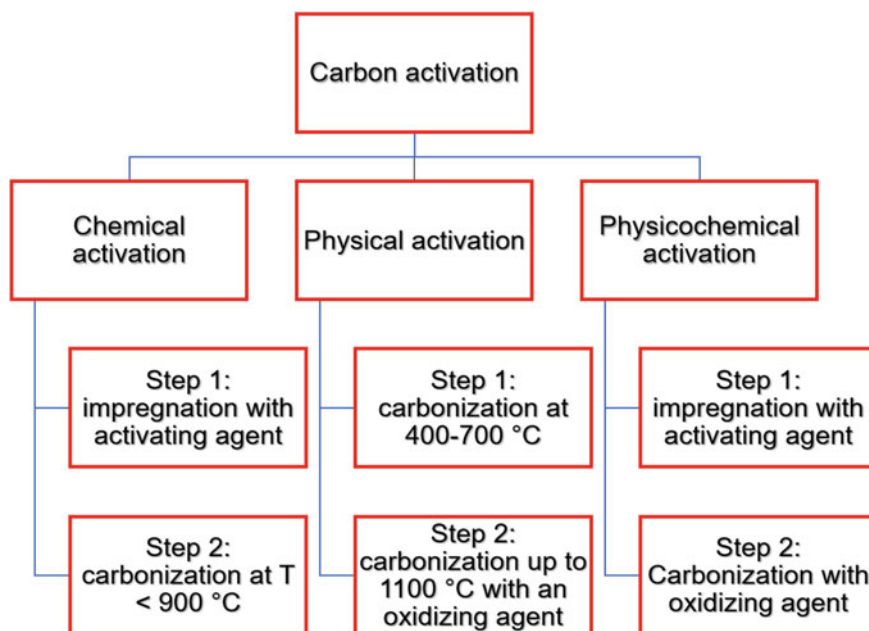


Fig. 1 Schematic representation of activated carbon production methods

increase in energy requirements. During the activation process, it is crucial to utilize an oxidizing agent such as steam, air, or CO_2 [14, 15]. Otherwise, physicochemical activation involves a combination of both physical and chemical activation. Essentially, the process involves saturating the biomass with a chemical activating agent and subjecting it to temperatures between 500 and 800 °C in the presence of an oxidizing agent, which determines the temperature range [16].

3 Reactor Types

There are different reactor technologies to convert a precursor into nanocarbons. The most widely used reactor types involve the use of electric resistances to increase the system's temperature, but recently, solar reactors (utilizing solar energy as the heat source) have been studied more extensively.

Electrical tubular reactors have found extensive application in the production of various types of nanocarbons from a wide range of precursors. This type of reactor utilizes electricity to generate heat, facilitating the transformation of the precursor into nanocarbon materials. These reactors offer several advantages, including precise temperature control, and their operating conditions can be electronically regulated through instrumentation systems. However, it has been reported that the use of electricity in these reactors significantly contributes to greenhouse gas emissions [17],

thus presenting an environmental concern and posing a challenge to the sustainability of nanocarbon production.

On the other hand, a solar reactor is a type of reactor that utilizes concentrated solar energy, either directly or indirectly, for heating purposes. This has been achieved through the application of concentrated solar technologies, operating within different temperature ranges (200–3000 °C). Solar reactors can be classified based on the method of heating reagents, either directly or indirectly. In Fig. 2, it can be observed that an indirectly heated reactor provides energy for the reaction in a slower manner, as the heat supplied must traverse from the heated external wall through the materials until it reaches the reactive part. Typically, these reactors are constructed using metal alloys, primarily stainless steel. Some drawbacks associated with this configuration include lower heating rates and high thermal stress in the materials due to non-homogeneous heat distribution caused by the linear heat distribution of concentrated solar technologies. One significant advantage of these reactors is their capability to operate at high pressures [18].

Conversely, a directly heated reactor is composed of materials with high transmittance, such as borosilicate, quartz, and tempered glass, which facilitate direct radiative heat transfer from the source to the reactive part. Direct heating reactors can achieve temperatures and heating rates of up to 3000 °C and 450 °C/min, respectively [3]. However, a drawback of using such window materials in solar reactors is their inability to withstand higher pressures without breaking, and the gases released during the reactions can contaminate the atmosphere and reduce the heating rate. Nevertheless, this issue can be mitigated by implementing a sweeping gas.

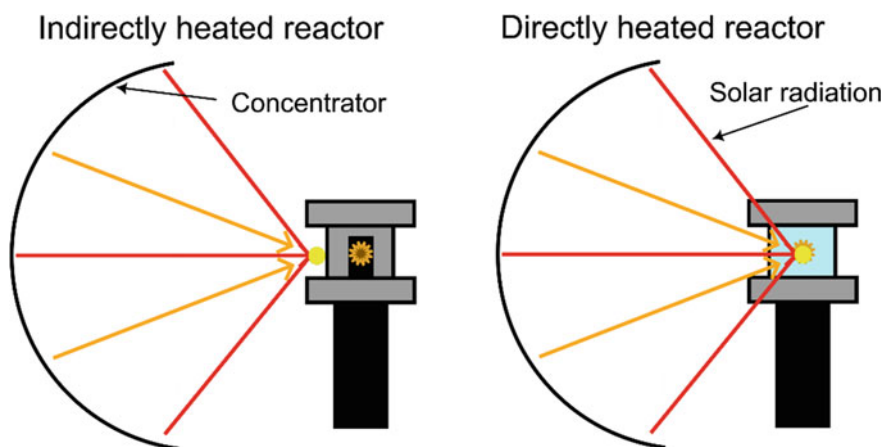


Fig. 2 Schematic representation of solar irradiated reactor types

4 Common Technologies for Diverse Nanocarbon Materials

Carbon has vast applications, and its production could assume several shapes or structure for task specific application. Nanoporous carbons or nanoarchitectonics have been of increasing appeal due to their exceptional characteristics such as high surface area, durability, lightweight, conductivity, and abundant oxygen groups that allows easy functionalization. In this section, the focus shifts to the discussion of nanoporous carbons, which includes carbon nanotubes, graphene, and nanocomposites, all of which represent noteworthy selections within the realm of carbon-based materials.

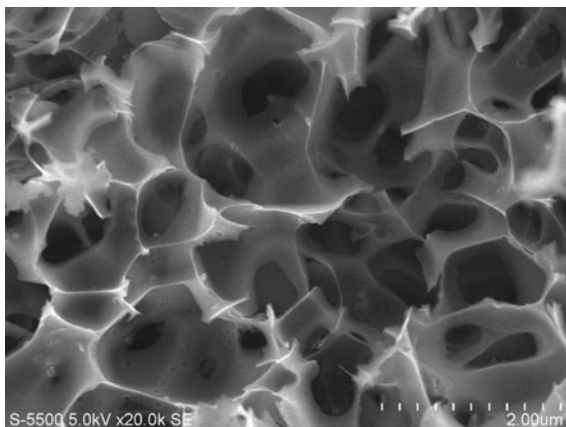
4.1 Nanoporous Carbon

Nanoporous carbons are derived from various sources, primarily through the utilization of an activating agent, as mentioned earlier in Sect. 2. The presence of porosity in these materials (Fig. 3) renders them well-suited for energy storage applications due to the advantageous electrical double layer (EDL) mechanism. This mechanism holds immense importance in devices like supercapacitors. Supercapacitors are composed of cells comprising two electrodes immersed in an electrolytic medium (liquid or solid-state) containing dissolved ions. These electrodes are separated by a dielectric material to prevent short circuits. The EDL phenomenon arises when the ions dissolved in the electrolyte are attracted to the carbon surface through electrostatic interactions, forming a closely situated layer. This phenomenon plays a crucial role in the storage of energy within the system [19]. In this context, enhanced porosity facilitates an increase in the specific surface area of carbon materials. This increased porosity allows for a higher specific surface area of carbon materials, enabling them to attract a greater quantity of ions and, consequently, achieve a higher capacity for energy storage through the electrical double layer (EDL) mechanism.

It is crucial to highlight that the porosity of carbon materials derived from a particular precursor varies when the production conditions, such as temperature, heating rate, and activating agent, differ. For instance, when carbon materials are obtained from agave leaves without any activating agent in the temperature range of 600–950 °C, specific surface areas range from 47 to 298 m²/g. However, when the carbon production process from this precursor is aided by the use of K₂CO₃, the specific surface area of the resulting materials dramatically increases to more than 2800 m²/g [20, 21].

Not only lignocellulosic precursors suitable for nanoporous carbon production, but it is also possible to utilize various abundant waste materials that contain carbon atoms in their composition. Diapers, for instance, are known to be abundant residues, particularly in densely populated urban areas. It has been demonstrated that these materials can be transformed into activated carbon through impregnation with H₃PO₄ followed by a thermal process within the temperature range of 400–600 °C [7]. The

Fig. 3 Representative micrograph of nanoporous carbon materials



resulting materials exhibit a hierarchical porosity, encompassing macro-, meso-, and micropores, along with a specific surface area of up to $936 \text{ m}^2/\text{g}$. These materials have been evaluated as supercapacitor electrodes and have displayed promising characteristics, including good energy retention and excellent coulombic efficiency. In a similar vein, another non-lignocellulosic material that has been tested as a nanoporous carbon precursor is wasp hives. These hives are constructed by wasps for temporary habitation before being abandoned. A recent study [6] have successfully demonstrated the production of highly porous carbon from this particular precursor, resulting in a specific surface area of $765 \text{ m}^2/\text{g}$. Furthermore, the resulting material was evaluated as a supercapacitor electrode and exhibited a specific capacitance of up to 225 F/g . Notably, it displayed superior electrochemical behavior compared to a commercially available activated carbon that underwent testing under identical conditions.

4.2 Carbon Nanotubes

The history of carbon nanotubes can be traced back to the 1990s when they were initially fabricated by Iijima and co-workers using an arc-discharge evaporation method [22]. As the name suggests, carbon nanotubes are one-dimensional tubular structures (Fig. 4) composed of sp^2 -hybridized carbon atoms [23]. Given their significant attributes, including excellent electrical conductivity, mechanical strength, thermal resistance, and chemical stability, carbon nanotubes are commonly utilized in energy storage applications, such as the fabrication of flexible (solid-state) supercapacitors, fuel cells and hydrogen storage [24].

Carbon nanotubes have been synthesized using various precursors and methodologies. For instance, carbon nanotubes have been derived from algal biochar through microwave-assisted synthesis [25]. In this particular case, the initial step involved

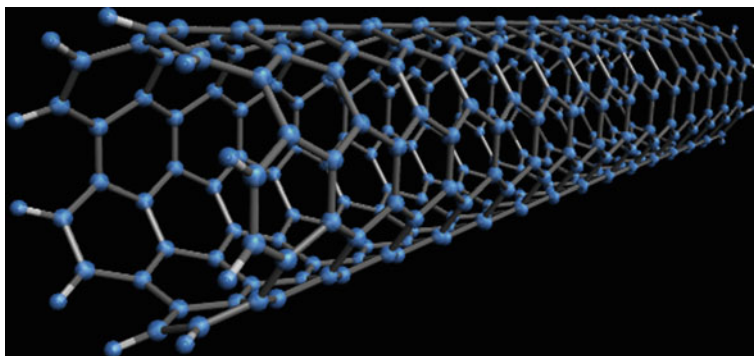


Fig. 4 Schematic representation of carbon nanotubes

pyrolysis of *Macrocystis pyrifera*, *Sarcothalia crispata*, and *Scenedesmus almeriensis* species at 600 °C (with a heating rate of 3 °C/min) for 3 h in the presence of nitrogen, resulting in the formation of biochar. Subsequently, the obtained biochars were subjected to treatment in a microwave oven operating at 2.45 GHz and 17 psi, with the addition of ferrocene as a catalyst. The synthesis process lasted for 5 min, and the irradiation ranged from 100 to 300 W, leading to temperatures between 80 and 100 °C. The resulting materials were identified as multiwall carbon nanotubes containing a substantial nitrogen content in their structure.

In addition to the utilization of plant-based materials, there have been endeavors to explore the use of real-world plastics as sustainable precursors for carbon nanotube production. The methodology employed for this purpose [26] involved the collection of plastic raw materials, namely polystyrene, polyethylene, polyethylene terephthalate, and polypropylene. These materials underwent a transformation process, converting them into carbon nanotubes through a system consisting of two furnace reactors that reached temperatures of up to 800 °C. The heating rate employed was 20 °C/min, and Fe@Al₂O₃ served as the catalyst. This process allowed a carbon yield of approximately 32% and a purity level of 93%. Another important advancement in environmentally conscious carbon nanotube production is the simultaneous generation of carbon nanotubes and hydrogen gas, as described in [27]. This process involved the catalytic conversion of biogas into a methane-rich gas utilizing Ni/CeO₂ as the catalyst. In the subsequent step, this methane-rich gas was chemically decomposed in an oven using CoMo/MgO as the catalyst, leading to the formation of carbon nanotubes and hydrogen gas. Through this procedure, multiwall carbon nanotubes with a purity level of 90% were successfully obtained.

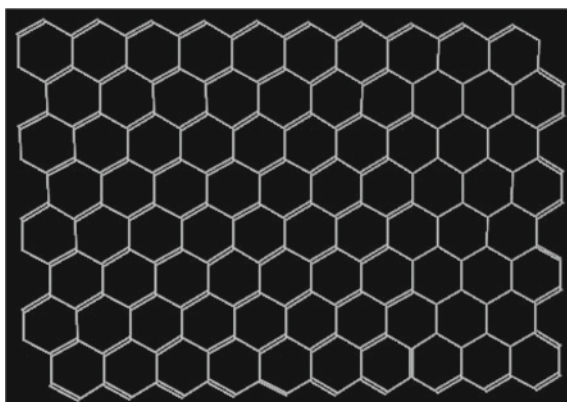
4.3 Graphene

The history of graphene began in 2004 when this material was first produced through mechanical exfoliation from graphite. Graphene is characterized by its ortho-hexagonal honeycomb-like structure (Fig. 5), which arises from carbon atoms exhibiting sp^2 hybridization and forming three chemical bonds with angles of 120° [28]. Thanks to its unique chemical structure, graphene exhibits intriguing properties, including high electron mobility, remarkable mechanical strength, exceptional electrical and thermal conductivity. These qualities make it highly suitable for a wide range of energy storage applications, including batteries, supercapacitors, hydrogen storage, among others [29].

Two primary forms of graphene commonly employed in energy storage applications are graphene oxide and reduced graphene oxide [30]. Graphene oxide is a material composed of single or multiple layers with oxygen-based functional groups incorporated into its structure. The presence of these functional groups leads to lower electrical conductivity. However, graphene oxide exhibits higher reactivity compared to graphene and serves as an excellent substrate for nanoparticles. Additionally, it is well-suited for use in both aqueous and organic solutions, making it a versatile choice for various applications. On the other hand, reduced graphene oxide is derived from the reduction of graphene oxide and can be obtained through various methods. As the name suggests, this material possesses fewer oxygen-based functional groups compared to graphene oxide. However, it is crucial to note that reduced graphene oxide differs from the pristine graphene structure, resulting in distinct properties between the two materials. Although the electrical conductivity of reduced graphene oxide is lower than that of graphene, the presence of oxygen-based functional groups in its structure enhances electron transfer.

Different methods have been reported for the production of graphene, and they can generally be classified into two main categories: bottom-up and top-down methods [31]. Bottom-up methods involve the construction of graphene using simple carbon molecules. These methods start with small carbon units and build up the graphene

Fig. 5 Schematic representation of graphene layer structure



structure. On the other hand, top-down methods involve extracting graphene oxide, which is a bulk material, from a carbon source or graphite. The top-down approach is widely recognized as the most popular method for producing graphene derivatives. Among these methods, three main routes to synthesize graphene-based materials, such as graphene oxide, can be mentioned: Brodie's method, Straudenmaier's method, and Hummer's method. The difference between these three methods lies in the ability to vary the oxidation degree through factors such as stoichiometry, reaction conditions (pressure, temperature, etc.), and the type of graphite used. Graphene oxide can be synthesized by oxidizing graphite or by using alternative forms or sources, whether they are synthetic or natural.

Hummer's method and its variations are among the techniques that have been employed for synthesizing graphene. For instance, it has been reported a preparation of graphene oxide from graphite [32] in which initially, graphite was combined with concentrated H_2SO_4 and NaNO_3 at low temperatures. KMnO_4 was gradually introduced to maintain the temperature below 5°C , and the mixture was stirred while deionized water was added. The oxidation reaction was augmented with additional water and H_2SO_4 solution. The resulting product underwent a series of washes, including treatment with an $\text{HCl} + \text{H}_2\text{O}$ solution, deionized water, and ethanol, until the pH reached a neutral level. Reduction of graphene oxide to graphene was accomplished through sonication in water and subsequent treatment with hydrazine hydrate. The reduced graphene oxide was purified by filtration and subsequently dried, yielding graphene powder. The resultant material exhibited excellent electrochemical performance, demonstrating a capacitance of 525 F/g at a scan rate of 30 mV/s in a 3-electrode system.

5 Characterization Techniques

Providing a comprehensive description of the properties of activated carbon continues to pose a challenge. As previously discussed, the attributes of activated carbon are predominantly influenced by the precursor and the specific procedure employed, leading to a divergence in properties among distinct samples. It is imperative to acquire and analyze these variations in order to maximize the efficient utilization of carbonaceous materials across applications including adsorption, electrochemistry, cosmetics, and various other intended purposes. Noteworthy characterization techniques for activated carbon encompass the assessment of textural properties, surface chemistry, and elemental composition of the carbon samples [33]. Next subsections will delve into detailed explanations of several of these techniques.

5.1 *Gasses Physisorption*

Describing the properties of activated carbon comprehensively remains a challenging task, as mentioned in previous sections. One of the key parameters that significantly impacts the behavior of carbon-based materials in energy storage is their surface area. Therefore, it becomes imperative to accurately measure this surface area.

The technique employed to measure the surface area of carbon materials is gas physisorption. This technique involves a pretreatment process that begins with purging the surface of the material. The procedure starts by placing the sample in a quartz cell, followed by the application of a vacuum and an increase in temperature. It is crucial to determine the upper temperature limit based on the specific material under analysis to prevent any thermal decomposition of the sample. The combined effect of vacuum and high temperature leads to the removal of particles from the surface of the material, enabling the measurement of its surface area. After the purging process, the sample is transferred to an analysis station where the pressure is carefully controlled. A new vacuum is generated, and a gas is injected into the system with the intention of being adsorbed onto the surface of the carbon material. Various pressures are applied to the system, while maintaining a constant temperature, in order to generate isotherms (Fig. 6a) that are conducive to the analysis of the textural properties of the material. The amount of gas that is adsorbed provides information about the surface area of the material. By measuring the quantity of gas adsorbed, it becomes possible to determine the surface area of the material under examination. Regarding the types of gases used for this technique, the most common ones are nitrogen and argon; however, it is also possible to use others such as helium, carbon dioxide, among others.

The isotherms obtained from this analysis indicate various properties of the carbon materials. For instance, they provide information about the size of the pores and the degree of interaction between the sample and the gas. The identified pores can be categorized as macropores (>50 nm), mesopores (2–50 nm), and micropores (<2 nm). Similarly, the shape of the isotherms can offer insights into the shape of the pores. For example, it can determine whether the pores are uniform, inkbottle shaped, exhibit network effects, or have blocked pores, among other effects [34].

5.2 *Chemical Composition and Functional Groups*

Chemical composition plays a crucial role in determining the performance of carbon-based materials for energy storage applications. Therefore, it is of utmost importance to understand the elemental constituents of these materials. Several methods can be employed for this purpose, including energy dispersive X-ray analysis, which is conducted concurrently with electron microscopy. This technique involves bombarding the material with high-energy electrons or X-rays and detecting and measuring the resulting emitted X-rays. The emitted radiation is unique to each

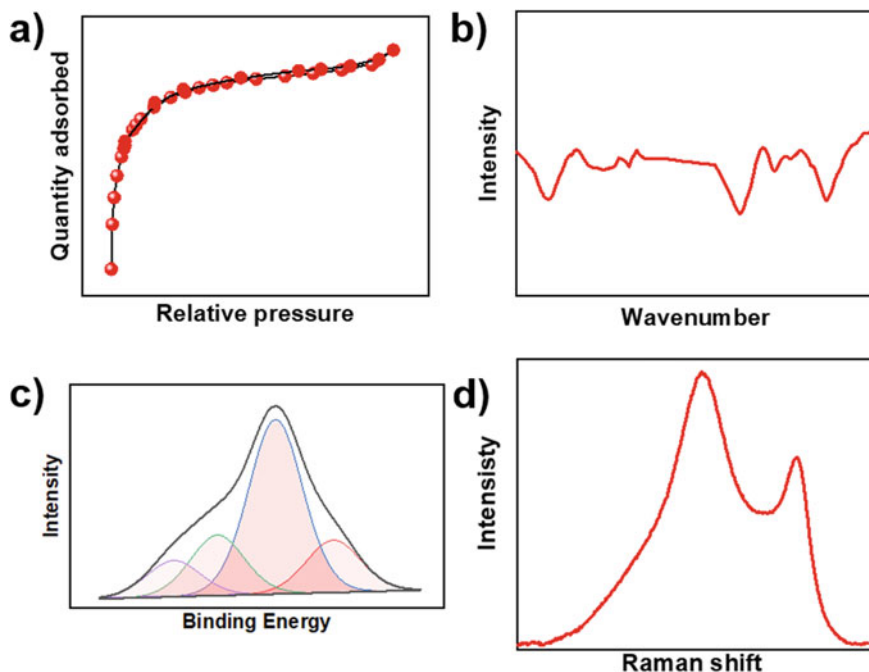


Fig. 6 Examples of responses obtained through different physicochemical characterizations of nanocarbon materials. **a** Gasses physisorption, **b** Fourier transform infrared spectroscopy, **c** photoelectron spectroscopy, **d** Raman spectroscopy

element, enabling the identification and quantification of elements and their concentrations. Another approach for characterizing carbon-based materials is CHNS/O elemental analysis, which involves the destructive combustion of the sample and the use of detectors to measure the amounts of carbon, hydrogen, nitrogen, and sulfur (oxygen is determined by difference) [6, 35].

Additionally, it is essential to determine the functional groups present in carbon samples. Two prominent techniques for this purpose are Fourier Transform Infrared Spectroscopy (FTIR) and X-ray Photoelectron Spectroscopy (XPS). FTIR involves the exposure of the sample to infrared radiation, causing specific frequencies of the radiation to be absorbed by the sample's molecules. The absorbed frequencies correspond to the characteristic vibrational modes of the chemical bonds within the molecules, each of which is distinct (Fig. 6b). The transmitted or reflected infrared radiation is then analyzed to generate a spectrum, representing the intensity of absorbed radiation as a function of wavelength or wavenumber. On the other hand, XPS utilizes a high-energy X-ray source directed at the sample's surface, resulting in the emission of photoelectrons from the sample's atoms. The energy of these emitted photoelectrons is measured to produce an XPS spectrum (Fig. 6c), which provides information about the binding energies specific to the elements and chemical environments present [35, 36].

5.3 Raman Spectroscopy

Raman spectroscopy is a valuable characterization technique employed to determine the physical and chemical properties of carbon materials. This analytical method involves directing a laser beam onto the surface of the sample to assess its vibrational modes and generate a corresponding spectrum. The resulting spectrum represents the intensity plotted against the Raman shift, which signifies the energy difference between the incident and scattered photons. Carbon materials typically exhibit characteristic responses within the Raman shift range of approximately $1300\text{--}1700\text{ cm}^{-1}$, manifesting as two distinct bands known as D and G (Fig. 6d). By nature, this technique provides insights into molecular vibrations encompassing stretching, bending, and rotational modes. These parameters facilitate the acquisition of information pertaining to the chemical bonds, molecular structures, and functional groups present in the carbon material. Among the notable advantages offered by this technique are the ability to obtain molecular-specific information, its non-destructive nature, and the requirement of only a small sample quantity for analysis, among others [37].

5.4 Electrochemical Characterization

Electrochemical characterization plays a crucial role in assessing the performance of carbon materials for energy storage applications. This characterization provides valuable insights into the suitability of carbon materials for integration into various energy storage systems. It is important for the utilization of this type of characterization that the carbon material be present as part of the electrodes that constitute the analysis system. Below are some of the key techniques used in this field:

- **Cyclic voltammetry:** This technique consists of applying an electrical potential to a working electrode, with another electrode serving as a reference, to obtain a corresponding measured current. It is useful for determining the redox behavior of chemical species present on the electrode and/or understanding the electrochemical properties of the carbon surface. The resulting plot, comparing the obtained current with the applied potential (Fig. 7a), is known as a cyclic voltammogram [38]. In the field of supercapacitors, this technique enables the determination of the capacitance of the carbon electrode through simple calculations. For a capacitive material, it is expected that the profile obtained exhibits a semi-rectangular shape, indicating energy storage across the entire potential window. Conversely, for a battery, well-defined redox peaks are observed due to the energy storage occurring through chemical reactions at specific potentials [39].
- **Galvanostatic charge/discharge:** This electrochemical method is based on applying a constant current to the system and monitoring the resulting voltage response over time (Fig. 7b). In other words, the system is charged and subsequently discharged. During the charging phase, the system receives the current, and energy is stored, resulting in a change in potential until a specified endpoint

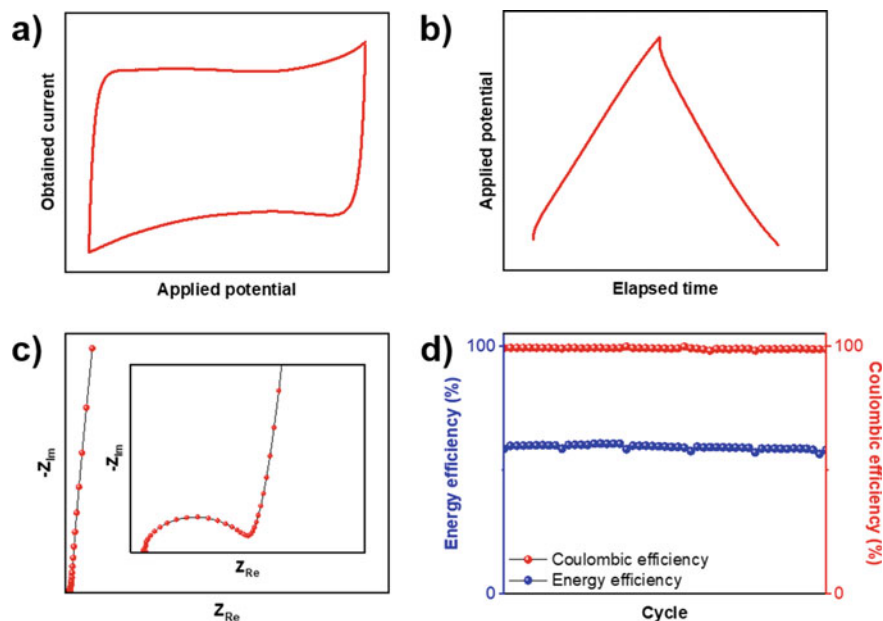


Fig. 7 Typical responses obtained for a supercapacitor through **a** cyclic voltammetry, **b** galvanostatic charge/discharge, **c** potentiometric electrochemical impedance spectroscopy, **d** efficiency measurement

is reached. Subsequently, the polarity of the current is inverted, and the system begins to discharge, releasing stored energy and causing the potential to decrease until a specified point or complete discharge of the system occurs. By analyzing the voltage response during both the charge and discharge phases, valuable information about the energy storage and conversion processes in the device can be obtained [40]. Parameters such as capacity, efficiency, power output, and voltage stability can be determined from the galvanostatic charge/discharge curves.

- Potentiometric electrochemical impedance spectroscopy:** Unlike the two previously mentioned methods, potentiometric electrochemical impedance spectroscopy employs alternating current instead of direct current. For this reason, this characterization technique utilizes a sinusoidal perturbation (usually in the range of ± 5 – 10 mV) and measures the resulting current response at different frequencies. This technique allows the acquisition of Nyquist plots (Fig. 7c) that illustrate the real contribution of impedance (resistance, Z_{Re}) and the imaginary contribution (reactance, Z_{Im}), which is associated with the capacitive or inductive behavior of the system. Similarly, potentiometric electrochemical impedance spectroscopy is useful for obtaining information about charge transfer kinetics, double-layer capacitance, adsorption/desorption phenomena, and diffusion processes. It finds wide application in corrosion studies, fuel cell research, battery characterization, and the development of electrochemical sensors [41, 42].

- **Coulombic and energy efficiencies:** Other important parameters commonly reported to gain a better understanding of the behavior of carbon materials for energy storage applications are coulombic and energy efficiencies (Fig. 7d). Coulombic efficiency measures the degree to which electrical charge is transferred during electrochemical processes. It can be expressed as the ratio of the actual amount of charge participating in the desired reaction to the total charge theoretically available. Supercapacitors typically exhibit values close to 100% for this parameter, while batteries often have values exceeding 80%. In contrast, energy efficiency represents the ratio of energy received by the electrode during the charging process to the amount of energy released during discharge. As anticipated, energy transfer processes exhibit efficiencies lower than 100% due to irreversible energy losses as heat resulting from non-reversible faradaic processes, the generation of decomposition products, blockage of material porosity, among other factors, resulting usually in energy efficiencies of ~60% [30, 43, 44].

6 Conclusions

Carbon-based materials can be obtained from a wide variety of precursors. However, it is always important to prioritize those that are more sustainable or have minimal environmental impact. Several parameters influence the production of these materials, with temperature, heating rate, and the type of activation employed being the most crucial. Furthermore, from a production method standpoint, it is also possible to explore alternatives in green chemistry, such as solar concentration processes to raise the temperature instead of using traditional energy sources that generate higher levels of harmful emissions to the environment.

Due to their versatility, various carbon-based materials have been employed for energy storage, including nanoporous carbons, graphene, carbon nanotubes, among others. These materials exhibit different properties that make them suitable for use in various devices that can adapt to specific requirements. To gain a better understanding of the behavior of carbon materials for energy storage, it is necessary to subject them to various characterization techniques. These techniques allow for the determination of parameters such as specific surface area, degree of order/disorder in the structure, chemical composition, functional groups, and electrochemical performance.

Acknowledgements This work was financed by Dirección General de Asuntos del Personal Académico (DGAPA-UNAM)-PAPIIT under project No. IA102522. A master's fellowship was granted to E. Duque-Brito through CONAHCYT. Authors also acknowledge the financial support of MCIN with funding from European Union NextGenerationEU (PRTR-C17.I1) within the Green Hydrogen and Energy Program-CSIC, as part of the CSIC Interdisciplinary Thematic Platform (PTI+) Transición Energética Sostenible+ (PTI-TRANSENER+). Authors also acknowledge the financial support of MICINN and the European Union under the NextGeneration EU Program to the FABSEE project (Iron-air batteries as cost-effective and sustainable electrochemical energy storage, TED2021-130279A-I00, call Proyectos de Transición Ecológica y Digital) and PRTR-C17.I1 within the Green Hydrogen and Energy Program-CSIC, as part of the CSIC Interdisciplinary Thematic Platform (PTI+) Transición Energética Sostenible+ (PTI-TRANSENER+).

References

1. Fic, K., Platek, A., Piwek, J., Frackowiak, E.: Sustainable materials for electrochemical capacitors. *Mater. Today* **21**, 437–454 (2018)
2. Bar-On, Y.M., Phillips, R., Milo, R.: The biomass distribution on earth. *Proc. Natl. Acad. Sci.* **115**, 6506–6511 (2018)
3. Ayala-Cortés, A., Arcelus-Arrillaga, P., Millan, M., Arancibia-Bulnes, C.A., Valadés-Pelayo, P.J., Villafán-Vidales, H.I.: Solar integrated hydrothermal processes: a review. *Renew. Sustain. Energy Rev.* **139**, 14–23 (2021)
4. Lobato-Peralta, D.R., Duque-Brito, E., Villafán-Vidales, H.I., Longoria, A., Sebastian, P.J., Cuentas-Gallegos, A.K., Arancibia-Bulnes, C.A., Okoye, P.U.: A review on trends in lignin extraction and valorization of lignocellulosic biomass for energy applications. *J. Clean. Prod.* **293**, 126123–126147 (2021)
5. Matveeva, V.G., Bronstein, L.M.: From renewable biomass to nanomaterials: does biomass origin matter? *Prog. Mater. Sci.* **130**, 100999–101039 (2022)
6. Lobato-Peralta, D.R., Amaro, R., Arias, D.M., Cuentas-Gallegos, A.K., Jaramillo-Quintero, O.A., Sebastian, P.J., Okoye, P.U.: Activated carbon from wasp hive for aqueous electrolyte supercapacitor application. *J. Electroanal. Chem.* **901**, 115777–115787 (2021)
7. Lobato-Peralta, D.R., Arias, D.M., Okoye, P.U.: Polymer superabsorbent from disposable diaper as a sustainable precursor for the development of stable supercapacitor electrode. *J. Energy Storage* **40** (2021)
8. Park, S.-J., Kim, K.-D.: Influence of activation temperature on adsorption characteristics of activated carbon fiber composites. *Carbon N. Y.* **39**, 1741–1746 (2001)
9. Ayinla, R.T., Dennis, J.O., Zaid, H.M., Sanusi, Y.K., Usman, F., Adebayo, L.L.: A review of technical advances of recent palm bio-waste conversion to activated carbon for energy storage. *J. Clean. Prod.* **229**, 1427–1442 (2019)
10. Doja, S., Pillari, L.K., Bichler, L.: Processing and activation of tire-derived char: a review. *Renew. Sustain. Energy Rev.* **155**, 111860–111881 (2022)
11. Sakhiya, A.K., Anand, A., Kaushal, P.: Production, activation, and applications of biochar in recent times. *Biochar* **2**, 253–285 (2020)
12. Ayala-Cortés, A., Lobato-Peralta, D.R., Arreola-Ramos, C.E., Martínez-Casillas, D.C., Pacheco-Catalán, D.E., Cuentas-Gallegos, A.K., Arancibia-Bulnes, C.A., Villafán-Vidales, H.I.: Exploring the influence of solar pyrolysis operation parameters on characteristics of carbon materials. *J. Anal. Appl. Pyrolysis* **140**, 290–298 (2019)
13. Fu, P., Hu, S., Xiang, J., Sun, L., Su, S., Wang, J.: Evaluation of the porous structure development of chars from pyrolysis of rice straw: effects of pyrolysis temperature and heating rate. *J. Anal. Appl. Pyrolysis* **98**, 177–183 (2012)
14. Reza, M.S., Yun, C.S., Afroze, S., Radenahmad, N., Bakar, M.S.A., Saidur, R., Taweekun, J., Azad, A.K.: Preparation of activated carbon from biomass and its' applications in water and gas purification, a review. *Arab. J. Basic Appl. Sci.* **27**, 208–238 (2020)
15. Ouyang, J., Zhou, L., Liu, Z., Heng, J.Y.Y., Chen, W.: Biomass-derived activated carbons for the removal of pharmaceutical micropollutants from wastewater: a review. *Sep. Purif. Technol.* **253**, 117536–117553 (2020)
16. Canales-Flores, R.A., Prieto-García, F.: Activation methods of carbonaceous materials obtained from agricultural waste. *Chem. Biodivers.* **13**, 261–268 (2016)
17. Ortiz, P., Kubler, S., Rondeau, É., McConky, K., Shukhobodskiy, A.A., Colantuono, G., Georges, J.P.: Greenhouse gas emission reduction in residential buildings: a lightweight model to be deployed on edge devices. *J. Clean. Prod.* **368**, 133092–133106 (2022)
18. Ayala-Cortés, A., Arcelus-Arrillaga, P., Millan, M., Okoye, P.U., Arancibia-Bulnes, C.A., Pacheco-Catalán, D.E., Villafán-Vidales, H.I.: Solar hydrothermal processing of agave bagasse: insights on the effect of operational parameters. *Renew. Energy* **192**, 14–23 (2022)
19. Muñiz, J., Cuentas-Gallegos, A.K., Robles, M., Guillén-López, A., Lobato-Peralta, D.R., Pascoe-Sussoni, J.E., Boddula, R., Khan, A., Asiri, A.M., Kolosov, A.E. (eds.): Lignin-derived materials for supercapacitors. In: *Handbook of Supercapacitor Materials*. Wiley-VCH (2022)

20. Lobato-Peralta, D.R., Pacheco-Catalán, D.E., Altuzar-Coello, P.E., Béguin, F., Ayala-Cortés, A., Villafán-Vidales, H.I., Arancibia-Bulnes, C.A., Cuentas-Gallegos, A.K.: Sustainable production of self-activated bio-derived carbons through solar pyrolysis for their use in supercapacitors. *J. Anal. Appl. Pyrolysis* **150**, 104901–104912 (2020)
21. Lobato-Peralta, D.R., Ayala-Cortés, A., Longoria, A., Pacheco-Catalán, D.E., Okoye, P.U., Villafán-Vidales, H.I., Arancibia-Bulnes, C.A., Cuentas-Gallegos, A.K.: Activated carbons obtained by environmentally friendly activation using solar energy for their use in neutral electrolyte supercapacitors. *J. Energy Storage* **52**, 104888–104898 (2022)
22. Iijima, S.: Helical microtubules of graphitic carbon. *Nature* **354**, 56–58 (1991)
23. Lv, R., Cruz-Silva, E., Terrones, M.: Building complex hybrid carbon architectures by covalent interconnections: graphene-nanotube hybrids and more. *ACS Nano* **8**, 4061–4069 (2014)
24. Ghodhbane, M., Ashraf, J.M., Karam, Z., Lonkar, S., Alshaya, A., Busà, C.: Cellulose nanofibers as a green binder for symmetric carbon nanotubes-based supercapacitors. *Electrochim. Acta* **461**, 142584 (2023)
25. Hidalgo, P., Navia, R., Hunter, R., Camus, C., Buschmann, A., Echeverría, A.: Carbon nanotube production from algal biochar using microwave irradiation technology. *J. Anal. Appl. Pyrolysis* **172**, 106017 (2023)
26. Zhu, Y., Miao, J., Zhang, Y., Li, C., Wang, Y., Cheng, Y., Long, M., Wang, J., Wu, C.: Carbon nanotubes production from real-world waste plastics and the pyrolysis behaviour. *Waste Manag.* **166**, 141–151 (2023)
27. Rattanaamonkulchai, R., Kludpantanapan, T., Nantapong, P., Srifa, A., Koo-Amornpattana, W., Chaiwat, W., Sakdaronnarong, C., Kiatphuengporn, S., Charinpanitkul, T., Assabumrungrat, S., Wongsakulphasatch, S., Eiad-ua, A., Sudoh, M., Watanabe, R., Fukuhara, C., Ratchahat, S.: Simultaneous production of hydrogen and carbon nanotubes from biogas: on the design of combined process. *Int. J. Hydrogen Energy* **47**, 14432–14452 (2022)
28. Wen, Y., Liu, H., Jiang, X.: Preparation of graphene by exfoliation and its application in lithium-ion batteries. *J. Alloys Compd.* **961**, 170885 (2023)
29. Boateng, E., Thiruppathi, A.R., Hung, C.-K., Chow, D., Sridhar, D., Chen, A.: Functionalization of graphene-based nanomaterials for energy and hydrogen storage. *Electrochim. Acta* **452**, 142340 (2023)
30. Liu, Z., Navik, R., Tan, H., Xiang, Q., Wahyudiono, Goto, M., Ibarra, R.M., Zhao, Y.: Graphene-based materials prepared by supercritical fluid technology and its application in energy storage. *J. Supercrit. Fluids* **188**, 105672–105688 (2022)
31. Omar, H., Malek, N.S.A., Nurfazianawatie, M.Z., Rosman, N.F., Bunyamin, I., Abdullah, S., Khusaimi, Z., Rusop, M., Asli, N.A.: A review of synthesis graphene oxide from natural carbon based coconut waste by Hummer's method. *Mater. Today Proc.* **75**, 188–192 (2023)
32. Padma Priya, R., Baradeswaran, A., Bagubali, A.: Energy storage improvement of graphene based super capacitors. *Mater. Today Proc.* 919–923 (2023)
33. Bläker, C., Muthmann, J., Pasel, C., Bathen, D.: Characterization of activated carbon adsorbents—state of the art and novel approaches. *ChemBioEng Rev.* **6**, 119–138 (2019)
34. Thommes, M., Kaneko, K., Neimark, A.V., Olivier, J.P., Rodriguez-Reinoso, F., Rouquerol, J., Sing, K.S.W.: Physisorption of gases, with special reference to the evaluation of surface area and pore size distribution (IUPAC technical report). *Pure Appl. Chem.* **87**, 1051–1069 (2015)
35. Ma, Z.H., Li, S., Dong, X.Q., Li, M., Liu, G.H., Liu, Z.Q., Liu, F.J., Zong, Z.M., Cong, X.S., Wei, X.Y.: Recent advances in characterization technology for value-added utilization of coal tars. *Fuel* **334**, 126637–126653 (2023)
36. Rotonnelli, B., Fernandes, M.-S.D., Bournel, F., Gallet, J.-J., Lassalle-Kaiser, B.: In situ/operando X-ray absorption and photoelectron spectroscopies applied to water-splitting electrocatalysis. *Curr. Opin. Electrochem.* **40**, 101314 (2023)
37. Ferrari, A.C., Robertson, J.: Interpretation of Raman spectra of disordered and amorphous carbon. *Phys. Rev. B* **61**, 14095–14107 (2000)
38. Elgrishi, N., Rountree, K.J., McCarthy, B.D., Rountree, E.S., Eisenhart, T.T., Dempsey, J.L.: A practical beginner's guide to cyclic voltammetry. *J. Chem. Educ.* **95**, 197–206 (2018)

39. Brousse, T., Bélanger, D., Long, J.W.: To be or not to be pseudocapacitive? *J. Electrochem. Soc.* **162**, A5185–A5189 (2015)
40. Lang, J., Matějová, L., Cuentas-Gallegos, A.K., Lobato-Peralta, D.R., Ainassaari, K., Gómez, M.M., Solís, J.L., Mondal, D., Keiski, R.L., Cruz, G.J.F.: Evaluation and selection of biochars and hydrochars derived from agricultural wastes for the use as adsorbent and energy storage materials. *J. Environ. Chem. Eng.* **9**, 105979–105995 (2021)
41. Taberna, P.L., Simon, P., Fauvarque, J.F.: Electrochemical characteristics and impedance spectroscopy studies of carbon-carbon supercapacitors. *J. Electrochem. Soc.* **150**, A292 (2003)
42. Navalpotro, P., Anderson, M., Marcilla, R., Palma, J.: Insights into the energy storage mechanism of hybrid supercapacitors with redox electrolytes by electrochemical impedance spectroscopy. *Electrochim. Acta* **263**, 110–117 (2018)
43. Lai, X., Zhou, L., Zhu, Z., Zheng, Y., Sun, T., Shen, K.: Experimental investigation on the characteristics of coulombic efficiency of lithium-ion batteries considering different influencing factors. *Energy* **274**, 127408–127414 (2023)
44. Laheäär, A., Przygocki, P., Abbas, Q., Béguin, F.: Appropriate methods for evaluating the efficiency and capacitive behavior of different types of supercapacitors. *Electrochem. Commun.* **60**, 21–25 (2015)

Electrochemical Properties of Nanocarbon



**Shilpa Pande, Bidhan Pandit, Shoyebmohamad F. Shaikh,
and Mohd Ubaidullah**

Abstract Carbon materials are essential for a wide variety of electrochemical utilisations due to the fact that their electron-transfer and charge-storage capabilities may be tuned. In order to rationally build various high-performance electrochemical devices, it is essential to engage in careful structural manipulation of carbon in order to control its chemical, electrical, and crystalline properties. This study focuses on three different forms of carbon nanomaterials that have recently gained interest in the field of electrochemistry. These are carbon nanofibres, carbon nanotubes (CNTs), and graphene. The focus of this chapter is on the ways in which the structural differences among these carbon nanomaterials influence the electrochemical activities they exhibit. In this Chapter, after providing a brief summary of the recent developments in the fields of Nano carbon and nanofibres, Nano carbon and composites for energy applications, and the future perspectives of Nano carbon electrochemistry, this study will move on to discuss these topics in more depth. Focus is placed on delineating the ways in which the electrical structure of carbon affects the electrochemical activity of the element. Notice some of the modification approaches applicable to over one utilization area through the examination of various electrochemical devices; as a result, structural manipulation approaches utilized in one class of electrochemical devices can be extended to other types of electrochemical devices.

Keywords Carbon nanofibre · Carbon nanotube · Sensing · Carbon nano particles · Graphene · Supercapacitors

S. Pande (✉)

Department of Applied Physics, Laxminarayan Innovation Technological University, Nagpur,
Maharashtra 440033, India
e-mail: sap7001@gmail.com

B. Pandit

Department of Materials Science and Engineering and Chemical Engineering, Universidad,
Carlos III de Madrid, Avenida de la Universidad 30, 28911 Leganés, Madrid, Spain

S. F. Shaikh · M. Ubaidullah

Department of Chemistry, College of Science, King Saud University, P.O. Box 2455,
Riyadh 11451, Saudi Arabia

1 Introduction

It is necessary to do research into the ever-evolving landscape of nanotechnology in order to acquire a comprehension of the current standing of these technologies. One subfield of nanotechnology, known as nanocarbons, is undergoing continuous development and expansion in search of applications that are not only effective but also novel, robust, and efficient and have the potential to fill the gaps left by newer technologies. In this context, the status of various nanocarbons should be evaluated on a frequent and ongoing basis so that the current condition can be observed and the outcomes of the future may be anticipated. Enhanced electrical and thermal conductivity, mechanical strength and transmissivity are some of the qualities that have been reported in these nanocarbons. These properties provide these nanocarbons applications in electronic devices, energy storage, drug carriers, biosensors, biomedicine, aerospace, and thermal management, amongst other fields.

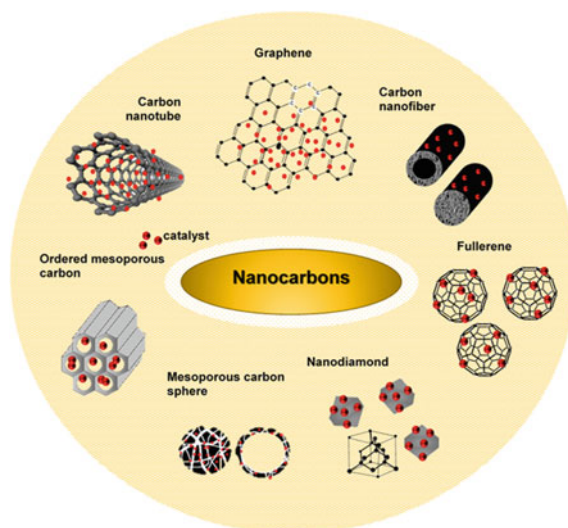
This chapter primarily focused on the Class of Nano carbons, nanofibres and their associated electronic structures and properties, 3D composite foams, Current Progress in the Fields of Nano carbon and nanofibres, Graphene, CNTs, Carbon Nanoparticles, Nano carbon and Composites for Energy Applications, Super capacitors, Future Perspectives of Nano carbon Electrochemistry, and finally, Conclusions.

1.1 Nanocarbons

The term “nanocarbons” is utilised to describe a wide variety of carbon-based materials that have dimensions, structures, and textures on the nanoscale [1]. Because of the dimensional constriction of the electronic structures, nanocarbons have physicochemical characteristics that are entirely their own. When compared to ceramics or synthetic organics, nanocarbons have several advantages, including being abundant, flexible, versatile, lightweight, and environmentally beneficial for a variety of applications (Fig. 1) [2, 3].

Nanocarbons, in general, exhibit outstanding intrinsic features (such as surface chemistry and electrical structures, for example), as well as extrinsic properties (such as specific surface area and shape, for example), which are imparted by the nanoscale confinement of their structures. As a result, synergistic catalytic performance can be achieved with better thermal and chemical stabilities, enhanced activity, and superior reusability by painting active catalyst (such as metal, oxide, and sulfide) onto nanocarbon. This will result in the catalyst having a longer lifespan. These nanocarbon composites have a wide variety of potential applications, some of which include photonics, nanomedicine, environmental remediation, energy storage, and industrial catalysis [5, 6].

Fig. 1 Overview of nanocarbons. Adapted with permission [4], Copyright 2018, Elsevier



1.2 Carbon Nanotubes (CNTs)

CNTs are one-dimensional, cylindrically rolled, solitary layers of carbon. The creation of ‘needle-like tubes’ of limited carbon structures is done by using an arc discharge evaporation technique. The generated carbon structures were eventually characterized as ‘multi-walled CNTs’. On the negative side of the electrode that was participating in the arc discharge, the creation of needle-like tubes was observed [2]. CNTs are essentially tubular structures that are manufactured by rolling up hexagonal sheets of carbon atoms or graphene. This process results in the formation of CNTs. These structures are only able to maintain their alignment and cohesion thanks to the presence of sp^2 bonds and the force of van der Waal. They can also be covered with half fullerene molecules on each end, which makes them even stronger than the sp^3 bonds despite the fact that their structure is completely unique [5].

Types of Carbon Nanotubes:

CNTs can be categorized into two distinct categories as shown in Fig. 2.

- *Single-walled CNTs* (SWCNT): Nanotubes made of single-walled carbon existing in a one-dimensional (1-d) configuration. Armchair and zig-zag shapes are two examples of SWCNTs.
- *Multi-walled CNTs* (MWCNT): It is made up of multiple CNTs arranged in a nesting pattern. This particular variety of nanotubes possesses two diameters: the first one is referred to as the outer diameter, while the second one is referred to as the inner diameter. Chiral multi-walled CNTs are a type of multi-walled CNTs [7].

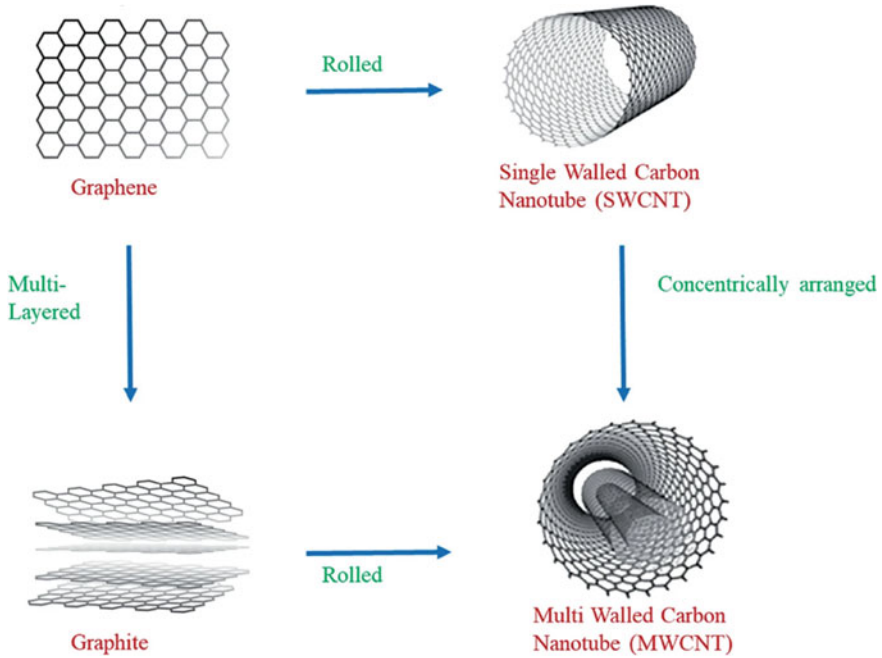


Fig. 2 Types of CNTs. Adapted with permission [7], Copyright 2023, Springer Nature

The following Table 1 can be utilised to provide an explanation of the characteristics of CNTs.

Table 1 Properties of carbon nanotubes

| Parameters | MWCNTs | SWCNTs |
|---|-------------------|-------------------|
| <i>Key parameters</i> | | |
| Aspect ratio | 50–4000 | Upto 10,000 |
| Typical diameter | 7–100 nm | 1–2 nm |
| Typical length | Upto 1 mm | Upto 1 mm |
| <i>Electronic structure properties</i> | | |
| Minimum working dosage as an anti-static additive | 0.5% | 0.01% |
| Thermal conductivity at room temperature | 2000–3000 W/(m k) | 3000–6000 W/(m k) |
| <i>Mechanical properties</i> | | |
| Tensile strength | 10–50 GPa | 50–100 GPa |
| Elastic modulus | 300–1000 GPa | 0–3000 GPa |

2 Nanofibers Electronic Structure and Properties, Class of Nano Carbons

In 1879, Thomas Edison was the first to successfully carbonise cotton and bamboo strands to create carbon fibres, which were then utilised in energy conversion and also storage, along with sensing devices, and also the reinforcing of composites. Hughes and Chamber [8] filed for a patent on gas pyrolysis to create nanofilaments of carbon in 1889. Carbon fibres were utilised in the areas of energy conversion and also storage, along with sensing devices, and also composite reinforcement. Tables 2 and 3 defines the properties of Nanofibers [6] and characteristics of different nanocarbon. When compared to conventional carbon fibre, the architectures of carbon nanofibres as shown in Fig. 3 can be described as having a few minor distinctions. These are renowned for their mechanical, along with electromagnetic shielding, as well as electrical, and also thermal stability with their existence at the nanoscale scale. Additionally, they are quite adaptable [9].

2.1 3D Composite Like Foams

Closed cell foams made of thermoplastics are traditionally produced using compression or injection moulding techniques. These processes call for tooling, which can be costly and time-consuming, to fabricate complicated parts. However, studies on additive manufacturing (AM) show that fused filament fabrication (FFF) is one of the methods most frequently employed to produce intricate functional parts [11, 12]. Additionally, additive manufacturing (AM) overcomes the conventional limitations on component size and may produce extremely complicated parts with no tooling expenses and minimal energy and also material usage [13]. Even though most polymers are already used in FFF-based 3D printing (3DP), the development of lightweight thermoplastic filaments for specialised applications remains in its early stages [14]. Due to its versatility in processing and ability to be employed in various engineering utilisations, thermoplastic composites are utilised in semi-structural and also many other engineering utilisations. Industrial 3D printers employ thermoplastic polymers as feedstock, such as polymethylmethacrylate, polylactide, acrylonitrile butadiene styrene, polycarbonate, and polyetherimide filaments made

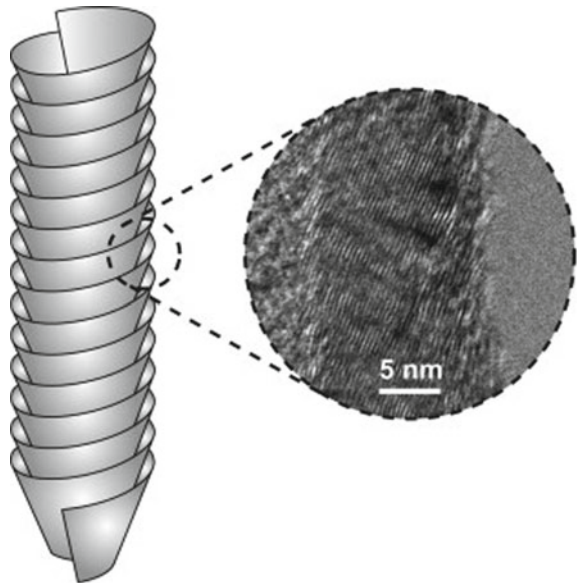
Table 2 Properties of nanofibres

| | |
|--|---------|
| Commercial name | XFM60 |
| Diameter (nm) | 200–600 |
| Length (μm) | 5–50 |
| Density (g/m^3) | 2.1 |
| Purity (%) | >70 |
| Surface area (m^2/g) | >18 |

Table 3 NanoCarbon types

| Nanocarbon | | |
|--|---|--|
| Graphene | Carbon nanotubes | Fullerene |
| Graphene was successfully demonstrated by Andre Gemi and Konstantina Novoselov from the University of Manchester in 2004 | CNTs are carbon-wall structured tubes with a diameter of less than 100 nm. They were identified by Sumio Lijima in 1991 | Eiji Osawa predicted the existence of C ₆₀ in 1970 and was observed in 1985 by Richard E. Smalley, Robert F. Curl, and Harold W. Kroto. Macroscopic synthesis is achieved in 1990 |
| 2-Dimensional structure | 1-Dimensional structure | 0-Dimensional structure |
| Mainly chemical vapor deposition | Mainly chemical vapor deposition | Mainly combustion and arc-discharge |
| Highly transparent and conductive, difficult transfer | Can be metallic and semiconducting Costly separation Difficult dispersion | Semiconducting, costly separation of higher number fullerene |
| Graphene Graphene oxide (GO) Reduced graphene oxide (RGO) | Single-walled CNT (SWCNT) Double-walled CNT (DWCNT) Multi-walled CNT (MWCNT) | Higher number Fullerene Fullerene derivates |

Fig. 3 Structure of nanofibres. Adapted with permission [10], Copyright 2011, Elsevier



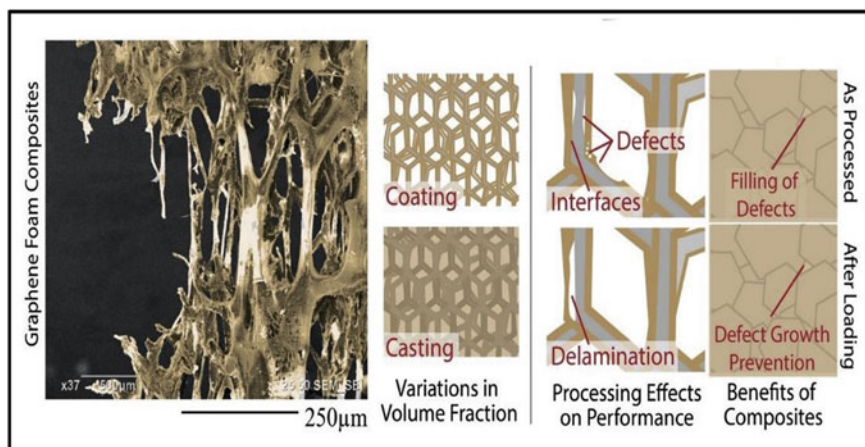


Fig. 4 3D composite foam. Adapted with permission [18], Copyright 2018, Elsevier

from their respective mixes [15, 16]. There have been few studies on 3D Graphene Foam-Reinforced Polymer composites as shown in Fig. 4 along with polymers like HDPE with polypropylene, and also polyamide along with polycaprolactone, and also polybutylene terephthalate, and others due to problems with warpage and delamination that can be resolved by using compounding techniques to add various inorganic/organic fillers [17, 18].

3 Current Progress in the Fields of Nanocarbon and Nanofibers

For creating an eco-friendly society within the biosphere, the development of environmentally friendly, non-harmful materials that are also capable of keeping pace with technological progress is not only extremely important but has also become a difficult undertaking. Therefore, green chemistry plays a significant role in achieving these goals, which are essential for a healthy society. For businesses, the number one concern is zero waste creation, waste avoidance, and effective resource utilisation. By reducing the use of harmful chemical substances in the development of beneficial chemical products [19], green chemistry is widely acknowledged to be a safer alternative to conventional chemical synthesis techniques.

Nowadays, due to the of carbon-based nanomaterials' unique properties like good electrical conductivity, along with ease in surface functionalization, as well as high mechanical strength, and also good thermal stability of carbon-based fullerenes CNTs, along with carbon fibres, as well as carbon quantum dots, and also graphene, they have attracted a lot of interest towards research and are utilised widely in a variety of utilisations. Therefore, within published literature, carbon nanomaterials

are utilised directly or even modified for the aforementioned purposes [19]. These materials have been referred to as wonder materials. Despite this, other synthesis pathways, such as chemical vapor deposition (CVD), along with plasma CVD, and also laser ablation, which are utilized for the synthesis of various carbon-based nanomaterials, are not exactly the easiest things to work with because they require the employment of complex procedures and pricey hydrocarbons, as well as other specific dangerous sources. It has been demonstrated experimentally that carbon-based nanoparticles have usefulness in remediation and sensing applications [20, 21]. There have been a few reports published in academic journals that describe a technique to recovering carbon-based nanomaterials that is both economical and kind to the environment. The creation of nanocomposites plays a key role in the advanced applications that are being utilised today for things like energy storage, electronic parts, environmental remediation, biomedicine, and so on [22]. Some of the applications are listed below [23].

Catalyst Support of Hydrogen Fuel Cells and Two-Electron ORR: As the demand for energy continues to rise, more and more people are becoming interested in the study of fuel cells. The major reactions that take place in hydrogen fuel cells are the hydrogen evolution reaction (HER)/oxygen evolution reaction (OER) and also the hydrogen oxidation reaction (HOR)/oxygen reduction reaction (ORR). A two-electron oxygen reduction reaction (ORR) also is vital in the creation of hydrogen peroxide (H_2O_2). In typical circumstances, the reaction that occurs when oxygen and hydrogen combine to form water is spontaneous, although the process itself is somewhat slow. As a result, the reactions require a catalyst in order to proceed more quickly.

Sensor Material of Wearable Devices: Real-time monitoring of the human body is possible with wearable electronics, which can provide information on the heart rate, sleep activities, calories burned, and stress level. These benefits have made wearable technology desirable and encouraged a variety of study. For the sensor materials, a thin, stretchable, flexible, and affordable material is crucial. Due to their exceptional conductivity, mechanical characteristics, etc., carbon-based materials, like CNFs and also CNTs have been researched as very stable and sensitive sensors.

Direct Contact Membrane Distillation: Researchers have been looking towards making freshwater from salt or contaminated water due to the lack of freshwater. Reverse osmosis is a traditional technology that uses a lot of energy but has limited uses. Due to its simple operating conditions (low temperature and pressure) and superior capabilities (high solute rejection, little mechanical needs), membrane distillation (MD) has become a viable alternative. With the simplest MD arrangement, direct contact membrane distillation (DCMD) is utilised extensively in the food and desalination processes.

Sensor Applications: Nanomaterial biosensor research is popular. Stacking, along with hydrogen bonding, and also hydrophobic interactions, along with Van der Waals, and also electrostatic forces allow these nanomaterials to interact non-covalently

with organic molecules. These interactions and hollowness make them good analytical candidates. Carbon nanoparticle electrodes are highly electrocatalytic. Nanobiosensors benefit from their high surface area and volume ratio. Its chemical stability and biocompatibility make it a preferred sensor material.

3.1 Fullerenes

Fullerenes are spheroidal molecules that are comprised entirely of carbon. The most well-known fullerene is C_{60} , which has 60 individual carbon atoms in its structure. Because of their nanoscale size and unusual electronic properties, they have been the focus of numerous investigations into their possible use in nanomedicine [24]. These applications include medication delivery, photodynamic therapy, antioxidant treatment, and even antiviral treatment.

Fullerenes can be manufactured by a variety of processes, the majority of which require the vaporization of graphite or other similar carbon sources. These processes include arc-evaporation, along with pyrolysis, as well as radio-frequency plasma, and also laser ablation, among others. In addition, the relatively low solubility of fullerenes necessitates the use of substantial amounts of organic solvents throughout the purifying process. As a result, the creation of environmentally friendly processes for their preparation is not at all a straightforward endeavour [25, 26]. The utilization of microwaves, on the other hand, can be advantageous in terms of reducing reaction times and also temperatures; nevertheless, even this practical advancement has not resolved the numerous issues that the industry faces in terms of producing fullerenes at minimal cost. One must keep in mind that fullerenes need to be derivatized in order for them to be water-soluble in concentrations that are significant for use in biomedical utilizations. As a result, chances for the environmentally friendly production of fullerenes may lie in the development of such derivatives. For example, hydrophilic polydopamine and also glutathione was utilised to solubilize fullerenes by simply mixing them in water. This was followed by dialysis and also freeze-drying so that the antioxidant activity of the fullerenes could be investigated [27]. A mixture containing fullerene and gallium oxide was subjected to a sonochemical treatment in water, which resulted in the production of nanostructured hybrids with possible uses in sensing. Without considering how to synthesise the fullerene core structure, these approaches just concentrate on derivatization. However, in a recent breakthrough, plastic trash was catalytically converted into a magnetic fullerene-based composite. The catalyst and precursor of magnetic nanoparticles, along with ferrocene, played a crucial role in this [28].

3.2 Graphene

As the class of graphene-based materials is so large and varied, it is essential to have a thorough understanding of the particular sort of structure that is being investigated and how it may be unique in comparison to previously published research on the subject [29, 30]. Although graphene has captivated the imagination of scientists for a number of applications in the medical field, unsolved difficulties exist in its extensive deployment on a worldwide industrial scale in order for it to widely reach the market. Nevertheless, significant work is being made in this area. There are several uses, but the ones relating to antibacterial properties are the ones that have received the most attention [31, 32]. When it comes to sensing applications, the one-of-a-kind features that graphene-based materials possess because of their two-dimensional structure are of utmost relevance. The biocompatibility of these materials has been the subject of extensive research, and the findings obtained so far are encouraging; nonetheless, because to the great variety of graphene-based materials, it is preferable to transition from descriptive to predictive toxicology [33].

In particular, the reviews [32] looked at the creation of a biomolecular corona on given graphene-based materials and also its implications for biodistribution and also cytocompatibility. Exfoliating graphite in the presence of a variety of dispersants is one of the many methods that may be utilised to make graphene; nonetheless, this method is now the most widely used. Graphene, on the other hand, is commonly oxidized to graphene oxide (GO) in order to provide good water dispersibility. This is a process for which environmentally friendly solutions are being researched. So, for instance, graphite's electrochemical oxidation in acidic water was successful in producing GO-based conductive materials in a matter of seconds [31]. Taking use of synergy with photochemistry could result in further improvements to the process. Figure 5 depicts different structures of graphene [31].

3.3 Diamane

The structural structure of diamane, a nano-allotrope of carbon, includes the presence of bilayer graphene that experiences sp^3 hybridization. The creation of covalent bonds between the carbon atoms and hydrogen atoms of the two sub-lattices during the hybridization is confirmed, resulting in the synthesis of a C_2H layer on one side and the formation of the diamane structure on the other side of the carbon layer [34]. In 2009, Chernozatonskii et al. [35] utilised theoretical simulation studies (Vienna Ab Initio Simulation Package (VASP)) to examine the synthesis, characteristics, and structure of diamane for the first time. They discovered that diamane, a diamond nanofilm, is created by hydrogenating bilayer graphene and has exceptional mechanical and electrical properties [35, 36].

Although the term "diamane" is frequently utilised by researchers, the diamane structure is also referred to by other names, including bilayer graphene, hydrogenated

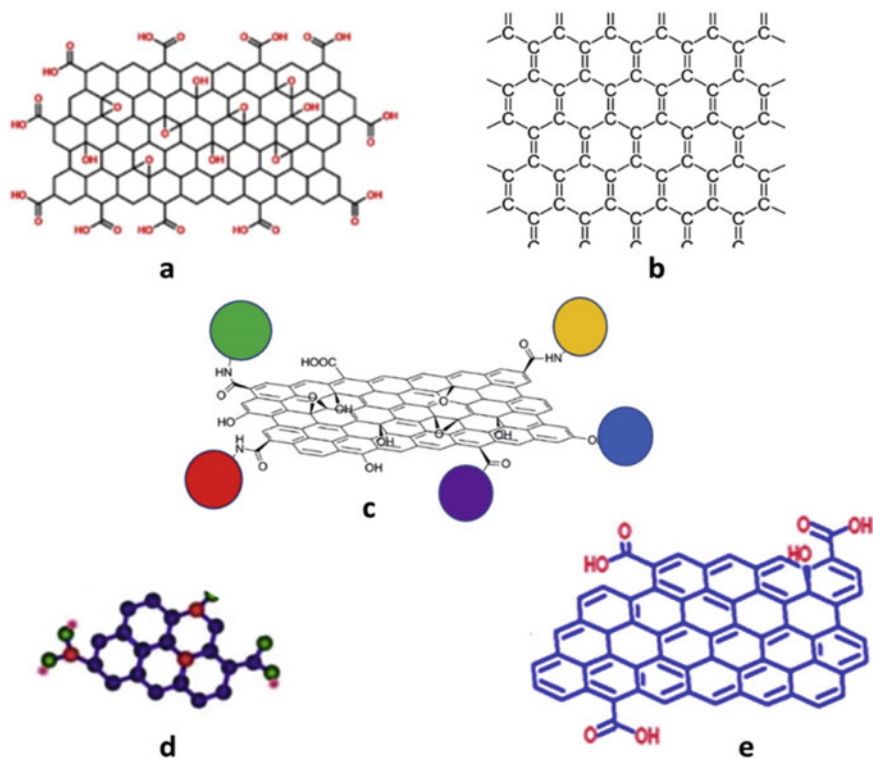


Fig. 5 Different structures of graphene. Adapted from Ref. [31]. Copyright The Authors, some rights reserved; exclusive licensee Elsevier. Distributed under a Creative Commons Attribution License 4.0 (CC BY) <https://creativecommons.org/licenses/by/4.0/>

bilayer graphene, hydrogenated few-layer graphene, and interlayer-bonded bilayer graphene [37]. Diamane is categorized as either Bernal stacking (the AB stacking sequence of diamane) or Lonsdaleite stacking (the AA stacking sequence of diamane) based on its shape. The most stable form of diamane in this situation is represented by Lonsdaleite stacking, and under pressure, 3D graphene crystals can also be created from them [35].

3.4 Carbon Nanotubes (CNT)

CNTs are essentially single-walled or multi-walled sheets of graphene, depending on how many sheets make up their walls. They can be considered graphene sheets that have been rolled up into a tube. They are identified as prospective materials to innovate inside the biochemical field, much like the other nanostructures. Despite the

Table 4 Properties of CNTs

| Properties | Parameter | Range |
|------------------------------|----------------------|------------------------|
| Density | Armchair (10.9) | 1.32 g/cm ³ |
| | Chiral (12.5) | 1.41 g/cm ³ |
| | Zig zag (16.0) | 1.33 g/cm ³ |
| Structure during equilibrium | Mean diameter | 1.3–1.5 nm |
| Interlayer distance | Arm chair | 3.37 Å ⁰ |
| | Chiral | 3.38 Å ⁰ |
| | Zig zag | 3.40 Å ⁰ |
| Lattice parameter | Arm chair (10.9) | 16.55 nm |
| | Chiral (12.5) | 16.53 nm |
| | Zig zag (16.0) | 16.53 nm |
| Elastic nature | Tensile strength | About 100 GPa |
| | Young's modulus | 1.0–1.27 TPa |
| Electrical behaviour | Conductance | 13 kΩ ⁻¹ |
| | Current density | 1015 A/m ² |
| Thermal property | Thermal conductivity | Around 2000 W/m K |
| | Mean free Path | Around 100 nm |

fact that functionalization can reduce nanostructures' toxicity, their physical resemblance to asbestos fibres has created many obstacles for their applications [38]. The academic community engaged in CNT research responded strongly, fearing additional barriers to innovation. The biocompatibility profiles of these nanomaterials vary widely depending on a number of criteria such as functionalization and also route of administration, and it was discovered that one specific form of CNT proved hazardous [39, 40].

The following Table 4 can be utilised to provide an explanation of the characteristics of CNT.

3.4.1 CNT with Metal-Oxides

Recently, numerous types of research is done looking at whether or not CNTs may be utilised as adsorbents. Research has been done looking into how CNTs can be utilised to filter contaminants out of water-based systems. Numerous laboratory investigations on the adsorption of dangerous chemical compounds and heavy metals have already been conducted out [41].

Purification and also activation or even functionalization of CNTs is needed and can be accomplished through oxidation treatment [42]. These processes are necessary for further enhancing the adsorption ability of CNTs. It is required to purify CNTs in order to get rid of the impurities that can frequently be found mixed in with them. Some examples of these impurities include catalyst particles, along with soot, as well

as amorphous carbon, and also other forms. As a result of their coating on CNTs' surfaces, impurities can lower the amount of adsorption that takes place, which in turn influences the amount of adsorption that takes place on the exterior surface of the nanotubes. Treatment of CNTs with an oxidising agent (like nitric acid, along with hydrogen peroxide, and also potassium permanganate, or even a mix of nitric acid and also sulfuric acid) results in an increase in hydrophilicity, which likely accounts for the improved adsorption ability. This is because the oxidation treatment increases the hydrophilicity of the CNTs. When CNTs are subjected to oxidation treatment, new functional groups are created on nanotubes' surface.

Recently, metal oxide nanoparticles supported by CNTs are the subject of intensive research. This research has revealed that these nanoparticles are an excellent adsorbent for removing heavy metal ions and harmful organic compounds from water, and that they can also function as catalysts.

3.4.2 Synthesis of CNT/Metal Sulfide Composites

CNTs' combination with metal sulphides is done in order to boost the electrocatalytic activity of CEs as well as their conductivity. CNTs' combination and metal sulphides (metals) produce a remarkable electron channel due to the CNT network's high electrical conductivity and the fact that metal sulphides improve electrochemical performance due to the electrocatalytic behavior that they exhibit [41, 43].

The Ni foam was cleaned with acetone, along with ethanol, and also deionized water (DI) for 10 min each, followed by ultrasonic etching with a 2 M HCl solution for 30 min, before the synthesis could begin. We mixed 0.05 g of MWCNT powder with 0.1 g of PVDF in 2 ml of N-Methyl-2-pyrrolidone (NMP) to make the counter electrode. Coating a piece of Ni foam (1.31.6 cm²) with the slurry required first thoroughly mixing the ingredients utilising a mortar and pestle. Sintered at 150 °C for 30 min, the resulting thin film is the carbon nanotube (CNT) electrode [3].

Figure 6a illustrates CNT/metal-sulfides. The electrons in CNT/metal-sulfides find the shortest path to accelerate charge transport and facilitate reduction of the polysulfide electrolyte compared to the bare CNT network, which encourages the enhanced electrocatalytic activity of the composite electrode material to enable higher QDSSC and SC performance (Fig. 6b). To deposit metal sulphides on the Ni-foam based CNT electrode, the simple solution method of chemical bath deposition (CBD) was utilised. Metal sources of 0.1 M CuSO₄·5H₂O (or NiSO₄·6H₂O, along with Pb(NO₃)₂, and also CoCl₂·6H₂O) and also sulphur sources of 0.4 M C₂H₅NS in 50 ml deionized water were used to create CuS, along with NiS, as well as PbS, and also CoS deposition solutions. The CuS and NiS solutions were next treated with 0.6 M C₂H₄O₂ while the CoS and also PbS solutions were treated with 0.4 M CH₄N₂O, both added drop by drop. CNT electrodes were dipped vertically into CuS, along with NiS, as well as PbS, and also CoS solutions for 90 min at 90 °C to create composite electrodes. The electrodes were taken out of the oven after deposition and washed with DI water and also ethanol. When everything was ready, it was dried at 100 °C overnight. The solutions of PbS, along with CuS, as well as

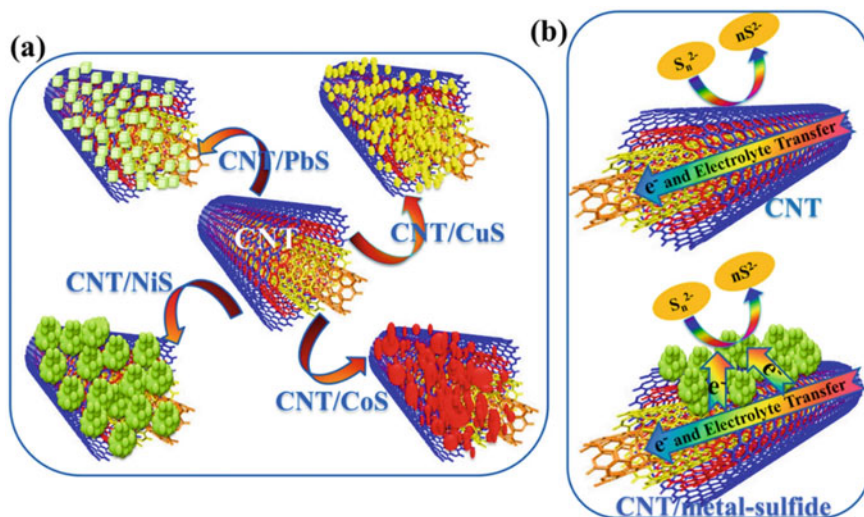


Fig. 6 **a** Schematic representation and **b** electron transfer process of CNT/metal sulphides. Adapted from Ref. [3]. Copyright The Authors, some rights reserved; exclusive licensee Springer Nature. Distributed under a Creative Commons Attribution License 4.0 (CC BY) <https://creativecommons.org/licenses/by/4.0/>

CoS, and also NiS were used to make the CNT/PbS, along with CNT/CuS, as well as CNT/CoS, and also CNT/NiS samples.

3.4.3 CNT with Chalcogenides

The chemistry behind CNTs' functionalization is well understood due to the high level of interest and research activity, which, along with their special characteristics, makes them ideal templates for assembling with other functional nanomaterials. Increasing the tunability of CNTs' physical, electrical, and optical characteristics has been shown to be possible by adding various organic or inorganic species to their surface. Nanocomposites and functional CNTs with novel or even tunable features may play a critical part in the miniaturisation procedure for nanoengineering and nanotechnology as the need for smaller, along with quicker, and also more efficient electronic devices increases. This covers the research and creation of novel catalyst materials, along with solar cell sensitization, and also nanobatteries, etc. Nanocomposites with semiconductor QDs covalently bound to CNTs have recently gained significant attention for use in these areas. In many applications, the unique ability of QDs to be tuned for key optical and electrical characteristics by changing their size is of tremendous importance. As promising semiconductors for utilisation in optoelectronic devices, multinary chalcogenide materials such as CuInS₂ (CIS), Cu(In,Ga)S₂ (CIGS), and Cu(In,Ga)Se₂ (CIGSe) are of great interest due to their

exceptional electronic and also optical properties (due to their characteristics as a direct band-gap semiconductor), precise control of these by straightforward modification of the preparation conditions (size, along with surface chemistry, and also composition), and also cost-effective [44].

3.4.4 CNT with HTS

High-temperature superconductors (HTS) feature layers that are extremely anisotropic, and their critical current density, J_c , is influenced by microstructural characteristics like connection between the grains and grain borders. Numerous researchers investigated the improvement of J_c using a variety of techniques, one of the most widely utilised being the substitution or addition of various nanomaterials. Due to the improved connectivity of the grain boundaries and an increase in their flux pinning capacities, the addition of nanomaterials enhances the electric transport parameters of HTS materials, such as the critical current density. It has been discovered that nanoparticles fill the spaces between the grains and have an impact on superconductivity through mechanisms that strongly bind the grain borders. While acting as impurities, these nanoparticles don't alter the structure of HTS materials [45].

Many researchers have also looked at the possibility of using carbon-based nanomaterials to enhance HTS performance, especially with regard to critical current density. Recently, there has been a surge of interest in increasing the J_c of these HTS materials by adding CNTs. It has been claimed that the vital current density increases by a factor of 10 when CNTs are added to $YBa_2Cu_3O_7$. These nanostructure phases are excellent traps for preventing flux mobility. J_c under the applied magnetic field likewise rises as a result. The addition of the CNT increases the electric transport capabilities between the grains without altering the materials' structural makeup by creating electrical networks between grains, as seen in the SEM image [45].

4 Nanocarbon and Composites for Energy Applications

Due to its unconventional characteristics, like their high power density, quick charging time, and also high cycling stability, super capacitors are employed as energy storage devices in electric vehicles, along with hybrid electric vehicles, as well as backup power cells, and also portable electronic gadgets. Pseudo capacitance and electrochemical double-layer capacitance are the two basic methods of energy storage in super capacitors. The mechanisms of faradic reactions are in charge of charge transfer in a pseudo capacitor. Pseudo capacitance can be seen in several metals, oxides, and conducting polymers. In contrast, inside electrochemical double-layer capacitance procedures, charges are always accumulated at the interface by the mechanism of electrolyte ion adsorption/desorption on electrode materials with a wide surface area. Therefore, carbon-based nanomaterials can be crucial in the

creation of super capacitors. Super capacitors made of Nano carbon are superior to conventional (metal-based) super capacitors in several ways, including high cycling stability, along with high power density, and also lower energy density requirements for battery use [46].

CNTs, which have excellent mechanical and electrical properties, have an exposed surface that can be functionalized to make them appropriate for energy storage. However, it has significant drawbacks, namely a moderate capacitance brought on by the low density of the nanomaterials. A different kind of energy-storing material is the lithium-ion battery, which stores energy as chemical energy. It is superior to capacitors in several ways, including high power density and reduced potential for greenhouse gas emissions. Since the structure of Nano carbon-based materials typically expresses some common factors, like the lithium amount reversibly incorporated into the carbon lattice, along with the faradic losses throughout the initial charge–discharge cycle, and also the voltage profile throughout charging and discharging, Nanocarbon materials and composites are utilised in lithium batteries [47]. Table 5 displays some Nano carbon-based compounds utilised in environmental and energy applications.

Supercapacitors:

To make super capacitors, electro spun carbon nanofibres are used, and they do so quite effectively. Electro spun CNFs can be produced with a variety of fibre diameters, porosities, and surface chemistries, which has several advantages for improving capacitor performance. Increasing the electrochemical capacitance of electrospun carbon nanofibres has been achieved through the manipulation of fibre morphology and also degree of graphitization via control of heat treatment conditions, utilisation of catalysts throughout carbonization and/or activation, and also selection and even combination of various polymer precursors like PAN/CA, along with PAN/PVP, and also PAN/pitch [48].

Electrospun carbon fibres' electrochemical capacitance may be greatly increased by the insertion of redox-active species due to the simultaneous use of two charge storage processes, along with electrical double layer and also redox reactions. Ruthenium-embedded carbon nanofibres were made by electrospinning fibres made of ruthenium(III) acetylacetonate and PAN in dimethylformamide (DMF), then stabilizing, carbonizing, and activating those fibres. After adding Ru nanoparticles to the carbon fibres, the specific capacitance significantly increased. Carbon nanofibres without Ru had a capacitance of 140 F/g, whereas an electrode with 7.31 wt% Ru had a capacitance of 391 F/g. The enlargement of the average pore diameter and the additional pseudo capacitance made available by the well-dispersed Ru nanoparticles were credited as having synergistic effects that increased electric double-layer capacitance [8, 48]. Additionally, the pseudo capacitive contribution from the electrochemically active polymer PPy led to a further increase in capacitance when polypyrrole (PPy) was coated on the MWCNT-loaded fibres. Another strategy for improving the electrochemical performance of electrospun CNFs is the encapsulation of many highly conductive components like CNTs and also metallic nanoparticles to increase electrical conductivity [8].

Table 5 Applications of Nano carbon based materials in energy and environmental field

| | Nanomaterials | Material used | Methods | Applications |
|--------------------------|--|---|--|--|
| Energy application | Carbon nanotubes (CNT) | Graphite, nanoplatelets, phase change materials | Melting/heating, sonicated | To prepare enhanced thermal conductive material |
| | Single wall carbon nanotube (SWCNT) | HNO ₃ , Ag/AgCl electrode, methylene blue | Absorption, drying, nitration | Application in biofuel |
| | Graphite powder | K ₂ S ₂ O ₅ , P ₂ O ₅ , H ₂ SO ₄ , KMnO ₄ , H ₂ O ₂ | Heating, drying, filtration, mixing | Fabricating of various micro electrical devices |
| | Porous carbon and hydrous RuO ₂ | Sulfuric acid | Oxidation, absorption | Supercapacitor for energy storage |
| | Graphene oxide graphene nanoplates | Polyethylene glycol, H ₃ PO ₄ , KMnO ₄ , H ₂ SO ₄ , HCL, H ₂ O ₂ | Heating, drying, filtration, mixing | To prepare higher thermal energy storage |
| Environment Applications | Multiwall carbon nanotube (MWCNT) | H ₂ SO ₄ , HNO ₃ (3:1) | Oxidation, filtration, drying | Heavy metal removal (cadmium reduction) |
| | | Ethanol ferrocene thiophene | Oxidation/reduction/pyrolysis | Ciprofloxacin reduction from aqueous solution |
| | Oxidized MWCNT | NH ₂ material | EDA, N-HATU, filtration, drying | Heavy metal removal (cadmium and lead reduction) |
| | Graphite oxide | Na ₂ S ₂ O ₃ | Oxidation, sonication, washed, dried | Heavy metal removal (mercury Hg ²⁺ reduction) |
| | | NaNO ₃ , H ₂ SO ₄ , KMnO ₄ , H ₂ O ₂ | Oxidation, filtration, washed, dispersed | Waste water treatment |

5 Future Perspectives of Nanocarbon Electrochemistry

Due to the one-of-a-kind characteristics, carbon nanomaterials have made significant contributions to the research, development, and advancement of electrochemical sensors and biosensors. When compared to traditional, non-nanostructured electrochemical systems, the innovative as well as the modified carbon-based probes frequently demonstrate significantly improved analytical performance. Electroanalytical approaches incorporating sensing and biosensing devices employing carbon nanostructure modified electrodes are displaying potential for utilisation in real-life

analytical detection. Particularly useful as electrode materials for electrochemical detection of a wide variety of analytes have been CNTs and diamond. Because of their one-of-a-kind characteristics, CNTs, diamonds, and diamond-like films have made significant contributions to the development of innovative nanostructured electrochemical sensors and biosensors. These sensors have improved analytical performance in comparison to conventional electrochemical sensing systems. In addition, before any prospective commercialization can take place, more accurate assessments of certain performance characteristics along with their application for sensing analytes inside samples taken from the actual world are required [49].

The boosted active surface area of CNTs and also the anti-fouling capability of diamond and also diamond-like surfaces are two examples of the novel properties of carbon nanomaterials that contribute to their impact in modern electrochemical systems beyond their analytical superiority. These properties help make diamond and diamond-like surfaces resistant to fouling. In addition, the authors expect that the continued development of novel, adaptable methodologies for the synthesis and functionalization of carbon nanomaterial will soon lead to an increasing number of significant electroanalytical applications in a variety of fields of interest, including rapid and also sensitive medical analyses, along with drug quality monitoring, and also food and environment security.

6 Conclusion

In conclusion, carbon-based sensors, along with electrocatalyst, as well as supercapacitors, and also LIBs share some electrochemical characteristics; some ways of manipulating carbon's structural properties apply generically to each application area. For example, one way to modulate electrochemical activity is to disturb the electronic structure of the material. This can be done through covalent (e.g., controlled oxidation, along with doping with heteroatoms, and also alteration of synthesis conditions) or even noncovalent (adsorption of surfactants or even poly-electrolytes) approaches. In addition to this, the architectural design plays a vital effect on the electrochemical performance as a whole. For instance, substrate-supported continuous carbon nanotube arrays (CNFs) that have outstanding mesh integrity demonstrate wide-range sensing capabilities. Also, vertically aligned carbon nanotube arrays along with graphene sheets offer both good rate performance and also high sensitivities.

References

1. Nayak, A.K., Tiwari, S.K. (eds.): Nanocarbon Allotropes Beyond Graphene. IOP Publishing (2023). <https://doi.org/10.1088/978-0-7503-5177-5>.

2. Talebian, S., Rodrigues, T., Das Neves, J., Sarmento, B., Langer, R., Conde, J.: Facts and figures on materials science and nanotechnology progress and investment. *ACS Nano* **15**, 15940–15952 (2021). <https://doi.org/10.1021/acsnano.1c03992>.
3. Muralee Gopi, C.V.V., Ravi, S., Rao, S.S., Eswar Reddy, A., Kim, H.J.: Carbon nanotube/metal-sulfide composite flexible electrodes for high-performance quantum dot-sensitized solar cells and supercapacitors. *Sci. Rep.* **7**, 1–12 (2017). <https://doi.org/10.1038/srep46519>.
4. Liang, Y.N., Oh, W.-D., Li, Y., Hu, X.: Nanocarbons as platforms for developing novel catalytic composites: overview and prospects. *Appl. Catal. A Gen.* **562**, 94–105 (2018). <https://doi.org/10.1016/j.apcata.2018.05.021>
5. Pandey, R., Tiwari, S.K.: Recent advances in nanocarbons: status and prospect. In: *Nanocarbon Allotropes Beyond Graphene*, pp. 1–1–1-57. IOP Publishing (2023). <https://doi.org/10.1088/978-0-7503-5177-5ch1>
6. Astié, V., Millon, C., Decams, J.-M., Bartaszyte, A.: Direct liquid injection chemical vapor deposition. In: *Chemical Vapor Deposition for Nanotechnology*. IntechOpen (2019). <https://doi.org/10.5772/intechopen.80244>
7. Gautam, R., Sahoo, A., Pant, K.K., Mohanty, K.: Graphene nanoparticles and their derivatives for oil spill treatment. In: *Materials Horizons: From Nature to Nanomaterials*, pp. 229–249. Springer Nature (2023). https://doi.org/10.1007/978-981-99-4382-1_11
8. Mao, X., Rutledge, G.C., Hatton, T.A.: Nanocarbon-based electrochemical systems for sensing, electrocatalysis, and energy storage. *Nano Today* **9**, 405–432 (2014). <https://doi.org/10.1016/j.nantod.2014.06.011>
9. Kim, S.K., Mao, A., Sen, S., Kim, S.: Fast Na-ion conduction in a chalcogenide glass-ceramic in the ternary system Na₂Se–Ga₂Se₃–GeSe₂. *Chem. Mater.* **26**, 5695–5699 (2014). <https://doi.org/10.1021/cm502542p>
10. Palmeri, M.J., Putz, K.W., Ramanathan, T., Brinson, L.C.: Multi-scale reinforcement of CFRPs using carbon nanofibers. *Compos. Sci. Technol.* **71**, 79–86 (2011). <https://doi.org/10.1016/j.compscitech.2010.10.006>
11. Yilmaz, A.C., Ozen, M.S., Sancak, E., Erdem, R., Erdem, O., Soın, N.: Analyses of the mechanical, electrical and electromagnetic shielding properties of thermoplastic composites doped with conductive nanofillers. *J. Compos. Mater.* **52**, 1423–1432 (2018). <https://doi.org/10.1177/0021998317752503>
12. Luo, J., Fang, C.-C., Wu, N.-L.: High polarity poly(vinylidene difluoride) thin coating for dendrite-free and high-performance lithium metal anodes. *Adv. Energy Mater.* **8**, 1701482 (2018). <https://doi.org/10.1002/aenm.201701482>
13. Jayavardhan, M.L., Bharath Kumar, B.R., Doddamani, M., Singh, A.K., Zeltmann, S.E., Gupta, N.: Development of glass microballoon/HDPE syntactic foams by compression molding. *Compos. Part B Eng.* **130**, 119–131 (2017). <https://doi.org/10.1016/j.compositesb.2017.07.037>
14. Bharath, H.S., Bonthu, D., Prabhakar, P., Doddamani, M.: Three-dimensional printed lightweight composite foams. *ACS Omega* **5**, 22536–22550 (2020). <https://doi.org/10.1021/acsomega.0c03174>
15. Gama, N., Ferreira, A., Barros-Timmons, A.: 3D printed cork/polyurethane composite foams. *Mater. Des.* **179**, 107905 (2019). <https://doi.org/10.1016/j.matdes.2019.107905>
16. Chatkunakasem, P., Luangjuntawong, P., Pongwisuthiruchte, A., Aumnate, C., Potiyaraj, P.: Tuning of HDPE properties for 3D printing. *Key Eng. Mater.* **773**, 67–71 (2018). <https://doi.org/10.4028/www.scientific.net/KEM.773.67>
17. Wang, S., De Clerck, K., Cardon, L.: Polylactic acid poly-3-hydroxybutyrate applications in extrusion based additive manufacturing. In: *International Conference on Polymers and Moulds Innovations*, pp. 1–5 (2018)
18. Idowu, A., Boesl, B., Agarwal, A.: 3D graphene foam-reinforced polymer composites—a review. *Carbon N. Y.* **135**, 52–71 (2018). <https://doi.org/10.1016/j.carbon.2018.04.024>
19. Khare, P., Singh, A., Verma, S., Bhati, A., Sonker, A.K., Tripathi, K.M., Sonkar, S.K.: Sunlight-induced selective photocatalytic degradation of methylene blue in bacterial culture by pollutant soot derived nontoxic graphene nanosheets. *ACS Sustain. Chem. Eng.* **6**, 579–589 (2018). <https://doi.org/10.1021/acssuschemeng.7b02929>

20. Gao, X., Han, S., Zhang, R., Liu, G., Wu, J.: Progress in electrospun composite nanofibers: composition, performance and applications for tissue engineering. *J. Mater. Chem. B*, **7**, 7075–7089 (2019). <https://doi.org/10.1039/C9TB01730E>
21. Wang, Y., Ding, Y., Guo, X., Yu, G.: Conductive polymers for stretchable supercapacitors. *Nano Res.* **12**, 1978–1987 (2019). <https://doi.org/10.1007/s12274-019-2296-9>
22. Kausar, A., Ahmad, I., Maaza, M., Eisa, M.H.: State-of-the-art of polymer/fullerene C60 nanocomposite membranes for water treatment: conceptions, structural diversity and topographies. *Membranes (Basel)* **13**, 27 (2022). <https://doi.org/10.3390/membranes13010027>
23. Wang, T., Chen, Z., Gong, W., Xu, F., Song, X., He, X., Fan, M.: Electrospun carbon nanofibers and their applications in several areas. *ACS Omega* **8**, 22316–22330 (2023). <https://doi.org/10.1021/acsomega.3c01114>
24. Wang, H., Wang, H.S., Ma, C., Chen, L., Jiang, C., Chen, C., Xie, X., Li, A.-P., Wang, X.: Graphene nanoribbons for quantum electronics. *Nat. Rev. Phys.* **3**, 791–802 (2021). <https://doi.org/10.1038/s42254-021-00370-x>
25. Kim, W.Y., Kim, K.S.: Prediction of very large values of magnetoresistance in a graphene nanoribbon device. *Nat. Nanotechnol.* **3**, 408–412 (2008). <https://doi.org/10.1038/nnano.2008.163>
26. Chen, Z., Narita, A., Müllen, K.: Graphene nanoribbons: on-surface synthesis and integration into electronic devices. *Adv. Mater.* **32**, 1–26 (2020). <https://doi.org/10.1002/adma.202001893>
27. Llinas, J.P., Fairbrother, A., Borin Barin, G., Shi, W., Lee, K., Wu, S., Yong Choi, B., Braganza, R., Lear, J., Kau, N., Choi, W., Chen, C., Pedramrazi, Z., Dumsloff, T., Narita, A., Feng, X., Müllen, K., Fischer, F., Zettl, A., Ruffieux, P., Yablonovitch, E., Crommie, M., Fasel, R., Bokor, J.: Short-channel field-effect transistors with 9-atom and 13-atom wide graphene nanoribbons. *Nat. Commun.* **8**, 633 (2017). <https://doi.org/10.1038/s41467-017-00734-x>
28. Koch, M., Ample, F., Joachim, C., Grill, L.: Voltage-dependent conductance of a single graphene nanoribbon. *Nat. Nanotechnol.* **7**, 713–717 (2012). <https://doi.org/10.1038/nnano.2012.169>
29. Li, Y., Liu, Q., Li, W., Meng, H., Lu, Y., Li, C.: Synthesis and supercapacitor application of alkynyl carbon materials derived from CaC₂ and polyhalogenated hydrocarbons by interfacial mechanochemical reactions. *ACS Appl. Mater. Interfaces* **9**, 3895–3901 (2017). <https://doi.org/10.1021/acscami.6b13610>
30. Cui, W., Zhang, M., Wang, N., He, J., Yu, J., Long, Y., Yan, S., Huang, C.: High-performance field-effect transistor based on novel conjugated P-o-Fluoro-p-alkoxyphenyl-substituted polymers by graphdiyne doping. *J. Phys. Chem. C* **121**, 23300–23306 (2017). <https://doi.org/10.1021/acs.jpcc.7b07364>
31. Tiwari, S.K., Sahoo, S., Wang, N., Huczko, A.: Graphene research and their outputs: status and prospect. *J. Sci. Adv. Mater. Devices* **5**, 10–29 (2020). <https://doi.org/10.1016/j.jsamd.2020.01.006>
32. Zhu, M.J., Kretinin, A.V., Thompson, M.D., Bandurin, D.A., Hu, S., Yu, G.L., Birkbeck, J., Mishchenko, A., Vera-Marun, I.J., Watanabe, K., Taniguchi, T., Polini, M., Prance, J.R., Novoselov, K.S., Geim, A.K., Ben Shalom, M.: Edge currents shunt the insulating bulk in gapped graphene. *Nat. Commun.* **8**, 14552 (2017). <https://doi.org/10.1038/ncomms14552>
33. Li, J., Xie, Z., Xiong, Y., Li, Z., Huang, Q., Zhang, S., Zhou, J., Liu, R., Gao, X., Chen, C., Tong, L., Zhang, J., Liu, Z.: Architecture of β -graphdiyne-containing thin film using modified Glaser-Hay coupling reaction for enhanced photocatalytic property of TiO₂. *Adv. Mater.* **29**, 1700421 (2017). <https://doi.org/10.1002/adma.201700421>
34. Li, J., Gao, X., Jiang, X., Li, X.-B., Liu, Z., Zhang, J., Tung, C.-H., Wu, L.-Z.: Graphdiyne: a promising catalyst-support to stabilize cobalt nanoparticles for oxygen evolution. *ACS Catal.* **7**, 5209–5213 (2017). <https://doi.org/10.1021/acscatal.7b01781>
35. Chernozatonskii, L.A., Demin, V.A., Kvashnin, D.G.: Fully hydrogenated and fluorinated bigraphenes–diamanes: theoretical and experimental studies. *C* **7**, 17 (2021). <https://doi.org/10.3390/c7010017>
36. Li, H., Li, Q., Wen, P., Williams, T.B., Adhikari, S., Dun, C., Lu, C., Itanze, D., Jiang, L., Carroll, D.L., Donati, G.L., Lundin, P.M., Qiu, Y., Geyer, S.M.: Retracted: colloidal cobalt

- phosphide nanocrystals as trifunctional electrocatalysts for overall water splitting powered by a zinc–air battery. *Adv. Mater.* **30** (2018). <https://doi.org/10.1002/adma.201705796>
37. Gao, X., Ren, H., Zhou, J., Du, R., Yin, C., Liu, R., Peng, H., Tong, L., Liu, Z., Zhang, J.: Synthesis of hierarchical graphdiyne-based architecture for efficient solar steam generation. *Chem. Mater.* **29**, 5777–5781 (2017). <https://doi.org/10.1021/acs.chemmater.7b01838>
 38. Chen, L., Hernandez, Y., Feng, X., Müllen, K.: From nanographene and graphene nanoribbons to graphene sheets: chemical synthesis. *Angew. Chem. Int. Ed.* **51**, 7640–7654 (2012). <https://doi.org/10.1002/anie.201201084>
 39. Hou, C., Wang, J., Du, W., Wang, J., Du, Y., Liu, C., Zhang, J., Hou, H., Dang, F., Zhao, L., Guo, Z.: One-pot synthesized molybdenum dioxide–molybdenum carbide heterostructures coupled with 3D holey carbon nanosheets for highly efficient and ultrastable cycling lithium-ion storage. *J. Mater. Chem. A* **7**, 13460–13472 (2019). <https://doi.org/10.1039/C9TA03551F>
 40. Liu, X., An, Y., Feng, J., Zhu, X., Li, F.: Preparation and properties of carbon nanofiber modified emulsified asphalt based on ultrasonication and surfactant and the impact of SBR and NH₄Cl. *Front. Mater.* **7**, 1–9 (2020). <https://doi.org/10.3389/fmats.2020.00209>
 41. Pandit, B., Pande, S.A., Sankapal, B.R.: Facile SILAR processed Bi₂S₃:PbS solid solution on MWCNTs for high-performance electrochemical supercapacitor. *Chinese J. Chem.* **37**, 1279–1286 (2019). <https://doi.org/10.1002/cjoc.201900222>
 42. Muralee Gopi, C.V.V., Ravi, S., Rao, S.S., Eswar Reddy, A., Kim, H.-J.: Carbon nanotube/metal-sulfide composite flexible electrodes for high-performance quantum dot-sensitized solar cells and supercapacitors. *Sci. Rep.* **7**, 46519 (2017). <https://doi.org/10.1038/srep46519>
 43. Pande, S.A., Pandit, B., Sankapal, B.R.: Facile chemical route for multiwalled carbon nanotube/mercury sulfide nanocomposite: high performance supercapacitive electrode. *J. Colloid Interface Sci.* **514**, 740–749 (2018). <https://doi.org/10.1016/j.jcis.2017.12.068>
 44. Voigt, D., Primavera, G., Uphoff, H., Rethmeier, J.A., Schepp, L., Bredol, M.: Ternary chalcogenide-based quantum dots and carbon nanotubes: establishing a toolbox for controlled formation of nanocomposites. *J. Phys. Chem. C* **126**, 9076–9090 (2022). <https://doi.org/10.1021/acs.jpcc.2c01142>
 45. Chong, T.V., Loh, S.K., Liow, C.H., Abd-Shukor, R.: Effects of carbon nanotubes addition on the superconducting properties and critical current density of NdBa₂Cu₃O_{7–δ}. *Appl. Phys. A* **128**, 740 (2022). <https://doi.org/10.1007/s00339-022-05877-3>
 46. Banerjee, R., Gebrekstos, A., Orasugh, J.T., Ray, S.S.: Nanocarbon-containing polymer composite foams: a review of systems for applications in electromagnetic interference shielding, energy storage, and piezoresistive sensors. *Ind. Eng. Chem. Res.* **62**, 6807–6842 (2023). <https://doi.org/10.1021/acs.iecr.3c00089>
 47. Radwan, A., Jin, H., He, D., Mu, S.: Design engineering, synthesis protocols, and energy applications of MOF-derived electrocatalysts. *Nano-Micro Lett.* **13**, 132 (2021). <https://doi.org/10.1007/s40820-021-00656-w>
 48. Zhong, M., Zhang, M., Li, X.: Carbon nanomaterials and their composites for supercapacitors. *Carbon Energy* **4**, 950–985 (2022). <https://doi.org/10.1002/cey2.219>
 49. Wang, Q., Zhou, Y., Zhao, X., Chen, K., Bingni, G., Yang, T., Zhang, H., Yang, W., Chen, J.: Tailoring carbon nanomaterials via a molecular scissor. *Nano Today* **36**, 101033 (2021). <https://doi.org/10.1016/j.nantod.2020.101033>

Tunability of Electrochemical Properties of Nanocarbon for Sustainable Energy



Kavitha Mulackampilly Joseph, Maliha Marzana, Ayush Raut,
and Vesselin Shanov

Abstract As the world transitions from fossil fuels towards more sustainable renewable energy options, carbon-based materials play a significant role due to the growing demand for portable energy devices (for wearable electronics) and heavy-duty energy sources (for power stations, long-distance transportation and electric vehicles). Current, commercially available carbon-based energy materials are inadequate to meet the energy requirements of a fossil fuel-free energy scenario. So, academia and industry are shifting their interest toward advanced materials like nanocarbons, including graphene, carbon nanotube, and fullerene for energy application. They all exhibit extraordinary properties due to their nanoscale dimensions and unique morphology. The tunability of physical, chemical, and electrochemical properties of nanocarbon are their significant features that make them ideal candidates for energy storage and conversion. Advanced tailoring approaches applicable to nanocarbons for energy storage applications are discussed here in detail. They include (a) heteroatom doping, (b) design of hierarchically structured nanocarbon, (c) construction of ionic channels within the material, and (d) growing metal compound-based nanoparticles on nanocarbon. Further, strategies like grafting fullerenes, patterning CNT films, and compositing graphene with CNT and PANI are explored in energy conversion applications like photovoltaics. The discussed electrocatalysis employs tuning methods like nanocarbon doping, porous templating, defect engineering, electrodeposition, and electro-reduction. On the other hand, fuel cell technology adopts tailoring methods like nanocarbon doping, porosity engineering, and graphitization metamorphosis. In summary, this study presents practical strategies that can be adopted for fabricating efficient and high-performance, next-generation energy conversion and storage devices using tailored nanocarbons.

K. M. Joseph · M. Marzana · A. Raut · V. Shanov (✉)

Department of Mechanical and Materials Engineering, University of Cincinnati, Cincinnati, OH, USA

e-mail: shanovvn@ucmail.uc.edu

V. Shanov

Department of Chemical and Environmental Engineering, University of Cincinnati, Cincinnati, OH, USA

Keywords Nanocarbon · Tunability · Renewable energy · Photovoltaics · Electrocatalysis · Fuel cell

1 Introduction

The Role of Nanocarbon in the Future Energy Scenario

A significant portion of our current society's energy supply relies heavily on fossil fuels. However, these resources are rapidly depleting, and the imperative to mitigate greenhouse gas emissions is calling for a reduction of their usage [1]. The main solution to this problem appears to be exploring alternative and renewable energy options to ensure sustainable progress. Thus, there is a necessity for transitioning toward renewable energy sources. While research facilities worldwide are dedicated to establishing the groundwork for the future energy landscape, the current focus revolves around creating novel, property-tailored nanomaterials that will facilitate the practical utilization of renewable energy sources. In this endeavor, carbon-based materials assume a pivotal role.

The future fossil-free energy landscape is centered around two primary components: energy conversion and energy storage. While various forms of renewable energy will have their contributions, solar energy will emerge as the predominant force in a sustained long-term energy outlook [2]. Carbon-based materials, while having a limited role in energy scenarios centered around fossil fuels, are expected to play a significant role in moving toward this novel energy paradigm. The evolving societal demand for concentrated, portable energy that can be distributed drives this shift. Graphite, widely used as an anode material, dominates commercial lithium-ion batteries. Supercapacitors rely solely on activated carbon as active material, and carbon black serves as a support for electrocatalysts in fuel cells. While these energy conversion and storage devices can be adapted for a future reliant on solar energy, their current performance falls short of meeting the requisites for a non-fossil fuel energy-dependent society. The future requires power not only for personal devices like cell phones, laptops, and cars but also for essential functions like power stations, long-distance transportation, lighting, and heating. This appears to be the driving force behind ongoing efforts in carbon materials research for advanced energy applications. Numerous factors contribute to the preference for carbon: it is cost-effective, eco-friendly, and abundant, and its various bonding configurations and structural forms facilitate the creation of a diverse range of new carbon materials. The nanocarbon materials are anticipated to assume a distinct role in the forthcoming energy scenario that conventional carbon sources cannot fulfill [3]. The various nanocarbon properties, like optical, electrical, mechanical, or morphological, are outstanding due to their uniquely high surface-to-volume ratio driven by their nanosized structure. This distinction presents an opportunity for significant advancements in energy conversion and storage capabilities when employing nanocarbon. The primary members of the

nanocarbon family are graphene, carbon nanotubes (CNTs), and fullerene. Structures like nanocage, nanofiber, nanoribbon, nano horn, and others with nanomorphology are derivatives of the primary nanocarbon members. A shared advantage of these new carbon materials lies in their reduced dimensions, distinct morphologies, and nanostructure-defined properties. Nanocarbons with sp^2 hybridized backbone possess a long range of highly ordered structures; however, they differ from conventional bulk graphite. Dimension in the nanoscale and unique morphology render them extraordinary properties encompassing greater surface area, advanced porous structure, high electrical conductivity, thermal conductivity, and remarkable mechanical properties that distinguish them from traditional bulk carbon forms [4–9].

2 Tuning Electrochemical Properties of Nano Carbons for Energy Storage

The tunability of physical, chemical, and electrochemical properties of nanocarbon is one of the most significant features that makes nanocarbon a potential candidate for energy storage applications. Major tailoring methods of nanocarbon structure are discussed below.

(a) Heteroatom Doped and Oxygen-Functionalized Nano Carbons

Introducing heteroatoms like N, S, B, P, and F within carbon nanostructures has been proven to be an effective strategy to enhance a wide variety of electrochemical performances, leading to improvement in hydrophilicity, porosity, charge density, inter-layer spacing, chemically active sites, and charge distribution properties. Heteroatom doping is cost-effective and does not add additional mass to the energy storage device. A schematic of the influence of heteroatom doping on the physicochemical properties of carbon nanostructure for energy application (specifically for supercapacitors) is given in Fig. 1a [10].

Nitrogen Doping: Nitrogen doping has become a common strategy to improve the energy storage performance in nanocarbons because the synthesis of N-doped nanocarbons is simple and easy. In addition, they improve hydrophilicity, electrical conductivity, and structural integrity and create electrochemically active sites. The higher electronegativity of nitrogen (3.04), in contrast to that of carbon (2.55), aids in improved adsorption of electrolyte ions. Additionally, introducing nitrogen into the lattice structure hinders the creation of an insulating inactive layer of hydrocarbons, which can detrimentally impact the performance of supercapacitors.

Oxygen Functionalization: Functionalization with oxygen, proven to enhance electrode performances, has received wide attention in the energy storage field. Though doped nanocarbons usually have greater oxygen content, the O/C ratio should be high enough to modify the carbon surface from hydrophobic to hydrophilic. Therefore, oxygen functionalization is employed as it is a simple and popular method to

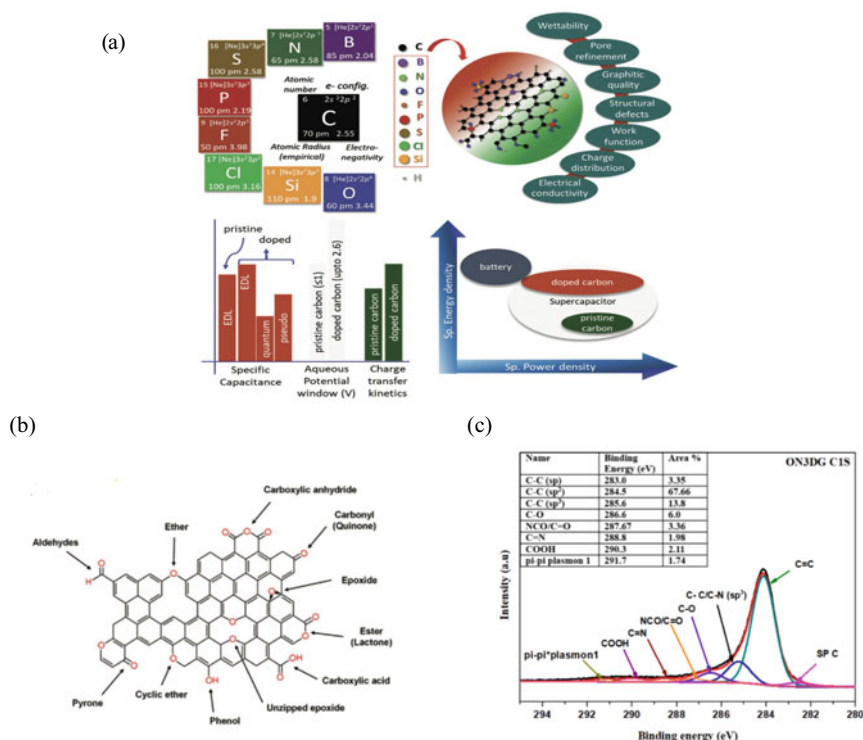


Fig. 1 **a** Schematic of doping in carbon and its influence on the physicochemical properties for energy applications. Reproduced with permission [10]. **b** Possible O-configuration in graphene matrix. Reproduced with permission [10]. **c** C1s spectra of N-doped and oxygen functionalized 3-Dimensional (3D) graphene. **d** SEM images of pristine (top) and N-doped graphene (bottom). **e** Water contact angle of N-doped 3D graphene before and after oxygen functionalization. **f** Cyclic voltammetry plot comparing pristine 3D graphene (P3DG), N-doped 3D graphene (N3DG), Oxygen functionalized, and N-doped 3D graphene (ON3DG) **g** Cyclic stability study on oxygen plasma functionalized, nitrogen-doped three-dimensional graphene (ON3DG). Reprinted with permission [11]

increase hydrophilicity and introduce oxygen functional groups. Figure 1b shows the numerous possible C–O linkages [10]. Most of the above concepts have been proved by our recent study on N-doped and oxygen plasma functionalized 3-dimensional (3D) graphene [11]. The results confirm the possibility of achieving higher capacitance and greater electrochemical performance by the synergistic effects of N–C, O–C, and NCO linkages (Fig. 1c).

The morphology of N-doped graphene (Fig. 1d bottom) exhibits a more open and densely porous structure than pristine 3D graphene (Fig. 1d top). The interconnected pores act as efficient channels for electrolyte-ion transport during electrochemical reactions.

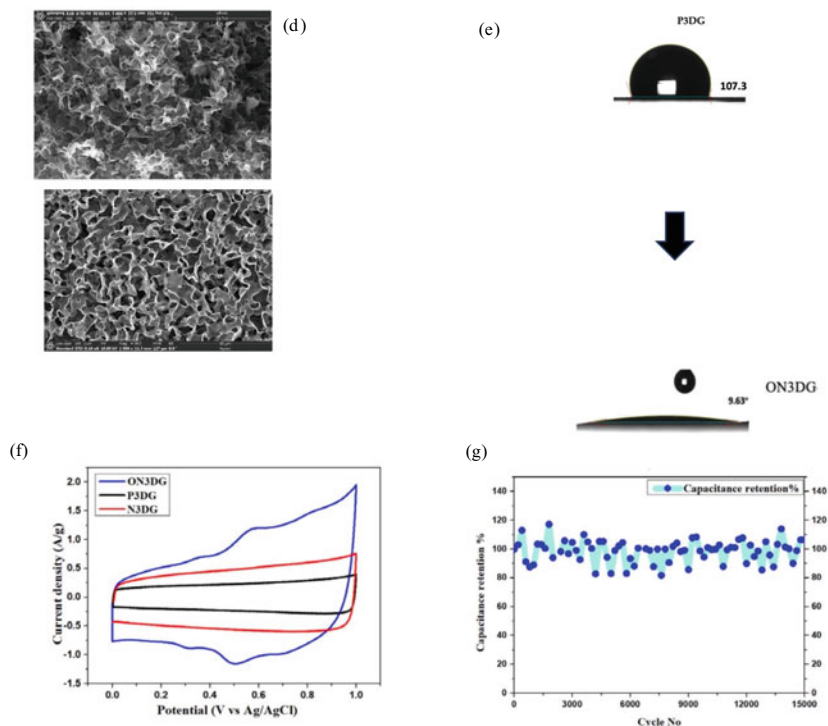


Fig. 1 (continued)

A huge improvement in hydrophilicity after plasma functionalization is proven by the water contact angle measurements (Fig. 1e). The increased wettability facilitates better electrode–electrolyte interactions. The interaction, in turn, accelerates the movement of electrolyte ions toward the surface, reducing the resistance to mass transfer, which leads to the formation of a more effective electrical double layer at the interface (Fig. 1f). The symmetric supercapacitor device fabricated from N-doped oxygen functionalized electrodes exhibits a high energy density of 54 Wh/kg and a power density of 1,224 W/kg at a current density of 0.5 A/g. The higher energy density is also due to ionic electrolytes with a wider voltage window. The device shows an impressive cycle life of 15,000 with a capacitance retention of 107%. (Fig. 1g).

(b) Designing Hierarchically Structured Carbon Material

Carbon-based nanocomposites featuring hierarchical structures offer substantial specific surface area, exceptional electrical conductivity, and synergistic effects that promote electrochemical reactions at interfaces. Building a hierarchical structure of carbon nanomaterials (HSCNs) involves a primary carbon matrix upon which nanocarbon units (0D nanospheres, 1D nanofibers/tubes, and 2D nanosheets) are built either by growing the subunits or integrating them into the primary carbon matrix.

Wang et al., in their detailed study on HSCNs, elaborated not only on the advantages of the hierarchical structure but also the enhancement in electrochemical performance in Lithium-ion Batteries (LIBs), Sodium-Ion Batteries (SIBs), supercapacitors (SCs), and Li–Sulfur (Li–S) batteries [12].

Recently, Li–S batteries have emerged as an important energy storage and power source for future electric vehicles due to their high theoretical capacity and energy density. However, pure sulfur cathodes suffer from practical issues like poor electrical conductivity, large volume expansion during cycling, and lithium polysulfide shuttling. HCNs with porous structure, when used to host sulfur cathode, can address the above issues because the pores can store sulfur, and the carbon matrix can increase the sulfur conductivity, reduce the volume change during the lithiation process, and hinder the shuttle effect of lithium polysulfides. Cui et al. [13], by using Anodic Aluminum Oxide (AAO) as a template, synthesized an array of hollow carbon nanofiber, which was used as sulfur host for Li–S batteries (Fig. 2a, b). The high length-to-diameter ratio of the nanofiber ($\sim 60 \mu\text{m}$ to $\sim 200 \text{nm}$) trapped the polysulfide and facilitated the transport speed of lithium ions. The nanofiber delivered a specific capacity of 1,560 mAh/g at a current density of 0.5 C, close to the theoretical capacity of sulfur of 1,672 mAh/g. Post-cycling (after 150 cycles) capacity was measured to be $\sim 700 \text{mAh/g}$ (Fig. 2c). These impressive results have been achieved thanks to the high sulfur loading and the addition of 0.1 M LiNO_3 to the electrolyte.

(c) Constructing Ionic Channel for Nanocarbon

Efficient energy storage using nanocarbon relies on the quick transport of ions, primarily determined by effective ionic channels in active electrodes. Mostly, the origin of ionic channels is from the nanocarbon pore structure, which can be created by controlled processing techniques. The commonly employed approaches for producing these pores and their associated outcome are outlined in Fig. 3a [14]. A notable illustration involves the creation of an electrode utilizing 3-D porous carbon frameworks (referred to as HGF or Holey Graphene Framework) as the scaffold for ion and electron conduction, combined with orthorhombic niobium oxide (Nb_2O_5) serving as the electrochemically active substance (Fig. 3b, c) [15]. The resulting

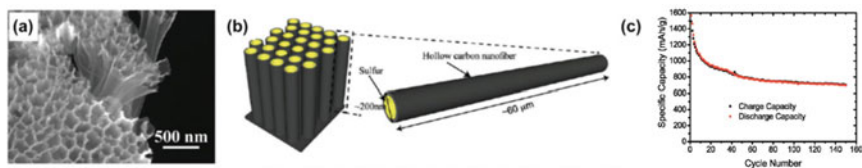


Fig. 2 **a** Hollow carbon nanofiber encapsulating sulfur after etching away the AAO template. **b** The schematic shows a high aspect ratio of the hollow carbon nanofiber for effective trapping of polysulfides. **c** Capacities of the carbon nanofiber-encapsulated sulfur electrode in electrolyte with LiNO_3 additive at C/5. Reproduced with permission [13]. Copyright 2011, American Chemical Society

electrode, comprising the porous 3D Nb₂O₅/HGF combination, exhibited impressive performance metrics. Notably, it achieved an excellent rate capacity of 139 mAh/g at a high current of 10 C, with a material loading of 11 mg/cm². This electrode also displayed remarkable stability over 10,000 charge–discharge cycles at 10 C, maintaining a Coulombic efficiency exceeding 99.9%. These outcomes highlight the durability of the established ionic pathways, representing a crucial advancement towards the practical utilization of high-power lithium-ion batteries (LIBs).

(d) Nanoparticle-Enhanced Multifunctional Nanocarbon

As discussed in the previous sections, though nanocarbons (NCs) are widely recognized for their potential as energy storage electrodes, they have limitations like low charge-storage capacity, chemical inactivity, and insufficient hydrophilicity. To find a solution for these issues, metal-based materials are being combined with carbon matrices, which can improve electrical conductivity and enhance electrical performance. Metal-based compounds, including metal oxides, nitrides, and chalcogenides, offer high storage capacity but suffer poor electrical conductivity and stability during

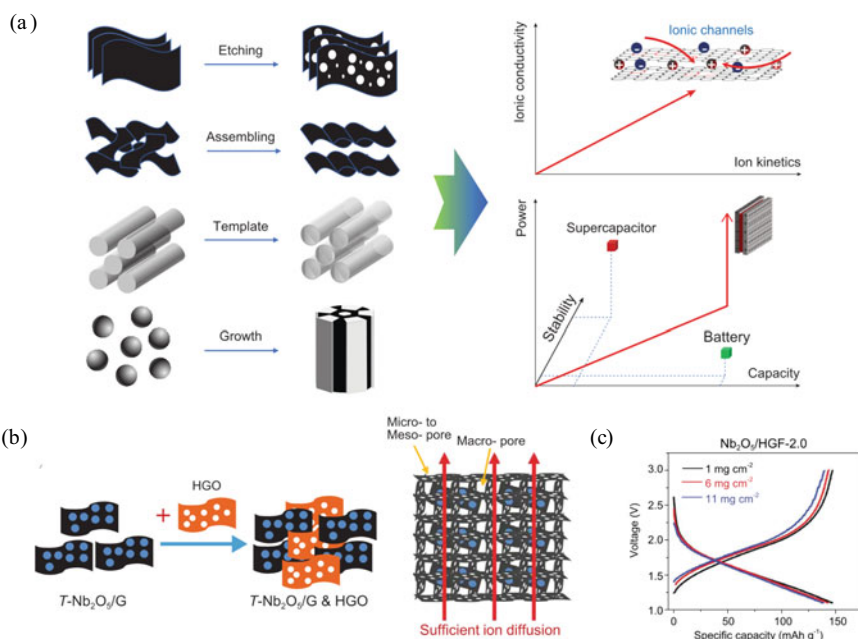


Fig. 3 **a** Common techniques for creating ionic pathways spanning from microscopic to macroscopic dimensions, each with specific objectives to enhance energy storage performances. Reprinted with permission [14] **b** Illustration of the two-step process to prepare 3D hierarchically porous composite architecture with efficient ion diffusion. **c** Galvanostatic charge–discharge curves for porous graphene/Nb₂O₅ with different mass loading. Reprinted with permission [15], Copyright 2017, American Association for the Advancement of Science

electrochemical cycling. To address this, nanoscale structuring is proposed as a synergistic solution to shorten the ion pathways, resulting in enhanced capacity and rate capability. Growing nanoparticles (NPs) on nanocarbons (NCs) is a rapidly evolving strategy for designing and making electrodes used in energy storage applications termed here as NPs/NC composites. The composites can be prepared by two common processes known as ex-situ and in situ, as given in Fig. 4a-c [16].

A recent example of NPs/NCs composite is described by Pei et al. as an anode for the next generation energy storage devices like potassium ion batteries (KIBs) [17].

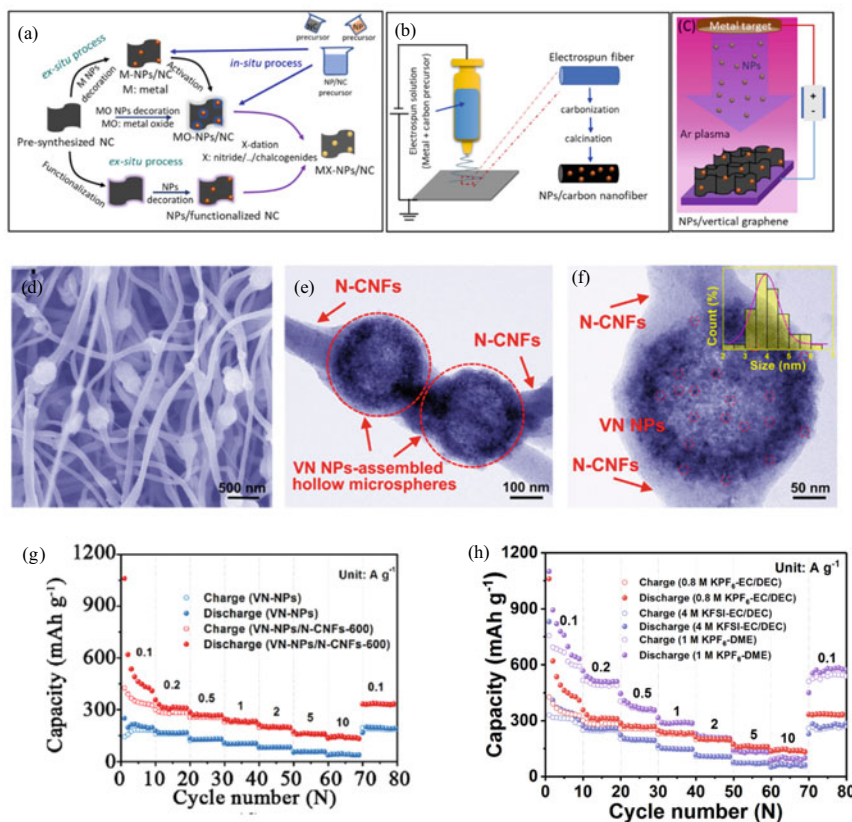


Fig. 4 a Schematic of various methods of NPs/NCs preparation. b Example of in situ process (NPs on carbon nanofiber). c Example of ex-situ process (NP decoration on vertical graphene by low-temperature DC plasma process). Reproduced with permission [16]. d Scanning electron micrographs. e, f Transmission electron micrograph of VN-NPs/N-doped CNFs-600. The inset of f shows particle size distribution. g Rate performance of VN-NPs/N-CNFs-600 and VN-NPs for K⁺ ion storage. h Rate performance of the VN-NPs/N-CNFs-600 electrode in various electrolyte concentrations. (0.8 M KPF₆-EC/DEC, 4 M KFSI-EC/DEC, and 1 M KPF₆-DME) electrodes. CNF: carbon nanofiber; KFSI: potassium bis (fluor sulfonyl) imide; EC: ethylene carbonate; DEC: diethyl carbonate; DME: dimethoxy ethane. Reproduced with permission [17]

Vanadium nitride (VN) nanoparticles, assembled into hollow microspheres within nitrogen-doped carbon nanofiber framework, delivered outstanding K^+ ion storage capabilities. The interconnection between the hollow microspheres of VN (NPs) with the N-doped CNF can be observed in Fig. 4d–f. The anode exhibited impressive rate capabilities for K^+ ion storage with varying current densities and also with various electrolyte concentrations (Fig. 4g, h). The nanocarbons structure, N-doped CNF in the composite shown above, played the following crucial roles: preventing the nanoparticles from clustering, establishing conductive pathways, and enhancing structural stability. The doping helped create active sites for electrochemical interactions with the K^+ ions, while the hollow structure facilitated greater contact between the nanoparticles and the electrolyte. The described composite also accommodated volume expansions during cycling and enabled effective electrolyte penetration. Beyond electrode material design, the other factors instrumental in remarkable K^+ ion storage include the choice of potassium salt, solvent, electrolyte concentration, and additives.

3 Tuning Electrochemical Properties of Nano Carbons for Energy Conversion

3.1 Photovoltaics (PV)

As mentioned, solar energy will emerge as a predominant and sustainable energy source. While selenium was the first element to be used in PV technology with an efficiency of 1%, the current PV market is dominated by Si-based solar cells with an efficiency of over 45%. Recently, various developments in solar cells can be witnessed in the form of thin-film PVs comprising of CIGS (Copper Indium Gallium Selenide), CdTe/CdS, DSSCs (Dyed and Sensitized Solar Cells), organic photovoltaics, and the latest hybrid Perovskites. All of the above can be grouped under the third-generation solar cells [18].

As the solar industry and research strive to fabricate high-efficiency solar cells, advanced materials are being explored to overcome the limitations of conventional materials. Nanocarbons like carbon nanotubes, graphene, fullerene, and other nanohybrids are among the advanced materials used in photovoltaic (PV) technology due to their exceptional photoelectric characteristics, abundant availability, strong optical absorption, and excellent thermal and electrical properties. Due to the above outstanding properties, they are employed in solar cells as electrodes, charged carrier transport media, and active or interfacial layers. A recent trend in DSSCs (Dyed and Sensitized Solar Cells) and PSC type (Perovskite Solar Cells) is engineering interfaces with carbon nanomaterials. This practice reduces the extensive usage of unstable or precious metals like platinum (Pt) and gold (Au) as counter electrodes (CR) or back electrodes, which raise production costs, posing commercial viability challenges. Recent advancements in tailoring nanocarbons for improving various

types of solar cells to enhance the efficiency and stability of photovoltaic technology are discussed below [18].

(a) Doped Nanocarbons for High-Performance Silicon-Based Solar Cells

The basic functioning of a solar cell is based on a p–n junction to convert sunlight photons to electricity. The junction is formed when semiconducting carbon contacts silicon, creating a C–Si heterojunction between p-type carbon and n-type Si. The utilization of carbon nanomaterials has the potential to overcome some limitations of silicon-based solar cells (SCs), which lack flexibility and transparency.

The doping of nanocarbons like fullerene (C60), CNTs, and graphene has been proven to increase solar cells' power conversion efficiency (PCE). PCE is a critical factor for every solar cell and can be defined as the ratio of the optical power incident on the cell to the electrical power output. In organic PV cells, Fullerene, or C60, is commonly used as an electron acceptor/transporter. Earlier studies of heterojunctions consisting of C60/p-Si and C60/n-Si heterojunctions displayed a poor PCE value below 0.1%. Later studies using a modified fullerene, n-type C60 with grafted tertbutyl ammonium iodide (TBAI) and p-type Si reported a high efficiency of 8.43% [18].

Similarly, for CNT films/Si heterojunctions, chemically doped CNT films demonstrated greater PCE values. For example, a CNT/NAFION with Si heterojunction solar cell exhibited a high efficiency of 15.25 and 18.9% in the front and back junctions design of solar cells, respectively. This is mainly due to an intermix NAFION layer, which acted as a CNT dopant and an anti-reflecting and passivation layer. The observed high efficiency is also due to the cell design, where a greater active area for the entire silicon wafer was available due to the front and back junction design [19].

Graphene is a potential candidate in the electronics industry thanks to its near-zero band gap, outstanding electron mobility (2.5×10^5 cm²/Vs), and transparency. Tailoring graphene properties can help achieve high PCE in graphene/Si heterojunction for the following reasons. (1) Increasing the work function of graphene can expand the junction's built-in potential. Here, P-type doping can increase the work function of graphene. (2) Tailoring the number of layers of graphene can control the transmittance, and (3) Adding an interfacial layer of GO/SiO₂ can increase the spectrum/band of light absorption. However, due to inhomogeneous oxide formation, the graphene/n-Si Schottky diode interface has an issue suppressing the tunneling current at the interface. Charge recombination at the interface is induced by the accumulated trap charges at low current, which leads to a low fill factor of the solar cell. The fill factor is the maximum achievable power in the solar cell at both open circuit voltage and short circuit current. The charge recombination gives rise to a non-linear I–V feature called an S-shaped kink in solar cells. Adhikari et al. [20] addressed this issue by increasing the carrier mobility at the interface accomplished by doping graphene. This approach helped transform the non-linear I–V to linear I–V. It increased the fill factor and efficiency, as shown in Fig. 5.

Figure 5a, b give the device's schematic with and without graphene, as further illustrated by the SEM image in Fig. 5c. Figure 5d presents the space-charge limited

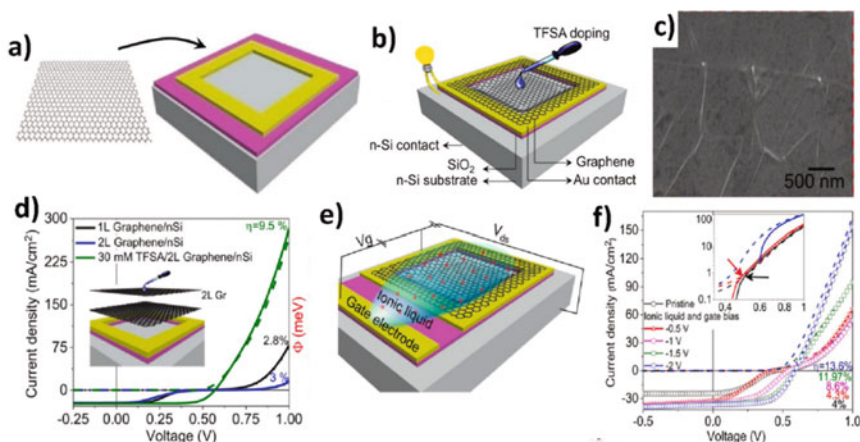


Fig. 5 Schematic of graphene/n-Si device structure **a** before and **b** after graphene transfer and chemical doping. **c** SEM images of graphene/n-Si. **d** Current density–voltage (J – V) characteristics of graphene/n-Si solar cells with one and two layers of graphene before and after doping with 1-ethyl-3-methylimidazolium bis (trifluoromethyl sulfonyl) imide (TFSA). **e** Schematic of graphene/n-Si device with Ionic Liquid (IL) and external bias configuration. **f** J – V characteristics of pristine and IL-doped graphene/n-Si at various gate voltages (V_g). The dashed and symbol lines indicate dark and illumination conditions, respectively. The inset shows a portion of the J – V curve in the log scale to highlight the crossing of the dark and illuminated J – V marked by black and red arrows. Reprinted with permission [20]

current, which yields a linear I – V curve after doping with Ionic Liquid (IL). The latter caused an increase in the material’s electrical conductivity, which enabled a decrease in the trap charge density. Figure 5e displays a schematic of the graphene being doped by IL called 1-ethyl-3-methylimidazolium bis (trifluoromethyl sulfonyl) imide (TFSA). The resultant IL-doped Graphene/n-Si structure was reported to give an efficiency of 13.6%. Further, current density–voltage (J – V) characteristics are presented in Fig. 5f. Nevertheless, the theoretical efficiency limit can be pushed further to 19% by optimizing various factors like graphene electrical conductance, silicon carrier density, and interface oxidation.

(b) Nanocarbon Tuning for Advanced Performing Dyed and Sensitized Solar Cells (DSSCs) and Perovskite Solar Cells (PSCS)

Dyed and Sensitized Solar Cells (DSSC) have significant potential as a renewable source due to their environmentally benign nature, low cost, and simple fabrication process. However, they reveal limitations that hinder their commercialization, like (a) highly expensive electrode materials (transparent conductive oxide (TCO) and Pt), (b) poor performance due to sluggish electron transport, and (c) recombination of charges. The counter electrode (CE) and the photoelectrodes in DSSCs consist of an important component called TCE or Transparent Conductive Electrode (TCE), usually made of Indium Tin Oxide (ITO) and Fluorine Doped Tin Oxide (FTO). They are used due to their low sheet resistance ($R_s = 5$ – $100 \Omega/\text{sq}$) and high optical

transparency (80–97% at 550 nm). However, they have drawbacks like (1) poor high-temperature stability, low salt and acid resistance, (3) high cost due to shortage of indium supplies, (4) low transparency in the IR region, (5) brittleness, and (6) defects created in the FTO devices leading to leakage. Nanocarbons, which can undergo tailoring and fine-tuning, are capable of addressing the above issues [18].

Patterned CNTs: CNT films subjected to network architecture exhibit a high aspect ratio, resulting in very low sheet resistance and high optical transmittance. A research group studied the different CNT forms as CEs wherein CNT in planar and microarray patterns was grown on n-type Si substrates by hot filament CVD process. The CNT-based CEs performed better than Pt-coated Si-based CEs, giving a PCE of 7.13 versus 6.29% [18].

Graphene Composites: Bilayer graphene composite comprised of graphene and MWCNT was used as CEs instead of Pt-based CEs in DSSCs. The bilayer electrode gave a better PCE of 4.1% than the Pt-based, which showed a PCE of 3.4%. Also, the bilayer electrode performed better than monolayer graphene and monolayer MWCNT individually. Mehmood et al. [18] reported a composite of graphene with PANI, which resulted in lower charge transfer resistance and better performance. The PANI/9% graphene electrode exhibited an efficiency of 7.45% and a charge transfer resistance of 20.1 Ω . The performance depended on the concentration of graphene in the composite.

Perovskite Solar Cells (PSCs) also hold great potential as future renewable energy devices due to their ease of fabrication and outstanding performance. However, short life and manufacturability issues hinder their commercialization. Nanocarbons, due to their uniqueness, are widely used in PSCs to overcome the above issues. Nanocarbon is a promising component in the future high-performing PSCs because it improves their stability. The latter is accomplished by the hydrophobic nature of the nanocarbon, which shields the PSC from humidity.

In PSCs, when conventional mesoporous TiO_2 is replaced with planar ZnO as an electron transport layer (ETL), it allows for scalability, resulting in cost savings and feasibility of low-temperature processing. However, during annealing, the perovskite materials get converted to lead iodide due to the presence of oxygen on the surface of the ETL layer. Hence, to tackle the issue, Ahmed et al. [21] added graphene quantum dots (GQD) to ZnO, forming a hybrid ETL layer of ZnO/GQD. The GQDs prevented the recombination of electron–hole pairs by extracting electrons from the perovskite film and passivating the oxygen agents on the surface of ZnO, thus avoiding the formation of PbI_2 . A hybrid ETL made of ZnO/GQD exhibited the highest PCE of 17.63%, and the long-term and thermal stability performance were satisfactory. During the long-term stability test, the ETL retained 80% of the PCE after exposure to 1,500 h of 60% relative humidity. In contrast, in thermal stability, the PCE retention was 90% after exposure to 80 °C for 1,500 h.

Although carbon materials research has brought enhancements in solar cell device life and efficiency, there are hurdles to overcome, including long service life, high yield, and cost-effective mass production.

3.2 *Electrocatalysis*

Electrocatalysis represents the co-mingling of two branches of physical chemistry, namely electrochemistry and catalysis. It is related to the electrochemical processes at the electrode surface where the catalysts function. Within this mechanism, electron (e^-) and ion movement at electrode interfaces break and forge bonds, converting chemical energy into electrical energy. This conversion allows for the accumulation of electrical energy, supporting environmentally friendly and sustainable energy technologies [22, 23]. These technologies play an important role in advancing high-performance electrochemical devices like sensors, lithium-ion batteries, and supercapacitors.

3.2.1 **Characteristics of Nanocarbons in Electrocatalysis**

Nanocarbon materials possess distinctive electrical, mechanical, and chemically modifiable characteristics owing to their specific shapes, porosities, and atomic arrangements. These attributes render nanocarbons exceptionally desirable as tailored materials in applications involving electrocatalysis, referred to as Electrocatalytic Nanocarbon (EN) [24, 25]. Therefore, in recent years, there has been a surge in scientific investigations documenting the remarkable effectiveness of EN across a range of reactions, including oxygen reduction reaction (ORR), oxygen evolution reaction (OER), nitrogen reduction reaction (NRR), carbon dioxide reduction reaction (CO_2RR), hydrogen evolution reaction (HER), and methanol oxidation reaction (MOR), as shown in Fig. 6. The interest in employing EN as electrocatalysts for energy conversion and chemical synthesis arises from several key aspects. Firstly, EN is an economical alternative to costly noble metal electrocatalysts due to its composition comprising readily available elements like carbon, nitrogen, and trace amounts of transition metals. Secondly, its molecular structure predominantly comprises sp^2 -hybridized graphitic carbon, rendering it an exceptional conductor with a rapid electron transfer rate. Thirdly, the synthesis process of EN allows for the substantial incorporation of different heteroatom dopants and catalytic designs into their molecular framework. This similarity to homogeneous electrocatalysts enables fine-tuning of the active site structure to enhance activity towards specific reactions. Lastly, the 3D hierarchical structure of EN, particularly in terms of porosity, can be readily tuned through synthetic techniques, providing extensive surface areas and abundant access to catalytic sites [25].

3.2.2 **Impact of Nanocarbon Structure Tuning on Electrocatalysis**

The tuning of the compositions and arrangements of nanocarbon materials through deliberate design and engineering involving various techniques can augment selectivity, reaction rates, and the overall efficiency of electrocatalytic processes [25].

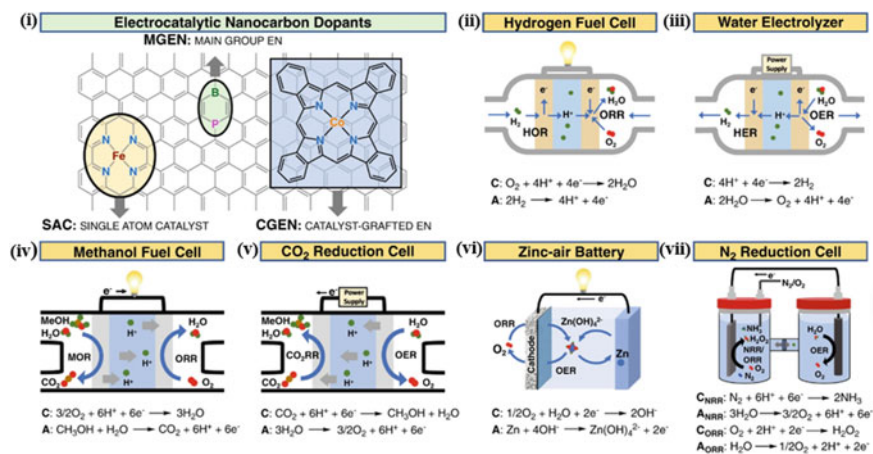


Fig. 6 Reactions and utilizations of tuned electrocatalytic nanocarbons (EN). (i) Exemplary configurations of 3 EN varieties. Employment of EN in (ii) Hydrogen fuel cells and (iii) Water electrolyzers to improve ORR, OER, and HER. (iv) Methanol fuel cells. (v) CO₂ reduction cells for MOR, CO₂RR, ORR, and OER. (vi) Cathode electrocatalysis in zinc-air batteries for ORR and OER. and (vii) nitrogen or oxygen reduction cells for NRR and 2e⁻ ORR, targeting electrochemical synthesis of NH₃ and H₂O₂, respectively. Reprinted with permission [25]

(a) Doping

Graphene, among other nanocarbon materials, is an exceptionally versatile candidate for electrocatalytic doping. For example, Zhou et al. conducted a remarkable experiment to produce microelectrodes with tuned nanocarbons. They achieved this by utilizing an electrocatalytic doping method on a self-assembled sequential arrangement of graphene oxide (GO), polydopamine (PDA), and iron(III) chloride (FeCl₃) solution, resulting in the creation of PDA/GO/Fe³⁺ microelectrodes [26]. These microelectrodes demonstrated advanced functionality as miniaturized electrochemical sensors, showcasing remarkable attributes such as superior thermal stability, structural integrity, sensitivity, electrical conductivity, and electrocatalytic properties. Moreover, the sensor could detect substances at concentrations as low as 82 nmol per liter within aqueous environments. This innovative approach holds the potential to open novel avenues in electrocatalytic nanocarbon-based sensors. Moreover, incorporating nitrogen effectively adjusts the electron densities of exposed active sites, developing high-performance nanocarbon-based electrocatalysts. As an illustration, Song and his collaborators formulated a composite by dispersing iron carbide onto nitrogen-doped graphene-like carbon nanosheets. This led to a significant enhancement in the rate and longevity of lithium-sulfur (Li-S) batteries [27]. Remarkably, these nanocarbon-based composites exhibited a specific capacity of 954.5 mA h/g after the initial cycle and maintained 439.9 mA h/g over 500 stable cycles. This exemplary structure, characterized by unique catalytic activity and conductivity, can be considered a remarkable model for electrocatalytic nanocarbon in high-performance Li-S batteries. Furthermore, Shu et al. devised a straightforward oxidation method to

achieve in-situ oxidation of a palladium–iridium alloy on nitrogen-doped graphene, resulting in a significant enhancement in methanol electro-oxidation activity ($1,374.8 \text{ mA mg}^{-1}$) and remarkable stability (retaining 44.9% of the current density after 500 cycles) [28]. Ali et al. also highlighted the potential of graphene-based nanomaterials as versatile bifunctional electrocatalysts, specifically for the comprehensive splitting of water into hydrogen and oxygen [29]. These materials offer distinctive attributes such as substantial surface area, abundant active sites, and facile syntheses of various co-doped nanomaterials.

(b) Porous Templating

The strategic utilization of porous templating is a crucial technique in fine-tuning nanocarbon structures. This process involves a precisely designed porous template to tailor porous carbon structures with a similar pattern to amplify the electrocatalytic capabilities. For example, Cheng et al. employed a simple impregnation-adsorption technique to create platinum solid-state supercapacitors combining micropore entrapment and nitrogen-doping methods onto a 3D hierarchical carbon nanocage support [30]. These carbon nanocage-based supercapacitors showcased a record-breaking Hydrogen Evolution Reaction (HER) performance with minimal overpotential, low Tafel slope, and long-term stability. In a separate study, Liu et al. introduced porosity-tuned carbon nanosheets for supercapacitors and Oxygen Reduction Reaction (ORR) activity. They included a process involving triethanolamine intercalation of layered peanut seed coats followed by thermal exfoliation and pyrolysis [31]. These sheets demonstrated elevated electrical conductivity (8.1 S cm^{-1}), exceptional ultra-high-rate capabilities, and remarkable stability after 20,000 cycles, positioning them as efficient cathodes for zinc–air batteries.

(c) Defect Engineering

The controlled introduction of defects in nanocarbon holds significant promise in tailoring their properties for electrocatalysis applications. For instance, Zhang et al. synthesized a flawed graphene-like carbon nanomaterial using cost-effective and widely available anthracite coal as the precursor [32]. This material displayed remarkable ORR activity, selectivity, and an impressive H_2O_2 production rate of $355.0 \text{ mmol L}^{-1} \text{ h}^{-1} \text{ cm}^{-2} \text{ g cat}^{-1}$ with nearly 100% Faraday efficiency. Additionally, Zhang et al. underscored the strong correlation between the ORR activities of ENs and the presence of defects and heteroatom dopants. As a reference, they experimented with pristine nanocarbons like graphite, graphene, and CNTs, which exhibited negligible ORR activity. In contrast, defect-engineered nanocarbons exhibited the highest ORR performance [33]. This result suggests that the arrangements of heteroatom dopants and diverse defects play a significant role in shaping the distinctive electronic structure of nanocarbons that leads to varied electrocatalytic activities.

(d) Electrodeposition

Electrodeposition is a technique used to modify and enhance the electrocatalytic properties of nanocarbon materials by selectively depositing desired substances onto

their surfaces through an electrochemical process. A possible alternative to graphene for generating catalytically active metal species through electrodeposition is electrospun carbon nanofibers (CNFs). For example, Hatton et al. described a method for electrodepositing Pt clusters of random size and shape onto CNF surfaces using several cyclic voltammetry scans. The created Pt/CNF revealed a much greater peak current density in the forward scan than a commercial Pt/C electrode, indicating increased methanol oxidation activity [23]. However, they also unveiled that while these electrospun CNFs might not function as standalone electrocatalysts, their potential can be unlocked through the electrodeposition of other materials, offering new possibilities. CNTs can also be tuned using electrodeposition, enabling their dual role as catalyst supports and metal-free catalysts. This holds for various fuel cell types, including direct methanol fuel cells, half cells, and proton exchange membrane fuel cells. To exemplify, Gao et al. conducted experiments involving Pt deposition on multi-walled carbon nanotubes through an ion exchange method, yielding excellent cathode electrocatalysts that exhibited enhanced performance in oxygen reduction reactions. These catalysts demonstrated a notably increased Pt utilization efficiency of 96.5% and greater oxygen reduction current even with a reduced Pt loading [34]. Furthermore, using an electrophoretic deposition approach, Kamat et al. established a reliable method for fabricating Pt electrodes supported by single-walled carbon nanotubes [35]. The substantial surface area, unique architecture, and inherent porosity of these nanocarbons enabled the use of relatively small quantities of Pt while still attaining impressive current outputs. Consequently, these electrodes displayed increased catalytic activity in the ORR and methanol oxidation processes.

(e) Electroreduction

Electroreduction is a process that involves the reduction of particular chemical species or molecules present in a solution onto the surface of nanocarbon materials to develop catalytically active sites for electrochemical reactions [36]. Among others, using tuned nanocarbon materials for electrocatalytic CO₂ reduction emerges as a crucial avenue in addressing global warming and promoting environmentally sustainable energy approaches [24]. This is why researchers are actively exploring and advancing this area of research. The utilization of single-layer graphene supports has shown significant promise in achieving selective CO₂ reduction. For example, Yu et al. have indicated that the creation and application of partially oxidized cobalt nanoparticles dispersed on nitrogen-doped single-layer graphene can significantly influence CO₂ reduction reactions [37]. The resultant materials displayed exceptional selectivity toward alcohol compounds and high yields of methanol and ethanol. Moreover, this resulted in an amplified current output, reduced overpotential of – 0.1 V, and sustained stability over a 10-h period of electrocatalysis. Another example is provided by Han et al., who introduced a method to develop defective graphene (DG) as a potential electrocatalyst. They initiated the process by nitrogen-doping graphene and subsequently removing the nitrogen, resulting in DG. This material is distinguished by its substantial presence of catalytically active sites and a

notable capability for CO₂ reduction [38]. Compared to pristine graphene, nitrogen-doped graphene, and edge-rich graphene, DG showcased superior performance with a reversible hydrogen electrode, higher capacity of CO₂ chemisorption, and notably higher current density. This result underscores the significant potential of defective graphene in driving electrocatalytic CO₂ reduction with an impressive faradaic efficiency of 84%, signifying a promising avenue in addressing carbon reduction in the atmosphere through enhanced catalytic methods.

(f) Metal-Free Electrocatalytic Nanocarbons for Sustainable Future

A major goal in environmental-friendly chemistry is to substitute expensive and precious metal catalysts with less expensive and more readily obtainable ones. Nanocarbon-based electrocatalysts play a great role in this matter to fabricate metal-free substitutions, as shown in Fig. 7. Li et al. significantly developed this area by synthesizing dual-doped carbon nanosheets like graphene containing sulfur and nitrogen. These sheets were accomplished using a simple pyrolysis procedure to produce metal-free electrocatalysts for ORR by combining melamine and dibenzyl sulfide [39]. The obtained carbon nanosheets displayed enhanced ORR reactivity and excellent durability. This straightforward method could yield additional metal-free ENs for various electrochemical applications, such as fuel cells and metal-air batteries linked to ORR. Moreover, Hu et al. suggested using N-doped CNTs with pristine CNTs as the core and N-doped carbon layers as the shell introduced as a great alternative to the widely used and valuable Pt in ORR [40]. They claimed that these carbon nanotube arrays with N-doping exhibit high electrical conductivity of 3.3 S cm⁻¹ and an elevated amount of N atoms on the surface of ordered mesoporous CNTs, resulting in an increment of ORR activity of 51 mV, which was better than Pt. This discovery generated a fascinating field of nanocarbon-based tailored, metal-free ORR electrocatalysts. The latter enabled anticipatory design and adjustable fabrication of microporous structures along with doping topologies enhancing the performance of fuel cells.

In conclusion, electrocatalysis is a transformative pathway toward unlocking the full potential of nanocarbon materials for energy applications. Researchers are paving the way for more efficient, sustainable, and environmentally friendly energy technologies by leveraging the intricate interplay between catalysts and nanocarbon structures.

3.3 Fuel Cells

In the quest for cleaner and more efficient energy solutions, fuel cells have emerged as a groundbreaking technology with the potential to revolutionize how we energize our world. A fuel cell operates by facilitating a continuous electrochemical process. It generates electricity by splitting hydrogen into protons and electrons at the anode. Protons travel through an electrolyte to the cathode, while electrons create an electric current. At the cathode, oxygen combines with protons and electrons to produce

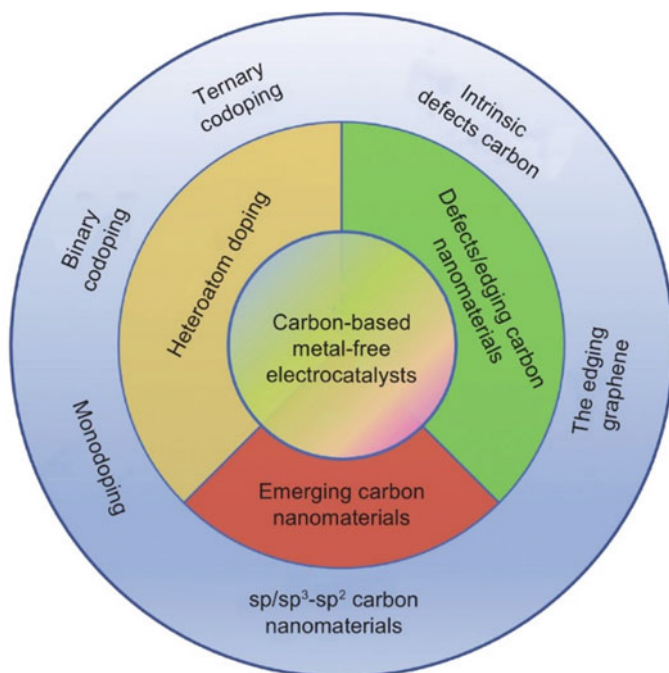


Fig. 7 Illustrative overview of nanocarbons as sustainable noble, metal-free electrocatalysts. Reprinted with permission [41]

water and heat, yielding clean electrical power with only water vapor as a byproduct. Improving fuel cells' efficiency involves enhancing ion conductivity, catalyst activity, power density, and current conductivity [42]. All these improvements have been explored by employing structurally adjusted nanocarbon materials.

3.3.1 Influence of Carbon Nanomaterial Structure Tuning on Fuel Cell Performance

Fuel cell technology has made amazing progress in recent years, with carbon nanomaterials playing a key role in improving fuel cell performance. The precise engineering of carbon nanomaterial structures is the main topic of this investigation, which also looks at how specific alterations and tuning methods can significantly impact the effectiveness and overall functionality of fuel cells.

(a) Porosity Engineering

Porosity engineering fine-tunes the electrochemical properties of nanocarbon for fuel cells by optimizing internal structures to enhance reactivity and transport efficiency. A functional loss occurs when oxygen cannot be transported to the electrode active sites in the micro pores due to the overflow of the pores (flooding).

The natural hydrophobicity and abundance of mesopores and macro pores in the nano carbons-derived catalyst can ensure the purity of the O₂ in the gas diffusion electrode. For instance, Peng et al. used pyrolysis to create customizable carbon nanoshells (CNS) with macro and mesoporous structures [43]. Fe–N/CNS catalysts developed based on CNS with varying microstructures demonstrated efficient oxygen/ion transport due to their hierarchical mesoporous/macroporous structure. This enhanced the Three-Phase Interface (TPI) in the Oxygen Reduction Reaction (ORR) catalyst layer. The CNS structure with linked transfer routes promoted strong ORR activity in a membrane-less Direct Formic acid Fuel Cell (DFFC). Moreover, in pursuit of efficient and high-performance catalytic activity and oxygen reduction for high-temperature Polymer Electrolyte Fuel Cell (PEFCs), Yang et al. created a strong Pt electrocatalyst based on a 3D nanoporous carbon (NanoPC) substrate. NanoPC/PyPBI/Pt-NPs where PyPBI denotes poly[2,2'-(2,6-pyridine)-5,5'-bibenzimidazole], which was deposited on PyPBI-wrapped NanoPC. The obtained FC device demonstrated exceptional electrochemical stability even after 10,000 start-up/shutdown cycles [44]. Due to the NanoPC's unique nanoporous shape, reactant diffusion was enhanced, and the power density of this catalyst gave excellent results, outperforming standard CB/PyPBI/Pt and CB/Pt catalysts where CB stands for Carbon Black).

(b) Graphitization Metamorphosis

Graphitization tunes carbon structure for fuel cell stability and conductivity. Carbon aerogels are attractive Pt supports in this case, but standard heat treatment or catalytic graphitization procedures have limits. The ideal carbon support for fuel cells requires significant graphitization to resist electrochemical corrosion, as well as mesoporous pore configurations for effective oxygen reduction. Although most nitrogen-doped mesoporous carbons lack stability and graphitization, carbon aerogels emerge as platinum (Pt) supports due to their adjustable features. Catalytic approaches are used to avoid excessive temperatures and improve carbon aerogel graphitization. Luo et al. used transition-metal salts (transition metals like Fe, Mn, and Cr) to convert carbon aerogel into graphene layers, thus minimizing carbon-coated metal impurities and enhancing stability [45]. This method, particularly when catalyzed by MnCl₂, produced promising Pt-supported catalysts with increased surface area, completed graphitization, and corrosion resistance for fuel cell cathodes. Additionally, Bock et al. investigated the effect of graphitization on thermal conductivity in Catalyst Layers (CLs) of proton exchange membrane fuel cells. They discovered that graphitized CLs have higher thermal conductivity (0.12–0.05 WK⁻¹ m⁻¹) at 10 bar pressure than non-graphitized CLs (0.061–0.006 WK⁻¹ m⁻¹) [46]. This increased thermal conductivity and helped improve the catalytic activity of fuel cells by tuning efficient charge transfer, stability, and power density. In addition, Qiao et al. created stable Porous Graphitic Carbon (PGC) by pyrolyzing 3D polymer hydrogel with Mn, displaying multilayer carbon sheets in flower-like nanoparticles [47]. The high graphitization, hierarchical porosity, and nitrogen doping of PGC improved Pt nanoparticle dispersion and corrosion resistance. The Pt/PGC catalyst demonstrated better stability in fuel cell testing, losing only minimal voltage after 5,000 cycles.

This was attributed to good graphitization, increased surface area, and porosity, along with nitrogen doping effects, resulting in the effective stabilization of Pt.

(c) Transforming Nanocarbon Lattices via Doping

Doping nanocarbon materials like CNT and graphene lead to adding foreign atoms, which can boost conductivity and catalytic activity for better fuel cell performance. According to Xu et al., the existence of various nitrogen (N) configurations in N-doped carbons, such as pyridinic-N, pyrrolic-N, graphitic-N, oxidized-N, and sp-hybridized N, is critical for the carbon's catalytic activity in the Oxygen Reduction Reaction (ORR) for fuel cells [48]. However, it is difficult to determine the effect of each configuration on the cathode reaction. This research group adjusted N-doping by varying pyrolysis temperature and Ar gas flow rate. They discovered the following catalytic activity sequence: pyridinic-N > pyrrolic-N > graphitic-N > oxidized-N > C (carbon), thus explaining the increased fuel cell power output. Moreover, Dai et al. developed a high-performance 3D nitrogen-doped carbon electrode (N-G-CNT + KB) for acidic fuel cells [49], where KB is "ketjenblack" carbon black. This electrode integrates nitrogen-doped graphene and nitrogen-doped carbon nanotubes, offering an expansive reaction area from N-doped graphene, enhanced conductivity via the CNT core, and efficient water and gas transport through the KB separator. The excellent energy dynamics and stability underscore the potential of heteroatom-doped carbon nanomaterials as promising electrocatalysts in acidic fuel cells. Apart from this, Hornberger et al. used a fluidized bed reduction reactor to create Pt electrocatalysts based on N-doped carbons with catalytic activity and stability equivalent to state-of-the-art PEMFC catalysts for the oxygen reduction reaction [50]. They investigated the effect of N-doping on Pt/N-C catalyst deterioration, discovering that while N-doping does not prevent carbon corrosion during high-potential cycling, it did improve cell performance under normal PEMFC operating circumstances. This study adds to our understanding of the effect of N-doped carbon catalyst supports on fuel cell performance.

(d) Electrode Evolution in Polymer Electrolyte Fuel Cells Based on Nanocarbon

Metal-based catalysts use porous carbon supports to boost the oxygen reduction capacity of polymer electrolyte fuel cells, while carbon nanotubes (CNT) and other nanocarbons act as carriers to improve catalyst efficiency. For example, Girishkumar et al. demonstrated significantly lower charge transfer resistance for carbon nanotube-based electrodes in hydrogen evolution reactions compared to Pt-supported carbon black electrodes, indicating higher catalytic activity and current density, thus offering the potential to reduce Pt usage. These metal-free nanocarbon-based electrocatalysts improve fuel cell performance by tuning efficient catalytic activity and eliminating the need for typical precious metal catalysts [51]. Further, Xue et al. recently combined zigzag graphene nanoribbons with carbon nanotubes as the backbone to contribute to higher FC efficiency. By doing this, they enhanced the nanocarbon current conductivity and reduced the resistance, achieving a peak power density of 520 mW mg^{-1} and a peak power field density of 161 mW cm^{-2} [52]. In conclusion, the precise

tuning of nanocarbon materials holds the key to unlocking the full potential of fuel cells, paving the way for a cleaner and more sustainable energy future.

4 Conclusions

The study confirms the huge potential of nanocarbon tailoring in energy conversion and storage applications. CNT and graphene have already shown great promise as electrode materials in supercapacitors and rechargeable batteries due to their high electrical conductivity and large specific surface area. Further, fullerene derivatives are widely used in Perovskite Solar Cells (PSCs) as electron acceptors in energy conversion devices like solar cells. CNTs and graphene are frequently employed as counter electrodes, presenting an alternative to Pt electrodes in Dyed and Sensitized Solar Cells (DSSC) due to their flexibility, low cost, and high catalytic activity. While large-scale synthesis, structure control, and enhancement of physical and chemical properties of nanocarbons will be the continuous focus and effort of industrialists and researchers in the energy applications arena, controlling nanocarbon structures is not easy on a large scale. For example, the reproducibility of SWCNT structure, repeatable production of defect-free MWCNT, and controlling the consistency in the size and number of graphene layers in a scaled-up production environment remain technological challenges. Despite a lot of problems that need to be solved, there is a huge possibility and plenty of room for new ideas and strategies in areas such as material design, synthesis routes, and device configuration involving nanocarbon tunability. All these are considered as primary tools to unlock the full potential of future energy harvesting and storage devices.

References

1. Sheng, Su.D., Centi, G.: A perspective on carbon materials for future energy applications. *J. Energy Chem.* **22**, 151–173 (2013)
2. Dai, L., Chang, D.W., Baek, J.B., Lu, W.: Carbon nanomaterials for advanced energy conversion and storage. *Small* **8**, 1130–1166 (2012)
3. Jariwala, D., Sangwan, V.K., Lauhon, L.J., Marks, T.J., Hersam, M.C.: Carbon nanomaterials for electronics, optoelectronics, photovoltaics, and sensing. *Chem. Soc. Rev.* **42**, 2824–2860 (2013)
4. Yang, Z., Ren, J., Zhang, Z., Chen, X., Guan, G., Qiu, L., et al.: Recent advancement of nanostructured carbon for energy applications. *Chem. Rev.* **115**, 5159–5223 (2015)
5. Inagaki, M., Orikasa, H., Morishita, T.: Morphology and pore control in carbon materials via templating. *RSC Adv.* **1**, 1620–1640 (2011)
6. Sunde, L., Goela, S.J.: *High Thermal Conductivity Materials*. Springer (2006)
7. Che, J., Çagin, Goddard, W.A.: Thermal conductivity of carbon nanotubes. *Nanotechnology*, 65–69 (2000)
8. Wen, Z., Li, J.: Hierarchically structured carbon nanocomposites as electrode materials for electrochemical energy storage, conversion, and biosensor systems. *J. Mater. Chem.* **19**, 8707–8713 (2009)

9. Frackowiak, E., Gautier, S., Gaucher, H., Bonnamy, S., Beguin, F.: Electrochemical storage of lithium multiwalled carbon nanotubes (1999)
10. Ghosh, S., Barg, S., Jeong, S.M., Ostrikov, K.: Heteroatom-doped and oxygen-functionalized nanocarbons for high-performance supercapacitors. *Adv. Energy Mater.* **10** (2020)
11. Joseph, K.M., Shanov, V.: Symmetric supercapacitor based on nitrogen-doped and plasma-functionalized 3D graphene. *Batteries* **8**, 258 (2022). <https://www.mdpi.com/2313-0105/8/12/258>
12. Wang, Y., Wang, Z., Yu, X., Li, B., Kang, F., He, Y.B.: Hierarchically structured carbon nanomaterials for electrochemical energy storage applications. *J. Mater. Res.* **33**, 1058–1073 (2018)
13. Zheng, G., Yang, Y., Cha, J.J., Hong, S.S., Cui, Y.: Hollow carbon nanofiber-encapsulated sulfur cathodes for high specific capacity rechargeable lithium batteries. *Nano Lett.* **11**, 4462–4467 (2011)
14. Ye, J., Simon, P., Zhu, Y.: Designing ionic channels in novel carbons for electrochemical energy storage. *Natl. Sci. Rev.* **7**, 191–201 (2020)
15. Sun, H., Mei, L., Liang, J., Zhao, Z., Lee, C., Fei, H., et al.: Three-dimensional holey-graphene/niobia composite architectures for ultrahigh-rate energy storage. <https://www.science.org>
16. Ghosh, S., Polaki, S.R., Macrelli, A., Casari, C.S., Barg, S., Jeong, S.M., et al.: Nanoparticle-enhanced multifunctional nanocarbons—recent advances on electrochemical energy storage applications. *J. Phys. D. Appl. Phys.* **55** (2022)
17. Pei, Y.R., Zhao, M., Zhu, Y.P., Yang, C.C., Jiang, Q.: VN nanoparticle-assembled hollow microspheres/N-doped carbon nanofibers: an anode material for superior potassium storage. *Nano Mater. Sci.* **4**, 104–112 (2022)
18. Deshmukh, M.A., Park, S.J., Hedau, B.S., Ha, T.J.: Recent progress in solar cells based on carbon nanomaterials. *Sol. Energy* **220**, 953–990 (2021)
19. Chen, J., Tune, D.D., Ge, K., Li, H., Flavel, B.S.: Front and back-junction carbon nanotube-silicon solar cells with an industrial architecture. *Adv. Funct. Mater.* **30** (2020)
20. Adhikari, S., Biswas, C., Doan, M.H., Kim, S.T., Kulshreshtha, C., Lee, Y.H.: Minimizing trap charge density towards an ideal diode in graphene-silicon Schottky solar cell. *ACS Appl. Mater. Interfaces* **11**, 880–888 (2019)
21. Ahmed, D.S., Mohammed, M.K.A., Majeed, S.M.: Green synthesis of eco-friendly graphene quantum dots for highly efficient perovskite solar cells. *ACS Appl. Energy Mater.* **3**, 10863–10871 (2020)
22. Banoth, P., Kandula, C., Kollu, P.: Introduction to electrocatalysts. In: *ACS Symposium Series*, 1432, pp. 1–37 (2022)
23. Mao, X., Rutledge, G.C., Hatton, T.A.: Nanocarbon-based electrochemical systems for sensing, electrocatalysis, and energy storage. *Nano Today* **9**, 405–432 (2014)
24. Melchionna, M., Fornasiero, P., Prato, M., Bonchio, M.: Electrocatalytic CO₂ reduction: role of the cross-talk at nano-carbon interfaces. *Energy Environ. Sci.* **14**, 5816–5833 (2021)
25. Askins, E.J., Zoric, M.R., Li, M., Luo, Z., Amine, K., Glusac, K.D.: Toward a mechanistic understanding of electrocatalytic nanocarbon. *Nat. Commun.* **12** (2021)
26. Zhou, H., Shi, T., Cai, W., Wu, D.: All-in-one coupling of 3D hybridized nanocarbon microelectrode for portable monitoring of doxycycline hyclate. *Talanta* **266**, 124926 (2024)
27. Song, C.L., Li, Z.H., Li, M.Z., Huang, S., Hong, X.J., Si, L.P., et al.: Iron carbide dispersed on nitrogen-doped graphene-like carbon nanosheets for fast conversion of polysulfides in Li–S batteries. *ACS Appl. Nano Mater.* **3**, 9686–9693 (2020)
28. Shu, J., Li, R., Lian, Z., Zhang, W., Jin, R., Yang, H., et al.: In-situ oxidation of Palladium-Iridium nanoalloy anchored on Nitrogen-doped graphene as an efficient catalyst for methanol electrooxidation. *J. Colloid Interface Sci.* **605**, 44–53 (2022)
29. Ali, A., Shen, P.K.: Recent progress in graphene-based nanostructured electrocatalysts for overall water splitting. *Electrochem. Energy Rev.* **3**, 370–394 (2020)
30. Cheng, X., Shen, Z., Jiao, L., Yang, L., Wang, X., Wu, Q., et al.: Tuning metal catalysts via nitrogen-doped nanocarbons for energy chemistry: from metal nanoparticles to single metal sites. *EnergyChem* **3**, 100066 (2021)

31. Liu, B., Yang, M., Yang, D., Chen, H., Li, H.: Graphene-like porous carbon nanosheets for ultra-high rate performance supercapacitors and efficient oxygen reduction electrocatalysts. *J. Power Sources* **456**, 227999 (2020)
32. Zhang, C., Zhang, J., Zhang, J., Song, M., Huang, X., Liu, W., et al.: Tuning coal into graphene-like nanocarbon for electrochemical H₂O₂ production with nearly 100% faraday efficiency. *ACS Sustain. Chem. Eng.* **9**, 9369–9375 (2021)
33. Zhang, J., Zhang, J., He, F., Chen, Y., Zhu, J., Wang, D., et al.: Defect and doping co-engineered non-metal nanocarbon ORR electrocatalyst. *Nanomicro Lett.* **13** (2021)
34. Wang, J., Yin, G., Shao, Y., Wang, Z., Gao, Y.: Platinum deposition on multiwalled carbon nanotubes by ion-exchange method as electrocatalysts for oxygen reduction. *J. Electrochem. Soc.* **154**, B687 (2007)
35. Girishkumar, G., Vinodgopal, K., Kamat, P.V.: Carbon nanostructures in portable fuel cells: single-walled carbon nanotube electrodes for methanol oxidation and oxygen reduction. *J. Phys. Chem. B* **108**, 19960–19966 (2004)
36. Zhu, M., Chen, J., Guo, R., Xu, J., Fang, X., Han, Y.F.: Cobalt phthalocyanine coordinated to pyridine-functionalized carbon nanotubes with enhanced CO₂ electroreduction. *Appl. Catal. B* **251**, 112–118 (2019)
37. Zhao, K., Liu, Y., Quan, X., Chen, S., Yu, H.: CO₂ electroreduction at low overpotential on oxide-derived Cu/carbon fabrics fabricated from metal organic framework. *ACS Appl. Mater. Interfaces* **9**, 5302–5311 (2017)
38. Han, P., Yu, X., Yuan, D., Kuang, M., Wang, Y., Al-Enizi, A.M., et al.: Defective graphene for electrocatalytic CO₂ reduction. *J. Colloid Interface Sci.* **534**, 332–337 (2019)
39. Li, J., Zhang, Y., Zhang, X., Huang, J., Han, J., Zhang, Z., et al.: S, N dual-doped graphene-like carbon nanosheets as efficient oxygen reduction reaction electrocatalysts. *ACS Appl. Mater. Interfaces* **9**, 398–405 (2017)
40. Yang, L., Shui, J., Du, L., Shao, Y., Liu, J., Dai, L., et al.: Carbon-based metal-free ORR electrocatalysts for fuel cells: past, present, and future. *Adv. Mater.* **31**, 1804799 (2019)
41. An, F., Bao, X.Q., Deng, X.Y., Ma, Z.Z., Wang, X.G.: Carbon-based metal-free oxygen reduction reaction electrocatalysts: past, present and future. *New Carbon Mater.* **37**, 338–354 (2022)
42. James, L., Andrew, D.: *Fuel Cell Systems Explained*. Wiley (2003)
43. Peng, Q., Lu, Q., Fu, Q., Zhang, L., Li, J., Zhu, X., et al.: A microstructure tuning strategy on hollow carbon nanoshells for high-efficient oxygen reduction reaction in direct formate fuel cells. *Int. J. Hydrog. Energy* **48**, 16678–16689 (2023)
44. Yang, Z., Moriguchi, I., Nakashima, N.: Durable Pt electrocatalyst supported on a 3D nanoporous carbon shows high performance in a high-temperature polymer electrolyte fuel cell. *ACS Appl. Mater. Interfaces* **7**, 9800–9806 (2015)
45. Luo, Y., Feng, J., Wang, L., Jiang, Y., Li, L., Feng, J.: Highly stable nanocarbon supported Pt catalyst for fuel cell via a molten salt graphitization strategy. *Int. J. Hydrog. Energy* **47**, 20494–20506 (2022)
46. Bock, R., Karoliussen, H., Pollet, B.G., Secanell, M., Seland, F., Stanier, D., et al.: The influence of graphitization on the thermal conductivity of catalyst layers and temperature gradients in proton exchange membrane fuel cells. *Int. J. Hydrog. Energy* **45**, 1335–1342 (2020)
47. Qiao, Z., Hwang, S., Li, X., Wang, C., Samarakoon, W., Karakalos, S., et al.: 3D porous graphitic nanocarbon for enhancing the performance and durability of Pt catalysts: a balance between graphitization and hierarchical porosity. *Energy Environ. Sci.* **12**, 2830–2841 (2019)
48. Liu, J., Song, P., Xu, W.: Structure-activity relationship of doped-nitrogen (N)-based metal-free active sites on carbon for oxygen reduction reaction. *Carbon N Y* **115**, 763–772 (2017)
49. Shui, J., Wang, M., Du, F., Dai, L.: N-doped carbon nanomaterials are durable catalysts for oxygen reduction reaction in acidic fuel cells. *Sci. Adv.* **1** (2015)
50. Hornberger, E., Merzdorf, T., Schmies, H., Hübner, J., Klingenhof, M., Gernert, U., et al.: Impact of carbon N-doping and Pyridinic-N content on the fuel cell performance and durability of carbon-supported Pt nanoparticle catalysts. *ACS Appl. Mater. Interfaces* **14**, 18420–18430 (2022)

51. Girishkumar, G., Rettker, M., Underhile, R., Binz, D., Vinodgopal, K., McGinn, P., et al.: Single-wall carbon nanotube-based proton exchange membrane assembly for hydrogen fuel cells. *Langmuir* **21**, 8487–8494 (2005)
52. Xue, L., Li, Y., Liu, X., Liu, Q., Shang, J., Duan, H., et al.: Zigzag carbon as efficient and stable oxygen reduction electrocatalyst for proton exchange membrane fuel cells. *Nat. Commun.* **9**, 3819 (2018)

One-Dimensional Carbon for Electrocatalytic Activities



Niharika Maley, Pratik Patel, Felipe M. de Souza, and Ram K. Gupta

Abstract One-dimensional (1D) carbon structures like carbon nanotubes (CNTs), carbon nanofibers (CNFs), and graphene ribbons, for instance, have drawn a lot of interest in the field of electrocatalysis because of their distinctive characteristics and superior electrochemical performance. The purpose of this chapter is to give a general review of the electrocatalytic properties of 1D carbon nanomaterials and their prospective uses in a range of energy conversion and storage technologies. The main attractive properties of these carbon structures are based on their satisfactory electrocatalytic activity for several processes due to their high surface area as well as conductivity. The first section provides a brief overview of some of the main theoretical aspects related to technologies such as water-splitting electrolyzers, fuel cells, and metal-air batteries. From that, some of their main electrochemical reactions such as hydrogen evolution reaction (HER), oxygen evolution reaction (OER), oxygen reduction reaction (ORR), and hydrogen oxidation reaction (HOR) are discussed based on the application of their respective electrochemical devices. The second section provides some of the main techniques and approaches utilized for the synthesis of 1D carbon-based materials while providing some of their main advantages and drawbacks. The third section provides an in-depth discussion of some of the most recent works from the literature under the scope of the electrochemical performance of 1D carbon-based materials and the main phenomena that justify their use in such technologies. Lastly, an outlook and future aspects regarding the main advantages and current hurdles on the use of 1D carbon-based material are provided to elucidate some of the main issues for the readers while providing some insight for future experimental design.

Keywords 1D carbon nanomaterials · Oxygen evolution reaction · Oxygen reduction reaction · Hydrogen evolution reaction · Electrolyzers · Fuel cells · Nanocomposites

N. Maley · P. Patel · R. K. Gupta (✉)
Department of Chemistry, Pittsburg State University, Pittsburg, KS 66762, USA
e-mail: ramguptamsu@gmail.com

N. Maley · P. Patel · F. M. de Souza · R. K. Gupta
National Institute for Materials Advancement, Pittsburg State University, Pittsburg, KS 66762, USA

© The Author(s), under exclusive license to Springer Nature Singapore Pte Ltd. 2024
R. K. Gupta (ed.), *NanoCarbon: A Wonder Material for Energy Applications*,
Engineering Materials, https://doi.org/10.1007/978-981-99-9935-4_5

1 Introduction

The ever-growing consumption of fossil fuels is a concerning matter worldwide as it can eventually lead to the exhaustion of this non-renewable resource along with severe environmental impacts. To address that, it is deemed necessary to utilize alternative sources of energy to diminish the burden of the excessive use of petrochemicals. Some examples include the generation of energy through solar radiation, wind, tide movement, waterfalls, and nuclear, for instance, which can serve as viable alternatives when utilized in conjunction. However, such sources of energy are intermittent and are influenced by geographical aspects. Because of that, more ways to generate energy are necessary. Part of the challenge lies in developing a technology that is efficient, eco-friendly, and can be reproduced on a large scale as such conditions can decrease the strain on non-renewable sources leading to a more sustainable future. Some of the technologies that can offer such conditions are water electrolyzers, fuel cells, and metal-air batteries for example. Water electrolyzers are a two-electrode system-based device that can perform the electrochemical water-splitting process. The cathode generates H_2 at the potential standard of 0 V known as hydrogen evolution reaction (HER) whereas the anode generates O_2 at +1.23 V known as oxygen evolution reaction (OER), in an ideal scenario. Given, the renewability of this process and zero carbon emission, water electrolyzers have been arduously researched as a viable technology for the generation of clean and renewable energy [1, 2]. The schematic of a water electrolyzer is presented in Fig. 1a. The fuel cells are devices that can convert chemical energy into electricity as, in most cases, H_2 can react with O_2 to generate electricity, heat, and H_2O as a byproduct. Hence, fuel cells can be complementary to a water electrolyzer as the H_2 generated by the latter can react with O_2 to generate energy from the former. In a fuel cell, the hydrogen oxidation reaction (HOR) occurs where H_2 is oxidized at the anode to generate H^+ or H_2O if the electrolyte is acidic or alkaline, respectively. Then, the electrons generated from the previous reaction can flow to the cathode where oxygen reduction reaction (ORR) occurs at which O_2 is reduced to H_2O or OH^- in acidic or alkaline electrolytes, respectively [3]. The schematic for a fuel cell is presented in Fig. 1b. Also, one of the emerging technologies that has been attracting the attention of the scientific community is metal-air batteries which are composed of a metallic anode, a cathode that can adsorb O_2 , and an electrolyte that is usually an aqueous or aprotic solution. During the discharging process, the metallic anode undergoes oxidation whereas O_2 undergoes reduction at the cathode. Particularly, metal-air batteries are attractive because they can potentially have a much higher energy density when compared to the current Li-ion batteries. Hence, optimizing its properties for large-scale use can be a convenient way to partially address the need for green and sustainable energy [4, 5]. The schematic of a typical metal-air battery is presented in Fig. 1c. The proper introduction and combination of these technologies can lead to a sustainable aspect for the generation of energy and decrease the burden on non-renewable sources.

The presented electrochemical devices are governed by mainly three electrochemical reactions which are HER, OER, HOR, and ORR. However, these reactions are

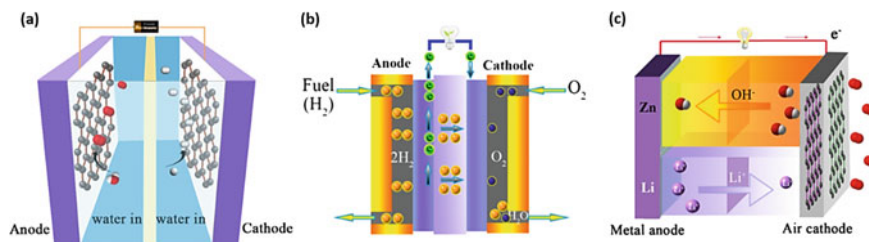


Fig. 1 Schematic of **a** water electrolyzer, **b** fuel cell, and **c** metal-air battery. Adapted with permission [6]. Copyright 2021, Elsevier

inherently sluggish, and, under practical conditions an extra voltage is required to overcome the thermodynamic barriers to these electrochemical reactions to occur, which is known as overpotential. Hence, most of the research is devoted to finding materials that can decrease the overpotential required to catalyze these reactions. Another challenge is that, even though some electrocatalysts can perform these electrochemical processes under feasible conditions they are usually composed of rare metals which makes it impractical for a large-scale scenario. Some examples include Pt or its alloys for HER and ORR, and IrO_2 or RuO_2 for OER. Hence, for these technologies to be properly implemented it is required to use materials that are readily available and cheaper. One of the promising candidates for that are carbon-based materials which can present high conductivity, versatile synthetical approaches, a broad range of chemical property tunability, and high chemical and electrochemical stability which makes them suitable materials for the electrocatalysis of HER, OER, and ORR processes [7–9]. The versatility of carbon materials can be noticed based on the plethora of its allotropes which aside from graphite, diamond, and amorphous carbon also include nanomaterials that go from 0D, 1D, 2D, and 3D which include, fullerenes, carbon nanotubes (CNTs), graphene, and graphene aerogels, respectively, to name a few. Based on that, this chapter is focused on the use of 1D carbon nanomaterials such as CNT, carbon nanofibers (CNF), and carbon nanoribbons (CNR), among others that can perform electrocatalytic processes. The inherent properties of these materials such as high conductivity, high surface area, electrochemical and chemical stability, and broad property tunability, associated with the abundance of carbon make them attractive to the scientific community in the field of electrocatalysis and energy storage. Based on that, some of the variations that have been recently performed on CNT are presented in Fig. 2. Under the line of the promising uses of 1D carbon materials, the next section describe some of the synthetic and characterization approaches followed by some of their recent applications regarding HER, OER, and ORR.

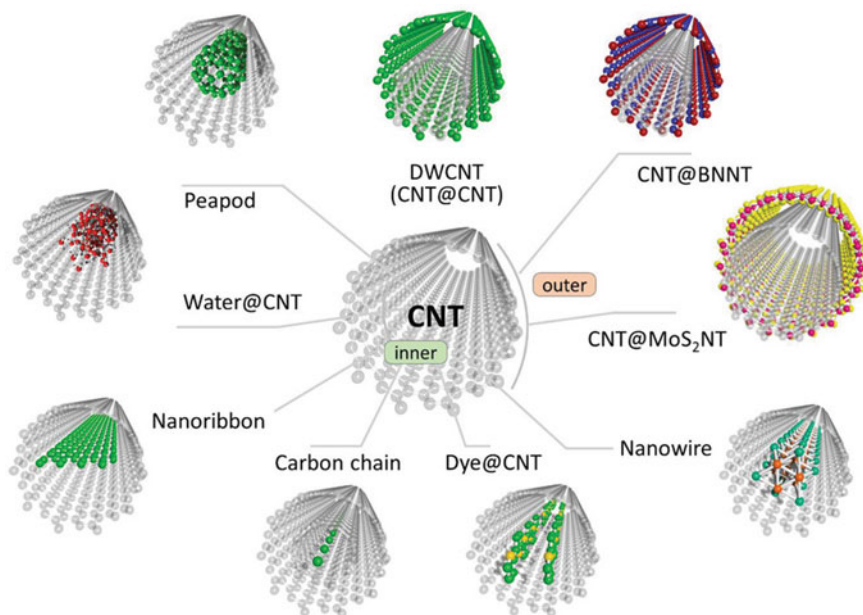


Fig. 2 Variations on the inner and outer layers of 1D carbon-nanostructures where some of the structures include: peapod (fullerene encapsulated within the tubular structure of CNT), double-walled carbon nanotubes (DWCNT), and boron nitride nanotube (BNNT). Adapted with permission [10]. Copyright 2021, John Wiley and Sons

2 Type, Synthesis, and Characterization of 1D Carbon

One of the factors that prompted the research on 1D carbon nanomaterials is their versatility in terms of synthetic approaches. Accompanied by that, the 1D carbon-based nanomaterials present some highly desirable features due to their wide versatility in terms of properties, structure, synthetic approaches, and applications. Among those there are CNTs, graphene nanoribbons (GNRs), CNFs, and carbon fibers (CFs). All these materials present a larger ratio between length and diameter or width. Alongside that, they can be characterized by the conjugated sp^2 hybridized carbons in their structure which enables high electronic conductivity. Also, the strong covalent carbon-carbon bonds throughout the structure provide high thermal, chemical, and electrochemical stability which greatly increase their robusticity for a plethora of applications. Along with that, their high surface area enables proper adsorption of ionic species that can contribute to energy storage properties. There are considerable distinctions between such materials. In this sense, CNTs can be obtained in the form of single CNTs (SCNTs) or as multi-walled CNTs (MWCNTs) which display different properties in terms of surface area, wettability, and mechanical properties. The GNRs consist of graphene strips with high lengths over a short width ratio. Such structure provides some differences when compared to graphene

as the decrease in width leads to a quantum confinement effect. Through that, its properties can present a wider degree of tunability when compared to other 1D and 2D carbon-based materials due to the variations in the energy values in its band gap attributed to the decrease in the width [11–13]. The CNF are also attractive materials given their inherent conductivity accompanied by relatively higher mechanical strength and low density, which makes them attractive for applications that require more robust conditions [14].

The variety of these carbon-based nanomaterials is attributed to the broad number of techniques available for their synthesis. Selecting the proper synthetic methods to obtain nanomaterials with the desired properties is a core part of the process. For that, the synthetic methods of nanomaterials can be divided into two large groups which are top-down and bottom-up. The top-down approaches consist of utilizing a bulk precursor and decreasing its size to the nanoscale. In this sense, some of the most used methods to obtain 1D nanomaterials are pyrolysis and ball milling. The bottom-up is based on obtaining a nanomaterial starting from an atom or molecule which can be performed through chemical vapor deposition (CVD), arc discharge, laser ablation, and electrospinning, among other methods. In most cases, bottom-up approaches tend to be used for the synthesis of 1D carbon nanomaterials. For example, CNTs can be synthesized through CVD, arc discharge, and laser ablation. The GNRs can be synthesized through template-assisted polymerization to direct its structure towards a 1D structure. Lastly, CNFs can also be synthesized through CVD, template-assisted synthesis, or electrospinning.

The selection of the proper method plays a critical role in the overall properties of the obtained material since several parameters can be varied. Through that, some of the variations include the introduction of heteroatoms during a doping process, compositing with nanomaterials or polymers, surface functionalization, increase in the number of defects, disorders, or voids, among many other factors [15–17]. Pyrolysis is a commonly employed method that consists of a thermochemical treatment of a carbon precursor that is decomposed at high temperatures under an inert atmosphere i.e., Ar or N₂. The schematic of a tube furnace for pyrolytic processes is presented in Fig. 3a. Aside from the relatively lower cost of this method it also allows a facile doping process by performing the pyrolysis of the carbon precursor along with a compound containing the desired heteroatoms. Some cases include N doping (i.e., melamine, urea, or ammonia), S doping (i.e., hydrogen sulfide, thiourea, or thiophene), and P doping (i.e., phosphoric acid), for instance. Aside from doping, the morphology of carbon-based nanomaterials can also be varied through the use of templates during the pyrolytic process which can include soft (i.e., 1,3,5-trimethylbenzene), hard (i.e., SiO₂), or highly porous templates such as metal–organic frameworks (MOFs) [18, 19]. Other parameters related to the pyrolysis technique include varying temperatures and ramping rate, reaction time, and gas composition. Such factors play a major role in the nanomaterial's surface area, porosity, morphology, and dopant concentration, among others [20]. One common case lies in finding the optimal temperature for the pyrolytic process as it can lead to a proper graphitization degree which directly influences the conductivity. However, excessive temperature can deteriorate such properties as it can induce a larger number

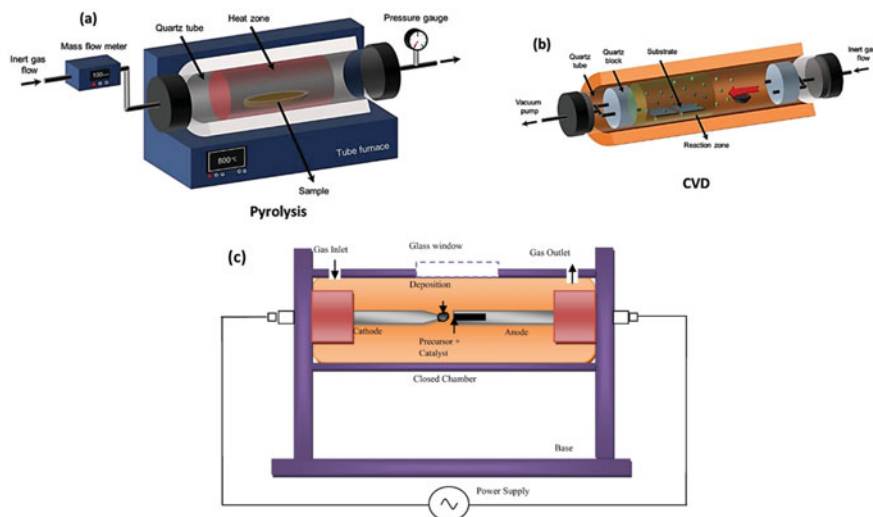


Fig. 3 Schematics for some of the most common techniques for the synthesis of 1D carbon-based materials through **a** pyrolysis and **b** CVD. Adapted with permission [30]. Copyright 2020, John Wiley and Sons. (c) Arc discharge. Adapted with permission [31]. Copyright 2014, Elsevier

of voids in the structure that can disrupt the conjugation degree and promote the formation of too many voids which can ultimately decrease the surface area. On top of that, relatively unstable dopant heteroatoms can be removed from the carbon matrix if the pyrolytic temperature is too high [21]. Even though pyrolysis is an accessible method the synthesis conditions often require relatively long reaction times which can be around several hours along with careful control of the parameters. Some previous studies have demonstrated the synthesis of CNTs through pyrolysis methods [22–26].

The synthesis of 1D carbon-based nanomaterials is often limited when considering top-down methods such as mechanical exfoliation, ball milling, laser ablation, and ultrasonication, among others. Bottom-up methods such as CVD, for instance, are better known to yield high-quality 1D carbon nanostructures. CVD is a versatile technique that can be used to synthesize several types of carbon-based nanomaterials, yet it is the most employed for the synthesis of CNTs [24, 27, 28]. The schematic for this process is presented in Fig. 3b. Alongside that, there are several variations of this technique which include hot-filament CVD (HFCVD), hot-wire CVD (HWCVD), aerosol-assisted CVD (ACVD), microwave plasma-enhanced (MWCVD), and liquid-injection (LICVD) [29]. Some of the main advantages of CVD over other techniques are related to the relatively lower temperature requirements which can range from 550 to 1000 °C and the capability to obtain aligned CNTs over a substrate. However, the nanostructure tends to be more defective under CVD when compared to arc discharge or laser evaporation methods. Yet, the latter methods require higher temperatures. Arc discharge is a method that consists of the

generation of a highly energetic electric arc in between two carbon-based electrodes at which the anode contains the carbon precursor material along with the catalyst whereas the cathode is often made of a graphite rod. The system is immersed in an inert atmosphere of He or Ar to prevent the oxidation of the carbon electrodes. After a voltage is applied to the system the electrodes are placed around 1–2 mm to allow for a steady discharge process. Through that, the arc current generates plasma that can reach temperatures to the range of 4000–6000 K causing the carbon precursor to sublime and migrate to the cathode leading to the formation of the CNT. The schematic for the arc discharge process is presented in Fig. 3c.

Several characterization techniques can be performed on nanomaterials. One of their most notorious aspects is their morphology which can be analyzed through scanning electron microscope (SEM) which provides a 2D image of the material's surface which allows the determination of nanomaterial's dimensions in terms of diameter, length, alignment, physical arrangement over the substrate along with other morphological aspects. Another related technique is transmission electron microscope (TEM) which allows for the analysis of the internal structure as well as crystallography aspects of the nanomaterial [32]. Through that, some of the structural defects, and internal diameter of CNTs, for example, can be determined through this characterization. The atomic force microscopy (AFM) provides a 3D image of the nanomaterial's surface which provides some information of their topography such as surface roughness, alignment, and organization of the nanomaterials along other aspects.

The spectroscopic characterizations are also extremely important for the elucidation of specific properties of nanomaterials. Raman spectroscopy provides some information regarding the vibrational modes of carbon bonds in a material which can be either graphitic or diamond types of carbons which are defined by the G and D bands, respectively. Through that, some of the levels of disorder and defects in the structure can be determined. Furthermore, knowing the degree of graphitic and diamond carbons in a material can provide information regarding their influence on the electrocatalytic properties which enables researchers since a larger degree of graphitic carbon improves the conductivity whereas diamond carbon can lead to some defects that can act as active sites for catalysis [33, 34]. The X-ray diffraction characterization can be used to determine the degree of organization through crystallinity along with the interlayer spacing between the nanostructures [35, 36]. X-ray photoelectron spectroscopy (XPS) is a widely used characterization as it can provide information regarding the chemical composition and the types of bonds present in the nanomaterial's surface. Alongside that, Fourier-transformed infrared (FTIR) is one of the most utilized spectroscopic characterizations as it can determine the presence of polarized organic groups on the material. Through that, the presence of moieties such as alcohol, aldehydes, carboxylic acids, amines, along any other polarized bonds can be identified. The UV–Vis–NIR spectroscopy consists of emitting light that covers a broad range of wavelengths that can be absorbed by the nanomaterial. Through that, some of its optical and electronic properties can be elucidated such as the calculation of band gap, for example. Gas adsorption analysis such as Brunauer–Emmett–Teller (BET) is an important characterization to obtain the surface area of a material, which

is a major factor for electrocatalytic performance. Lastly, theoretical studies are also a valuable tool for the description of the electronic properties of nanomaterials, one of the most employed characterizations in that regard is density functional theory (DFT), which among other things, can be used to calculate the theoretical band gap which are related to the electrocatalytic efficiency and the mechanism at which it takes place. Based on that, it is notable that there are several characterization techniques available as each one can provide a piece of information to aid in the property elucidation of a given material.

3 Applications of One-Dimensional Carbon as Electrocatalysts

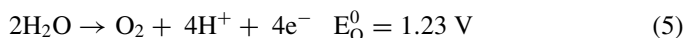
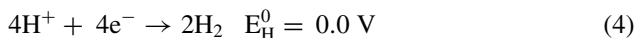
The water splitting reaction leads to the evolution of O_2 and H_2 which can be described by the global Reaction (1).



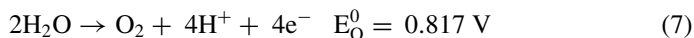
This reaction can be divided into two half cells, which are HER and OER that occur on the cathode (reduction) and anode (oxidation) electrodes of an electrolyzer, respectively. Such reactions can occur in either alkaline or acidic media. In this sense, in an alkaline environment, the HER and OER can be presented by Reactions (2) and (3), respectively. Where E_H^0 and E_O^0 are the standard half-cell potentials at 1 atm and 25 °C.



In an acidic environment, the HER and OER can be presented by Reactions (4) and (5), respectively.



In a neutral environment, the HER and OER can be presented by Reactions (6) and (7), respectively.



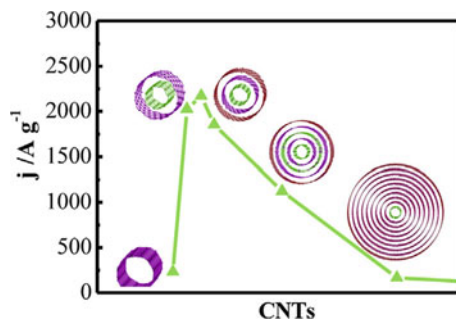
Based on that, for the water-splitting process to occur the cell potential (E_{cell}^0) has to be applied. For that, $E_{\text{cell}}^0 = E_{\text{O}}^0 - E_{\text{H}}^0$, thus the E_{cell}^0 is 1.23 V. Yet, it is worth noting that the water splitting process is more favorable in alkaline and acid media due to the larger populations of OH^- and H^+ which are active species for the occurrence of reactions. Because of that, in neutral conditions, the water splitting has relatively lower kinetic energy due to the relatively high stability of the water itself as the Gibbs free energy required for the overall process is around 237.21 kJ/mol. Following that, transition metal oxides are often used as electrocatalysts for water-splitting processes. However, they usually display relatively high electric resistance and low electrochemical stability. Such drawbacks can be countered by combining them with carbon-based nanomaterials. Through that, the inherently high surface area, porosity, conductivity, and electrochemical stability of these carbon-based nanomaterials can optimize the overall electrocatalytic performance. Some examples of that include the use of NiFeO_x [37], NiO_x [38–40], MnO_x [41], and CoO_x [42].

3.1 Nanocarbon for OER

The OER process is a half-cell reaction of the electrochemical water-splitting that takes place on the anode electrode characterized by the release of O_2 . However, the complexity and sluggishness of this reaction have been an aim of the study as there are still further studies to fully elucidate the reaction mechanisms along with finding feasible electrocatalysts for this process. Under this situation, carbon-based nanomaterials have been considered good candidates for this process given their broad versatility in several aspects including chemical modifications. Some of these approaches are (i) defect engineering to better expose the active sites [43]; (ii) precise control of the amount of heteroatoms in the nanostructure to promote a proper charge distribution on the basal plane that can lead to the improvement of electrocatalytic activity [44]; (iii) compositing of carbon-based nanomaterials along with other components such as transition metal derivatives that can enhance the electron transfer processes and diminish the aggregation that tends to occur with carbon [44, 45]; (iv) tuning of the pore size and structure also influences the ion diffusion and electron transfer processes [46]. There is often a combination of these four approaches to lead to an optimized electrochemical performance. Based on these cases some studies have demonstrated the effect of ORR catalysis concerning the number of outer layers in a CNT. In this sense, a previous report described that CNTs presenting around 2 to 3 concentric tubes can display a more satisfactory activity for OER when compared to SWCNT and MWCNTs [47].

From that, it was observed, for OER, that following the order of the number of concentric tubes going from MWCNT, SWCNT to 2–3 walled CNT there was an increase in current density at a voltage of 1.8 V that went from 1.6, 5.9, and 56 mA/cm². The proposed explanation for this observation was that a CNT presenting around 2 to 3 internal tubes could facilitate electron transport through tunneling between the outer wall with the inner tubes. Such an effect could promote the adsorption of

Fig. 4 CNTs' activity towards OER is based on the number of walls in their structure in 1 M KOH at 1.8 V vs. reference hydrogen electrode (RHE) at a rotating rate of 2000 rpm, scan rate of 1 mV/s and 0.025 mg/cm². Adapted with permission [50]. Copyright 2015, Elsevier



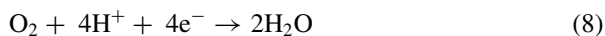
active species of OER at the outer wall while promoting electron transport to the inner walls [48, 49]. For the case of SWCNT, such an effect could not take place as it was proposed that despite the fast electron transfer the active species would not be properly adsorbed to the SWCNT's surface which resulted in a decrease in the electrocatalytic activity towards OER. The schematics for this process are presented in Fig. 4.

Another example was presented by Zhao et al. [51] who obtained a N-doped carbon-based material that was suitable for OER electrocatalysis as it displayed an overpotential of 0.38 V when reaching 10 mA/cm². The electrocatalytic properties arise due to the presence of the different types of N in the carbonaceous structure such as pyridinic and quaternary, which can promote a stronger polarization of electrons on the adjacent carbons which facilitates the adsorption of reactive species for the catalysis. Another similar study was presented by Li et al. [52] who performed the doping process on MWCNT which was followed by partial unzipping of the nanotubes through oxidation and high-temperature treatment in the presence of NH₃. This approach led to the formation of a graphene-like structure attached to the inner 1D tubes which served as active sites for the ORR process in both alkaline and acid environments. This study demonstrated a viable way to dope the structure of a carbon-based 1D/2D nanomaterial without jeopardizing the conductivity, which plays a major role in the electron transfer steps related to the electrocatalytic mechanism. Based on that, Lu et al. [53] fabricated a composite electrocatalyst for both OER and ORR which was based on a CNT/graphene nanoribbon doped with N containing Co₃O₄ nanoparticles over its surface (Co₃O₄/N-CNT-GNR). Their study demonstrated that there was a considerable increment in electrocatalysis towards OER in alkaline media (0.1 M KOH) with an onset potential of 1.51 V which corresponded to an overpotential of around 280 mV. Also, the overpotential at 10 mA/cm² was 360 mV which was lower than state-of-art Ir/C electrocatalysts done in that study. Yet, upon testing the electroactive materials separately there was a decrease in overall electrocatalytic performance which suggested that the combination of both Co₃O₄ with N-CNT-GNR promoted an advantageous complementary effect. Such improvement was attributed to the composite's morphology as the carbon matrix functioned as a pathway for electrons due to its high conductivity. Along with that, the porous surface of the N-CNT-GNR served as a proper support as it allowed higher loads of

Co₃O₄ to be incorporated. Lastly, it was proposed that the doping with N also positively influenced the electrocatalytic activity. Hence, the combination of factors such as the linear and porous structure of N-CNT-GNR along with the higher loading and proper distribution of Co₃O₄ throughout its surface along with the N-doping led to an improvement in OER performance. The authors also utilized the same composite to analyze the ORR electroactivity. For that, the Co₃O₄/N-CNT-GNR presented 40 mV of onset potential. Along with that, the composite presented a half wave potential ($E_{1/2}$) of around 0.81 V at 1600 rpm which was more positive when compared to the value obtained for the Pt/C according to the authors. Based on that, it was proposed that the catalytic site for ORR originated from the synergy between Co and C atoms. In this sense, in a previous work performed by Dai et al. [54], it was proposed through X-ray absorption near edge structure (XANES) that there was the formation of Co–N–C and Co–O–C bonds which could vary the electronic density among the C, O, and Co-leading to an improvement in ORR electrocatalytic response.

3.2 Nanocarbon for ORR

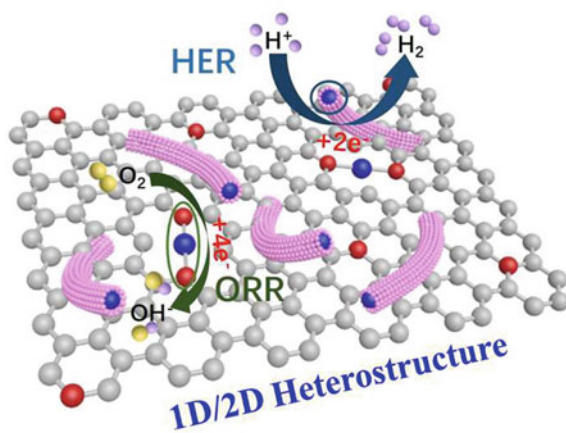
The need to find electrocatalysts that can serve as alternatives to rare metals is a decisive factor for the introduction of technologies such as electrolyzers, fuel cells, and metal-air batteries. As discussed, there are several electrochemical reactions related to the production of energy from H₂O. Based on that, it is known that, in an electrolyzer, two complementary reactions take place one being HER and the other OER which are reduction and oxidation processes that generate H₂ and O₂, respectively. On the other hand, in a fuel cell, there are two complementary reactions which are ORR and HOR. In this sense, ORR is a reduction reaction in which O₂ is converted to H₂O as presented in Reaction (8), whereas HOR is an oxidation reaction based on the conversion of H₂ into H⁺ as presented in Reaction (9).



Considering the nature of these processes there are some similarities between HER and ORR which, even though are half reactions from different processes in water splitting and fuel cells, respectively, are both reduction reactions. Based on that, the electrochemical mechanism at which they take place is based on the gaining of electrons which can be catalyzed by certain types of electroactive materials. In this sense, carbon-based materials that present high surface area, tunable porous structure, and high conductivity can fit for such applications as electrocatalysts. Alongside that, introducing transition metals such as Fe, Co, Cu, and Ni, for instance, are also viable ways to promote a variation in the electronic density of the surrounding carbon atoms that can promote some degree of electrocatalytic activity. Similarly, the doping

process with N can induce a similar effect given its relatively higher electronegativity than carbon creating a polarization on their covalent bond that facilitates the adsorption of electroactive species during the catalysis process [55, 56]. Under this premise, the combination of factors such as favorable morphology, electronic polarization, and high conductivity have been demonstrated to generally improve the electrocatalytic activity allowing such materials to approach and sometimes even surpass the performance of some rare metal-based electroactive materials. Based on that, Yang et al. [57] obtained a 1D/2D hybrid nanocarbon-based material of CNT and graphene respectively that was doped with both Co and N, hence obtaining a composite named Co–N/N–CNT/N–G with the schematics presented in Fig. 5. The material was then utilized to fabricate an electrode that was used for the electrocatalysis of both ORR and HER. Within this line, for ORR it presented an $E_{1/2}$ of 0.85 V against RHE along with good electrochemical stability. The satisfactory electrocatalytic performance for the Co–N/N–CNT/N–G was attributed to the presence of CoN_x species that were attached to the carbonaceous matrix, which allowed for the adsorption of electroactive species from the ORR process along with efficient electron transport from the conducting carbon, which made it as effective active sites for ORR [58, 59]. For HER, the nanocomposite Co–N/N–CNT/N–G displayed an overpotential of 123 mV at a current density of 10 mA/cm^2 along with excellent stability in acidic media ($0.5 \text{ M H}_2\text{SO}_4$). It could be observed that the other tested composites such as Co–N/G and Co–N/N–CNT prepared in the study displayed lower electrocatalytic activity towards HER. Such an effect was initially attributed to the smaller population of CoN_x . On top of that, there was a decrease in the surface area of Co–N/G and Co–N/N–CNT when compared to C–N/N–CNT/N–G. Through that, it was concluded that CoN_x species displayed better electro-catalytic activity towards ORR whereas the metallic Co wrapped on CNTs supported by the graphene layers displayed the best electro-catalytic for HER. Another important factor is that the combination of the 1D and 2D nanostructures of carbon can prevent aggregation and therefore better expose the electroactive sites to perform both ORR and HER [60, 61].

Fig. 5 Schematics for the electroactive 1D/2D composite for both ORR and HER based on Co, N-doped CNT/graphene. Adapted with permission [57]. Copyright 2018, Royal Society of Chemistry



3.3 Nanocarbon for HER

The electrocatalytic production of H_2 through water splitting reaction is a highly desired process as it can lead to an economically viable and sustainable way to obtain an eco-friendly and highly efficient fuel. Likewise the other electrochemical reactions, there are several ways to promote the improvement of electrocatalytic activity by compositing carbon-based materials with transition metal derivatives such as CoP nanocrystals/CNT, N_2P nanoparticles/CNT, among others [62, 63]. HER has relatively better kinetics than OER given that the former requires two electrons to occur whereas the latter needs four, which makes it inherently sluggish. Despite that, one of the challenges of HER surrounding its mechanisms lies in the differences in the process based on the environment in which it takes place. For example, in acidic media, the catalysis is based on the optimal interaction between the catalyst's surface with H^+ species, whereas in alkaline media is based on the equilibrium of the interaction of the electrocatalysts with H_2O and OH^- [64]. Zhang et al. [65] proposed the synthesis of a CoP nanosheet/CNT (CoP-NS/CNT). The interaction between CoP and CNT was enhanced by promoting the oxidation of the CNT through Hummer's method along with the addition of sodium dodecyl sulfate (SDS) to increase the dispersibility of CNT. The components were then placed in a Teflon-lined autoclave reactor at $160\text{ }^\circ\text{C}$ at 12 h. Then, a phosphorization process was performed through the vaporization of red P powder to form the CoP nanosheet over the CNT. The detailed synthetical procedure is presented in Fig. 6.

From that, the electrochemical characterizations for the CoP-NS/CNT presented a Tafel slope of 57 mV/dec which suggested that the HER process presented fast

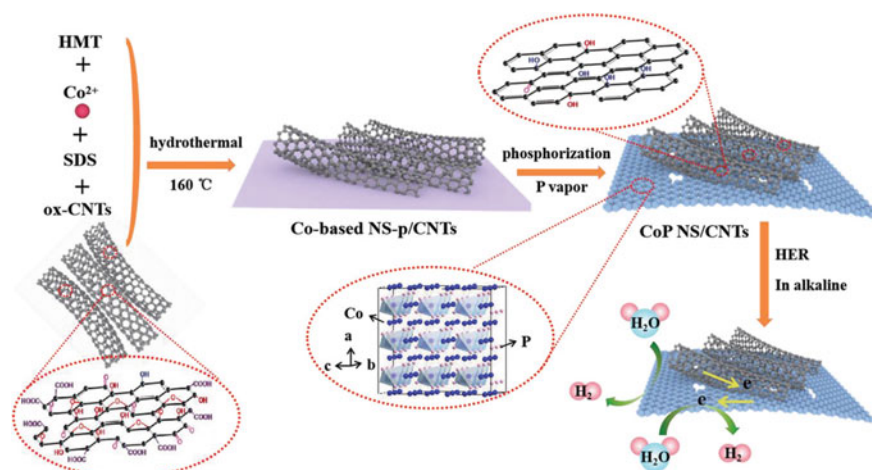


Fig. 6 Schematic for the synthesis of CoP-NS/CNT through hydrothermal followed by doping with P through solid/gas-phase vaporization. The nanohybrid composite was utilized as electrocatalysts for HER in alkaline media. Adapted with permission [65]. Copyright 2019, John Wiley and Sons

kinetics along with a low overpotential of 68 mV at 10 mA/cm². The satisfactory performance of HER can be attributed to several factors. It was proposed that the surface area was optimized due to the presence of hexamethylenetetramine (HMT) which could lead to the formation of ammonia during the hydrothermal process promoting the formation of small pores into the CNT's surface. In this sense, the active sites could be more exposed. The presence of SDS aided in the dispersion of CNTs which allowed it to be properly grafted onto CoP nanosheet structure. Through that, a better electron transfer process could occur, likely playing a role in the HER performance. Another factor was alkaline media which required the H–O–H bonds to be broken for the adsorption of H* afterwards. However, this process can be less favorable than the reduction of H₃O⁺ [66]. Yet, the wettability of the CoP-NS/CNT was an important step for the electrocatalysis. Based on that the proposed mechanism is presented through Reactions (10)–(12).



4 Conclusion

The 1D carbon nanomaterials such as graphene nanoribbons, CNTs, and CNFs have been demonstrated to be promising components for the fabrication of electrocatalysts for several reactions given their versatility in terms of synthetical approaches and tunability in terms of properties. In that sense, one of the most utilized methods for the synthesis of CNTs through CVD has reached the industry. Even though it is inherently limited it is a viable approach to obtain aligned CNT nanostructures that can be grown in a plethora of substrates. Also, the several parameters that can be modified during the synthetical process account for great versatility in the overall process leading to nanomaterials with a vast range of properties. Furthermore, 1D carbon-based nanomaterials are compatible with several components such as transition metal derivatives, conducting polymers as well and other carbon-based nanomaterials. Such variations allow for a considerably high number of materials available that can be utilized in different types of electrocatalytic processes such as HER, OER, ORR, and HOR, among others. Yet, despite such versatility in terms of synthetical process, compositive, and application their performance might not be satisfactory when employed as neat materials. Their properties can drastically enhance when composited with transition metal derivatives. Such improvement can be mostly attributed to the synergy that arises through the combination of such materials as the carbon matrix can provide a suitable platform for the electron transfer

steps and the transition metal serves as the electroactive site for the electrochemical process. There are several nuances in this process since the 1D carbon matrix must present an optimized porosity to properly arrange the transition metal derivative on its surface by providing intimate contact between the two. Also, carbon-based materials are inherently hydrophobic, hence decorating their surface with polarized nanoparticles, functionalizing with polar groups, and improving their surface area are important aspects to facilitate their interaction with the electrolytes which usually consist of either alkaline or acidic solutions. On the other hand, these carbon-based materials present relatively high electrochemical stability, which serves as an important factor for long-term usage. Despite the several advantages of the use of such materials, there are challenges in terms of the full elucidation of the mechanistic processes surrounding some of the electrochemical reactions that can help in the design of novel electrocatalysts. Also, carbon-based materials present a tendency to agglomerate, which even though can be addressed by the approaches mentioned, can still jeopardize the electrochemical performance. Despite those drawbacks, there has been appreciable progress in the use of 1D carbon-based materials in electrocatalytic processes. Such findings are extremely important since the use of these materials in technologies such as electrolyzers, fuel cells, and metal-air batteries is highly desired for a more sustainable future. In that sense, a more sustainable way to harvest energy can be obtained leading to a decrease in the strain applied on petrochemicals and non-renewable sources. Thus, encouraging further research on this type of material can aid in not only more sustainable but also efficient energy storage and energy production devices.

References

1. Roger, I., Shipman, M.A., Symes, M.D.: Earth-abundant catalysts for electrochemical and photoelectrochemical water splitting. *Nat. Rev. Chem.* **1**, 0003 (2017)
2. Zou, X., Zhang, Y.: Noble metal-free hydrogen evolution catalysts for water splitting. *Chem. Soc. Rev.* **44**, 5148–5180 (2015)
3. O'hayre, R., Cha, S.-W., Colella, W., Prinz, F.B.: *Fuel Cell Fundamentals*. Wiley (2016)
4. Deng, Y.-P., Jiang, Y., Liang, R., Zhang, S.-J., Luo, D., Hu, Y., Wang, X., Li, J.-T., Yu, A., Chen, Z.: Dynamic electrocatalyst with current-driven oxyhydroxide shell for rechargeable zinc-air battery. *Nat. Commun.* **11**, 1952 (2020)
5. Tan, P., Chen, B., Xu, H., Zhang, H., Cai, W., Ni, M., Liu, M., Shao, Z.: Flexible Zn- and Li-air batteries: recent advances, challenges, and future perspectives. *Energy Environ. Sci.* **10**, 2056–2080 (2017)
6. Wang, J., Kong, H., Zhang, J., Hao, Y., Shao, Z., Ciucci, F.: Carbon-based electrocatalysts for sustainable energy applications. *Prog. Mater. Sci.* **116**, 100717 (2021)
7. Jiang, H., Gu, J., Zheng, X., Liu, M., Qiu, X., Wang, L., Li, W., Chen, Z., Ji, X., Li, J.: Defect-rich and ultrathin N doped carbon nanosheets as advanced trifunctional metal-free electrocatalysts for the ORR, OER and HER. *Energy Environ. Sci.* **12**, 322–333 (2019)
8. Li, W., Liu, J., Zhao, D.: Mesoporous materials for energy conversion and storage devices. *Nat. Rev. Mater.* **1**, 16023 (2016)
9. Jiao, Y., Zheng, Y., Jaroniec, M., Qiao, S.Z.: Design of electrocatalysts for oxygen- and hydrogen-involving energy conversion reactions. *Chem. Soc. Rev.* **44**, 2060–2086 (2015)

10. Cambré, S., Liu, M., Levshov, D., Otsuka, K., Maruyama, S., Xiang, R.: Nanotube-based 1D heterostructures Coupled by van der Waals forces. *Small* **17**, 2102585 (2021)
11. Li, X., Wang, X., Zhang, L., Lee, S., Dai, H.: Chemically derived, ultrasmooth graphene nanoribbon semiconductors. *Science* (80–) **319**, 1229–1232 (2008)
12. Jiao, L., Zhang, L., Wang, X., Diankov, G., Dai, H.: Narrow graphene nanoribbons from carbon nanotubes. *Nature* **458**, 877–880 (2009)
13. Cai, J., Ruffieux, P., Jaafar, R., Bieri, M., Braun, T., Blankenburg, S., Muoth, M., Seitsonen, A.P., Saleh, M., Feng, X., Müllen, K., Fasel, R.: Atomically precise bottom-up fabrication of graphene nanoribbons. *Nature* **466**, 470–473 (2010)
14. Ren, J., Li, F.F., Lau, J., González-Urbina, L., Licht, S.: One-pot synthesis of carbon nanofibers from CO₂. *Nano Lett.* **15**, 6142–6148 (2015)
15. Zhao, H., Wang, J., Chen, C., Chen, D., Gao, Y., Saccoccio, M., Ciucci, F.: A bi-functional catalyst for oxygen reduction and oxygen evolution reactions from used baby diapers: α -Fe₂O₃ wrapped in P and S dual doped graphitic carbon. *RSC Adv.* **6**, 64258–64265 (2016)
16. Wei, X., Luo, X., Wang, H., Gu, W., Cai, W., Lin, Y., Zhu, C.: Highly-defective Fe–N–C catalysts towards pH-Universal oxygen reduction reaction. *Appl. Catal. B Environ.* **263**, 118347 (2020)
17. Wang, J., Ciucci, F.: In-situ synthesis of bimetallic phosphide with carbon tubes as an active electrocatalyst for oxygen evolution reaction. *Appl. Catal. B Environ.* **254**, 292–299 (2019)
18. Guo, H., Feng, Q., Zhu, J., Xu, J., Li, Q., Liu, S., Xu, K., Zhang, C., Liu, T.: Cobalt nanoparticle-embedded nitrogen-doped carbon/carbon nanotube frameworks derived from a metal–organic framework for tri-functional ORR, OER and HER electrocatalysis. *J Mater Chem A* **7**, 3664–3672 (2019)
19. Zhang, H.-M., Zhao, Y., Zhang, Y., Zhang, M., Cheng, M., Yu, J., Liu, H., Ji, M., Zhu, C., Xu, J.: Fe₃O₄ encapsulated in porous carbon nanobowls as efficient oxygen reduction reaction catalyst for Zn-air batteries. *Chem. Eng. J.* **375**, 122058 (2019)
20. Santori, P.G., Speck, F.D., Li, J., Zitolo, A., Jia, Q., Mukerjee, S., Cherevko, S., Jaouen, F.: Effect of pyrolysis atmosphere and electrolyte pH on the oxygen reduction activity, stability and spectroscopic signature of Fe_{Nx} moieties in Fe–N–C catalysts. *J. Electrochem. Soc.* **166**, F3311 (2019)
21. Zhang, L.-M., Wang, Z.-B., Zhang, J.-J., Sui, X.-L., Zhao, L., Gu, D.-M.: Honeycomb-like mesoporous nitrogen-doped carbon supported Pt catalyst for methanol electrooxidation. *Carbon N Y* **93**, 1050–1058 (2015)
22. Zahid, M.U., Pervaiz, E., Hussain, A., Shahzad, M.I., Niazi, M.B.K.: Synthesis of carbon nanomaterials from different pyrolysis techniques: a review. *Mater. Res. Exp.* **5**, 52002 (2018)
23. Acomb, J.C., Wu, C., Williams, P.T.: Control of steam input to the pyrolysis-gasification of waste plastics for improved production of hydrogen or carbon nanotubes. *Appl. Catal. B Environ.* **147**, 571–584 (2014)
24. Arnaiz, N., Gomez-Rico, M.F., Martin Gullon, I., Font, R.: Production of carbon nanotubes from polyethylene pyrolysis gas and effect of temperature. *Ind. Eng. Chem. Res.* **52**, 14847–14854 (2013)
25. Chung, Y.-H., Jou, S.: Carbon nanotubes from catalytic pyrolysis of polypropylene. *Mater. Chem. Phys.* **92**, 256–259 (2005)
26. Kukovitsky, E.F., L'vov, S.G., Sainov, N.A., Shustov, V.A.: CVD growth of carbon nanotube films on nickel substrates. *Appl. Surf. Sci.* **215**, 201–208 (2003)
27. Kobayashi, Y., Nakashima, H., Takagi, D., Homma, Y.: CVD growth of single-walled carbon nanotubes using size-controlled nanoparticle catalyst. *Thin Solid Films* **464–465**, 286–289 (2004)
28. Ying, L.S., Bin Mohd Salleh, M.A., Mohamed Yusoff, H.B., Abdul Rashid SB, Razak J.B.A.: Continuous production of carbon nanotubes—a review. *J. Ind. Eng. Chem.* **17**, 367–376 (2011)
29. Manawi, Y.M., Ihsanullah, S.A., Al-Ansari, T., Atieh, M.A.: A review of carbon nanomaterials' synthesis via the chemical vapor deposition (CVD) method. *Materials (Basel)* **11**, 822 (2018)
30. Wang, J., Kim, J., Choi, S., Wang, H., Lim, J.: A review of carbon-supported nonprecious metals as energy-related electrocatalysts. *Small Methods* **4**, 2000621 (2020)

31. Arora, N., Sharma, N.N.: Arc discharge synthesis of carbon nanotubes: comprehensive review. *Diam. Relat. Mater.* **50**, 135–150 (2014)
32. Pantano, M.F., Kuljanishvili, I.: Advances in mechanical characterization of 1D and 2D nanomaterials: progress and prospects. *Nano Exp.* **1**, 022001 (2020)
33. Moo, J.G.S., Veksha, A., Oh, W.-D., Giannis, A., Udayanga, W.D.C., Lin, S.-X., Ge, L., Lisak, G.: Plastic derived carbon nanotubes for electrocatalytic oxygen reduction reaction: effects of plastic feedstock and synthesis temperature. *Electrochem. Commun.* **101**, 11–18 (2019)
34. Luo, H., Zhang, X., Zhu, H., Zhang, K., Yang, F., Xu, K., Yu, S., Guo, D.: Tailoring d-band center over electron traversing effect of NiM@C-CoP (M=Zn, Mo, Ni, Co) for high-performance electrocatalysis hydrogen evolution. *J. Mater. Sci. Technol.* **166**, 164–172 (2023)
35. Xia, B.Y., Yang, P., Sun, Y., Wu, Y., Mayers, B., Gates, B., Yin, Y., Kim, F., Yan, H.: One-dimensional nanostructures: synthesis, characterization, and applications. *Adv. Mater.* **15**, 353–389 (2003)
36. Mu, J., Chen, B., Guo, Z., Zhang, M., Zhang, Z., Zhang, P., Shao, C., Liu, Y.: Highly dispersed Fe₃O₄ nanosheets on one-dimensional carbon nanofibers: synthesis, formation mechanism, and electrochemical performance as supercapacitor electrode materials. *Nanoscale* **3**, 5034–5040 (2011)
37. Gong, M., Li, Y., Wang, H., Liang, Y., Wu, J.Z., Zhou, J., Wang, J., Regier, T., Wei, F., Dai, H.: An advanced Ni–Fe layered double hydroxide electrocatalyst for water oxidation. *J. Am. Chem. Soc.* **135**, 8452–8455 (2013)
38. Yu, X., Hua, T., Liu, X., Yan, Z., Xu, P., Du, P.: Nickel-based thin film on multiwalled carbon nanotubes as an efficient bifunctional electrocatalyst for water splitting. *ACS Appl. Mater. Interfaces* **6**, 15395–15402 (2014)
39. Zhou, X., Xia, Z., Zhang, Z., Ma, Y., Qu, Y.: One-step synthesis of multi-walled carbon nanotubes/ultra-thin Ni(OH)₂ nanoplate composite as efficient catalysts for water oxidation. *J. Mater. Chem. A* **2**, 11799–11806 (2014)
40. Cheng, Y., Shen, P.K., Jiang, S.P.: NiOx nanoparticles supported on polyethylenimine functionalized CNTs as efficient electrocatalysts for supercapacitor and oxygen evolution reaction. *Int. J. Hydrogen Energy* **39**, 20662–20670 (2014)
41. Mette, K., Bergmann, A., Tessonier, J.-P., Hävecker, M., Yao, L., Ressler, T., Schlögl, R., Strasser, P., Behrens, M.: Nanostructured manganese oxide supported on carbon nanotubes for electrocatalytic water splitting. *ChemCatChem* **4**, 851–862 (2012)
42. Wu, J., Xue, Y., Yan, X., Yan, W., Cheng, Q., Xie, Y.: Co₃O₄ nanocrystals on single-walled carbon nanotubes as a highly efficient oxygen-evolving catalyst. *Nano Res.* **5**, 521–530 (2012)
43. Jia, Y., Zhang, L., Du, A., Gao, G., Chen, J., Yan, X., Brown, C.L., Yao, X.: Defect graphene as a trifunctional catalyst for electrochemical reactions. *Adv. Mater.* **28**, 9532–9538 (2016)
44. Jiao, Y., Zheng, Y., Davey, K., Qiao, S.-Z.: Activity origin and catalyst design principles for electrocatalytic hydrogen evolution on heteroatom-doped graphene. *Nat. Energy* **1**, 16130 (2016)
45. Deng, J., Ren, P., Deng, D., Bao, X.: Enhanced electron penetration through an ultrathin graphene layer for highly efficient catalysis of the hydrogen evolution reaction. *Angew. Chemie Int. Ed.* **54**, 2100–2104 (2015)
46. Chen, X., Paul, R., Dai, L.: Carbon-based supercapacitors for efficient energy storage. *Natl. Sci. Rev.* **4**, 453–489 (2017)
47. Zhang, L., Jia, Y., Gao, G., Yan, X., Chen, N., Chen, J., Soo, M.T., Wood, B., Yang, D., Du, A.: Graphene defects trap atomic Ni species for hydrogen and oxygen evolution reactions. *Chem* **4**, 285–297 (2018)
48. Cheng, Y., Lee, S., Gu, Z., Ho, K., Zhang, Y., Huang, Y., Chow, J.C., Watson, J.G., Cao, J., Zhang, R.: PM2.5 and PM10-2.5 chemical composition and source apportionment near a Hong Kong roadway. *Particuology* **18**, 96–104 (2015)
49. Cheng, Y., Zhang, J., Jiang, S.P.: Are metal-free pristine carbon nanotubes electrocatalytically active? *Chem. Commun.* **51**, 13764–13767 (2015)
50. Cheng, Y., Xu, C., Jia, L., Gale, J.D., Zhang, L., Liu, C., Shen, P.K., Jiang, S.P.: Pristine carbon nanotubes as non-metal electrocatalysts for oxygen evolution reaction of water splitting. *Appl. Catal. B Environ.* **163**, 96–104 (2015)

51. Zhao, Y., Nakamura, R., Kamiya, K., Nakanishi, S., Hashimoto, K.: Nitrogen-doped carbon nanomaterials as non-metal electrocatalysts for water oxidation. *Nat. Commun.* **4**, 2390 (2013)
52. Li, Y., Zhou, W., Wang, H., Xie, L., Liang, Y., Wei, F., Idrobo, J.-C., Pennycook, S.J., Dai, H.: An oxygen reduction electrocatalyst based on carbon nanotube–graphene complexes. *Nat. Nanotechnol.* **7**, 394–400 (2012)
53. Lu, X., Chan, H.M., Sun, C.-L., Tseng, C.-M., Zhao, C.: Interconnected core–shell carbon nanotube–graphene nanoribbon scaffolds for anchoring cobalt oxides as bifunctional electrocatalysts for oxygen evolution and reduction. *J. Mater. Chem. A* **3**, 13371–13376 (2015)
54. Liang, Y., Li, Y., Wang, H., Zhou, J., Wang, J., Regier, T., Dai, H.: Co₃O₄ nanocrystals on graphene as a synergistic catalyst for oxygen reduction reaction. *Nat. Mater.* **10**, 780–786 (2011)
55. Yu, H., Fisher, A., Cheng, D., Cao, D.: Cu, N-codoped hierarchical porous carbons as electrocatalysts for oxygen reduction reaction. *ACS Appl. Mater. Interfaces* **8**, 21431–21439 (2016)
56. Lai, Q., Zheng, L., Liang, Y., He, J., Zhao, J., Chen, J.: Metal–organic-framework-derived Fe–N/C electrocatalyst with five-coordinated Fe–Nx sites for advanced oxygen reduction in acid media. *ACS Catal.* **7**, 1655–1663 (2017)
57. Yang, L., Lv, Y., Cao, D.: Co, N-codoped nanotube/graphene 1D/2D heterostructure for efficient oxygen reduction and hydrogen evolution reactions. *J Mater Chem A* **6**, 3926–3932 (2018)
58. Yin, P., Yao, T., Wu, Y., Zheng, L., Lin, Y., Liu, W., Ju, H., Zhu, J., Hong, X., Deng, Z.: Single cobalt atoms with precise N-coordination as superior oxygen reduction reaction catalysts. *Angew. Chemie* **128**, 10958–10963 (2016)
59. Han, Y., Wang, Y.-G., Chen, W., Xu, R., Zheng, L., Zhang, J., Luo, J., Shen, R.-A., Zhu, Y., Cheong, W.-C., Chen, C., Peng, Q., Wang, D., Li, Y.: Hollow N-doped carbon spheres with isolated cobalt single atomic sites: superior electrocatalysts for oxygen reduction. *J. Am. Chem. Soc.* **139**, 17269–17272 (2017)
60. Fan, Z., Yan, J., Zhi, L., Zhang, Q., Wei, T., Feng, J., Zhang, M., Qian, W., Wei, F.: A three-dimensional carbon nanotube/graphene sandwich and its application as electrode in supercapacitors. *Adv. Mater.* **22**, 3723–3728 (2010)
61. Chen, P., Xiao, T.-Y., Qian, Y.-H., Li, S.-S., Yu, S.-H.: A nitrogen-doped graphene/carbon nanotube nanocomposite with synergistically enhanced electrochemical activity. *Adv. Mater.* **25**, 3192–3196 (2013)
62. Liu, Q., Tian, J., Cui, W., Jiang, P., Cheng, N., Asiri, A.M., Sun, X.: Carbon nanotubes decorated with CoP nanocrystals: a highly active non-noble-metal nanohybrid electrocatalyst for hydrogen evolution. *Angew. Chemie Int. Ed.* **53**, 6710–6714 (2014)
63. Pan, Y., Yang, N., Chen, Y., Lin, Y., Li, Y., Liu, Y., Liu, C.: Nickel phosphide nanoparticles–nitrogen-doped graphene hybrid as an efficient catalyst for enhanced hydrogen evolution activity. *J. Power. Sourc.* **297**, 45–52 (2015)
64. Zhang, B., Liu, J., Wang, J., Ruan, Y., Ji, X., Xu, K., Chen, C., Wan, H., Miao, L., Jiang, J.: Interface engineering: the Ni(OH)₂/MoS₂ heterostructure for highly efficient alkaline hydrogen evolution. *Nano Energy* **37**, 74–80 (2017)
65. Zhang, Y., Wang, Y., Wang, T., Wu, N., Wang, Y., Sun, Y., Fu, L., Du, Y., Zhong, W.: Heterostructure of 2D CoP Nanosheets/1D carbon nanotubes to significantly boost the alkaline hydrogen evolution. *Adv. Mater. Interfaces* **7**, 1901302 (2020)
66. Wang, J., Xu, F., Jin, H., Chen, Y., Wang, Y.: Non-noble metal-based carbon composites in hydrogen evolution reaction: fundamentals to applications. *Adv. Mater.* **29**, 1605838 (2017)

Graphene as a Metal-Free Catalyst—Recent Case Studies



T. Stach, A. Seif, and U. Burghaus

Abstract One can encounter some skepticism about clean, non-functionalized, defect-free graphene being a catalyst for gas-surface reactions at ultra-high vacuum (UHV). We will describe a few successful literature examples, focusing on our own recent work, to illustrate that graphene indeed can act as a catalyst. Experimental and theoretical results will be described. Our own work concerns the decomposition of small sulfur compounds (SO_2 , H_2S , thiophene) on epitaxial graphene characterized in UHV by surface science experimental and theoretical techniques. Desulfurization catalysis has some overlap with energy-related applications. Other recent works from other groups concern the surface chemistry of organic compounds, as well as the dissociation of hydrogen on corrugated graphene. This book chapter does not provide a comprehensive review, however. A few liquid phase studies, work on powder samples, electrochemistry, and photoelectrochemistry works are mentioned but not discussed in any detail. The case studies focus on defect-free and clean (not functionalized), epitaxial graphene as the catalyst studied at UHV.

Keywords Metal-free heterogeneous catalysis · Graphene · Experimental surface science · Small sulfur compounds · Density functional theory

T. Stach · U. Burghaus (✉)

Department of Chemistry and Biochemistry, North Dakota State University, Sugihara Hall, 1311 Albrecht Blvd, Fargo, ND 58102, USA

e-mail: uwe.burghaus@ndsu.edu

URL: <http://www.uweburghaus.us>

A. Seif

Dipartimento Di Fisica E Astronomia, Università Di Padova, Via Marzolo 8, 35131 Padova, Italy

1 Introduction

1.1 Motivation

Metal-free heterogeneous catalysis using carbon catalysts is an intriguing alternative to traditional chemical synthesis [1–5]. Because carbon materials are practically inexhaustible and as such sustainable, in contrast to precious metals. In addition, the functionalization of carbon materials is already widely used today which could result in highly selective catalysts reducing side reactions, waste products, and increasing energy efficiency. The concept of noble metal-free catalysis dates back many years, [1–4, 6, 7] but was so far mostly explored in liquid/solid phase reactions such as organic synthesis or electro chemistry. However, gas-surface reactions are preferred for large-scale industrial processes, generating less waste due to easier separation of products and catalyst. A scientifically interesting allotrope of carbon is graphene (Gr). In general, two-dimensional (2D) crystals are currently a highly regarded research area [5, 8–10]. However, surface reactions on pristine graphene have not been studied much in detail at ultra-high vacuum (UHV) using surface science techniques. The current literature is dominated by synthetic liquid/solid phase processes, theory, and engineering type works on powders at high pressure. Indeed, it is relatively simple to synthesize multilayer (!) “graphene”/graphene oxide flakes in bulk quantities. However, already a stack of a few layers of graphene shows basically the same properties as bulk graphite [11] (e.g., HOPG—Highly Ordered Pyrolytic Graphite), i.e., the intrinsic surface properties of graphene cannot be studied on thick “graphene” flakes in liquid solutions. Generally, the UHV environment guarantees ultra-clean samples. Unexpectedly, recently it turned out that even clean, non-functionalized and defect free graphene is chemically reactive for a few processes [12–14]. In some of these studies, graphene was epitaxially grown on metal single crystals (Ni, Ru) which was according to density functional theory calculations (DFT) important for graphene’s reactivity enhancement [12, 14]. However, graphene on nonmetallic substrates (such as SiO₂, graphene/SiC, etc.) could also be tested for catalytic activity. Recent DFT studies now include the effect of the substrate which does allow potentially to tune graphene’s reactivity [15–17]. One could consider other 2D crystals as metal-free catalysts such as silicene (2D-silicon) or germanene which have greater chemical reactivity than graphene due to sp²/sp³ hybridization and differences in the π bonding as compared to graphene. The drawback of overwhelming reactivity, however, is that the reactions become likely stoichiometric and not catalytic. The restriction of the book chapter to a few references, does not allow to include in detail the many other strategies to develop environmentally sound catalysts such as utilizing non-noble metals, reducing catalyst loadings, etc. The book chapter focuses on UHV studies on non-functionalized graphene, exploring graphene’s intrinsic catalytic properties. However, in a broader perspective, working on the catalysis of graphene may extend the use of graphene beyond the utilization of its remarkable electronic and mechanical properties.

1.2 How Can Graphene Become a Catalyst—Possible Mechanisms?

Let's consider possible mechanisms explaining why a carbon-based system becomes a catalyst. Searching the literature, several ideas for possible mechanisms become apparent.

- (1) **Defects.** According to DFT studies, Refs. [18, 19] defects in graphene create carbon atoms with dangling bonds (i.e. unpaired valence electrons) which enhance graphene's reactivity. For example, the dissociation of C_6H_5OH (phenol) [18] and H_2S (hydrogen sulfide), [19, 20] were noted to be catalyzed by defected graphene. In that case, free-standing graphene was catalytically active. Thus, here the substrate seems unimportant. Importantly, if correct, defect enhanced reactivity should also be present for non-metallic substrates allowing for truly metal free catalysis. Depending on annealing temperature and other preparation details, the defect density of grain boundaries (extended defects) can become significant, as shown in scanning tunnelling microscopy (STM) studies specifically for graphene/ruthenium (short Gr/Ru) [21]. However, defect free graphene can be made (see Sect. 2.2). Also, it seems from DFT studies that only very specific defects make graphene reactive. On real samples, those defects are unlikely present in large enough concentrations to dominate graphene's reactivity.
- (2) **Geometrical induced electronic structure effects.** Graphene growth on some single crystal supports results in the formation of a Moiré pattern caused by a graphene layer incommensurate to the support. In other words, C atoms are either properly or improperly aligned with the support atoms (these sites are usually termed top-fcc and top-hcp sites, i.e., face-centered-cubic and hexagonal-close-packed, respectively) [22]. The different sites can show different chemical activities, Ref. [22] e.g., the properly aligned C atoms act as nucleation sites for metal clusters [23]. Photoelectron spectroscopy (XPS) can in principle distinguish top-fcc, and top-hcp sites [22, 24]. For non-surface chemists, this may appear as a rather subtle effect, but let's recall, however, that graphene on e.g., ruthenium is a single crystal that even grows over step edges [10, 25–31]. That system can be made virtually defect free.
- (3) **Hybridization.** Based on experimental data about CO adsorption on graphene/nickel [22, 32] another mechanism was recently suggested by theory [15–17]. For that system, a hybridization of graphene's C(p) and Ni(3d) orbitals was predicted by DFT, increasing the binding energy of CO (consistent with experimental data). The process is catalytic since graphene was not consumed [22, 32]. Hybridization effects (and strong substrate interactions) are dominant for some metallic substrates. E.g., similar hybridization effects have been seen for graphene/Ru in a photoemission study [24]. In most basic terms, hybridization implies electron transfer, Ref. [33] i.e., this could lead also to the dissociation of adsorbates. These effects will unlikely be present for nonmetallic substrates, however.

- (4) **Polarization.** Approximately 10 years back, the adsorption of water on epitaxial graphene was a hot topic area. Back then theoretical works suggested that some of the van der Waals interactions from a substrate are transmitted through graphene. Thus, the polarization of the substrate can affect surface properties of graphene [11]. Polarization effects are not per se restricted to metallic substrates but, e.g., nonmetals such as glass or silica used as a substrate also can affect van der Waals interactions [11]. Thus, that mechanism also could be relevant for nonmetallic systems. Initially, polarization effects were considered for weak molecularly interacting species. But conceptually, dipole–dipole interactions between an adsorbate and catalyst enhance in general their interaction and may promote chemical reactions.
- (5) **Functionalization.** In this book chapter we focus on model studies on pristine non functionalized graphene. Therefore, only briefly, synthetic organic or electro chemistry studies often use carbon flakes in liquid solutions rather than graphene. These flakes are functionalized which determines the reactivity. For example, when graphene oxide is formed, the sp^2 hybridized graphene changes to a sp^3 . In principle, C- sp^2 and C- sp^3 can be distinguished in XPS by chemical shifts (as large as 1 eV) [34]. DFT studies have shown that the oxidation of graphene can form a few different oxygen-containing functional groups (epoxide, hydroxyl, and carboxyl) [35]. These reactive functional groups in graphene oxide can make it a reactive material. Many published DFT works describe the mechanism by which a functionalization modifies the reactivity of graphene.
- (6) **Bending, rippling and corrugation effects.** For epitaxial graphene, the roughness of the substrate can result in non-flat, bend graphene [36]. That out-of-plane corrugation can potentially affect graphene's reactivity. That the curvature of carbon layers affects its electronic properties is well-known from carbon nanotubes [28]. Graphene ripples can form on non-metallic substrates.
- (7) **Acceptor/donor interactions.** Literature seems to indicate that in particular sulfur compounds are reactive on clean and defect free graphene (in UHV and also in the liquid phase) [18–20] despite that alkanes, benzene, CO_2 , CO, H_2 are unreactive (adsorb molecularly) on Gr/Ru (and Gr/Ni) in UHV. That raises the question, what is special about sulfur? Conceptually, the sulfur atom in these sulfur compounds has a d orbital which may act at the same time as an electron acceptor from Ru/G and as an electron donor to the antibonding orbital of e.g., S–H bonds. Charge transfer into antibonding states dissociates the adsorbate. Sulfur, located in the 3rd row of the periodic table, has empty d-orbitals that are better accessible compared to elements in the 2nd row (see Sect. 2.3.2b for details). Also, the d orbital of S is highly polarized.

2 Case Studies

2.1 *Molecular Adsorption of Small Gas Phase Species on Graphene*

In comparison with the reactive interactions discussed in the following sections, most small gas phase species adsorbed at UHV on epitaxial graphene remain intact, i.e., these just adsorb molecularly including alkanes, benzene, CO₂, CO, water for graphene grown on Ru(0001) and CO on Ni(111) [22, 32, 37–42]. For CO/graphene-Ni, enhanced binding strength was present, apparently related to hybridization effects (see mechanism 3 in Sect. 1.2) [22, 32]. Enhancement of binding strength also is present for CO₂ on graphene oxide, Ref. [43] likely due to enhanced polarization compared with graphene. Rippled graphene seems reactive towards H₂ dissociation [13].

2.2 *Synthesizing Defect Free Epitaxial Graphene*

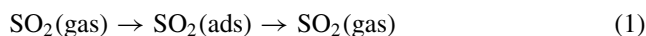
Interestingly, benzene does dissociate on Ru(0001) (according to C₆H₆(gas) → 3H₂(gas) + 6C(ads)), but once a single carbon layer is formed, dissociation ceases and benzene interacts just molecularly with graphene/Ru [39, 40]. Thus, graphene growth is self-terminating making sure that only single layer graphene forms. Consequently, using adsorption/desorption cycles to form graphene/Ru from benzene, by monitoring the desorption of H₂ (as the dissociation product) one can monitor exactly the completion of the graphene layer. Once the H₂ desorption signal disappears, single layer graphene is completed. Importantly, an eventual residual H₂ signal correlates with vacancy defect sites in the graphene/ruthenium layer. However, virtually vacancy defect free graphene can be synthesized on Ru(0001) using adsorption/desorption cycles; referred in the following as “low temperature preparation” (LT-prep) [40]. The ability to study defect free systems is important since a number of mechanisms suggested theoretically (see mechanism 1 in Sect. 1.2) describe various defects as active sites on graphene. STM studies show that the LT-prep graphene does have grain boundary defects, however [21, 23, 44]. Those grain boundary defects can be eliminated by a one-step synthesis where e.g., benzene is dosed on ruthenium at high temperature (“high temperature preparation”, HT-prep). In summary, vacancy defect free and grain boundary free single layer graphene can be grown on Ru(0001).

2.3 Dissociative Adsorption of Sulfur Compounds on Graphene

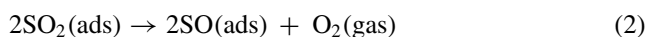
2.3.1 Adsorption and Reaction of Sulfur Dioxide (SO₂) on Graphene

Unexpectedly, SO₂ does dissociate on graphene/ruthenium besides that numerous other gas phase species (alkanes, benzene, CO₂, CO, water, H₂ see Sect. 2.1) just adsorb intact using the same graphene preparation, the same experimental set-up, and the same vacuum system in these studies [12]. The kinetics of the SO₂ dissociation was characterized by TDS (thermal desorption spectroscopy) which is a simple temperature ramping technique. Here, gas is adsorbed onto a sample in a UHV chamber at low temperature where the desorption/reaction rate is zero. Next, the sample temperature is ramped up and simultaneously desorbing species are detected with a mass spectrometer. In regular TDS experiments, usually just one mass is monitored, but one also can register a few masses simultaneously (multi-mass TDS).

Figure 1 depicts the results of multi-mass SO₂ TDS experiments as compared with the gas phase SO₂ fragmentation pattern [12]. If the pattern would agree (same intensity for the same mass peaks), then the adsorption/desorption would purely be molecular according to

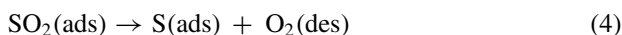


with gas and ads denoting gas-phase species and adsorb species, respectively. However, the SO(gas) and O(gas) signals detected in TDS are larger than expected from the gas phase (Fig. 1). And, the sulfur signal does agree with expectations from gas-phase data, i.e., no extra sulfur is found in the gas phase. The latter indicates that sulfur if formed, does not desorb. These kinds of data allow for suggesting a kinetics mechanism as follows. Sulfur dioxide could simply decompose such as



forming the extra SO and O₂ gas seen experimentally. Also, the SO₂ parent mass was detected [12]. Thus, a molecular adsorption pathway is present as well. From intensity ratios a reaction probability of 0.5 was estimated, meaning that half of the SO₂ molecules dissociate on the surface [12].

Indeed, sulfur was seen left behind on the surface after TDS experiments using Auger electron spectroscopy (AES, see Fig. 2). Thus, one must add:



AES data allow to estimate the sulfur coverage which turned out to be about half of a monolayer (ML) for typical experimental conditions (see Ref. [12] for details). The

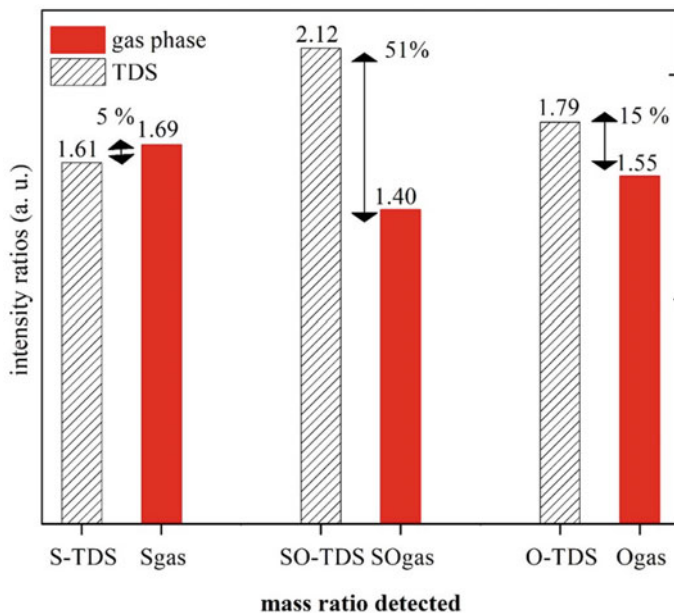


Fig. 1 Multi-mass SO₂ TDS (thermal desorption spectroscopy) data as compared with the gas phase SO₂ fragmentation pattern. Adapted with permission [12], Copyright (2021) AIP publishing

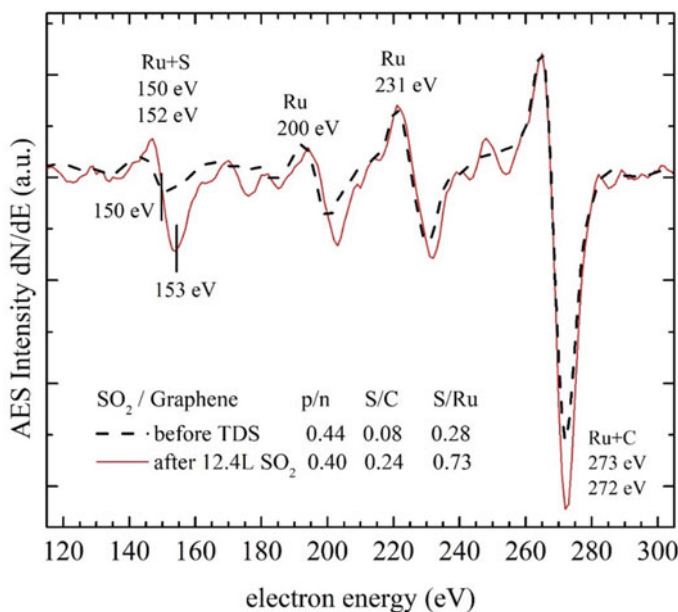


Fig. 2 Auger electron spectra (AES) collected before and after adsorbing SO₂ on graphene/ ruthenium (Adapted with permission [12], Copyright (2021) AIP publishing

reaction probability and sulfur concentration are much larger than the experimentally determined defect concentration (<1% ML) which rules out vacancy defects as the active sites. For SO₂, experiments were only run on LT-prep samples.

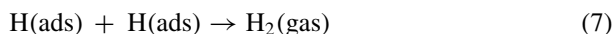
Since carbon and ruthenium AES lines overlap, the positive to negative AES peak ratio at 273 eV is used to determine the carbon concentration on the surface [23]. Accordingly, an increase of carbon on the surface was detected after SO₂ adsorption/desorption experiments. First, graphene does not decompose due to SO₂ adsorption. Second, as control experiments revealed, the increase in carbon is caused by the AES system. The micro-CMA based AES is rather short. Therefore, carbon that desorbs from the filament of the AES electron gun (which is in line of sight to the sample) adsorbs on the sample. Meanwhile the manufacturer of this system seems to have fixed this problem by using a different filament for the electron gun of the AES system. For the H₂S and thiophene projects (see next sections), a different, larger AES spectrometer was used which does not suffer from this contamination effect.

2.3.2 Adsorption and Reaction of Hydrogen Sulfide (H₂S) on Graphene/ruthenium

(a) Experimental Results for H₂S-graphene/ruthenium

For H₂S adsorption on graphene/ruthenium only the parent mass and H₂ desorption were detected by TDS [45]. In addition, adsorb sulfur was seen after adsorption/desorption of H₂S by AES. The system remained reactive for H₂S dissociating even when the surface was sulfur covered. For that reaction, nearly identical data were obtained for the LT-prep and HT-prep. Thus, vacancy defect sites and grain boundaries can be ruled out as active sites. Recall again, that the vacancy defect density of our samples is virtually zero. The AES carbon/ruthenium signal did not change upon H₂S adsorption. Thus, H₂S adsorption also does not generate defects in graphene. One could imagine other active sites besides graphene and sulfur on graphene. But RuO, graphene oxide, or RuS₂ were not formed. The presence of oxygen would lead to an oxygen AES peak at 500 eV [43] which was not present. Although RuS₂ is a known desulfurization catalyst, it can only form on vacancy defect sites. In addition, no significant desorption of water or CO (due to uptake from the residual gas in the UHV system) were seen. The missing CO desorption again indicates that vacancy defects are absent since CO does adsorb on Ru but not on Gr/Ru (at ~100 K).

Because only H₂S and H₂ desorption was detected, the mechanism is simply given by:



where H_2S dissociation is 1st order in the hydrogen sulfide concentration (see Eq. (6)). Assuming that H_2S dissociation likely occurs at the same temperature as the H_2 desorption (~ 125 K), the activation energy would amount to (28.5–31.2) kJ/mol (with typical 1st order pre-factor of $1 \times 10^{13}/\text{sec}$).

The recombinative desorption of H_2 would be a 2nd order reaction (see Eq. (7)). In that case, and with a preexponential of $10^{21} \text{ cm}^2/(\text{mol sec})$, [46] the H_2 desorption energy would be (45.5–50.0) kJ/mol. However, the TDS data [45] are indicative of 0th order kinetics. For 0th order H_2 desorption, one would obtain an activation energy for H_2 desorption of 7.4 kJ/mol and a pre-factor of $7.0 \times 10^{10}/\text{sec}$ (see Figure S6 in Ref. [45]). Generally, 0th order kinetics appears when a two-phase regime is formed. E.g., sulfur clusters form on the surface and are covered with hydrogen due to reaction Eq. (6). H_2 starts to desorb along the rim of the islands which are refilled by H_2 from terrace sites. Therefore, the desorption of H_2 along the rim sites of sulfur clusters becomes H_2 coverage independent. Coverage independent kinetics is 0th order.

Typical reaction probabilities and sulfur concentrations were estimated as 0.8 and 0.5 ML, respectively (see supplemental to Ref. [45]). Again, these numbers are much larger than any defect density one could imagine.

The molecular adsorption pathway corresponds to a binding energy of 33.9 kJ/mol (for a 1st order pre-factor of $1 \times 10^{13}/\text{sec}$). At large exposures, H_2S forms condensed layers desorbing at 110–120 K.

Sulfur could be removed by Ar^+ sputtering which, however, also destroyed the graphene layer. Similarly, sulfur could be cleaned off the surface by oxygen annealing (Fig. 3), but then RuO or graphene oxide were formed (according to AES) and prolonged annealing also removes the graphene layer. Therefore, unfortunately, a catalytic cycle cannot easily be formed for that system at UHV. Perhaps atomic hydrogen cleaning would do the trick, but a hydrogen doser was not available. Figures 3 and 4 depict more details of cleaning the surface by oxygen annealing. According to Fig. 3, oxygen annealing gradually also removes graphene from the surface. Based on the positive to negative AES peak ratio at 273 eV, Ref. [23] after annealing in 1000 L of O_2 , clean ruthenium is obtained. Figure 4 seems to indicate that sulfur remains mostly on the surface as long as some carbon is present. When clean ruthenium is obtained (at 1000 L O_2), also sulfur diminishes fast. One may speculate that carbon and sulfur compete for the oxygen with carbon having a greater reaction rate. This could indicate that indeed RuS is formed while the graphene layer breaks down (due to O_2 annealing) and vacancy defects form. RuS is likely more inert than carbon patches on ruthenium. That too would explain why relatively large exposures of oxygen are needed to clean the surface. In case of very large sulfur surface concentrations, some of that sulfur could be cleaned off just by UHV annealing, but not all of it.

(b) DFT Modelling of H_2S -graphene/ruthenium

The dissociation of H_2S also was considered using DFT (density functional theory) [45]. Through theoretical investigations using GGA (Generalized Gradient Approximation) calculations and the Perdew–Burke–Ernzerhof (PBE-D) approach augmented

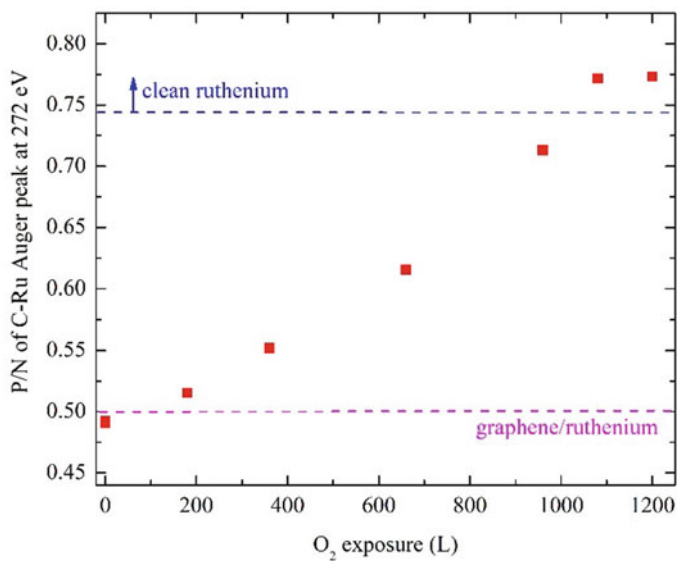


Fig. 3 Sample cleaning. The AES carbon signal decreases as a function of oxygen annealing time of a sulfur contaminated graphene/ruthenium surface (The total oxygen exposure is depicted) [47]

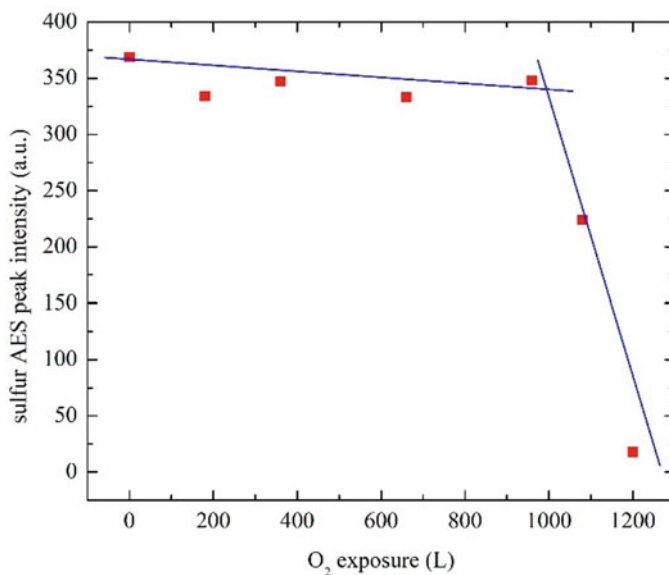
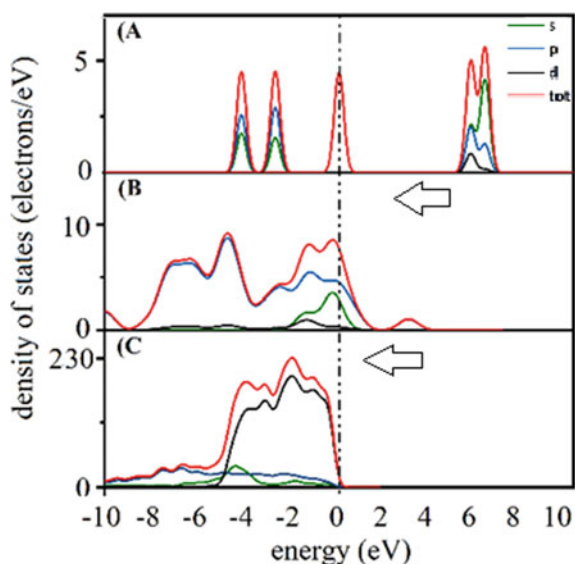


Fig. 4 Sample cleaning. The AES sulfur signal as a function of oxygen annealing time (The total oxygen exposure is depicted) [47]

with long-range van der Waals (vdW) effects proposed by Grimme, we delve into the mechanisms and reaction pathways of this process. This analysis provides a fundamental understanding of the catalytic behavior of graphene with ripples supported by a substrate. By examining the molecular adsorption pathway, it was observed that the adsorption energy of H_2S on graphene/ruthenium depends on the adsorption site, primarily due to the pronounced corrugation resulting from the lattice mismatch between graphene and the Ru(0001) substrate. The most stable adsorption configurations ranged from -39.8 kJ/mol for adsorption in the “valleys” to -25.7 kJ/mol for adsorption at the “on top” sites. Experimental evidence reveals broad TDS peaks (see Fig. 1 in Ref. [45]), suggesting the presence of different adsorption sites and lateral interactions. The averaged adsorption energy over these sites (-33 kJ/mol) aligns well with the experimental estimate for the α -peak (-33.9 kJ/mol) at saturation coverage. Comparatively, the adsorption energy is significantly higher for epitaxial Gr/Ru compared to free-standing Gr (-16 kJ/mol), indicating the substantial influence of the Ru substrate. The enhanced molecular binding can be attributed to charge transfer, polarization, and van der Waals forces, which induce a surface dipole moment in the corrugated Gr. The calculations reveal that H_2S dissociation is energetically unfavorable on defect-free, unsupported Gr. However, the presence of the Ru substrate renders the dissociated configuration energetically favorable, with a reduced activation energy compared to the undissociated state. Notably, when examining the complex geometry of nanorippled graphene without the Ru substrate, a high energy barrier of approximately 350 kJ/mol is encountered, underscoring the significance of both the geometric and electronic effects of the Ru substrate for this reaction. The calculated activation energy aligns well with the experimental estimate of around 30 kJ/mol, confirming the agreement between simulations and the observed dissociation process. To gain insight into the dissociation mechanism, an electronic-structure analysis was performed. Charge transfer upon adsorption weakens the covalent bonding between H and S, facilitating H_2S dissociation. As displayed in Fig. 5, when H_2S is adsorbed on the Gr/Ru surface, its antibonding orbitals effectively hybridize with the 4d orbitals of Ru, enhancing reactivity. In contrast, this effect is nearly absent in adsorption on free-standing Gr, as some antibonding states remain above the Fermi level, indicating that the S–H bonds are not easily broken. Consequently, electron transfer to the antibonding orbitals is more pronounced on Gr/Ru than on free-standing Gr, resulting in increased reactivity of H_2S . The valley sites of corrugated Gr serve as electron donor centers, efficiently trapping H_2S and promoting dissociation through interfacial charge transfer. Following dissociation, the H_2 molecule desorbs more readily than the S atom from Gr/Ru, leading to the presence of S atoms on the surface, which can aggregate into sulfur clusters.

In summary, our findings demonstrate that nanorippled graphene supported by a Ru substrate exhibits higher reactivity compared to unsupported graphene, owing to a complex interplay between geometric and electronic effects. Notably, the electronic effects were found to be significant in the dissociation of the H_2S molecule.

Fig. 5 The figure presents the Partial Density of States (PDOS) of H₂S, including the total and s, p, and d orbitals, in different configurations: **a** as a free molecule, **b** adsorbed on graphene (Gr), and **c** adsorbed on graphene supported by a Ru substrate (Gr/Ru). The zero line on the energy axis corresponds to the Fermi energy (EF). Adapted with permission [45], Copyright (2021) AIP publishing



2.3.3 Adsorption and Reaction of Thiophene (C₄H₄S) on Graphene

Thiophene is one of the standard probe molecules for testing desulfurization catalysts. It is beyond the scope of this book chapter to go into any details; the literature for many different surfaces is extensive, although it seems that graphene has not been considered so far. Interestingly, also C₄H₄S dissociates on defect free graphene/Ru [47]. (1) TDS multi mass pattern deviates from gas phase thiophene. In fact, gas phase species are detected which are not part of the gas phase fragmentation pattern of C₄H₄S. (2) Sulfur and carbon remain on the surface after thiophene TDS.

Since the reaction pathways and possible side reactions of C₄H₄S dissociation on graphene/Ru are complex, we did collect reactive mass scans at constant temperature. These experiments allow for detecting all masses ranging from hydrogen ($m/e = 1$) to the parent (molecular) mass of thiophene ($m/e = 84$) within one minute or so. Rather than collecting TDS scans one by one for 84 different masses. To correct for thiophene's gas phase fragmentation pattern and the UHV background, such a mass scan detected at the lowest possible surface temperature (where graphene is non-reactive) was subtracted from mass scans collected at higher temperatures. Figure 6 shows one example. The mass scan is dominated by the masses $m/e = 2$ (H₂), 26 (C₂H₂), and 58 (C₂H₂S). This suggests that the adsorbed thiophene (C₄H₄S) dissociates into acetylene (C₂H₂ with parent mass $m/e = 26$) and thioketene (C₂H₂S, $m/e = 58$) via the pathway:



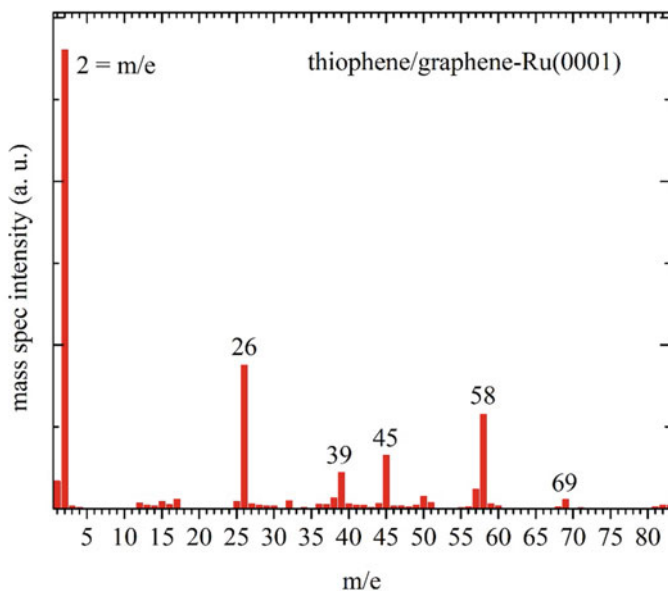


Fig. 6 Isothermal mass scan at 140 K where 1×10^{-8} torr thiophene were leaked into the vacuum chamber with a graphene/ruthenium(0001) sample present [47]. A similar mass scan collected at 100 K was removed as a background. Thus, the thiophene gas phase fragmentation pattern and the UHV background were removed, i.e., only the mass peaks generated by surface reactions are shown (The scan is not corrected for sensitivity factors of the ionizer or the mass spec transmission factor. Thus, the hydrogen signal is overexposed by a factor of roughly 16 in case of H_2S , see supplemental to Ref. [45])

Briefly, along this pathway, the adsorbed thiophene likely forms α -carbene as an intermediate which then subsequently dissociates into acetylene and thioketene. Part of the formed thioketene could adsorb and further dissociate in adsorbed sulfur and carbon (as detected by AES) as well as hydrogen gas (Fig. 6). That mechanism was suggested in a DFT study [48]. For further details, see Ref. [47]. First experiments suggest that graphene on silica is none reactive using the same small sulfur compounds.

2.4 Dissociative Adsorption of Hydrogen on Graphene

2.4.1 Experimental Results for H_2 /graphene

Only a handful other examples are currently known where non-functionalized graphene displays catalytic properties for gas-phase processes [13, 14]. An intriguing, very recent example (that also may have implications for energy related applications of graphene) is the experimental finding that defect free (in the traditional sense)

and clean graphene efficiently dissociates molecular hydrogen [13]. In addition, the isotope exchange reaction of H_2 and D_2 was detected [13]. The reactivity of graphene was attributed to geometrical effects (see next section), i.e., graphene not being perfectly flat but rippled. Raman spectroscopy was employed for rippled and pristine graphene to detect adsorbed hydrogen atoms. The Raman D-peak is indicative of sp^3 bound hydrogen atoms. The ripples are induced by certain rough substrates such as SiO_2 whereas these are missing when bulk graphite is used as a substrate for graphene. This study is not a traditional surface science project, in fact the sample was exposed to one bar hydrogen gas at 600 °C for 2 h, but it does provide an interesting and important example of a gas-surface reaction well known for many other surfaces. The above room temperature treatment is needed to circumvent an activation barrier.

2.4.2 Theoretical Results for H_2 /graphene

In this section, we focus on theoretical studies from the literature that primarily investigate how the behavior of intact (defect free) graphene, both geometrically and electronically, is influenced by the substrate. These investigations, utilizing DFT, provide insights into how controlled modifications at the atomic level of the graphene surface can enhance or modify its reactivity in specific catalytic reactions. It should be noted that graphene monolayers are inherently characterized by their lack of complete flatness, primarily due to thermal fluctuations (flexural phonons) and unavoidable local strain. These factors give rise to the formation of static nanoscale wrinkles and ripples on the graphene surface [13]. While defected or functionalized graphene flakes can exhibit catalytic activity towards the dissociation of certain molecules, Ref. [13] intact and defect-free graphene is highly regarded for its ability to engineer properties through appropriate strategies. For example, combining graphene with electron-rich sources such as metals can enhance the driving force for reactivity, as explained at least in one of the mentioned mechanisms in a previous section (see Sect. 1.2). To gain a better understanding, let us begin by examining a few noteworthy studies that have already been published on this subject, including the work of Geim's group [13]. Computational investigations, specially supported by DFT calculations, have shed light on the catalytic reactivity of intact graphene. In a seminal study published in Ref. [13] the electronic structures of graphene were examined by analyzing the shape of ripple, revealing intriguing findings. According to the simulations, when the height (h) of the corrugation (also known as ripple) in graphene exceeds a threshold ratio of 0.07 relative to its radius (R), a significant enhancement in its chemical activity is observed. It was shown that functionalization can stabilize ripples via strong strains, close to the breaking of carbon-carbon bonds. However, if original corrugations are small enough, such that typical h/R is smaller than 0.07, the ripples will disappear after elimination of the substrate. Furthermore, as the curvature of the ripples increases, midgap states emerge, leading to a substantial rise in chemisorption energy. In a recent study conducted by the research group of Geim, Ref. [13] they demonstrated that a rippled graphene sheet can act as a catalyst for the

reaction between H_2 and D_2 , producing HD as the resulting product. The detection of HD serves as compelling evidence for hydrogen dissociation on graphene from a H_2/D_2 isotope mixture. Furthermore, this reaction allows for a comparison between graphene and known catalysts. Interestingly, few-layer graphene displayed lower efficiency in HD production compared to monolayer graphene. This observation aligns with the fact that few-layer graphene possesses a smoother surface with fewer ripples than monolayer graphene. This comparative investigation involving hexagonal boron nitride nanosheets (BNNS) and graphene as catalysts highlighted that the energy barrier (E_b) for the hydrogen dissociation pathway decreases with an increase in the curvature of nanoripples. Graphene nanoripples exhibited a significant reduction in the energy barrier, reaching values as low as 0.4 eV for specific curvatures ($h/R \approx 12\%$). Conversely, hBN nanoripples demonstrated an energetically unfavorable reaction, with the central position being unfavorable across the entire range of h/R considered. The study also analyzed the evolution of bond lengths and strengths along the hydrogen dissociation pathway. It was observed that the dissociation of H_2 on graphene ripples required a shorter elongation of H–H bonds compared to h-BN ripples. Additionally, the reaction on graphene ripples could occur at a greater distance from the surface. These factors contribute to a lower energy cost for the reaction on graphene compared to h-BN. The bonding strengths of atomic hydrogen to graphene and hBN ripples were further examined using the crystal orbital Hamilton population (COHP) method. Graphene ripples exhibited bonding states below the Fermi level, as illustrated in Fig. 7, indicating a stable adsorption configuration. In contrast, h-BN ripples displayed a notable antibonding component in the occupied states, leading to a less stable adsorption configuration and higher total energy. Overall, the DFT analysis in the given work revealed that graphene with nanoripples exhibits higher reactivity compared to hBN due to its lower energy barrier, shorter elongation of H–H bonds, ability to accommodate longer distances from the surface, and stronger bonding strengths. These factors contribute to graphene's enhanced capability for hydrogen dissociation, rendering it more reactive than h-BN. Importantly, these results have significant implications for various previously reported observations in the literature. For instance, nanoripples may play a crucial role in graphene oxidation, which predominantly occurs on monolayers and wrinkles but has remained unexplained until now. They also concluded that nanoripples could play a more significant role in catalysis compared to commonly considered factors such as vacancies, edges, and residual functional groups on the surface of graphene. The findings presented above indicate a substantial disparity in the chemical and catalytic activities between graphene and hBN monolayers, particularly in the case of hydrogen. However, when dealing with more complex molecules with bonding energies higher than that of H–H, the situation may change. For instance, in the case of H_2S dissociation, neither flat nor rippled graphene alone can efficiently facilitate the robust reactivity required for breaking S–H bonds (see Sect. 2.2.2b). Instead, additional driving forces such as charge transfer, potentially from a substrate, are necessary to facilitate the desired reactivity.

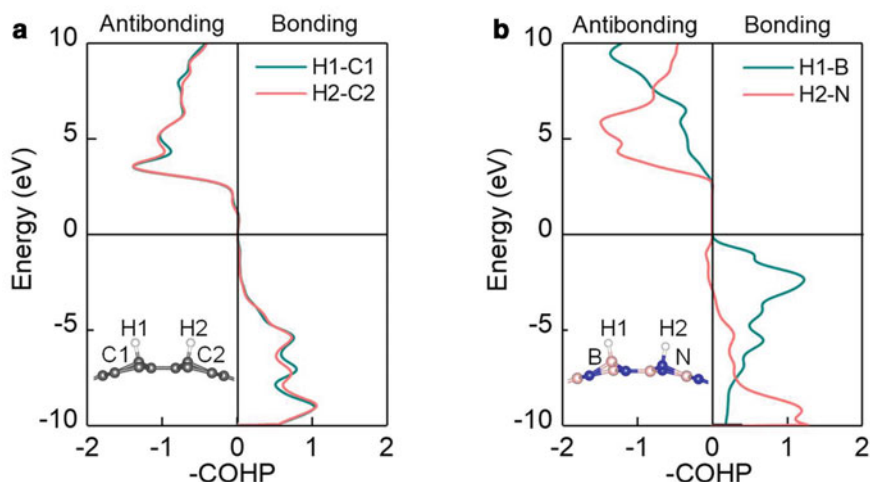


Fig. 7 The figure illustrates the results of Crystal Orbital Hamilton Population (COHP) bonding analysis showing the interaction of hydrogen adatoms with **a** graphene and **b** hBN ripples ($t/D = 12\%$). Insets: Atomic structures with hydrogen adatoms adsorbed at the central position for graphene and hBN ripples. Adapted from Ref. [13]. Copyright (2023) by P. Z. Suna, W. Q. Xiong, A. Bera, I. Timokhin, Z. F. Wu, A. Mishchenko, M. C. Sellers, B. L. Liu, H. M. Cheng, E. Janzen, J. H. Edgar, I. V. Grigorieva, S. J. Yuan, and A. K. Geim, some rights reserved; exclusive licensee PNAS. Distributed under a Creative Commons Attribution License 4.0 (CC BY) <https://creativecommons.org/licenses/by/4.0/>

2.5 Other Surface Reactions on Clean Graphene at UHV

A somewhat exotic, perhaps, example, but there aren't too many known today, is the polymerization of 1,3,5-tris(4-bromophenyl)benzene via dehalogenation on graphene/Ni(111) [14]. That system was studied at UHV using primarily STM and DFT. The goal apparently is to synthesize covalent organic networks, i.e., self-assembled molecular monolayers. The bromobenzene dissociation needed for the polymerization is catalyzed by graphene/Ni(111) [14]. Also for that example, the activation energy on graphene/Ni(111) is smaller than for freestanding graphene.

Another exotic but successful example of graphene acting as a catalyst in UHV is the formation of a C–C bond between cyanomethylene (i.e., $-\text{CH}_2\text{CN}$) and TCNQ (7,7,8,8-tetracyano-p-quinodimethane which is $(\text{NC})_2\text{CC}_6\text{H}_4\text{C}(\text{CN})_2$) also studied in UHV by STM and DFT. Here graphene facilitates charge transfer between the surface and the adsorbates [49]. The catalytically formed molecule was manipulated with the STM tip, forming a molecular magnetic switch.

3 Conclusions

As noted, this short book chapter focuses on reactive gas-surface interactions on clean, defect free graphene monolayers preferentially studied at UHV. Many more liquid phase studies on thick “graphene” flakes and projects on powder samples at high pressure have already been published. The decomposition of several small sulfur compounds has been characterized experimentally at UHV and in DFT calculations. So far metallic substrates were still used simply because it is experimentally simpler to synthesize graphene that way. Thus, it remains to be tested if graphene’s reactivity e.g., towards decomposition of sulfur compounds, is conserved for truly metal free systems. Known today already is that H₂ dissociates on rippled graphene/SiO₂ which indeed is a metal free catalyst [13].

Regarding similarities and differences in the decomposition kinetics of SO₂, H₂S, and C₄H₄S, sulfur dioxide does obviously not lead to H₂ desorption, but the other molecules do, where H₂ desorbs at about the same temperature, namely at ~120 K. H₂ desorption seems to follow 0th order kinetics. Adsorbed extra carbon is not seen for SO₂ and H₂S as well as the C-AES region does not change at all, i.e., graphene remains intact. All molecules decompose to adsorbed sulfur that is difficult to clean off. At the time this chapter had to be finished, detailed DFT calculations were available only for H₂S-graphene/ruthenium and reproduce the experimental findings well.

Acknowledgements A.S acknowledges funding from Fondazione Cariparo, Progetti di Eccellenza 2017, “Engineering van der Waals Interactions: Innovative paradigm for the control of Nanoscale Phenomena”. The Fargo group acknowledges a teaching assistant position from NDSU as well as partial support via donations from RBD Instruments, Inc and Princeton Scientific Corp., both located in the US.

References

1. Schreiner, P.R.: Metal-free organocatalysis through explicit hydrogen bonding interactions. *Chem. Soc. Rev.* **32**, 289–296 (2003)
2. Qi, W., Su, D.: Metal-free carbon catalysts for oxidative dehydrogenation reactions. *ACS Catal.* **4**, 3212–3218 (2014)
3. Tang, Y., Liu, Z., Dai, X., Yang, Z., Chen, W., Ma, D., Lu, Z.: Theoretical study on the Si-doped graphene as an efficient metal-free catalyst for CO oxidation. *Appl. Surf. Sci.* **308**, 402–407 (2014)
4. Wu, S., Yu, L., Wen, G., Xie, Z., Lin, Y.: Recent progress of carbon-based metal-free materials in thermal-driven catalysis. *J. Energy Chem.* **58**, 318–335 (2021)
5. Burghaus, U.: Can graphene act as a (noble) metal-free catalyst? *Curr. Phys. Chem. (CPC)* **12**, 2–10 (2022). <https://www.eurekaselect.com/article/120800>
6. Wang, Y., Li, H., Yao, J., Wanga, X., Antonietti, M.: Synthesis of boron doped polymeric carbon nitride solids and their use as metal-free catalysts for aliphatic C–H bond oxidation. *Chem. Sci.* **2**, 446–450 (2011)

7. Sun, F., Liu, J., Chen, H., Zhang, Z., Qiao, W., Long, D., Ling, L.: Nitrogen-rich mesoporous carbons: highly efficient, regenerable metal-free catalysts for low-temperature oxidation of H₂S. *ACS Catal.* **3**, 862–870 (2013)
8. Burghaus, U.: Gas-surface interactions on two-dimensional crystals. *Surf. Sci. Rep.* **74**, 141–177 (2019)
9. Burghaus, U.: Adsorption of water on two-dimensional crystals: water/graphene and water/silicatene. *Inorganics* **4**, 10 (2016). <http://www.mdpi.com/2304-6740/4/2/10/pdf>
10. Batzill, M.: The surface science of graphene: metal interfaces, CVD synthesis, nanoribbons, chemical modifications, and defects (review). *Surf. Sci. Rep.* **67**, 83–115 (2012)
11. Shih, C.J., Strano, M.S., Blankschtein, D.: Wetting translucency of graphene. *Nat. Mater.* **12**, 866 (2013)
12. Stach, T., Johnson, M.C., Stevens, S., Burghaus, U.: Adsorption and reaction kinetics of SO₂ on graphene: an ultra-high vacuum surface science study. *J. Vac. Sci. Technol., A* **39**, 042201 (2021)
13. Suna, P.Z., Xiong, W.Q., Bera, A., Timokhin, I., Wu, Z.F., Mishchenko, A., Sellersa, M.C., Liud, B.L., Chengd, H.M., Janzene, E., Edgare, J.H., Grigorievaa, I.V., Yuanc, S.J. Geim, A.K.: Unexpected catalytic activity of nanorippled graphene. *PNAS* **120** (2023)
14. Morchutt, C., Bjork, J., Krotzky, S., Gutzler, R., Kern, K.: Covalent coupling via dehalogenation on Ni(111) supported boron nitride and graphene. *Chem. Commun.* **51**, 2440–2443 (2015)
15. Ambrosetti, A., Silvestrelli, P.L.: Communication: enhanced chemical reactivity of graphene on a Ni(111) substrate. *J. Chem. Phys.* **144**, 111101 (2016)
16. Silvestrelli, A.A., Luigi, P.: Cooperative effects of N-doping and Ni(111) substrate for enhanced chemical reactivity of graphene: the case of CO and O₂ adsorption. *J. Phys. Chem. C* **123**, 31050–31056 (2019)
17. Ambrosetti, A., Silvestrelli, P.L.: Toward tunable CO adsorption on defected graphene: the chemical role of Ni(111) and Cu(111) substrates. *J. Phys. Chem. C* **121**, 19828–19835 (2017)
18. Widjaja, H., Oluwoye, I., Altarawneh, M., Hamra, A.A.B., Lim, H.N., Huang, N.M., Yin, C.Y., Jiang, Z.T.: Phenol dissociation on pristine and defective graphene. *Surf. Sci.* **657**, 10–14 (2017)
19. Borisova, D., Antonov, V., Proykova, A.: Hydrogen sulfide adsorption on a defective graphene. *Int. J. Quantum Chem.* **113**, 786–791 (2013)
20. Faye, O., Raj, A., Mittal, V., Beye, A.C.: H₂S adsorption on graphene in the presence of sulfur: a density functional theory study. *Comput. Mater. Sci.* **117**, 110–119 (2016)
21. Donner, K., Jakob, P.: Structural properties and site specific interactions of Pt with the graphene/Ru(0001). *J. Chem. Phys.* **131**, 164701 (2009)
22. Celasco, E., Carraro, G., Smerieri, M., Savio, L., Rocca, M., Vattuone, L.: Influence of growing conditions on the reactivity of Ni supported graphene towards CO. *J. Chem. Phys.* **146**, 104704 (2017)
23. Xu, Y., Semidey-Flecha, L., Liu, L., Zhou, Z., Goodman, D.W.: Exploring the structure and chemical activity of 2-D gold islands on graphene moire/Ru(0001). *Faraday Discuss.* **152**, 267 (2011)
24. Preobrajenski, A.B., Ng, M.L., Vinogradov, A.S., Mårtensson, N.: Controlling graphene corrugation on lattice-mismatched substrates. *Phys. Rev. B* **78**, 073401 (2008)
25. Wintterlin, J., Bocquet, M.L.: Graphene on metal surfaces. *Surf. Sci.* **603**, 1841–1852 (2009)
26. Sua, D.S., Perathoner, S., Centi, G.: Catalysis on nano-carbon materials: going where to? *Catal. Today* **186**, 1–6 (2012)
27. Planeix, J.M., Coustel, N., Coq, B., Brotons, V., Kumbhar, P.S., Utartre, R.D., Eneste, P.G., Ernier, P.B., Alayan, P.M.: Application of carbon nanotubes as supports in heterogeneous catalysis. *J. Am. Chem. Soc.* **116**, 7935 (1994)
28. Burghaus, U.: Gas-carbon nanotubes interactions: a review of surface science studies on CNTs. *Research Trends, Nova Science (New York)* (2009). ISBN 978-1-60692-236-1
29. Wehling, T.O., Katsnelson, M.I., Lichtenstein, A.I.: Adsorbates on graphene: Impurity states and electron scattering (review). *Chem. Phys. Lett.* **476**, 125–134 (2009)
30. Dresselhaus, M.S., Jorio, A., Saito, R.: Characterizing graphene, graphite, and carbon nanotubes by Raman spectroscopy. *Ann. Rev. Condens. Matter Phys.* **1**, 89–108 (2012)

31. Bostwick, A., McChesney, J., Ohta, T., Rotenberg, E., Seyller, T. Horn, K.: Experimental studies of the electronic structure of graphene. *Progr. Surf. Sci.* **84**, 380–413 (2009)
32. Smerieri, M., Celasco, E., Carraro, G., Lusuan, A., Pal, J., Bracco, G., Rocca, M., Savio, L., Vattuone, L.: Enhanced chemical reactivity of pristine graphene interacting strongly with a substrate: chemisorbed carbon monoxide on Graphene/Nickel(111). *ChemCatChem* **7**, 2328–2331 (2015)
33. Wang, Y., Shen, Y., Zhou, Y., Xue, Z., Xi, Z., Zhu, S.: Heteroatom-doped graphene for efficient NO decomposition by metal-free catalysis. *ACS Appl. Mater. Interfaces* **10**, 36202–36210 (2018)
34. Zebda, A., Sabbah, H., Ababou-Girard, S., Solal, F., Godet, C.: Surface energy and hybridization studies of amorphous carbon surfaces. *Appl. Surf. Sci.* **254**, 4980–4991 (2008)
35. Su, C., Loh, K.P.: Carbocatalysts: graphene oxide and its derivatives. *Acc. Chem. Res.* **46**, 2275–2285 (2013)
36. Singh, R., Scheinecker, D., Ludacka, U., Kotakoski, J.: Corrugations in free-standing. *Nanomaterials* **12**, 3562 (2022)
37. Chakradhar, A., Burghaus, U.: Adsorption of water on graphene/Ru(0001)—an experimental ultra-high vacuum study. *Chem. Commun.* **50**, 7698–7701 (2014)
38. Chakradhar, A., Sivapragasam, N., Nayakasinghe, M.T., Burghaus, U.: Support effects in the adsorption of water on CVD graphene: an ultra-high vacuum adsorption study. *Chem. Commun.* **51**, 11463–11466 (2015)
39. Chakradhar, A., Sivapragasam, N., Nayakasinghe, M.T., Burghaus, U.: Adsorption kinetics of benzene on graphene: an ultra-high vacuum study. *J. Vac. Sci. Technol., A* **34**, 021402 (2016)
40. Chakradhar, A., Trettel, K.M., Burghaus, U.: Benzene adsorption on Ru(0001) and graphene/Ru(0001)—How to synthesize epitaxial graphene without STM or LEED? *Chem. Phys. Lett.* **590**, 146–152 (2013)
41. Sivapragasam, N., Nayakasinghe, M.T., Burghaus, U.: Adsorption of n-butane on graphene/Ru(0001)—A molecular beam scattering study. *J. Vac. Sci. Technol., A* **34**, 041404 (2016)
42. Sivapragasam, N., Nayakasinghe, M.T., Chakradhar, A., Burghaus, U.: Effects of the support on the desorption kinetics of n-pentane from graphene: an ultra-high vacuum adsorption study. *J. Vac. Sci. Technol., A* **35**, 061404 (2017)
43. Sivapragasam, N., Nayakasinghe, M.T., Burghaus, U.: Adsorption kinetics and dynamics of CO₂ on Ru(0001) supported graphene oxide. *J. Phys. Chem. C* **120**, 28049–28056 (2016)
44. Pan, Y., Gao, M., Huang, L., Liu, F., Gao, H.J.: Directed self-assembly of monodispersed platinum nanoclusters on graphene Moiré template. *Appl. Phys. Lett.* **95**, 093106 (2009)
45. Stach, T., Seif, A., Ambrosetti, A., Silvestrelli, P.L., Burghaus, U.: Enhancing the reactivity of clean, defect-free epitaxial graphene by the substrate—experiment and theory. *J. Vac. Sci. Technol., A* **41**, 062201 (2023)
46. Waugh, K.C.: *Catal. Today* **53**, 161 (1999)
47. Stach, T., Seif, A., Ambrosetti, A., Silvestrelli, P.L., Burghaus, U.: Adsorption and reaction of thiophene on graphene/ruthenium—experiment and theory. *J. Phys. Chem. C* (2024) in press.
48. Li, T., Zhang, H., Li, Y., Li, J., Wang, J., Xiao, J.: Theoretical study on the unimolecular pyrolysis of thiophene and modeling. *ACS Omega* **6**, 20471–20482 (2021)
49. Navarro, J.J., Pizarra, M., Nieto-Ortega, B., Villalva, J., Ayani, C.G., Díaz, C., Calleja, F., Miranda, R., Martín, F., Pérez, E.M. Parga, A.L.V.D.: Graphene catalyzes the reversible formation of a C–C bond between two molecules. *Sci. Adv.* **4**, eaau9366 (2018)

3D Graphene: A Nanocarbon Innovation in Electrochemical Sensor Technology



Sahar Foroughirad, Behnaz Ranjbar, and Zahra Ranjbar

Abstract Nanocarbons, a diverse category of nanoscale carbon materials, have transformed scientific and industrial fields. Graphene, a remarkable nanocarbon, stands out due to its exceptional mechanical, electrical, and thermal properties. Three-dimensional (3D) graphene, with greater surface area and conductivity than its 2D counterpart, has gained recent popularity. In electrochemical sensing, the key component is the electrochemical electrode, driving chemical reduction reactions and generating signals. 3D graphene-based structures, featuring tailored meso- and micropores, offer interconnected hierarchical architectures, high surface area, intrinsic electrical conductivity, and a high signal-to-noise ratio, making them ideal electrochemical sensors. Two main fabrication strategies produce 3D graphene: 3D graphene aerogels and 3D graphene foams, each suited for different applications. Graphene foam's interconnected structure finds uses in electrochemical biosensors, adsorbents, supercapacitors, strain sensors, flexible electronics, space vehicle protection, EMI and microwave shielding, dampers, thermal interface materials, and flame-resistant materials. Incorporating nanomaterials like magnetite, doped elements, carbon nanotubes, and MXenes enhances these graphene-based structures. This chapter explores modification methods and applications of various 3D graphene-based structures as electrochemical sensors and offers insights into future synthesis and application prospects.

Keywords Nanocarbons · 3D graphene · Electrochemical sensor · Aerogel · Carbon nanotubes

S. Foroughirad

Faculty of Polymer Engineering, Sahand University of Technology, 51335-1996 Tabriz, Iran
Borna Chemi Arya Knowledge-Based Co., 5197817169 Tabriz, Iran

B. Ranjbar

Radsys Pooshesh Knowledge-Based Co, 1668836471 Tehran, Iran

Z. Ranjbar (✉)

Faculty of Surface Coating and Novel Technologies, Institute for Color Science and Technology,
1668836471 Tehran, Iran
e-mail: ranjbar@icrc.ac.ir

1 Introduction

Nanocarbons represent a diverse and fascinating class of carbon-based materials on the nanoscale. These materials, encompassing fullerenes, carbon nanotubes, graphene, and other carbon allotropes, have become a central focus in the field of nanotechnology. Their unique properties, such as high surface area, mechanical strength, and electrical conductivity, have paved the way for groundbreaking applications in various fields, including electronics, energy storage, and sensing. Among the various forms of nanocarbons, graphene has emerged as a particularly promising material. As a single layer of carbon atoms arranged in a two-dimensional honeycomb lattice, graphene exhibits high flexibility, remarkable electrochemical stability, significant specific surface area, and three-dimensional porosity, leading to high mass transfer rates and storage capacity [1]. Graphene-based nanomaterials can be synthesized in various dimensions, such as quantum dots (0D), nanofibers (1D), nanosheets (2D), and 3D stacks and gels with tailored properties. The pure graphene's thermal conductivity, attributed to its hole structure, sets it apart from other derivatives like graphene oxides. Classifying graphene as metal, semi-metal, or non-metal remains a challenge, but it best fits the semi-metal structure due to its low band gaps [2].

3D graphene nanostructures, a specific form of nanocarbon, have exceptional properties for application in electronic devices, overcoming drawbacks faced with other graphene-based materials. Issues such as low storage capacity, high agglomeration tendency in solvents, and the zero-gap nature of graphene as a semi-metal can be successfully addressed by employing 3D graphene structures [1]. The most common method for preparing 3D graphene involves stacking 2D graphene nanosheets. The resulting 3D graphene possesses low density, high mechanical and thermal properties, high specific surface area, and well-distributed porosity. Various types of 3D graphene structures, such as graphene foams, aerogels, and core-shell structures, have been developed according to research [2].

While the synthesis methods for 3D graphene structures are discussed in previous chapters, this chapter will focus on the applications of 3D graphene-based structures in fields like fuel cells, batteries, supercapacitors, biomedical, separation, solar cells, etc. Specifically, we will review different components of an electrochemical sensor and their fabrication procedures, followed by the application of 3D graphene nanomaterials in electrochemical sensors. A detailed discussion will be provided on the related reaction mechanisms of 3D graphene nanostructures as a component in electrochemical sensors.

2 Electrochemical Sensors

The electrochemical sensing technique is remarkably considered a promising technique in sensor fabrications. Electrochemical sensors can be fabricated at low cost, with simple instruments and can provide rapid response, with high sensitivity and

selectivity. These sensors are capable of analyzing various species including organic/inorganic structures, metallic compounds, ions, and neutral species [3]. Conventional electrodes which were fabricated with no modifications, had many drawbacks in application. They showed no signals at low concentrations as they had low sensitivity and they usually displayed broad peak by which the analysis of samples with close potentials together, were almost impossible [4]. In the last decade, the modification of conventional electrodes put a spotlight on employing electrochemical sensing techniques as a promising candidate in various applications. The modifications are most often carried out by the incorporation of nanostructures into the as-prepared electrodes. These modified electrodes can possess fascinating characteristics such as high sensitivity and selectivity, low production cost, fast detection, and accurate quantification analysis of the target molecule [3]. Metallic nanowires, non-metallic nanomaterials, nanostructured polymers, carbon nanotubes, and graphene-based structures are the most applicable nanostructures in electrode modifications.

3 3D Graphene-Based Electrochemical Sensors

2D graphene structures, known as graphene nanosheets, are one of the hottest topics in the field of electrochemical sensing due to their characteristic properties. high specific surface area of about $2630 \text{ m}^2 \text{ g}^{-1}$, tremendous electrical conductivity of 200 S m^{-1} , mechanical and thermal durability, and good chemical resistance are some of the most critical properties of 2D graphene nanosheets [5]. However, some drawbacks were faced while employing 2D graphene structures. The high agglomeration tendency of the nanosheets is considered the most practical issue of these nanostructures. Due to π - π interactions, 2D nanosheets are highly attracted toward agglomeration which dramatically decreases the specific surface area and thus the electron transfer efficiency of the structure.

Fabrication of 3D graphene nanostructures can effectively overcome the aforementioned issue, leading to structures with high specific surface area and fascinating conductivity which facilitates electron transfer leading to quick and accurate sensing of the target molecule [6]. For example, El-Kady et al. [7], could prepare an electrode for the high specific surface area of $1520 \text{ m}^2 \text{ g}^{-1}$ with the aid of 3D graphene structures. For this purpose, they used the restacking technique as well as laser induction for reducing graphene and stacking them as a 3D structure. Moreover, Li et al. [8], could synergistically improve the electrode conductivity and capacity, by incorporating gold nanoparticles into the graphene network structure. The conductivity was reported to be enhanced by about two orders of magnitude, reaching more than 10^6 S m^{-1} . The graphene-based electrode sensitivity was reported to be improved by Araujo et al. [9]. The electrochemical sensor was employed for the detection of picric acid and the lowest detection limit for sensing was reported to be 0.48 mM . In another study, by Vanegas et al. [10], a novel electrochemical sensor was fabricated based on graphene structures for rapid, selective, and sensitive detection of biogenic amines. The detection limit was reported to be $11.6 \text{ } \mu\text{mol L}^{-1}$ and the response

time was measured to be about 7 s which makes the prepared electrode a promising candidate for applications in rapid sensing technology.

3.1 Geometrical Classifications of 3D Graphene-Based Structures

The various 3D graphene nanostructures are classified into two major groups, in this chapter, regarding their chemical structures: (1) Solo 3D structures of graphene and (2) Their hybrid structures with other nanomaterials such as magnetite nanoparticles, carbon nanotubes, and other metallic or polymeric nanostructures. The subgroups are then separated according to the geometrical structure of the final 3D nanomaterial.

3.1.1 Solo 3D Structures of Graphene

The 3D graphene nanostructures can be classified into 2 main groups regarding their synthesis procedures. Randomly oriented 3D porous structures are mainly prepared by self-assembly technique and hierarchical structures in which uniform 3D structures such as foams and sponges are obtained by the templating approach.

3.1.2 Crumpled Ball Structures of 3D Graphene

Graphene-based 3D hydrogels and monoliths can be fabricated with the aid of self-assembly techniques, which include hydrothermal, laser engraving, and chemical reduction approaches. In all of these strategies, the graphene-based 2D structure is physically or chemically treated to be assembled and prepared 3D nanostructure based on graphene nanosheets [5, 11]. The physical treatment and graving of the surface with laser-based approaches are fully discussed by Vivaldi et al. [12]. The surface of the electrode can be engineered by adjusting the laser properties. The radiation of UV laser pulses onto the polymeric surfaces such as polyimide, induces a local heat of about 1700 °C as well as pressure up to 500 mJ cm⁻². The high temperature and pressure can effectively break the available aromatic structure bonds (C = O, C–N, C–H, and C–O bonds) and make new graphene-based structures followed by gas release. Moreover, metallic salts such as FeCl₃ can be added to the resin precursor, for obtaining a 3D graphene structure with good conductivity and high specific surface area [12]. Ball-shaped 3D structures of graphene are highly attractive as in this structure, graphene 2D nanosheets are assembled onto a specific core structure, which limits their further aggregation issues. Moreover, these porous 3D structures can provide abundant surfaces for ion and molecule transportation which is a critical point for applications of electrochemical-based sensing devices or storage systems. The obtained 3D graphene-based balls and spheres can be employed in

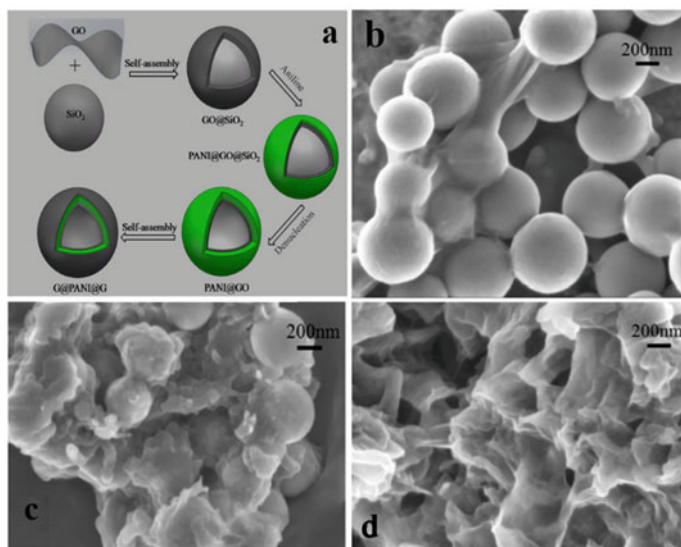


Fig. 1 a Schematic illustration of the synthesis procedure of G@PANI@G, SEM images of b GO@SiO₂, c PANI@GO@SiO₂ and d G@PANI@G. Adapted with permission [14], Copyright 2015, American Chemical Society

various devices in which the principal reactions are electrochemical ones including sensors, fuel cells, batteries, electrocatalytic reactions, etc. [13]. A robust ball-shaped core-double shell structure was reported by Liu et al. [14], the core and the outer shell were prepared with graphene, and the interlayer shell was designed to be polyaniline. The balls were prepared via a self-assembly approach. At first, GO@SiO₂ was synthesized by the Stober process, in the next step, surface modification was carried out to introduce amine to the surface of GO@SiO₂. The as-prepared polyaniline graphene oxide (denoted as PANI@GO) was added to the core mixture followed by the reduction of GO for obtaining G@PANI@G structure as represented in Fig. 1a. HF aqueous solution was employed for SiO₂ removal. SEM images at various stages of the fabrication are represented in Fig. 1b-d.

The obtained structure was reported to be resistant to shrinkage or swelling, with a high specific capacity of about 683 F g⁻¹ and outstanding cycling stability of about 93% after 1000 cycles, making it a promising candidate for electrode applications.

3.1.3 Hierarchical Structures of 3D Graphene

On the other hand, hierarchical 3D graphene structures including foams and sponges are usually obtained via templating strategies. In this method, a specific template is chosen, polystyrene beads for instance, on top of which the assembly of graphene nanosheets is carried out. The process is continued by the elimination of the template

molecule, leading to a highly porous 3D structure based on graphene [15]. The template approach mainly consists of 3 main steps: (1) the graphene oxides are assembled on top of the chosen template; (2) the 3D graphene is produced on the template via various chemical approaches including chemical vapor deposition (CVD), (3) the elimination of the template will result in 3D graphene-based structure with high porosity and specific surface area. As a typical example in this regard, Zhu et al. [16], has recently reported the fabrication of 3D graphene electrode for application in lithium-ion batteries. For this purpose, the commercial Ni foam was washed thoroughly with deionized (DI) water and acetone. To remove the oxidized layer of the foam, it was heated up to 900 °C under H₂ and Ar gases and then cooled down to the ambient temperature. The graphene layer was produced onto the treated Ni foam, via the CVD method. The 3D graphene foam was obtained by template removal. For this purpose, a diluted solution of nitric acid at about 45 °C was prepared and the foam was immersed in it. The elimination of Ni resulted in soft 3D graphene foam. The Ni commercial foam was also employed for further treatment to make a 3D hierarchical graphene structure with nanoholes. The procedure was carried out with the aid of a self-made instrument which is fully discussed in the article. The obtained sensor was characterized, and its electrochemical behavior was fully investigated. The current density was set to be 200 mA g⁻¹ and the cut-off voltage was 2 V. The discharge capacity for graphene Ni foam (denoted as G-NF) was measured to be 1700 mAh g⁻¹, which was much higher than Ni foam with no graphene coating. The bare graphene foam (GF) was obtained by the elimination of Ni. About 99.5% weight loss could make the free graphene foam, a promising candidate for applications in portable sensing devices. Moreover, by eliminating Ni, the inside pores of GF became accessible, leading to discharge capacity enhancement from 1700 mAh g⁻¹ to 2800 mAh g⁻¹. From the obtained results, it was obvious that the increase in graphene surface can influence the electrochemical performance of the obtained cathode. For a deep insight into this phenomenon, a graphene foam with expanded surface area (E-GF) was prepared by making hierarchical pores into the Ni foam, and by making nanoholes into the graphene layers (P-E-GF). These two treatments could effectively enhance the surface area and thus the discharge capacity of the cathode to 4300 mAh g⁻¹ and 7400 mAh g⁻¹, respectively.

3.1.4 Combined Strategies for Preparation of 3D Graphene

A new strategy based on the synergistic effect of self-assembly and templating was reported by Liu et al. [17]. In this article, a novel approach was introduced for the fabrication of graphene-based anode electrodes for Li and Na storage. For this purpose, the commercial Ni foam was immersed into the micro-sized GO suspension, followed by sonication for better diffusion of the suspension into the foam micropores. In the next step, the overnight dried foam was immersed into a specific mixture of nanosized GO and polystyrene beads with an average diameter of 0.5 μm. The etching procedure was then carried out to obtain free 3D graphene foam with graphene nanowires. The nanowires were obtained by self-assembly of nanosized

graphene onto the microsized interconnected graphene foam. Figure 2 represents the schematic illustration of the mentioned process as well as the SEM image of the prepared structure.

Electrochemical investigations were carried out to assess the quantitative performance of the prepared electrode. The results are represented in Fig. 3. The first discharge capacity of the anode was calculated to be 734.7 mAhg^{-1} at the rate of 0.1 C ($0.1 \text{ C} = 37.2 \text{ mAhg}^{-1}$). The next charge capacity was reduced to 545.6 mAhg^{-1} , as a result of solid electrolyte interface layer formation. The reversible capacity of the 3D graphene hierarchical structure with nanowires (abbreviated as 3DGNW) was compared to that of the 3D porous graphene structure (abbreviated as 3DPG). The results revealed that the fabrication of a hierarchical 3D structure can increase the transportation of Li ions and thus enhance the anode performance. The cycling stability of 3DGNW showed an increase up to the 400th cycle which remained unchanged at about 467 mAhg^{-1} during the next cycles to 1000 repeated cycles. The specific capacity was measured to increase continuously for 3DPG in all 1000 cycles. The increase in specific capacity during repeated cycles is a known phenomenon that is attributed to the formation of polymer film on top of the graphene surface. The results showed that this has no negative effect on the Li storage performance of the battery.

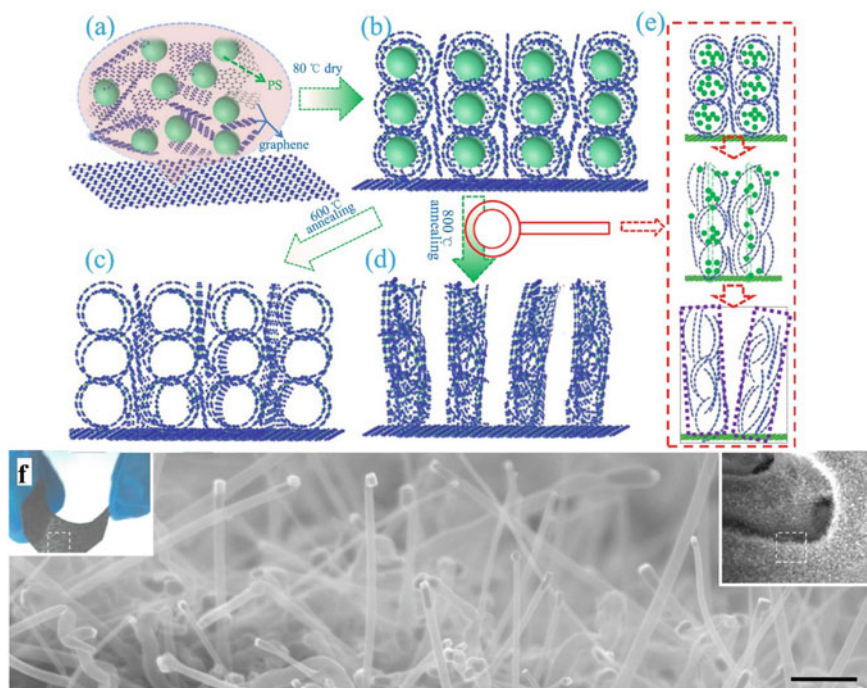


Fig. 2 Schematic representation of graphene nanowire fabrication. **a–e** and SEM image of 3D graphene nanowires **f**. Adapted with permission [17], Copyright 2017, Elsevier

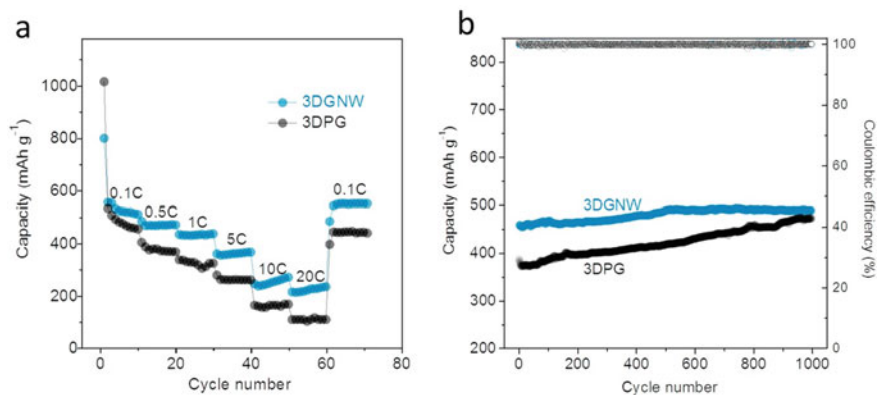


Fig. 3 lithium storage performance of 3D graphene nanowires. **a** Rate capability of 3DGNW and 3DPG at various C rates of 0.1, 1, 3, 5, 10, and 20 C. **b** Capacity retention of the 3DGNW and 3DPG electrodes at 1 C. Adapted with permission [17] Copyright 2017, Elsevier

3.2 Hybrid 3D Structures of Graphene

The functionality and chemical structure of the graphene nanostructures can be modified by incorporation of other nanostructures such as nanopolymers, iron oxide nanoparticles, carbon-based nanotubes, etc. This modification can be carried out during the reduction and assembly of the 2D nanosheets. This approach, simultaneous assembly and functionalization procedure, can result in functionalized hybrid hydrogels with fascinating properties [15]. The following will be a detailed discussion on modified graphene-based nanostructures.

3.3 Doped Structures of Graphene

Many elements such as Nitrogen and Boron and Cobalt are doped to graphene-based-3D nanostructures to enhance their catalytic and electrochemical performance. For instance, Jiang et al. [18], have synthesized graphene microspheres with hollow structures, in which Boron and Nitrogen were co-doped. The obtained structure was assessed for further application as an electrocatalyst of Oxygen Reduction Reactions (ORRs). The amino-modified SiO₂ nanoparticles with high porosity were employed as sacrificial templates. The GO was synthesized onto the surface of silica nanoparticles and then the homogeneous solution of NH₃BF₃ was added to the GO@SiO₂ core-shell structured mixture and the resultant suspension was hydrothermally treated for 12 h at 180 °C. A further calcination procedure was carried out to enhance the conductivity of the samples. The obtained structure was immersed in HF solution for the illusion of the silica template. The electrochemical performance

of the hollow spheres was assessed by cyclic voltammetry. For assessing the reactivity of the samples toward O_2 , the Oxygen or Nitrogen-saturated KOH solution with a concentration of 0.1 M was chosen. The difference between the two cyclic voltammetry curves of N_2 and O_2 suggested the specific attraction of the electrode toward oxygen. Other electrochemical analyses revealed that the obtained electrode can act more efficiently than the commercially available ones in ORRs. The N and B doped structures could enhance the adsorption of the Oxygen and the hollow structure provided higher available surface area to the electrolyte and thus reduce the overpotential of the ORRs. The fabricated electrode was reported to be a good candidate for further applications in fuel cells.

3.4 Graphene-Carbon Nanotube

Luo et al. [19], have recently reported the fabrication of a special 3D graphene structure, with a caterpillar shape, hybridized with carbon nanotubes (CNTs) to obtain a high-performance electrocatalyst. For this purpose, the 3D graphene oxide hydrogels with nanoscroll structure were obtained followed by the annealing at 750 °C for obtaining 3D graphene nanoscrolls. After that, by introducing ethane gas to the mixture at the same temperature, the CNTs were prepared onto the 3D graphene structure via the CVD method. Co-MoSe₂-3D graphene@CNTs were prepared after that, with a facile solvothermal method. The various structures were denoted as Co-MoSe₂-GNS@CNT-y (y = 1, 2, 3, 4) according to the various amounts of MoSe₂, from about 71 wt% to 87 wt%, respectively. Moreover, various amounts of Co were doped onto the structure which was represented by zCo-MoSe₂-GNS@CNT (z = 1, 2, 3, 4) according to the Mo: Co molar ratios. For better attachment of Co-doped MoSe₂ onto the CNT brushes, Ni nanoparticles were employed and encapsulated into the tip of the CNT brushes. Figure 4 represents the schematic illustration of the step-by-step synthesis procedure and FESEM and TEM images of the 3D graphene-based nanostructure.

The goal of this research was to prepare a porous 3D structure for better electron transportation and the encapsulation of Ni nanoparticles could provide an effective surface for Co-MoSe₂ decoration and thus better electron traversing through CNTs resulting in lower catalytic energy barrier and more efficient hydrogen evolution reaction catalyst. Electrochemical investigations were carried out to assess the performance of the electrode kinetic and interface reactions., the Co-MoSe₂-GNS@CNT had the smallest Tafel slope, Fig. 5a, suggesting rapid discharge reaction in which the electrochemical desorption is the rate-limiting step. The hierarchical 3D graphene-based nanostructure was responsible for electron transfer rate enhancement. Moreover, the presence of 3D graphene@CNTs could increase the conductivity. The Co-MoSe₂-GNS@CNT nanocomposite showed the smallest semicircle in the Nyquist plots, Fig. 5b, with $R_{ct} = 3.2 \Omega$. This reveals the facile charge transfer between the electrolyte and electrocatalyst interface which improves the rate of the reaction.

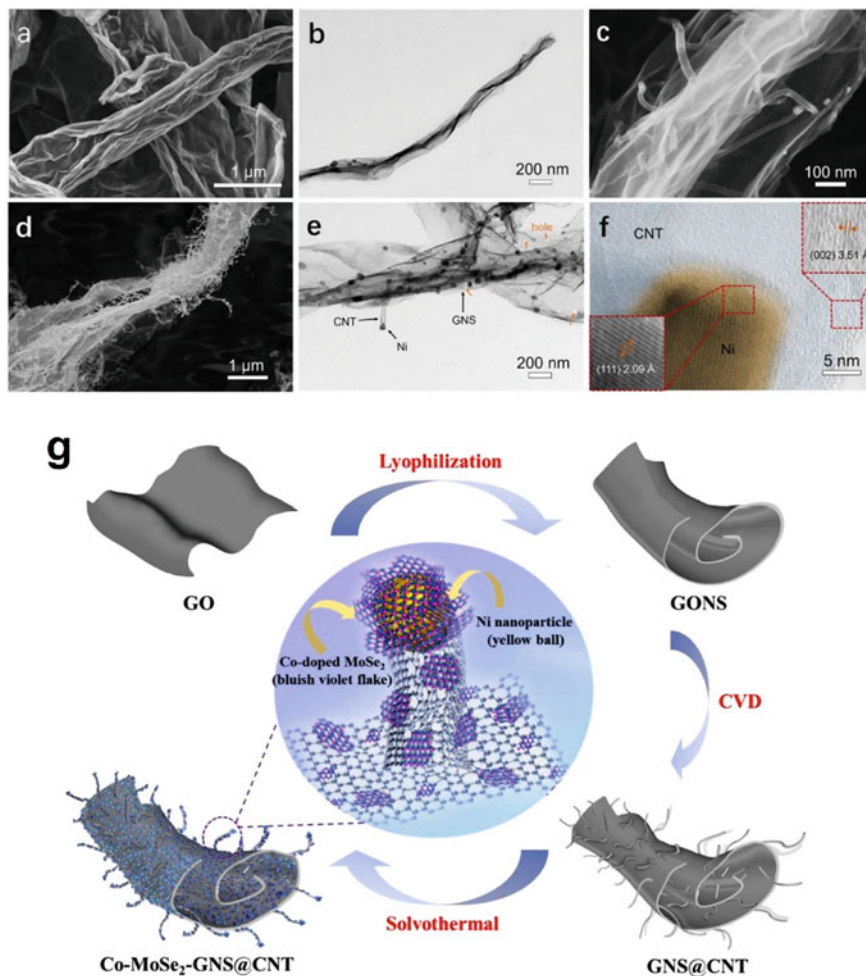


Fig. 4 TEM and FESEM images for: **a** and **b** GNS, **c–e** GNS@CNT, and HRTEM image of GNS@CNT. **g** Schematic illustration of the synthesis procedure for Co-MoSe₂-GNS@CNT. Adapted with permission [19], Copyright 2023, Elsevier

The unique 3D structure possessed excellent performance in both acidic and alkaline media, with high specific surface area with hierarchical pores which could effectively enhance the charge transfer and rate of the electrochemical reactions. This structure provided a new insight for preparing novel graphene-based-3D structures for electrochemical purposes including sensors and energy storage devices.

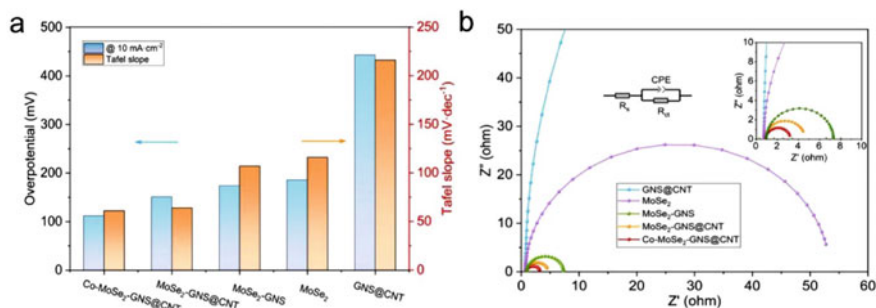


Fig. 5 a corresponding overpotential at 10 mAcm⁻² and value of the Tafel slope for different catalysts, b Nyquist plots. All measurements are in 0.5 mol L⁻¹ H₂SO₄. Adapted with permission [19], Copyright 2023, Elsevier

3.5 Graphene-Fe₃O₄

The incorporation of magnetic nanoparticles into graphene-based systems is one of the hottest topics these days. Magnetic nanoparticles such as magnetite (Fe₃O₄) can be introduced into the graphene via two main methods: *in-situ* and *ex-situ* synthesis methods [20]. In the *ex-situ* method, the magnetite and the graphene-based structure are synthesized, separately, and then the final composite is prepared via mechanical mixing, solvothermal methods, or other grafting approaches. On the other hand, in the *in-situ* method, the magnetite nanoparticles are synthesized directly onto the graphene nanosheets, making a seeded nanosheet structure. In a typical example of an *in-situ* approach carried out by Cong et al. [21], ferrous ions were employed for the *in-situ* reduction of graphene oxide and then the Fe₃O₄ nanoparticles and α-FeOOH nanorods were directly synthesized onto the graphene nanosheets. In this study, FeSO₄ salt was added to the graphene oxide suspension at 90 °C in an oil bath, after the first hour, the black floating resultant was observed which could be attributed to reduced graphene oxide. This was confirmed by XPS analysis in which the C-C bond peak was improved and the bonds containing O such as C=O and C-O were increased in intensity. With continuing the reaction, after 6 h, the black cylindrical hydrogel was prepared. The advantage of this method was that the scaling-up could be easily carried out resulting in the fabrication of 3D graphene hydrogel for further applications. In another study by Ershadi et al. [20], the *ex-situ* method was employed for the synthesis of amino-modified magnetite nanoparticles. The synthesized magnetic nanoparticles were then introduced to the 3D graphene framework. The results revealed that the electrodes based on magnetic 3D graphene have better electrochemical performance in comparison to bare Fe₃O₄ electrodes. Better nanoparticle distribution and less aggregation are responsible for this phenomenon. In this way, the rapid ion and electron transfer from GO to magnetite nanoparticles can increase the electrochemical performance, moreover, the higher porosity could be provided by the presence of magnetite nanoparticles leading to more surface of

contact between the electrolyte and the electrode and more available space for volume change in charge/discharge cycles.

Figure 6 represents the electrochemical performance of the optimum sample denoted as $\text{Fe}_3\text{O}_4\text{-E/rGO}$. The voltammograms of the sample at various rates and the calculation of the current constants are shown in Fig. 6a and b. The contribution for each supposed mechanism, diffusion-controlled reactions, and capacitive reactions, are calculated in Fig. 6c, and the percentage for each mechanism is measured, in Fig. 6d and e. At the cathode, reduction represented by peak A, about 90% of the produced current was due to the diffusion of the ions and the rest is provided by adsorption.

On the other hand, at the anode electrode, the oxidation denoted as peak B, especially at higher rates, the capacitive reactions become the most dominant mechanism leading to faster kinetic reaction in comparison to diffusion-controlled mechanism. The higher specific surface area and better porosity are responsible for this observation [20].

Zhao et al. [22], have reported the synthesis of hierarchical 3D structure based on magnetite nanoparticles and GO nanosheets. In this study, *in-situ* synthesis of Fe_3O_4 was carried out by which the magnetite nanoparticles were completely bonded to graphene oxide nanosheets, enhancing the specific surface area by mesoporous structure. The combination of magnetite mesoporous structure as well as macropores of rGO could synergistically improve the electrochemical performance of the composite. The specific capacity of the fabricated electrode was reported to be as

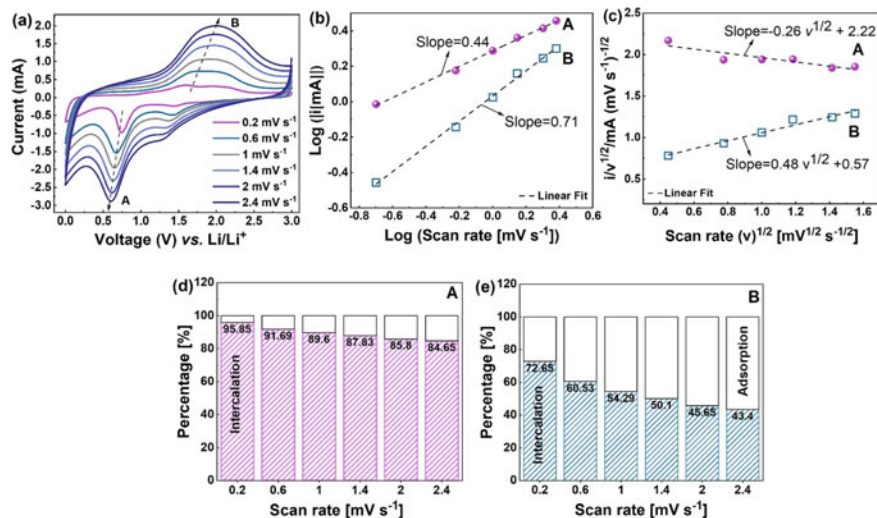


Fig. 6 a CV curves for $\text{Fe}_3\text{O}_4\text{-E/rGO}$ sample at various rates, b log–log plot for reduction and oxidation current peaks specific rates, c $\sqrt{i/v}$ dependence on the square root of scan rate, d and e percentage contribution for each proposed mechanisms of capacitive and intercalation reactions. Adapted with permission [20], Copyright 2022, Elsevier

high as 551 mAh g^{-1} after 2000 repeated cycles at a current density of 2 A g^{-1} . Further investigations through the dominant mechanism revealed that the capacitive reactions are the most effective mechanism, leading to fast ion and charge transfer through the electrode, making this nanocomposite a promising candidate for applications in lithium-ion batteries. In another study by Tian et al. [23], a novel 3D structure of graphene-based magnetite aerogel was prepared and then employed for lithium-ion storage applications. The N-doped graphene aerogel nanocomposite, abbreviated as $\text{Fe}_3\text{O}_4/\text{NGA}$, was prepared through the following steps: (I) The commercially prepared GO was obtained and incorporated for the synthesis of the nanocomposite. (II) The iron (III) phthalocyanine (FePc) and GO were both dispersed in deionized water. The weight ratio of FePc: GO was set to be 1:1, 1:1.5, and 1:2. The mixture was then heated at $180 \text{ }^\circ\text{C}$ for 12 h during which the GO was reduced to rGO, the Fe_3O_4 nanoparticles were synthesized in situ and the N element which was present in the phthalocyanine was assembled onto the rGO to make $\text{Fe}_3\text{O}_4/\text{N-doped rGO}$ aerogel. (II) For improved electrochemical performance, further annealing was carried out at $700 \text{ }^\circ\text{C}$ for three hours. The obtained 3D structure was employed as an anode electrode in lithium-ion batteries. The optimized sample, with a FePc: GO ratio of 1:1.5, revealed outstanding electrochemical performance and cyclic stability with a specific capacity of about 1185 mAh g^{-1} at a current density of 1 A g^{-1} after 500 continuous charge/discharge cycles.

There are many similar studies in which the graphene oxide properties are improved by the incorporation of magnetite nanoparticles onto the graphene aerogel. Other properties rather than electrochemical performance can be thermal, mechanical, catalytic, etc. Jalaly et al. [24], could improve the thermal and mechanical performance of 3D graphene-based structures by introducing Fe_3O_4 nanoparticles into the system. Magnetite nanoparticles at various contents, 0–30 wt.%, were encapsulated into graphene nanosheets via the ex-situ method. The compressive strength of 6.85 kPa could be obtained at 20 wt.% of Fe_3O_4 and the best mechanical strength was obtained at 10 wt.% of Fe_3O_4 . Liu et al. [25], could also report the successful synthesis of 3D graphene structure with magnetite incorporation, for better catalytic performance. Highly active Fe_3O_4 sites could effectively improve charge and mass transfer through the composite. The most applicable achievement of this research was limiting the metal-leaching issue which was faced when metal–organic frameworks are employed.

3.6 Graphene-MXene

MXenes, as a two-dimensional material, have recently attracted a lot of interest because of their unique electrical, chemical, and physical properties such as high hydrophilicity, thermal stability, surface area, and electrical conductivities, being environmentally friendly and unique layered morphology. Due to these characteristics, they are appropriate for electronic applications, catalysis, and energy storage devices. Their structure contains carbonitrides, nitrides, or metal carbides which

are added to two-dimensional nanomaterials groups. MXenes general formula is $M_{n+1}X_nT_x$, i.e., n is an integer between 1–3 and T is surface functional groups ($-F$, $-OH$ and $=O$). In MXene, M represents various transition metals like Mo, Cr, Nb, Ti, Sc, V, etc., and X represents nitrogen and/or carbon. Calcination and alkalization treatment can also be carried out to make changes to the functional groups based on the nature of the application. The number of MXenes is being expanded with increasing various synthetic methods and they are highly employed for fabrication of hybrid 3D graphene-based nanostructures. Gu et al. [26], synthesized a three-dimensional hybrid film based on graphene and MXene ($Ti_3C_2T_x$) via a simple mixing drying technique as an electrochemical biosensor to be used in glucose sensing. The pore size is an important parameter for immobilizing the enzymes and of course biosensing performance. They tuned the internal pore sizes by changing in MXene and graphene ratios. The more graphene content, the more porous the structure. It was shown that the 1:2 and 1:3 ratio in MXene: graphene showed better sensing results. In another research work, Feng et al. [27], also made a three-dimensional glucose sensor based on graphene, $Ti_3C_2T_x$ MXene, and gold nanoparticles. They used self-reduction and mixing-freeze-drying methods to build a carrier for the immobilization of glucose oxides for better sensing efficiency. As we mentioned before, the pore size has a great influence on sensing performance. Just like Gu et al. [26], they also controlled the pore's structure by changing the MXene to graphene ratio. Adding gold nanoparticles can reduce the redox potential and increase the electron transport efficiency along with the porous sensor structure. The sensor they made showed a good and repeatable sensitivity at $2 \mu M$ until 0.4 mM glucose concentration equal to $169.49 \mu A/(mM \cdot cm^2)$. This sensor can be potentially applied in biochemistry, drug analysis, and clinical diagnostics. Ma et al. [28], made a highly conductive porous aerogel material based on reduced graphene oxide and MXene. These two important properties made the composite a good candidate to be used as a pressure sensor. The sensor they made showed high repeatability over 10,000 times, below 200-ms response, and high sensitivity around 22.5 kPa^{-1} . A Ti_3C_2 MXene/graphene oxide nanocomposite was synthesized by Zheng et al. [29]. They applied this nanocomposite for making inkjet-printed hydrogen peroxide biosensors. They showed that their printable nanocomposite showed outstanding electrochemical sensing properties.

In another research work, Xie et al. [30], made an electrochemical sensor based on MXene and reduced graphene oxide (rGO) for carbendazim sensing. They used rGO to enhance the sensing performance of MXene. Carbendazim or methylbenzimidazol-2-ylcarbamate is a broad-spectrum benzimidazole fungicide and can be considered a toxic material. This material is widely utilized in seed, soil, and foliar treatment. It could be harmful to human health even in low amounts. Accordingly, the determination of carbendazim in vegetables and fruits is very important. The authors showed that MXene/graphene composite can be used as a reliable candidate as a carbendazim sensor. They utilized graphene as spacers in MXene sheets. Graphene spacers isolate the sheets and prevent them from restacking leading to an elevation in the interlayer spacing between MXene layers. It leads to an increase in structural robustness, electrical conductivity, and specific capacities.

The MXene nanosheet which is a water-soluble two-dimensional substrate inhibits graphene aggregation. The sensor that they made showed a low limit of detection (LOD) of about 0.67 nM and a linear and wide sensing range between 2 nM and 10 μ M. They checked their laboratory outcomes with the actual orange juice and cucumber samples and got reliable results. Aziz et al. [31], reviewed the effect of wearable sensors based on graphene and MXene on the environment. Because of their high electrocatalytic activity and surface area, they can be utilized in biochemical and biophysical sensors. They mentioned that although MXene and graphene have perfect sensing performance, their environmental impacts, biological toxicity, and biocompatibility need more investigation, especially in in-vivo studies.

Wang et al. [32], who proposed a roadmap for the future of MXene-based materials, introduced graphene/MXene composite, a candidate to be used in biosensors. On the other hand, Mostafavi et al. [33], specially reviewed the applications of MXene/graphene in biomedical and electrochemical biosensors. They believed that these kinds of sensors show low detection limit, fast response time (just about 15 ms to be recovered), high stability and performance. Liu et al. [33], synthesized a three-dimensional aerogel based on MXene/rGO/SnO₂ by the hydrothermal process as an electrochemical sensor for the detection of formaldehyde. The sensor they made showed perfect reversibility, fast response/recovery rate, good selectivity, and linearity between 10 and 200 ppm. They attribute the high sensing efficiency to the presence of p-n junctions, their composition, and their special three-dimensional structure. Wang et al. [33], have recently made a flexible three-dimensional electrochemical sample based on MXene and graphene for sensing uric acid, dopamine, and ascorbic acid. They showed the proposed sensor could mention the amount of uric acid, dopamine, and ascorbic acid precisely with no overlap. Furthermore, it showed a good approach for the wearable continuous yet non-invasive monitoring system for human well-being. It is also washable-free, user-friendly, and skin-adaptable.

4 Future Perspective of 3D Graphene-Based Sensors

Electrochemical-based electrodes are highly employed in various fields including, energy storage devices, selective adsorption of analytes, fuel cells, etc. for assuring accurate measurement, traditional electrochemical sensors require the attachment and immobilization of the eluent, or analyte, to the surface of the electrode. This was time-consuming, and limited the activity of the analytes, specifically when the adsorbate was a bio-based species and also the reusability of the electrode was dramatically affected. New strategies are recently emerged in electrode fabrication, in which there is no need for the adsorbate to be immobilized. Homogeneous electrochemical sensors (HESs) are a new class of sensors in which there is no need for immobilization of the analyte [34].

HESs are a subcategory of electrochemical sensors that the accurate detection of the analyte quantity can be accrued with no immobilization. This detection lies on many strategies such as the change in configuration of the electroactive dye which

is attached to the electrode [35, 36], intercalation of the attached dyes [37], or the controlled release of the attached dyes into the homogeneous media by which high effective and accurate probe electrode can be fabricated for highly sensitive detection of analytes [38]. The aforementioned technique is a promising one for the fabrication of electrochemical sensors, for the detection of various analytes. The approach is facile, cost-effective, fast, and accurate, however, there is just a limited number of research that focused on this method, during the past few years. Homogeneous electrodes are fabricated for the detection of inhibitors [39], pesticides [40], heavy metal ions [41], antibiotics [42], and biomarkers [43]. Many strategies and applications were discussed in this chapter, for the synthesis and application of 3D graphene-based nanostructures, however, no research could be found on incorporation of 3D graphene-based structures in immobilized-free electrodes. Moreover, it seems that there is a gap in the fabrication of HESs for applications in fuel cells, batteries, and other storage devices. By employing the free-immobilization technique in the fabrication of 3D graphene-based electrodes, novel and highly effective electrochemical-based electrodes can be fabricated, which can open a new insight into the world of electrochemical sensors.

5 Conclusion

Exceptional properties such as electrical, mechanical, and thermal properties have put graphene under the spotlight of research. Compared with two-dimensional graphene-based materials, three-dimensional graphene-based structures have a more specific surface area and higher porosity, which means that more target molecules can be loaded onto the structure. Moreover, many factors such as contact resistance, aggregation, and restacking tendency can be controlled in 3D graphene leading to higher electrical conductivity in application. Electrode, as a critical part of the sensing system in electrochemical sensors, can be designed with the aid of 3D graphene-based nanostructures. For this purpose, a tailor-made architecture of 3D graphene with interconnected mesopores and micropores is incorporated into the electrode fabrication. The obtained electrode is reported to have outstanding properties including, high surface area, fast kinetic and mass transportation, intrinsic electrical conductivity, high sensitivity and selectivity, etc. making them a promising candidate for applications in various fields such as solar cells, storage devices, separation, biomedical and electrochemical sensors. Two main categories of 3D graphene structures are fully discussed in the chapter 3D structures which are prepared by self-assembly of graphene nanosheets, and hierarchical structures by which graphene-based foams and sponges are fabricated. Each aforementioned structure has its application, for example, foams and sponges are widely used in adsorbents, biosensing materials, flexible sensors, super-capacitors, strain sensors, aerospace vehicles, and flame-resistant materials. Various nanomaterials can be incorporated into the 3D graphene frameworks to enhance their properties. These nanomaterials can be named magnetite nanoparticles, carbon nanotubes, MXenes, and doped structures of graphene. By fabrication

of these hybrid structures, many new properties, such as magnetic response, can be introduced to the system. Moreover, already existing features such as mechanical and electrical conductivity, can be remarkably improved. This can guarantee the performance of the fabricated electrode in electrochemical sensing devices. In this chapter, we discussed strategies for the fabrication of various hybrid structures of 3D graphene-based nanomaterials, and some of the most highlighted research in each category were included for better insight. At the end, we took a look into the future perspective of electrochemical sensing materials and their new potentials, in synthesis and applications.

References

1. Wang, H., Yuan, X., Zeng, G., Wu, Y., Liu, Y., Jiang, Q., Gu, S.: Three-dimensional graphene-based materials: Synthesis and applications from energy storage and conversion to electrochemical sensor and environmental remediation. *Adv. Colloid Interface Sci.* **221**, 41–59 (2015)
2. Makwana, M.V., Patel, A.M.: Recent Applications and Synthesis Techniques of Graphene. *Micro Nanosyst.* **14**(4), 287–303 (2022)
3. Asadian, E., Ghalkhani, M., Shahrokhian, S.: Electrochemical sensing based on carbon nanoparticles: A review. *Sensors Actuators, B Chem.* **293**(April), 183–209 (2019)
4. Baig, N., Sajid, M., Saleh, T.A.: “Recent trends in nanomaterial-modified electrodes for electroanalytical applications”, *TrAC - Trends Anal. Chem.* **111**, 47–61 (2019)
5. Lu, L.: Recent advances in the synthesis of three-dimensional porous graphene and its applications in the construction of electrochemical (bio)sensors for small biomolecule detection. *Biosens. Bioelectron.* **110**(March), 180–192 (2018)
6. Xu, J., Wang, Y., Hu, S.: Nanocomposites of graphene and graphene oxides: Synthesis, molecular functionalization and application in electrochemical sensors and biosensors. A review. *Microchim. Acta* **184**(1), 1–44 (2017)
7. El-Kady, M.F., Strong, V., Dubin, S., Kaner, R.B.: Laser scribing of high-performance and flexible graphene-based electrochemical capacitors. *Science (80-.)*. **335**(6074), pp. 1326–1330 (2012)
8. Li, R.Z., Peng, R., Kihm, K.D., Bai, S., Bridges, D., Tumuluri, U., Wu, Z., Zhang, T., Compagnini, G., Feng, Z., Hu, A.: High-rate in-plane micro-supercapacitors scribed onto photo paper using: In situ femtolaser-reduced graphene oxide/Au nanoparticle microelectrodes. *Energy Environ. Sci.* **9**(4), 1458–1467 (2016)
9. de Araujo, W.R., Frasson, C.M.R., Ameku, W.A., Silva, J.R., Angnes, L., Paixão, T.R.L.C.: Single-Step reagentless laser scribing fabrication of electrochemical Paper-Based analytical devices. *Angew. Chemie - Int. Ed.* **56**(47), 15113–15117 (2017)
10. Vanegas, D.C., Patiño, L., Mendez, C., de Oliveira, D.A., Torres, A.M., Gomes, C.L., McLamore, E.S.: Laser scribed graphene biosensor for detection of biogenic amines in food samples using locally sourced materials. *Biosensors* **8**(2), 42 (2018)
11. Tehrani, F., Bavarian, B.: Facile and scalable disposable sensor based on laser engraved graphene for electrochemical detection of glucose. *Sci. Rep.* **6**(June), 1–10 (2016)
12. Vivaldi, F.M., Dallinger, A., Bonini, A., Poma, N., Sembranti, L., Biagini, D., Salvo, P., Greco, F., Di Francesco, F.: Three-Dimensional (3D) Laser-Induced graphene: structure, properties, and application to chemical sensing. *ACS Appl. Mater. Interfaces* **13**(26), 30245–30260 (2021)
13. Nazarian-Samani, M., Kim, H.K., Park, S.H., Youn, H.C., Mhamane, D., Lee, S.W., Kim, M.S., Jeong, J.H., Haghight-Shishavan, S., Roh, K.C., Kashani-Bozorg, S.F., Kim, K.B.: Three-dimensional graphene-based spheres and crumpled balls: Micro- and nano-structures, synthesis strategies, properties and applications. *RSC Adv.* **6**(56), 50941–50967 (2016)

14. Liu, X., Wen, N., Wang, X., Zheng, Y.: A High-performance hierarchical graphene@polyaniline@graphene sandwich containing hollow structures for supercapacitor electrodes. *ACS Sustain. Chem. Eng.* **3**(3), 475–482 (2015)
15. Li, C., Shi, G.: Three-dimensional graphene architectures. *Nanoscale* **4**(18), 5549–5563 (2012)
16. Zhu, X., Wu, Y., Wang, Z., Wang, Y., Man, Z., Wen, X., Lv, Z., Wang, X.: Hierarchical architecture: A novel, facile and cost-efficient strategy to boost electrochemical performance of Li-O₂ battery cathodes. *Chem. Eng. J.* **450**(P4), 138462 (2022)
17. Liu, X., Chao, D., Su, D., Liu, S., Chen, L., Chi, C., Lin, J., Shen, Z.X., Zhao, J., Mai, L., Li, Y.: Graphene nanowires anchored to 3D graphene foam via self-assembly for high performance Li and Na ion storage. *Nano Energy* **37**(February), 108–117 (2017)
18. Jiang, Z., Zhao, X., Tian, X., Luo, L., Fang, J., Gao, H., Jiang, Z.J.: Hydrothermal synthesis of boron and nitrogen codoped hollow graphene microspheres with enhanced electrocatalytic activity for oxygen reduction reaction. *ACS Appl. Mater. Interfaces* **7**(34), 19398–19407 (2015)
19. Luo, H., Gao, H., Zhang, X., Yang, F., Liu, C., Xu, K., Guo, D.: Caterpillar-like 3D graphene nanoscrolls@CNTs hybrids decorated with Co-doped MoSe₂ nanosheets for electrocatalytic hydrogen evolution. *J. Mater. Sci. Technol.* **136**, 43–53 (2023)
20. Ershadi, M., Javanbakht, M., Brandell, D., Ahmad Mozaffari, S., Molaei Aghdam, A.: Facile Synthesis of Amino-functionalized Mesoporous Fe₃O₄/rGO 3D Nanocomposite by Diamine compounds as Li-ion Battery Anodes. *Appl. Surf. Sci.*, **601**, p. 154120 (2022)
21. Cong, H.P., Ren, X.C., Wang, P., Yu, S.H.: Macroscopic multifunctional graphene-based hydrogels and aerogels by a metal ion induced self-assembly process. *ACS Nano* **6**(3), 2693–2703 (2012)
22. Zhao, P., Jiang, L., Li, P., Xiong, B., Zhou, N., Liu, C., Jia, J., Ma, G., Zhang, M.: Tailored engineering of Fe₃O₄ and reduced graphene oxide coupled architecture to realize the full potential as electrode materials for lithium-ion batteries. *J. Colloid Interface Sci.* **634**, 737–746 (2023)
23. Tian, L., Xie, Y., Lu, J., Hu, Q., Xiao, Y., Liu, T., Davronbek, B., Zhu, X., Su, X.: Self-assembled 3D Fe₃O₄/N-Doped graphene aerogel composite for large and fast lithium storage with an excellent cycle performance. *J. Electroanal. Chem.* **922**(June), 116763 (2022)
24. Jalaly, M., Hosseini, R., Bakhshi, A., Chehelamirani, M.: Self-assembly synthesis of 3D graphene/nano-Fe₃O₄ hybrid aerogels with improved mechanical and thermal properties. *J. Alloys Compd.* **902**, 163718 (2022)
25. Liu, M., Liu, Y., Liu, X., Chu, C., Yao, D., Mao, S.: Peroxydisulfate activation by 2D MOF-derived Ni/Fe₃O₄ nanoparticles decorated in 3D graphene oxide network. *Sep. Purif. Technol.* **301**(May), 121967 (2022)
26. Gu, H., Xing, Y., Xiong, P., Tang, H., Li, C., Chen, S., Zeng, R., Han, K., Shi, G.: Three-Dimensional porous Ti₃C₂T_x MXene–Graphene hybrid films for glucose biosensing. *ACS Appl. Nano Mater.* **2**(10), 6537–6545 (2019)
27. Feng, L., Qin, W., Wang, Y., Gu, C., Li, X., Chen, J., Chen, J., Qiao, H., Yang, M., Tian, Z., Yin, S.: Ti₃C₂T_x MXene/Graphene/AuNPs 3D porous composites for high sensitivity and fast response glucose biosensing. *Microchem. J.* **184**, 108142 (2023)
28. Ma, Y., Yue, Y., Zhang, H., Cheng, F., Zhao, W., Rao, J., Luo, S., Wang, J., Jiang, X., Liu, Z., Liu, N., Gao, Y.: 3D synergistical MXene/Reduced graphene Oxide aerogel for a piezoresistive sensor. *ACS Nano* **12**(4), 3209–3216 (2018)
29. Zheng, J., Diao, J., Jin, Y., Ding, A., Wang, B., Wu, L., Weng, B., Chen, J.: An inkjet printed Ti₃C₂-GO electrode for the electrochemical sensing of hydrogen peroxide. *J. Electrochem. Soc.* **165**(5), B227 (2018)
30. Xie, Y., Gao, F., Tu, X., Ma, X., Xu, Q., Dai, R., Huang, X., Yu, Y., Lu, L.: Facile synthesis of MXene/Electrochemically reduced graphene oxide composites and their application for electrochemical sensing of carbendazim. *J. Electrochem. Soc.* **166**(16), B1673 (2019)
31. Aziz, A., Asif, M., Ashraf, G., Iftikhar, T., Hussain, W., Wang, S.: Environmental significance of wearable sensors based on MXene and graphene. *Trends Environ. Anal. Chem.* **36**, e00180 (2022)

32. Wang, Q., Han, N., Shen, Z., Li, X., Chen, Z., Cao, Y., Si, W., Wang, F., Ni, B.-J., Thakur, V.K.: MXene-based electrochemical (bio) sensors for sustainable applications: Roadmap for future advanced materials. *Nano Mater. Sci.* **5**(1), 39–52 (2022)
33. Mostafavi, E., Irvani, S.: MXene-Graphene composites: a perspective on biomedical potentials. *Nano-Micro Lett.* **14**(1), 130 (2022)
34. Li, H., Qi, H., Chang, J., Gai, P., Li, F.: Recent progress in homogeneous electrochemical sensors and their designs and applications. *TrAC - Trends Anal. Chem.* **156**, 116712 (2022)
35. Feng, Z., Zhao, R.J., Lu, Z.H., Jia, L.P., Ma, R.N., Zhang, W., Shang, L., Xue, Q.W., Wang, H.S.: Construction of aptasensors for sensitive detection of 8-OH-dG based on a diffusion mediated electrochemiluminescence quenching effect. *Chem. Commun.* **56**(75), 11074–11077 (2020)
36. Ni, J., Lin, H., Yang, W., Liao, Y., Wang, Q., Luo, F., Guo, L., Qiu, B., Lin, Z.: Homogeneous electrochemiluminescence biosensor for the detection of RNase a activity and its inhibitor. *Anal. Chem.* **91**(22), 14751–14756 (2019)
37. Zhang, J., Wu, D.Z., Cai, S.X., Chen, M., Xia, Y.K., Wu, F., Chen, J.H.: An immobilization-free electrochemical impedance biosensor based on duplex-specific nuclease assisted target recycling for amplified detection of microRNA. *Biosens. Bioelectron.* **75**, 452–457 (2016)
38. Huang, X., Bian, X., Chen, L., Guo, L., Qiu, B., Lin, Z.: Highly Sensitive homogeneous electrochemiluminescence biosensor for alkaline phosphatase detection based on Click Chemistry-Triggered branched hybridization chain reaction. *Anal. Chem.* **93**(29), 10351–10357 (2021)
39. Ge, L., Hong, Q., Li, H., Li, F.: A laser-induced TiO₂-decorated graphene photoelectrode for sensitive photoelectrochemical biosensing. *Chem. Commun.* **55**(34), 4945–4948 (2019)
40. Qi, H., Li, H., Li, F.: Aptamer Recognition-Driven homogeneous electrochemical strategy for simultaneous analysis of multiple pesticides without interference of color and fluorescence. *Anal. Chem.* **93**(21), 7739–7745 (2021)
41. Ge, L., Hong, Q., Li, H., Liu, C., Li, F.: Direct-Laser-Writing of metal Sulfide-Graphene nanocomposite photoelectrode toward sensitive photoelectrochemical sensing. *Adv. Funct. Mater.* **29**(38), 1–10 (2019)
42. Wang, X., Dong, S., Gai, P., Duan, R., Li, F.: Highly sensitive homogeneous electrochemical aptasensor for antibiotic residues detection based on dual recycling amplification strategy. *Biosens. Bioelectron.* **82**, 49–54 (2016)
43. Chang, J., Wang, X., Wang, J., Li, H., Li, F.: Nucleic Acid-Functionalized Metal-Organic framework-based homogeneous electrochemical biosensor for simultaneous detection of multiple tumor biomarkers. *Anal. Chem.* **91**(5), 3604–3610 (2019)

Nanocomposites of Carbon for Dye-Sensitized Solar Cell Applications



Kulandai Velu Ramanathan, Vishnu Vardhana Chary, Shantikumar V. Nair, and Dhamodaran Santhanagopalan

Abstract Efforts to make low-cost photovoltaic devices are a major part of today's energy conversion research. The abundant, cheap, highly conductive, and easy-to-tune nature of carbon allotropes makes carbon-based nanocomposites more attractive to use in dye-sensitized solar cells (DSSC). DSSCs are photo electrocatalytic solar cells that have a device architecture involving a nanoparticulate electron transport layer (ETL) which accommodates an adequate quantity of photo-active dye molecules in their mesoporous morphology where the major transport is diffusion-based. Accession of carbon-based nanocomposite materials in the ETL matrix is well-researched as they enable linear electron transport pathways. Carbon-based nanocomposites are known for their conductivity and tunability in the regimes of work function and catalytic activities. Foremost research involves nanocomposites of carbon allotropes as a replacement for the high-cost traditional Platinum counter electrode used in DSSC devices for effective regeneration. In this chapter, we will provide insight into the application of various carbonaceous nanocomposite materials both in the photo-anode and counter electrodes of a DSSC.

Keywords Dye-sensitized solar cells · Carbon · Counter electrode · Electron transport layer · Composites

K. V. Ramanathan · V. V. Chary · S. V. Nair · D. Santhanagopalan (✉)
Amrita School of Nanosciences and Molecular Medicine, Amrita Vishwa Vidyapeetham,
Ponekkara, Kochi, Kerala—682041, India
e-mail: dsgopalan20710@aims.amrita.edu

© The Author(s), under exclusive license to Springer Nature Singapore Pte Ltd. 2024
R. K. Gupta (ed.), *NanoCarbon: A Wonder Material for Energy Applications*,
Engineering Materials, https://doi.org/10.1007/978-981-99-9935-4_8

139

1 Introduction

1.1 *Types of Nanocomposite Carbons*

1.1.1 Allotropes of Carbon

The importance of carbon in photovoltaic (PV) technologies stems from its diverse roles that elevate the effectiveness, stability, and economic viability of converting solar energy. Although carbon does not itself produce electricity within PV systems, its distinctive characteristics and uses assume pivotal functions. Being a cost-efficient and widely available resource, carbon plays a role in diminishing the production expenses of PV panels. Furthermore, its lightweight and flexible characteristics harmonize with the increasing need for adaptable and portable energy alternatives.

These materials act as conduits for charge transport and electrodes, effectively ferrying and accumulating charge carriers produced through photon absorption. Diverse carbon structures, encompassing fullerenes and carbon nanotubes (CNT) at the nanoscale, graphene, and graphene oxide (GO) at the microscale, and porous material like activated carbon or amorphous carbon (AC) at the macroscale display a distinctive capacity to support crucial functions within PV systems [1–3].

1.1.2 CNT-Based Nanocomposites

CNT are widely researched from the day it was found by accident. The characteristics of CNTs are very attractive as a low-cost component in multiple devices such as opto-electronic devices, nano-electronic devices, thermo-electric devices, energy storage devices, and many more. The use of CNTs helps charge transport in these systems due to CNT's high conductivity and unique one-dimensional transport pathways. As a composite with other materials like polymers, metal nanoparticles, and transition metal compounds, other properties of CNT like electrochemical activity, and defect sites can be engineered for tuneable activity. Researchers have used single-walled CNT (SWCNT), double-walled CNT (DWCNT), and multi-walled CNT (MWCNT) as a conducting interface between the electron transport layer and the front electrode in multiple solar cell device structures. High conductivity and surface area of CNTs are major attractions for the reduction process via catalytic methods in any electrochemical device. Thus, CNTs are combined with metal oxides like TiO_2 , SnO_2 , and ZnO vastly to improve their overall conductivity. The ability to accommodate other materials like polymers, nanoparticles, and bulk materials to form a composite makes it attractive as a counter electrode used in a DSSC [4].

1.1.3 Graphene and Graphene Oxide-Based Nanocomposites

Graphene is a 2-dimensional material with a thickness of a single atomic layer. Electrical conductivity and optical transmittance of graphene are well researched and have been used in multiple optoelectronic devices to reduce cost and increase performance. PV is one other field where graphene is actively being used to replace the existing component of a solar cell. As a sheet of carbon, graphene has a Dirac point bandgap and a smooth plane. Introducing oxygen in to the matrix of the unique honeycomb structure, GOs are formed. GO is a semiconducting material generally prepared via chemical methods using reagents such as KMnO_4 and subsequent reduction to prepare reduced graphene oxide (r-GO). Graphene and GO/r-GO have been used along with metal oxides, metal nanoparticles, polymers, and other carbon allotropes to form composites which are used in solar cell devices to improve charge transport properties and catalytic activities. Composites of graphene are used as a replacement for Pt counter electrodes used in DSSC devices. In a study, nanocomposites comprising ZnO, ZnO/rGO (with varying weight percentages of rGO in the composites: 0, 0.01, 0.1, 0.5, and 1%), and Sr-doped ZnO/rGO (with nanoparticle stoichiometry $\text{Zn}_{1-x}\text{Sr}_x\text{O}$: $x = 0, 0.02, 0.04, 0.06, \text{ and } 0.08$) were produced and examined for their performance as DSSCs. The $\text{Zn}_{0.92}\text{Sr}_{0.08}\text{O/rGO}$ -based DSSC achieved the highest values for both the short-circuit current density (J_{SC}) at 18.4 mA cm^{-2} and the efficiency (η) at 7.90% [5].

1.1.4 Amorphous Carbon-Based Nanocomposites

AC is a low-cost, most commonly available resource of carbon allotropes. Tuneable properties of AC like surface area and pore size play a vital role in its usage in various applications. AC can be categorized into three types such as macro, meso and microporous based on their porosity. The porosity of AC is tuned by varying the particle size and synthesis process. Nanoscale AC gives microporous structures when coated over a surface whereas bulk AC gives a macro-porous network. This interconnected matrix of AC helps in charge transport and the exceptional surface sites make AC one of the top contenders to platinum counter electrodes used in DSSCs [6].

1.1.5 Carbon Black-Based Nanocomposites

Carbon black (CB) is thermally stable material with a high corrosion resistance against liquid electrolytes. CB is actively used in energy storage and conversion devices due to its high conductivity and the nature to effectively collect charges from various functional materials. The use of CB in DSSCs is well studied, CB used as counter electrodes and as electrically active material in photo anodes are widely reported. The synthesis techniques used were different and a common conclusion from the literature shows CB layers with less than $10 \mu\text{m}$ thick counter electrodes

have higher performance than thicker layers. CB mixed with TiO_2 and other metal oxides, increases the J_{SC} of the device by efficiently collecting the photo-generated charges. Multiple composites of CB with transition metal compounds like TiN, SnO_2 , TiC, etc., metal nanoparticles, and other carbon allotropes were studied to replace Pt counter electrode in DSSCs [7].

1.1.6 Carbon Nanofoam Based Nanocomposites

Carbon nanofoam is a unique three-dimensional nano-structural variant of carbon. Within this nanofoam, carbon atoms are organized into a complex hexagonal arrangement that spans three dimensions. This intricate arrangement is frequently likened to that of aerogel. Notably, carbon nanofoam showcases exceptional attributes, including an expansive surface area and a visually transparent framework. The transformation of 2D graphene into a 3D graphene nanofoam network has yielded impressive improvements in solar cell efficiency. This advancement is particularly evident in the context of DSSCs based on graphene nanofoam. These DSSCs have been meticulously developed and scrutinized, with a focus on their environmental robustness, lack of toxicity, cost-effectiveness, and potential applicability for commercial purposes [8].

1.2 Dye-Sensitized Solar Cells

DSSCs are a part of third generation excitonic solar cells. The working principle of excitonic solar cells widely varies from a typical first- and second-generation solar cell. Unlike traditional single-junction solar cells, DSSCs work based on a bulk heterojunction structure. DSSCs are photo-electrochemical devices consisting of an organic light sensitizer to absorb the incoming photons and generate excitons. At the photoexcited state of the sensitizer, electrons are inserted into an n-type mesoporous network of a wide band gap nano particular semiconductor, and holes are regenerated by the redox reaction of a liquid electrolyte. These photo-generated charges are then availed by the electrodes. The electron transport mechanism in a DSSC is dependent on diffusion-based Brownian motions.

1.2.1 Architecture

The DSSC operates through a series of intricate steps that culminate in the conversion of sunlight into usable electrical energy. This process involves a careful orchestration of components and physical phenomena. The journey commences with the absorption of sunlight by organic dye molecules adsorbed to the surface of the semiconductor material used to transport the electrons generated through the photoexcitation process. Here the dye molecules act as a sensitizer with the ability to absorb solar

spectrum. The absorbed photons are then converted into excitonic pairs consisting of an electron in the conduction band and a hole in the valence band of the dye. These free electrons are injected into the conduction band of the semiconductor material, commonly titanium dioxide (TiO_2), forming the photoanode. The architecture of the DSSC facilitates the conduction of these separated electrons through the mesoporous structure of the semiconductor material [9].

In short, DSSCs follow a sandwich structure where the device is locked between a transparent conducting oxide (TCO) electrode (anode) and a counter electrode (cathode) to collect holes. It consists of an electron transport layer of wide bandgap nano particular n-type material coated in a mesoporous way, a light-sensitive organic dye to create excitons as a sensitizer, and an ionic electrolyte with a redox couple matching the LUMO of the organic dye. This electrolyte transports the photogenerated holes and is known as the hole transport layer (HTL). Finally, a counter electrode with high electrocatalytic activity to reduce the ionic electrolyte efficiently.

1.2.2 Photoanode or Electron Transport Layer (ETL)

At the core of a DSSC lies a comprehensive architecture that intricately orchestrates the conversion of sunlight into electrical energy. The journey begins with a TCO, often composed of materials like Fluorine-doped Tin Oxide (FTO) or Indium Tin Oxide (ITO). This TCO coated substrate serves as the foundation, allowing sunlight to penetrate while furnishing a conductive surface for the movement of electrons as the front electrode. All DSSC devices require an interfacial layer to adsorb the dye molecules and transfer the photo-generated electrons to the TCO electrode. This layer is called ETL or photoanode. Wide band gap oxide materials are the most preferred ETL used in any DSSC device. The most commonly used ETLs are TiO_2 , SnO_2 and ZnO nano particles. The dye molecules are adsorbed to the surface of these wide bandgap oxide semiconductors. To achieve high dye adsorption, a mesoporous nanoparticle network has been adopted as the standard structure for any material used as a photoanode.

1.2.3 Sensitizer

Sensitizers, at the heart of DSSCs, wield a critical role in the initial stages of solar energy conversion. These organic molecules are carefully chosen for their unique ability to interact with sunlight and facilitate the process of photon absorption. Their absorption maxima are fine-tuned to match AM1.5 solar spectrum to allow them to harness the incoming solar energy. Most commonly used light sensitizer in a DSSC device is an organic dye with a general structure of $\text{ML}_2(\text{X})_2$ where M corresponds to a Ruthenium metal, L corresponds to 2,2'-bipyridyl-4,4'-dicarboxylic acid and X represents a halide, cyanide, thiocarbamate and other suitable compounds. However, the ruthenium-based cis-bis (iso-thiocyanato)-bis (2, 2'-bipyridyl-4, 4'-dicarboxylato)

Ru (II) bis-tetrabutylammonium also known as N719 is used widely as the sensitizer. N719 dye has maximum photon absorption peaks at 380 nm and 518 nm in the visible spectrum of solar irradiance, making it one of the major contenders in both exterior and interior energy conversion fields. The field of sensitizers is vast and continuously evolving, with researchers exploring novel organic dyes, metal complexes, and other molecular structures to enhance efficiency and stability.

1.2.4 Ionic Electrolyte or Hole Transport Layer (HTL)

The performance of a solar cell depends on the balance between the movement of electrons and holes. If recombination occurs within the active layer, the energy generated by the photons is lost. An ionic liquid electrolyte (commonly I^-/I^{3-}) is introduced between the counter electrode and photoanode. As the photogenerated electrons are injected into the ETL layer, the positive counterparts of the excitons are accumulated in the dye molecule. This accumulation of holes in the dye leads to the degradation of the organic dye. The I^- ions of the redox couple are ready to be oxidized by effectively replacing the electrons in the HOMO of the dye. Whereas, the abundant I^{3-} ions are efficiently reduced by the counter electrode. This process of combining holes and electrons through the HTL is called regeneration and it plays a vital role in stabilizing a DSSC device. The choice of materials for the HTL is critical, they should have harmonized redox potential compatible with the specific dye used as the sensitizer.

1.2.5 Counter Electrode (CE)

The CE, also known as the cathode, plays a pivotal role in preventing a solar cell from charge exhaustion. CE is often made of high-work function metals to form an ohmic contact for hole transport. In the case of DSSCs, the use of liquid electrolytes implies that the CE should also possess high electrocatalytic activity and abundant active sites along with its superior conductivity to enhance the reduction reaction. Commonly used materials include metals like platinum (Pt), conductive carbon materials, conductive polymers, and conducting metal oxides. Developing counter-electrode materials that balance high catalytic activity, stability, and cost-effectiveness is an ongoing challenge in DSSC research. The device architecture was explained in Fig. 1 [10, 11].

1.2.6 Shortcomings of DSSCs

DSSCs, while holding promise as efficient solar energy conversion devices, are not without their limitations. These shortcomings impact their overall performance and practical viability for widespread adoption. However, the cost of production of a DSSC panel for commercial use is higher than other potential technologies due to

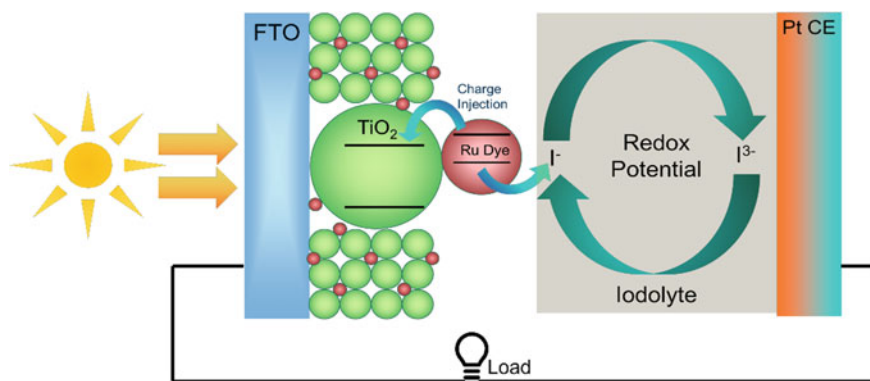


Fig. 1 Working principle of a DSSC

the use of Pt CE. Also, most of the injected charge carrier are typically lost in the mesoporous network of the photoanode due to diffusion-based transport. The lifetime of a free electron is much lower than the time it takes to reach the front electrode. These are the significant drawbacks of a DSSC along with their other limitations such as dye degradation upon over exposure, liquid electrolyte stability and reliability. This chapter discusses about how carbon allotropes are used to overcome these limitations of a DSSC conversion device.

2 Discussion

2.1 Electron Transport Layer (ETL)

Acting as a conduit for the efficient movement of electrons generated through the photoconversion process, the ETL assumes a critical function within the framework of a DSSC. Its intricate task of fine-tuning electron transport significantly contributes to ameliorating the cell's quantum efficiency, rendering it a paramount component in the intricate dance of photogenerated charges within the solar cell architecture. Current studies are underway to modify the physical chemistry of ETL constituents with the aim of enhancing the overall efficiency.

2.1.1 Nanocomposite CNT with TiO_2

Tae et al. successfully engineered DSSCs utilizing a novel approach involving the incorporation of TiO_2 -coated MWCNT (TiO_2 -CNTs) (Fig. 2). In contrast to a standard TiO_2 cell, the altered TiO_2 cell containing 0.1 wt.% TiO_2 -coated CNTs (TiO_2 -CNTs) exhibited a notable enhancement of approximately 50% in the conversion

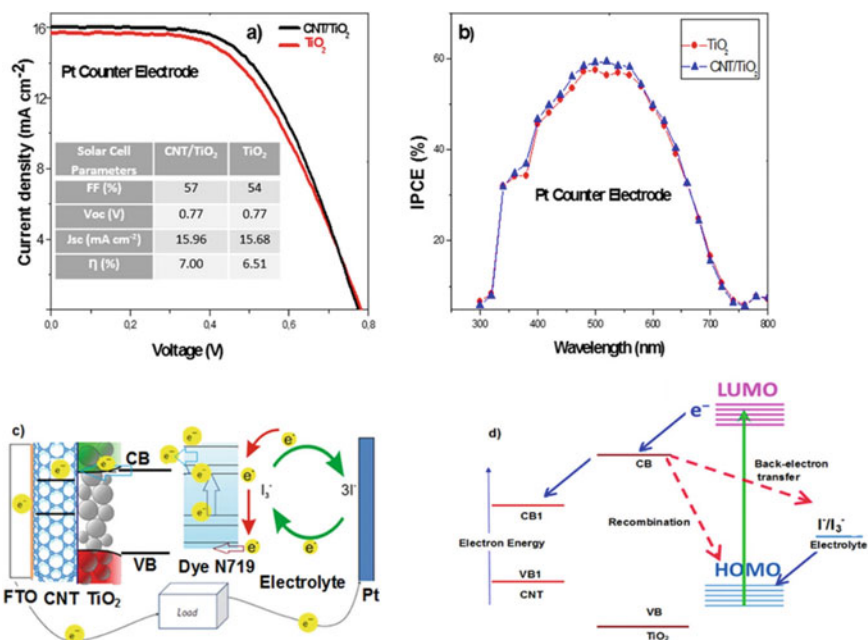


Fig. 2 **a** J-V characteristics, **b** Quantum efficiency, **c** DSSC schematics and **d** Band alignment diagram of DSSC device with CNT—TiO₂ photoanode. Adapted with permission [13]. Copyright 2016, Scientific Reports, Springer Nature. Adapted from reference [13]. Copyright Kilic, B. et al., some rights reserved; exclusive licensee [Scientific Reports, Springer Nature]. Distributed under a Creative Commons Attribution 4.0 International (CC by 4.0)

efficiency value. The increase in J_{sc} is attributed to the heightened interconnectivity observed between the TiO₂ particles and CNTs within the porous film. This phenomenon substantially improved the efficiency of electron transfer throughout the film within DSSCs [12].

Ghartavol and colleagues documented the construction of DSSCs utilizing photoanodes composed of TiO₂ and 1D core-shell structures formed by CNTs encapsulated TiO₂ (CTH). The primary responsibility for charge separation is predominantly assumed by TiO₂ in CTH structures, while the transport is taken care by CNT rods. An interesting observation emerges wherein the fill factor (FF) of the devices remains consistent between 61.9 and 62.1 although V_{oc} and J_{sc} exhibited an upward trend with an elevated CTH: TiO₂ ratio. The power conversion efficiency (PCE) of the devices exhibits fluctuations corresponding to alterations in the CTH: TiO₂ weight ratio attaining its peak value at 0.3 wt.% CTH concentration demonstrating an efficiency of 7.94% with 17.26 mA.cm⁻² J_{sc} . Consequently, the anticipated gains from the enhanced conductivity of CTH affect the dye adsorption in the TiO₂ structure. This reduction in dye adsorption has a detrimental influence on exciton generation. The findings elucidated the intricate relationship between material properties, charge

transport mechanisms, and the delicate balance that governs the efficiency of dye-sensitized solar cells [14]. This confirms the aid of CNTs in electron transport within the mesoporous matrix of photoanode.

2.1.2 Nanocomposite Graphene/r-GO and GO with TiO₂

The 2D layered material is attractive due to its surface transport abilities. Eshaghi et. al conducted a study involving TiO₂ photoanodes with 0.5, 1, 1.5, and 2 wt.% of graphene as a composite. The J_{SC} of the cells exhibited an incremental rise in tandem with the increasing graphene concentration. This ascent culminated in an apex value of 8.83 mA.cm⁻² at a graphene concentration of 1.5 wt.%. However, beyond this juncture, the J_{SC} experienced a downward trend, tapering off to 3.615 mA.cm⁻² as the graphene concentration escalated further to 2 wt.%. In contrast, the V_{OC} demonstrated a relatively stable behavior, with minimal variations observed across the range (0.61–0.68 V). The presence of graphene engenders a more facile pathway for electron mobility, leading to the initial surge in J_{SC}. However, as the graphene concentration exceeds an optimal threshold, the lack of dye adsorption and potential adverse interactions contribute to the subsequent downturn in J_{SC} [15]. Madhavan et.al, worked with graphene TiO₂ nanofibers-based photoanode to have a conformal presence of graphene sheets in the bulk of the ETL. They used an electrospinning approach to form graphene-incorporated TiO₂ and TiO₂/ZnO nanofibers, through this they achieved graphene embedded metal oxide fibers. The charge transport was improved with the addition of graphene and J_{SC} increased from 6.3 mA.cm⁻² to 9.4 mA.cm⁻² and from 13.9 mA.cm⁻² to 16.2 mA.cm⁻² and the devices attained PCEs of 7.6% [16, 17]. GO with the more oxygen groups made strong coupling with metal oxide semiconductors used in DSSCs. The presence of this coupling helped in better interfaces between TiO₂ and GO, minimizing the recombination loss. Research groups have achieved efficiencies of 7.83% with the use of commercial GO incorporated in the bulk of TiO₂ photoanode. The addition of GO into TiO₂ increases the overall pore volume and pore size of the photoanode film escalating the surface area. When dye adsorption of these films is characterized, it is found that TiO₂ films with GO have dye molecules up to 0.198 μmol.cm⁻² whereas pristine TiO₂ has only 0.122 μmol.cm⁻² adsorption. Nevertheless, the use of r-GO with few COO-bonds attached to the surface is more preferred for DSSC photoanodes than the pure graphene. Integration of r-GO with mesoporous TiO₂ increases the adsorption and aids in charge transport, unlike GO whose conductivity is less. PCEs of 11.8% are obtained by utilization of r-GO and 3D r-GO nanosheets in the photoanodes. This clearly displays the competency of r-GO with metal oxides as a superior photoanode for DSSC solar cells [18]. Fig. 3 (a-d) shows SEM images of the composites and (e & f) displays the device performance with CNF/G-TiO₂ composites [19].

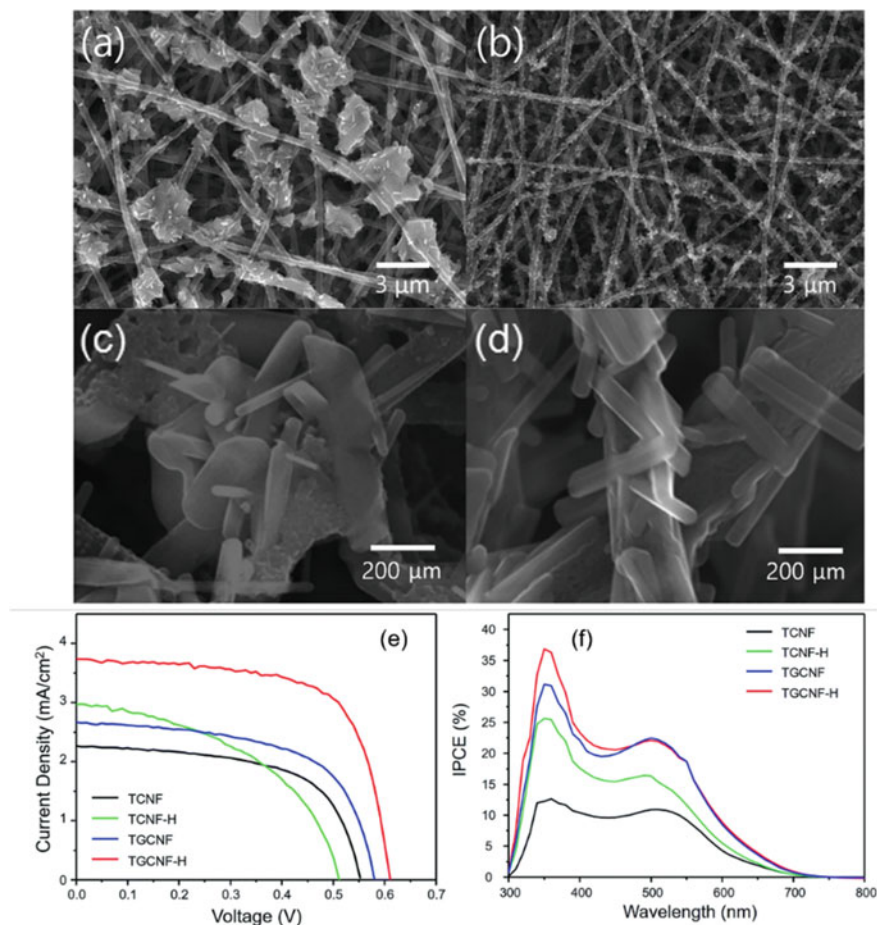


Fig. 3 a–d SEM images, e J–V characteristics, and f quantum efficiency of CNF with Graphene TiO₂ Composite Photoanode. Adapted with permission [19]. Copyright 2017, RSC Advances, RSC. Adapted from reference [19]. Copyright Lee, Hoik. et. al, some rights reserved; exclusive licensee [RSC Advances, RSC]. Distributed under a Creative Commons Attribution 3.0 (CC by 3.0)

2.1.3 Nanocomposite Fullerenes with TiO₂

In a study conducted by Hun and his team, they introduced a novel approach to enhance the efficiency of DSSCs by leveraging a specific fullerene derivative known as PC61BM (6,6-phenyl C₆₀ butyric acid methyl ester). This fullerene derivative, renowned for its electron-accepting properties, was strategically utilized for the surface modification of arrays of TiO₂ nanotubes. By integrating PC61BM onto the surface of TiO₂ nanotube arrays, the researchers aimed to optimize the electron transport and separation processes within the DSSCs. The inherent characteristics of PC61BM, including its excellent electron-accepting nature, make it a

suitable candidate for facilitating efficient charge transfer within the photoanode material. This approach holds significant potential for advancing the performance of DSSCs, as the tailored modification of the TiO₂ nanotube arrays with the fullerene derivative lead to enhanced electron mobility and reduced recombination of charge carriers. The incorporation of PC61BM onto the TiO₂ nanotube surface acts as a crucial step in enhancing the photoconversion efficiency, ultimately contributing to the overall effectiveness of the solar cell. The untreated samples and those coated with PC61BM were immersed in a solution containing 0.3 mM N719 dye dissolved in ethanol for 24 h. Following the immersion period, the samples were carefully washed with ethanol to remove any excess dye and ensure a controlled experimental condition. Pt-coated FTO glasses were employed as CEs in the experimental setup. The photoanode, which had absorbed the dye, and the Pt-coated FTO glasses were positioned with a separation achieved using a 60- μm surlyn film. The reduction in total resistance resulting from the PC61BM coating primarily stemmed from the reduction in charge transfer resistance occurring at the interface between the TiO₂ nanotubes and the liquid electrolyte and notably, the resistance at the interface of the counter electrode exhibited minimal change as a consequence of the PC61BM coating. Upon increasing the concentration from 3 mg/ml to 6 mg/ml, there was a concurrent decrease observed in both the J_{SC} from 5.47 mA/cm² to 5.06 mA/cm² and the PCE from 1.44% to 1.38%. The presence of the PC61BM interlayer led to an increase in the J_{sc} , indicating enhanced charge generation and transport. However, it was noted that the V_{oc} experienced a slight reduction with the introduction of the PC61BM interlayer [20].

2.2 Counter Electrode (CE)

Different allotropes of carbon in its pristine form are used as counter electrodes for DSSC devices. The electrocatalytic activity of carbonaceous materials makes them suitable as a counter electrode, however, the disadvantages have to be accounted. CNT as it is having a very high linear electrical conductivity with a large surface area is appropriate for electrolyte reduction, yet SWCNT and hollow structure MWCNT have smooth basal planes with fewer defects making them barely apt for electrocatalytic activity. Along with low catalytic activity, both SWCNT and MWCNT have a high packing fraction blocking the ions of the electrolyte from being reduced efficiently. Graphene and graphite are well known for their high surface area (2600 m²g⁻¹), electrical and thermal stability. Graphene is prone to oxygen vacancies and defects with amplified hole mobility and corrosive corrosive-resistant nature making it viable as a CE. Graphene demonstrates equivalent charge transfer resistance (R_{ct}) values compared to that of Pt and lower R_{ct} when doped with halogens like Cl, Br and I. With these reduced R_{ct} the device FF were improved to 71.3% and a PCE of 10.31%. AC are known for their porosity and fine control over the specific surface area. By changing the particle size of AC, a diverse range of surface area and porosity can be acquired. The catalytic activity of any material is dependent on the

surface defect states created by vacancies and dislocations. As AC can be tuned to our needs, multiple groups have synthesized micro, meso, and macroporous carbon with surface areas vary between $489 \text{ m}^2\text{g}^{-1}$ to $3000 \text{ m}^2\text{g}^{-1}$. The R_{ct} varies from $4.8 \Omega.\text{cm}^{-2}$ to $1.32 \Omega.\text{cm}^{-2}$ appropriate for electrolyte reduction process worthy for DSSC devices. CB is widely studied as a viable CE for DSSC cells. Based on the size of the particle and the thickness of the film coated over a conducting substrate determined the device's performance. Higher thickness ($14.7 \mu\text{m}$) with smaller particles results in PCEs as high as 9.1% compared to that of Pt CEs. CBs are known for their high surface area to volume ratio, which helps the in-electro reduction of Iodine electrolytes with numerous active sites in the mesoporous network. Carbon nanofibers (CNF) have linear structures with a one-dimensional length extending up to several centimetres whose diameter varies between a few nanometres to a few hundred nanometres. CNFs also have a hollow active type with a cylindrical structure at the edges of the fibers. Following a sp^2 hybridization, CNFs are graphitic in nature with excellent directional electrical conductivity and have numerous morphologies like tubes, cones, cups, etc. CNF used as CE for DSSCs shows promising results when coated over a conducting oxide substrate. They also have low R_{ct} values due to their stacking morphology, however, this also amplified the series resistance of the CNF films coated. Resulting in deteriorating the overall performance of the device [21–23]. Fig. 4(a-h) displays the SEM images of carbon-carbon composite counter electrodes while (i & j) shows the device performance [24].

2.2.1 Carbon Metal Composites

Hybridization of carbon allotropes with metal nanoparticles has been proven to improve the electrocatalytic activity of the composite as well as retain its rich surface area and conductivity. Pure CNTs without any dopants or composites with indigenous catalytic activity give rise to DSSC devices with PCE ranging from 3.5% to 7.59%. Their one-dimensional structure helps in linear charge transport and their unique structure surges the electrolyte—CE interaction. Nitrogen-doped CNTs have better intrinsic activity and an increased number of active sites due to the lattice distortions created by the dopants. Metal nanoparticles such as Ni, Co, Fe, and Pt are incorporated into Nitrogen-doped and undoped SWCNTs and MWCNTs show higher catalytic activity with good electrochemical performance with the power conversion efficiency ranging between 7.75% to 9.55%. Graphene in its present state proves to be a better CE and can replace Pt in DSSCs, researchers have created hybrid graphene CE with varying concentrations of Pt. Graphene/Pt CE used in a DSSC shows a PCE of 7.88% with 0.15 wt.% of Pt added. Other transition metal chalcogenides like MoS_2 and CoS_2 were also used as the composite with graphene to induce better electrocatalytic activity in the CE. Resulting composite electrodes with R_{ct} values of $4.94 \Omega.\text{cm}^{-2}$ and $5.05 \Omega.\text{cm}^{-2}$ and device efficiencies were comparable to traditional Pt CE [23, 26]. Fig. 5(a & b) shows the device performance with PtFe-Graphene composite as counter electrode [25] while Fig 5(c & d) displays the SEM image

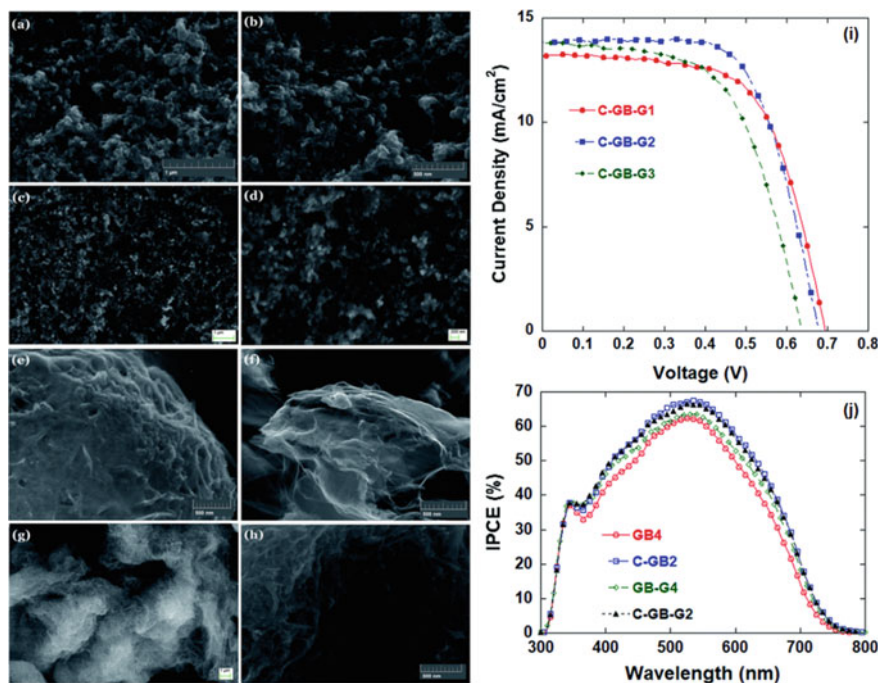


Fig. 4 SEM, J-V and Quantum Efficiency characteristics of Carbon—carbon composite Counter electrodes for DSSC. Adapted with permission [24]. Copyright 2019, RSC Advances, RSC. Adapted from reference [24]. Copyright Zhang. et.al, some rights reserved; exclusive licensee [RSC Advances, RSC]. Distributed under a Creative Commons Attribution-Non-Commercial 3.0 (CC BY-NC 3.0)

of Cu-Polypyrrole-CNT composite and its device performance as counter electrode [27].

Hybridization of CB constructs multiple functionalities in a CE to improve the device's operational dynamics. Use of Pt nanoparticles as a composite material, researchers have achieved higher efficiency like 6.72% with a Pt content of 1.5wt%. This is due to the mutual contribution of CB + Pt nanoparticles in the redox reaction. This efficiency was higher than both pristine CB and pristine Pt CE with 3.76% and 6.63% respectively. Nanocomposites of metal alloys like Pd-Co and NiCu nanoparticles electrospun along with CNFs show promising results with 3.75% PCE of a DSSC device. The bimetallic alloys increase the catalytic activity of the CNF yet fail to reduce the series resistance of the fibers. This affects the charge transport dynamics at the rear end of the device [28, 29].

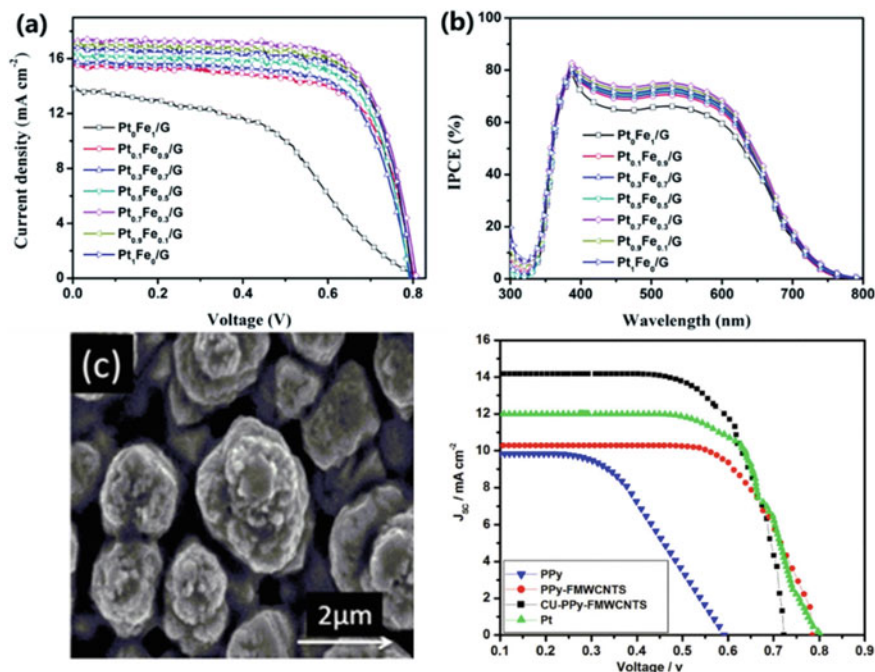


Fig. 5 **a** Device performance, **b** Quantum efficiency of PtFe alloy with Graphene composite counter electrode. Adapted with permission [25]. Copyright 2021, RSC Advances, RSC. Adapted from reference [25]. Copyright Cao, Xiaoyu. et.al, some rights reserved; exclusive licensee [RSC Advances, RSC]. Distributed under a Creative Commons Attribution-Non-Commercial 3.0 Unported (CC BY-NC 3.0), **c** and **d** SEM micrograph and J-V characteristics of Cu-Polypyrrole with CNT counter electrode. Adapted with permission [27]. Copyright 2021, Scientific Reports, Springer Nature. Adapted from reference [27]. Copyright Rafique, Shaista. et.al, some rights reserved; exclusive licensee [Scientific Reports, Springer Nature]. Distributed under a Creative Commons Attribution 4.0 International (CC by 4.0)

2.2.2 Carbon—Polymer Composites

Polymers are widely used in synthesis of carbon allotrope-based CE as binders while conducting polymers are used as composite materials to enhance catalytic activity and provide further active sites for the liquid electrolyte. Such commonly used conducting polymers are polyaniline (PANI), polypyrrole (PPy) and Poly(3,4-ethylenedioxythiophene) (PEDOT). These polymers are used as CE as such without any allotropes of carbon, nevertheless, carbon–polymer hybrids help in the intercalation of electrolyte ions into the structure of the CE. Polymers help not only in charge mobility but also in the stabilization of the carbon allotropes. Studies conducted by synthesizing SWCNTs with PANI results in providing large active surface sites for electrocatalysis and achieved a remarkable efficiency of 7.81% due to the porosity of PANI with 4% SWCNT compound. Also, PPy/MWCNTs have resulted in higher

PCEs of DSSCs. CNTs wrapped with PEDOT create better charge mobility and core-shell nanostructures with CNT cores and PEDOT shells were also studied as CE. Providing an aligned morphology of CNT-PEDOT augmented the regeneration process and amplified the device performance to 8.3%. This endorses the use of polymer CNT composites as CE for DSSC devices are a sound replacement for Pt CEs.

To increase the electrocatalytic activity of graphene, more basal plane sites must be functionalized since the electronic conductivity of graphene is restricted only to in-plane charge transfers. Composites of conducting polymers like PANI and PPy with graphene sheets are examined as CEs for DSSC devices. Especially nano-graphite/PANI composite used as a CE performed way better and achieved a PCE of 7.07%. Due to the smooth defect-free basal planes of graphene, other functional materials like GO and r-GO are considered to make composites with polymers. Such composites with r-GO are mostly transparent and have a good electrochemical activity creating new ways for DSSCs in indoor applications. This transparent nature of r-GO/PANI electrodes and translucent windows with power conversion technologies are now a possibility. PPy was doped with quantum dots of r-GO improving the charge transport properties of the composite. AC with its rich surface-active sites is more stable with the addition of conducting polymers. These polymers also provide transport pathways for the charges to effectively reach the electrolyte ions. PEDOT:PSS with AC paste has been observed as a CE for DSSC demonstrating an enrichment in charge collection increasing the J_{SC} of the device. Dual doping via the addition of metal nanoparticles along with the polymers increases the catalytic activity of the CE by reducing the R_{ct} and increasing the device efficiency up to 6.01% (Fig. 6).

CB added with conducting polymers not only acts as a CE but also acts as a conducting substrate. This composition can be directly applied over a glass slide to form a thin film and used as a CE. Multiple carbon allotropes like graphite and CB are mixed together with PANI showing promising results with a PCE of 7.01% and the series resistance was as low as 8Ω and R_{ct} was found to be $3.9 \Omega \text{ cm}^{-2}$. CNF with polymers like polyoxy-ethylene tridecylether (POETE) was studied by research groups as a binder for CE preparation part. These composites have a faster triiodide reduction rate with a low R_{ct} compared to the traditional electrodes. CNFs by itself adopt a fibrous network and can be easily electro-spun to various designs over a substrate or as a substrate with the help of certain polymers [30]. From this, we can conclude that carbon polymer counter electrodes are a viable replacement for the high-cost platinum electrode used in the DSSC PV devices.

2.2.3 Carbon—Transition Metal Compounds Composites:

Fig. 6(a & b) shows the TEM images of C-transition metal composite Fig. 6(c & d) unveils the device performance [31]. Transition metal compounds comprises of two major categories that are used in DSSCs for CE applications. They are transition metal oxides and transition metal chalcogenides. Various transition metal oxides like nickel oxide (NiO), molybdenum oxide (MoO_3), tungsten oxide (WO_2), etc., have

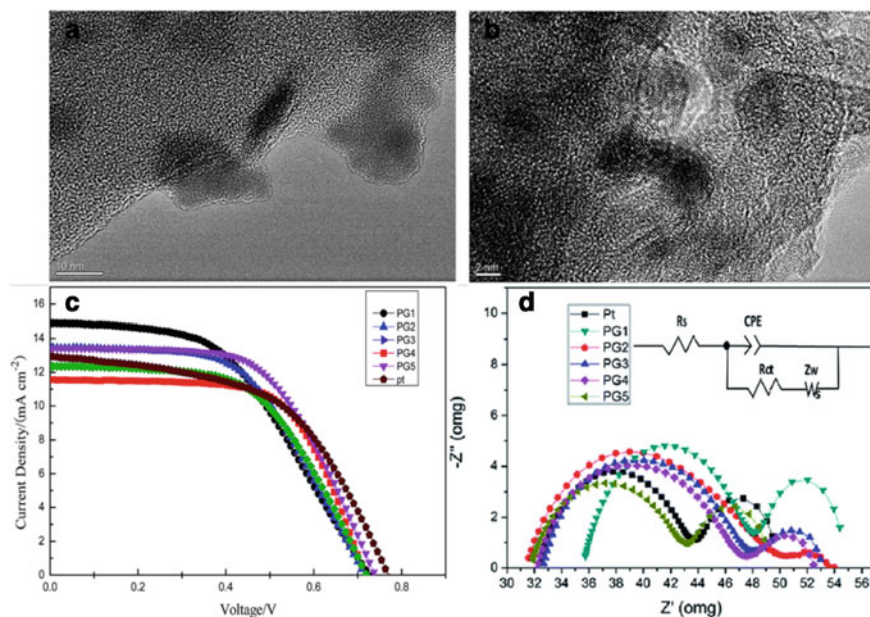


Fig. 6 **a** and **b** TEM images of Ni nanoparticles with PANI and Graphene composite, **c** IV characteristics and **d** electrochemical impedance of different compositions of Ni nanoparticles with PANI and Graphene composites compared with Pt CE. Adapted with permission [31]. Copyright 2018, RSC Advances, RSC. Adapted from reference [31]. Copyright Chen, Xin. et.al, some rights reserved; exclusive licensee [RSC Advances, RSC]. Distributed under a Creative Commons Attribution-Non-Commercial 3.0 Unported (CC BY-NC 3.0)

good catalytic activity yet, lack electrical conductivity due to their high resistive band structure. Carbon allotropes are recognized for their superior conductivity and directional transport pathways. CNTs in adjunct with p-type transition metal oxides like NiO have low charge transfer resistance and high electrocatalytic activity between the electrolyte and the composite, which helps in charge collection and increases the efficiency of DSSC to 7.63% which is higher than the reference device with Pt CE (6.72%). Other metal oxides like TiO₂ and La₂O₃ synthesized along with SWCNT and MWCNT were employed as CE for DSSC devices with N719 dye sensitizer, the resultant PCEs were around 5% with different ratios of oxides and CNTs. Graphene in general comes as r-GO and the amount of reduction process taking place on GO is crucial in the interaction between CE and electrolyte. Graphene mixed with metal oxides like CuO and WO₂ shows reduced R_{ct} and also graphene enhanced the conductivity of these metal oxides. This type of nanoparticular counter electrodes shows a PCE of about 3.40% which is not comparable with that of Pt CE [32, 33]. Transition metal chalcogenides like MoS₂, WS₂, CoS, VS₂, NiS, MoSe₂, etc., are some of the commonly investigated materials used as a carbon composite for CEs of DSSCs. CNT-MoS₂ composites are investigated by Wu and team who found that the charge transport resistance is very low along with a large surface area escalating the

catalytic activity of the CE and achieving a PCE of 7.36%. With this as a base, various groups investigated the role of TMDCs with CNT as CE and achieved good conversion efficiencies. CVD-grown graphene/CoS₂ was used as a CE due to their low R_{ct} values of $5.5 \Omega \cdot \text{cm}^{-2}$. Composites like NiSe/r-GO films are transparent and are used to achieve a maximum efficiency of 9.35% with a low R_{ct} of $0.75 \Omega \cdot \text{cm}^{-2}$. MoS₂/AC CEs are widely used in DSSC solar cells due to the facile way of synthesizing AC from many natural resources. Multiple carbonaceous composites of transition metal compounds were analysed to acquire a replacement for Pt based CEs [34]. Fig. 7 shows the device performance of VO₂-CNF composite counter electrode comparison with platinum counter electrode.

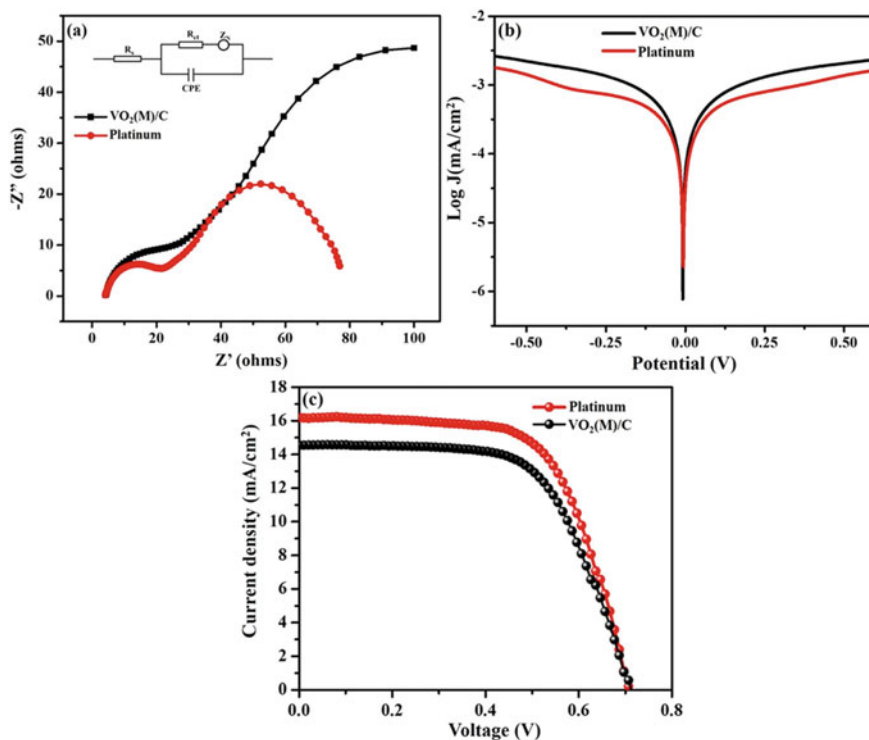


Fig. 7 a Electrochemical impedance, b Tafel polarization plot and c J-V device characteristics of VO₂-CNF composite counter electrode. Adapted with permission [35]. Copyright 2019, Scientific Reports, Springer Nature. Adapted from reference [35]. Copyright Gnanasekar, Subashini. et al., some rights reserved; exclusive licensee [Scientific Reports, Springer Nature]. Distributed under a Creative Commons Attribution 4.0 International (CC by 4.0)

3 Conclusions

The aim of the chapter was to provide a summary of the use of carbon allotrope and their composites in DSSCs. Most metal oxide semiconductors are poor conductors compared to the conductive allotropes of carbon. The addition of highly conductive carbon to the photoanode provides a percolated pathway for electrons toward the front electrode. The addition of a specific ratio of conductive carbon demonstrates elevated charge collection in the photoanode along with adequate dye adsorption. Carbonaceous composites with metal nanoparticles, transition metal compounds, and polymers are used as CEs that show a significant increase in performance due to their hybrid nature to incorporate multiple quirks. Other materials support carbon allotropes to attain better porosity and increase active sites in the overall surface of the CEs to improve the electro-catalytic activity. However, no material or carbon composite has a substantial surge in efficiency of DSSCs when compared to Pt CE.

Acknowledgements KVR acknowledges the fellowship from Amrita Vishwa Vidyapeetham and the authors are indebted to the institute for the support.

References

1. Ram, Babu, Hiroshi Mizuseki.: C568: A new two-dimensional sp²-sp³ hybridized allotrope of carbon. *Carbon* **158**, Republic of Korea, Elsevier Ltd. (2020)
2. Burchfield, Larry A., Mohamed Al Fahim, Richard S. Wittman, Francesco Delodovici, Nicola Manini.: Novamene: A new class of carbon allotropes. *Heliyon* **3**(2), USA, Elsevier Ltd. (2017)
3. Ding, Xian-Yong, Chao Zhang, Dong-Qi Wang, Bing-Sheng Li, Qingping Wang, Zhi Gen Yu, Kah-Wee Ang, Yong-Wei Zhang. A new carbon allotrope: T5-carbon. *Scripta Materialia* **189**, China, Elsevier Ltd. (2020)
4. Janani, Murugesan, Pillalamarri Srikrishnarka, Shantikumar V. Nair, Sreekumaran Nair, A.: An in-depth review on the role of carbon nanostructures in dye-sensitized solar cells. *J. Mater. Chem. A* **3**(35), India, RSC Publishing (2015)
5. Savari, Rojan, Jalal Rouhi, Omid Fakhar, Saeid Kakoei, Davoud Pourzadeh, Okhtay Jahanbakhsh, Saeid Shojaei.: Development of photo-anodes based on strontium doped zinc oxide-reduced graphene oxide nanocomposites for improving performance of dye-sensitized solar cells. *Ceram. Int.*, **47**(22), Iran, Elsevier Ltd. (2021)
6. Eguchi, Takuto, Shinya Kato, Naoki Kishi, Tetsuo Soga. Effect of thickness on photovoltaic properties of amorphous carbon/fullerene junction. *AIMS Materials Science*, **9**(3), Japan, AIMS Press (2022)
7. Kim, Jung-Min, Shi-Woo Rhee.: Electrochemical properties of porous carbon black layer as an electron injector into iodide redox couple. *Electrochimica acta* **83**, South Korea, Elsevier Ltd. (2012)
8. Kausar, Ayesha, Ishaq Ahmad, Tingkai Zhao, M.H. Eisa, Aldaghri. O.: Graphene nanofoam based nanomaterials: manufacturing and technical prospects. *Nanomanufacturing* **3**(1), Pakistan, MDPI (2023)
9. Nazeeruddin, Md K., Etienne Baranoff, and Michael Grätzel. "Dye-sensitized solar cells: A brief overview. *Sol. Energy*, **85**(6), Switzerland, Elsevier Ltd. (2011)
10. Bera, S., Sengupta, D., Roy, S., Mukherjee, K.: Research into dye-sensitized solar cells: a review highlighting progress in India. *J. Phys.: Energy* **3**(3), India, IOPscience (2021)

11. Munukutla, L.V., Htun, A., Radhakrishnan, S., Main, L., Kannan, A.M., Tiwari, A., Boukherroub, R., Sharon, M., "Solar Cell Nanotechnology", "Dye-Sensitized Solar Cells": USA. Scrivener Publishing, Wiley (2013)
12. Lee, Tae Young, Prashant S. Alegaonkar, Ji-Beom Yoo. Fabrication of dye sensitized solar cell using TiO₂ coated carbon nanotubes. Thin solid films **515**(12), Republic of Korea, Elsevier Ltd. (2007)
13. Kilic, Bayram, Sunay Turkdogan, Aykut Astam, Oguz Can Ozer, Mansur Asgin, Hulya Cebeci, Deniz Urk, Selin Pravadihi Mucur.: Preparation of carbon nanotube/TiO₂ mesoporous hybrid photoanode with iron pyrite (FeS₂) thin films counter electrodes for dye-sensitized solar cell. Sci. Rep. **6**(1), Turkey, Springer Nature (2016)
14. Ghartavol, H.M., Mohammadi, M.R. Afshar, A., Li. Y.: On the assessment of incorporation of CNT-TiO₂ core-shell structures into nanoparticle TiO₂ photoanodes in dye-sensitized solar cells. Photochem. Photobiol. Sci. **18**, Iran, Springer Nature (2019)
15. Eshaghi, Akbar, Abbas Ail Aghaei.: Effect of TiO₂-graphene nanocomposite photoanode on dye-sensitized solar cell performance. Bull. Mater. Sci. **38**(5), Pakistan, Elsevier Ltd. (2015)
16. Madhavan, Asha Anish, Annapoorna Mohandas, Antonio Licciulli, K.P. Sanosh, P. Praveen, R. Jayakumar, Shantikumar V. Nair, A. Sreekumaran Nair, Avinash Balakrishnan.: Electrospun continuous nanofibers based on a TiO₂-ZnO-graphene composite. RSC advances, **3**(47), India, RSC Publishing (2013)
17. Madhavan, Asha Anish, Sujith Kalluri, Daya K. Chacko, T.A. Arun, Sivakumar Nagarajan, Kavasseri RV Subramanian, A. Sreekumaran Nair, Shantikumar V. Nair, Avinash Balakrishnan. Electrical and optical properties of electrospun TiO₂-graphene composite nanofibers and its application as DSSC photo-anodes. RSC advances, **2**(33), India, RSC Publishing (2012)
18. Pallikkara, Athira, and Kala Ramakrishnan.: Efficient charge collection of photoanodes and light absorption of photosensitizers: A review. Int. J. Energy Res. **45**(2), India, Wiley (2021)
19. Lee, Hoik, Tomoki Nagaishi, Duy-Nam Phan, Myungwoong Kim, Ke-Qin Zhang, Kai Wei, Ick Soo Kim. Effect of graphene incorporation in carbon nanofiber decorated with TiO₂ for photoanode applications. RSC advances, **7**(11), Japan, RSC Publishing (2017)
20. Park, Hun, Woong-Rae Kim, Changduk Yang, Ho-Gi Kim, and Won-Youl Choi. "Effect of a fullerene derivative on the performance of TiO₂-nanotube-based dye-sensitized solar cells. J. Nanosci. Nanotechnol. **12**(2), Korea, American Scientific Publishers (2012)
21. Samantaray, Manas R., Abhay Kumar Mondal, Govindhasamy Murugados, Sudhagar Pitchaimuthu, Santanu Das, Raihana Bahru, and Mohd Ambri Mohamed. "Synergetic effects of hybrid carbon nanostructured counter electrodes for dye-sensitized solar cells: A review. Materials, **13**(12), India, MDPI (2020)
22. Ding, Shuang, Chaoqiao Yang, Jie Yuan, Huijin Li, Xianli Yuan, Min Li.: An overview of the preparation and application of counter electrodes for DSSCs. RSC advances **13**(18), China, RSC Publishing (2023)
23. Karim, Nayab Abdul, Umer Mehmood, Hafiza Fizza Zahid, Tahira Asif. Nanostructured photoanode and counter electrode materials for efficient Dye-Sensitized Solar Cells (DSSCs). Sol. Energy **185**, Pakistan, Elsevier Ltd. (2019)
24. Zhang, Shihan, Jingsha Jin, Dan Li, Zhiqiang Fu, Shufang Gao, Shubo Cheng, Xiangxiang Yu, Yan Xiong.: Increased power conversion efficiency of dye-sensitized solar cells with counter electrodes based on carbon materials. RSC advances, **9**(38), PR China, RSC Publishing (2019)
25. Cao, Xiaoyu, Qingyu Shen, Yefei Zhuang, Guoce Zhuang, Xiaobo Chen.: Atmospheric plasma reaction synthesised Pt_xFe_{1-x}/graphene and TiO₂ nanoparticles/graphene for efficient dye-sensitized solar cells. RSC advances, **11**(12), PR China, RSC Publishing (2021)
26. Theerthagiri, Jayaraman, Arumugam Raja Senthil, Jagannathan Madhavan, Thandavarayan Maiyalagan.: Recent progress in non-platinum counter electrode materials for dye-sensitized solar cells. Chem. Electro. Chem , **2**(7), India, Chemistry Europe (2015)
27. Rafique, Shaista, Imran Rashid, Rehana Sharif.: Cost effective dye sensitized solar cell based on novel Cu polypyrrole multiwall carbon nanotubes nanocomposites counter electrode. *Scientific Reports*, **11**(1), Pakistan, Springer Nature (2021)

28. Wu, Jihuai, Zhang Lan, Jianming Lin, Miaoliang Huang, Yunfang Huang, Leqing Fan, Genggeng Luo, Yu Lin, Yimin Xie, Yuelin Wei. Counter electrodes in dye-sensitized solar cells. *Chem. Soc. Rev.* **46**(19), China, RSC Publishing (2017)
29. Chen, Ming, Leng-Leng Shao. Review on the recent progress of carbon counter electrodes for dye-sensitized solar cells. *Chem. Eng. J.* **304**, China, Elsevier Ltd. (2016)
30. Chen, Xin, Jing Liu, Kun Qian, and Jihui Wang.: Ternary composites of Ni–polyaniline–graphene as counter electrodes for dye-sensitized solar cells. *RSC advances*, **8**(20), China, RSC Publishing (2018)
31. Saranya, K., Md Rameez, and A. Subramania.: Developments in conducting polymer based counter electrodes for dye-sensitized solar cells–An overview. *Eur. Polym. J.* **66**, India, Elsevier Ltd. (2015)
32. Ahmad, Iftikhar, Joseph E. McCarthy, Mazhar Bari, and Yurii K. Gun'ko. “Carbon nanomaterial based counter electrodes for dye sensitized solar cells.” *Sol. Energy* **102**, Ireland, Elsevier Ltd. (2014)
33. Shahzad, Nadia, Tahira Perveen, Diego Pugliese, Sirajul Haq, Nusrat Fatima, Syed Muhammad Salman, Alberto Tagliaferro, and Muhammad Imran Shahzad.: Counter electrode materials based on carbon nanotubes for dye-sensitized solar cells. *Renew. Sustain. Energy Rev.* **159**, Pakistan, Elsevier Ltd. (2022)
34. Thomas, Sara, Deepak, T.G., Anjusree, G.S., Arun, T.A., Shantikumar Nair, V., Sreekumaran Nair, A.: A review on counter electrode materials in dye-sensitized solar cells. *J. Mater. Chem. A* **2**, 13, India, RSC Publishing (2014)
35. Gnanasekar, Subashini, Pratap Kollu, Soon Kwan Jeong, Andrews Nirmala Grace.: Pt-free, low-cost and efficient counter electrode with carbon wrapped VO₂ (M) nanofiber for dye-sensitized solar cells. *Sci. Rep.* **9**(1), India, Springer Nature (2019)

Nanocarbon for Electrocatalysis



Yingna Chang, Tian Zhang, and Guoxin Zhang

Abstract Electrocatalytic utilization of renewable energy is vital for realizing carbon neutralization of our globe and sustainably fueling human society. Heteroatom-doped carbon nanomaterials (CNMs) have received considerable interest in recent years due to their potential application as electrocatalysts in various renewable energy conversion and storage technologies such as fuel cells, water splitting, nitrogen fixation, etc. This review presents an overview of the recent progress in the tunable synthesis, characterizations, and electrocatalytic properties of heteroatom-doped CNMs. The focus will be laid on the effects of different heteroatoms, the synergy of multiple doping elements, and treating conditions on the electrocatalytic performance of CNMs towards fundamental electrocatalytic reactions including oxygen reduction reaction (ORR), oxygen evolution reaction (OER), hydrogen evolution reaction (HER), CO₂ reduction reactions (CO₂RR), nitrogen fixation reactions (NRR), etc. Moreover, the review highlights the current understanding of the underlying mechanisms of heteroatom doping on the electrocatalytic properties of CNMs. Finally, the opportunities and challenges associated with the applications of heteroatom-doped CNMs as electrocatalysts in practical energy conversion devices are discussed.

Keywords Heteroatom doping · Nanocarbon · Charge redistribution · Electrocatalysis · Clean energy utilization

Y. Chang

Institute of New Energy on Chemical Storage and Power Sources, College of Applied Chemistry and Environmental Engineering, Yancheng Teachers University, Yancheng 224000, China

T. Zhang · G. Zhang (✉)

College of Energy Storage Technology, Shandong University of Science and Technology, Qingdao 266590, Shandong, China

e-mail: zhanggx@sdust.edu.cn

1 Introduction

Energy is not just the material basis for human survival, it is also an important driver of social progress and development. But in recent years, traditional fossil energy sources have been unable to fulfill the needs of human production and life, mainly in two aspects: firstly, due to massive exploitation and over-consumption, the problem of energy shortage is becoming increasingly serious; secondly, the burning process of fossil energy sources produces a large amount of toxic and harmful gases, which brings pollution to the environment [1]. The development of a new energy system that is environmentally friendly, efficient, and safe is the way to alleviate the energy crisis and protect the environment.

Electrochemical technologies, such as fuel cells, metal-air batteries, water electrolysis for hydrogen production, nitrogen reduction, etc., are used as means for clean energy storage and conversion. These technologies react separately at the cathode and anode, and chemical energy can be converted into electrical energy, resulting in a continuous supply of renewable and green energy [2]. In the field of electrochemistry, catalysts play a pivotal role in enhancing the conversion efficiency and selectivity of the reaction process. Precious metal-based catalysts such as Pt, Ir, Pd, Os, Rh, and Ru, have been widely adopted in renewable energy technologies. However, noble metal-based catalysts still have several drawbacks, including high cost, instability under operating conditions, and susceptibility to gas poisoning [3]. Recent advancements in 3d transition metal-based catalysts have shown a potential to reduce dependence on precious metal catalysts; however, their cost remains prohibitive for large-scale applications. In addition, non-precious metal catalysts are prone to oxidation in the air and may undergo unexpected morphological/structural changes during aging, leading to unsatisfactory long-term stability [4]. Thus, the development of sustainable and high-performance catalysts using the abundant resources available is a pressing and meaningful endeavor to overcome the limitations of current catalysts.

In recent years, carbon nanomaterials have shown tremendous potential as efficient metal-free catalysts to replace metals due to their cost-effectiveness, good conductivity, tunable structure and composition, environmental friendliness, and strong tolerance to acidic/alkaline environments. The incorporation of non-metallic dopant atoms such as B, N, P, and S into the carbon framework induces charge redistribution on adjacent carbon atoms, thereby enhancing the catalytic activity of the material [5]. Since the pioneering work of Dai and colleagues in 2009 on vertically aligned N-doped carbon nanotubes (CNTs) arrays as metal-free catalysts for the oxygen reduction reaction (ORR), numerous research activities on metal-free doped carbon have ensued [6]. It has been demonstrated that metal-free dopant carbon materials (CNMs) can catalyze the hydrogen evolution reaction (HER) and produce clean fuel (H_2) through water electrolysis, assist in the ORR for energy generation/conversion in fuel cells, facilitate the oxygen evolution reaction (OER) in metal-air batteries for energy storage, enable the $2e^-$ ORR for the production of H_2O_2 (an energy carrier and green oxidant), and promote the N_2 reduction reaction (NRR) for the synthesis

of NH_3 at room temperature. These findings have paved the way for the potential large-scale application of renewable energy technologies.

Despite significant progress in the synthesis of CNMs with excellent catalytic properties through serendipitous discovery or trial-and-error approaches, there is a lack of fundamental understanding of the structure and doping diversity of the induced active sites in CNMs. It is crucial to understand the doping-induced active sites and their effects on the catalytic activity of CNMs for the rational design of efficient catalysts. The electronic and geometrical properties of CNMs are investigated to reveal potential mechanisms controlling their catalytic behavior. Moreover, the doping diversity in CNMs provides a platform for tailoring their properties, allowing for the optimization of specific catalytic reactions. Thus, this chapter intends to provide an introduction to the electrocatalytic mechanisms of CNMs the design principles of metal-free doped carbon catalysts, and the current challenges and future perspectives in this field.

2 Synthesis of Heteroatom-Doped Carbon Materials

Carbon materials show potential applications in energy storage and catalysis because of their abundance of storage on the earth, inexpensive price, excellent electrical conductivity, and tunable structure and morphology. Conventional carbon materials include graphene, carbon nanotubes, carbon fibers, activated carbon, carbon aerogels, porous carbon, etc. However, pure carbon materials have fewer active sites, which causes them to exhibit poor electrocatalytic activity, thereby limiting their application in catalysis and energy storage. Heteroatom doping is a method of replacing certain carbon lattice atoms with heteroatoms. Due to the difference in electronegativity between carbon and heteroatoms, the doping process usually redistributes the charge density and spin density of the carbon atoms in the lattice, which effectively modulates the figure of merit and increases the adsorption of reactants at specific locations, and endows it with new electrochemical activities [7]. In particular, doped carbon materials have shown high electrocatalytic activity in areas such as fuel cells, water electrolysis, and the NRR for energy storage and conversion.

2.1 *Single Heteroatom-Doped Carbon Materials*

The commonly used doping elements include N, B, O, F, P, S, Cl, Br, I, and Se. The local geometry near dopant atoms changes doping due to the difference in atomic radii between the dopant and carbon atoms. When the size difference between the dopant atom (such as Se, Br, I) and the carbon atom is significant, this spatial distortion significantly reduces the catalytic activity [8–10]. The electronegativity and atomic radius of N are similar to that of C, N atoms and C atoms are more easily

replaced, and N is the most extensively studied dopant atom in carbon nanomaterials. In 1999, the synthesis method of N-doped carbon nanotubes (N-CNTs) was first reported through the thermal decomposition of iron phthalocyanine (FePc) precursor containing carbon and nitrogen atoms [11]. In 2009, Dai et al. [6] successfully synthesized vertically aligned N-doped carbon nanotubes (VA-NCNTs) through the thermal decomposition of FePc under an ammonia atmosphere. The residual iron catalyst was removed through electrochemical purification to obtain metal-free VA-NCNTs suitable for the ORR. The metal-free VA-NCNTs exhibited a lower overpotential (-0.08 V vs Ag/AgCl) compared to commercial Pt/C, demonstrating improved CO tolerance and stability. This work also demonstrated the potential of using N-doping as a method to design and develop efficient metal-free catalysts, opening up a new avenue for research in non-metal carbon-based materials. To simplify the synthesis steps and reduce the cost of nitrogen-doped carbon materials, Sheng et al. [12] mixed inexpensive melamine with graphite oxide to synthesize N-doped graphene with excellent ORR performance through a baking method. X-ray photoelectron spectroscopy (XPS) analysis revealed that the doped nitrogen atoms accounted for approximately 10.1% of the composition, with nitrogen mainly existing in the form of pyridinic-N. Atomic force microscopy (AFM) analysis showed that the thickness of the nitrogen-doped graphene sheets was only 1.0 nm. Huang et al. [13] developed a simple method to prepare highly conductive and highly N-doped hierarchical porous carbon by carbonizing N-containing Schiff base polymers. Organic components of the polymers with a benzene ring structure promoted the formation of more sp²-graphitized carbon, which facilitated the increase of electrical conductivity. The N-doped graded porous carbon calcined at 900 °C under NH₃ atmosphere has a high nitrogen content of 7.48 at%, a large specific surface area of 1613.2 m²/g, and a high electrical conductivity of 2.7 S/cm.

However, at present, there is still significant controversy regarding the active sites of nitrogen-doped carbon and the effective types of nitrogen atoms (pyridinic-N, pyrrolic-N, graphitic-N) that generate these active sites, and no clear explanation has been provided. Professor Junji Nakamura from the University of Tsukuba addressed this issue by designing four different types of N-doped model catalysts using ion beam etching: pyridinic-N-doped model catalyst (pyri-HOPG), graphitic-N-doped model catalyst (grap-HOPG), edge-eroded model catalyst (edge-HOPG), and pure model catalyst (clean-HOPG) [14]. These catalysts were utilized to test the ORR activity of various N-doped graphite models, allowing for the determination of effective N-doping species. Through the utilization of these model catalysts, the research team discovered that under acidic conditions, the effective catalytic nitrogen species in N-doped carbon materials were pyridinic-N. Furthermore, they identified that the active sites for ORR catalytic activity were located near the pyridinic-N nitrogen species adjacent to carbon atoms. Nonetheless, ongoing research aims to provide a clearer understanding of the mechanisms underlying the catalytic activity of N-doped carbon materials, specifically the types of nitrogen species that facilitate enhanced performance in ORR.

Unlike N atoms with abundant electrons, B dopants lack electrons but can alter the electrically neutral state of sp²-hybridized carbon, resulting in positively charged sites

favorable for oxygen adsorption. We employed a green strategy involving polymer dehalogenation to synthesize boron-doped carbon materials (O-BC) and investigated their 2-electron ORR properties [15]. By experimentally adjusting the dosage of the boron source (H_3BO_3) and annealing temperature, we optimized the catalytic activity of O-BC materials. Electrochemical tests demonstrated that the optimal O-BC sample exhibited up to 98% selectivity towards H_2O_2 ; in an alkaline electrolytic cell of the H-type, the average yield of H_2O_2 was $412.8 \text{ mmol}^{-1} \text{ h}^{-1}$. As illustrated in Fig. 1, density functional theory calculations further supported our findings, revealing that the boron atom bonded to an oxygen atom is the most favorable active site. This active site achieved the lowest Gibbs free energy difference (ΔG) of 0.03 eV during the adsorption process of O_2 reduction.

Compared to N and B doping, S doping exhibits distinct changes in the electronic density due to its electron-donating nature [16]. The introduction of S also leads to enhanced local reactivity in carbon materials through the presence of lone pairs of electrons. Sun et al. [17] firstly applied S-doped carbon nanospheres (S-CNS) for electrochemical nitrogen reduction reduction (NRR). S-CNS achieved NH_3 yield of $19.07 \text{ ug}_{\text{NH}_3}^{-1} \text{ h}^{-1}$, significantly higher than undoped carbon nanospheres ($3.7 \text{ ug}_{\text{NH}_3}^{-1} \text{ h}^{-1}$). The incorporation of S atoms increased the number of catalytic active sites in the materials, facilitating the adsorption of N_2 molecules and promoting

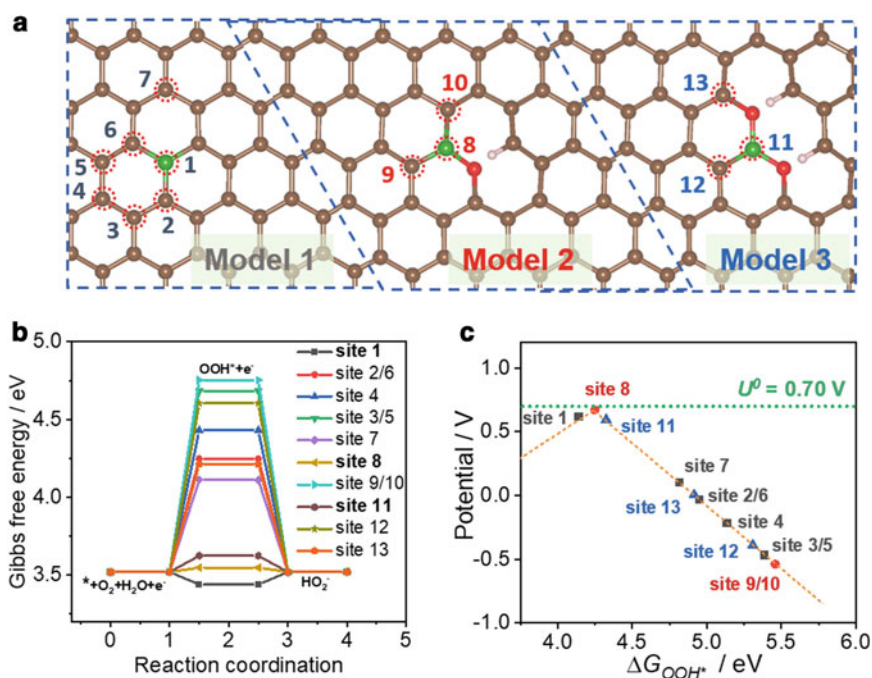


Fig. 1 DFT results of the $2e^-$ ORR activities on O-BC. Adapted with permission [15]. Copyright (2022) Springer

NRR. In comparison to N, B, and S, P has a lower electronegativity and a larger covalent radius. P doping can effectively modify the structure of carbon, introducing more active sites into the carbon framework. For instance, Wen et al. [18] synthesized large-scale two-dimensional phosphorus-doped carbon nanosheets (2D-PPCN) using phosphorus pentoxide and glucose as precursors via a multifunctional templating approach. 2D-PPCN exhibited a high phosphorus content and exceptional porosity, enabling efficient ions and energy transfer within the framework. Consequently, catalysts based on 2D-PPCN demonstrated catalytic activities comparable to commercial Pt/C and Ir/C for both ORR and oxygen evolution reaction (OER) in half-cell testing. It should be noted that the P-C bond length of 1.79 Å is significantly longer than the C-C bond length (1.42 Å), which suggests that the sole doping of phosphorus may cause severe structural deformation in the carbon framework. Therefore, phosphorus doping is generally combined with other elements in carbon frameworks.

2.2 *Binary Heteroatom-Doped Carbon Materials*

Although carbon nanomaterials doped with individual impurity atoms such as N, B, F, O, S, or P have been proven to be promising non-metal catalysts for various reactions, the synergistic effects arising from the electronic interactions between different dopants can further enhance their performance through co-doping N with other impurity atoms [19]. The most common approach is co-doping N with a second element such as B, S, P, F, or Si to improve the electrochemical properties of carbon nanomaterials. Furthermore, there are also ternary-doped carbon materials, such as B, N, and P ternary doping, as well as N, P, and S ternary doping, which can offer additional advantages.

B, N co-doped carbon is one of the earliest materials studied for investigating the synergistic effects of different dopant atoms. As early as 2000, Bai et al. [20] synthesized B, N co-doped carbon nanofibers using bias-assisted hot-filament chemical vapor deposition (CVD) at room temperature, where some of the carbon atoms in the graphite layers were replaced by boron or nitrogen atoms. In 2011, Dai et al. [21] used melamine and boron salts as precursors to synthesize vertically aligned B, N co-doped carbon nanotubes (VA-BCN) and applied them for the first time in the ORR. Due to the synergistic effects between carbon nanotubes and B, N co-doped atoms, the resulting VA-BCN electrode exhibited higher electrocatalytic activity for ORR in alkaline media compared to carbon nanotubes doped solely with boron or nitrogen. In addition to forming active sites by coupling with neighboring carbon atoms, the synergistic interaction between adjacent N and B atoms can further enhance charge transfer efficiency and catalytic activity during the doping process of carbon materials for ORR. Theoretical results indicate that in the N-C-B doping configuration, the electron-donating N atoms polarize the C atoms, providing additional electrons to neighboring B atoms. This not only increases the electron occupancy of the materials but also improves the adsorption performance of doped carbon materials on O₂ in alkaline solutions.

Boric acid and NH_3 are commonly used as dopant sources for the synthesis of B, and N co-doped carbon materials. However, under high-temperature annealing, they tend to form boron nitride, which has poor conductivity and exhibits significant inertness for most electrochemical reactions. Based on this, Liang et al. [22] prepared N, S co-doped graphene (N-S-G) by heating a mixture of graphene oxide (GO), melamine, and benzyl disulfide under an inert gas atmosphere. The alkaline ORR catalytic activity of N-S-G was found to be comparable to Pt/C. Density functional theory (DFT) calculations revealed that carbon atoms surrounding nitrogen with high charge density serve as active sites for ORR in N-doped graphene, while positively charged sulfur is considered the catalytic center for S-doped graphene. When both sulfur and nitrogen are doped into graphene, N-S-G exhibits optimal ORR catalytic activity, attributed to the synergistic effects of N and S co-doping and the redistribution of spin and charge density, resulting in the formation of active sites for adsorbing H^* and HOO^* reaction intermediates in the materials. Bandosz et al. [23] recently studied N, S co-doped polymer-derived carbon (CPSN), and S-doped polymer-derived carbon (CPS) as electrocatalysts for CO_2 reduction reactions (CO_2RR). CPSN exhibited higher faradaic efficiency (FE) than CPS for the reduction of CO_2 to CO and CH_4 . The positively charged carbon atoms near the pyridinic N and S dopants were identified as the main active sites for CO_2RR . These active sites stabilized the negatively charged intermediate $\text{CO}_2^{\bullet-}$ during the initial steps of CO_2RR . Due to the lower electronegativity of S compared to N, the positive charge on the carbon atoms adjacent to S was lower than those adjacent to pyridinic N. Considering the low cost and ease of large-scale synthesis of N, S co-doped graphite materials, they are expected to be excellent candidates for the next generation of fuel cell electrode materials and demonstrate significant potential in applications such as metal-air batteries and CO_2RR .

In addition, P has been reported to improve the electrochemical activity of N-doped nanocarbon materials. Zheng et al. [24] have found that doping P into the carbon lattice effectively reduces the free energy barrier (ΔG_{H^*}) of the HER and thus promotes the H^* adsorption by DFT calculations, where the pyridine-N and P co-doping model shows the lowest absolute value of negative ΔG_{H^*} ($|\Delta G_{\text{H}^*}| = 0.08 \text{ eV}$). Consequently, N, P co-doped graphene has higher HER activity in acidic and alkaline solutions compared to N or P mono-doped graphene. Theoretical calculations indicated that co-doping N and P introduced additional active sites, resulting in enhanced catalytic efficiency. Furthermore, Zhao et al. [25] synthesized N, P co-doped carbon nanonetworks using a thermal decomposition method involving molecular precursor self-assembly (MPSA/GO). The charge delocalization and edge effects of the carbon atoms contributed to exceptional ORR activity in acidic media for the N, P co-doped carbon nanonetworks. This represents the first reported dual-functional non-metal catalyst. It is assembled into zinc-air batteries with high power density (310 W g^{-1}) and excellent stability.

The co-doping heteroatoms can introduce additional active sites into the carbon lattice; thus, researchers aim to further enhance the catalytic activity of carbon materials by introducing more types of heteroatoms. Zhang et al. [26] reported the efficient

synthesis of ternary B, N, and P-doped porous carbon materials via polymer dehalogenation strategy (Fig. 2a). The atomic contents of B, N, and P, as characterized by XPS, are 11.5, 1.1, and 0.8%, respectively, yet intriguingly resulting in limited water splitting activity due to the overwhelmingly presented B dopant (Fig. 2b–f). Zhang et al. Razmjooei et al. [27] synthesized N, S, and P tri-doped carbon materials (N, S, P-rGO), which exhibited higher positive onset potential (0.93 V vs RHE) compared to N, S co-doped rGO and P doped rGO. The introduced P synergistically interacts with N, S co-doped rGO by forming active P–N bonds, thereby enhancing the graphitic order and specific surface area for ORR catalysis. Recently, Pham et al. [28] synthesized N, F, S tri-doped reduced graphene oxide (N, F, S-rGO) by thermally decomposing a mixture of perfluorosulfonic acid, dimethyl, and S-doped rGO. The N, F, and S-rGO exhibited excellent ORR catalytic activity in rotating disk electrode tests. While the co-doping of multiple heteroatoms in carbon materials contributes to improving their electrochemical activity, determining the active sites for electrochemical activity remains a significant challenge. Compared to extensively studied co-doped carbon materials, there is limited discussion in the literature on ternary or multiple-doped carbon materials, representing an important area for future research.

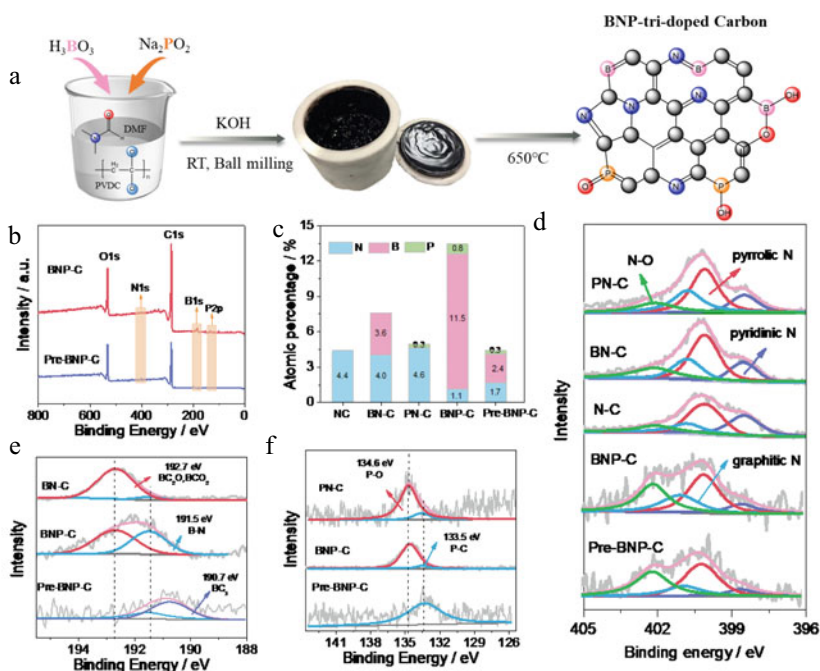


Fig. 2 a Graphical scheme for the synthesis of ternary BNP-C via polymer dehalogenation strategy. b–f XPS analysis of N–C, BN-C, PN-C, BNP-C, and Pre-BNP-C. Adapted with permission [26]. Copyright (2020) Elsevier

2.3 Preparation of Doped Carbon Materials

The synthesis methods of doped carbon materials can be divided into in-situ doping and post-doping. In-situ doping refers to the direct pyrolysis of biomass and organic precursors containing dopant atoms. Common in-situ doping methods include the template method, activation method, chemical vapor deposition method, and activation method. For example, Yan et al. [29] synthesized N-doped carbon materials using an ionic liquid ([BMIM][Br]) as the carbon source and mesoporous silica as the template. The In-situ doping method is simple, requiring only the selection of suitable carbon precursors for pyrolysis treatment. However, it is difficult to precisely control the dopant content and doping form in carbon materials.

Post-doping involves first carbonizing the raw materials and then further processing to achieve impurity doping. For instance, carbon precursors are synthesized into N-doped carbon materials through high-temperature calcination in an NH_3 gas atmosphere. Mixing carbon precursors with a boron source, followed by calcination or arc discharge, leads to the synthesis of B-doped carbon materials. The dopant content and pore structure of carbon materials can be controlled by adjusting the calcination temperature and the amount of doping source [30, 31].

Heteroatom-doped carbon materials are usually synthesized using ultra-high-temperature pyrolysis, where high-temperature pyrolytic synthesis, in addition to the problems of high energy consumption and the production of a variety of toxic gases, produces materials with a chemical structure that is less predictable than that of conventional organic synthesis. For comparison, conventional organic synthesis methods typically involve lower temperatures. Therefore, post-synthesis modification of available carbon materials with nitrogen-containing reagents, preferably at low temperatures, can also yield heteroatom-doped carbon materials.

Furthermore, Zhang et al. [32] discovered that halogenated polymers can de-functionalize halogenated groups in the presence of inorganic bases at room temperature to form cyclic carbons via a C-C coupling reaction (Fig. 3). The halogenated polymers have high reactivity at the moment of de-functionalization during the reaction process, and when a doping source is added during the reaction process, these highly reactive sites form covalent bonds with the contacted heteroatoms to synthesize the doped carbon materials. Subsequently, the materials are further carbonized through calcination to improve the conductivity of the materials, giving them better electrochemical performance. This dehalogenation approach is one of the post-doping methods. Moreover, Zhang et al. [33] synthesized N-doped carbon with polyvinyl dichloride (PVDC) as the carbon source, N, N-dimethylformamide (DMF) as the nitrogen source, and KOH as the dehalogenation agent (Fig. 4). These synthesized materials were then applied in areas such as ORR and supercapacitors.

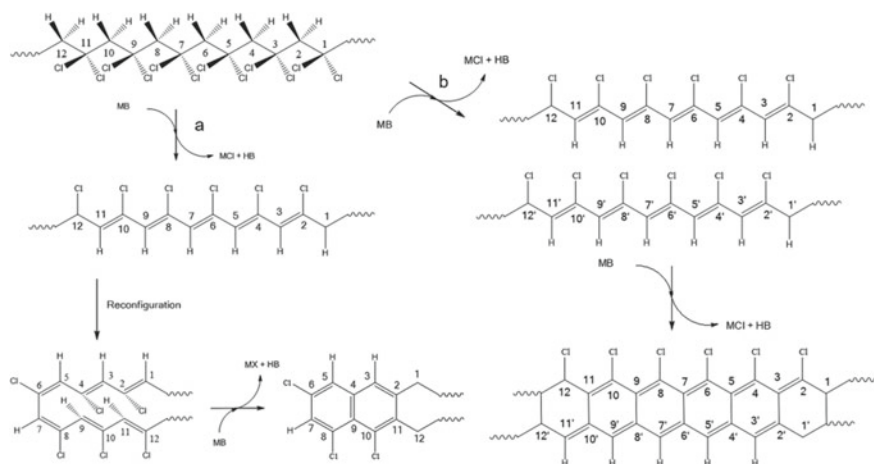


Fig. 3 Schematic diagram of polymer dehalogenation reaction mechanism, M = alkali metal or alkali earth metal, B = strong alkaline group [32]. Reproduced with permission [32]. Copyright (2016) Wiley

3 Electrochemical Applications of Heteroatom-Doped Carbon Materials

3.1 Metal-Air Battery

The main bottleneck in metal-air batteries is the slow ORR behavior of the air electrode (cathode). Currently, noble metals are the most efficient ORR catalysts, but their expensive cost limits their development. Introducing heteroatoms into carbon materials is a method to create efficient catalysts. Wang et al. [34] prepared nitrogen-doped porous carbon (NPC) with graded micropores and a large surface area by ball-milling polymerization and pyrolysis. The optimized NPC (NPC-1000) prepared at 1000 °C showed excellent ORR activity with onset potentials and half-wave potentials of 0.9 and 0.82 V, respectively (compared to reversible hydrogen electrodes), which were only about 30 mV lower than that of Pt/C. A rechargeable zinc-air battery assembled using NPC-1000 and NiFe layered double hydroxide. The open-circuit voltage was 1.43 V. The discharge curves and corresponding power density of the ZAB catalyzed by NPC-1000 are comparable to those of Pt/C, suggesting the superior activity of NPC-1000 (Fig. 5). Zhu et al. [35] synthesized N, F co-doped carbon materials (NF@CB) by direct pyrolysis of a mixture of carbon black, polytetrafluoroethylene, and melamine. Due to the synergistic interaction between N and F atoms, NF@CB served as an air electrode catalyst for zinc-air batteries, achieving a voltage of 0.852 V at 20 mA cm⁻² and displaying over 49 h of cycling stability. Wang et al. [36] proposed a simple alkali activation method to prepare N-doped carbon materials (NKCNP-900) with specific surface area and pore structure. The introduced

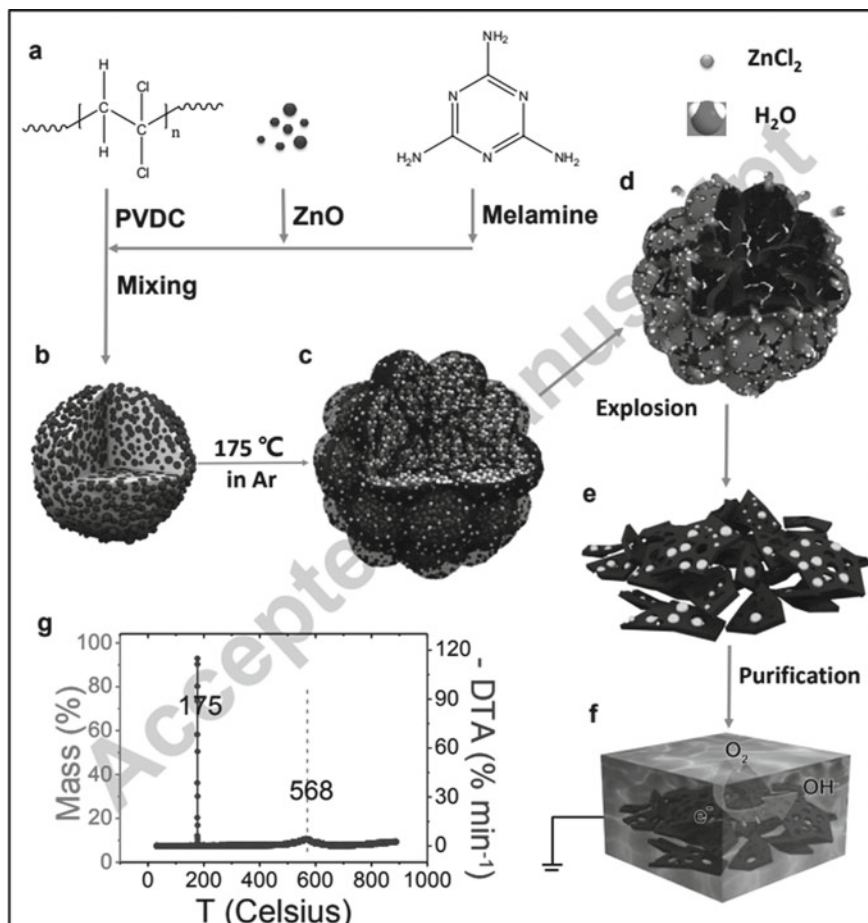


Fig. 4 Graph depiction for the fabrication of hierarchical Porous N-Doped nanocarbon, and ORR applications. Reproduced with permission [33]. Copyright (2016) Elsevier

nitrogen atoms increased the quantity of pyridinic-N, pyrrolic-N, and edge defect sites in the carbon materials, further enhancing its electrochemical performance. Theoretical calculations revealed that the amount of N doping and edge defects were related to the electrochemical activity of the materials. NKCNP-900 exhibited excellent half-wave potential for ORR (0.79 V) and demonstrated a high energy density of 889.0 Wh kg⁻¹ for a zinc-air battery with an extended lifespan.

Recently, Park et al. [37] prepared composites of ethylenediamine-derived N-doped carbon nanotubes with thermally reduced graphene oxide (TRGO/NCNT) using injection chemical vapor deposition. The N-doped carbon nanotubes in TRGO/NCNT are uniformly distributed on graphene sheets and connected to multiple graphene sheets. This interconnection not only enhanced its electronic conductivity but also created a porous structure between graphene sheets, facilitating the diffusion

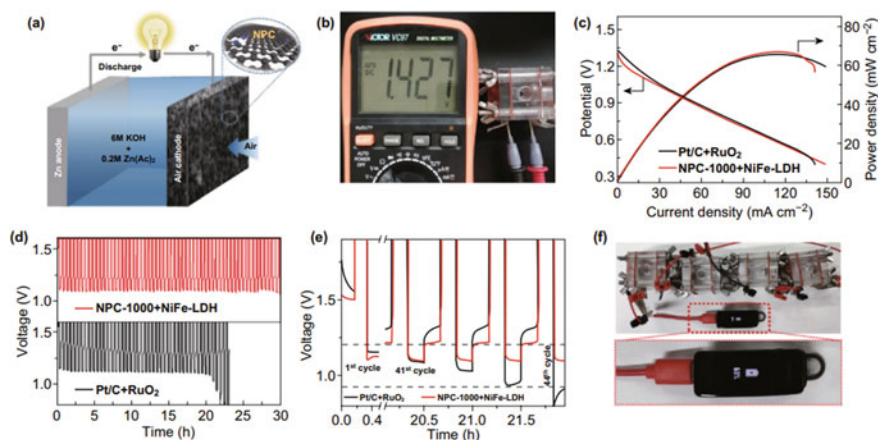


Fig. 5 The performance of NPC-1000-based Zn-air batteries. Reproduced with permission [34]. Copyright (2020) springer nature. Distributed under a creative commons attribution license 4.0 (CC BY)

of ions and O_2 . Electrochemical tests showed that the peak ORR current catalyzed by TRGO/NCNT was higher than that of thermally reduced graphene oxide with a stronger onset potential, indicating that TRGO/NCNT has higher ORR activity. This indicates that heteroatom doping is beneficial to enhance the ORR activity of the materials. Furthermore, the current density of TRGO/NCNT at 1.0 V (relative to the saturated calomel electrode) was about 27.8 mA cm^{-2} , which was superior to that of N-doped carbon nanotubes and Pt/C. This study confirms that the combination of doped carbon with other types of carbon is an effective strategy for creating bifunctional composite catalysts for chargeable and dischargeable metal-air batteries. Xu et al. [38] synthesized two-dimensional N-doped carbon nanotube/graphene hybrids (GNCNTs) by in situ growth of metal-organic framework compounds on graphene oxide followed by roasting and used as efficient bifunctional catalysts for zinc-air batteries. The GNCNTs exhibit excellent catalytic activity and reaction durability because of the synergy effects arising from the hierarchical structure and heteroatom doping. The assembly of GNCNTs into zinc-air batteries achieved a high power density of 253 mW cm^{-2} and a specific capacity of $801 \text{ mAh g}_{\text{Zn}}^{-1}$. Additionally, the flexible solid-state rechargeable zinc-air battery assembled from this catalyst with a high discharge power density of 223 mW cm^{-2} could power 45 light-emitting diodes. In conclusion, both single and binary-doped atoms, along with their unique porous structures, can effectively enhance catalytic activity for ORR or a combination of ORR and OER, making them efficient methods for preparing high-performance catalysts for metal-air batteries.

3.2 Fuel Cells

ORR is a critical component of fuel cells. The most prominent explanation for the catalytic activity of ORR in metal-free heteroatom-doped carbon materials is the charge polarization of the covalent bonds between carbon and the dopant elements due to the differences in electronegativity between the different elements. Dai et al. [39] demonstrated that N-doped graphene/carbon nanotube composite (N-G-CNT) as a cathode catalyst in acidic PEM fuel cells exhibited exceptionally high limiting current (2000 A g^{-1}) and a peak power density of 300 W g^{-1} . Due to the strong acid-corrosion resistance of carbon materials compared to most transition metal catalysts, N-G-CNT also demonstrated remarkable durability in acidic PEM fuel cells even when using pure H_2/O_2 gas. Yang et al. [40] successfully synthesized N, S co-doped multi-walled carbon nanotubes rich with edge defects by controlled nanoscale cutting techniques. The study found that carbon catalysts with higher edge content exhibited superior ORR catalytic activity. The edge sites provided anchoring points for heteroatoms, accelerating ORR kinetics. Sun et al. [41] first synthesized F-doped carbon black (CB-F) for ORR, with ORR performance comparable to Pt/C, but at a significantly lower cost around ten thousand times cheaper than Pt or other materials and with abundant availability, suggesting potential for commercial applications. These findings highlight that in practical PEM fuel cells, carbon-based non-metal catalysts can serve as low-cost, efficient, and durable ORR catalysts, holding substantial market potential.

3.3 Water Splitting for Producing Hydrogen

Water splitting is an effective method for hydrogen production in the future, involving the cathodic hydrogen evolution reaction (HER) and the anodic OER. To mitigate the overpotential of electrode reactions and accelerate reaction rates, the utilization of electrocatalysts is crucial. Precious metals like Pt, Ir, and Ru serve as excellent electrolysis catalysts, but their high cost and limited availability hinder widespread practical application. In recent years, CNMs have shown significant potential as electrocatalysts. Heteroatoms such as N, B, P, and S can effectively modulate the electronic and chemical properties of carbon materials.

Dai et al. [42] harnessed the characteristics of polydopamine to synthesize N, S co-doped multi-walled carbon nanotubes (N, S-CNT) for use as catalysts for water electrolysis. In this process, dopamine underwent polymerization under alkaline conditions to form polydopamine, which adhered to the CNTs. Subsequently, sulfur was introduced into the polydopamine through a sulfur addition reaction, resulting in the formation of N, S-CNT upon high-temperature treatment. Electrochemical tests revealed that the overpotentials for hydrogen evolution and oxygen evolution reactions were 0.45 V and 0.36 V at a current density of 10 mA cm^{-2} , respectively.

Theoretical calculations indicated that the N, S co-doping induced spin density variations in carbon atoms, promoting the adsorption of intermediates during the water electrolysis process. Additionally, Qiao et al. [43] demonstrated by theoretical calculations of the free energy distribution of HER on different co-doped graphene sheets that co-doping of the two elements with the largest electronegativity difference (e.g., N and P) resulted in the highest HER activity. For carbon catalysts doped with N/S, N/P, and N/B separately, the catalytic activity is largely dependent on the electronically active surface area (EASA). In addition, the enhanced charge density of S-doped carbon atoms can stabilize H* intermediates on N/S co-doped carbon of HER. Li et al. [44] put forward a spontaneous gas-foaming strategy to synthesize N-doped ultrathin carbon nanosheets (NCNs) through simple one-step carbonization of citric acid and NH₄Cl. At the optimal pyrolysis temperature (carbonization at 1000 °C) and precursor mass ratio (1:1), the synthesized sample of NCN-1000-5 exhibits an ultrathin lamellar structure, an ultrahigh specific surface area (1793 m² g⁻¹) and an abundance of edge defects. It shows superior ORR activity (onset potential), even better than that of commercial Pt/C, and the E_{onset} and measured potentials in the alkaline electrolyte at a current density of 10 mA cm⁻² are 1.55 and 1.64 V, respectively, slightly lower than that of IrO₂ (1.48 V and 1.59 V) but comparable to that of many of OER advanced catalysts. Moreover, it is also highly active and stable against HER in acidic media, having almost the same positive E_{onset} as Pt/C (0.03 V), and at a current density of 10 mA cm⁻², the NCN-1000-5 (0.09 V) obtains a potential that is only 51 mV more negative than that of Pt/C. DFT calculations revealed that the intrinsically active sites of ORR, OER, and HER are carbon atoms located at the edge of the armchair and adjacent to the graphite N dopant.

3.4 CO₂ Reduction Reactions

Carbon-based catalyst materials exhibit excellent catalytic performance closely associated with heteroatom doping. For instance, the introduction of N into carbon-based materials can show excellent electrical conductivity and more active sites. Therefore, the preparation of doped carbon-based catalysts has been an important research direction in the field of CO₂ electrochemical reduction. Zheng et al. [45] obtained N-doped carbon materials enriched with pyrrole-type nitrogen by selectively etching pyridine-type and graphite-type nitrogen in N-doped carbon nanotubes using high-temperature water vapor etching. Through the high-temperature steam treatment, the proportion of pyrrole-type nitrogen increased from 22.1% before treatment to 55.9%. The catalytic system exhibited a maximum selectivity of 88% for CO production during CO₂ reduction reaction (CO₂RR) at -0.5 V versus RHE. Wang et al. [46] synthesized F-doped carbon (FC) catalyst by thermally decomposing a commercial BP 2000 mixed with polytetrafluoroethylene as the fluorine source. The FC catalyst exhibited a maximum Faradaic efficiency of 90% at a low overpotential of -0.51 V and a small Tafel slope of 81 mV dec⁻¹. The partial current density of H₂ on FC was lower than that on pristine carbon, indicating the suppression of the HER by F doping

into the carbon lattice. Experimental measurements and DFT calculations showed that F doping can modulate the electronic cloud structure of carbon atoms, increase the number of active sites in carbon materials, enhance their adsorption capacity for COOH* intermediates, and suppress the adsorption of HER intermediates, significantly enhancing the electrocatalytic performance for CO₂RR. Furthermore, the CO₂ decomposition cell equipped with FC achieved a solar-to-chemical efficiency of 13.6%.

Han et al. [47] synthesized N, P co-doped carbon aerogel (NPCA) capable of reducing CO₂ to CO. The Faradaic efficiency of NPCA can reach 99.1%, with a partial current density of $-143.6 \text{ mA cm}^{-2}$. NPCA exhibits higher electrochemical active surface area and overall electronic conductivity compared to N- or P-doped carbon aerogels, enabling efficient electron transfer for the reduction of CO₂ to its free radical anion or other key intermediates. The theoretical calculations revealed that the pyridine-N species exhibited high activity for CO₂ reduction to CO, while the co-doping of P and N significantly suppressed the HER, thus enabling high current densities and Faradaic efficiency. Despite numerous recent studies on CO₂RR, the reaction mechanism and nature of active sites in heteroatom-doped carbon catalysts remain unclear. Employing a combined experimental and theoretical approach is crucial to gaining a deeper understanding and better catalyst design principles for optimizing CO₂RR. In this context, metal-free doped carbon deserves further exploration to improve our understanding of complex electrocatalytic processes and to facilitate the development of efficient carbon-based catalysts for CO₂ reduction.

3.5 N₂ Reduction Reaction

Electrocatalytic nitrogen reduction reaction has attracted research attention as one of the alternative methods to the Haber-borsch process. However, most catalysts face the dilemma of low efficiency of NH₃ synthesis. The introduction of heteroatoms into carbon materials to distort their structure and increase the positive charge density on neighboring carbon atoms can endow them with excellent NRR catalytic performance.

Zeng et al. [48] fabricated F-doped carbon materials by pyrolysis of a mixture of UiO-66 and poly(tetrafluoroethylene), and introduced F atoms into a three-dimensional porous carbon skeleton. Because of the different electronegativity of F (3.98) and C (2.55) atoms, Lewis acid sites are easily formed between F and C atoms, and the repulsive effect of Lewis acid sites with proton H inhibits the electrocatalytic hydrogen production process, thereby enhancing the pathway of selective reduction of NH₃ by N₂. Electrochemical tests indicated that the F-doped carbon had a product content as high as 54.8% at -0.2 V , which is three times higher than that of the pristine carbon skeleton, and its NH₃ yield reached $197.7 \text{ ug}_{\text{NH}_3} \text{ mg}^{-1} \text{ h}^{-1}$ at -0.3 V (RHE). Subsequently, the Cl-doped reduced graphene (Cl-RGO) is synthesized by Zhu et al. [49] The Cl-RGO achieves a high NH₃ yield of $70.9 \text{ ug}_{\text{NH}_3} \text{ mg}^{-1} \text{ h}^{-1}$ at -0.3 V (RHE) with a Faraday efficiency of 5.97%. Experimental and

theoretical calculations indicate that Cl doping facilitates the enhancement of N_2 adsorption in the defective structure, and the electronegativity of chlorine can cause the electron redistribution of adjacent carbon atoms, which is favorable to NRR. The strong electron affinity of the B atom can act as a Lewis acid site to capture the lone pair of electrons in nitrogen and activate the inert N_2 molecule. In this, Du et al. [50] fabricated B-doped carbon materials including B-doped carbon fibers (B/CNFs), P, B co-doped carbon fibers (P-B/CNFs), and S, B co-doped carbon fibers (S-B/CNTs) by electrostatic spinning process and chemical vapor deposition method. Electrochemical tests showed that S-B/CNTs exhibited Faraday efficiency up to 22.4% and NH_3 yield of $0.22 \text{ } \mu\text{mol}^{-1} \text{ h}^{-1} \text{ cm}^{-2}$ in 0.5 M K_2SO_4 electrolyte at -0.7 V . Furthermore, the catalysts exhibited excellent catalytic stability. Theoretical calculations show that S doping leads to a change in the center of the P_z orbital of B, which facilitates the adsorption of N_2 at the S-C-B site and lowers the energy barrier for the formation of *NNH by protonation in the first step.

4 Conclusions and Perspectives

The core of green and renewable energy technologies, such as fuel cells, metal-air batteries, water splitting, and chemical conversion, is crucial for achieving global carbon neutrality. Until now, noble metals such as Pt, Ir, Ru, and Pd have been reported as highly efficient electrocatalysts. However, the high cost and scarcity of these precious metals hinder the commercialization of renewable energy technologies. CNMs have been widely studied in the field of energy conversion and storage due to multiple advantages such as low cost, high electronic conductivity, morphological and structural tunability, and strong tolerance to acidic/alkaline media as a metal alternative for efficient metal-free catalysis. By controlling the content and types of heteroatom precursors, CNMs can generate various coexisting active sites for multiple catalytic functions. These significant advantages have led to the development of multifunctional CNMs capable of simultaneously catalyzing different electrochemical reactions, such as ORR, OER, HER, NRR, and CO_2RR . Their catalysis performance can be further improved by rationally designing the carbon structure as well as the physicochemical defects in the carbon lattice and edges.

Despite the encouraging progress achieved so far, there is still a lack of fundamental understanding of the doping effects and structural diversity of such carbon catalysts, particularly in terms of the molecular structure of the active center (e.g., dopant type, position, distribution) and the specific doping effects that control the electrocatalytic reaction. While DFT calculations can provide a basic theoretical foundation for the working mechanisms of dopants, there still exists a significant gap between current theoretical models and practical systems. Elucidation of the factors controlling the electrochemical behavior of catalytic active centers in CNMs poses a temporary challenge, but in the meantime opportunities for precise control and guidance of catalytic activity through active center modification and interfacial functionalization. Furthermore, the catalysis performance of CNMs needs to

be further enhanced to meet the requirements of industrial applications. Through continued research efforts, we believe that CNMs will achieve commercial success and surpass metal-based catalysts in the competitive renewable energy technology market.

5. References

1. Chia, X., Pumera, M.: Characteristics and performance of two-dimensional materials for electrocatalysis. *Nat. Catal.* **1**, 909–921 (2018)
2. Ji, Y., Du, J., Chen, A.: Review on heteroatom doping carbonaceous materials toward electrocatalytic carbon dioxide reduction. *Trans. Tianjin Univ.* **28**, 292–306 (2022)
3. Liang, L., Jin, H., Zhou, H., Liu, B., Hu, C., Chen, D., Wang, Z., Hu, Z., Zhao, Y., Li, H.-W., He, D., Mu, S.: Cobalt single atom site isolated Pt nanoparticles for efficient ORR and HER in acid media. *Nano Energy* **88**, 106221 (2021)
4. Hu, C., Dai, L.: Doping of carbon materials for metal-free electrocatalysis. *Adv. Mater.* **31**, e1804672 (2019)
5. Gao, K., Wang, B., Tao, L., Cuning, B.V., Zhang, Z., Wang, S., Ruoff, R.S., Qu, L.: Efficient metal-free electrocatalysts from N-doped carbon nanomaterials: mono-doping and co-doping. *Adv. Mater.* **31**, e1805121 (2019)
6. Gong, K., Du, F., Xia, Z., Durstock, M., Dai, L.: Nitrogen-doped carbon nanotube arrays with high electrocatalytic activity for oxygen reduction. *Science* **323**, 760–763 (2009)
7. Yang, J., Xiang, F., Guo, H., Wang, L., Niu, X.: Honeycomb-like porous carbon with N and S dual-doping as metal-free catalyst for the oxygen reduction reaction. *Carbon* **156**, 514–522 (2020)
8. Zou, W.S., Kong, W.L., Zhao, Q.C., Zhang, J., Zhao, X., Zhao, D., Wang, Y.Q.: A composite consisting of bromine-doped carbon dots and ferric ions as a fluorescent probe for determination and intracellular imaging of phosphate. *Mikrochim. Acta* **186**, 576 (2019)
9. Zhao, Y., Wei, J., Vajtai, R., Ajayan, P.M., Barrera, E.V.: Iodine doped carbon nanotube cables exceeding specific electrical conductivity of metals. *Sci. Rep.* **1**, 83 (2011)
10. Zhang, C., Bai, J., Ma, L., Lv, Y., Wang, F., Zhang, X., Yuan, X., Hu, S.: Synthesis of halogen doped graphite carbon nitride nanorods with outstanding photocatalytic H₂O₂ production ability via saturated NH₄X (X = Cl, Br) solution-hydrothermal post-treatment. *Diam. Relat. Mater.* **87**, 215–222 (2018)
11. Huang, S., Dai, L., Mau, A.W.H.: Patterned growth and contact transfer of well-aligned carbon nanotube films. *J. Phys. Chem. B* **103**, 4223–4227 (1999)
12. Sheng, Z., Shao, L., Chen, J., Wang, F., Xia, X.: Catalyst-free synthesis of nitrogen-doped graphene via thermal annealing graphite oxide with melamine and its excellent electrocatalysis. *ACS Nano* **5**, 4350–4358 (2011)
13. Wang, P., Qi, X., Zhao, W., Qian, M., Bi, H., Huang, F.: Nitrogen-doped hierarchical few-layered porous carbon for efficient electrochemical energy storage. *Carbon Energy* **3**, 349–359 (2020)
14. Guo, D., Shibuya, R., Akiba, C., Saji, S., Kondo, T., Nakamura, J.: Active sites of nitrogen-doped carbon materials for oxygen reduction reaction clarified using model catalysts. *Science* **351**, 361–365 (2016)
15. Chang, Y., Li, J., Ma, J., Liu, Y., Xing, R., Wang, Y., Zhang, G.: Oxygenated boron-doped carbon via polymer dehalogenation as an electrocatalyst for high-efficiency O₂ reduction to H₂O₂. *Sci. China Mater.* **65**, 1276–1284 (2022)
16. Guo, Y., Zeng, Z., Zhu, Y., Huang, Z., Cui, Y., Yang, J.: Catalytic oxidation of aqueous organic contaminants by persulfate activated with sulfur-doped hierarchically porous carbon derived from thiophene. *Appl. Catal. B Environ.* **220**, 635–644 (2018)

17. Xia, L., Wu, X., Wang, Y., Niu, Z., Liu, Q., Li, T., Shi, X., Asiri, A.M., Sun, X.: S-Doped carbon nanospheres: an efficient electrocatalyst toward artificial N₂ fixation to NH₃. *Small Methods* **3**, 1800251 (2018)
18. Lei, W., Deng, Y.-P., Li, G., Cano, Z.P., Wang, X., Luo, D., Liu, Y., Wang, D., Chen, Z.: Two-dimensional phosphorus-doped carbon nanosheets with tunable porosity for oxygen reactions in Zinc-air batteries. *ACS Catal.* **8**, 2464–2472 (2018)
19. Yan, X., Liu, H., Jia, Y., Zhang, L., Xu, W., Wang, X., Chen, J., Yang, D., Yao, X.: Clarifying the origin of oxygen reduction activity in heteroatom-modified defective carbon. *Cell Rep. Phys. Sci.* **1**, 100083 (2020)
20. Bai, X.D., Wang, E.G., Yu, J., Yang, H.: Blue–violet photoluminescence from large-scale highly aligned boron carbonitride nanofibers. *Appl. Phys. Lett.* **77**, 67–69 (2000)
21. Wang, S., Iyyamperumal, E., Roy, A., Xue, Y., Yu, D., Dai, L.: Vertically aligned BCN nanotubes as efficient metal-free electrocatalysts for the oxygen reduction reaction: a synergistic effect by co-doping with boron and nitrogen. *Angew. Chem. Int. Ed.* **50**, 11756–11760 (2011)
22. Liang, J., Jiao, Y., Jaroniec, M., Qiao, S.Z.: Sulfur, and nitrogen dual-doped mesoporous graphene electrocatalyst for oxygen reduction with synergistically enhanced performance. *Angew. Chem. Int. Ed.* **51**, 11496–11500 (2012)
23. Li, W., Seredych, M., Rodriguez-Castellon, E., Bandosz, T.J.: Metal-free nanoporous carbon as a catalyst for electrochemical reduction of CO₂ to CO and CH₄. *ChemSuschem* **9**, 606–616 (2016)
24. Zheng, Y., Jiao, Y., Li, L., Xing, T., Jaroniec, M., Qiao, S.: Toward the design of synergistically active carbon-based catalysts for electrocatalytic hydrogen evolution. *ACS Nano* **8**, 5290–5296 (2014)
25. Zhang, J., Qu, L., Shi, G., Liu, J., Chen, J., Dai, L.: N, P-codoped carbon networks as efficient metal-free bifunctional catalysts for oxygen reduction and hydrogen evolution reactions. *Angew. Chem. Int. Ed.* **55**, 2230–2234 (2016)
26. Chang, Y., Shi, H., Yan, X., Zhang, G., Chen, L.: A ternary B, N, P-Doped carbon material with suppressed water splitting activity for high-energy aqueous supercapacitors. *Carbon* **170**, 127–136 (2020)
27. Razmjooei, F., Singh, K.P., Song, M.Y., Yu, J.-S.: Enhanced electrocatalytic activity due to additional phosphorus doping in nitrogen and sulfur-doped graphene: a comprehensive study. *Carbon* **78**, 257–267 (2014)
28. Van Pham, C., Klingele, M., Britton, B., Vuyyuru, K.R., Unmuessig, T., Holdcroft, S., Fischer, A., Thiele, S.: Tridoped reduced graphene oxide as a metal-free catalyst for oxygen reduction reaction demonstrated in acidic and alkaline polymer electrolyte fuel cells. *Adv. Sustain. Syst.* **1**, 1600038 (2017)
29. Lin, T., Chen, I., Liu, F., Yang, C., Bi, H., Xu, F., Huang, F.: Nitrogen-doped mesoporous carbon of extraordinary capacitance for electrochemical energy storage. *Science* **350**, 1508–1513 (2015)
30. Panchakarla, L.S., Subrahmanyam, K.S., Saha, S.K., Govindaraj, A., Krishnamurthy, H.R., Waghmare, U.V., Rao, C.N.R.: Synthesis, structure, and properties of boron- and nitrogen-doped graphene. *Adv. Mater. NA-NA* (2009)
31. Niu, L., Li, Z., Hong, W., Sun, J., Wang, Z., Ma, L., Wang, J., Yang, S.: Pyrolytic synthesis of boron-doped graphene and its application as electrode material for supercapacitors. *Electrochim. Acta* **108**, 666–673 (2013)
32. Zhang, G., Wang, L., Hao, Y., Jin, X., Xu, Y., Kuang, Y., Dai, L., Sun, X.: Unconventional carbon: alkaline dehalogenation of polymers yields N-doped carbon electrode for high-performance capacitive energy storage. *Adv. Funct. Mater.* **26**, 3340–3348 (2016)
33. Zhang, G., Luo, H., Li, H., Wang, L., Han, B., Zhang, H., Li, Y., Chang, Z., Kuang, Y., Sun, X.: ZnO-promoted dechlorination for hierarchically nanoporous carbon as superior oxygen reduction electrocatalyst. *Nano Energy* **26**, 241–247 (2016)
34. Guo, B., Ma, R., Li, Z., Guo, S., Luo, J., Yang, M., Liu, Q., Thomas, T., Wang, J.: Hierarchical N-doped porous carbons for Zn-air batteries and supercapacitors. *Nano-micro lett.* **12**, 20 (2020)

35. Zhu, P., Gao, J., Chen, X., Liu, S.: An efficient metal-free bifunctional oxygen electrocatalyst of carbon co-doped with fluorine and nitrogen atoms for rechargeable Zn-air battery. *Int. J. Hydrogen Energy* **45**, 9512–9521 (2020)
36. Wang, Q., Lei, Y., Zhu, Y., Wang, H., Feng, J., Ma, G., Wang, Y., Li, Y., Nan, B., Feng, Q., Lu, Z., Yu, H.: Edge defect engineering of nitrogen-doped carbon for oxygen electrocatalysts in Zn-air batteries. *ACS Appl. Mater. Interfaces* **10**, 29448–29456 (2018)
37. Park, H.W., Lee, D.U., Liu, Y., Wu, J., Nazar, L.F., Chen, Z.: Bi-functional N-doped CNT/graphene composite as highly active and durable electrocatalyst for metal-air battery applications. *J. Electrochem. Soc.* **160**, 2244–2250 (2013)
38. Xu, Y., Deng, P., Chen, G., Chen, J., Yan, Y., Qi, K., Liu, H., Xia, B. Y.: 2D nitrogen-doped carbon nanotubes/graphene hybrid as bifunctional oxygen electrocatalyst for long-life rechargeable Zn-air batteries. *Adv. Funct. Mater.* **30**, 1906081 (2019)
39. Shui, J., Wang, M., Du, F., Dai, L.: N-doped carbon nanomaterials are durable catalysts for oxygen reduction reaction in acidic fuel cells. *Sci. Adv.* **1**, e1400129 (2015)
40. Yang, Q., Xiao, Z., Kong, D., Zhang, T., Duan, X., Zhou, S., Niu, Y., Shen, Y., Sun, H., Wang, S., Zhi, L.: New insight to the role of edges and heteroatoms in nano carbons for oxygen reduction reaction. *Nano Energy* **66**, 104096 (2019)
41. Sun, X., Zhang, Y., Song, P., Pan, J., Zhuang, L., Xu, W., Xing, W.: Fluorine-doped carbon blacks: highly efficient metal-free electrocatalysts for oxygen reduction reaction. *ACS Catal.* **3**, 1726–1729 (2013)
42. Qu, K., Zheng, Y., Jiao, Y., Zhang, X., Dai, S., Qiao, S.: Polydopamine-inspired, dual heteroatom-doped carbon nanotubes for highly efficient overall water splitting. *Adv. Energy Mater.* **7**, 1602068 (2017)
43. Qu, K., Zheng, Y., Zhang, X., Davey, K., Dai, S., Qiao, S.: Promotion of electrocatalytic hydrogen evolution reaction on nitrogen-doped carbon nanosheets with secondary heteroatoms. *ACS Nano* **11**, 7293–7300 (2017)
44. Jiang, H., Gu, J., Zheng, X., Liu, M., Qiu, X., Wang, L., Li, W., Chen, Z., Ji, X., Li, J.: Defect-rich and ultrathin N doped carbon nanosheets as advanced trifunctional metal-free electrocatalysts for the ORR, OER, and HER. *Energy Environ. Sci.* **12**, 322–333 (2019)
45. Cui, X., Pan, Z., Zhang, L., Peng, H., Zheng, G.: Selective etching of nitrogen-doped carbon by steam for enhanced electrochemical CO₂ reduction. *Adv. Energy Mater.* **7**, 1701456 (2017)
46. Xie, J., Zhao, X., Wu, M., Li, Q., Wang, Y., Yao, J.: Metal-free fluorine-doped carbon electrocatalyst for CO₂ reduction outcompeting hydrogen evolution. *Angew. Chem. Int. Ed.* **57**, 9640–9644 (2018)
47. Chen, C., Sun, X., Yan, X., Wu, Y., Liu, H., Zhu, Q., Bediako, B.B.A., Han, B.: Boosting CO₂ electroreduction on N, P-co-doped carbon aerogels. *Angew. Chem. Int. Ed.* **59**, 11123–11129 (2020)
48. Liu, Y., Li, Q., Guo, X., Kong, X., Ke, J., Chi, M., Li, Q., Geng, Z., Zeng, J.: A highly efficient metal-free electrocatalyst of F-doped porous carbon toward N₂ electro reduction. *Adv. Mater.* **32**, e1907690 (2020)
49. Huang, P., Cheng, Z., Zeng, L., Yu, J., Tan, L., Mohapatra, P., Fan, L.-S., Zhu, Y.: Enhancing nitrogen electroreduction to ammonia by doping chlorine on reduced graphene oxide. *ACS Catal.* **10**, 14928–14935 (2020)
50. Wen, Y., Zhu, H., Hao, J., Lu, S., Zong, W., Lai, F., Ma, P., Dong, W., Liu, T., Du, M.: Metal-free boron and sulfur co-doped carbon nanofibers with optimized p-band centers for highly efficient nitrogen electroreduction to ammonia. *Appl. Catal. B Environ.* **292**, 120144 (2021)

Graphene-Based Electrocatalysts



Touba Rezaee Adriani and Ali A. Ensafi

Abstract The utilization of electrochemical conversion and energy storage has become feasible in tackling the growing concerns related to energy and environment. One of the primary challenges in the practical application of these devices is the sluggishness of their reaction kinetics. There should be a heightened focus on examining electrocatalysts that exhibit superior efficiency and enhance kinetics rate. Graphene is one of the most extensively researched electrode materials for electrochemical applications among advanced nanomaterials. The incorporation of graphene with nanomaterials can make it easier to take advantage of the material's inherent features. Particularly, graphene and graphene derivatives have been utilized as templates for the synthesis of numerous noble-metal nanocomposites, which have demonstrated exceptional performance in electrocatalytic applications, such as the sensors, ORR, OER, HER, CO₂RR, SCs, and so on. In this chapter, we undertake an examination of the progress made in the development of graphene and its composites-based electrodes for the electrocatalytic field.

Keywords Electrocatalyst · Carbon-based materials · Graphene · Sensors · Biosensors

1 Introduction

The global community is confronted with a pressing concern known as the energy crisis, which has emerged as a significant challenge due to the exponential increase in energy use and the gradual exhaustion of traditional energy equipment [1, 2]. Electricity, which is the most extensively utilized energy source, is predominantly generated by the combustion of fossil fuels such as petroleum, coal, and natural gas.

T. R. Adriani · A. A. Ensafi (✉)

Department of Chemistry, Isfahan University of Technology, 84156-83111 Isfahan, Iran

e-mail: ensafi@iut.ac.ir; aensafi@uark.edu

A. A. Ensafi

Department of Chemistry & Biochemistry, University of Arkansas, Fayetteville, AR 72701, USA

© The Author(s), under exclusive license to Springer Nature Singapore Pte Ltd. 2024

179

R. K. Gupta (ed.), *NanoCarbon: A Wonder Material for Energy Applications*,
Engineering Materials, https://doi.org/10.1007/978-981-99-9935-4_10

The combustion of fossil fuels results in the generation of substantial quantities of toxic gases, which contribute to the pollution of marine ecosystems and food webs, in addition to the emission of carbon dioxide that influences climate change [3]. Electrocatalyst active sites can be employed to mitigate excessive electrical energy consumption. This technology holds significant promise in addressing our impending energy demands and mitigating the challenges posed by climate change.

Electrocatalysts play a vital role in facilitating the efficient conversion between electrical and chemical energies, thereby enabling the implementation of water, carbon, and nitrogen cycles dependent on renewable energy sources. The desired electrocatalysts should exhibit exceptional performance in terms of activity, stability, and product selectivity, while simultaneously reducing or eliminating the reliance on precious metals [4]. At least three factors should be met at the same time by the catalytically active sites of desirable electrocatalysts. (i) It is imperative that the catalysts possess a substantial level of intrinsic activity. (ii) The catalysts must have a significant density on their surfaces. (iii) The catalysts should be readily accessible to molecules participating in the reaction. The advantages stem from the fact that electrocatalytic processes can be used to transform surplus and off-peak electricity into chemical bonds in molecules. This opens several potential commercial opportunities.

Some surface sites contribute to catalyst activity, known as catalytic active sites. Determining catalytic sites is of great significance in furthering our understanding of electrocatalytic reactions and promoting the advancement of improved electrocatalysts. The usual approach utilized for the identification of active sites in heterogeneous catalysts entails the production of catalysts with various sizes, employing the scanning transmission electron microscopy (STEM) analysis. There exists a clear correlation between the dimensions of catalyst particles and the number of corners and edges they possess, which subsequently impacts their catalytic activity [5]. Porous electrocatalysts are a significant category of materials that exhibit a variety of properties that enable efficient electrocatalysis. The presence of carbon-based materials (CBMs) can lead to the formation of electrocatalytic active sites, owing to their inherent properties. The objective is accomplished through the manipulation of the charge distribution and spin density of neighboring CBMs, as well as the optimization of their adsorption and desorption properties concerning essential intermediate species. The utilization of defect engineering can be employed as a strategy to activate the π electrons present in undoped CBMs, thus leading to the generation of active sites that facilitate electrocatalysis.

Recent studies have further confirmed the importance of dopant-induced and intrinsic defect sites in CBMs concerning their electrocatalytic activity. To date, a variety of SACs including, platinum (Pt), palladium (Pd), ruthenium (Ru), iridium (Ir), molybdenum (Mo), and iron (Fe), have been successfully prepared to facilitate a wide range of electrochemical reactions. The main cause of this phenomenon can be ascribed to the unique characteristic of metal atoms that exist in isolation at the atomic scale, frequently attached to supporting materials. Recently, single-atom catalysts (SACs)-based CBMs have emerged as highly promising materials for electrocatalysis in a diverse array of applications.

The establishment of effective coordination between metal atoms and support materials, such as CBMs, has the potential to generate electrocatalytically active sites exhibiting significant levels of activity. These catalysts' high electro-catalytic activity is often due to their strong metal-support interactions. These interactions change the local coordination environment, regulate metal atom-support material electronic transfer, and increase reaction intermediate chemisorption energies.

CBMs, like carbon quantum dots (CQDs), nanowires, nanotubes ((CNTs) (multi-wall carbon nanotubes (MWNTs)), single-wall carbon nanotubes (SWCNTs), fibers, and graphene, graphene oxide (GO) are predicted to play crucial roles in overcoming obstacles and making advances in catalysis process. The fundamental cause of this phenomenon can be attributed to their distinct composition and inherent characteristics, which include large specific surface area, electrochemical and chemical inertness, and good biocompatibility, on the other hand, straightforward synthesis procedures have boosted research in life science, energy, and environmental domains. Graphene, an up-and-coming star in the fields of material science and technology, is speculated to be capable of resolving a wide variety of critical problems. It has been demonstrated that graphene possesses a substantial variety of fascinating features, some examples of which are as follows: charge transport mobility ($\sim 10,000 \text{ cm}^2 \text{ V}^{-1} \text{ s}^{-1}$), excellent chemical stability ($\sim 1.0 \text{ TPa}$), and huge specific surface area. In addition, given its exceptional mechanical strength and flexibility, outstanding thermal and electrical conductivity ($\sim 5000 \text{ Wm}^{-1} \text{ K}^{-1}$), optical transparency ($\sim 97\%$), and remarkable electronic characteristics [6].

The electrical characteristics of graphene exhibit variations based on the number of layers and the relative arrangement of atoms in neighboring layers, often known as stacking order. Double-layer graphene can have a stacking order of AA (atoms on top of each other) or AB (second layer atoms on top of first layer hexagon center). Several techniques have been devised for the synthesis of this promising graphene material, including the Hummers method, chemical vapor deposition (CVD), direct liquid exfoliation, and others [7, 8]. From the perspective of condensed matter physics, graphene is composed of carbon atoms bound together through sp_2 hybridization of their atomic orbitals, specifically s, px, and py orbitals. This hybridization results in the formation of three robust σ bonds between each carbon atom and its three neighboring atoms.

Graphene can be divided into two-dimensional (2D) and three-dimensional (3D) materials, with carbon atoms arranged in a honeycomb-like hexagonal lattice [6]. Specifically, the design of 3D graphene that is formed through the assembly of 2D has significant attention has been drawn to 3D graphene due to its unique features and ability to retain 2D graphene properties. Some notable characteristics of this 3D material include the ability to modify pore shapes, high mechanical strength, and exceptional electronic conductivity. Based on these fascinating characteristics, 3D graphene as a catalyst or electrocatalyst support has already met a number of the prerequisites for consideration as an advanced catalyst process, which contributes more to the improvement of catalytic performance. It should be noted that the 3D confinement of electrocatalytic components graphene stabilizes catalytic active sites. In addition to the described here, the use of 3D graphene offers catalysis benefits:

(i) 3D graphene modified with functional groups such as $-\text{NH}_2$, $-\text{COOH}$, and $-\text{OH}$ directly contributes to catalysis. (ii) The utilization of defect-related or heteroatom-doped 3D graphene has demonstrated commendable efficacy in catalytic reactions, particularly in the domain of electrocatalysis. (iii) 3D graphene is widely recognized as a substrate that enhances catalytic functions, including metal oxides, phosphides, chalcogenides, and nitrides. (iv) The utilization of 3D graphene has been seen to serve as cocatalysts to enhance the efficiency of photocatalytic reactions. For modifying graphene's electronic/optical properties, heteroatom doping is a simple method for creating n-type, p-type, or hybrid graphene. Similar variations are also observed in other parameters, such as thermal conductivity and thermal expansion. The incorporation of foreign elements such as nitrogen (N), boron (B), and sulfur (S) into support materials has been shown to enhance their electrical properties and catalytic performance [9, 10]. Carbon materials have been widely utilized as support materials to stabilize single-metal catalytic sites, owing to their numerous significant advantages. Vital progress has been made in the past decade regarding the application of graphene-based electrocatalyst materials in various electrochemical reactions. These reactions include the solar cells (SCs), oxygen reduction reaction (ORR), hydrogen evolution reaction (HER), oxygen reduction reaction (ORR), carbon dioxide reduction reaction (CO_2RR), and oxygen evolution reaction (OER), supercapacitors, sensors, and biosensors (Fig. 1).

2 Application

2.1 Solar Cells

Fossil fuels possess the characteristic of being non-renewable resources, with their reserves undergoing depletion at a rate that surpasses the discovery or creation of new reserves. The advancement of clean and sustainable energy sources is crucial to address the continuously growing global energy needs resulting from rapid economic growth and the expanding world population. At present, there is a significant focus on the extensive investigation of emerging technologies for energy conversions, such as SCs and fuel cells, as well as energy storage, including super-capacitors. The performance of these devices is heavily influenced by the materials utilized. Several electrocatalysts exhibiting specific nanostructures and significant surface/interface areas have been successfully synthesized for utilization in energy-related devices. CBMs have been significant in driving industrial and technical progress since the onset of the previous century. In contrast to conventional energy materials, carbon nanostructures demonstrate distinctive features that are influenced by their size and surface characteristics. These qualities, which include morphological, electrical, optical, and mechanical attributes, contribute to the improved performance of energy conversion processes. In recent times, significant endeavors have been undertaken to explore

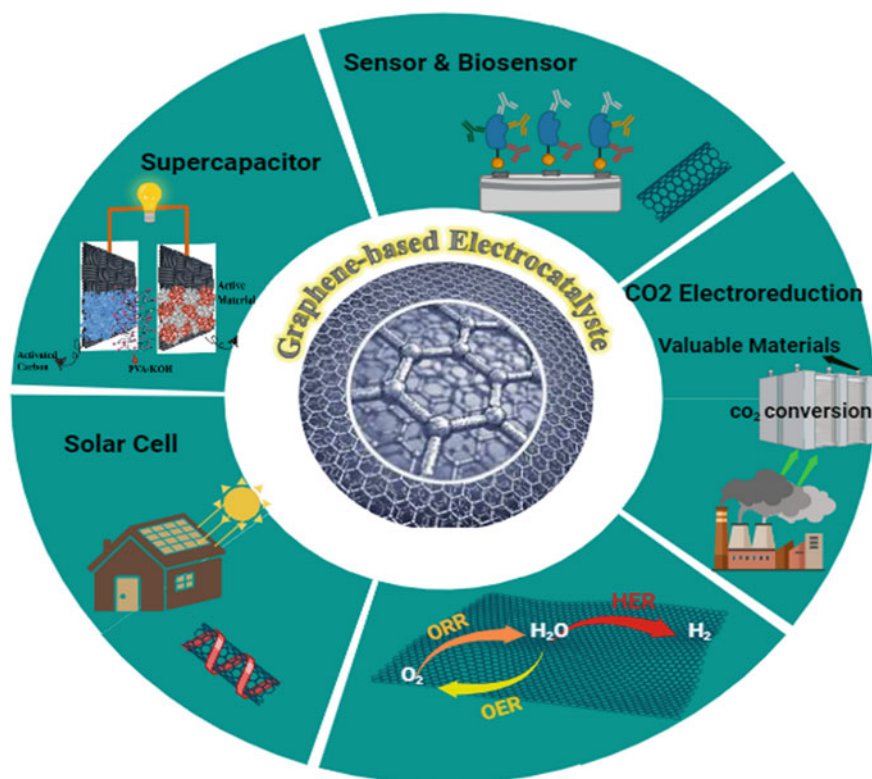


Fig. 1 Electrocatalysts application of graphene

the potential applications of graphene in energy-related devices and enhance their efficiency, processability, stability, and cost-effectiveness.

There is a projected demand for the global energy supply to undergo a twofold increase by the year 2050. In typical photovoltaic cells, inorganic semiconductors like amorphous silicon, gallium arsenide, and sulfide salts are commonly utilized to directly produce free electrons and holes from photon absorption. Although (semiconductor III–V) inorganic multijunction SCs have achieved over 40% power conversion efficiency (PCE) in the lab. Their widespread use is limited due to challenges in modifying their bandgap and high costs associated with elaborate fabrication processes at elevated temperatures and vacuum [11]. The cost of inorganic SCs remains prohibitively high in comparison to conventional grid electricity, hindering their competitiveness. Dye-sensitized solar cells (DSSCs) are a new subtype of photovoltaic cells that employ a sensitizer molecule, typically in the form of dye molecules, to convert sunlight into electrical energy. The most current reported peak PCE achieved for a DSSC stands at 12.3%. Even though DSSCs now exhibit lower efficiency compared to silicon SCs, their affordability and straightforward manufacturing process have rendered them highly appealing for “low-density” purposes,

such as rooftop solar collectors. As elucidated in this section, graphene has been employed in nearly all constituents of a DSSC. Given the inherent properties of great transparency and excellent conductivity exhibited by graphene, numerous research groups have utilized graphene as a transparent cathode in DSSCs.

Claudia et al. directed their attention on examining the technical viability of utilizing graphene synthesized through CVD as a potential substitute for tin oxides inside the photoanode component of DSSCs. This study represented the pioneering utilization of graphene as the photoanode transparent conductor in a tin oxide-free DSSC, where ZnO serves as the mesoporous semiconductor. The superior optical transparency exhibited by graphene led to the generation of higher open circuit voltage and short circuit current density compared to devices utilizing FTO [12].

The utilization of organic or polymer materials as alternative ways has garnered significant interest due to their advantageous characteristics such as cost-effectiveness, lightweight nature, flexibility, and capacity to be processed. Unlike inorganic SCs, conjugated polymers with graphene commonly form bound electron-hole pairs termed excitons during photon absorption at ambient temperature. Active layers in polymer solar cells (PSCs) are often a mixture of donor and acceptor materials that are sandwiched between a cathode and an anode [13].

Fei Pan et al. fabricated a solution-processable n-doped graphene cathode interfacial material (CIM) PDINO-G was formulated for organic solar cells (OSCs) through the incorporation of graphene into the conventional PDINO ((N, N-dimethylammonium N-oxide) propyl perylene di imide) material. PDINO-G CIM with n-doping exhibited enhanced conductivity, decreased work function, diminished charge recombination, and augmented charge extraction rate. The impact of the charge injection material (CIM) on the photovoltaic efficiency of organic solar cells (OSCs) was investigated using a photovoltaic model system consisting of PTQ10 as the donor and IDIC-2F as the acceptor. The organic solar cells (OSCs) utilizing PTQ 10: IDIC-2F with PDINO-G CIM exhibited the highest power conversion efficiency (PCE) of 13.01%. This PCE was notably improved compared to the devices lacking graphene modification on the PDINO CIM, which achieved a PCE of 12.23% [14]. During illumination, photoinduced charge transfer between donor and acceptor generates electrons and holes, which travel to and are collected by the cathode and anode. To enhance the efficiency of charge collection by the electrodes, it is common practice in perovskite solar cells (PSCs) to incorporate an electron extraction layer between the cathode and the active layer, as well as a hole-extraction layer between the anode and the active layer. The most popular transparent electrode in PSCs, indium tin oxide (ITO), has several drawbacks including its high production cost and its fragility. Another disadvantage of using ITO electrodes is the limited amount of indium in nature. To investigate their involvement in PSCs, nitrogen and sulfur functionalized GQDs were produced using a hydrothermal technique. These GQDs were subsequently employed to modulate the interfacial characteristics of all-inorganic CsPbBr₂ PSC. The highest possible efficiency of carbon-electrode-based the highest possible CsPbBr₂ PSCs with excellent long-term stability is achieved through the interaction between GQDs and under-coordinated Pb²⁺ ions, based on Lewis's acid-base chemistry. This interaction effectively reduces the detrimental non-radiative

recombination, particularly for functionalized QDs-tailored PSCs. As a result, the efficiency of these PSCs reaches 9.80% [15].

2.2 Cathodic Reaction: ORR, HER, ECR

The cathode catalyst, which is involved in the ORR and HER is a crucial component in both fuel cells and metal-air batteries, as it significantly influences their performance. Efficiency in transforming chemical energy into electrical energy is one of the performance characteristics of energy devices. The factors that are commonly considered in evaluating the performance of a system include energy efficiency, cycling life, kinetic reaction, and other relevant parameters. The effective conversion of molecular oxygen (O_2) to water (H_2O) plays a pivotal role in various energy systems, encompassing essential biological processes such as respiration and photosynthesis, as well as developing energy technologies. This section presents a short overview of the fundamental aspects of the ORR, encompassing mechanism and catalytic materials. The process of ORR can occur in two pathways. The first is a four-electron process where oxygen interacts directly with electrons and protons to produce water. The second is a less efficient two-step, two-electron approach that involves the formation of hydrogen peroxide ions as an intermediary. The ORR would exhibit a sluggish rate in the absence of a catalyst at the cathode [16].

Pt nanoparticles (NPs) have historically been recognized as the most effective catalyst for the ORR. However, electrodes based on Pt are prone to time-dependent drift and deactivation caused by carbon monoxide (CO). The exorbitant expense associated with Pt catalysts poses a significant barrier to the widespread adoption of fuel cells in commercial settings. Recently, there has been a significant surge in research endeavors aimed at mitigating or substituting Pt-based electrodes in ORR. To enhance the effectiveness and productivity of Pt catalysts, a commonly employed strategy involves the immobilization of Pt constituents onto a cost-effective and highly conductive substrate. CBMs, specifically graphene, are extensively employed as a carbon substrate for Pt catalysts due to their notable attributes of possessing a large surface area and being economically advantageous. The researchers from the Xin Tong group investigated three different categories of graphene materials, which were utilized as support materials for immobilizing Pt through a wet impregnation technique. The superior ORR performance found in this study can be due to the decreased size and minimized aggregation of Pt NPs that are immobilized on the graphene sheets. This process led to the fabrication of catalysts known as Pt/graphene catalysts.

The influence of the composition of supporting materials on catalytic performance was examined and elucidated through the utilization of DFT simulation. The surface characteristics of graphene materials have the potential to influence both the size and distribution of Pt on the surface, as well as alter the electrical structure of Pt [17]. Seonghee Kim's group investigated the utilization of a pyridinic-N doped few-layer

graphene material that encapsulates a cobalt catalyst (Co-N/C) as a promising electrocatalyst for rechargeable seawater batteries (SWBs), as shown in (Fig. 2). The presence of Cl^- ions on the metal surface has been observed to have a detrimental effect on the catalytic activity, resulting in a decrease in reaction kinetics. This is attributed to the interference caused by Cl^- ions in the cleavage of O–O bonds during the oxygen reduction reaction (ORR), thereby altering the reaction mechanism from a 4-electron process to a 2-electron process. This study represents the inaugural utilization of a meticulously designed interface dipole moment in cobalt-graphene heterojunctions to impede the ingress of negatively charged chloride ions through Coulombic repulsion. In the experimental investigation, it was shown that the catalytic activity of a certain configuration of N-doped graphene-encapsulated cobalt (Co 4 mmol-N/C) with several layers exhibited exceptional performance in both alkaline and seawater environments [18]. The performance of catalyst is typically influenced by ion transport. Therefore, an optimal catalyst for ORR in seawater should possess both corrosion resistance and high activity. This can be achieved by repelling chloride ions (Cl^-) and attracting hydrogen ions (H^+) to its surface. Furthermore, theory and experimental research have shown that heteroatom-doped graphene nanomaterials, like those doped with nitrogen, can change their electronic properties and chemical reactivity. Also, these nanomaterials that have been doped can have new functions. So, they are seen as a very hopeful group of electrocatalysts for ORR that don't use noble metals.

Joseph H. Dumont et al. have conducted a study whereby they have successfully synthesized catalysts composed of nitrogen-doped GO. These catalysts exhibit

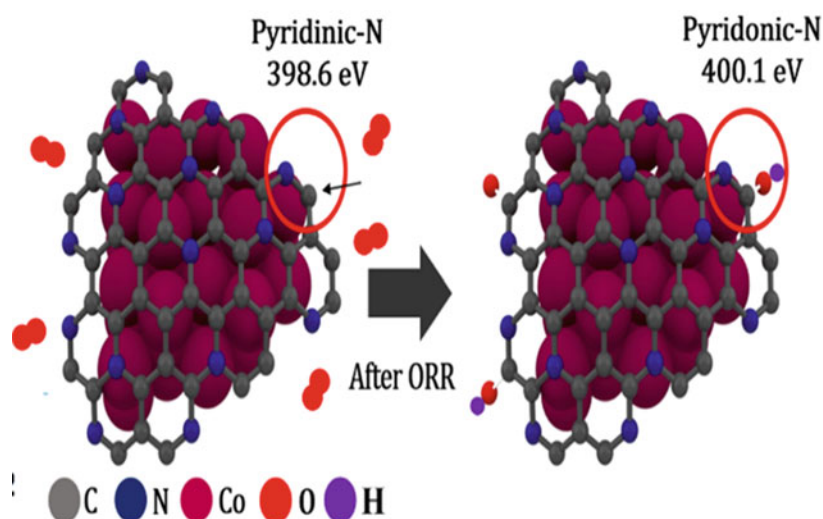


Fig. 2 Illustration of the conversion of pyridinic-N to pyrrolic-N in Co 4 mmol-N/C after cycling test. Adapted with permission [20], Copyright (2022), Elsevier

increased activity and four-electron selectivity for the ORR, achieved through the implementation of the simplest solvent and electrochemical treatments. The selection of solvents, guided by Hansen's solubility parameters, significantly influences the morphological characteristics of functionalized graphene materials. This influence is observed through two main mechanisms: (i) the creation of microporous voids in the graphitic sheets, resulting in the formation of edge defects, and (ii) the induction of a 3D structure within the graphitic sheets, which enhances the ORR. The experiment revealed a significant level of ORR activity in an alkaline electrolyte. The ORR activity commenced at an onset potential of around 1.1 V and reached a half-wave potential of 0.84 V compared to the reversible hydrogen electrode (RHE). In addition, the results of long-term stability potential cycling experiments demonstrated a little decrease in the half-wave potential (<3%) for both N₂- and O₂-saturated solutions. Moreover, the selectivity towards the four-electron reduction was enhanced after 10,000 cycles [19].

The HER is a notable electrocatalytic process that takes place at the cathode of electrolyzes employed in the process of water splitting. The process is of utmost importance in facilitating the generation of hydrogen gas (H₂) through the utilization of water. Two distinct reaction pathways lead to the HER, known as the Volmer-Tafel mechanism and the Volmer-Heyrovsky mechanism. The determination of the possible reaction way and rate-determining step (RDS) at an active site can be achieved by the application of experimental Tafel slope analysis [20]. The general rate of the HER reaction depends considerably on how well the adsorbed H* species bind to the surface. According to the Sabatier principle, an effective catalyst for the hydrogen evolution reaction (HER) should have weak binding interactions between the hydrogen species (H*) and its active sites. In recent years, significant progress has been achieved in the development of alternative electrocatalysts that do not rely heavily on Pt or contain reduced levels of Pt [21].

Numerous breakthroughs in this field have been achieved using knowledge about active sites and reaction mechanisms of HER on various catalysts. Graphene-based catalysts have exhibited superior environmental compatibility in terms of reduced heavy metal contamination and cost-effectiveness, as compared to conventional catalysts [22, 23]. Graphene-based catalysts commonly demonstrate four fundamental structural advantages in the context of the HER: (I) Efficient delivery of electrolytes to the active sites is facilitated by a significant surface area. (II) A significant level of electrical conductivity is necessary to provide rapid catalytic reaction kinetics. (III) Graphene-based catalyst exhibits a notable degree of chemical stability, enabling its structural integrity to be maintained even under the harsh conditions encountered during electrocatalysis. (IV) The presence of oxygen-containing groups in GO contributes to its improved dispersibility in different solvents. Additionally, these groups can establish chemical interactions with other materials, leading to the formation of desirable designs characterized by high conductivity and stability.

The incorporation of metal NPs and alloys with graphene is facilitated by the exceptional electrical conductivities, robust mechanical strengths, and efficient charge transfer that occurs between the catalyst and graphene material. The electrochemical features of graphene-based catalysts can be modified effectively by

different methods such as doping with heteroatom. Doping can be accomplished through two methods: carbonization of heteroatom-enriched compounds in an inert atmosphere, or post-treatment involving the use of toxic gases. Nitrogen as a dopant has garnered attention. In their groundbreaking study, Wenxin Li et al. successfully synthesized a novel core shell structure known as NiSe₂@nitrogen-doped graphene (NiSe₂@NG). This structure consists of NiSe₂ NPs that are enclosed within ultra-thin graphene shells, which have been doped with nitrogen. The graphene shells are generated from a Ni-based metal–organic framework. In both alkaline and acidic conditions, the hybrid has a relatively low onset potential of -163 mV (or -171 mV) compared to the RHE. Additionally, it demonstrates a minor overpotential of 201 mV (or 248 mV) vs. RHE at a current density of -10 mA cm⁻². Notably, it possesses a low Tafel slope of 36.1 mV dec⁻¹ (or 74.2 mV dec⁻¹). The exceptional catalytic performance of the hybrid can be ascribed to its distinctive core–shell structure. This architecture not only enhances conductivity and generates a multitude of active sites to boost electrocatalytic activity, but also ensures the chemical and structural stability of the NiSe₂ core, thereby enhancing the overall stability of the electrocatalyst [24].

Mohd. Khalid et al. have reported a method for the simultaneous electro-reduction of GO, ruthenium chloride, and gold chloride precursors in a single step. This method does not require any pre- or post-mechanical, hydrothermal, or carbonization processes. The objective of this study was to prepare a homogeneous structure by anchoring ruthenium (Ru) and gold (Au) NPs onto RGO, which serves as an efficient electrocatalyst for the HER. The Ru Au-RGO catalyst has remarkable HER activity, as evidenced by an overpotential of 56 mV at a current density of 10 mA cm⁻² [25].

In the future decades, fossil fuels will probably remain the predominant energy source. The inordinate consumption and subsequent emissions of carbon dioxide (CO₂) have resulted in significant challenges relating to resources, the environment, and climate change, also known as global warming [26]. The utilization of direct electrochemical CO₂ reduction (ECR) for the production of fuels and chemical substrates, such as hydrocarbons, shows potential as an early-stage technique to mitigate the adverse effects and decrease the atmospheric CO₂ concentration. Graphene is commonly used as a support for active phases (NPs or nanosheets) due to its large accessible surface areas and high conductivity. It has been discovered that the incorporation of metallic species (such as Ni, Fe, Co, Zn, Mn, Ru, Rh, Ir, Os, Ag, Cu, and Pt) into graphene significantly enhances the electrocatalytic activity of CO₂ reduction. In this study, Tooba et al. reported a highly effective electrocatalyst composed of copper (Cu) and tin (Sn) supported on nitrogen-doped graphene (NG). This catalyst demonstrates remarkable performance in the reduction of carbon dioxide (CO₂) across a broad range of potentials. The CuSn alloy NPs were synthesized on a substrate of NG using a hydrothermal approach to achieve a homogeneous distribution of the alloy nanoparticles. The electrocatalytic reduction of CO₂ into C1 products was conducted using a CuSn NP catalyst with a Cu/Sn ratio of 0.175 . The catalyst exhibited a high faradaic efficiency (FE) of around 93% at an overpotential of 1.0 V versus RHE. This efficiency was significantly greater than that observed for the individual Cu and Sn catalysts, which were 32% and 58% , respectively. This study

describes a novel approach that employs inexpensive non-noble metals as electrocatalysts with exceptional efficiency for the reduction of CO_2 in aquatic environments [27].

2.3 Anodic Reaction: OER

The current leading approach to produce hydrogen is the process of water splitting. The crucial complementary reaction for these processes is the OER, which entails the production of oxygen at the anode. The reaction kinetics of OER are inherently slow due to the involvement of many proton-coupled electron transfer stages. To overcome this limitation, an efficient electrocatalyst is necessary to enhance the pace of the reaction. The electro-oxidation chemical reactions that occur in acidic and alkaline environments exhibit minor variations due to the involvement of different reactive species [28]. In acidic settings, the reactive species involved is H_2O , while in alkaline conditions, it is OH^- .

To establish design principles for OER catalysts that exhibit improved activity and stability, it is crucial to undertake thorough mechanistic investigations on the surfaces of the catalysts, regardless of the operational conditions in which OER electrocatalysts are utilized. The RDS can be assessed by analyzing the Tafel slope derived from the polarization curve. There is a prevailing pattern wherein the latter stage of the reaction induces a heightened transfer coefficient, subsequently resulting in a diminished Tafel slope and accelerated kinetics. The correlation between the activity and stability of OER catalysts poses a challenge. Typically, materials that possess enhanced catalytic activity for the OER tend to display heightened susceptibility to surface structural instability during OER, which frequently leads to the dissolution of cations. Graphene and related materials have the potential to enhance the stability of these catalysts.

In 2023, Ibrahim Khan et al., present the development of water-splitting electrodes that are both self-supported and exhibit long-term stability. As can be seen clearly in Fig. 3, this is achieved through the decorating of NPs onto a 3D porous structure known as laser-induced graphene (3D-LIG). The 3D-LIG electrodes are uniformly decorated with CuO and Pt NPs by an electrochemical technique that does not require the use of binders. The electrodes are subjected to individual analysis to determine their long-term performance in terms of OER and HER activities. This paper shows such a design, HER reaction on Cu-3D-LIG paired with OER reaction over Pt-3D-LIG. The 3D-LIG has a porous and wrinkled architecture, which results in a significant increase in surface area. This unique structure also promotes the easy flow of electrolytes via the channels. The electrodes demonstrate exceptional electrochemical durability when subjected to demanding alkaline conditions [29].

An electrocatalytic OER process of tri-metal atoms (Ni, Fe, Co) embedded nitrogen-doped graphene monolayer and coordinated with pyridine nitrogen atoms was investigated by Chen Ma et al. The objective of this study is to evaluate the stability of dual-metal and tri-metal sites and to quantitatively analyze the charge

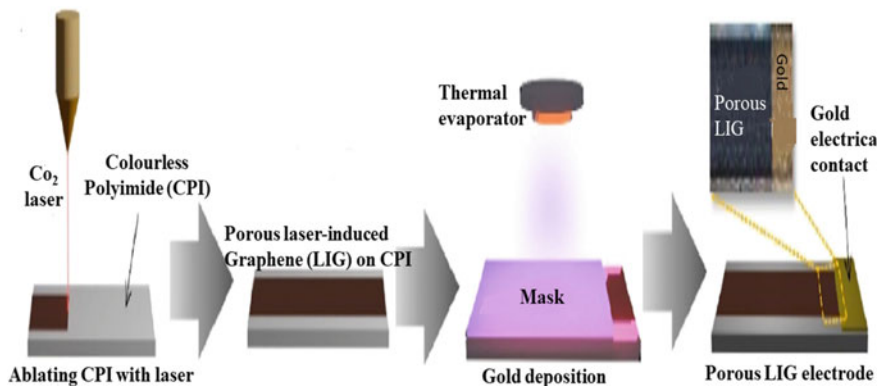


Fig. 3 Schematic image of the process of fabricating a three-dimensional laser-induced graphene (3D-LIG) electrode. Adapted with permission [30], Copyright (2023), Elsevier

redistribution of doped structures by the utilization of Bader charge analysis. The aforementioned discoveries provided significant insight into the relationship between metal-active sites and catalytic activity. [30].

2.4 Energy Storage Device: Supercapacitors

Supercapacitors (SCs) have substantial potential in facilitating the conversion and storage of electrochemical energy. SCs are electrochemical instruments that possess the ability to store energy and subsequently discharge it with notable power capacity and elevated current density within a brief temporal duration [31]. The fundamental concept underlying energy storage in a supercapacitor is either: (I) The accumulation of electrostatic charge at the electrode–electrolyte interface (electric double-layer capacitance) or (II) charge transfer to the layer of redox molecules that sit on the surface of the electrode (also known as pseudo capacitance) [32]. The efficacy of these systems is intrinsically linked to the properties of the materials utilized. Hence, the integration of material technology assumes a crucial role in enabling the advancement of SCs [33].

Extensively investigated materials for SCs electrodes encompass CBMs, metal oxides, and conducting polymers. The study of electrochemical devices has focused a lot of attention on CBMs because they enhance the electrode's electrical conductivity by increasing the mobility of the electron produced during the redox reaction. The latter will increase the electrode's ability to absorb electrolytes, hence reducing the polarization effect. Electrode materials made of CBMs have been used due to their extensive surface area, improved conductivity corrosion resistance, which allows them to operate based on electric double layer capacitance [34].

CBMs extraordinary chemical stability over a broad temperature range in both acidic and basic environments makes them highly desirable for use as electrodes in electrochemical energy devices. Due to the distinctive properties exhibited by graphene, significant attention has been directed to exploring the potential applications of graphene in the field of high-performance SCs. With a theoretical surface area of $2.63 \times 106 \text{ m}^2 \text{ kg}^{-1}$, graphene is a viable material for SCs electrodes due to its superior conductivity, tunable microstructure, and thermal/mechanical durability. Nithin Joseph Panicker et al. demonstrated a novel supercapacitor electrode material consisting of a band-gap controlled h-BN/rGO wrapped CdS/PPy. This material demonstrates exceptional performance in terms of specific capacitance, power density, and cycling stability. The compound was produced using a hydrothermal technique in conjunction with a chemical oxidative polymerization mechanism. The use of the h-BN/rGO-CdS core-shell structure effectively mitigates the phenomenon of swelling and shrinking in CdS, hence enhancing the electrochemical performance and stability of the SCs electrode [35]. Another study conducted by Jilei Liui's group fabricated NiCo₂S₄/nitrogen and sulfur dual-doped 3D holey-reduced GO (NiCo₂S₄/N, S-HRGO) composite structures using a two-step hydrothermal method for synthesis. As displayed in Fig. 4, TEM and HRTEM of the final stages of the composite show excellent distribution of this material. The enhanced super capacitive performance of the NiCo₂S₄/N, S-HRGO composite can be attributed to the utilization of 3D interconnected and highly conductive holey-reduced GO with a mesopore-rich structure, which facilitates fast electron/ion transport [36].

2.5 *Sensors and Biosensors*

An electrochemical sensor refers to a device or apparatus utilized to ascertain the observable existence, concentration, or amount of an analyte. The measurement of the electric current that is generated by chemical reactions within the electrochemical system is the fundamental principle underlying the detection of analytes by electrochemical sensors. The fundamental components of an electrochemical sensor consist of two essential elements: a chemical recognition system, which is accountable for the identification of the analyte species, and a physicochemical transducer, which facilitates the conversion of chemical interactions into electrical signals. The detection and display of these signals can be simply achieved through the utilization of modern electrical devices. The electrochemical reactions taking place at the electrode's surface interface between the recognition element and the target/binding analyte result in the formation of an electrical double layer. This potential is subsequently quantified by converting the chemical reactions into a measurable electrochemical signal using a recognition element and a sensor transducer. Electrochemical sensors have notable characteristics such as heightened sensitivity, rapid response time, affordability, instrumental simplicity, the potential for downsizing, and incorporation into portable devices.

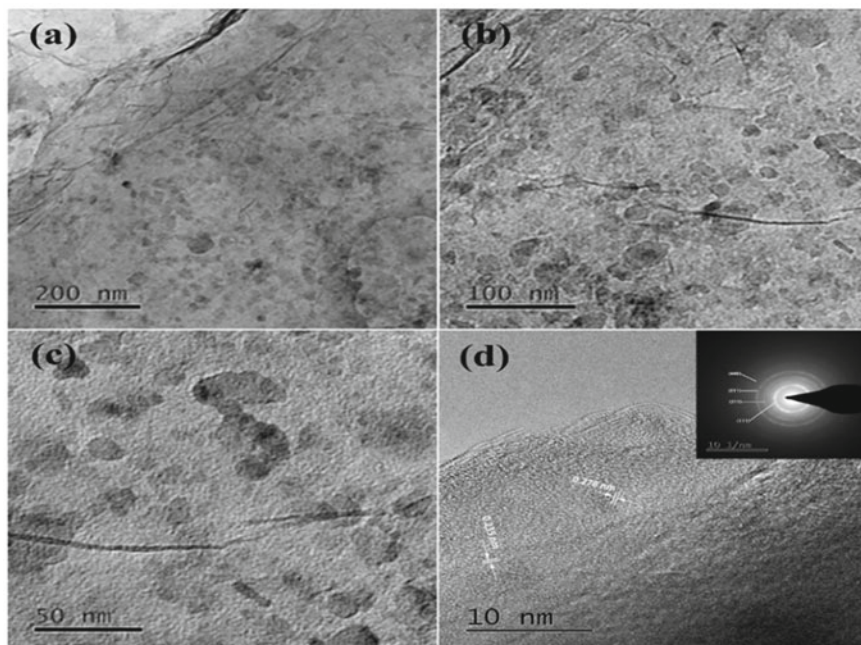


Fig. 4 a–c TEM pictures captured at various magnifications of the $\text{NiCo}_2\text{S}_4/\text{N}$, S-HRGO sample. **d** HRTEM picture of the $\text{NiCo}_2\text{S}_4/\text{N}$, S-HRGO sample, and the inset is corresponding SAED pattern. Adapted with permission [35], Copyright (2021), Elsevier

Additionally, electrochemical systems can detect a diverse array of substances, encompassing organic, inorganic, ionic, and neutral molecules, as well as metal ions [37]. The combination of CBMs and their characteristics has led to powerful electrochemical sensing platforms using “CBMs-modified electrodes” for determining various analyte species. The electrochemical sensor has undergone significant advancements over time due to its notable efficiency, straightforward functionality, and particularly, its adaptability to various chemical, physical, and biological attributes. The categorization of electrochemical sensors is based on the specific electroanalytical technique employed for the quantification of chemical interactions. The main categorizations encompass conductometric, voltammetric, and potentiometric sensors. The utilization of graphene-based nanohybrids has been widely recognized as a highly promising approach in the field of electrochemical sensing. When they were used as modifiers, the combination of these intriguing features has the potential to not only augment the kinetics of electron transfer and reduce overpotential but also boost sensitivity by increasing the peak current. Graphene has been widely used to detect and determine many analytes, including pharmaceutical formulations, biological species, and heavy metals, because of their superior properties. Usually, it is vital to apply alterations to graphene to produce GO or RGO. The underlying justification

behind this is: (I) the surface functional group of the original graphene is too minuscule to form strong bonds with other substances and, (II) the compound possesses a delocalized p-electron system and exhibits a significant surface area, rendering it prone to agglomeration and resistant to dispersion. Considering this, the functionalization and dispersion of graphene nanosheets are of the utmost significance for the application to which they will ultimately be put. As previously stated, hybrid CBMs, such as RGO composites, have already demonstrated enormous potential for electrochemical sensor construction due to their exceptional catalytic capabilities, making them emerge high-performance materials in the electrochemical sensor area. Sanaz Ghanbari et al. conducted an experimental procedure wherein RGO was subjected to functionalization through an amidation reaction with L-arginine (L-Arg), resulting in the bonding of the support and amino acid. The addition of a strong ligand, L-Arg, onto the electrode surface, resulted in the fabrication of a highly efficient catalytic sensor capable of detecting Pb(II) ions by differential pulse anodic stripping voltammetry (DP ASV). The findings of this study have emphasized the potential of RGO as a viable substrate for optical and electrochemical sensors. The electrochemical sensor that was proposed exhibits a broad linear range and a limit of detection of 0.06 nM, enabling the convenient identification of Pb(II) even in the presence of other cations [38].

Graphene-based modified electrodes have detected and determined organic pollutants and carcinogenic compounds like pesticides, anti-bacterial and anti-fungal agents, phenolic compounds, organophosphate insecticides, and toxic pharmaceutical and personal care ingredients. From the perspective of the graphene-based nanocomposite, electrochemical sensors may be categorized into two groups: “non-enzymatic sensors” and “biosensors”. Electrochemical biosensors possess the capability to identify a diverse range of biomolecules within the human body, including but not limited to glucose, cholesterol, uric acid, lactate, DNA, hemoglobin, blood ketones, and other relevant substances. To accomplish this objective, it is imperative to establish a proficient electrical connection between the active redox centers (enzymes, DNA, antigen, and so on), and the surface of the electrode. The first case pertains to electrodes that have been modified with graphene-based nanocomposite and are utilized for the analysis of samples connected to biology. The second situation involves sensing platforms that incorporate bioreceptors, such as enzymes and aptamers, capable of detecting certain biological substances. The utilization of graphene as an electron mediator in the development and production of biosensing platforms incorporating redox proteins is facilitated by their redox properties, high electrical conductivity, and biocompatibility.

Yusuf Dilmac et al. investigated a study wherein they deposited gold nanoparticles (AuNPs) onto carboxylated graphene oxide (GO-COOH) for the purpose of electrochemical oxidation, as well as enzyme-free voltammetric and amperometric measurement of glucose. The GO-COOAu modified glassy carbon electrode (GCE) demonstrated superior sensitivity and stability when used for glucose electro-oxidation in alkaline environments. The working electrodes were subjected to electrochemical characterization through the utilization of cyclic voltammetry (CV), electrochemical impedance spectroscopy (EIS), and amperometry techniques. The GO-COO

Au/GCE sensor exhibited exceptional electro-catalytic efficiency in the oxidation of glucose, demonstrating a linear range from 0.02 to 4.48 mM ($R^2 = 0.9919$) at a potential of +0.35 V shown in (Fig. 5). Additionally, the sensor had a low limit of detection (LOD) of 6 μM and a high sensitivity of 20.218 $\mu\text{A mM}^{-1} \text{cm}^{-2}$ [39]. In this study, Sopit Phetsang et al. successfully established a straightforward electrochemical synthesis method for producing a nanocomposite film consisting of Pt, RGO, and poly (3-aminobenzoic acid) (Pt/rGO/P3ABA) on a screen-printed carbon electrode (SPCE). Furthermore, explored the potential application of this nanocomposite film in the construction of highly sensitive amperometric biosensors. Electro polymerization of P3ABA, co-electrodeposition of rGO and Pt, and GO reduction to rGO were done using cyclic voltammetry. A Pt/rGO/P3ABA-modified SPCE demonstrated effective electrocatalytic oxidation of H_2O_2 and can be used to produce glucose and cholesterol biosensors by integrating glucose oxidase (GOx) and cholesterol oxidase (ChOx). Under the optimized experimental parameters, specifically at a working potential of +0.50 V, the biosensors that were proposed exhibited highly desirable linear responses to glucose and cholesterol. These linear responses were observed within the concentration ranges of 0.25–6.00 mM for glucose and 0.25–4.00 mM for cholesterol. The biosensors demonstrated sensitivities of 22.01 and 15.94 $\mu\text{A mM}^{-1} \text{cm}^{-2}$ for glucose and cholesterol, respectively. Additionally, the biosensors exhibited low detection limits (LODs) of 44.3 and 40.5 μM for glucose and cholesterol, respectively [40].

In 2022, Mantian Xue et al. fabricated a robust array of bioelectronic sensors based on graphene comprised of more than 200 integrated graphene-based sensing devices, custom-built speeds readout circuits, and portable, and trustworthy measurements. The platform provides a reversible, highly sensitive, and real-time response for sodium, potassium, and calcium ions in complex solutions despite variations in device performance [41]. In 2018, Thiago C et al. demonstrated the procedure for

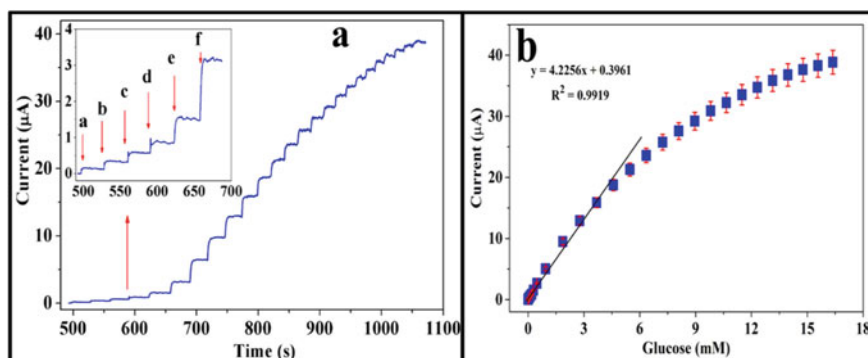


Figure 5. Amperometry responses of the GO-COOAu/GCE electrode to different concentrations of glucose (0.02 (a), 0.04 (b), 0.06 (c), 0.08 (d), 0.1 (e), and 0.2 mM glucose (f)) were measured at a potential of +0.35 V. (b) The calibration curve was generated for the amperometry technique of glucose measurement. Adapted with permission [38], Copyright (2020), John Wiley and Sons

synthesizing GO and then reducing it utilizing carbon NPs, without the use of standard chemical reducing agents or external energy sources. The endocrine disruptor bisphenol A was detected by using a printed carbon electrode coated with the rGO-CNPS nanomaterial. The SPE-rGO-CNPS electrode presented an excellent response for bisphenol A at concentrations varying from 7.5×10^{-9} to 2.6×10^{-7} mol L⁻¹ in PBS, pH 7 with sensitivity 189.5 μ mol L⁻¹ and a detection limit of 1×10^{-9} mol L⁻¹. The electrode demonstrated exceptional performance, even when exposed to significant phenolic interferences. Consequently, it was employed to quantify the concentration of bisphenol A in drinking water stored in plastic bottles [42].

3 Conclusion

To accomplish efficient electrochemical energy storage and conversion, it is essential to develop electrocatalysts with both high activity and low cost. Graphene-based materials have distinctive structures and characteristics, rendering them potentially suitable electrocatalysts. This study primarily examines the current advancements in graphene materials for electrocatalysis. The scope of the chapter encompasses several aspects, including catalytic properties, functional modification, and electrocatalytic applications specifically ORR, OER, HER, CO₂RR, SCs, supercapacitors and sensors, and biosensors.

References

1. Sumabat, A.K., Lopez, N.S., Yu, K.D., Hao, H., Li, R., Geng, Y., Chiu, A.S.F.: Decomposition analysis of Philippine CO₂ emissions from fuel combustion and electricity generation. *Appl. Energy* **164**, 795–804 (2016)
2. Cho, H.H., Strezov, V.: A comparative review on the environmental impacts of combustion-based electricity generation technologies. *Energy Fuels* **34**, 10486–10502 (2020)
3. Liu, J., Xue, Y., Zhang, M., Dai, L.: Graphene-based materials for energy applications. *MRS Bull.* **37**, 1265–1272 (2012)
4. Garlyyev, B., Fichtner, J., Piqué, O., Schneider, O., Bandarenka, A.S., Calle-Vallejo, F.: Revealing the nature of active sites in electrocatalysis. *Chem. Sci.* **10**, 8060–8075 (2019)
5. Chen, H., Liang, X., Liu, Y., Ai, X., Asefa, T., Zou, X.: Active site engineering in porous electrocatalysts. *Adv. Mater.* **32**, 1–32 (2020)
6. Novoselov, K.S., Geim, A.K., Morozov, S.V., Jiang, D., Zhang, Y., Dubonos, S.V., Grigoriva, I.V., Firsov, A.A.: Electric field effect in atomically thin carbon films. *Science* **306**, 666–669 (2016)
7. Obraztsov, A.N.: Chemical vapour deposition: making graphene on a large scale. *Nat. Nanotechnol.* **4**, 212–213 (2009)
8. Li, D., Müller, M.B., Gilje, S., Kaner, R.B., Wallace, G.G.: Processable aqueous dispersions of graphene nanosheets. *Nat. Nanotechnol.* **3**, 101–105 (2008)
9. Wang, H., Maiyalagan, T., Wang, X.: Review on recent progress in nitrogen-doped graphene: synthesis, characterization, and its potential applications. *ACS Catal.* **2**, 781–794 (2012)
10. Dai, L., Xue, Y., Qu, L., Choi, H.J., Baek, J.B.: Metal-free catalysts for oxygen reduction reaction. *Chem. Rev.* **115**, 4823–4892 (2015)

11. Green, M.A., Emery, K., King, D.L., Igari, S., Warta, W.: Solar cell efficiency tables (version 24). *Prog. Photovoltaics Res. Appl.* **12**, 365–372 (2004)
12. Villarreal, C.C., Sandoval, J.I., Ramnani, P., Terse-Thakoor, T., Vi, D., Mulchandani, A.: Graphene coupled to fluorine-doped tin oxide as transparent conductor in ZnO dye-sensitized solar cells. *J. Environ. Chem. Eng.* **10**, 107551 (2022)
13. Tang, C.W., Vanslyke, S.A.: Organic electroluminescent diodes. *Appl. Phys. Lett.* **51**, 913–915 (1987)
14. Pan, F., Sun, C., Li, Y., Tang, D., Zou, Y., Li, X., Bai, S., Wei, X., Lv, M., Chen, X., Li, Y.: Solution-processable n-doped graphene-containing cathode interfacial materials for high-performance organic solar cells. *Energy Environ. Sci.* **12**, 3400–3411 (2019)
15. Zhou, Q., Tang, S., Yuan, G., Zhu, W., Huang, Y., Li, S., Lin, M.: Tailored graphene quantum dots to passivate defects and accelerate charge extraction for all-inorganic CsPbIBr₂ perovskite solar cells. *J. Alloys Compd.* **895**, 162529 (2022)
16. Wang, X., Zhi, L., Müllen, K.: Transparent, conductive graphene electrodes for dye-sensitized solar cells. *Nano Lett.* **8**, 323–327 (2008)
17. Tong, X., Zhan, X., Gao, Z., Zhang, G., Xie, Y., Tian, J., Ranganathan, H., Li, D., Claverie, J.P., Sun, S.: Effect of the metal-support interaction in platinum anchoring on heteroatom-doped graphene for enhanced oxygen reduction reaction. *Chem. Commun.* **1**, 11519–11522 (2022)
18. Kim, S., Ji, S., Yang, H., Son, H., Choi, H., Kang, J., Li, O.L.: Near surface electric field enhancement: Pyridinic-N rich few-layer graphene encapsulating cobalt catalysts as highly active and stable bifunctional ORR/OER catalyst for seawater batteries. *Appl. Catal. B Environ.* **310**, 121361 (2022)
19. Dumont, J.H., Martinez, U., Artyushkova, K., Purdy, G.M., Dattelbaum, A.M., Zelenay, P., Mohite, A., Atanassov, P., Gupta, G.: Nitrogen-doped graphene oxide electrocatalysts for the oxygen reduction reaction. *ACS Appl. Nano Mater.* **2**, 1675–1682 (2019)
20. Diard, J.P., Landaud, P., Le Gorrec, B., Montella, C.: Calculation, simulation and interpretation of electrochemical impedance. Part II. Interpretation of Volmer-Heyrovsky impedance diagrams. *J. Electroanal. Chem.* **255**, 1–20 (1988)
21. McKone, J.R., Sadtler, B.F., Werlang, C.A., Lewis, N.S., Gray, H.B.: Ni-Mo nanopowders for efficient electrochemical hydrogen evolution. *ACS Catal.* **3**, 166–169 (2013)
22. Wang, Y., Su, H., He, Y., Li, L., Zhu, S., Shen, H., Xie, P., Fu, X., Zhou, G., Feng, C., Zhao, D., Xiao, F., Zhu, X., Zeng, Y., Shao, M., Chen, S., Wu, G., Zeng, J., Wang, C.: Advanced electrocatalysts with single-metal-atom active sites. *Chem. Rev.* **120**, 12217–12314 (2020)
23. Cao, L., Luo, Q., Liu, W., Lin, Y., Liu, X., Cao, Y., Zhang, W., Wu, Y., Yang, J., Yao, T., Wei, S.: Electrocatalytic hydrogen evolution. *Nat. Catal.* **2**, 134–141 (2019)
24. Li, W., Yu, B., Hu, Y., Wang, X., Yang, D., Chen, Y.: Core-shell structure of NiSe₂ Nanoparticles@Nitrogen-Doped graphene for hydrogen evolution reaction in both acidic and alkaline media. *ACS Sustain. Chem. Eng.* **7**, 4351–4359 (2019)
25. Khalid, M., Zarate, X., Saavedra-Torres, M., Schott, E., Maria Borges Honorato, A., Rafe Hatshan, M., Varela, H.: Electro-reduced graphene oxide nanosheets coupled with RuAu bimetallic nanoparticles for efficient hydrogen evolution electrocatalysis. *Chem. Eng. J.* **421**, 129987 (2021)
26. Khalili, S., Afkhami, A., Madrakian, T.: Environmental Electrochemical simultaneous treatment approach: electro-reduction of CO₂ at Pt/PANI @ ZnO paired with wastewater electro-oxidation over PbO₂. *Appl. Catal. B Environ.* **328**, 122545 (2023)
27. Xiong, W., Yang, J., Shuai, L., Hou, Y., Qiu, M., Li, X., Leung, M.K.H.: CuSn alloy nanoparticles on nitrogen-doped graphene for electrocatalytic CO₂ reduction. *ChemElectroChem* **6**, 5951–5957 (2019)
28. Liang, Y., Li, Y., Wang, H., Zhou, J., Wang, J., Regier, T., Dai, H.: Co₃O₄ nanocrystals on graphene as a synergistic catalyst for oxygen reduction reaction. *Nat. Mater.* **10**, 780–786 (2011)
29. Khan, I., Baig, N., Bake, A., Haroon, M., Ashraf, M., Al-Saadi, A., Tahir, M.N., Wooh, S.: Robust electrocatalysts decorated three-dimensional laser-induced graphene for selective alkaline OER and HER. *Carbon N. Y.* **213**, 118292 (2023)

30. Ma, C., Feng, J., Xia, C., Du, C., Chen, X., Pang, B., Dong, H., Yu, L., Dong, L.: Theoretical insights into multi-metal atoms embedded nitrogen-doped graphene as efficient bifunctional catalysts for oxygen reduction and evolution reactions. *Appl. Surf. Sci.* **605**, 154714 (2022)
31. Zhang, L., Zhao, X.S.: Carbon-based materials as supercapacitor electrodes. *Chem. Soc. Rev.* **38**, 2520–2531 (2009)
32. Adriyani, T.R., Ensafi, A.A., Rezaei, B.: Flexible and sewable electrode based on Ni—Co @ PANI—salphen composite—coated on textiles for wearable supercapacitor. *Sci. Rep.* **13**, 19772 (2023)
33. Verma, R.U.: Generalized relaxed proximal point algorithms involving relative maximal accretive models with applications in Banach spaces. *Commun. Korean Math. Soc.* **25**, 313–325 (2010)
34. Ramadas, A., Dinesh, A., Shankaranarayana, M., Rani, M., Venkatesh, K., Patil, J.M., Mohan, C.B., Basavarajiah, H., Yogesh, K.: Functionalized graphene-MoO₂ frameworks: an efficient electrocatalyst for iron-based redox flow battery and supercapacitor application with enhanced electrochemical performances. *J. Phys. Chem. Solids* **171**, 110990 (2022)
35. Panicker, N.J., Ajayan, P.M., Sahu, P.P.: Band-gap tuned hexagonal-boron nitride/reduced graphene oxide superlattice wrapped cadmium sulfide/Polypyrrole nanocomposite as an efficient supercapacitor electrode material. *J. Energy Storage* **56**, 105901 (2022)
36. Liu, J., Chen, X., Zhu, Y., Chen, R., Yuan, W.: NiCo₂S₄/nitrogen and sulfur dual-doped three-dimensional holey-reduced graphene oxide composite architectures as high-rate battery-type cathode materials for hybrid supercapacitors. *Vacuum* **190**, 110302 (2021)
37. Goud, K.Y., Kumar, S., Gobi, K.V., Kim, K.: Biosensors and bioelectronics progress on nanostructured electrochemical sensors and their recognition elements for detection of mycotoxins: a review. *Biosens. Bioelectron.* **121**, 205–222 (2018)
38. Ghanbari, S., Ahour, F., Keshipour, S.: An optical and electrochemical sensor based on l-arginine functionalized reduced graphene oxide. *Sci. Rep.* **12**, 1–14 (2022)
39. Dilmac, Y., Guler, M.: Fabrication of non-enzymatic glucose sensor dependent upon Au nanoparticles deposited on carboxylated graphene oxide. *J. Electroanal. Chem.* **864**, 114091 (2020)
40. Phetsang, S., Jakmunee, J., Mungkornasawakul, P., Laocharoensuk, R., Ounnunkad, K.: Sensitive amperometric biosensors for detection of glucose and cholesterol using a platinum/reduced graphene oxide/poly(3-aminobenzoic acid) film-modified screen-printed carbon electrode. *Bioelectrochemistry* **127**, 125–135 (2019)
41. Xue, M., Mackin, C., Weng, W.H., Zhu, J., Luo, Y., Luo, S.X.L., Lu, A.Y., Hempel, M., McVay, E., Kong, J., Palacios, T.: Integrated biosensor platform based on graphene transistor arrays for real-time high-accuracy ion sensing. *Nat. Commun.* **13**, 1–11 (2022)
42. Canevari, T.C., Rossi, M.V., Alexiou, A.D.P.: Development of an electrochemical sensor of endocrine disruptor bisphenol A by reduced graphene oxide for incorporation of spherical carbon nanoparticles. *J. Electroanal. Chem.* **832**, 24–30 (2019)

Electrocatalytic Properties of Fullerene-Based Materials



Emilia Grądzka

Abstract This chapter provides a comprehensive review of research related to the electrocatalytic properties of fullerenes and their derivatives. The paper begins with general information about problems that occur in electrocatalysis and its role in the modern technology of clean energy sources. Next, general information about fullerenes and their derivatives is presented. Additionally, their role in many applications is mentioned. An electrocatalytic area is noticed. Thus, chemical processes based on the electrocatalytic properties of fullerenes, and their derivatives are described. The electrocatalytic activity of materials such as doped, exo-, and endohedral fullerenes is described. Additionally, fullerene-like materials or materials formed from fullerenes are mentioned. Composite materials of fullerenes and carbon nanostructures, metal–organic frameworks, metal oxides, metallic nanoparticles, or bimetallic systems are discussed. Their electrocatalytic performance is compared to commercial catalysts used in these systems. To date, many different catalytic systems have been studied, and this scientific area is very broad. Recently, carbon nanomaterials have been studied intensively due to their unusual chemical and physical properties. Among them, special attention has also been paid to fullerenes as pure carbon allotropes with unique structures and properties.

Keyword Fullerenes · Electrocatalytic properties, · Oxygen reduction reaction, · Hydrogen evolution reaction, · Oxygen evolution reaction, · Methanol oxidation reaction, · Catalyst

1 Introduction

Currently, electrocatalysis plays a key role in today's world due to the global energy crisis, which forces the use of "clean" energy sources such as fuel cells, which use the chemical energy of hydrogen or other fuels. Fuel cells have many potential practical applications. They can be used in a wide range of fuels and feedstocks and can

E. Grądzka (✉)

Faculty of Chemistry, University of Białystok, Ciołkowskiego 1K, 15-245 Białystok, Poland
e-mail: emilia@uwb.edu.pl

provide power for systems as large as a utility power station and as small as a laptop computer. However, their efficiency is hindered by the sluggish kinetics of electrode reactions. Thus, scientists are searching for new catalysts with excellent activities for oxygen and/or hydrogen and alcohol that can substantially outperform the catalytic activity and long-term electrochemical stability properties of conventional benchmark catalysts. Mostly, carbon black is used as a catalyst support [1]. However, during fuel cell operation, carbon undergoes electrochemical oxidation to oxidized carbon and eventually to CO_2 when it is subjected to high acidity, high potential, high humidity, and high temperature ($\sim 80^\circ\text{C}$). Carbon corrosion results in the detachment of noble metal nanoparticles from the electrode or the ripening of larger aggregates. Oxidation of the carbon support can also lead to changes in surface hydrophobicity that can cause gas transport difficulties [2]. Therefore, increasing attention has been given to solving carbon corrosion by finding another alternative material. Recently, special attention has been given to carbon nanostructures such as carbon nanotubes, graphene, and fullerenes due to their high surface area and electrical conductivity. Among these supports, fullerene could be a good choice due to its high surface area and high thermal and mechanical stability [3].

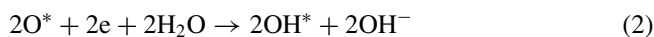
Fullerenes are one of the groups of carbon allotropes. They are zero-dimensional (0D) hollow spherical carbon spheres characterized by a closed-cage structure with no edges. The first fullerene, C_{60} , was discovered in 1985, but the family of fullerenes includes a wide range of carbon-based molecules with different numbers of carbon atoms and symmetries. They are built from pentagon and hexagon rings. The most stable fullerenes are those in which each pentagon is surrounded by hexagons. Their well-defined structure, unique chemical, optical, and electronic properties, high electron affinity, and high physicochemical stability provide them with many practical applications [3]. The main advantage of fullerenes over other carbon nanomaterials is their well-defined molecular structure, which can be easily covalently modified. Extensive progress in organic chemistry research on fullerene facilitates the production of a variety of fullerene derivatives with different structures and physicochemical properties. Additionally, the polyhedral structure of fullerenes containing many bonding sites provides an opportunity for a wide range of covalent modifications. Moreover, they can also be polymerized. Polymeric structures containing fullerene moieties represent a particularly large class of materials with unique properties. Due to the empty space inside the fullerene structure, fullerene can enclose many species. Recently, unfolding fullerenes have been shown to generate a carbon matrix with rich topological defects and active sites, which may facilitate binding with other heteroatoms. Fullerenes also exhibit a high affinity for constructing supramolecular assemblies [4].

The large number of different fullerene-based material properties provides many potential practical future applications, among which the significant applications are related to systems that exhibit electrocatalytic properties in the many chemical processes described below.

2 Oxygen Reduction Reaction

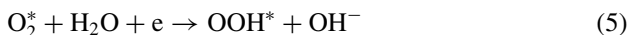
Currently, rapid technological progress provides large-scale production of new and fast devices that need efficient storage systems, such as fuel cells, batteries, or supercapacitors. Fuel cells and metal – air batteries are promising technologies, especially for automotive industries, due to their high energy densities, low operating temperature, and environmental compatibility. The main problem that occurs in fuel cells and metal-air batteries is the slow kinetics of the oxygen reduction reaction (ORR) at the cathode, which limits their efficiency [5]. Due to the sluggish rate of the ORR reaction, it has been the most intensively studied last time [5, 6]. The second problem is the corrosion of the carbon support. The most popular catalysts are carbon black-supported platinum nanoparticles (Pt/C), but their corrosion under fuel cell operating conditions drastically affects the performance of PEMFCs (proton-exchange membrane fuel cells). Pt/C degradation includes the two aspects of the catalyst (Pt) and one aspect of the carbon support, which influence each other. Pt catalyzes the oxidation of carbon, and the oxidation of carbon further accelerates Pt sintering [5, 7]. The application of Pt-based catalysts is also hindered by Pt's high cost and its sensitivity to deactivation in the presence of CO [8]. Thus, much attention has been given to improving the efficiency of Pt-based catalysts or to searching for new more-effective catalysts. Apart from platinum, palladium has also been studied thus far. However, Pd nanoparticles resulted in lower activity than Pt catalysts [5].

Recently, it was demonstrated that pristine fullerenes or fullerene-based materials can be used as efficient electrocatalytic systems. Such an approach based on mesoporous fullerene C₆₀ and a copper/copper oxide catalyst (MFC₆₀/Cu/Cu₂O) was proposed by Saianand and coworkers [9]. The copper anchored in mesoporous fullerene displays excellent catalytic properties due to the synergistic effects arising from the well-defined and robust structures and contact interface with the catalytic metal nanoparticles. Mesoporous fullerene decorated with Cu/Cu₂O exhibited superior electrocatalytic properties toward the oxygen reduction reaction with onset potential, diffusion-limiting current density, and stability higher than pristine nonmodified mesoporous C₆₀. This system was also characterized by high selectivity with exclusive four-electron transfer pathways. The high ORR performance of MFC₆₀/Cu/Cu₂O has two sources: (i) a hierarchical porous structure with a high surface area tuned by Cu and (ii) enhanced electrical conductivity due to the presence of Cu, which can facilitate ORR activity. Thus, more ORR active sites can be exposed to molecular oxygen, and the mass transport resistance may decrease significantly due to the appropriate structure. Sufficient exposure of ORR active sites can create shorter channel lengths, resulting in high electrochemical activity of the electrocatalyst. For the four-electron transfer process, there can be two possible dissociative pathways.





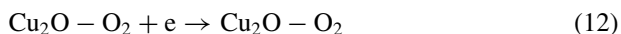
and an associative 4e pathway,



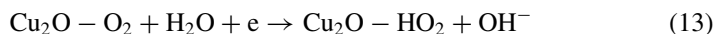
or an associative 2e pathway



mechanism in alkaline solutions, where * represents the catalytic active site on the surface. This mechanism involves the initial adsorption of O_2 and then O–O bond cleavage to form two adsorbed atomic O^* species. The O^* species are transformed to water or OH^- through the gaining of two protons and two electrons to form OH^* , and OH^- is eventually formed by the addition of two electrons. In the case of the $\text{MFC}_{60}/\text{Cu}/\text{Cu}_2\text{O}$ system, where high electrocatalytic activity derives from the synergistic effect of the porous C_{60} and catalyst Cu, Eq. (4) may proceed with the following first-order rate-determining step:



The rate-limiting first electron transfer reaction involved the adsorbed O_2 to form superoxide on Cu_2O (Eq. (12)), with a concurrent reaction with water:



Mao and coworkers performed a comprehensive computational study of the catalytic activities of various fullerenes and fullerene fragment species by using density functional theory (DFT) and computational hydrogen electrode (CHE)

methods [8]. They showed that pentagon rings play a crucial role in boosting catalytic activities for the oxygen reduction reaction. The active sites associated with more pentagon rings show stronger adsorption toward O^* , OH^* and OOH^* species. However, the fundamental chemical mechanism underlying the remarkable catalytic effect of the pentagon rings toward the ORR is still not fully understood. It was shown that fullerene-based fragments exhibit higher electrocatalytic activity toward the ORR than fullerenes. The highest electrocatalytic activity and suitable adsorption-free energy of OH^* and OOH^* species were observed in the case of C_{60} -frag1 and C_{60} -frag2 (Fig. 1). This can be attributed to the high-energy HOMO orbitals induced by the low-symmetry fullerene fragment structures.

The combination of experimental and theoretical methods by Sanad and coworkers [10], who studied spheroidal C_{60} and C_{70} fullerenes and tubular C_{90} , C_{96} and C_{100} fullerenes, showed that C_{96} displayed the highest oxygen reduction reaction activity close to the state-of-the-art Pt/C benchmark. Both the onset potential and halfway potential were like those obtained in the case of Pt/C. It was found that the valence band of C_{96} is closer to the standard water splitting and oxygen reduction reaction standard potentials (Fig. 2a), which indicates the potential capability of C_{96} to reduce oxygen. The density of states (DOS) calculations showed a high density of states near the Fermi level in the case of C_{90} , C_{96} , and C_{100} , supporting the high electrocatalytic activity of the fullertubes, as shown in Fig. 2b. Figure 2c shows the Gibbs free energy and ORR reaction intermediates for both C_{96} and Pt/C. Free energy calculations showed that the limiting elementary step for the ORR is OH_{ads} , which has a small energy barrier in the case of C_{96} and thus its more favorable adsorption to the C_{96} surfaces.

Theoretical studies were also performed for heteroatom-doped fullerenes such as $C_{59}N$, $C_{59}P$, $C_{59}Si$, $C_{59}B$ and $C_{59}S$ [11]. It was shown that combining curvature, unique defects, and suitable dopants should be a promising strategy to explore

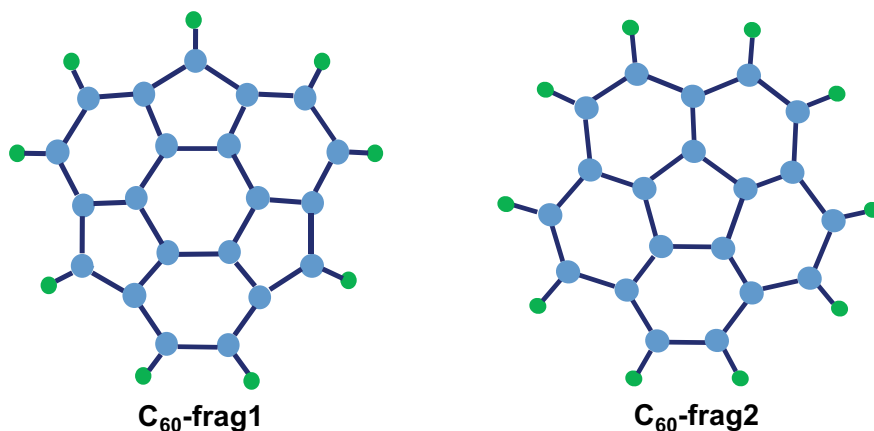


Fig. 1 Two C_{60} -based fragment structures with H passivation at the edges. The blue spheres represent C atoms, and the green spheres represent H atoms

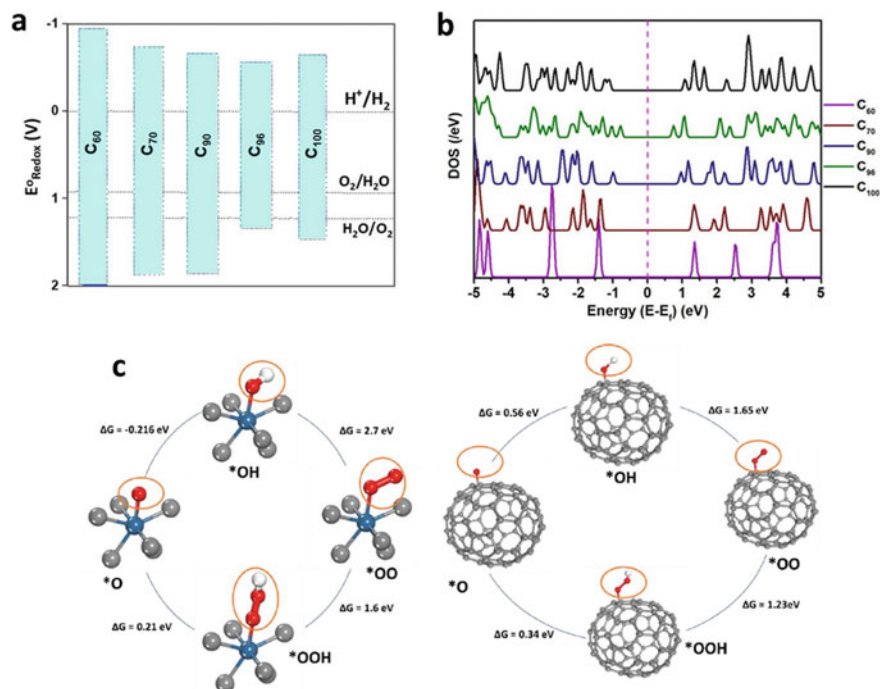


Fig. 2 **a** Experimental band structures of C_{60} , C_{70} , C_{90} , C_{96} , and C_{100} . **b** Density of states of C_{60} , C_{70} , C_{90} , C_{96} , and C_{100} . **c** Gibbs free energy of the oxygen reduction reaction calculated using benchmark Pt/C and C_{96} molecular catalyst. Adapted with permission [10], Copyright (2022), Wiley-VCH GmbH

advanced fullerene-based metal-free electrocatalysts. Promising results were also obtained in the case of codoped transition metal M and heteroatom N_4 in vacancies of fullerene ($M-N_4-C_{64}$), where such metals as Fe, Co, and Ni were studied [12]. Mulliken charge analysis shows that the metal center is the reaction site of the ORR and that the electron transfer from the metal center to N_4-C_{64} is the largest in the case of $Fe-N_4-C_{64}$. From a theoretical point of view, endohedral metalofullerenes also exhibit good electrocatalytic performance [13]. A significant improvement was also obtained by the formation of composites of fullerenes with different carbon nanostructures, such as carbon nanotubes [14] and graphene [15]. High ORR electrocatalytic activity was also reported for fullerene C_{60} encapsulated inside imidazolate framework-8 (ZIF-8) [16].

Additionally, fullerene-like carbons have been demonstrated as effective electrode materials for electrocatalytic reactions. Gao and coworkers proposed a nitrogen-doped fullerene-like shell (Fig. 3) as an efficient electrocatalytic system for the oxygen reduction reaction [17]. The N-doped carbon material (NDCS) was prepared by using a facile method with fallen ginkgo leaves, which are naturally available and constantly renewable as carbon and nitrogen precursors. The NDCS was shown

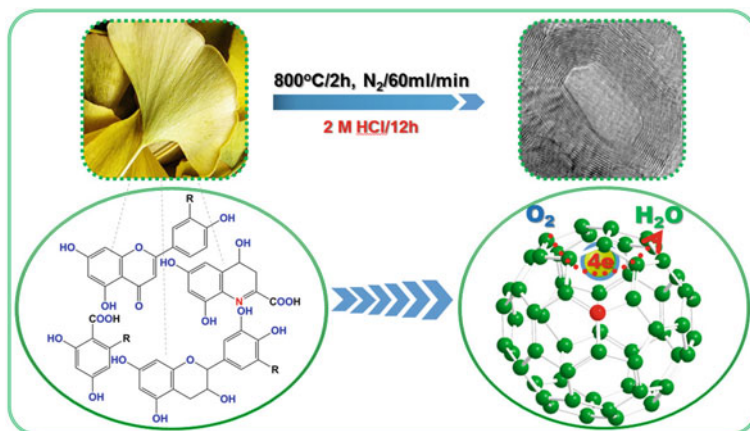


Fig. 3 Illustrated procedure for fabricating N-doped fullerene-like carbon shells from organic-rich fallen ginkgo leaves. Adapted with permission [17], Copyright (2015), Elsevier

to catalyze a four-electron transfer process for the ORR with much higher electrocatalytic activity, lower overpotential, smaller crossover effect, and better long-term operation stability than commercially available platinum-based electrodes in alkaline electrolytes.

N-induced charge delocalization could change the chemisorption mode of O_2 from the usual end-on adsorption at the nanocarbon surface, named the Pauling model, to side-on adsorption, described as the Yeager model, on the nitrogen-doped nanocarbon electrodes. The parallel diatomic adsorption could effectively weaken the O–O bonding to facilitate the ORR. Doping carbon nanostructures with nitrogen heteroatoms can efficiently create metal-free active sites for the electrochemical reduction of O_2 . In N-doped fullerenes, charge transfer occurs between the N and C atoms, resulting in an unbalanced charge distribution in the carbon cage skeleton. Thus, N-doped fullerene-like carbons seem to be the best type for electrocatalysis [17, 18].

Promising electrocatalytic properties can also be obtained by the incorporation of carbon structure by additional, other than nitrogen, atoms such as sulfur [19], phosphorous [20] or ferric [21]. The solid-state growth of fullerene-derived carbon nanotubes from Fe- C_{60} hierarchical microstructures at different temperatures is shown in Fig. 4a. Depending on the synthesis temperature, different structures of synthesized materials were obtained (Fig. 4b). The largest number of carbon nanotubes exhibiting curved and entangled structures was obtained in the case of synthesis carried out at 730 °C (MN7-10/3). These nanotubes of 10–12 nm in diameter have less than seven layers of walls with a lattice distance of 0.34 nm, corresponding to the (002) plane of graphite. Figure 4c shows cyclic voltammetric curves of all synthesized materials and Pt/C catalyst indicative of superior ORR performance in the case of MN7-10/3. This material has the most positive potential corresponding

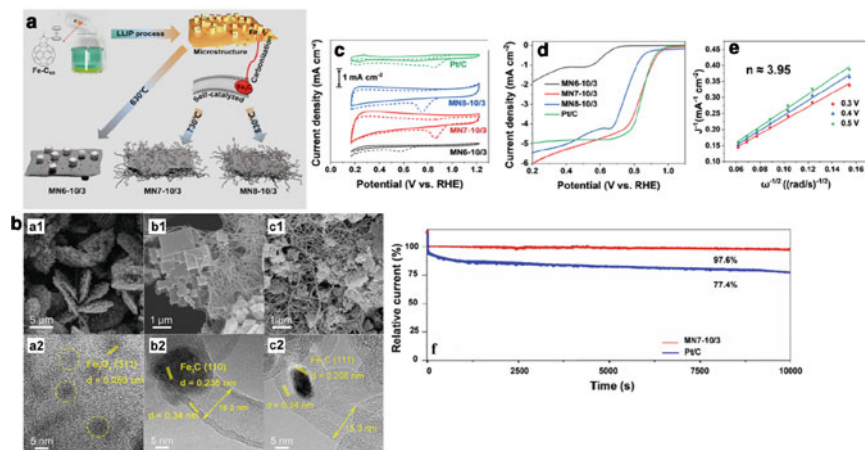


Fig. 4 X **a** Illustration of the in situ growth from fullerene derivative Fe-C₆₀ to carbon nanotubes. **b** SEM images of (a1) MN6-10/3, (b1) MN7-10/3, and (c1) MN8-10/3 and TEM images of (a2) MN6-10/3, (b2) MN7-10/3, and (c2) MN8-10/3. **c** CV curves of MN6-10/3, MN7-10/3, MN8-10/3, and Pt/C in N₂- (dotted line) and O₂-saturated (solid line) 0.1 M KOH solutions (scanning rate: 10 mV s⁻¹). **d** LSV curves of MN6-10/3, MN7-10/3, MN8-10/3, and Pt/C at 1600 rpm in O₂-saturated 0.1 M KOH solutions (scanning rate: 10 mV s⁻¹). **e** Electron transfer numbers calculated based on K-L plots. **f** Stability of MN7-10/3 and Pt/C. Adapted with permission [21], Copyright (2022), American Chemical Society

to the oxygen reduction reaction. Moreover, it exhibited the highest half-wave potential and the largest onset potential (Fig. 4d) among all synthesized systems. These values are comparable to those obtained for commercial Pt/C catalysts. The average electron transfer number estimated at operating voltages from 0.3 to 0.5 V is approximately 3.95 (Fig. 4e), which indicates a preferential four-electron ORR process. The long-term stability performance of MN7-10/3 was also significantly higher than that of the Pt/C benchmark (Fig. 4f).

3 Methanol/Ethanol Oxidation Reaction

Finally, direct methanol (DMFC) or ethanol (DEFC) fuel cells have received increasing attention and have been extensively studied as promising energy conversion devices to replace current fossil fuels. The sources of methanol and ethanol are abundant and have good electrochemical activity due to their eco-friendly nature, facile storage, cost-efficiency, and easy transport of gaseous hydrogen fuel [22]. The most common catalyst used for methanol oxidation is platinum. However, the short lifespan due to the formation of poisoned CO intermediates during the irreversible reaction in alcohol oxidation, high cost and low abundance are key problems that hinder the commercialization of alcohol fuel cells. Increasing attention has

been given to fullerenes and other carbon nanostructures because they are attractive support materials for alcohol fuel cells due to their extraordinary physical properties, abundance, processability, environmental friendliness and relative corrosion stability in both acidic and basic conditions [23, 24]. The Pt or Pd-fullerene hybrid catalyst exhibits significantly enhanced electrocatalytic activity and stability for the alcohol oxidation reaction compared to the unsupported Pt or commercial catalyst. Fullerene derivatives such as fulleropyrrolidine [25], fullerene ammonium iodide [26] or polyhydroxy fullerenes [27] have been studied as carbon supports. Promising electrocatalytic properties toward ethanol oxidation were also obtained for palladium nanoparticles supported on hydroxypropyl- β -cyclodextrin-modified C₆₀ fullerene [28]. The carbon support area was extended to fullerene derivative composites with carbon nanostructures. Such an approach was proposed by Zhang and coworkers [29], who fabricated graphene oxide-multisubstituted fulleropyrrolidone hybrid materials as a support deposition of Pd nanoparticles.

Moreover, bi and trimetallic catalytic materials [22] and Pt- or Pd-free catalysts based on fullerenes have been formed [24]. Bhavani and coworkers [24] proposed a nanocomposite material employing gold nanoparticles and fullerene-C₆₀ at a glassy carbon electrode (AuNP@reduced-fullerene-C₆₀/GCE) as an anode for high-performance oxidation of methanol (Fig. 5). Fullerene-C₆₀ was manually dropped on a pretreated GCE electrode and partially electroreduced in KOH to make it more conductive. Gold nanoparticles (AuNPs) were deposited on a reduced-fullerene-C₆₀ modified electrode under cyclic voltammetric conditions. In the obtained catalyst, AuNPs are uniformly distributed on the reduced fullerene surface. The cyclic voltammetric response of AuNP@reduced-fullerene-C₆₀/GCE is characterized by two well-defined peaks (Fig. 5B), indicating the facile oxidation of methanol, whereas fullerene-C₆₀/GCE and GCE do not exhibit these signals. The forward voltammetric peak corresponds to the oxidation of methanol, and the reverse peak reveals the formation of intermediates. This material also exhibits good linearity between the peak current and scan rate, indicating that the oxidation reaction of methanol is diffusion controlled. Compared to other catalytic systems based on Pd or Pt, it exhibits superior electrocatalytic properties. This result shows that the addition of gold nanoparticles to fullerene could enhance electrocatalytic properties due to the change in electronic structure and the improvement in the electrochemically active surface area. Changes in the electronic structure of the catalyst are strongly associated with the secondary oxidation peak in the reverse scan. This peak can be attributed to the inability of the gold atoms' surface to equilibrate with the lattice atoms after the reduction of the blocking oxide film. This consequently leads to superior catalytic activity by the exposed high-energy sites (Fig. 5A). The presence of hydrogen adsorption and desorption peaks confirms the availability of many active sites at the surface of the electrocatalyst. The enhancement in the anodic peak corresponds to the desorption of hydrogen, also suggesting the potential catalytic tendency of AuNP@reduced-fullerene-C₆₀/GCE for methanol electro-oxidation. This electrocatalyst also exhibits low charge transfer resistance (Fig. 5D) due to its high surface area and conductivity.

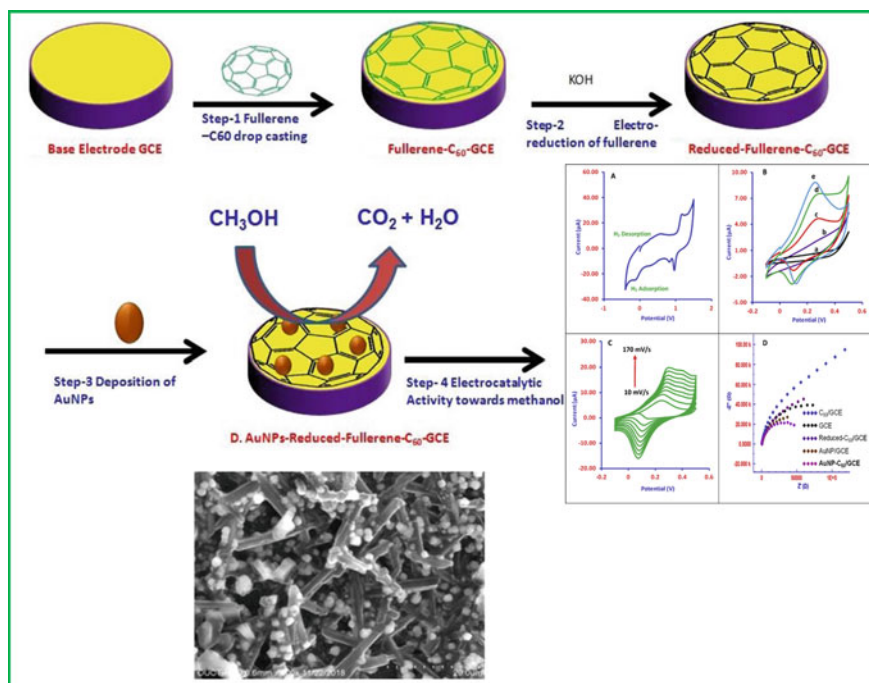


Fig. 5 Schematic illustration of the preparation of the electrocatalyst/electrode and methanol oxidation performance. **A** CV of AuNP-reduced-fullerene- C_{60} catalyst recorded in 0.5 M H_2SO_4 in the potential scan -0.3 V -1.5 V. **B** CVs of fullerene- C_{60}/GCE (a), GCE (b), reduced-fullerene- C_{60}/GCE (c), AuNP/GCE (d) and AuNP-reduced-fullerene- C_{60}/GCE (e) in 1 M methanol containing 1 M NaOH. **C** Effect of scan rate on the voltammetric behavior of methanol at AuNP-reduced-fullerene- C_{60}/GCE . **D** EIS plots of all five electrodes in 1 M methanol containing 1 M NaOH. Adapted with permission [24], Copyright (2019), Elsevier

4 Hydrogen and Oxygen Evolution Reactions

Because of accelerated global warming due to the accumulation of greenhouse gases, the most promising fuel is hydrogen. Unlike fossil fuels, the combustion of hydrogen does not produce greenhouse gases that contaminate the natural environment but only water vapor. Hydrogen can be generated by splitting water with excess renewal energy in an electrolyzer. Electro-catalytic water splitting, which is a reverse process of fuel cell reactions, involves the cathodic hydrogen evolution reaction (HER) and the anodic oxygen evolution reaction (OER). Both reactions require efficient catalysts to accelerate the reaction kinetics to make the electrolyzer practically feasible (Fig. 6) [30].

Noble Pt is the most used catalyst due to its high exchange current density and small Tafel slope. However, the high cost of Pt prohibits its commercial application for sustainable hydrogen and oxygen production [32]. Thus, much attention has been given to the preparation of low-cost, stable, and effective catalytic materials. Among

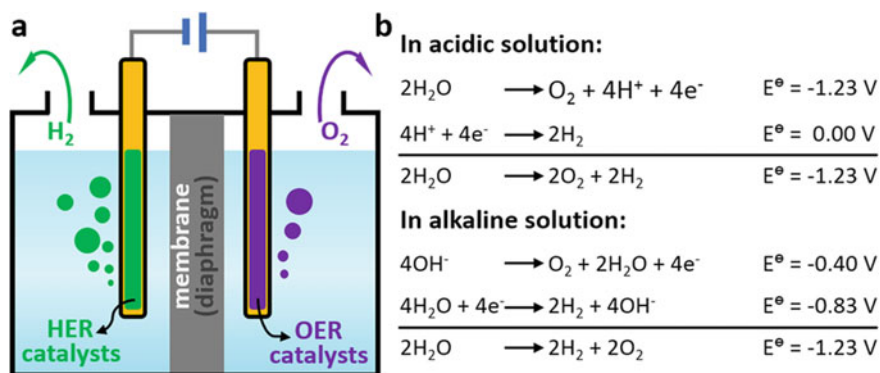
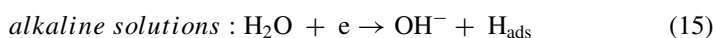
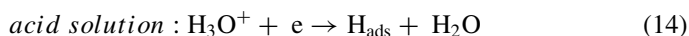


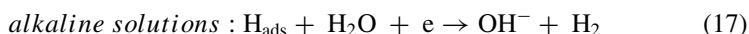
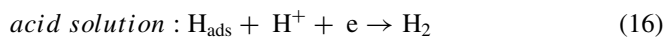
Fig. 6 X **a** Scheme of conventional water electrolyzers. **b** Water splitting reactions under acidic and alkaline conditions. Adapted with permission [31], Copyright (2018), American Chemical Society

different carbon materials, such as carbon nanotubes or graphene, fullerenes have been adopted for the improvement of hydrogen and oxygen evolution reactions.

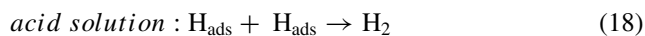
The hydrogen evolution reaction includes the adsorption and removal of adsorbed hydrogen atoms on the electrode surface. The first step of the hydrogen evolution reaction is the discharge of H_3O^+ or H_2O dependent on the pH to produce a hydrogen atom absorbed on the catalyst's surface (Volmer reaction):



The second step can be two possible pathways. One is the electrochemical desorption step, described as the Heyrovsky reaction:



The other is the Tafel recombination reaction involving two adsorber hydrogen atoms:



These are competitive processes, and a good catalyst should have an ideal balance between binding and releasing of adsorbed reaction intermediates [30].

Narwade and coworkers showed for the first time the electrocatalytic activity of C_{60} decorated with Ag nanoparticles [33] toward hydrazine oxidation, which is one of the fuel cell reactions for hydrogen generation. The obtained electrocatalytic activity is comparable to that of Pt in acidic, neutral and basic media. The product of oxidation is characterized by no emission of CO_2 or CO, which suggests that it is an environmentally eco-friendly hydrogen generation system. Next, studies devoted to the hydrazine oxidation reaction were expanded to C_{60} nanocomposites functionalized with ethylenediamine (EDA@ C_{60}) [34].

Electrocatalytic studies of the hydrogen evolution reaction using a combination of experimental and theoretical methods were performed for a series of endohedral fullerenes (EMFs), such as $Gd_3N@I_h(7)-C_{80}$, $Y_3N@I_h(7)-C_{80}$, $Lu_3N@I_h(7)-C_{80}$, $Sc_3N@I_h(7)-C_{80}$, $Sc_3N@D_{5h}(6)-C_{80}$, $Sc_3N@D_{3h}(5)-C_{78}$, and $Sc_3N@D_3(6140)-C_{68}$ [35]. From all of them, the best catalytic performance toward the generation of molecular hydrogen was obtained for $Sc_3N@D_3(6140)-C_{68}$ (Fig. 7), which exhibited the lowest onset potential, high mass activity and excellent electrochemical stability. The high catalytic activity of the $Sc_3N@D_3(6140)-C_{68}$ catalyst derives from the relatively high negative charge densities on the pentalene groups, which can favor the adsorption of the intermediate catalytic species and significantly improve the catalytic HER rates. The superior intrinsic catalytic performance was also verified by double-layer capacitance studies, which showed that the obtained capacitance for $Sc_3N@D_3(6140)-C_{68}$ is significantly higher than the capacitance of other endohedral fullerenes and comparable to those of low-dimensional hydrogen HER catalysts. This suggests a high number of accessible catalytic sites on the catalyst surface. It was shown that in the case of other materials, such as $Sc_3N@I_h(7)-C_{80}$, $Sc_3N@D_{3h}(5)-C_{78}$, $Sc_3N@D_{5h}(6)-C_{80}$, $Gd_3N@I_h(7)-C_{80}$, $Y_3N@I_h(7)-C_{80}$, and $Lu_3N@I_h(7)-C_{80}$, the HER catalytic activities are similar, indicating that their structural variations, based mainly on the nature of the metal, symmetries, and degree of pyramidalization of the metal clusters, do not play a significant role in their catalytic performances. For $Gd_3N@I_h(7)-C_{80}$, $Sc_3N@I_h(7)-C_{80}$, $Sc_3N@D_{3h}(5)-C_{78}$, and $Sc_3N@D_{5h}(6)-C_{80}$, a very high Tafel slope was observed, indicating that the Volmer step mainly controls the catalytic processes, leading to sluggish kinetics on the fullerene surfaces. The observed decrease in the Tafel slope in the case of $Sc_3N@D_3(6140)-C_{68}$, $Lu_3N@I_h(7)-C_{80}$, and $Y_3N@I_h(7)-C_{80}$ suggests better HER activity based on the Volmer-Heyrovsky pathway.

A drastic improvement in the electrocatalytic HER properties of van der Waals 1 T-MoS₂/ C_{60} heterostructures was obtained by the formation of well-organized arrays of C_{60} molecules in a very narrow fullerene concentration range [36]. The modulation of the MoS₂- C_{60} and C_{60} - C_{60} interactions at specific ratios allowed us to obtain one of the lowest onset overpotential values among low-dimensional nonprecious HER nanomaterials. Density functional theory calculations of the electronic structures of different pristine fullerenes, such as C_{60} , C_{76} , C_{84} , and C_{100} , show that C_{76} fullerene exhibits the most convenient electronic structure suitable for the HER. This molecule is characterized by the lowest bandgap energy. Therefore, the formation of the C_{76}/Ni catalyst results in a drastic decrease in the free energy compared to bare C_{76} and bare nickel foam. The electron density difference (EDD) calculations showed

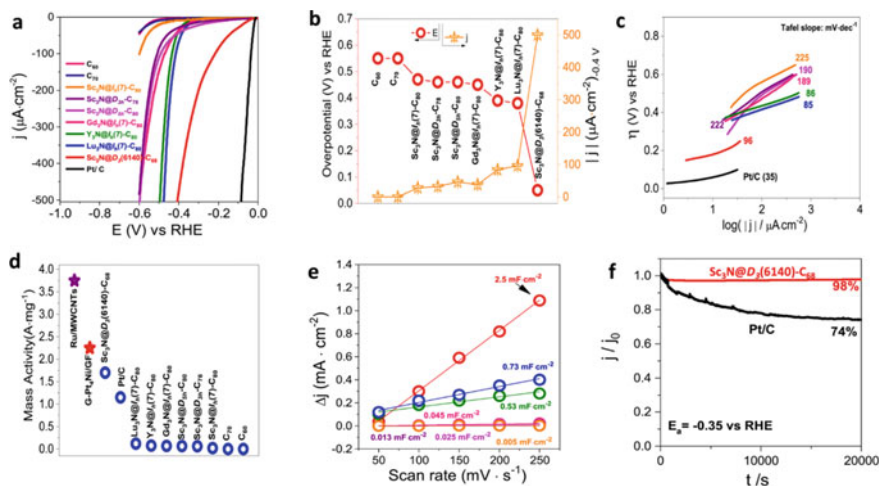


Fig. 7 **a** LSVs of HER for C_{60} , C_{70} , $Gd_3N@I_h(7)-C_{80}$, $Y_3N@I_h(7)-C_{80}$, $Lu_3N@I_h(7)-C_{80}$, $Sc_3N@I_h(7)-C_{80}$, $Sc_3N@D_{5h}(6)-C_{80}$, $Sc_3N@D_{3h}(5)-C_{78}$, and $Sc_3N@D_3(6140)-C_{68}$ and Pt/C at $2 \text{ mV}\cdot\text{s}^{-1}$ in $0.5 \text{ M H}_2\text{SO}_4$. **b** Onset overpotential and current density HER values for C_{60} , C_{70} , $Gd_3N@I_h(7)-C_{80}$, $Y_3N@I_h(7)-C_{80}$, $Lu_3N@I_h(7)-C_{80}$, $Sc_3N@I_h(7)-C_{80}$, $Sc_3N@D_{5h}(6)-C_{80}$, $Sc_3N@D_{3h}(5)-C_{78}$, and $Sc_3N@D_3(6140)-C_{68}$. **c** Corresponding Tafel plots of the EMFs and Pt/C. **d** Mass activity values of EMFs, Pt/C and other state-of-the-art catalysts at -0.4 V vs. RHE. **e** Δj vs. scan rate for the EMF catalysts. **f** $I-t$ curves for $Sc_3N@D_3(6140)-C_{68}$ and Pt/C. Adapted with permission [35], Copyright (2021), American Chemical Society

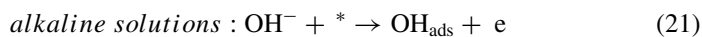
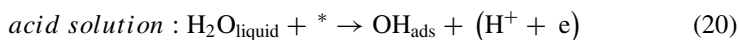
charge redistribution at the C_{76}/Ni interface, where the electron density increased on fullerene and decreased on nickel, indicating the synergistic effect between C_{76} and Ni foam, allowing electron transfer from nickel to C_{76} and acting as a superior bifunctional catalyst. The C_{76}/Ni catalyst exhibited an HER overpotential comparable to that obtained for the benchmark Pt/C catalyst [37].

Excellent catalytic activities were found in theoretical studies for $M@C_{60}$ ($M = \text{Na, K, Rb, Cs, Sc, Ti, Mn, Fe}$) endohedral metallofullerenes [38]. These studies showed that charge transfer from the metal to the C_{60} cage can enhance the adsorption of hydrogen on endohedral metallofullerenes during hydrogen evolution. The high electrocatalytic activity is attributed to the charge transfer between the metal atom and the C_{60} cage. The electronic structure analysis showed that the charge transfer from the metal to C_{60} modified the charge distribution of the C_{60} cage, which enhanced the adsorption of H-atoms on $M@C_{60}$. Promising catalytic properties toward the hydrogen evolution reaction were obtained for *p*- and *n*-doped inorganic fullerene MoS_2 with an onion-like morphology [39]. The obtained excellent HER activity in both basic and acidic media provides better strategies for designing electrocatalysts for many practical applications, such as electrolyzers for proton exchange membrane fuel cells operating over a wide pH range.

Because HER activity is limited by the participation of only Pt surfaces in contact with the electrolyte in the hydrogen evolution process, increasing attention has been given to reducing the size of bulk Pt or Pt nanoparticles to single atoms, which achieves nearly 100% Pt utilization in catalytic processes. For the first time, the formation of single-atom platinum anchored on C₆₀ fullerene was proposed. In this system, C₆₀ was used as an electron-accepting support to anchor Pt atoms (Fig. 8). Highly loaded and highly dispersed Pt catalysts (Pt/C₆₀) were synthesized at room temperature with different molar ratios of C₆₀ to Pt(bis(dibenzylidenoacetone)platinum). The inner structure was a Pt-C₆₀ polymer, and the Pt sites were confined by two C₆₀ molecules [40]. The sp²-hybridized carbon surface of C₆₀ is sufficiently reactive with metals due to the presence of electron-deficient olefinic C = C bonds (i.e., more π-electron delocalization), to which metal atoms can bind in an η²-C₆₀ π-type bonding mode. The Pt atoms were mainly in a divalent form, indicating that atomically dispersed Pt single atoms predominate and prefer to be tetracoordinated. Therefore, one Pt atom binds to two C₆₀ in an η²-C₆₀ π-type bonding mode. The best electrocatalytic properties were obtained for the Pt/C₆₀-2 catalyst formed in the toluene solution with a C₆₀ to Pt(bis(dibenzylidenoacetone)platinum) ratio of 2:1. This system exhibited an amorphous spherical-like structure (Fig. 8b) with many single Pt atoms and some Pt clusters (Fig. 8c). First, the excellent HER activity of Pt/C₆₀-2 was derived from the highly loaded and highly dispersed atomic Pt active sites, which maximized the utilization of Pt atoms. Moreover, the charge redistribution between Pt and C₆₀ delivers favorable adsorption energy toward H₂O* and H*. The experimental results were confirmed by theoretical calculations. As shown in the exemplary results presented in Fig. 8d, the adsorption of H₂O occurs almost spontaneously for Pt/C₆₀-2 and P₁₃ clusters, while a high energy barrier of 0.35 eV needs to be overcome in the case of the Pt (111) surface. The observed ΔG*H value close to 0 eV is typical for ideal HER catalysts. Although the adsorption of H₂O on the Pt₁₃ cluster occurs spontaneously, the adsorption of H* on the Pt₁₃ cluster needs to overcome a high energy barrier of 1.35 eV, which greatly hinders the efficient formation of H₂ molecules. However, the connection of Pt₁₃ to C₆₀ significantly enhances H* adsorption. These results open new perspectives in the new generation of electrocatalytic systems.

A significant accelerating hydrogen evolution reaction was also obtained for fullerene lattice-confined ruthenium nanoparticles coupled with single ruthenium atoms [39].

The oxygen evolution reaction involves a four-electron transfer and is much more complicated than the HER. The OER can be divided into four steps. The first step is the formation of adsorbed OH (OH*) on the catalysts with the first electron transfer:



The second step is the transformation of OH* to O*:

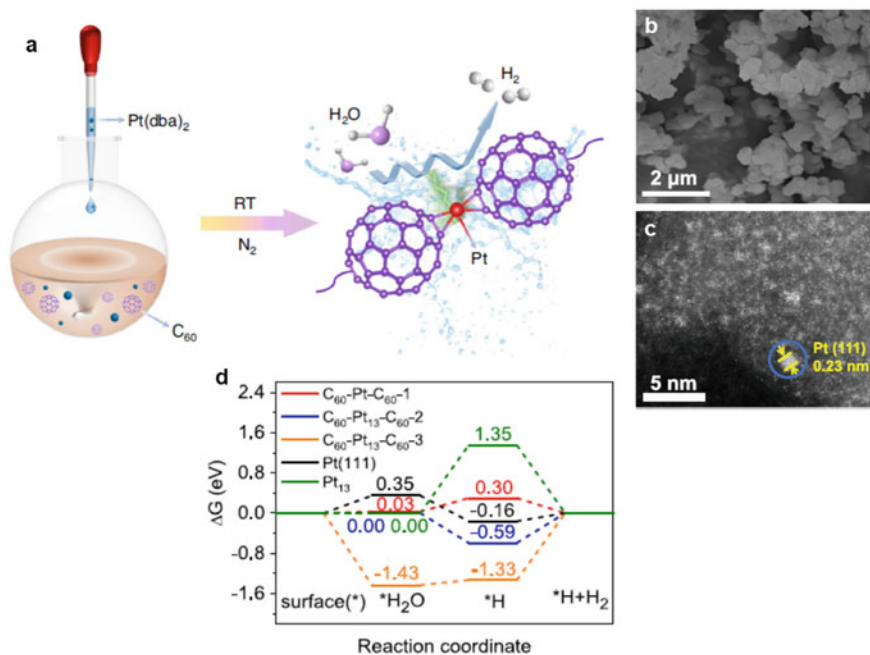
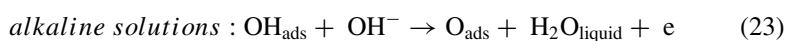
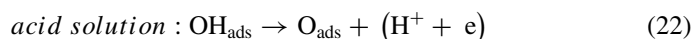
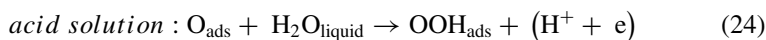


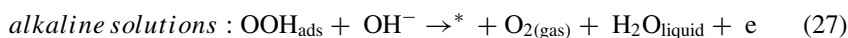
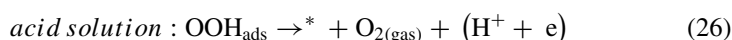
Fig. 8 X **a** Synthetic scheme of Pt/C₆₀ catalyst formation. **b** SEM and **c** HAADF-STEM images of Pt/C₆₀. **d** Calculated adsorption energies of H₂O and H on the surface for C₆₀-Pt-C₆₀-1, C₆₀-Pt₁₃-C₆₀-2, C₆₀-Pt₁₃-C₆₀-3, Pt (111), and Pt₁₃ clusters. Adapted with permission [40], Copyright (2023), Nature



The third step is the transformation of O* to OOH* with another H₂O molecule or OH⁻:



The last step is the release of O₂. Each step occurs with the release of one electron:



The overpotentials of the OER can be determined by the reaction free energies of all four steps. The sluggish four-electron transfer kinetics of the OER hinder its practical application [30].

Munawar and coworkers proposed a facile and simple synthesis method for a catalyst composed of a bimetallic sulfide nanocomposite and fullerene CeNdS/C₆₀ [40]. The covered C₆₀ over CeNdS provides a strong interface between CeNdS and C₆₀. This system exhibits a very small overpotential, a small Tafel plot and good stability. The high OER activity derives from the high surface area of CeNdS/C₆₀ with porous channels. Additionally, the increase in the superb intrinsic OER catalytic activity is associated with the presence of Nd and C₆₀ ions in the CeNdS/C₆₀ catalyst and large active sites by the Ce⁴⁺ and Ce³⁺ peroxidation step with a low overpotential. The synergistic effect between CeNdS and C₆₀ improves the electronic structure and energy barrier and enhances the catalytic active sites.

In the area of oxygen evolution reaction studies, doped fullerenes take place. Theoretical studies showed that compared with pristine fullerene C₇₀, both B and N heteroatom doping of this carbon cage can reduce the oxygen evolution reaction overpotential value and improve OER performance [41]. Promising results toward the oxygen evolution reaction were found for fullerene C₆₀ with an embedded transition metal atom coordinated by three carbon atoms (TM-C₆₀, where TM = Fe, Co, or Ni) in theoretical studies [42]. The TM-C₆₀ system combines the charge reservoir character of C₆₀ with the catalytic activity of metal for electrocatalysis. The performed calculations showed that the electrocatalytic activity of TM-C₆₀ with 0-3e⁺ charge states exhibits a volcano-shaped trend, while in the case of Co-C₆₀ with a 1e⁺ charge state, the lowest overpotential was observed. This suggests that the charge state greatly affects the catalytic activity, which can be interpreted as the charge state changing the interactions between the active site and reactant species and finally resulting in the variation in catalytic activity.

Some of the studied electrocatalysts exhibit bifunctional properties, and they can effectively accelerate both the HER and OER [30], OER and ORR [43] or OER and photochemical processes of pollutant elimination [44]. The ORR, OER and HER activities can also be combined in one catalytic material. Thus far, such properties have been found in such systems as metal-free catalysts composed of C₆₀-adsorbed single-walled carbon nanotubes [14]. The metal-free boron carbon nitride nanosheets/C₆₀ catalyst exhibits multifunctional electrocatalytic properties for hydrogen evolution/oxidation reactions (HER/HOR) and oxygen evolution/reduction reactions (OER/ORR) [45].

5 Other Electrocatalytic Activity

Fullerenes play an important role as a component of electrode materials in all-vanadium redox flow batteries. It was found that the addition of C₇₆ fullerene to hydrated tungsten oxide (HWO) boosts the electrode kinetics toward the VO₂⁺/VO₂⁺ redox reaction. Moreover, the composite material showed a significant inhibitory

effect on the parasitic chlorine evolution reaction due to the W-OH functional groups. The parasitic chlorine evolution reaction is a significant problem for third-generation all-vanadium redox flow batteries in which a mixed acid-based electrolyte ($\text{H}_2\text{SO}_4/\text{HCl}$) is used [46].

Endohedral fullerenes with embedded transition metal atoms, such as Fe, Co, or Ni, coordinated by three carbon atoms can be effective electrocatalysts in the nitrogen reduction reaction (NRR), a very important reaction that is a source of NH_3 , which is an important energy carrier for fuel cell applications [42]. Noncovalently functionalized graphene oxide by a p-methoxy zinc porphyrin-fullerene derivative can be used as an electrocatalyst for the reduction of hydrogen peroxide [47]. Such a sensor exhibits high sensitivity and a low limit of detection. Excellent electrocatalytic properties toward the electrocatalytic oxidation of ascorbic acid were obtained for coil-like fullerene (C_{60})-doped polyaniline acid [48].

6 Conclusions

Electrocatalysis is an inherent, very important pillar of modern technology. The increase in the greenhouse effect resulting from large amounts of pollutants emitted by cars and other systems forces the search for alternative clean fuels and energy sources. Among them, a special place is dedicated to fuel cells. However, these systems need catalysts that will accelerate processes that occur on their electrodes and thus increase their efficiency. Apart from the catalyst, electrode material supports also play an important role in fuel cell operation. Commonly used carbon black is very sensitive to many factors and is destroyed during fuel cell operation. Thus, both the acceleration of electrode reactions and the stable performance of the carbon support are research objects. In both cases, fullerenes can be applied due to their unique structure, many possibilities of transformations, and excellent physical and chemical properties. The studies presented in this work showed the promising properties of fullerenes and their derivatives as electrocatalytic systems. They can compete with commercially produced platinum or palladium catalysts both in the case of electrocatalytic properties and stability performance. The unique structure and properties of fullerenes are inspirations for the formation of fullerene-like inorganic materials that also exhibit excellent catalytic properties.

References

1. Kobayashi, A., Fujii, T., Takeda, K., Tamoto, K., Kakinuma, K., Uchida, M.: Effect of Pt Loading percentage on carbon blacks with large interior nanopore volume on the performance and durability of polymer electrolyte fuel cells. *ACS Appl. Energy Mater.* **5**, 316 (2022)
2. Perazzolo, V., Grądzka, E., Durante, C., Pilot, R., Vicentini, N., Rizzi, G.A., Granozzi, G., Gennaro, A.: Chemical and electrochemical stability of nitrogen and sulphur doped mesoporous carbons. *Electrochim. Acta* **197**, 251 (2016)

- Georgakilas, V., Perman, J.A., Tucek, J., Zboril, R.: Broad family of carbon nanoallotropes: classification, chemistry, and applications of fullerenes, carbon dots, nanotubes, graphene, nanodiamonds, and combined superstructures. *Chem. Rev.* **115**, 4744 (2015)
- Grądzka, E., Wysocka-Zołopa, M., Winkler, K.: Fullerene-based conducting polymers: n-dopable materials for charge storage application. *Adv. Energy Mater.* **10**, 2001443 (2020)
- Perini, L., Durante, C., Favaro, M., Perazzolo, V., Agnoli, S., Schneider, O., Granozzi, G., Gennaro, A.: Metal–support interaction in platinum and palladium nanoparticles loaded on nitrogen-doped mesoporous carbon for oxygen reduction reaction. *ACS Appl. Mater. Interfaces* **7**, 1170 (2015)
- Brandiele, R., Durante, C., Grądzka, E., Rizzi, G.A., Zheng, J., Badocco, D., Centomo, P., Pastore, P., Granozzi, G., Gennaro, A.: One step forward to a scalable synthesis of platinum–yttrium alloy nanoparticles on mesoporous carbon for the oxygen reduction reaction. *J. Mater. Chem. A* **4**, 12232 (2016)
- Hara, M., Lee, M., Liu, Ch-H., Chen, B-H., Yamashita, Y., Uchida, M., Uchida, H., Watanabe, M.: Electrochemical and Raman spectroscopic evaluation of Pt/graphitized carbon black catalyst durability for the start/stop operating condition of polymer electrolyte fuel cells. *Electrochim. Acta* **2012**, 70, 171.
- Mao, K., Zhang, W., Dai, J., Zeng, Z.C.: Carbon fragments as highly active metal-free catalysts for the oxygen reduction reaction: a mechanistic study. *Nanoscale* **11**, 19422 (2019)
- Saianand, G., Gopalan, A.I., Lee, J.C., Sathish, C., Gopalakrishnan, K., Unni, G.E., Shanbhag, D., Dasireddy, V.D.B.C., Yi, J., Xi, S., Al-Muhtaseb, A.H., Vinu, A.: Mixed copper/copper-oxide anchored mesoporous fullerene nanohybrids as superior electrocatalysts toward oxygen reduction reaction. *Small* **16**, 1903937 (2020)
- Sanad, M.F., Franklin, H.M., Ali, B.A., Puente Santiago, A.R., Nair, A.N., Chava, V.S.N., Fernandez-Delgado, O., Allam, N.K., Stevenson, S., Sreenivasan, S.T., Echegoyen, L.: Cylindrical C₉₆ Fullertubes: a highly active metal-free O₂-reduction electrocatalyst. *Angew. Chem. Int. Ed.*, 61, e202116727 (2022)
- Wang, Y., Jiao, M., Song, W., Wu, Z.: Doped fullerene as a metal-free electrocatalyst for oxygen reduction reaction: a first-principles study. *Carbon* **114**, 393 (2017)
- Yang, S., Zhao, C., Qu, R., Cheng, Y., Liu, H., Huang, X.: Probing the activity of transition metal M and heteroatom N4 co-doped in vacancy fullerene (M–N₄–C₆₄, M = Fe Co, and Ni) towards the oxygen reduction reaction by density functional theory. *RSC Adv.* **11**, 3174 (2021)
- Chen, X., Zhang, H., Lai, N.: Endohedral metallofullerenes Mn@C₆₀ (M = Mn Co, Ni, Cu; n = 2–5) as electrocatalysts for oxygen reduction reaction: a first-principles study. *J. Mater. Sci.* **55**, 11382 (2020)
- Chen, X., Zhang, H., Li, X.: Mechanisms of fullerene and single-walled carbon nanotube composite as the metal-free multifunctional electrocatalyst for the oxygen reduction, oxygen evolution, and hydrogen evolution. *Molecular Catalysis* **502**, 111383 (2021)
- Guan, J., Chen, X., Wei, T., Liu, F., Wang, S., Yang, Q., Lu, Y., Yang, S.: Directly bonded hybrid of graphene nanoplatelets and fullerene: facile solid-state mechanochemical synthesis and application as carbon-based electrocatalyst for oxygen reduction reaction. *J. Mater. Chem. A* **3**, 4139 (2015)
- Basu, O., Mukhopadhyay, S., De, A., Das, A., Das, S.K.: Tuning the electrochemical and catalytic ORR performance of C₆₀ by its encapsulation in ZIF-8: a solid-state analogue of dilute fullerene solution. *Mater. Chem. Front.* **5**, 7654 (2021)
- Gao, S., Wei, X., Fan, H., Li, L., Geng, K., Wang, J.: Nitrogen-doped carbon shell structure derived from natural leaves as a potential catalyst for oxygen reduction reaction. *Nano Energy* **13**, 518 (2015)
- Gong, K., Du, F., Xia, Z., Durstock, M., Dai, L.: Nitrogen-doped carbon nanotube arrays with high electrocatalytic activity for oxygen reduction. *Science* **323**, 760 (2009)
- He, Z., Wei, P., Chen, N., Han, J., Lu, X.: N, S-Co-doped porous carbon nanofiber films derived from fullerenes (C₆₀O) as efficient electrocatalysts for oxygen reduction and a Zn–air battery. *Chem. Eur. J.* **27**, 1423 (2021)

20. Meng, F., Wang, S., Jiang, B., Ju, L., Xie, H., Jiang, W., Ji, Q.: Coordinated regulation of phosphorus/nitrogen doping in fullerene-derived hollow carbon spheres and their synergistic effect for the oxygen reduction reaction. *Nanoscale* **14**, 10389 (2022)
21. Yu, A., Peng, Z., Li, Y., Zhu, L., Peng, P., Li, F.F.: Fullerene-derived carbon nanotubes and their electrocatalytic properties in oxygen reduction and Zn–air batteries. *ACS Appl. Mater. Interfaces* **14**, 42337 (2022)
22. Bhavani, K.S., Anusha, T., Kumar, J.V.S., Kumar Braham, P.: Enhanced electrocatalytic activity of methanol and ethanol oxidation in alkaline medium at bimetallic nanoparticles electrochemically decorated fullerene-C₆₀ nanocomposite electrocatalyst: an efficient anode material for alcohol fuel cell applications. *Electroanalysis*, 33, 97 (2021)
23. Huang, H., Wang, X.: Recent progress on carbon-based support materials for electrocatalysts of direct methanol fuel cells. *J. Mater. Chem. A* **2**, 5266 (2014)
24. Bhavani, K.S., Anusha, T., Kumar Braham, P.: Fabrication and characterization of gold nanoparticles and fullerene-C₆₀ nanocomposite film at glassy carbon electrode as potential electrocatalyst towards the methanol oxidation. *Int. J. Hydrogen. Energy*, 44, 25863 (2019)
25. Zhang, X., Ma, L.X.: Electrochemical fabrication of platinum nanoflakes on fulleropyrrolidine nanosheets and their enhanced electrocatalytic activity and stability for methanol oxidation reaction. *J. Power. Sources* **286**, 400 (2015)
26. Lin, Z., Wang, H., Lei, M.: Solvent engineering of highly conductive and porous fullerene ammonium iodide for immobilizing Pd nanoparticles with enhanced electrocatalytic activity toward ethanol oxidation. *Electrocatalysis*, 10, 524 (2019)
27. Almeida, C.V.S., Almagro, L.E., Valerio Neto, E.S., Coro, J., Suarez, M., Eguiluz, K.I.B., Salazar-Banda, G.R.: Polyhydroxylated fullerenes: an efficient support for Pt electrocatalysts toward ethanol oxidation. *J. Electroanal. Chem.* 878, 114663 (2020)
28. Zhang, Q., Bai, Z., Shi, M., Yang, L., Qiao, J., Jiang, K.: High-efficiency palladium nanoparticles supported on hydroxypropyl- β -cyclodextrin modified fullerene [60] for ethanol oxidation. *Electrochim. Acta* **177**, 113 (2015)
29. Zhang, X., Zhang, J.W., Xiang, P.H., Qiao, J.: Fabrication of graphene-fullerene hybrid by self-assembly and its application as support material for methanol electrocatalytic oxidation. *Reaction. Appl. Surf. Sci.* 440, 477 (2018)
30. Zhang, L., Xiao, J., Wang, H., Shao, M.: Carbon-based electrocatalysts for hydrogen and oxygen evolution reactions. *ACS Catal.* **7**, 7855 (2017)
31. You, B., Sun, Y.: Innovative strategies for electrocatalytic water splitting. *Acc. Chem. Res.* **51**, 1571 (2018)
32. Pavel, C.C., Ceconi, F., Emiliani, C., Santiccioli, S., Scaffidi, A., Catanorchi, S., Comotti, M.: Highly efficient platinum group metal free based membrane-electrode assembly for anion exchange membrane water electrolysis. *Angew. Chem. Int. Ed.* **53**, 1378 (2014)
33. Narwade, S.S., Mulik, B.B., Mali, S.M., Sathe, B.R.: Silver nanoparticles sensitized C₆₀(Ag@C₆₀) as efficient electrocatalysts for hydrazine oxidation: Implication for hydrogen-generation reaction. *Appl. Surf. Sci.* **396**, 939 (2017)
34. Narwade, S.S., Mali, S.M., Tanwade, P.N., Chavan, P.P., Munde, A.V., Sathe, B.R.: Highly efficient metal-free ethylenediamine-functionalized fullerene (EDA@C₆₀) electrocatalytic system for enhanced hydrogen generation from hydrazine hydrate. *New J. Chem.* **46**, 14004 (2022)
35. Santiago, A.R.P., Sanad, M.F., Moreno-Vicente, A., Ahsan, M.A., Ceron, M.R., Yao, J.R., Sreenivasan, S.T., Rodriguez-Forteza, A., Poblet, J.M., Echegoyen, L.: A new class of molecular electrocatalysts for hydrogen evolution: catalytic activity of M₃N@C_{2n} (2n = 68, 78, and 80) fullerenes. *J. Am. Chem. Soc.* **143**, 6037 (2021)
36. Santiago, A.R.P., He, T., Eraso, O., Ahsan, M.A., Nair, A.N., Chava, V.S.N., Zheng, T., Pilla, S., Fernnandez-Delgado, O., Du, A., Sreenivasan, S.T., Echegoyen, L.: Tailoring the interfacial interactions of van der Waals 1T-MoS₂/C₆₀ heterostructures for high-performance hydrogen evolution reaction electrocatalysis. *J. Am. Chem. Soc.* **142**, 17923 (2020)
37. Hasan, M.H., Khedr, G.E., Allam, N.K.: C₇₆ nanospheres/Ni foam as high-performance heterostructured electrocatalysts for hydrogen evolution reaction: unveiling the interfacial interaction. *ACS Appl. Nano Mater.* **5**, 15457 (2022)

38. He, T., Gao, G., Kou, L., Will, G., Du, A.: Endohedral metallofullerenes (M@C₆₀) as efficient catalysts for highly active hydrogen evolution reaction. *J. Catal.* **354**, 231 (2017)
39. Luo, T., Huang, J., Hu, Y., Yuan, C., Chen, J., Cao, L., Kajiyoshi, K., Liu, Y., Zhao, Y., Li, Z., Feng, Y.: Fullerene lattice-confined Ru nanoparticles and single atoms synergistically boost electrocatalytic hydrogen evolution reaction. *Adv. Funct. Mater.* **33**, 2213058 (2023)
40. Munawar, T., Bashir, A., Nadeem, M.S., Mukhtar, F., Manzoor, S., Ashiq, M.N., Khan, S.A., Koc, M., Iqbal, F.: Electrochemical performance evaluation of bimetallic sulfide nanocomposite with fullerene (CeNdS/C₆₀) for efficient oxygen evolution reaction (OER). *Energy Fuels* **37**, 1370 (2023)
41. Yang, S., Cheng, Y., Liu, H., Huang, X.: Heteroatom-doped fullerene C₇₀ as non-metal electrocatalysts for oxygen reduction and oxygen evolution from computational study. *Diam. Relat. Mater.* **2022**, 108954 (2022)
42. Xiao, H., Li, H., Li, X., Jiang, J.: Effect of the charge state on the catalytic activity of a fullerene-based molecular electrocatalyst: a theoretical study. *J. Phys. Chem. Lett.* **13**, 7392 (2022)
43. Chen, X., Huang, S., Zhang, H.: Bimetallic alloys encapsulated in fullerenes as efficient oxygen reduction or oxygen evolution reaction catalysts: a density functional theory study. *J. Alloys Compd.* **894**, 162508 (2022)
44. Bashir, A., Munawar, T., Mukhtar, T., Nadeem, M.S., Manzoor, S., Ashiq, M.N., Khan, S.A., Koc, M., Iqbal, F.: Dual-functional fullerene supported NiO-based nanocomposite: efficient electrocatalyst for OER and photocatalyst for MB dye degradation. *Mater. Chem. Phys.* **293**, 126886 (2023)
45. Ahsan, M.A., He, T., Eid, K., Abdullah, A.M., Curry, M.L., Du, A., Puente Santiago, A.R., Echegoyen, L., Noveron, J.C.: Tuning the intermolecular electron transfer of low-dimensional and metal-free BCN/C₆₀ electrocatalysts via interfacial defects for efficient hydrogen and oxygen electrochemistry. *J. Am. Chem. Soc.* **143**, 1203 (2021)
46. El Diwany, F.A., Al Najjar, T., Allam, N.K., El Sawy, E.N.: Tungsten oxide/fullerene-based nanocomposites as electrocatalysts and parasitic reactions inhibitors for VO²⁺/VO₂⁺ in mixed-acids. *Sci. Rep.* **12**, 14348 (2022)
47. Fan, S., Yang, J., Wei, T., Zhang, J., Zhang, N., Chai, M., Jin, X., Wu, H.: Zinc porphyrin-fullerene derivative noncovalently functionalized graphene hybrid as interfacial material for electrocatalytic application. *Talanta* **160**, 713 (2016)
48. Bai, L., Chen, Y., Bai, Y., Chen, Y., Zhou, J., Huang, A.: Fullerene-doped polyaniline as new redox nanoprobe and catalyst in electrochemical aptasensor for ultrasensitive detection of *Mycobacterium tuberculosis* MPT64 antigen in human serum. *Biomaterials* **133**, 11 (2017)
49. Chhetri, M., Gupta, U., Yadgarov, L., Rosentsveig, R., Tenne, R., Rao, C.N.R.: Effects of p- and n-type doping in inorganic fullerene MoS₂ on the hydrogen evolution reaction. *ChemElectroChem* **2016**, 3 (1937)
50. Zhang, R., Li, Y., Zhou, X., Yu, A., Huang, Q., Xu, T., Zhu, L., Peng, P., Song, S., Echegoyen, L., Li, F.F.: Single-atomic platinum on fullerene C₆₀ surfaces for accelerated alkaline hydrogen evolution. *Nat. Commun.* **14**, 2460 (2023)

Nanocomposites of Carbon as Electrocatalyst



Veena Mounasamy and Ponpandian Nagamony

Abstract Earnest efforts in developing electrochemical energy production, conversion, and storage devices to meet the energy requirements globally routes to the research and development of highly efficient and sustainable electrocatalysts. The escalated physicochemical characteristics and ease in tunability of carbon material and its allotropes (viz., graphene, graphite, carbon nanotubes, carbon quantum dots, nano diamond, etc.) facilitated to exercise of its remarkable footprints in the electrocatalytic applications. Due to the trade-off between its conductivity and intrinsic activity, carbon materials are often combined with several metal oxides, sulfides, nitrides, or carbides and form their respective composites. In addition to their enhanced conductivity and stability, carbon nanocomposites will exhibit higher catalytic activity due to their higher surface-to-volume ratio which is crucial for an electrocatalyst. In this chapter, several carbon nanocomposites electrocatalysts used in water splitting (OER, ORR and HER), fuel cells (methanol and proton exchange membrane) and air batteries (lithium and zinc) applications are majorly discussed.

Keywords Carbon allotropes · Energy conversion and production · Water splitting · Air batteries · Fuel cells

1 Introduction to Electrocatalyst

The electrochemical energy sector gained significant interest over decades owing to the demand for sustainable and renewable energy devices. Electrocatalysts are indispensable entities in electrochemical energy devices. The catalysts involved in the electrochemical reactions are called electrocatalysts. The electrocatalysts are responsible for a number of electrochemical applications such as oxygen evolution reaction (OER), oxygen reduction reaction (ORR) and hydrogen evolution reaction (HER) in water splitting [1], carbon dioxide reduction reaction (CRR) [2], lithium and zinc air batteries [3, 4], methanol and proton exchange membrane fuel cells [5,

V. Mounasamy · P. Nagamony (✉)

Department of Nanoscience and Technology, Bharathiar University, Coimbatore 641 046, India
e-mail: ponpandian@buc.edu.in

6]. In the electrochemical process, the electrocatalysts are usually electrodes that are involved in facilitating the charge transfer reactions and chemical transformations carried either at their surfaces or interfaces. Mainly, the electrocatalysts decrease the activation energy of the charge transfer reaction, thereby improving the reactivity of the electrochemical process. Nanomaterials play a vital role as an efficient electrocatalyst owing to their higher surface-to-volume ratio leading to larger reactivity, efficient interfacial activity, higher adsorption and desorption of ions, improved rate of reaction etc. Several class of nanomaterials viz., metal oxides, sulphides, nitrides, carbides, metal free catalysts and noble metals are largely explored towards electrocatalyst applications. Majority of the studies proved that carbon-based materials integrated to the above class of nanomaterials or standalone carbon-based materials (viz., graphene oxides, carbon quantum dots, carbon nanotubes etc.) are highly regarded as electrocatalyst and provided significant performance in electrochemical process.

2 Carbon Based Electrocatalyst

Right from the first industrial revolution carbon acts as an integral part in the materials development in various streams of energy sector. Carbon nanomaterials exhibits in various allotropic forms namely graphite, graphene, quantum dots, nanotubes, nano diamond and various forms such as porous carbon, activated carbon, etc. and is applied in various applications as shown in Fig. 1. The characteristics of carbon based materials such as its electrical conductivity, chemical stability in alkaline and acidic medium, highly abundant, thermal stability, high durability, cost effective and less toxic makes it well suitable for electrocatalyst [7]. The noble metals such as ruthenium, platinum and iridium were used as an efficient electrocatalysts until the discovery of the carbon electrocatalysts. The exploration of carbon and carbon composite electrocatalyst replaced the expensive noble metal based electrocatalysts retaining its electrocatalytic efficiency that is suitable for large scale employability. The carbon based electrocatalysts improve the kinetics of the reaction thereby increasing the reactivity of the electrochemical process.

2.1 Graphite

The chemical and electronic properties of the carbon nanomaterials can be very well tuned by doping the heteroatoms such as boron, nitrogen, and oxygen into its graphitic network. The doping also helps in altering the electronic distribution in g-C₃N₄ [8]. The limitation of graphite are its intercalation kinetics and surface passivation which could be tackled by making it as nanocomposite with other materials. The surface functional groups of graphite acts as a key role in improving the catalytic activities [9].

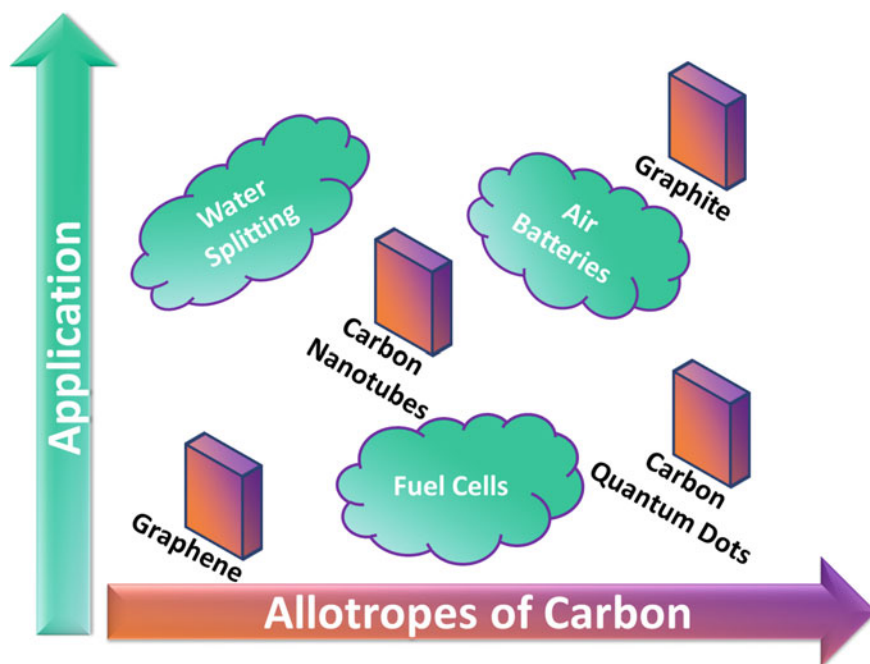


Fig. 1 Schematic representation of carbon electrocatalyst and its applications

2.2 Graphene

The invention of graphene revolutionized the materials research and development for several applications due its characteristic functional properties. Graphene, an allotrope of carbon, atomically thin sheets of carbon, having C–C bond length of ~ 1.42 Å exhibits tremendous outstanding properties such as flexibility, electronic properties, ultra-thin structure and so on [10]. Graphene is one of the potential electrocatalysts boosting electrochemical reactions. Graphene can be well defined as carbon atoms with sp^2 hybridization in a hexagonal framework with two-dimensional sheet structure. In other words, the exfoliated graphite sheets render graphene sheet. By stacking, rolling and wrapping process graphene can be converted to 3D, 1D and 0D structures [11]. Due to its excellent physical characteristics, graphene is employed as electrocatalyst for various application and its significance as electrocatalyst have been reviewed by N. Shaari et al. [7]. The types of graphene-based material are shown in Fig. 2a.

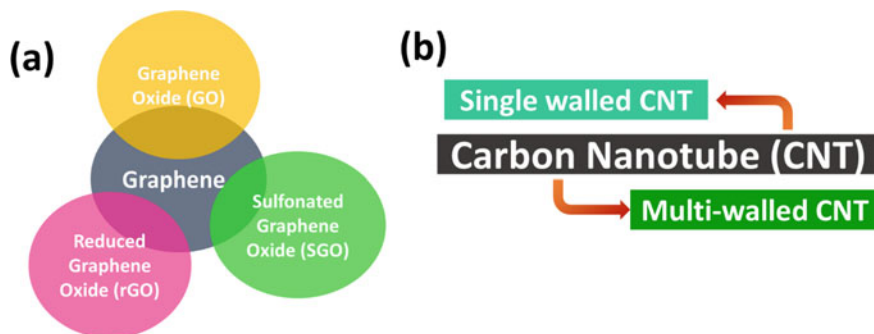


Fig. 2 **a** Types of graphene-based materials, **b** Types of carbon nanotubes

2.3 Carbon Nanotubes

Carbon nanotubes are 1D nanostructures with the length being in few micrometres with nanoscale tube diameter. The types of carbon nanotubes are given in Fig. 2b. The geometry of carbon nanotubes is distinctive that are bonded by sp^2 carbon-carbon chemical bonds. Gedefaw Asmare Tafete et al., reported the works of carbon nanotube electrocatalyst in detail. The structural uniqueness of carbon nanotubes provide enhanced electronic conductivity, mechanical and chemical stability [12].

2.4 Carbon Quantum Dots

The carbon quantum dots are zero dimensional unique quasi spherical nanoparticles of size less than 10 nm. They have better surface properties with π - π stacking, higher surface area, higher crystallization and larger diameter, higher solubility, robustness, and chemical inertness. In energy conversion applications, graphene quantum dots are widely used usually with heteroatom doping enhancing oxidation and reduction reactions. Graphene quantum dots are usually less than 30 nm in size having few atomic layer thickness and mainly used in luminescence applications [11].

3 Carbon Nanocomposites

Due to its outstanding properties, carbon-based materials are often incorporated with several class of materials including metals, metal oxides, metal organic frameworks etc. Due to its higher surface to volume ration influencing the surface activity and conductivity carbon-based materials are largely employed in electrocatalytic applications. Applications involving carbon-based electrocatalyst, mainly energy storage and conversions are discussed in this chapter.

4 Applications

Electrocatalyst is the major element in an electrochemical process and it acts as an electrode. Depending on the applications, electrocatalyst acts either as anode or cathode. The electrochemical activity occurs either at surface or interfaces of the electrodes. They can be either homogeneous such as platinum or heterogeneous material. A brief study on the applications involving electrocatalyst such as water splitting (OER, ORR and HER), fuel cells (methanol and proton exchange membrane fuel cells) and batteries (zinc air, lithium air and lithium-ion batteries) are discussed in this chapter.

4.1 Water Splitting

Hydrogen economy is at the growing phase due to its scope of green energy production from water. Water splitting is one of the wonders in the chemistry which opened a wider path towards renewable energy production eliminating fossil fuels. Oxygen evolution reaction (OER), hydrogen evolution reaction (HER) and oxygen reduction reaction (ORR) are major reactions that need to be realized and improved for a better performance water splitting. The electrocatalysts plays a major role in deciding the efficiency of the electrochemical reactions involved in water splitting reaction.

4.1.1 Oxygen Evolution Reaction (OER)

OER, four electron transfer reaction occurring at anode with sluggish kinetics is one of the biggest challenges in electrochemical water splitting. Hence, a material with higher electronic conductivity and charge transport characteristics are preferred to be an OER electrocatalyst. In that row, several single and mixed metal oxides are employed in water splitting application. In addition, reports suggest that incorporating carbon-based materials with metal oxides will compliment metal oxides in improving the surface area, influencing the catalytic activity etc.

Fengcui shen et al., studied the catalytic activity of $\text{CoV}_2\text{O}_6\text{-V}_2\text{O}_5/\text{N-doped rGO}$ synthesized by direct carbonization of its precursors towards OER. The $\text{CoV}_2\text{O}_6\text{-V}_2\text{O}_5/\text{N-doped rGO}$ nanocomposite was coated on glassy carbon electrode which acts as working electrode and its electrocatalytic activity was studied in 1 M KOH saturated using nitrogen. The studies revealed that $\text{CoV}_2\text{O}_6\text{-V}_2\text{O}_5/\text{N-doped rGO}$ nanocomposite required an overpotential of 239 mV at the current density of 10 mA cm^{-2} . The Tafel slope value (49.7 mV dec^{-1}) of $\text{CoV}_2\text{O}_6\text{-V}_2\text{O}_5/\text{N-doped rGO}$ nanocomposite which is lower than other compared electrocatalysts in this work revealed that indicates exhibits better reaction kinetics due to its faster charge transport and improved surface area. The cyclic stability was observed for over 1000 cycles at the scan rate of 100 mV/s in the potential 1.3 and 1.5 (V versus

RHE). The durability of the $\text{CoV}_2\text{O}_6\text{-V}_2\text{O}_5/\text{N-doped rGO}$ nanocomposite was also confirmed using chronoamperometry. The turnover frequency (TOF) was found to be 1.80 s^{-1} representing the better performance of the electrocatalyst. Therefore, this work proved that $\text{V}_2\text{O}_5/\text{N-doped rGO}$ nanocomposite as an excellent electrocatalyst for OER with higher TOF and lower overpotential [13].

Xiaolin Xing et al., studied the OER as well as ORR performance of manganese vanadium oxide–N-doped reduced graphene oxide ($\text{MnVO}_x@/\text{N-rGO}$) composite synthesized using hydrothermal synthesis. The OER studies were studied using linear sweep voltammetry and electrochemical impedance spectroscopy by coating $\text{MnVO}_x@/\text{N-rGO}$ on carbon fibre paper in 1 M KOH. The $\text{MnVO}_x@/\text{N-rGO}$ nanocomposite rendered an overpotential of 1.65 V at 10 mA/cm^2 with Tafel slope value of 271 mV. The over-all oxygen activity was determined by finding the potential difference ($\Delta E_{\text{OER}} - \Delta E_{\text{ORR}}$) between OER and ORR potential at the current density of 10 mA/cm^2 . The $\text{MnVO}_x@/\text{N-rGO}$ yielded $\Delta E_{\text{OER}} - \Delta E_{\text{ORR}}$ value of 0.85 V versus RHE. This minimum potential difference implies the better oxygen activity of the $\text{MnVO}_x@/\text{N-rGO}$ catalyst [14].

Hybrid electrocatalysts plays a significant role in improving the electrochemical efficiency due to its synergistic effects. Several reports on electrocatalysts involving more than two materials are found in literature which emphasize on the individual material's advantages complimenting the composite.

A work on two step gas phases synthesized $\text{Co}_3\text{O}_4\text{-MnO}_2\text{-CNT}$ nanocomposite as OER electrocatalyst was reported by Kungeng Xie et al. As the metal oxides limits the conductivity compared to noble metals, usually carbon- based materials are incorporated with metal oxides to improve the conductivity and reduce the charge transfer resistance as well. In this work, $\text{Co}_3\text{O}_4\text{-MnO}_2\text{-CNT}$ nanocomposite was treated with nitric acid (HNO_3) at $200 \text{ }^\circ\text{C}$ and the electrochemical characteristics were studied. The $\text{Co}_3\text{O}_4\text{-MnO}_2\text{-CNT}$ nanocomposite exhibited good catalytic performance at the current density of 10 mA/cm^2 and the cyclic stability was found over a period of around 37 h. This work proved that employing $\text{Co}_3\text{O}_4\text{-MnO}_2\text{-CNT}$ nanocomposite as electrocatalyst would yield a scalable electrode helping large scale production [15].

4.1.2 Hydrogen (H_2) Evolution Reaction (HER)

The ardour for electrochemical water splitting research is purely for H_2 production to enable green energy society. For several decades, splitting H_2O into H_2 and O_2 is prevailing using electrolysis method. But developing a method suitable for large scale production, low cost and environmentally safe procedures are challenging and hence still research is moving towards developing the same. Though metal oxide possesses several advantages in terms of its availability, cost, nanostructured morphology, stability and better catalytic behaviour, its wider band gap limits its electronic conductivity. Hence, usually carbon-based materials are incorporated with metal oxides to increase the electrocatalytic activity of the material. The HER is a cathodic reaction in the water electrolysis reaction. In their work, Bishal Das et al.,

reported photocatalytic hydrogen evolution reaction of metal complex (VO (acac)₂) and dual (sodium and sulfur) doped graphitic carbon nitride (VNS-GC). The VNS-GC composite exhibited a hydrogen evolution rate of 310.63 $\mu\text{mol g}^{-1} \text{h}^{-1}$ in the presence of platinum co-catalyst. The results support the better cyclability as well as photoactivity of the metal complex/carbon composite [16].

Yanping Zhu et al., reported one pot synthesis of tungsten nitride and nitrogen-rich graphene-like carbon nanocomposite (WN-NRC) that are hierarchically arranged and employed it as an electrocatalyst for HER. The electrochemical characteristics of WN-NRC was studied in a three-electrode system in 0.5 M H₂SO₄. From linear sweep voltammetric studies, it was found that WN-NRC exhibited an overpotential of 255 mV at 10 mA cm⁻², which is very much less compared to its bulk counterpart which had an overpotential of 492 mV. It shows that the nanocomposites of WN-NRC are excellent catalyst for HER due to its increased active sites. In addition, the counter electrode also plays a vital role in deciding the electrocatalytic activity of the catalyst. In this work, the catalytic activity of WN-NRC was found to be high when platinum counter electrode was used compared to the graphite rod counter electrode. The charge transfer resistance (R_{CT}) observed from electrochemical impedance spectroscopy indicated that the R_{CT} value of WN-NRC is lower due to its porous morphology than its bulk particles. The work provides a rational for scalable synthesis of WN-NRC and its application as electrocatalyst in hydrogen evolution reaction [17].

4.1.3 Oxygen Reduction Reaction (ORR)

The ORR is a crucial process in electrochemical conversion process such as fuel cells and batteries. Deshuang Yu et al., reported metal organic framework (MOF) based electrocatalyst cobalt nano- particles encapsulated in nitrogen-doped carbon and carbon nanotube (Co/N-CCN) for ORR application as well as its employability for OER. The ORR characteristics of Co/N-CCN was studied using rotating disk electrode (RDE) and rotating ring disk electrode (RRDE) in 0.1 M KOH. The RDE study showed that the Co/N-CCN exhibited onset potential and half wave potential of 0.924 and 0.81 V respectively. The better efficiency of Co/N-CCN towards ORR is due to the presence of active pyridine-N and graphitic-N in the MOF and carbon nanotube network. The work also supports the use of Co/N-CCN composite in Zn-air battery applications [18].

Yu Pan et al., reported the electrochemical characteristics of palladium/iron nanoparticles supported by carbon towards ORR. Usually, noble metals are better catalytic agents in electrochemical studies. That way, Pd plays a huge role in the catalytic performance. In addition to catalytic activity, the conductivity and reduction in overpotential are the major factors to support the electrocatalysis. In this work, the addition of iron to the palladium decreased the overpotential of the composite and the carbon improved he charge transfer due to its surface properties. The consistency of the electrocatalyst was studied using linear sweep voltammetry where even

after 50 scans, the trend remained same showing the stability and durability of the electrocatalyst [19].

4.2 Fuel Cells

The fuel cells play an important role in meeting energy demands in global arena. Basically, fuel cells convert chemical to electrical energy in an electrochemical process. There are several types of fuel cells such as alkaline, phosphoric acid, molten carbonate and solid oxide fuel cells in addition to methanol and proton exchange membrane fuel cells. In this chapter, the carbon-based nanocomposites employed as electrocatalyst in methanol and proton exchange membrane fuel cells are discussed.

4.2.1 Methanol Fuel Cells

The demand for sustainable and clean energy sources has led to the development of research and development in methanol fuel cells. To commercialize methanol fuel cells as an efficient energy source, its expensive applicability due to the use of platinum anode and sluggish kinetics remains as its challenging factor. To overcome this, research on carbon-based materials and its composites are widely studied in recent times which possess good electrocatalytic activity, higher surface to volume ratio and better stability during chemical reactions. An extensive discussion on the progress and challenges in carbon-based materials (mesoporous carbon, carbon black, carbon nanofibers, carbon nanotubes, graphene) as anodes for methanol oxidation reaction was reported by Huajie Huang et al. [20].

In addition to these major carbon materials, other carbon materials such as carbon aerogel and carbon paper were also studied as an electrocatalyst towards ethanol oxidation reaction for the fuel cells applications. The materials such as nitrogen doped carbon, CeO_2 , MnO_2 , TiO_2 and conducting polymers such as polyaniline and poly(2-amino-5-mercapto-1,3,4-thiadiazole) are studied largely as an efficient co-catalyst of carbon for methanol oxidation reaction. B. Rajesh et al., reported Pt- WO_3 /carbon nanotube composite for the methanol oxidation in acidic medium. Self-poisoning due to CO production at the time of dehydrogenation remains a challenging task in selecting the anode catalyst in the methanol oxidation reaction. Hence, this work reports that the Pt/ WO_3 provides better stability during the catalytic reaction of methanol oxidation. But Pt/ WO_3 lower activity in the catalytic reaction. Hence, in this work, Pt/ WO_3 were loaded inside carbon nanotubes and CNT/Pt- WO_3 coated on glassy carbon electrodes were used for electrochemical studies towards methanol oxidation reaction. In the forward scan, at room temperature condition, the methanol oxidation onset potential started at + 0.1 V and higher current density of 98.5 mA/cm² was obtained at + 0.7 V versus Ag/AgCl without any self-poisoning at the reverse scan. Zhenyu Sun et al., reported the methanol oxidation electrochemical performance of Pt-Ru/ CeO_2 /multiwalled carbon nanotube composite. In this work,

the Pt-Ru/CeO₂ were attached to the surface of multiwalled carbon nanotube through sonication method. The electrochemical characteristics of Pt-Ru/CeO₂/multiwalled carbon nanotube composite towards methanol oxidation were studied using cyclic voltammetry and chrono-amperometry in 0.5 M H₂SO₄. The electrochemical surface area of Pt-Ru/CeO₂/MWNT (122.4 m² g⁻¹) was found to be higher than Pt-Ru/MWNT (77.4 m² g⁻¹) and Pt/MWNT (36.6 m² g⁻¹). From chrono-amperometric studies, it was found that the oxidative current of the Pt-Ru/CeO₂/MWNT nanocomposite was higher than the Pt-Ru/MWNT and Pt/MWNT inferring that the methanol oxidation reaction was better for Pt-Ru/CeO₂/MWNT than other catalysts [5].

Yuehe Lin et al., reported an interesting work on low temperature fuel cells using Pt/CNT synthesized in supercritical fluid. The self-poisoning of the electrodes occurring in the middle of the methanol oxidation reaction can be understood using the difference between forward (I_f) and reverse anodic peak current (I_b). Higher the I_f/I_b value, better the methanol oxidation to CO₂. This work suggested that the use of CNT with Pt reduced the catalyst poisoning as well as increased the surface activity due to the increased surface area of CNT and decrease in overpotential [21].

4.2.2 Proton-Exchange Membrane Fuel Cells (PEMFC)

In a view to develop eco-friendly energy sources, research on PEMFC is on a larger interest in global arena. The PEMFC consists of an anode where the hydrogen will be oxidized and a cathode where the oxygen will be reduced and an electrolyte membrane. The proton is migrated from anode to cathode through proton exchange membrane. There are two types of PEMFC depending on the temperature namely low temperature PEMFC (60–80 °C) and high temperature PEMFC (110–180 °C). The high temperature PEMFC provides higher proton conductivity with better chemical and thermal stability. In addition, high PEMFC also offers low permeability towards fuel and carbon monoxide poisoning occurring at low temperature PEMFC is controlled in high PEMFC. To overcome its lower power density limitation in PEMFC, focus on developing efficient catalyst is believed to deliver better performance. Platinum is the ideally used catalyst for PEMFC applications. But, due to its cost and availability as well as poisoning limitations, Pt is often supported by carbon-based materials. Hence, recently carbon based electrocatalyst is studied at a larger scale to enhance the PEMFC performance. The Pt/C also delivers attractive electrocatalytic activity improving the cell performance. Among various carbon-based materials, carbon nanotubes (CNT) are majorly used for PEMFC application owing to its nanoscale morphology, higher surface area, better stability and corrosion resistance in addition to higher electrical conductivity. Both single wall and multi walled CNTs exhibit higher surface area improving the electrochemical activity.

Weimin Zhang et al. studied the electrocatalytic performance of Pt/CNT nanocomposite synthesized using microwave heating towards PEMFCs. The CNT were functionalized and the difference in electrocatalytic performance of raw and functionalized CNT were studied. The Pt/CNT electrodes with functionalized CNT exhibited an electrochemical active surface area of 72.9 m²/g and the Pt/CNT electrodes with

unfunctionalized CNT exhibited an electrochemical active surface area of $48.2 \text{ m}^2/\text{g}$. This shows that the CNT electrodes which are functionalized possess better catalytic activity towards proton membrane exchange fuel cells [22].

A. Leela Mohana Reddy et al., reported electrochemical performance of Pt/SWNT (single wall nanotube)–Pt/C (carbon) nanocomposite towards PEMFC. The enhanced electrochemical performance of Pt/SWNT–Pt/C was found when 50 wt % Pt/SWNT + 50 wt % Pt/C was taken as both anode and cathode where 20% of Pt was loaded. The uniform distribution of Pt/C over Pt/SWNT was observed in this study using transmission electron microscopy. The PEMFC performance with a potential of 540 mV exhibited a current and power density of 485 mA cm^{-2} and 262 mW cm^{-2} . The performance of Pt/SWNT was found to be better than Pt/C indicating the advantages of SWNT. The membrane with thickness of $89 \text{ }\mu\text{m}$ exhibited a membrane resistance of $0.1072 \text{ }\Omega \text{ cm}^2$. The study exhibited Pt/SWNT as a better cathode catalyst than Pt/C with enhanced electron transfer and higher catalytic activity [6]. In addition to being an electrocatalyst, carbon/chromium composite coating as bipolar plates in PEMFC yielded better interfacial conductivity as well as anticorrosive property. Elisabete I. Santiago et al., reported the use of PtMo/C composite as electrocatalyst for PEMFC. The Mo/C diffusion layer helped in lowering the CO concentration in the electrodes hence promoting the CO tolerance of PtMo/C composite. The performance of Mo/C in reducing the CO concentration was also confirmed using gas chromatographic technique [23].

4.3 Batteries

4.3.1 Lithium Air (Li-Air) Batteries

Littauer and Tsai introduced lithium air batteries in the year 1976. Due to its higher theoretical energy density Li-O₂ batteries are considered as a good choice for electrochemical power source. For a material to exhibit better electrochemical performance towards Li-O₂ battery must be exhibit a better catalytic activity towards ORR. In that case, noble metals like platinum (Pt), usually exhibit effective ORR activity. As the noble metals as ORR catalyst are expensive and challenging to employ in real-time, carbon-based materials plays a vital role as its alternative. Oi Lun Li discussed the challenges and prospects in using carbon electrodes towards lithium air battery applications. The role of electrolyte (aqueous, non-aqueous, hybrid (aqueous/non aqueous) and solid electrolytes) also plays an important role in the functioning of the electrocatalyst. Carbon materials are often used as cathode in Li-air batteries where the cell voltage drop occurs [4].

Co₃O₄ doped hollow carbon nanospheres were grown in-situ by Wang et al., and employed it for lithium-air battery application. Co₃O₄/nitrogen-doped hollow carbon nanospheres was used as air electrode in coin type Li-O₂ battery. The incorporation of Co₃O₄ into carbon composite are believed to reduce the overpotential and improve catalytic activity. The carbon nanospheres used in this works supports

electron mobility as well as develops nucleation sites for the transition metal oxides. The synthesized Co_3O_4 /nitrogen-doped hollow carbon nanospheres exhibited mesoporous structures with the surface area of $278.3 \text{ m}^2\text{g}^{-1}$ helping faster transport of oxygen and increasing the reactivity supporting the discharge reactions. The specific discharge capacity of the nanocomposite was about 3325 mAhg^{-1} . The work also discussed the limitation of the cyclic stability of the synthesized nanocomposite. Hence, by improving the stability and optimizing the electrode efficient air-batteries as bifunctional catalysts can be achieved [24].

The electrochemical performance of $\delta\text{-MnO}_2$ /N-rGO towards the studies on Li-O_2 battery was discussed by Awan Zahoor et al. The porous nature, higher theoretical energy density, abundance, ease in ion transportation makes MnO_2 as a better electrocatalyst to be used in Li-O_2 battery application. In this work, the battery specific capacity of $\delta\text{-MnO}_2$ /N-rGO nanocomposite was found to be 5250 mAhg^{-1} . The $\delta\text{-MnO}_2$ /N-rGO electrodes also exhibited better discharge capacity of 3300 mA h g^{-1} at 0.1 mA cm^{-2} . The N-graphite species combined with $\delta\text{-MnO}_2$ in this work acted as a better ORR catalyst with improved reaction kinetics and energy conversion efficiency [25]. Masoumeh Salehia et al., studied the effect of rGO/CNT nanocomposite with specific surface area of $564.48 \text{ m}^2/\text{g}$ as electrocatalyst for Li-air batteries application. The work yielded better cyclability for about 50 cycles and at 100 mA/g it delivered the capacity of 9000 mA h/g . At 50 mA/g , the discharge capacity of $12,350 \text{ mA h/g}$ is obtained. The work also employed constant current and constant current/voltage discharge method [26].

The carbon materials are usually doped using nitrogen to make it as an effective electrochemical catalyst in terms of improved electron conductivity and durability as well as surface active sites. Hence, doping carbon with nitrogen while synthesizing nanocomposites with transition metal oxides is one of the effective strategies in enhancing the electrocatalytic performance.

4.3.2 Zinc Air (Zn-Air) Batteries

Due to its high theoretical energy density and low cost than Li-air batteries research on zinc-air (Zn-air) batteries gained significant attention in energy storage applications specifically for rechargeable batteries [27, 28]. In addition, Zn based materials are highly stable, abundantly available, less toxic and cost effective. Due to its physicochemical properties, electrical conductivity and its cost-effectiveness, carbon-based materials are widely used as a bifunctional catalyst for Zn-air battery applications [29]. Daolan Liu et al. reported the recent advances in Zn-air batteries using carbon based bifunctional catalyst [3].

Qing Qin et al. reported the multifunctional catalytic activity (OER, HER, ORR and Zn-air battery) of nitrogen and phosphorous co-doped carbon-supported Fe nanocomposite prepared through one-pot pyrolysis approach. In this work, carbon has been derived from tannic acid which is highly helpful in adsorbing properties. The developed nanocomposite exhibited an overpotential of about only 75 mV at 10 mA/cm^2 towards HER catalysis. The charge and discharge voltage gap was found

to be less at longer cycles which makes this nanocomposite an ideal candidature for the Zn-air battery application [30]. Xiaopeng Han et al., reported NiCo_2S_4 /nitrogen doped carbon nanotubes as an efficient bifunctional catalyst with better performance than the ideal RuO_2 and Pt/C electrodes with lower overpotential of about 0.63 V corresponding to charge/discharge and cyclability of 150 cycles. The nitrogen doped carbon nanotubes facilitated the surface conductivity as well as adsorption [31]. Sun et al., reported the synthesis and electrochemical studies of reduced graphene oxide/carbon black/amorphous cobalt borate (rGO/CB/Co-B) nanocomposites towards rechargeable Zn-air batteries. Herein, sandwich like structure of the nanocomposite with surface area of $1052.3 \text{ m}^2 \text{ g}^{-1}$ is developed where the graphene oxide sheets are separated by cobalt borate that are densely packed. The nanocomposite exhibited minimum charge transfer resistance followed by the higher diffusion kinetics from the LSV polarization. From the Koutecky–Levich plot signified that the synthesized rGO/CB/Co-B nanocomposite exhibited four electron transfer and rGO/Co-B exhibited two electron transfer pathways with the electron transfer number of 3.93 and 2.76 respectively. It shows that the addition of carbon black in rGO/CB/Co-B nanocomposite helps in enhanced conductivity and decreases the Lewis acidity making them thermodynamically favourable. The study proved that the rGO/CB/Co-B nanocomposite is an efficient catalyst towards OER as well as ORR and hence has been taken forward as a better cathode for Zn-air battery. In the primary study, the rGO/CB/Co-B nanocomposite exhibited a steady discharge curve up to 2000 min and also the battery exhibited the power density of $\sim 76 \text{ mW cm}^{-2}$. The rechargeable Zn-air battery made up of rGO/CB/Co-B nanocomposite was stable in 124 h cycling at the current density of 10 mA/cm^2 . The room temperature synthesized sandwich rGO/CB/Co-B nanocomposite exhibited lower discharge voltage and voltage gap at charging as well as discharging proving that the carbon based electrocatalyst as a robust Zn-air battery electrode [32].

Yan et al. reported an interesting perovskite/carbon nanocomposites synthesized using gel auto-combustion method as an electrocatalyst for oxygen reduction reaction in Zn-air batteries. The synthesized $\text{La}_{0.99}\text{MnO}_{3.03}/\text{C}$ nanocomposite exhibited a specific surface area of $120 \text{ m}^2 \text{ g}^{-1}$ with pore volume of $0.401 \text{ cm}^3 \text{ g}^{-1}$. The perovskite carbon composite delivered the energy and power density of $0.401 \text{ cm}^3 \text{ g}^{-1}$ and 430 mW cm^{-2} respectively with a stability along 340 h at current density of 10 mA/cm^2 [33].

4.3.3 Lithium-Ion (Li-Ion) Batteries

Due to its layered structures, vanadium pentoxide (V_2O_5) is widely used in applications involving adsorption and diffusion kinetics including sensors, supercapacitors and batteries [34, 35]. It is largely employed as cathode material in Li-ion battery application. The layered structure helps in efficient lithium intercalation and deintercalation. In addition to the advantage of layered V_2O_5 , integrating carbon-based materials will enhance the electrocatalytic performance due to its larger surface area, conductivity and chemical stability. Yifang Zhang et al., reported the

synthesis of dodecahedron-shaped carbon framework encapsulated by V_2O_5 making carbon/ V_2O_5 nanocomposites and employed it as a cathode material for lithium-ion batteries. The as-synthesized carbon/ V_2O_5 nanocomposite exhibited higher porosity with homogeneous structure. With change in calcination temperature in the synthesis process, carbon/ V_2O_5 nanocomposites exhibited varied surface morphology because of varied carbon combustion at different temperatures. The work reported better electrochemical performance of carbon/ V_2O_5 nanocomposite than pure V_2O_5 because of synergistic performance of carbon and oxide. The carbon/ V_2O_5 nanocomposite exhibited specific capacity of 121.6 mAhg^{-1} , whereas pure V_2O_5 rendered a specific capacity of only 20 mAh/g . In addition, from electrochemical impedance spectroscopy it was noticed that the charge transfer resistance (R_{CT}) of is 267.9Ω lower than V_2O_5 electrodes which exhibited the R_{CT} value of 638.8Ω . The Li^+ ions diffusion coefficient of carbon/ V_2O_5 nanocomposite was also found to be 2–4 times higher than the V_2O_5 electrodes [36].

Bin Sun et al., reported V_2O_5 nanosphere/MWCNT electrocatalyst as cathode material for Li-ion battery. In this work, V_2O_5 and MWCNT are arranged layer-by-layer with V_2O_5 having thickness of $\sim 2\text{--}3 \mu\text{m}$ and MWCNT having thickness of $\sim 1 \mu\text{m}$ and the whole stack possessed thickness of about $\sim 20 \mu\text{m}$. From cyclic voltammetric studies of V_2O_5 /MWCNT undergone a multistep reduction process corresponding to V^{+5} signifying the phase changes from $\alpha\text{-}V_2O_5 \rightarrow \epsilon\text{-}Li_{0.5}V_2O_5 \rightarrow \delta\text{-}Li V_2O_5 \rightarrow \gamma\text{-}Li_2V_2O_5$. Good reversibility of oxidation and reduction was noticed for three cycles and the galvanostatic charge/discharge cycles were also found to be consistent. The reversible capacity of about 275 mAh/g was observed after 50 cycles. The work reports that the layered structure had good stability and cyclability helping better lithiation/delithiation due to its electrostatic interaction. Hence, the layered V_2O_5 /MWCNT electrode can be used as an efficient electrocatalyst for Li-ion batteries [37]. Hongbin Zhao et al., reported the electrochemical characteristics of V_2O_5 /rGO and VO_2 /rGO and exhibited better cyclic stability and specific capacity towards Li-ion battery studies. The specific surface area of V_2O_5 /rGO and VO_2 /rGO were found to be $64 \text{ cm}^2/\text{g}$ and $35 \text{ cm}^2/\text{g}$ using BET studies. The rGO helped to increase the surface area of vanadium oxides which will improve the electrocatalytic activity of the composite cathode material. Even after 100 cycles, the discharge specific capacity of V_2O_5 /rGO was 171 mAh/g , which is 1.3 times greater than pure V_2O_5 implying the higher electrocatalytic activity of rGO. In addition to specific capacity, the addition of rGO to V_2O_5 also improved the cyclic stability of the nanocomposite. Hence, V_2O_5 /rGO was found to be a potential candidate as carbon composite for Li-ion battery application [38].

Linfei Zhang et al. reported V_2O_5 -C- SnO_2 synthesized using hydrothermal method as anodes for Li-ion batteries. In this work, glucose is used as carbonating agent and V_2O_5 and SnO_2 are linked to carbon to achieve high power and energy density. The nanocomposite retained reversible capacity of 800 mAh/g after 100 cycles which proved the cyclic stability of the synthesized nanocomposite material. The resistance was calculated from electrochemical impedance spectroscopy which showed lower resistance for the V_2O_5 -C- SnO_2 than V_2O_5 / SnO_2 . The work showed

that the carbon addition to V_2O_5/SnO_2 improved its reverse cyclic stability and rate capability suitable for Li-ion battery application [35].

4.4 Carbon Dioxide (CO_2) Reduction

Two major challenges prevailing in this century is global climate change and energy demand. To enjoy a sustainable environment both these challenges must be met using renewable energy sources. Carbon dioxide (CO_2) one of the major greenhouse gas responsible for climate change must be controlled or converted to any useful gas/or fuels. In that row, the research is carried out widely to covert CO_2 to fuels even before its release into the environment. The electrocatalyst plays a major role in electrochemical reduction of CO_2 and several reports indicate that carbon based electrocatalyst are efficient electrocatalyst for the CO_2 reduction. Xing Zhi et al. reported the interfacial electron transfer characteristics of graphitic carbon nitride (g- C_3N_4)/graphene doped with heteroatom boron, nitrogen, oxygen and phosphorous towards CO_2 reduction reaction through density functional theory (DFT) computational analysis. The work suggested that the carbon atom (C1) in the g- C_3N_4 , acts as an active site and the graphene provides better conductivity in the reaction. Increase in electron transfer was observed when nitrogen is doped with graphene. The strong adsorption capacity of g- C_3N_4 towards CO_2 makes it an ideal material for CO_2 reduction reaction [2].

Xunyu Lu et al., reported the CO_2 reduction of covalently bonded g- C_3N_4 /multiwall carbon nanotube nanocomposite. The bonding between carbon and nitrogen of multiwall carbon nanotube and g- C_3N_4 acted as core active sites for CO_2 reduction reaction. The highlights of g- C_3N_4 /multiwall carbon nanotube nanocomposite is its conductivity, active sites due to C-N bonding, increased specific surface area and mainly the aggregation of g- C_3N_4 could be hampered through multiwall carbon nanotube addition which results in higher surface area improving the catalytic performance for better CO_2 reduction reaction [8].

M. Nur Hossain et al. reported copper/reduced graphene oxide (Cu/rGO) nanocomposite for CO_2 reduction. The work also studied the Faradaic efficiency of the Cu/rGO catalyst using chemical oxygen demand for the first time. The chemical oxygen demand method which is different from CO_2 reduction, measures the total number of electrons taken part in the conversion of CO_2 gas to any other gas or fuel. While coming to the electrochemical characteristic study, linear sweep voltammetry and chronoamperometry are majorly used to understand the electrochemical behaviour of Cu/rGO nanocomposite. From the study it was found that the Cu/rGO nanocomposite exhibited minimum onset potential and better energy density compared to pure Cu nanoparticles as well as pure rGO implying that the synergistic effect of Cu/rGO nanocomposite plays a tremendous role in influencing the catalytic activity. From electrochemical impedance spectroscopy, the charge transfer resistance of Cu/rGO nanocomposite was found to be 355.40 Ω/cm , whereas R_{CT} value of pure Cu nanoparticles was 612.90 Ω/cm . In addition to R_{CT} value, the constant phase element value of Cu/rGO nanocomposite (1817.60 $\mu F/cm$) was also higher

than pure Cu nanoparticles (427.38 $\mu\text{F}/\text{cm}$) and rGO (781.40 $\mu\text{F}/\text{cm}$). For better electrochemical performance, the electrocatalyst must possess lower R_{CT} value and higher constant phase element value and hence the values observed in this work proves that Cu/rGO nanocomposite is an efficient electrocatalyst. In the cathodic potential range -0.4 to -0.6 V, it was found that carbon monoxide (CO) production from CO_2 was increased. This work confirmed that Cu/rGO nanocomposite exhibited higher Faradaic efficiency and lower overpotential making Cu/rGo a better candidate for CO_2 reduction [39].

5 Summary and Future Perspectives

The research on efficient electrocatalyst is thriving among researchers worldwide due to the demand for sustainable energy devices. The existing efficient electrocatalyst that are into commercialization are majorly noble metals (Pt, Ru, Ir) which are expensive and less abundant. In order to overcome these limitations of the existing electrodes, carbon-based materials are explored at a larger scale. The carbon-based nanocomposites with heteroatom doping, introducing functional groups, developing composites with metal oxides and sulphides are found to be effective. Though carbon-based materials are making a revolution in developing renewable energy devices, understanding the mechanisms underlying the improved electrocatalytic activity while making carbon integrated composites needs further exploration.

References

1. Mounasamy, V., Srividhya, G., Ponpandian, N.: Well-defined 2D transition vanadium pentoxide (V_2O_5) flat nanorods with large-scale synthesis feasibility as an electrocatalyst for the oxygen evolution reaction (OER). *Energy Adv.* **2**, 784–788 (2023). <https://doi.org/10.1039/D3YA00100H>
2. Zhi, X., Jiao, Y., Zheng, Y., Qiao, S.Z.: Impact of Interfacial Electron Transfer on Electrochemical CO_2 Reduction on Graphitic Carbon Nitride/Doped Graphene. *Small* **15**, 1–7 (2019). <https://doi.org/10.1002/sml.201804224>
3. Liu, D., Tong, Y., Yan, X., Liang, J., Dou, S.X.: Recent advances in Carbon-Based bifunctional Oxygen catalysts for Zinc-Air batteries. *Batter. Supercaps.* **2**, 743–765 (2019). <https://doi.org/10.1002/batt.201900052>
4. O.L. Li, T. Ishizaki, Development, challenges, and prospects of carbon-based electrode for lithium-air batteries, Elsevier Inc., (2018). <https://doi.org/10.1016/B978-0-12-813794-9.00004-1>.
5. Sun, Z., Wang, X., Liu, Z., Zhang, H., Yu, P., Mao, L.: Pt–Ru/CeO₂/Carbon nanotube nanocomposites: an efficient electrocatalyst for direct methanol fuel cells. *Langmuir* **26**, 12383–12389 (2010). <https://doi.org/10.1021/la101060s>
6. Leela Mohana Reddy, A., Ramaprabhu, S.: Pt/SWNT-Pt/C nanocomposite electrocatalysts for proton-exchange membrane fuel cells, *J. Phys. Chem. C.* **111** (2007) 16138–16146. <https://doi.org/10.1021/jp066985+>.

7. Shaari, N., Kamarudin, S.K.: Graphene in electrocatalyst and proton conduction membrane in fuel cell applications: An overview. *Renew. Sustain. Energy Rev.* **69**, 862–870 (2017). <https://doi.org/10.1016/j.rser.2016.07.044>
8. Lu, X., Tan, T.H., Ng, Y.H., Amal, R.: Highly selective and stable reduction of CO₂ to CO by a graphitic carbon nitride/carbon nanotube composite electrocatalyst. *Chem. - A Eur. J.* **22**, 11991–11996 (2016). <https://doi.org/10.1002/chem.201601674>
9. Kessler, F.K., Zheng, Y., Schwarz, D., Merschjann, C., Schnick, W., Wang, X., Bojdys, M.J.: Functional carbon nitride materials-design strategies for electrochemical devices, *Nat. Rev. Mater.* **2** (2017). <https://doi.org/10.1038/natrevmats.2017.30>
10. Ghany, N.A.A., Elsharif, S.A., Handal, H.T.: Revolution of Graphene for different applications: State-of-the-art. *Surfaces and Interfaces.* **9**, 93–106 (2017). <https://doi.org/10.1016/j.surfin.2017.08.004>
11. Kaur, M., Kaur, M., Sharma, V.K.: Nitrogen-doped graphene and graphene quantum dots: A review on synthesis and applications in energy, sensors and environment. *Adv. Colloid Interface Sci.* **259**, 44–64 (2018). <https://doi.org/10.1016/j.cis.2018.07.001>
12. Tafete, G.A., Thothadri, G., Abera, M.K.: A review on carbon nanotube-based composites for electrocatalyst applications. *Fullerenes Nanotub. Carbon Nanostructures.* **30**, 1075–1083 (2022). <https://doi.org/10.1080/1536383X.2022.2028278>
13. Shen, F.C., Wang, Y., Tang, Y.J., Li, S.L., Wang, Y.R., Dong, L.Z., Li, Y.F., Xu, Y., Lan, Y.Q.: CoV₂O₆-V₂O₅ coupled with porous N-Doped reduced graphene oxide composite as a highly efficient electrocatalyst for oxygen evolution. *ACS Energy Lett.* **2**, 1327–1333 (2017). <https://doi.org/10.1021/acsenergylett.7b00229>
14. Xing, X., Liu, R., Cao, K., Kaiser, U., Zhang, G., Streb, C.: Manganese vanadium Oxide-N-doped reduced graphene oxide composites as oxygen reduction and oxygen evolution electrocatalysts. *ACS Appl. Mater. Interfaces* **10**, 44511–44517 (2018). <https://doi.org/10.1021/acsami.8b16578>
15. Xie, K., Masa, J., Madej, E., Yang, F., Weide, P., Dong, W., Muhler, M., Schuhmann, W., Xia, W.: Co₃O₄-MnO₂-CNT hybrids synthesized by HNO₃ vapor oxidation of catalytically Grown CNTs as OER electrocatalysts. *Chem Cat Chem* **7**, 3027–3035 (2015). <https://doi.org/10.1002/cctc.201500469>
16. Das, B., Gogoi, D., Devi, M., Dhar, S.S., Peela, N.R.: Synergistic effect of metal complex and dual doped graphitic carbon nitride for superior photocatalytic hydrogen evolution. *Energy Fuels* **35**, 15223–15233 (2021). <https://doi.org/10.1021/acs.energyfuels.1c01732>
17. Zhu, Y., Chen, G., Zhong, Y., Zhou, W., Shao, Z.: Rationally designed hierarchically structured tungsten nitride and Nitrogen-Rich Graphene-Like carbon nanocomposite as efficient hydrogen evolution electrocatalyst, *Adv. Sci.* **5** (2018). <https://doi.org/10.1002/advs.201700603>
18. Yu, D., Ilango, P.R., Han, S., Ye, M., Hu, Y., Li, L., Peng, S.: Metal-organic framework derived Co@NC/CNT hybrid as a multifunctional electrocatalyst for hydrogen and oxygen evolution reaction and oxygen reduction reaction. *Int. J. Hydrogen Energy* **44**, 32054–32065 (2019). <https://doi.org/10.1016/j.ijhydene.2019.10.149>
19. Pan, Y., Zhang, F., Wu, K., Lu, Z., Chen, Y., Zhou, Y., Tang, Y., Lu, T.: Carbon supported Palladium-Iron nanoparticles with uniform alloy structure as methanol-tolerant electrocatalyst for oxygen reduction reaction. *Int. J. Hydrogen Energy* **37**, 2993–3000 (2012). <https://doi.org/10.1016/j.ijhydene.2011.11.042>
20. Huang, H., Wang, X., Jiang, S.P., Deng, N., Yoon, Y.S., Aricò, A.S., Spinelli, P., Jiang, L., Wang, C., O'Hayre, R., Kang, F., Yoshikawa, H., Ueda, S., Kobayashi, K., Sham, T.-K., Sun, X., Scardaci, V., Ferrari, A.C., Coleman, J.N.: Recent progress on carbon-based support materials for electrocatalysts of direct methanol fuel cells. *J. Mater. Chem. A.* **2**, 6266–6291 (2014). <https://doi.org/10.1039/C3TA14754A>
21. Lin, Y., Cui, X., Yen, C., Wai, C.M.: Platinum/carbon nanotube nanocomposite synthesized in supercritical fluid as electrocatalysts for low-temperature fuel cells. *J. Phys. Chem. B* **109**, 14410–14415 (2005). <https://doi.org/10.1021/jp0514675>
22. Zhang, W., Chen, J., Swiegers, G.F., Ma, Z.F., Wallace, G.G.: Microwave-assisted synthesis of Pt/CNT nanocomposite electrocatalysts for PEM fuel cells. *Nanoscale* **2**, 282–286 (2010). <https://doi.org/10.1039/b9nr00140a>

23. Santiago, E.I., Batista, M.S., Assaf, E.M., Ticianelli, E.A.: Mechanism of CO tolerance on Molybdenum-Based electrocatalysts for PEMFC. *J. Electrochem. Soc.* **151**, A944–A949 (2004). <https://doi.org/10.1149/1.1753579>
24. Wang, J., Fan, M., Tu, W., Chen, K., Shen, Y., Zhang, H.: In situ growth of Co₃O₄ on nitrogen-doped hollow carbon nanospheres as air electrode for lithium-air batteries. *J. Alloys Compd.* **777**, 944–953 (2019). <https://doi.org/10.1016/j.jallcom.2018.11.062>
25. Zahoor, A., Faizan, R., Elsaid, K., Hashmi, S., Butt, F.A., Ghouri, Z.K.: Synthesis and experimental investigation of δ -MnO₂/N-rGO nanocomposite for Li-O₂ batteries applications. *Chem. Eng. J. Adv.* **7**, 100115 (2021). <https://doi.org/10.1016/j.cej.2021.100115>
26. Salehi, M., Shariatinia, Z., Sadeghi, A.: Application of RGO/CNT nanocomposite as cathode material in lithium-air battery. *J. Electroanal. Chem.* **832**, 165–173 (2019). <https://doi.org/10.1016/j.jelechem.2018.10.053>
27. Qin, Y., Ou, Z., Xu, C., Zhang, Z., Yi, J., Jiang, Y., Wu, J., Guo, C., Si, Y., Zhao, T.: Progress of carbon-based electrocatalysts for flexible zinc-air batteries in the past 5 years: recent strategies for design, synthesis and performance optimization, *Nanoscale Res. Lett.* **16** (2021). <https://doi.org/10.1186/s11671-021-03548-5>.
28. Fu, G., Tang, Y., Lee, J.M.: Recent advances in Carbon-Based bifunctional oxygen electrocatalysts for Zn–Air batteries. *ChemElectroChem* **5**, 1424–1434 (2018). <https://doi.org/10.1002/celec.201800373>
29. Wei, Q., Fu, Y., Zhang, G., Sun, S.: Rational design of carbon-based oxygen electrocatalysts for zinc–air batteries. *Curr. Opin. Electrochem.* **4**, 45–59 (2017). <https://doi.org/10.1016/j.coelec.2017.09.006>
30. Qin, Q., Jang, H., Li, P., Yuan, B., Liu, X., Cho, J.: A Tannic Acid-Derived N-, P-Codoped Carbon-Supported Iron-Based nanocomposite as an advanced trifunctional electrocatalyst for the overall water splitting cells and Zinc-Air batteries. *Adv. Energy Mater.* **9**, 1803312 (2019). <https://doi.org/10.1002/aenm.201803312>
31. Han, X., Wu, X., Zhong, C., Deng, Y., Zhao, N., Hu, W.: NiCo₂S₄ nanocrystals anchored on nitrogen-doped carbon nanotubes as a highly efficient bifunctional electrocatalyst for rechargeable zinc-air batteries. *Nano Energy* **31**, 541–550 (2017). <https://doi.org/10.1016/j.nanoen.2016.12.008>
32. Sun, J., Yang, D., Lowe, S., Zhang, L., Wang, Y., Zhao, S., Liu, P., Wang, Y., Tang, Z., Zhao, H., Yao, X.: Sandwich-Like reduced graphene Oxide/Carbon Black/Amorphous cobalt borate nanocomposites as bifunctional cathode electrocatalyst in rechargeable Zinc-Air batteries. *Adv. Energy Mater.* **8**, 1–9 (2018). <https://doi.org/10.1002/aenm.201801495>
33. Yan, Z., Sun, H., Chen, X., Fu, X., Chen, C., Cheng, F., Chen, J.: Rapid low-temperature synthesis of perovskite/carbon nanocomposites as superior electrocatalysts for oxygen reduction in Zn-air batteries. *Nano Res.* **11**, 3282–3293 (2018). <https://doi.org/10.1007/s12274-017-1869-8>
34. Mounasamy, V., Mani, G.K., Tsuchiya, K., Madanagurusamy, S.: Nanoimprint assisted free standing porous vanadium oxide nanosheet based ammonia sensor. *Appl. Surf. Sci.* **541**, 148271 (2021). <https://doi.org/10.1016/j.apsusc.2020.148271>
35. Zhang, L., Yang, M., Zhang, S., Wu, Z., Amini, A., Zhang, Y., Wang, D., Bao, S., Lu, Z., Wang, N., Cheng, C.: V₂O₅-C-SnO₂ hybrid nanobelts as high performance anodes for Lithium-ion batteries. *Sci. Rep.* **6**, 33597 (2016). <https://doi.org/10.1038/srep33597>
36. Zhang, Y., Pan, A., Wang, Y., Wei, W., Su, Y., Hu, J., Cao, G., Liang, S.: Dodecahedron-Shaped porous vanadium oxide and carbon composite for High-Rate lithium ion batteries. *ACS Appl. Mater. Interfaces* **8**, 17303–17311 (2016). <https://doi.org/10.1021/acsami.6b04866>
37. Sun, B., Huang, K., Qi, X., Wei, X., Zhong, J.: Rational Construction of a functionalized V₂O₅ Nanosphere/MWCNT Layer-by-layer nanoarchitecture as cathode for enhanced performance of Lithium-Ion batteries. *Adv. Funct. Mater.* **25**, 5633–5639 (2015). <https://doi.org/10.1002/adfm.201502382>
38. Zhao, H., Pan, L., Xing, S., Luo, J., Xu, J.: Vanadium oxides-reduced graphene oxide composite for lithium-ion batteries and supercapacitors with improved electrochemical performance. *J. Power. Sources* **222**, 21–31 (2013). <https://doi.org/10.1016/j.jpowsour.2012.08.036>

39. Hossain, M.N., Wen, J., Chen, A.: Unique copper and reduced graphene oxide nanocomposite toward the efficient electrochemical reduction of carbon dioxide. *Sci. Rep.* **7**, 1–10 (2017). <https://doi.org/10.1038/s41598-017-03601-3>

Graphene-Based Fuel Cells



Suba Lakshmi Madaswamy, N. Veni Keertheeswari,
and Ragupathy Dhanusuraman

Abstract Graphene has received much attention in energy conversion devices due to its remarkable properties such as unique thermal, mechanical, electronic, and chemical properties. Also, graphene has an isolated layer of carbon hexagons with Sp^2 hybridized C–C bonds with electron clouds. Thin flakes made of a few layers of carbon atoms, such as mono-layer graphene, can be very significant from an engineering perspective due to their intriguing structural and physical properties as well as their potential for exciting technology applications. Hybrid structures based on graphene have been used to create a wide range of effective and long-lasting fuel cell energy systems. Graphene in fuel cell technology exhibits excellent catalytic performance in potential applications of fuel cell devices. This chapter focuses on the fuel cell device used by graphene and how graphene is used in contemporary fuel cell technology, including in electrodes.

Keywords Graphene · Catalytic performance · Fuel cell

1 Graphene—Historical Overview

A two-dimensional crystalline carbon ‘Graphene’ is either a multiple connected layer of atoms forming a honeycomb (hexagonal) lattice or a single layer of carbon. Graphene is a much-hyped honeycomb 2D lattice of carbon atoms, which is the

S. L. Madaswamy

Department of Chemistry, V.V. Vanniaperumal College for Women, Virudhunagar, Tamil Nadu 626001, India

N. V. Keertheeswari · R. Dhanusuraman (✉)

Department of Chemistry, Nano Electrochemistry Lab (NEL), National Institute of Technology Puducherry, Karaikal, Puducherry 609609, India
e-mail: ragu@pondiuni.ac.in; ragu.nitpy@gmail.com

R. Dhanusuraman

Nano Electrochemistry Laboratory (NEL), Central Instrumentation Facility (CIF), School of Physical, Chemical and Applied Sciences, Pondicherry University, Puducherry 605014, India

strongest, lightest, and thinnest substance widely known and the finest heat and electrical conductor ever discovered—and the list proceeds. It is the tiniest item ever made, being a million times thinner than a human hair. Even though graphene is flexible and lightweight, it is also the world's strongest substance (stronger than steel by 200 times). Konstantin Novoselov and Andre Geim of the University of Manchester and colleagues extracted graphene (single-layer) in 2004 using an exceedingly easy way of exfoliation from graphite. Their “scotch-tape method” involved using adhesive tape to remove a graphite sample's top layers and then applying them to a substrate material. When the tape was removed, some single-layer graphene remained on the substrate. Producing graphene is not a difficult operation by itself; every time someone draws with a pencil on paper, the pencil trace contains a small amount of multilayer and single-layer graphene. The Manchester group isolated graphene flakes, and examined their physical properties. They demonstrated that electrons in graphene had high mobility, and were utilized in electronic applications [1, 2].

The graphene substrate was naturally coated by a thin transparent layer of silicon dioxide on a silicon wafer by a process called either micromechanical cleavage or the Scotch tape technique for which Geim and Novoselov were awarded the Nobel Prize in Physics in 2010. It was discovered that single-layer graphene provided a strong enough optical contrast with silicon dioxide to make the graphene visible under a normal optical microscope. Graphene also conducts electricity more quickly than most other materials and, when piled in layers, forms graphite, which is also present in pencils [3].

2 Structure of Graphene

Carbon, the earliest element discovered by humanity remains one of the most fascinating chemical elements. Carbon materials are used for a wide range of applications due to their unique diversity of forms and features, which range from chemical bonding between carbon atoms to nanostructures, crystallite alignment, and microstructures. Carbons three-dimensional (3D) crystalline forms are graphite and diamond. Graphite is made up entirely of Sp^2 hybridized bonds, whereas diamond is made up entirely of Sp^3 hybridized bonds. Diamond's carbon atoms are organized in a face-centered cubic (fcc) crystal structure. The exceptional physical properties of diamonds are due to the strong covalent bonding between their atoms (Sp^3 hybridization).

Graphite has a lamellar (planar, layered) structure, unlike diamond. Carbon atoms are organized in a hexagonal lattice in each layer with a separation of 0.142 nm (Sp^2 hybridization), and the distance between planes (layers) is 0.335 nm. Graphite has two known forms, (hexagonal) and (rhombohedral), which are extremely similar. The forces within the lateral planes of lamellar structures are substantially stronger than the forces between the planes. All graphitic forms, such as three-dimensional graphite, one-dimensional carbon nanotubes, and zero-dimensional fullerenes, are descended from graphene. Graphite, carbon nanotubes (CNT), fullerene (C60), and

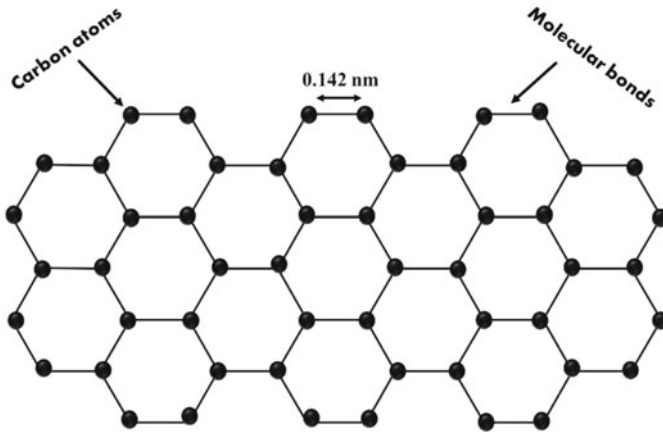


Fig. 1 Schematic structure of the graphene sheet

other related materials (carbon fiber (CF), amorphous carbon (AC), and charcoal) all contain the fundamental structural component known as graphene. A single atom forms each vertex of the 2D, atomic-scale hexagonal lattice known as graphene, which is an allotrope of carbon. The carbon–carbon bond has a length of roughly 0.142 nm, which is shown in Fig. 1.

Each lattice comprises three solidly connected linkages that combine to create a sturdy hexagonal framework. The electrical conductivity of graphene is mostly attributed to the bond connection located vertically to the lattice plane. Because of its tightly packed carbon atoms and a sp^2 orbital hybridization, which combines the orbitals s , p_x , and p_y to produce the σ -bond, graphene is stable. The final p_z electron creates the π -bond. The bonds join to form the π -band and π^* -bands. The majority of the notable electrical characteristics of graphene are attributed to the half-filled band that permits free-moving electrons. Graphene derivatives such as graphene oxide (GO), and reduced graphene oxide (rGO) possess unique features, which are revealed in Fig. 2 [4, 5].

A unit structure of graphene is composed of graphite, carbon nanotubes, and fullerene, as well as aromatic molecules of unlimited size, like planar polycyclic aromatic hydrocarbons. Carbon atoms bind with adjacent carbon atoms via Sp^2 hybridization to create a benzene ring, with each atom donating an unpaired electron. The thickness of graphene is 0.35 nm, which is 1/200,000th the diameter of human hair. Graphene structure is however relatively stable. The link between carbon atoms is strong enough to endure external stress through a twisting lattice plane, preventing atom reconfiguration. Graphene has a constrained nanoribbon structure, producing an energy barrier near the center point because of lateral charge flow. The energy barrier increases as the width of the nanoribbon decreases. Thus, the energy barrier can be controlled by the width of the graphene nanoribbon, which is a desirable feature for possible graphene-based electrical devices. Furthermore, like CNTs, graphene edges

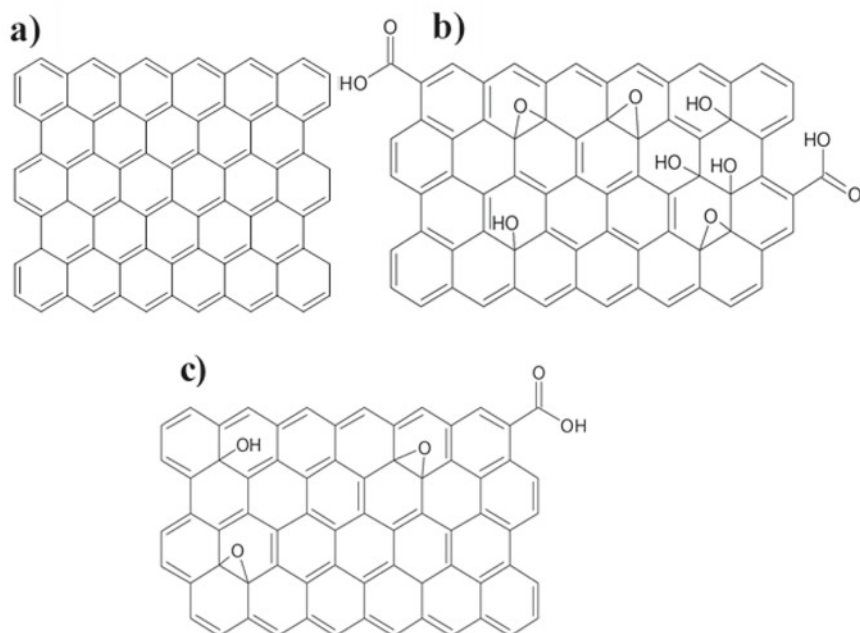


Fig. 2 Structure of **a** Graphene, **b** Graphene oxide (GO), and **c** Reduced graphene oxide (rGO)

may be categorized as zigzag or armchairs based on distinct carbon chains, as seen in Fig. 3a–c [5, 6].

3 The Versatile Properties of Graphene

Graphene's characteristics are distinct due to its all-carbon structure and nanoscale shape. Graphene possesses exceptional mechanical, electrical, optical and thermal characteristics [6–9]. Graphene is very light, weighing only 0.77 mg per square meter. It has the most surface area of any substance since it has a single 2D sheet. When left alone, graphene sheets stack to create graphite, the most durable 3D form of carbon in typical conditions. Graphene has a high electrical mobility, and electrons behave similarly to photons in terms of movement. Graphene's electrical mobility has been demonstrated to be extraordinarily high, with previously published findings exceeding $15,000 \text{ cm}^2 \text{ V}^{-1} \text{ s}^{-1}$ and theoretically potential limits of $200,000 \text{ cm}^2 \text{ V}^{-1} \text{ s}^{-1}$ (constrained by the dispersion of acoustic photons in graphene). The electronic properties of the electrons, which function as massless charge carriers with exceptionally great mobility, are responsible for this. The thermal conductivities of low dimensional carbon materials like graphene and carbon nanotubes, which range from 3000 to 6000 W/m/K [6–13].

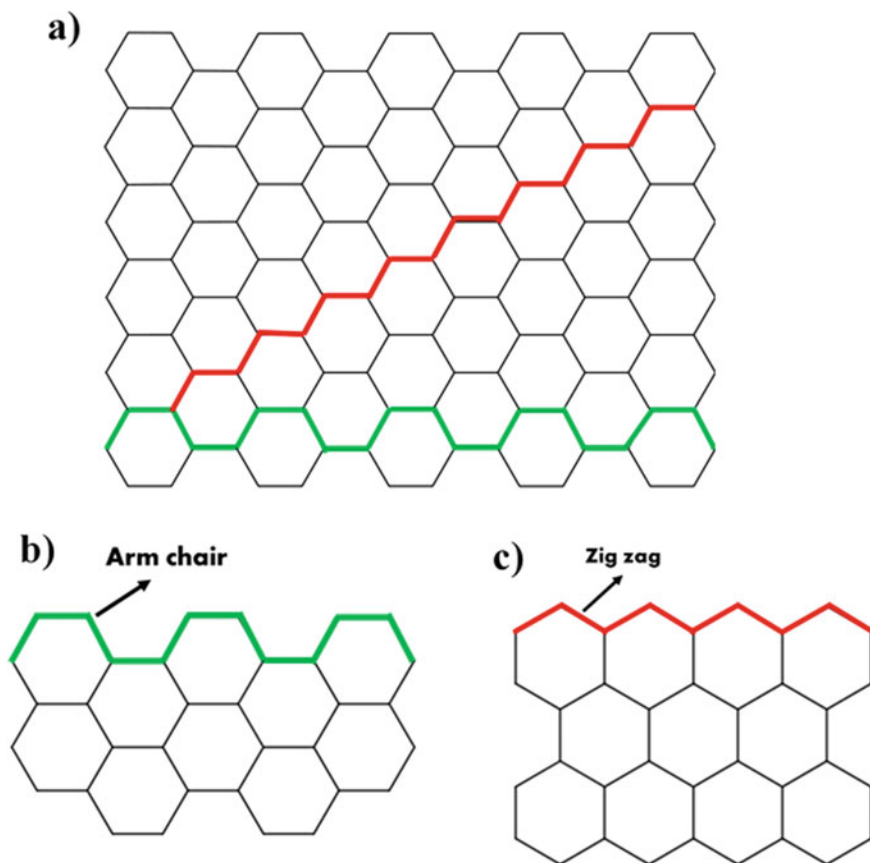


Fig. 3 a Honeycomb lattice of Graphene both directions (armchair and zigzag), b armchair structure of graphene, and zigzag structure of graphene

4 Synthesis of Graphene, Graphene-Based Electrocatalysts and Membrane

In 2004, Geim and Novoselov performed ground-breaking studies on two-dimensional graphene utilizing the scotch tape technique. For graphene production, both bottom-up and top-down techniques are possible. For example, chemical vapour deposition develops graphene in silicon carbide (bottom-up), whereas the mechanical exfoliation method is the mechanism by which graphite is broken down into graphene (top-down) [14–19].

4.1 Synthesis of Graphene

Exfoliation is a peeling process that is performed in graphite to create layers of graphene. The graphene layers were then peeled away from the graphite using scotch tape. Using graphite foils, plates, rods, and powders as electrodes in an aqueous or non-aqueous electrolyte and applying an electric current to promote electrode expansion are the key components of the Electrochemical exfoliation method. A basic method for producing graphene is the thermal breakdown of silicon carbide (SiC). High temperatures cause Si to desorb, leaving C atoms remaining to create a few layers of graphene. The CVD development of graphene was accomplished using cold-wall and hot-wall reaction chambers. The development of graphene in this approach is quick, excellent quality, and requires little power [14–19].

4.2 Synthesis of Graphene-Based Electrocatalysts

Graphene is a promising electrocatalyst supporting material for composite electrocatalysts owing to the material's enormous surface area, superior electric conductivity, and electrochemical stability. In order to anchor metal or metal oxide on the graphene substrate as well as conducting polymer and other carbon-based materials, several physical or chemical techniques, such as chemical reduction, thermal treatment, hydrothermal or solvothermal processes, self-assembly, and electrochemical processes, have been studied.

Chemical reduction is a typical method for producing graphene-supported metal catalysts that use a variety of reducing chemicals such as ethylene glycol (EG), sodium citrate, sodium borohydride (NaBH_4), and GO (or rGO). As well as In general, doping with heteroatoms (e.g., S, N, B, and P) is an excellent method for increasing graphene's intrinsic catalytic activity by producing additional active centers or modifying carbon atom charge density. For example, created a unique NG with a 3D porous nanostructure. The 3D graphene material was discovered to have more accessible active sites, exceptional, durability, and catalytic activity. Furthermore, the electron-accepting capacity of N atoms contributed significantly to the exceptional electrocatalytic ORR performance. Graphene-based electrocatalysts are very suitable electrocatalysts for all applications such as energy storage and conversion (Supercapacitor, Batteries, and Fuel cells), sensor, and biomedical applications (drug delivery, cancer therapy, and biological imaging) [20–23].

4.3 Synthesis of Graphene-Based Membranes

Graphene oxide's (GO) strong proton conductivity, chemical stability, and outstanding mechanical qualities make it a perfect filler material for fuel cell polymer

membranes. To make GO-polymer composites, in situ intercalative polymerization and solution intercalation are two common techniques. GO is combined with liquid monomer precursors in the in situ intercalative polymerization process, and the polymerization is subsequently initiated by an initiator under regulated circumstances. Epoxy and polyaniline (PANI) are two common polymers that are in situ polymerized with graphene. Using sonication or mechanical mixing, the well-dispersed soluble polymer and GO were rejoined to form a composite during the solution intercalation process. This method is simple and widely utilized in the manufacture of GO-polymer composites. Due to its higher proton conductivity and low permeability to reactant species, GO may be used directly as a proton electrolyte in fuel cells in addition to the creation of GO-polymer composites [24–26].

5 Graphene-Based Materials for Fuel Cell

5.1 *Electrochemical Energy Conversion Device: Fuel Cell*

Our daily lives necessitate the use of energy. A rapid increase in overall population and consistent personal income growth are two variables that contribute to increased energy consumption. The global population is expected to surpass 8.7 billion by 2035, implying that an extra 1.6 billion people would require energy. Due to this rapid development of economic growth, supplying energy cannot satisfy the increasing demand, as well as fossil resource depletion such as coal, petrol, oil, and environmental pollution, are worldwide.

The fundamental challenge is growing energy consumption and declining fossil fuel availability, as well as concerns about the impact of traditional fossil fuels on human health. There is an urgent need to replace existing non-renewable fossil fuels with green alternatives and sustainable energy. It has been observed that worldwide renewable energy generation is increasing. According to research of the literature, a renewable electricity capacity of around 1560 GW was used by the end of 2013, nearly doubling the 895 GW reported at the beginning of 2004. However, the conversion of energy devices is necessary for automobile industry applications. Over the past decades, clean and sustainable energy technologies (solar energy, wind energy, and biomass fuels) have been rapidly developed along with energy conversion technologies have also been on the rise. Electrochemical energy is an electrochemical process of conversion between chemical energy and electrical energy. In most electrochemical energy technologies, the electrode and electrolyte materials must possess the required ionic and electronic transport properties and a great deal of research is still to be performed at a fundamental level to study and optimize the electrochemistry of candidate materials, composites, and assemblies (such as catalyst and interface designs). As a result, the curtailment strategy was used to fix these costly problems and prevent further escalation. Aside from the energy storage approach, fuel cell

technology is one of the most current technologies that gives a quick solution to the aforementioned challenges.

The dynamic application of fuel cell technology is mainly for the insistence of global energy such as fossil fuel depletion, biomass, natural gas, and environmental pollution. The basic principle of the fuel cell was discovered by William Grove in 1839. The fuel cell converts fuel into electricity through an electrochemical reaction in which, the only products are heat, carbon dioxide, and water. Conversion paths of chemical energy to electrical energy have many steps. The conventional method of converting the chemical energy of fuel into heat energy and this heat energy is converted into mechanical energy, which in turn is converted into electrical energy. It has an efficiency of about 30% because of a minimum of three intermediate steps to attain energy. Whereas the fuel cell which converts the chemical energy of a fuel and an oxidant (pure oxygen or air) directly into electricity has a higher efficiency of about 80% without any intermediate steps involved. Water and heat are the only components of the electrochemical processes of a hydrogen fuel cell engine. Carbon dioxide emissions can be minimized by exploiting the better energy efficiency of fuel cell engines if hydrogen is produced from hydrocarbon reforming or electrolyzers driven by fossil-based electricity. Emissions may be lowered to zero if hydrogen is produced using sustainable energy sources such as wind, solar thermal, and nuclear power.

Fuel cell benefits include high efficiency and reliability, multi-fuel capability, durability, scalability, noise-free, and ease of maintenance. Hence, fuel cells find wider characteristics such as being portable, stationary, and power for transportation [27–30].

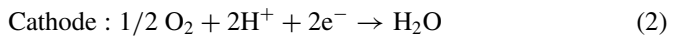
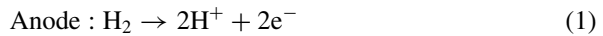
5.2 Types of Fuel Cell

Since the discovery of this technology, several fuel cell types have been studied and developed. Fuel cells are usually classified in terms of the type of electrolyte, chemical reactions, and operating temperature (low and high-temperature fuel cells). The classification of fuel cells. Low-temperature fuel cells which operate at a temperature range of 80–200 °C. They are Polymer Electrolyte Membrane Fuel Cells (PEMFC), Phosphoric Acid Fuel Cells (PAFC), Direct Methanol Fuel Cells (DMFC), and Alkaline Fuel Cells (AFC). High-temperature fuel cells such as Solid Oxide Fuel Cell (SOFC) and Molten Carbonate Fuel Cell (MCFC) operate at temperatures in the range 600–1000 °C. Each type of fuel cell has its own problem which can be overcome by other types of fuel cells [31].

5.3 Working Principle of Fuel Cell System

The fuel cell is an energy conversion device that interconverts chemical energy to electrical energy. The cathode, anode, electrolyte, membrane, and external circuit known as the load are the major components of a typical fuel cell system, which is illustrated in Fig. 4.

Despite the complicated setup, the functioning of the fuel cell system is easy. The anode will be fed with hydrogen fuel (or any other fuel) indefinitely, while the cathode will be fed with the oxidant in the air. The hydrogen supplied is diverted into two kinds in the anode: the hydrogen positive ion, H^+ , and the hydrogen negative ion, H^- . The electrolyte separates the cathode and anode pathways conceptually. The electrolyte only permitted the H^+ ions to pass from the anode to the cathode and acted as an insulator to prevent the H^- ions from traveling. The three primary reaction stages that occur at the anode and cathode in the fuel cell system are depicted in the equations below.



Modeling a fuel cell system is worthwhile because it is a useful tool for improving the design of the fuel cell by gaining a better knowledge of the internal operating

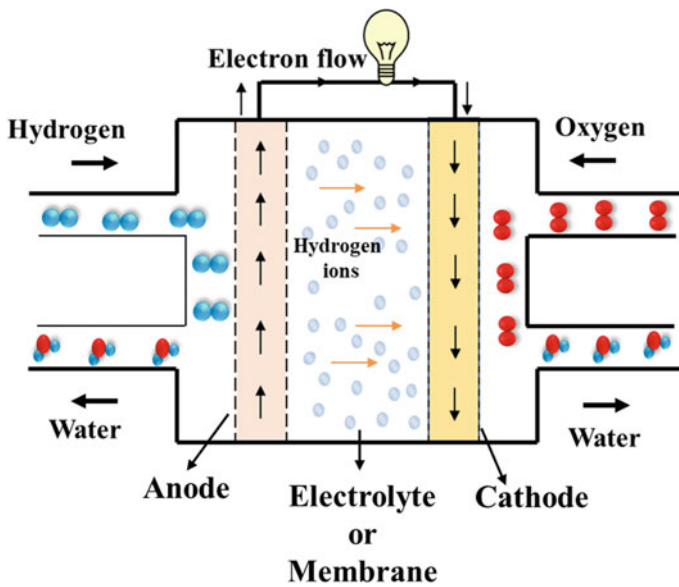


Fig. 4 A basic schematic structure of a fuel cell system

mechanism. Running a modeled fuel cell is faster and less expensive than running a real-scale system, which aids in the design process. Over the last 10 years, substantial research efforts have been devoted to the development of realistic computational fuel cell models [32–34].

5.4 Role of Graphene in Electrocatalytic Reactions

5.4.1 Substrate

Graphene has a large specific surface area for a 2D material. Furthermore, it is proved that some functional groups, such as O- and N- containing functional groups, may operate on the surface of graphene. On the one hand, functional groups serve as nucleation sites in the formation of metal nanoparticles or single atoms. However, it is also proved that these functional groups are advantageous for attaching metal nanoparticles. As a result, graphene may be widely used as an appropriate substrate for loading single-atom metal nanoparticles to significantly boost their electrocatalytic efficiency [35].

5.4.2 Active Center

Graphene, in addition to functioning as a substrate, may also operate as an active center to enhance electrochemical processes. Despite its high potential for electrocatalytic processes, graphene's catalytic activity remains much lower than that of metal nanocatalysts. Heteroatom doping is an efficient method for significantly altering the electronic characteristics of graphene in order to improve its catalytic activity. Furthermore, nitrogen (N) and phosphorous (P) co-doping can control their electrical conductivity and surface characteristics to function as catalytically active sites, significantly boosting electrocatalytic performance [35].

5.4.3 Conductor

The electrical conductivity of graphene is $1 \times 10^5 \text{ S m}^{-1}$. As a result, graphene may be used as an excellent conductor to increase the electrical conductance of hybrid catalyst composites. When graphene is combined with another material, such as metal or metal oxide, the resultant composite has a better conductivity than graphene. This increased electrocatalytic activity [35].

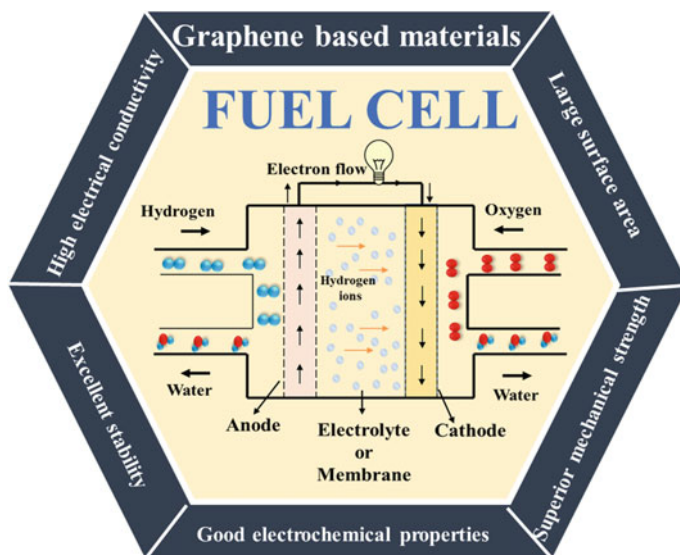


Fig. 5 Schematic illustration of fuel cell system incorporating graphene-based materials in each component

5.5 Graphene-Based Materials for Fuel Cell

The vast specific area, excellent electrochemical stability, strong electrical conductivity, and quick recovery of platinum catalysts make graphene a promising choice for energy conversion applications. Graphene is important in fuel cell technology because of its appealing features. The fuel cell is gaining a lot of interest as a potential alternative energy source. Because fuel cells are an environmentally benign method of producing water, heat, and electricity, with no pollutants or harmful by-products, many studies are currently concentrating on lowering the cost and increasing the efficiency of fuel cells. The cathode, anode, and separation membrane are the three main components of a fuel cell. Graphene-based electrocatalyst is an essential material in these main components due to its properties (Fig. 5) [35–50].

5.5.1 Graphene-Based Anode Electrocatalysts for Fuel Cell

Graphene-based materials have high electrical conductivity, vast surface area, and adjustable anchoring sites that can boost inert metal dispersion and enable charge mobility in fuel oxidation. There has been a lot of work put into developing effective graphene-supported electrocatalysts for methanol oxidation reaction (MOR), ethanol oxidation reaction (EOR), solid oxide fuel cell (SOFC), and formic acid oxidation reaction (FAOR). Because of their fast charge transfer rate and biocompatibility,

graphene-based materials are especially promising as anodes for microbial fuel cells (MFC) [39–44].

Graphene—Noble Metal Hybrids

As previously stated, graphene has several potential electrochemical uses, particularly for fuel cell applications such as methanol and ethanol oxidation reactions. Methanol, a liquid fuel with a high volumetric energy density that is easy to carry and store, may be used to power DMFCs directly, although its electrochemical reactivity is lower than that of hydrogen. Furthermore, the chemical intermediates easily obstruct the active sites of frequently employed platinum-based catalysts. Pt nanoparticles can be immobilized in graphene-based materials to improve their activity and durability for MOR.

For example, Eunyoo and Okata et al. have investigated Pt catalysts supported on GNS. Pt/GNS were created using a platinum precursor $[\text{Pt}(\text{NO}_2)_2(\text{NH}_3)_2]$ and GNS powder. Inductively coupled plasma (ICP) analysis determines the loading quantity (about 20 wt.%) of Pt clusters to GNS, which is essentially similar to Pt on activated carbon (Pt/C, Vulcan XC-72R) for fair comparison. When compared to the Pt/carbon black catalyst, the Pt/GNS electrocatalyst demonstrated particularly high activity for the methanol oxidation process. Among the tested catalyst samples, the Pt/GNS electrocatalyst had a markedly distinct profile for CO oxidation. It is discovered that Pt particles smaller than 0.5 nm in size develop on GNS, acquiring the particular electronic structures of Pt and altering its catalytic activities. MOR current–potential curves in $1 \text{ mol dm}^{-3} \text{ CH}_3\text{OH} + 0.05 \text{ mol dm}^{-3} \text{ H}_2\text{SO}_4$ for Pt/carbon black, Pt/GNS, and PtRu/carbon black. The quantity of metals was 0.0169 mg for Pt/carbon black and Pt/GNS, and 0.0184 mg for PtRu/carbon black Per apparent area of the electrode. For Pt/carbon black, Pt/GNS, and PtRu/carbon black, the onset potential of methanol oxidation was 0.6, 0.5, and 0.4 V relative to the reference hydrogen electrode (RHE), respectively. According to the findings of this work, GNS is projected to be a novel carbon support material capable of changing the catalytic characteristics of Pt fuel cell catalysts [39].

Ethanol is a renewable energy source that may be created from agricultural waste or biomass. Ethanol has a greater mass-energy density (8.01 kWh kg^{-1}) and lower toxicity than methanol (6.07 kWh kg^{-1}). Noble metals, like MOR, are necessary to break the C–C bond in ethanol in order to complete oxidation and prevent overpotential loss. Graphene-based materials are excellent supports for increasing noble metal dispersion and facilitating charge transfer. For example, Lifeng and Gari colleagues produced Pt and Pt-Ru nanoparticles on graphene sheets and examined their electrocatalytic performance for methanol and ethanol oxidation. In terms of diffusion efficiency, oxidation potential, forward oxidation peak current density, and the ratio of the forward peak current density to the reverse peak current density, graphene-supported Pt and Pt-Ru nanoparticles outperform the widely used Vulcan XC-72R carbon black catalyst supports in both methanol and ethanol electro-oxidations. For example, the forward peak current density of methanol oxidation for graphene- and

carbon black-supported Pt nanoparticles is 19.1 and 9.76 mA/cm², respectively, with ratios of 6.52 and 1.39; the forward peak current density of ethanol oxidation for graphene- and carbon black-supported Pt nanoparticles is 16.2 and 13.8 mA/cm², respectively, with ratios of 3.66 and 0.90. These findings suggest that graphene sheets can be used as catalyst supports in both direct methanol and ethanol fuel cells [40].

Graphene—Alloy Hybrids

Bimetallic nanoparticles have piqued the interest of researchers due to their superior catalytic characteristics when compared to single nanoparticles. Nickel-palladium alloy nanoparticles over graphene nanosheets (NiPd alloy NPs/GNS) are synthesized by Karthikeyan and Jayaraman et al. utilizing an ammonia-hydrazine technique in a surfactant-free hydrothermal procedure. NiPd alloy NPs/GNS are a novel type of electrocatalyst with improved activity and stability in formic acid and ethanol oxidation processes. According to research, bimetallic alloy nanoparticles have better catalytic activity than monometallic catalysts in electro-oxidation processes. The enhanced activity is mostly due to the robust assembly of bimetallic NiPd alloy NPs on graphene sheets. The innovative NiPd alloy NPs/GNS catalysts offer a new approach to improving electro-catalytic performance in next-generation fuel cells [41].

As an alternative energy conversion technique, the solid oxide fuel cell is a viable possibility. In this regard, graphene-included composite anode materials were synthesized using a solid-state reaction with anode composition Al_{0.1}Ni_{0.2}Zn_{0.7} oxides, and varying quantities of 1 wt.%, 1.3 wt.%, and 1.5 wt.% graphene were subsequently integrated in the resulting composite material. A direct current (DC) four-probe approach was used to assess electrical conductivity as a function of temperature from 300 to 650 °C, and the highest value was reported to be 0.53 Scm⁻¹ at 370 °C with 1.3% graphene inclusion. With 1.3% graphene inclusion, the highest power density was 375 mWcm⁻² at 600 °C. Even at lower temperatures 330–370 °C, a substantial improvement in conductivity from 0.42 to 0.52 S cm⁻¹ was seen for the sample containing 1.3% graphene concentration. The decreased activation energy of 0.09 eV shows that graphene-incorporated nanostructured material improves electrical conductivity and cell performance. In the H₂/air gaseous settings, the highest values of OCV were 0.95 V and power density was 375 mWcm⁻² at 600 C for the same sample with 1.3% wt ratio graphene. Based on the data presented above, it was determined that the ANZ-1.3%G composition is optimised in all aspects and is a viable anode material for low temperature SOFC applications. This graphene-incorporated study will be used as a starting point for the SOFC research community to explore for similar materials in order to improve fuel cell performance [42].

Functionalized Graphene Hybrids

Graphene or graphene-doped heteroatom hybrid materials improve electrocatalytic performance for use in fuel cells. Karim and Rahnavardi researched reduced graphene oxide (RGO) and nitrogen-doped RGO (N-RGO), which are generated electrochemically and then decorated with palladium nanoparticles through a solvothermal technique to produce Pd/RGO and Pd/NRGO. The bare RGO and NRGO electrodes are the most active for the oxygen reduction reaction (ORR) and ethanol tolerance, with the best Tafel slope and onset potential. However, the resulting Pd/NRGO electrocatalyst exhibits superior electrocatalytic performance in both ORR and ethanol oxidation reaction (EOR), with higher peak current density and lower Tafel slope than Pd/RGO, which can be attributed to Pd/NRGO's higher electrochemical active surface area ($53 \text{ m}^2 \text{ g}^{-1}$) than Pd/RGO's ($41 \text{ m}^2 \text{ g}^{-1}$). The fundamental reason for Pd/NRGO's increased efficiency is due to its larger electrochemical surface area and nitrogen doping of graphene [43].

Alper and colleagues disclosed polyoxometalate (NaPWO) functionalized graphene quantum dots (GQDs) with several mono-metallic and bi-metallic nanoparticles such as platinum nanoparticles (PtNPs), palladium nanoparticles (PdNPs), and platinum-palladium nanoparticles (Pt-PdNPs), simple and cost-effective catalysts have been developed. The Pt-PdNPs/NaPWO/GQDs also had a larger peak current for methanol oxidation than similar PdNPs/NaPWO/GQDs and PtNPs/NaPWO/GQDs, indicating greater electro-catalytic activity [44].

5.5.2 Graphene-Based Cathode Electrocatalysts for Fuel Cell

Cathode materials are critical components for the commercialization of fuel cell systems. Currently, the most well-known cathode materials for the oxygen reduction process (ORR) are pricey noble metals such as platinum (Pt), gold (Au), ruthenium (Ru), and their alloys. Pt is the most extensively researched noble metal as an electrocatalyst. However, it is prohibitively costly and has a finite supply on Earth. As a result, at least one of the three solutions must exist. One strategy is to increase surface area using nanoparticles to reduce the need of costly catalysts. Another option is to look for less cost but more efficient metal catalysts to replace pricey noble metals. The final step is to create effective metal-free catalysts. However, Pt-based catalysts have a low tolerance for carbon monoxide toxicity and fuel crossover. To make fuel cells one of the most promising energy sources, a new class of materials with cheap cost, high efficiency for ORR, and strong durability is required. In this context, carbon-based metal-free electrocatalysts with high catalytic activity, extended cycle stability, reduced poisoning impact, and anode crossover are being developed [45–49].

Graphene-Supported ORR Electrocatalysts

Graphene-based materials are more conductive in nature that are commonly used as supports for metal nanoparticles, allowing electrons to transfer to the electrode surface. For example, Muhammad et al., reports an effective technique for improving fuel cell conductivity and performance at low temperatures in solid oxide fuel cell by partially integrating graphene in the $\text{Li}_{0.1}\text{Cu}_{0.2}\text{Zn}_{0.7}$ -oxide (LCZ) composite. The outstanding performance of graphene-incorporated LCZ is attributable to the favorable charge transport routes with low area-specific resistance. The electrical conductivities of all materials are determined using the DC four-probe method, and LCZ-1.5% graphene exhibits an excellent conductivity of 3.5 S/cm in air atmosphere at 450 C with a minimum value of 0.057 cm^2 area-specific resistance (ASR) that demonstrates significantly good performance [45].

Three-dimensional graphene nanosheets (3D-GNS) were employed as cathode catalysts for microbial fuel cells (MFCs) functioning in neutral conditions, according to Santoro et al. In comparison to activated carbon (AC), 3D-GNS catalysts demonstrated superior performance in neutral medium oxygen electroreduction with high current densities and reduced hydrogen peroxide production. With three distinct loadings (2, 6, and 10 mg cm^2), 3D-GNS was combined into air-breathing cathodes based on AC. In MFCs, 3D-GNS performed best, with power densities of 2.059 0.003 Wm^{-2} , 1.855 0.007 Wm^{-2} , and 1.503 0.005 Wm^{-2} for loadings of 10, 6, and 2 mg cm^2 , respectively [46]. Iron- and nitrogen-functionalized graphene (Fe-Ne-G) as a non-precious metal catalyst is synthesized by Sizhe Li et al. using a simple thermal treatment of a Fe salt, graphitic carbon nitride (gC_3N_4), and chemically reduced form of graphene. The activity of the prepared electrocatalysts towards oxygen reduction reaction (ORR) as measured by linear sweep voltammetry shows that the Fe-Ne-G catalyst has a higher positive onset potential and higher reduction current densities than the pristine graphene (P-G) catalyst, indicating that the Fe-Ne-G catalyst has improved ORR activity. More crucially, the Fe-Ne-G-MFC has a maximum power density of 1149.8 mW m^{-2} , which is 2.1 times that of the Pt/C-MFC (561.1 mW m^{-2}) and much higher than that of the P-G-MFC (109 mW m^{-2}). These findings show that the Fe-Ne-G catalyst has the potential to be a viable alternative to the more expensive Pt catalyst in practical MFC applications [47].

Noori and colleagues employed graphene/Vulcan XC as conductive support and V_2O_5 as a catalyst in MFCs for bioelectricity recovery from fish market effluent. The electrocatalytic activity of a low-cost V_2O_5 -NRs catalyst coupled with graphene is notably improved, leading to increased power production and organic matter elimination in MFC. When compared to expensive platinum, the larger power generated by MFC employing a very low-cost $\text{V}_2\text{O}_5/\text{rGO}$ cathode makes it a suitable candidate for MFC scale-up [48].

5.5.3 Graphene-Based Membranes

The electrolytes used in a fuel cell must have strong conductivity of ions, electrical non-conductance, and low reactant accessibility. Nafion is the most often utilized polymeric film in PEMFCs because of its strong conductivity of proton and chemical retainability. However, humid circumstances, operating temperature, and fuel crossover concerns restrict its performance. Graphene-root compounds have been investigated as a cartridge to improve polymer membrane ionic conductance and minimize gas passable, as well as conductivity of proton in electrolytes for fuel cells.

Graphene-based materials are routinely utilized to increase the conductivity of ions and gas impermeability to the membrane of the polymer. The composite membranes outperform typical polymer membranes in terms of conductivity of ions, fuel gas possibility, mechanical toughness, and chemical retained, boosting fuel cell performance and durability. Graphene was synthesized by Ghosh et al. using chemical oxidation followed by thermal exfoliation of natural graphite. The chemical treatment of the synthesized graphene resulted in functionalized graphene (FG). As-grown graphene and FG were characterized and employed as Pt support materials. Precipitation was used to create catalysts with 20% Pt/G and 20% Pt/FG. When compared to the commercial carbon-supported platinum catalyst, the electrochemical surface area of the FG-supported platinum catalyst was found to be more than 45% larger. The new catalyst (Pt/G and Pt/FG) was substantially more stable than the commercial Pt/C. Using the catalysts, the membrane electrode assembly was created and tested in a PEMFC. The greatest power densities of the fuel cell were determined to be 314, 426, and 455 mW cm⁻², respectively, employing Pt/C, Pt/G, and Pt/FG [49].

Synthesized nanocomposites (F-GO/Nafion) are proposed as a viable proton exchange membrane (PEM) substitute for high temperature PEM fuel cell. The GO nanosheets were synthesised from natural graphite peel using a modified Hummer's technique and functionalized with 3-mercaptopropyl trimethoxysilane (MPTMS) as the sulfonic acid functional group precursor. A simple solution casting approach was used to create F-GO/Nafion composite membranes. Proton conductivity and single-cell test findings showed that F-GO/Nafion membranes (4 times) outperformed recast Nafion at 120 °C with 25% humidity [50].

6 Conclusion

We summarised graphene's history, structural characteristics, production process, and use to fuel cells in this chapter. Graphene and its derivative's unique chemical and physical properties (heteroatom-doped graphene, graphene oxide, and functionalized graphene) have imitated enormous efforts and made remarkable activity toward fuel cell applications, primarily graphene-based anodes, graphene-based cathodes, and graphene-based membranes for fuel cells. Graphene-supported catalysts promote a wide range of electrochemical reactions, including ORR, MOR, EOR, and FAOR.

Low-temperature polymer membrane-based fuel cells benefit greatly from graphene-based materials.

References

1. Geim, A.K.: Graphene prehistory. *Phys. Scr.* 014003, (2012)
2. Madurani, K.A., Suprpto, S., Machrita, N.I., Bahar, S.L., Illiya, W., Kurniawan, F.: Progress in graphene synthesis and its application: history, challenge and the future outlook for research and industry. *ECS J. Solid State Sci. Technol.* **9**, 093013 (2020)
3. Randviir, E.P., Brownson, D.A., Banks, C.E.: A decade of graphene research: production, applications and outlook. *Mater. Today* **17**, 426–432 (2014)
4. Zhen, Z., Zhu, H.: *Structure and Properties of Graphene*, pp. 1–12. Graphene Academic Press (2018)
5. Rao, C.N.R., Biswas, K., Subrahmanyam, K.S., Govindaraj, A.: Graphene, the new nanocarbon. *J. Mater. Chem.* **19**, 2457–2469 (2009)
6. Kan, E., Li, Z., Yang, J.: Graphene nanoribbons: geometric, electronic, and magnetic properties. *Phys. Appl. Graphene-Theory* **10**, 14112 (2011)
7. Urade, A.R., Lahiri, I., Suresh, K.S.: Graphene properties, synthesis and applications: a review. *JOM* **75**, 614–630 (2023)
8. Xu, Z.: *Fundamental Properties of Graphene*, pp. 73–102. Graphene Academic Press (2018)
9. Zhu, Y., Murali, S., Cai, W., Li, X., Suk, J.W., Potts, J.R., Ruoff, R.S.: Graphene and graphene oxide: synthesis, properties, and applications. *Adv. Mater.* **22**, 3906–3924 (2010)
10. Papageorgiou, D.G., Kinloch, I.A., Young, R.J.: Mechanical properties of graphene and graphene-based nanocomposites. *Prog. Mater. Sci.* **90**, 75–127 (2017)
11. Neto, A.C., Guinea, F., Peres, N.M., Novoselov, K.S., Geim, A.K.: The electronic properties of graphene. *Rev. Mod. Phys.* **81**, 109 (2009)
12. Falkovsky, L.A.: Optical properties of graphene. *J. Phys. Conf. Ser.* **129**, 012004 (2008)
13. Pop, E., Varshney, V., Roy, A.K.: Thermal properties of graphene: fundamentals and applications. *MRS Bull.* **37**, 1273–1281 (2012)
14. Bhuyan, M.S.A., Uddin, M.N., Islam, M.M., Bipasha, F.A., Hossain, S.S.: Synthesis of graphene. *Int. Nano Lett.* **6**, 65–83 (2016)
15. Choi, W., Lahiri, I., Seelaboyina, R., Kang, Y.S.: Synthesis of graphene and its applications: a review. *Crit. Rev. Solid State Mater. Sci.* **35**, 52–71 (2010)
16. Santhiran, A., Iyngaran, P., Abiman, P., Kuganathan, N.: Graphene synthesis and its recent advances in applications—a review. *C* **7**, 76 (2021)
17. Hur, S.H., Park, J.N.: Graphene and its application in fuel cell catalysis: a review. *Asia-Pac. J. Chem. Eng.* **8**, 218–233 (2013)
18. Bhuyan, M.S.A., Uddin, M.N., Islam, M.M., Bipasha, F.A., Hossain, S.S.: Synthesis of graphene. *Int. Nano Lett.* **6**, 65–83 (2016)
19. Van Bommel, A.J., Crombeen, J.E., Van Tooren, A.: LEED and Auger electron observations of the SiC (0001) surface. *Surf. Sci.* **48**, 463–472 (1975)
20. Huang, X., Qi, X., Boey, F., Zhang, H.: Graphene-based composites. *Chem. Soc. Rev.* **41**, 666–686 (2012)
21. Razaq, A., Bibi, F., Zheng, X., Papadakis, R., Jafri, S.H.M., Li, H.: Review on graphene-, graphene oxide-, reduced graphene oxide-based flexible composites: from fabrication to applications. *Materials* **15**, 1012 (2022)
22. Lin, Z., Waller, G.H., Liu, Y., Liu, M., Wong, C.P.: 3D Nitrogen-doped graphene prepared by pyrolysis of graphene oxide with polypyrrole for electrocatalysis of oxygen reduction reaction. *Nano Energy* **2**, 241–248 (2013)
23. Olszowska, K., Pang, J., Wrobel, P.S., Zhao, L., Ta, H.Q., Liu, Z., Trzebicka, B., Bachmatiuk, A., Rummeli, M.H.: Three-dimensional nanostructured graphene: synthesis and energy, environmental and biomedical applications. *Synth. Met.* **234**, 53–85 (2017)

24. Liu, G., Jin, W., Xu, N.: Graphene-based membranes. *Chem. Soc. Rev.* **44**, 5016–5030 (2015)
25. Hu, S., Lozada-Hidalgo, M., Wang, F.C., Mishchenko, A., Schedin, F., Nair, R.R., Hill, E.W., Boukhvalov, D.W., Katsnelson, M.I., Dryfe, R.A., Grigorieva, I.V.: Proton transport through one-atom-thick crystals. *Nature* **516**, 227–230 (2014)
26. Lee, D.C., Yang, H.N., Park, S.H., Kim, W.J.: Nafion/graphene oxide composite membranes for low humidifying polymer electrolyte membrane fuel cell. *J. Membr. Sci.* **452**, 20–28 (2014)
27. Sharaf, O.Z., Orhan, M.F.: An overview of fuel cell technology: fundamentals and applications. *Renew. Sust. Energ. Rev.* **32**, 810–853 (2014)
28. Sazali, N., Wan Salleh, W.N., Jamaludin, A.S., Mhd Razali, M.N.: New perspectives on fuel cell technology: a brief review. *Membranes* **10**, 99 (2020)
29. Perry, M.L., Fuller, T.F.: A historical perspective of fuel cell technology in the 20th century. *J. Electrochem. Soc.* **149**, S59 (2002)
30. Iqbal, M.Z., Rehman, A.U., Siddique, S.: Prospects and challenges of graphene based fuel cells. *J. Energy Chem.* **39**, 217–234 (2019)
31. Larminie, J., Dicks, A., McDonald, M.S.: *Fuel cell systems explained*. Chichester, UK J. Wiley **2**, 207–225 (2003)
32. Carrette, L., Friedrich, K.A., Stimming, U.: *Fuel cells: principles, types, fuels, and applications*. *ChemPhysChem* **1**, 162–193 (2000)
33. O'hayre, R., Cha, S.W., Colella, W., Prinz, F.B.: *Fuel Cell Fundamentals*. Wiley & Sons (2016)
34. Fan, L., Tu, Z., Chan, S.H.: Recent development of hydrogen and fuel cell technologies: a review. *Energy Rep.* **7**, 8421–8446 (2021)
35. Yang, P., Yang, X., Liu, W., Guo, R., Yao, Z.: *Graphene-Based Electrocatalysts for Advanced Energy Conversion*. GEE (2022)
36. Xia, B., Yan, Y., Wang, X., Lou, X.W.D.: Recent progress on graphene-based hybrid electrocatalysts. *Mater. Horiz.* **1**, 379–399 (2014)
37. Su, H., Hu, Y.H.: Recent advances in graphene-based materials for fuel cell applications. *Energy Sci. Eng.* **9**, 958–983 (2021)
38. Iqbal, M.Z., Siddique, S., Khan, A., Haider, S.S., Khalid, M.: Recent developments in graphene based novel structures for efficient and durable fuel cells. *Mater. Res. Bull.* **122**, 110674 (2020)
39. Yoo, E., Okata, T., Akita, T., Kohyama, M., Nakamura, J., Honma, I.: Enhanced electrocatalytic activity of Pt subnanoclusters on graphene nanosheet surface. *Nano Lett.* **9**, 2255–2259 (2009)
40. Dong, L., Gari, R.R.S., Li, Z., Craig, M.M., Hou, S.: Graphene-supported platinum and platinum–ruthenium nanoparticles with high electrocatalytic activity for methanol and ethanol oxidation. *Carbon* **48**, 781–787 (2010)
41. Gopalsamy, K., Balamurugan, J., Thanh, T.D., Kim, N.H., Hui, D., Lee, J.H.: Surfactant-free synthesis of NiPd nanoalloy/graphene bifunctional nanocomposite for fuel cell. *Compos. B Eng.* **114**, 319–327 (2017)
42. Ahmad, K., Ahmad, M.A., Raza, R., Khan, M.A., Rehman, Z.U., Abbas, G.: Graphene incorporated nanocomposite anode for low temperature SOFCs. *Electron. Mater.* **48**, 7507–7514 (2019)
43. Kakaei, K., Rahnavardi, M.: Synthesis of nitrogen-doped reduced graphene oxide and its decoration with high efficiency palladium nanoparticles for direct ethanol fuel cell. *Renew. Energy* **163**, 1277–1286 (2021)
44. Çolak, A.T., Eren, T., Yola, M.L., Beşli, E., Şahin, O., Atar, N.: 3D polyoxometalate-functionalized graphene quantum dots with mono-metallic and bi-metallic nanoparticles for application in direct methanol fuel cells. *J. Electrochem. Soc.* **163**, 1237 (2016)
45. Ahmad, M.A., Ahmad, K., Li, H., Gassoumi, A., Raza, R., Saleem, M., Jafri, S.H.M., Abbas, G.: Synergistic electrochemical properties of graphene incorporated LCZ-oxide cathode for low temperature solid oxide fuel cell. *Crystals* **13**, 434 (2023)
46. Santoro, C., Kodali, M., Kabir, S., Soavi, F., Serov, A., Atanassov, P.: Three-dimensional graphene nanosheets as cathode catalysts in standard and supercapacitive microbial fuel cell. *J. Power Sources* **356**, 371–380 (2017)
47. Li, S., Hu, Y., Xu, Q., Sun, J., Hou, B., Zhang, Y.: Iron-and nitrogen-functionalized graphene as a non-precious metal catalyst for enhanced oxygen reduction in an air-cathode microbial fuel cell. *J. Power Sources* **213**, 265–269 (2012)

48. Noori, M.T., Mukherjee, C.K., Ghangrekar, M.M.: Enhancing performance of microbial fuel cell by using graphene supported V_2O_5 -nanorod catalytic cathode. *Electrochim. Acta* **228**, 513–521 (2017)
49. Ghosh, A., Basu, S., Verma, A.: Graphene and functionalized graphene supported platinum catalyst for PEMFC. *Fuel Cells*. **13**, 355–363 (2013)
50. Zarrin, H., Higgins, D., Jun, Y., Chen, Z., M. Fowler.: Functionalized graphene oxide nanocomposite membrane for low humidity and high temperature proton exchange membrane fuel cells. *J. Phys. Chem. C* **115**, 20774–20781 (2011)

Nanocomposites of Carbon for Fuel Cells



James F. Amaku and Raymond Taziwa

Abstract A vast number of resources have been invested into the design of intermediate and low-temperature fuel cells such as the microbial fuel cell (MFC), proton exchange membrane fuel cell (PEMFC), direct borohydride fuel cell (DBFC), and direct methanol fuel cell (DMFC). This class of fuel cells has displayed varied limitations owing to their respective principal components. Hence, the need to investigate different materials and nanocomposites with the capacity to enhance the performance of fuel cells. Due to the exceptional properties of carbon molecules in their nano state, nanocarbons have gained global attention as catalyst supports in fuel cell applications. The triumphs and challenges of the application of carbon nanotube-based electrocatalysts in fuel cell technology have been presented in this book chapter. This chapter will review the application of carbon-based nanocomposite materials in the intermediate processes of MFC, PEMFC, DBFC, DMFC, and other recently designed fuel cells. Comparative study of the mechanism of action, applications, yield, merits, and demerits of various carbon-based nanocomposite materials will be assessed. Recent advances in important cutting-edge synthetic routes will be assessed. The sole purpose of this work is to act as a substantive reference for the application of carbon-based nanocomposite fuel cell energy generation reviews.

Keywords Nanocomposite · Fuel cells · Electrocatalyst · Graphene · Fullerene · Aerogel

1 Introduction

The recent technological advances with increasing global industrialization, demand a high volume of energy to function effectively. The global dependence on hydrocarbon-based fossil fuels, as her basic source of energy, has resulted in the depletion of fossil fuel resources, and this is a potential threat to the well-being of

J. F. Amaku (✉) · R. Taziwa

Department of Applied Science, Faculty of Natural Science, Engineering and Technology, Walter Sisulu University, Old King William Town Road, Potsdam Site, East London 5200, South Africa
e-mail: famaku@wsu.ac.za

man. Apart from the advantages of using fossil fuel as an energy source, man and his environment have faced significant hurdles due to the emissions of CO, SO_x, NO_x, and particulate matter [1]. In 2015, about 7, 8, and 85% of energy were sourced from renewable energy, nuclear energy, and fossil fuels respectively in the USA [1]. Meanwhile, 12, 27, and 56%, of the energy consumed in Germany (in 2006) were sourced from renewable, nuclear, and fossil fuels respectively [2]. The statistical data plainly demonstrates the world's overreliance on fossil fuels, which might be disastrous for global health and the environment. Therefore, it is essential to diversify the world's energy sources by utilizing technology that is pollution-free, reasonably priced, and renewable.

Fuel cells have demonstrated the capacity to be an effective and sustainable energy source with the capacity to convert chemicals to electrical energies with little or no secondary pollutants. With years of intensive and innovative development of fuel cell technology, this green energy source has demonstrated the capacity to serve as an alternative to conventional energy generation technology. These devices are classified based on the operating temperature and nature of the employed electrolyte. Some of these are solid oxide fuel cell (SOFC), alkaline fuel cell (AFC), direct methanol fuel cell (DMFC), molten carbonate fuel cell (MCFC), proton exchange membrane fuel cell (PEMFC) and phosphoric acid fuel cell (PAFC) [3]. Owing to the abundance of fuel sources, portability, low system temperature and little or no pollutant emissions, PEMFC and DMFCs are considered an ideal power source. The basic component of PEMFC and DMFC include the electrocatalyst that is needed to speed up the electrochemical process, the anode (for methanol or hydrogen oxidation) and the cathode (reduction of oxygen). The effectiveness of any electrochemical process in a fuel cell is a function of the suitability of its electrocatalyst. Iridium, platinum, lead, and their alloys are commonly used in fuel cells, and this could be due to their high efficiency. On the contrary, these catalysts are scarce sourced and expensive. Hence, it is imperative to design a cost-effective electrocatalyst with superior electrochemical activity for fuel cell application. To achieve this, stakeholders have invested resources in the search for porous catalyst supports in the design of fuel cell applications. In the quest to validate the implication of support in electrocatalyst design, carbon nanotubes (CNTs), carbon black, single-walled carbon nanotubes (SWCNTs), graphene, multiwalled carbon nanotubes (MWCNTs), graphite, Nafion-carbon (NC), and other forms of carbons have been employed [4].

However, good catalyst supports for PEMFC and DMFC should demonstrate good stability against redox attack, excellent surface activity, outstanding conductivity, high porosity, and robust surface area. Several porous materials have been examined as catalyst support amongst which porous carbon was found worthy due to their interchangeable carbon framework, biocompatibility, porosity, electrical conductivity, mechanical strength, cost-effectiveness, chemical stability, and surface area, which was found to match the desired physicochemical characteristics of a perfect catalyst support [5].

To reduce the cost of operating a potable fuel cell via the reduction in the amount of non-precious metal catalysts employed, carbon support-based electrocatalysts are thereby fabricated for commercial purposes. However, the efficiency of this class

of electrocatalyst was observed to decline due to the deterioration of the carbon support. To mitigate the catalytic failure due to the structural limitation of most electrocatalysts, robust synthetic routes have been used to obtain nanoporous carbon-based electrocatalysts with adjustable physicochemical properties. Furthermore, the application of nano-casting and self-assembly of organic molecules methods in the fabrication of superior carbon-based electrocatalysts with unique properties have been reported. Meanwhile, the integrated hard and soft template technique has been used to fabricate mesoporous carbon. A substantial amount of review papers has been published on the application of nanocomposite of carbon as an electrocatalyst in various fuel cells. Hence, this study aims to methodically provide an overview of the nanocomposite of carbon proposed as electrocatalyst support for fuel cell applications. Recent advances in important cutting-edge synthetic routes will be reviewed. It is our aim to present this piece as a reference tool for beginners and established researchers.

2 Types of Fuel Cells

Fuel cells are classified based on the operating temperature of the system and the type of electrolyte employed. Due to the variation in their operating conditions, the efficiency of fuel cells is known to vary. To gain extensive insight into how to enhance the efficiency of fuel cells using carbon-based nanocomposites, basic knowledge of simple fuel cells must be assessed. The engineering design of proton exchange membrane fuel cells displayed two basic compartments which include the catalyst layers and the gas diffusion layers. This membrane-electrode assembly technology is known to use palladium, iridium, gold, platinum, ruthenium or alloys of these metals as its catalysts and can operate effectively at a relatively low temperature with high power density and low cost of operation [6]. The constrained operational temperature range, susceptibility of the catalyst to CO poisoning and expensive nature of the metal catalyst are the demerits of PEMFC. Hence, the need to optimize the application of metal catalysts calls for the inclusion of porous carbon-base support [7]. Another efficient fuel cell with a similar fundamental design as PEMFC is the phosphoric acid fuel cell (PAFC). On a global scale, PAFCs are the most advanced and marketed fuel cell. This could be attributed to its capacity to resist contaminants, elevated power density and robust efficiency of operation. PAFCs consist of bipolar plates that were fabricated from graphite, liquid phosphoric acid as an electrolyte and a diffusion chamber (consisting of platinum/carbon). The drawback to the application of PAFCs in automobiles includes the high cost of the metal catalyst, huge warm-up time and poisoning of the anode. Massive generation of power at high temperature (600 °C) involving the application of eutectic (a mixture of molten carbonates and alkalis salt) solution as the electrolyte is the unique characteristic of molten carbonate fuel cells (MCFCs) [8]. MCFCs are stationary energy-generating sources with approximately 80% maximum efficiency [9]. This fuel cell employs coal, natural gas or bio-fuels as fuel and is considered to be green and renewable

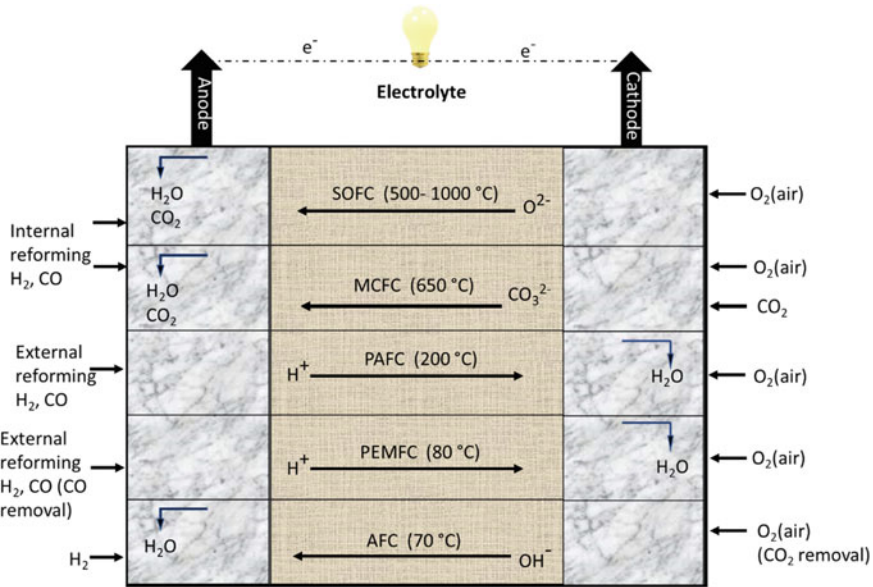


Fig. 1 Different types of fuel cells and their working condition

due to its carbon capture and storage characteristics [9]. Meanwhile, the application of MCFCs is limited due to corrosion tendency and low power density. The most economical fuel cell is the alkaline fuel cells (AFCs) which function effectively with the elimination of heat, H_2O and electrical power as byproducts [10]. AFCs make employs nickel and concentrated potassium hydroxide as their electrocatalyst and electrolyte respectively. However, a promising outcome was reported when noble metals were employed as catalysts in the operation of AFCs. Moderate operating cost, 60% efficiency and elevated oxide reduction at the anode are the advantages of AFCs [11]. Solid oxide fuel cells (SOFCs) are high-power generating cells that operate at ~ 1000 C with solid nonporous metal oxide as electrolytes [12]. SOFCs function with 60% efficiency for a long duration with high electrical power and a vast amount of heat as a by-product (Fig. 1).

2.1 Graphene-Based Electrode Materials

Graphene consists of a unit atom-carbon sheet that is held together by SP^2 hybridization. Layers of graphene can be rolled into graphene sheets (2D) and flower balls (fullerene) (3D). This material can be sourced as graphene liquid, graphene powder or graphene film. These forms of graphene are essentially due to the condition of synthesis. Graphene is synthesized using different synthetic paths and they include electrochemical, oxidation–reduction, chemical vapour deposition (CVD) (epitaxial

growth), mechanical stripping and heating methods amongst others. There are other synthetic routes that have been optimized for the fabrication of graphene. The goal of many stakeholders is to obtain a graphene material that fits their application with superior physicochemical properties. The unique thermal, chemical, and physical properties of this material present graphene as a promising candidate for applications in different energy devices. Meanwhile, graphene-based materials have demonstrated superior mechanical properties, robust electrical conductivity and excellent surface area that surpassed the estimated surface area obtained for single-walled carbon nanotubes [4]. The application of graphene in energy devices (catalyst support) has gained massive attention and this is due to its extraordinary properties [13]. The physicochemical characteristic of graphene confers on this material the ability to support metal catalysts with a hierarchical structural framework that supports high loading of metal catalysts (Fig. 2).

The application of graphene in the design of electrocatalyst and membrane for fuel cells have been reported with merit and drawback. Outstanding oxidation of methanol was observed using an electrocatalyst fabricated from Pt-loaded N-graphene for

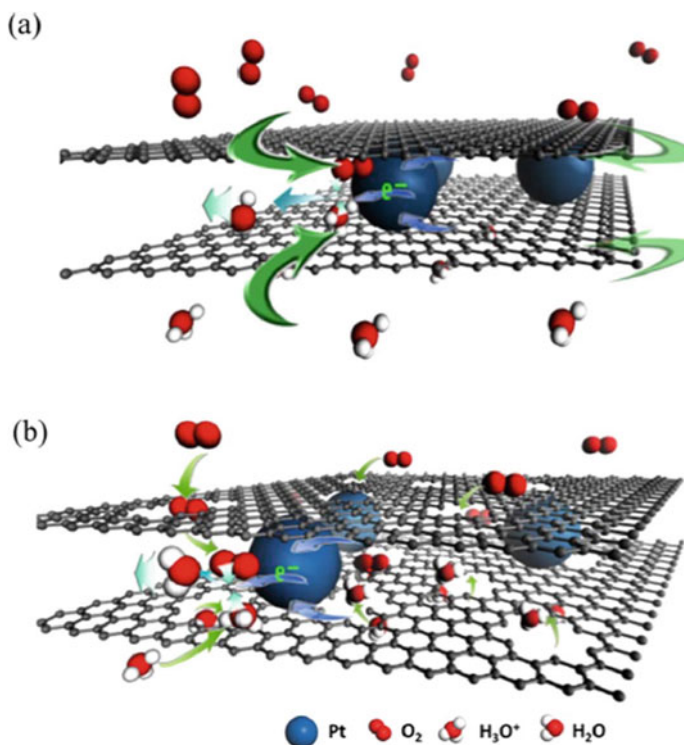


Fig. 2 Porous graphene-supported Pt catalysts for proton exchange membrane fuel cells. Adapted with permission [13], Copyright (2014) Elsevier

PEMFC. The thermally treated (180 °C) nitrogen-doped graphene was further modified with functionalized multiwalled carbon nanotubes (MWCNTs). The electrocatalyst obtained was noticed to have a current and power density of 1.20 A cm^{-2} and 704 mW cm^{-2} respectively. We believe that the application of MWCNTs containing pore-trapped Pt metals will further enhance the efficiency of the electrocatalyst [14]. Meanwhile, Co_3O_4 @graphene microspheres and reduced graphene oxide-nickel foam have displayed excellent performance in biosensor [15] and microbial fuel cell [16] applications. On the other hand, Pt-loaded graphene aerogel showed distinct efficiency as an anode for microbial fuel cells [17].

In a one-pot reaction in which ascorbic acid was employed as a reductant in the fabrication of graphene decorated with Pt-nanoclusters, the composite exhibited good stability and electrocatalytic characteristics against the oxidation of methanol [18]. Meanwhile, the fabrication of Pt-clusters anchored on graphene nanosheet was noticed to exhibit enhanced catalytic activity than Pt/carbon black and better tolerance to CO in hydrogen oxidation reactions [19]. Lei et al. successfully fabricated Pt/graphene catalysts by making use of polydiallyldimethyl ammonium as a Pt dispersant, the uniform dispersion of Pt on the graphene was observed to enhance the catalytic characteristics of the composite [20]. Cu and Pt-doped ionic-liquid-assisted graphene was successfully fabricated and was noticed to have superior stability and electrocatalytic properties [21]. Furthermore, the application of graphene in the design of electrocatalysts has been reported amongst which include Pt/G nanocomposites [22], Pt/GNS [23], Pd/graphene nanosheet [24], graphene/carbon cloth [25] and FeTsPcgraphene [26]. On the other hand, graphene has also demonstrated promising potential in the space of membranes for fuel cells. The graphene-based membrane was observed to have good selectivity, robust conducting performance within a wide temperature range and high-power density.

2.2 Carbon Nanotubes (CNTs)

Carbon nanotubes (CNTs) are one-dimensional materials with nanoscale measurements. This cylindrically structured carbon material is known to have a diameter-to-length ratio of 1:28,000,000 with exceptional optical, mechanical, magnetic, chemical, and electronic properties [27]. Hence, the demand for CNTs in different applications is quite amazing. The poor solubility of CNTs is a drawback to their application in some fields. Notwithstanding the solubility status of CNTs, surface modification of CNTs via chemical treatment (acidification) provides a leeway to the application of CNTs on surfaces that requires homogeneous dispersion of CNTs. In fuel cells, CNTs have played a vital role in the design of electrocatalysts. This was observed with improved catalyst performance that resulted in larger current density, elevated transmission capacity, robust corrosion resistance, improved stability, and cost-effectiveness. Lin et al. [28], successfully synthesized Pt/RuO₂-0.56H₂O/CNT catalyst exhibiting superb efficiency for direct methanol electrooxidation. The incorporation of the CNTs was noticed to enhance the microstructure and the power

output of the electrocatalyst. Notwithstanding the cellular toxicity of CNTs, a surface-based modification of CNTs can present carbon nanotubes as a value-added material for microbial fuel cell design. Wei and co-workers [29] produced MoS₂/CNTs nanocomposite with strong electrocatalytic activity and improved biocompatibility when employed in microbial fuel cells. The composite was observed to exhibit superior power density ($645 \pm 32 \text{ mW m}^{-2}$) with a moderate start time. Abbasi and group [30] developed a composite (CNT@SiO₂-PWA) as a membrane for direct methanol fuel cells. The Nafion-assisted composite demonstrated good electrocatalytic activity via fast proton transmission with reduced methanol permeability. A similar observation was made using ZrO₂-CNT nano-filler modified Nafion® membrane [31] and Nafion/SCNTs-SUCNTs composite [32]. Meanwhile, using the chemical oxidative method CNT/polypyrrole nanocomposite was carefully fabricated and assessed for catalytic activity using microbial fuel cells, the novel nanocomposite was noticed to exhibit approximately 113 mW m^{-2} and 21% power density and coulombic efficiency [33].

2.3 Multi-Walled Carbon Nanotubes (MWCNTs)-Based Materials

Polypyrrole-modified nanocomposite (MWCNT-MnO₂/PPy) was fabricated and coated on carbon cloth using an electrochemical technique. Good electrical conductivity and band gap were recorded for the electrode. The application of MWCNT-MnO₂/PPy as an anode in microbial fuel cells demonstrated good adaptability, enhanced power density and robust biocompatibility. The authors opined that the incorporation of the MWCNTs aided the microstructure and enhanced the active surface area of the nanocomposite. Hence the electrocatalytic properties of the nanocomposite were greatly enhanced [34]. Another report demonstrating the uniqueness of MWCNTs in fuel cell design was noticed in the fabrication of sGNR via the instantaneous opening and sulfonation of MWCNTs technique. The nanocomposite membrane showed good durability and water retention. Hence, the proton transmission was improved resulting in enhanced current (840 mA cm^{-2}) and power (660 mW cm^{-2}) density output [35]. Mirzaei et al. employed the hydrothermal method to produce MWCNTs decorated with Pt. The nanohybrid was further used to fabricate membrane electrode assemblies with high stability and excellent electrochemical activity [36]. The application of noble metal nanoparticles (MN) and MN-graphene composite in fuel cells have been vastly assessed and the outcome showed room for improvement. In the light of existing literature, Jha et al. successfully fabricated PtRu/graphene/MWCNTs composite as a value-added electrocatalyst for direct methanol fuel cell. The nanocomposite demonstrated enhanced power density (68 mW cm^{-2}) and the authors believed that the incorporation of the functionalized MWCNTs altered the microstructure and the morphology which resulted in a synergy and better electrocatalytic activity [37]. A similar nanocomposite (Ni/

Cu/Mo@MWCNTs) was produced by making use of the chronological wetness impregnation technique supported with a freeze-drying procedure. The nanocomposite (40% of ternary alloy (Ni/Mo/Cu) anchored on MWCNTs)) displayed good electrocatalytic activity when employed in alkaline direct methanol fuel cells [38].

2.4 Single-Walled Carbon Nanotube-Based Materials

The unique physicochemical properties of single-walled carbon nanotubes (SWCNTs) have increased their application in various fields. Amongst these qualities, the structural benefit, excellent surface area, unique electrical potential, robust catalytic properties, and mechanical characteristics have presented SWCNTs as value-added material in fuel cell design. Shukla and group fabricated nanocomposite membranes using the solution cast method. The electrocatalyst prepared from single-walled carbon nanotubes and polyaminobenzene sulfonic acid demonstrated enhanced power density (150 mWcm^{-2}), better durability over a period of 100 h, reduced methanol passage and enhanced proton conductivity when assessed in a direct methanol fuel cell [39] (Fig. 3). Hu and co-workers discovered that the encapsulation of fullerene, iron and potassium in SWCNTs will significantly distort the electronic states of CNTs. They opined that the material loaded into the SWCNTs will make nanotubes to be either more positive or negative. Meanwhile, the electron (n-type) doped SWNT prefers the four-electrons procedure, which produces little H_2O_2 , but the hole (p-type) doped SWNT prefers the two-electrons route, which produces a lot of H_2O_2 . As a result, they determined that modifying the carbon atoms of SWCNTs to make them more negative or positive would favour the four-electrons pathway (n-type) and the two-electrons route (p-type), respectively [40]. Meanwhile, in the electrochemical oxidation of methanol, Pt-loaded SWCNTs were observed to exhibit excellent electrocatalytic activity with robust power density [41].

2.5 Fullerene-Based Electrode Materials

The allotrope of carbon Buckminsterfullerene or C_{60} is an unpopular material in industrial fabrication processes. This is own to its difficult and expensive synthetic route. However, the unique structural stability, exceptional electron-accepting ability and robust electron transporting characteristics of fullerene have drawn the attention of researchers towards the application of fullerene in fuel cell design. Studies have shown that material with undesirable physicochemical properties can be turned into unique material with exceptional quality via chemical modification. Neelakandan and group reported the application of sulfonated fullerene polymer membranes in direct methanol fuel cells. Besides the exceptional proton conductivity of this electrocatalyst, the sulfonated fullerene polymer membranes exhibited high resistance to methanol transportation. Meanwhile, the authors attributed the high stability of

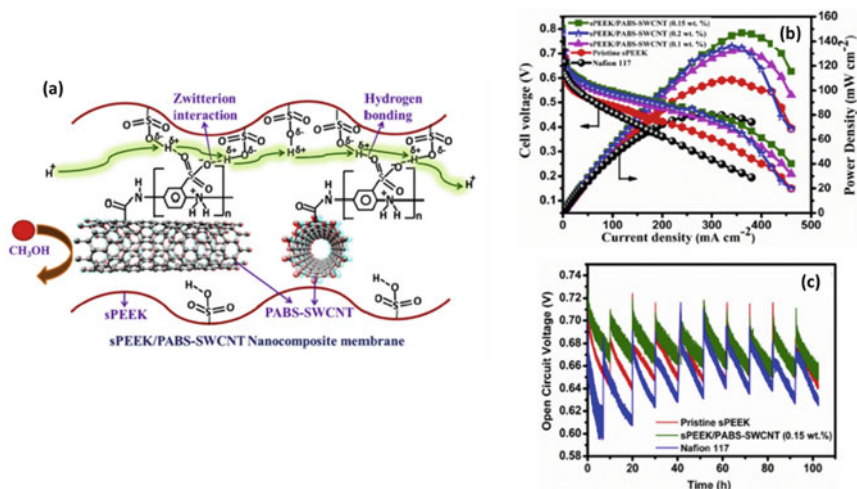


Fig. 3 **a** The nanocomposite membrane representing the zwitterion and hydrogen bonding interactions of PABS-SWCNT with a sulfonic acid group of sPEEK enhancing the transport of proton. **b** DMFC performance of sPEEK/PABS-SWCNT nanocomposite membrane, sPEEK and Nafion. The enhanced performance for sPEEK/PABS-SWCNT (0.15 wt %) is seen in comparison to pristine sPEEK and Nafion 117. **c** A comparison of the durability of sPEEK/PABS-SWCNT (0.15 wt %), sPEEK and Nafion membranes in DMFC reveal better durability for composite compared to pristine sPEEK and Nafion 117. Adapted with permission [39], Copyright (2019) Elsevier

the fullerene-supported electrocatalyst against oxidation to its radical scavenging behaviour. This electrolyte membrane demonstrated 0.332 S cm^{-1} proton conductivity at $80 \text{ }^\circ\text{C}$ and 74.38 mW cm^{-2} power density at $60 \text{ }^\circ\text{C}$ [42]. Another fullerene-based polymer electrolyte was prepared by Rambabu and Bhat for application in direct methanol fuel cells. In their study, the solution cast methodology technique was used to fabricate a superior polymer electrolyte consisting of sulfonated fullerene and sulfonated polyether ether ketone. The composite membrane electrolyte exhibited 96.3 mS/cm proton conductivity, $1.73 \times 10^{-7} \text{ cm}^2/\text{s}$ methanol permeability 103 mW/cm^2 peak power density. The incorporation of sulfonated polyether ether ketone onto the surface of sulfonated fullerene is displayed in Fig. 4 [43]. Meanwhile, Rambabu and group also synthesized a polymer electrolyte membrane for direct methanol fuel cell application. The membrane was obtained via the amalgamation of functionalized fullerene and Nafion ionomer. The membrane electrocatalyst demonstrated enhanced proton conductivity due to the availability of $-\text{SO}_3\text{H}$ groups, good methanol permeability and a peak power density of 146 mW cm^{-2} [44].

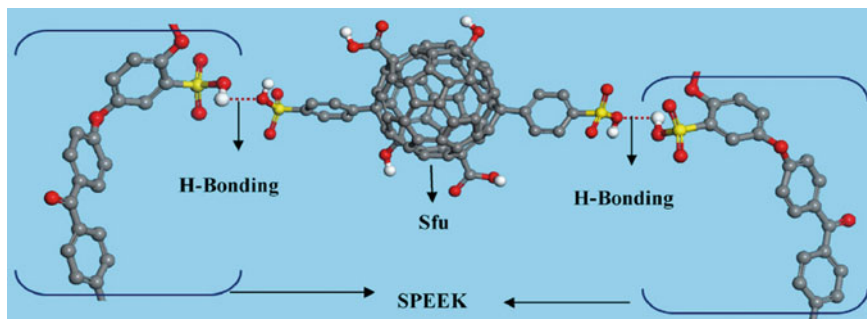


Fig. 4 Ball-stick model representing hydrogen bonding interaction between sPEEK and sulfonated fullerene. Adapted with permission [43], Copyright (2015) Elsevier

2.6 Aerogels-Based Electrode Materials

Aerogels are mesoporous solid foams with hierarchical structural characteristics, high surface area and low density. Aerogel is synthesized via polymerization followed by crosslinking to form a wet gel that is thereafter freeze-dried and thermally treated (Fig. 5). As catalyst support, carbon-based aerogels have demonstrated enhanced electrocatalytic activity due to their unique properties. Besides its application as a support, aerogels can be modelled to function as a self-standing aerogel with the potential to function as a support and catalyst in one platform. Abdelwahab and Abdelwahab reported the fabrication of black phosphorous/palladium functionalized carbon aerogel nanocomposite exhibiting highly efficient ethanol electrooxidation capacity. The carbon aerogel was prepared via sol–gel method and the hybrid obtained was noticed to sustain exceptional catalytic activity with a mass peak current density of 8376 mA mg^{-1} . The authors opined that the application of the aerogel as support provided high catalyst dispersibility and leaching inhibition. This resulted in spontaneous ethanol electrooxidation reaction kinetics [45]. The design of the electrocatalyst is an integral part of fuel cell design that make the overall process affordable and desirable. Carbon aerogels can be designed to sustain a bifunctional characteristic with the ability to catalyze oxygen-reduction reaction (ORR) and oxygen-evolution reaction (OER) (Fig. 5) [46]. This further demonstrates the robust nature of carbon aerogels as support in the fabrication of superior electrocatalysts for fuel cell applications. Another interesting finding in the quest to obtain an effective electrocatalyst was reported by Jiang et al. The group used the one-step fast reduction technique to fabricate carbon aerogel-supported platinum-nickel catalysts. This electrocatalyst demonstrated exceptional capacity for oxygen reduction reaction (ORR) with elevated mass and specific activities of $0.25 \text{ A mg}_{\text{Pt}}^{-1}$ and 4.69 A m^{-2} respectively [47].

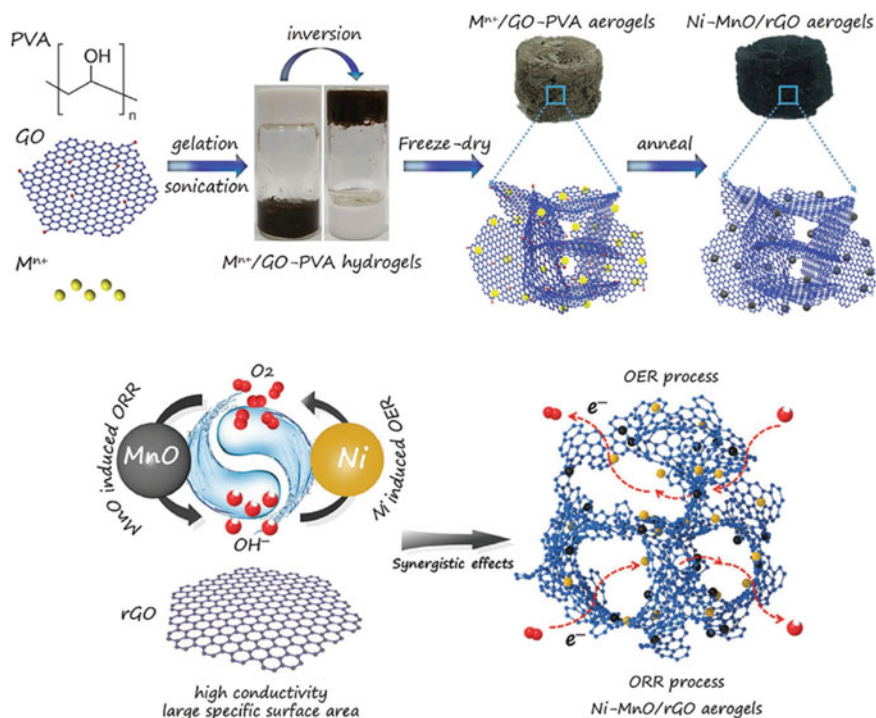


Fig. 5 Schematic illustration of the preparation of Ni-MnO/rGO aerogels and the bifunctional characteristics. Adapted with permission [46], Copyright (2017) Elsevier

2.7 Nanosheets of Carbon

Carbon nanosheets are forms of carbon with an ultrahigh surface-to-volume ratio. This unique material is commonly synthesized via self-assembly, chemical vapour deposition, templating, solvothermal synthesis and physical or chemical exfoliation methods. Meanwhile, due to the robust stability, excellent mechanical strength, high specific surface area, exceptional conductivity, easy preparation and functionalization, significant attention has been given to the application of carbon nanosheets in fuel cell design. This study aims to assess the effectiveness of carbon nanosheets in the design of electrocatalysts for fuel cells. The conventional path to enhance the efficiency of carbon nanosheets as support in electrocatalytic design is via the incorporation of nanoparticles and the covalent or non-covalent modification.

Zhong et al. used the facile in-situ growth technique to affix molybdenum disulfide onto carbon nanotubes and the product was thereafter anchored on the sulfonated polyether ether ketone (sPEEK) matrix which is depicted here in Fig. 6a. The membrane obtained exhibited enhanced dispersibility, good compatibility and improved mechanical strength. The group also reported a significant decrease in methanol permeability of the composite membrane which was observed to have

exceptional fuel cell accomplishment with a high peak power density of 98.5 mW cm^{-2} at 70°C (Fig. 6) [48]. Another study involving the application of carbon-based nanosheets as efficient electrocatalyst support in the design of microbial fuel cells was reported by Lai and co-workers. The study employed a cutting-edge synthetic route that involves chemisorption, calcination, and photodeposition in the fabrication of a zeolitic imidazole framework (Ag-Fe-N/C) electrocatalyst. Meanwhile, the fuel cell performance of the electrocatalyst demonstrated tremendous power generation with a maximum power density of $523 \pm 7 \text{ mWm}^{-2}$ and longstanding stability [49]. On the other hand, Masih et al. reported a novel synthetic approach (casting process) for the fabrication of cellulose acetate-strengthened graphene oxide nanosheets for fuel cell applications. The composite was utilized as a proton exchange membrane and was reported to sustain excellent tensile strength, improved proton conductivity and exceptional membrane performance. The membrane was reported to have a maximum power density of 519 mW/cm^{-2} . Hence, the study provided a synthetic path for the fabrication of cost-effective and nature-friendly membranes for application in proton exchange fuel cell technology [50].

The electrochemical characteristics of carbon-based electrode materials employed in fuel cell applications were summarized in Table 1. We observed that the variation of power and current density for the different electrodes may be associated with the quality and quantity of the basic materials used in the fabrication of the

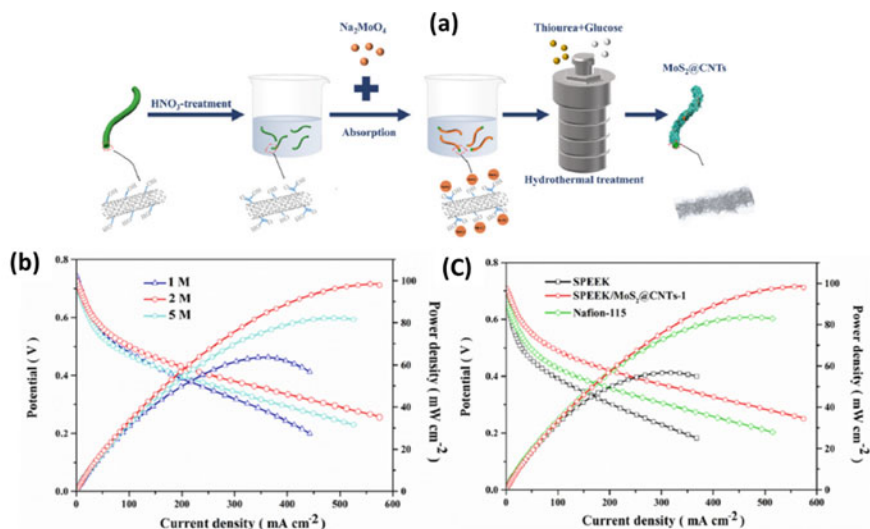


Fig. 6 Schematic illustration of MoS₂@CNTs preparation procedure. Power density curves and polarization curves of DMFCs using **a** sPEEK/MoS₂@CNTs-1 composite membrane with 1, 2 and 5 M methanol and **b** pristine sPEEK, sPEEK/MoS₂@CNTs-1 and Nafion 115 membrane with 2 M methanol at 70°C . Adapted with permission [48], Copyright (2022) Elsevier

electrodes. We also believe that the form of carbon used as support may have significant implications on the efficiency of the overall electrochemical process. Carbon-based aerogels demonstrated exceptional current density and we therefore recommend further research on the application of this form of carbon support in the design of electrocatalysts for different fuel cells.

Table 1 Studies on nanocomposites of carbon employed in the construction of electrodes for fuel cells

| Forms of carbon | Electrodes | Power density/current density/ specific activity | References |
|-----------------|---|---|------------|
| Graphene | Pt/NG180 + MWNT | 704 mW cm ⁻² | [14] |
| | GA/Pt | 1460 mW m ⁻² | [17] |
| | PtNCs/graphene | 62.5 mA mg ⁻¹ | [18] |
| | Pt/GNS | 0.80 mA cm ⁻² | [19] |
| | Pt/graphene-PDDA | 1.63 mA cm ⁻² | [20] |
| | Pt _{0.17} Cu _{0.83} /graphene | 780 mA mg ⁻¹ | [21] |
| | Pd@GN | 1.75 kWg ⁻¹ | [24] |
| | graphene/carbon cloth | 52.5 mW m ⁻² | [25] |
| | FeTsPc-graphene | 817 mW m ⁻² | [26] |
| CNTs | Pt/RuO ₂ -0.56H ₂ O/CNT | 0.60 mA mg ⁻¹ | [28] |
| | MoS ₂ /CNTs | 645 ± 32 mW m ⁻² | [29] |
| | Nafion/SCNTs-SUCNTs | 0.343 W cm ⁻² | [32] |
| | CNT/PPy | ~113 mW m ⁻² | [33] |
| MWCMTs | MWCNT-MnO ₂ /PPy | 1125.4 mW m ⁻² | [34] |
| | SPEEK/sGNR | 660 mW cm ⁻² | [35] |
| | Pt/MWCNT MEA | 160 mW cm ⁻² | [36] |
| | Pt/(50 wt% f-MWNT + 50 wt% f-G) | 68 mW cm ⁻² | [37] |
| SWCNTs | sPEEK/PABS-SWCNT | 150 mW cm ⁻² | [39] |
| Fullerene | BSPAEEKs/s-Fu | 74.38 mW cm ⁻² | [42] |
| | Sulfonated fullerene | 103 mW/cm ² | [43] |
| | Nafion-FF | 146 mW cm ⁻² | [44] |
| Aerogels | BP/Pd/CA | 8376 mA mg ⁻¹ | [46] |
| | Pt ₃ Ni/CA | 4.69 A m ⁻² | [47] |
| Nanosheets | SPEEK/MoS ₂ @CNTs | 98.5 mW cm ⁻² | [48] |
| | Ag-Fe-N/C | 523 ± 7 mWm ⁻² | [49] |
| | CA/GO | 519 mW/cm ⁻² | [50] |

3 Conclusion

To attain the high energy demand calls for the diversification of energy sources. Electrochemical technology has demonstrated the capacity to provide clean and sustainable energy. However, the sustainability of the electrochemical process greatly relies on the efficiency and stability of the electrocatalyst employed. Electrocatalysts are either self-sustained or designed using a support. The design of cost-effective and nature-friendly carbon-based electrocatalysts for various fuel cell technology has been substantively investigated. In the quest to obtain high-efficient electrocatalysts, synthetic routes such as self-assembly, chemical vapour deposition, templating, pyrolytic, casting, polymerization, solvothermal, and crosslinking amongst others have been employed. Meanwhile, authors generally hold the opinion that effective functionalization improves the dispersions of nanoparticles on the carbon support and increases the surface areas, which may result in enhanced electrochemical properties and exceptional stability of electrocatalysts. This chapter demonstrated the successful application of various forms of carbon (carbon aerogels, carbon nanosheet, fullerene, SWCNTs, carbon nanotubes, graphene, MWCNTs) in the fabrication of carbon-based composite electrodes. This chapter also revealed the cost-effectiveness and the improved fuel cell potential of carbon-based electrocatalysts as several authors compared the synthesized electrocatalyst to the commercial electrodes in these regards. Hence, the fabrication of novel carbon-based electrocatalysts using a cost-effective and scalable synthetic route should be encouraged. Finally, this chapter conveys the significant progress made in designing low-cost carbon-based electrocatalysts for different fuel cells. However, the pilot scale study for large-scale commercial applications, its stability assessment and financial implications have not been exhaustively addressed. Hence, the drawback should be investigated in the future.

Acknowledgements The authors thank the anonymous reviewers for their helpful comments. We are grateful for financial support from the Walter Sisulu Directorate of Research and Innovation and Eskom Tertiary Education Support (TESP). In addition, the authors are grateful for the excellent support of WSU staff members.

Funding This research was funded by the Walter Sisulu University grant for Renewable Energy Technologies RNA, and Tertiary Education Support Program (TESP), Eskom Holdings SOC Limited Reg. No. 2002/015527/06.

References

1. Sreethawong, T., Chatsiriwatana, S., Rangsunvigit, P., Chavadej, S.: Hydrogen production from cassava wastewater using an anaerobic sequencing batch reactor: effects of operational parameters, COD: N ratio, and organic acid composition. *Int. J. Hydrog. Energy* **35**, 4092–4102 (2010)
2. Asif, M., Muneer, T.: Energy supply, its demand and security issues for developed and emerging economies. *Renew. Sustain. Energy Rev.* **11**, 1388–1413 (2007)

3. Carrette, L., Friedrich, K.A., Stimming, U.: Fuel cells: Principles, types, fuels, and applications. *ChemPhysChem* **1**, 162–193 (2000)
4. Shaari, N., Kamarudin, S.: Graphene in electrocatalyst and proton conduction membrane in fuel cell applications: an overview. *Renew. Sustain. Energy Rev.* **69**, 862–870 (2017)
5. Chang, H., Joo, S.H., Pak, C.: Synthesis and characterization of mesoporous carbon for fuel cell applications. *J. Mater. Chem.* **17**, 3078–3088 (2007)
6. Kar, K.K., Rana, S., Pandey, J.: *Handbook of Polymer Nanocomposites Processing, Performance and Application*. Springer (2015)
7. Wang, Y., Chen, K.S., Mishler, J., Cho, S.C., Adroher, X.C.: A review of polymer electrolyte membrane fuel cells: technology, applications, and needs on fundamental research. *Appl. Energy* **88**, 981–1007 (2011)
8. Barbir, F.: *PEM Fuel Cells: Theory and Practice*. Academic Press 2012
9. Vielstich, W., Gasteiger, H.A., Yokokawa, H.: *Handbook of Fuel Cells: Advances in Electrocatalysis, Materials, Diagnostics and Durability, Volumes 5 and 6*. Wiley & Sons 2009
10. Iqbal, M.Z., Rehman, A.-U., Siddique, S.: Prospects and challenges of graphene based fuel cells. *J. Energy Chem.* **39**, 217–234 (2019)
11. Merle, G., Wessling, M., Nijmeijer, K.: Anion exchange membranes for alkaline fuel cells: a review. *J. Membr. Sci.* **377**, 1–35 (2011)
12. Singh, M., Zappa, D., Comini, E.: Solid oxide fuel cell: decade of progress, future perspectives and challenges. *Int. J. Hydrog. Energy* **46**, 27643–27674 (2021)
13. Cheng, K., He, D., Peng, T., Lv, H., Pan, M., Mu, S.: Porous graphene supported Pt catalysts for proton exchange membrane fuel cells. *Electrochim. Acta* **132**, 356–363 (2014)
14. Jafri, R.I., Rajalakshmi, N., Dhathathreyan, K., Ramaprabhu, S.: Nitrogen doped graphene prepared by hydrothermal and thermal solid state methods as catalyst supports for fuel cell. *Int. J. Hydrog. Energy* **40**, 4337–4348 (2015)
15. Yang, M., Jeong, J.-M., Lee, K.G., Lee, S.J., Choi, B.G.: Hierarchical porous microspheres of the CO₃O₄@ graphene with enhanced electrocatalytic performance for electrochemical biosensors. *Biosens. Bioelectron.* **89**, 612–619 (2017)
16. Si, P., Huang, Y., Wang, T., Ma, J.: Nanomaterials for electrochemical non-enzymatic glucose biosensors. *RSC Adv.* **3**, 3487–3502 (2013)
17. Zhao, S., Li, Y., Yin, H., Liu, Z., Luan, E., Zhao, F., Tang, Z., Liu, S.: Three-dimensional graphene/Pt nanoparticle composites as freestanding anode for enhancing performance of microbial fuel cells. *Sci. Adv.* **1**, e1500372 (2015)
18. Ji, K., Chang, G., Oyama, M., Shang, X., Liu, X., He, Y.: Efficient and clean synthesis of graphene supported platinum nanoclusters and its application in direct methanol fuel cell. *Electrochim. Acta* **85**, 84–89 (2012)
19. Yoo, E., Okada, T., Akita, T., Kohyama, M., Honma, I., Nakamura, J.: Sub-nano-Pt cluster supported on graphene nanosheets for co tolerant catalysts in polymer electrolyte fuel cells. *J. Power. Sources* **196**, 110–115 (2011)
20. Lei, M., Liang, C., Wang, Y., Huang, K., Ye, C., Liu, G., Wang, W., Jin, S., Zhang, R., Fan, D.: Durable platinum/graphene catalysts assisted with polydiallyldimethylammonium for proton-exchange membrane fuel cells. *Electrochim. Acta* **113**, 366–372 (2013)
21. Liu, Y., Huang, Y., Xie, Y., Yang, Z., Huang, H., Zhou, Q.: Preparation of highly dispersed CuPt nanoparticles on ionic-liquid-assisted graphene sheets for direct methanol fuel cell. *Chem. Eng. J.* **197**, 80–87 (2012)
22. Liu, X., Yi, L., Wang, X., Su, J., Song, Y., Liu, J.: Graphene supported platinum nanoparticles as anode electrocatalyst for direct borohydride fuel cell. *Int. J. Hydrog. Energy* **37**, 17984–17991 (2012)
23. Cho, S., Yang, H., Lee, D., Park, S., Kim, W.: Electrochemical properties of Pt/graphene intercalated by carbon black and its application in polymer electrolyte membrane fuel cell. *J. Power. Sources* **225**, 200–206 (2013)
24. Hsieh, C.-T., Gu, J.-L., Chen, Y.-C., Tzou, D.-Y.: Pulse microwave synthesis of palladium catalysts on graphene electrodes for proton exchange membrane fuel cells. *Electrochim. Acta* **98**, 39–47 (2013)

25. Liu, J., Qiao, Y., Guo, C.X., Lim, S., Song, H., Li, C.M.: Graphene/carbon cloth anode for high-performance mediatorless microbial fuel cells. *Biores. Technol.* **114**, 275–280 (2012)
26. Zhang, Y., Mo, G., Li, X., Ye, J.: Iron tetrasulfophthalocyanine functionalized graphene as a platinum-free cathodic catalyst for efficient oxygen reduction in microbial fuel cells. *J. Power. Sources* **197**, 93–96 (2012)
27. de la Zerda, A., Liu, Z., Zavaleta, C., Bodapati, S., Teed, R., Vaithilingam, S., Ma, T.-J., Oralkan, O., Chen, X., Khuri-Yakub, B.T.: Enhanced sensitivity carbon nanotubes as targeted photoacoustic molecular imaging agents. In: *Photons Plus Ultrasound: Imaging and Sensing 2009*. SPIE (2009)
28. Cao, L., Scheiba, F., Roth, C., Schweiger, F., Cremers, C., Stimming, U., Fuess, H., Chen, L., Zhu, W., Qiu, X.: Novel nanocomposite Pt/RuO₂-xH₂O/carbon nanotube catalysts for direct methanol fuel cells. *Angew. Chem.* **118**, 5441–5445 (2006)
29. Guo, W., Li, X., Cui, L., Li, Y., Zhang, H., Ni, T.: Promoting the anode performance of microbial fuel cells with nano-molybdenum disulfide/carbon nanotubes composite catalyst. *Bioprocess Biosyst. Eng.* 1–12 (2022)
30. Molla-Abbasi, P., Janghorban, K., Asgari, M.S.: A novel heteropolyacid-doped carbon nanotubes/Nafion nanocomposite membrane for high performance proton-exchange methanol fuel cell applications. *Iran. Polym. J.* **27**, 77–86 (2018)
31. Sigwadi, R., Dhlamini, M., Mokrani, T., Nemavhola, F.: Enhancing the mechanical properties of zirconia/Nafion® nanocomposite membrane through carbon nanotubes for fuel cell application. *Heliyon* **5**, e02112 (2019)
32. Vinothkannan, M., Kim, A.R., Ryu, S.K., Yoo, D.J.: Structurally modulated and functionalized carbon nanotubes as potential filler for Nafion matrix toward improved power output and durability in proton exchange membrane fuel cells operating at reduced relative humidity. *J. Membr. Sci.* 649, 120393 (2022)
33. Ghasemi, M., Daud, W.R.W., Hassan, S.H., Jafary, T., Rahimnejad, M., Ahmad, A., Yazdi, M.H.: Carbon nanotube/polypyrrole nanocomposite as a novel cathode catalyst and proper alternative for Pt in microbial fuel cell. *Int. J. Hydrog. Energy* **41**, 4872–4878 (2016)
34. Mishra, P., Jain, R.: Electrochemical deposition of MWCNT-MnO₂/PPy nano-composite application for microbial fuel cells. *Int. J. Hydrog. Energy* **41**, 22394–22405 (2016)
35. Shukla, A., Bhat, S.D., Pillai, V.K.: Simultaneous unzipping and sulfonation of multi-walled carbon nanotubes to sulfonated graphene nanoribbons for nanocomposite membranes in polymer electrolyte fuel cells. *J. Membr. Sci.* **520**, 657–670 (2016)
36. Mirzaei, F., Parnian, M.J., Rowshanzamir, S.: Durability investigation and performance study of hydrothermal synthesized platinum-multi walled carbon nanotube nanocomposite catalyst for proton exchange membrane fuel cell. *Energy* **138**, 696–705 (2017)
37. Jha, N., Jafri, R.I., Rajalakshmi, N., Ramaprabhu, S.: Graphene-multi walled carbon nanotube hybrid electrocatalyst support material for direct methanol fuel cell. *Int. J. Hydrog. Energy* **36**, 7284–7290 (2011)
38. Nazal, M.K., Olakunle, O.S., Al-Ahmed, A., Merzougui, B., Abualkibash, A., Sultan, A., Yousaf, A.B., Zaidi, S.J.: Precious metal free Ni/Cu/Mo trimetallic nanocomposite supported on multi-walled carbon nanotubes as highly efficient and durable anode-catalyst for alkaline direct methanol fuel cells. *J. Electroanal. Chem.* **823**, 98–105 (2018)
39. Shukla, A., Dhanasekaran, P., Sasikala, S., Nagaraju, N., Bhat, S.D., Pillai, V.K.: Nanocomposite membrane electrolyte of polyaminobenzene sulfonic acid grafted single walled carbon nanotubes with sulfonated polyether ether ketone for direct methanol fuel cell. *Int. J. Hydrog. Energy* **44**, 27564–27574 (2019)
40. Hu, R., Wu, C., Hou, K., Xia, C., Yang, J., Guan, L., Li, Y.: Tailoring the electrocatalytic oxygen reduction reaction pathway by tuning the electronic states of single-walled carbon nanotubes. *Carbon* **147**, 35–42 (2019)
41. Wu, G., Xu, B.-Q.: Carbon nanotube supported Pt electrodes for methanol oxidation: a comparison between multi- and single-walled carbon nanotubes. *J. Power Sources* **174**, 148–158 (2007)

42. Neelakandan, S., Liu, D., Wang, L., Hu, M., Wang, L.: Highly branched poly (arylene ether)/surface functionalized fullerene-based composite membrane electrolyte for DMFC applications. *Int. J. Energy Res.* **43**, 3756–3767 (2019)
43. Rambabu, G., Bhat, S.D.: Sulfonated fullerene in sPEEK matrix and its impact on the membrane electrolyte properties in direct methanol fuel cells. *Electrochim. Acta* **176**, 657–669 (2015)
44. Rambabu, G., Nagaraju, N., Bhat, S.D.: Functionalized fullerene embedded in Nafion matrix: a modified composite membrane electrolyte for direct methanol fuel cells. *Chem. Eng. J.* **306**, 43–52 (2016)
45. Abdelwahab, I., Abdelwahab, A.: Black phosphorous/palladium functionalized carbon aerogel nanocomposite for highly efficient ethanol electrooxidation. *RSC Adv.* **12**, 31225–31234 (2022)
46. Fu, G., Yan, X., Chen, Y., Xu, L., Sun, D., Lee, J.M., Tang, Y.: Boosting bifunctional oxygen electrocatalysis with 3D graphene aerogel-supported Ni/MnO particles. *Adv. Mater.* **30**, 1704609 (2018)
47. Jiang, L.-L., Zeng, M., Wang, C.-Y., Luo, Z.-H., Li, H.-Y., Yi, Y.: Pt-Ni alloy catalyst supported on carbon aerogel via one-step method for oxygen reduction reaction. *J. Solid State Electrochem.* 1–10 (2022)
48. Zhong, F., Zeng, Z., Liu, Y., Hou, R., Nie, X., Jia, Y., Xi, J., Liu, H., Niu, W., Zhang, F.: Modification of sulfonated poly (etherether ketone) composite polymer electrolyte membranes with 2D molybdenum disulfide nanosheet-coated carbon nanotubes for direct methanol fuel cell application. *Polymer* **249**, 124839 (2022)
49. Lai, B.L., Xiao, Z.H., Jiang, P.Y., Xie, Y., Li, N., Liu, Z.Q.: Two-dimensional Ag-Fe-N/C nanosheets as efficient cathode catalyst to improve power-generation performance of microbial fuel cells. *ChemElectroChem* **9**, e202101699 (2022)
50. Madih, K., El-Shazly, A.H., Elkady, M.F., Aziz, A.N., Youssef, M.E., Khalifa, R.E.: A facile synthesis of cellulose acetate reinforced graphene oxide nanosheets as proton exchange membranes for fuel cell applications. *J. Saudi Chem. Soc.* **26**, 101435 (2022)

Carbon Nanomaterials as One of the Options for Hydrogen Storage



B. Viswanathan

Abstract For the Hydrogen economy, cost-effective and safe storage of hydrogen assumes importance. Among the various modes of storage, solid-state storage has definite advantages for mobile and stationary applications. However, among the probable solid-state materials, the desired levels of storage (~6 Weight %) can be possible in carbon materials suitably modified with activation centers. A variety of modifications of carbon materials have been examined for hydrogen storage. However, the search has to continue till the desired levels of storage under ambient conditions are achieved.

Keywords Hydrogen storage · Carbon nanomaterials · Graphene · Activation centers · Carbon allotropes · Solid-state storage

1 Introduction

The energy needs of the world have been centered around carbon-based materials for a number of centuries. There are various forms of carbon materials that are available. It appears that the variety of carbon forms may be endless, and a simple classification is given in Table 1.

Five decades ago, a concept based on the Hydrogen Economy has been evolving and the transformation towards this economy essentially depends on the three components namely generation, storage, and delivery of hydrogen. There are consistent attempts to generate hydrogen from the decomposition of water (from renewable sources) and this pursuit is an ongoing exercise to make this process economically feasible, though the desired level of success is still to be achieved. Commonly available methods for the storage of hydrogen, namely in high-pressure gas cylinders (up to 800 bar) and as liquid hydrogen in cryogenic tanks (at 21 K) are energy inefficient and not safe for certain applications, especially for mobile applications. Hydrogen

B. Viswanathan (✉)

Department of Chemistry, National Centre for Catalysis Research, Indian Institute of Technology, Madras 600036, India

e-mail: bviswanathan@gmail.com

Table 1 A classification scheme for carbon allotropes, molecular crystals, and derived forms

| Sp ³ | Sp ² | Sp ¹ |
|--|---|--|
| Diamond Cubic Hexagonal | Graphite Hexagonal Rhombohedral | Carbyne A-Carbyne B-Carbyne Chaoite |
| Sp ³ + Sp ² + Sp ¹ | Sp ⁿ (3 < n > 1, n ≠ 2) | |
| Mixed forms of carbon | Intermediate forms of carbon | Intermediate forms of carbon |
| Amorphous carbon Glassy carbon Carbon black Adamantine carbon | 3 > n > 2 Fullerene C _x X = 60, 70, 84 (When x = ∞, n = 2) Carbon onions Carbon nanotubes | 2 > n > 1 Cyclo (N) carbons N = 18, 24,30 (When N = ∞, n = 1) |

adsorption/absorption on solid materials with high specific surface area and chemically bonded in covalent and ionic bonds appears to be attractive. Materials such as metal hydrides, alloys, complex hydrides, and high surface area porous materials are showing an affinity for ab(ad)sorbing large amounts of hydrogen. However, each of these storage materials suffers from some particular drawbacks. These materials crystallize in closed packed configurations giving rise to tetra-/octahedral- or other voids thus possibly restricting one hydrogen species per void space at room temperature and atmospheric pressure, which means the weight percent of storage capacity depends on the atomic or molecular weight of the nature of solid storage medium. In the solid-state hydrogen storage, hydrogen is bonded by either physical forces (Physical adsorption or van der Waals forces), e.g., MOF and carbon-based materials, or chemical forces (chemisorption involving chemical bonds), e.g., hydrides, imides, and nitrides. Physisorption has the advantages of higher energy efficiency and faster adsorption/desorption cycles, whereas chemisorption results in the adsorption of larger amounts of gas but in some cases, is not reversible and requires higher temperatures to release the adsorbed gas which is not suitable for mobile applications.

The development of hydrogen storage materials with lightweight, high capacity, high stability, and better safety is imperative for portable electronics and transport applications. Carbon-based materials with different (allotropic) forms and chemical affinity are favorable for hydrogen storage application due to their low atomic weight, high surface area, porous nature, and higher safety characteristics. Carbon can be hybridized in Sp, Sp², and Sp³ bonds, and exist in 0D, 1D, 2D, and 3D forms. Additionally, chemical and physical properties of these materials can be altered by using its different sources, composites, functional derivatives, or doping with other elements. It may possess pores of different shapes and sizes, which are ideal physisorption/ad(ab)sorption sites for hydrogen storage. In the following, the hydrogen storage capacities of different carbon nanostructures, including activated carbon, graphite, graphene, CNTs, fullerene, and CNFs, are discussed. The attempts to store on modified (especially metal loaded) carbon materials also will be considered. Recent and

relevant efforts for improving the hydrogen storage capacities are also considered. There are a variety of these materials and nature has shown that this is one of the potential storage media for hydrogen (in the form of hydrocarbons) and also shown that storage can go up to 25 weight percent (as in methane). However, one must be aware these hydrocarbon molecules are covalent in nature and thus may not readily release hydrogen when required as in transport applications. In this presentation, the scope of carbon materials for hydrogen storage application is considered.

The microporosity of carbon materials is not directly related to hydrogen storage application but a nearly linear relationship has been realized with respect to BET surface area, typical plots can be seen in the following reference and references cited therein [1]. There have been many attempts to modify the surface of carbon materials so that the storage capacity can be increased. One such attempt deals with the presence of heteroatoms on the surface of carbon materials for various reasons like the possibility of dissociating molecular hydrogen or facilitating the spill-over process. However, the current situation with respect to hydrogen storage in carbon materials with heteroatoms can be stated that typically N-doping is only apparent when considering the hydrogen uptake as a function of microporosity (rather than total porosity). This possibly leads to the conclusion that pores larger than the micropore size range have a lesser role in hydrogen storage capacity.

The advanced design and testing of carbon materials for energy storage devices appear to be important. The main shortcomings of these materials are related to irreversible capacity loss, big voltage crosstalk, and low density [2]. Novel composites containing multifunctional nanostructured carbon and other dopants can synergistically take advantage of the combination of ordered building block units with other desired properties. Since most physisorption is involved in this process of hydrogen storage, only a small amount of hydrogen could be stored even at a pressure of 90 bar. Obviously, temperature (~room temperature) will have an almost negligible effect on hydrogen storage capacity.

2 Activated Carbon

Activated carbon is one of the widespread and commercially used porous carbon materials, consisting of graphite crystallites and amorphous carbon. It has been used for centuries as an adsorbent due to its good adsorption capacity, high specific surface area (up to $\sim 3000 \text{ m}^2/\text{g}$), porous structure, inertness, surface reactivity, and thermal stability. The pores range from micro to macro size with an abundance of micro-sized pores of $<1 \text{ nm}$. Due to its widespread pores, it is a potential material for hydrogen storage. In general, the hydrogen adsorption on such materials is proportional to the specific surface area (SSA) and pore volume. Several research efforts are devoted to finding the hydrogen uptake in activated carbon materials with different pore sizes, pore volume, and specific surface area. Most of the experimental findings have demonstrated the hydrogen storage capacity of activated carbon as 2.5 and 5.5 wt.% at low pressure (1–10 bar) and high pressure (up to 60 bar), respectively. It was

observed that at 100 bar and room temperature, the hydrogen uptake of activated carbon was <1 wt.%, even with a highly porous structure and high specific surface area. It has been observed by different researchers that the optimum pore size in activated carbon for hydrogen storage is 0.6 nm. Table 2 shows the experimental results reported (compiled) of hydrogen storage capacity of activated carbons at different temperatures and pressure conditions. Different chemical treatments and doping of activated carbon were also utilized to improve the hydrogen uptake of activated carbon materials. However, they do not meet the U.S. Department of Energy (DOE) target, and further efforts are needed to realize their potential for enhanced hydrogen storage capacity.

One can assess that the highest value of excess adsorption of hydrogen reported for a commercial activated carbon is around 5 wt.% at 77 K and pressures from 3 to 6 MPa. In the case of activated carbons prepared on a laboratory scale, the best value obtained is ~7 wt.% at 77 K and 20 MPa. Most of the studies reported in the literature mainly concentrated on increasing the surface area of the activated carbon (by an appropriate method for (mostly chemical) activation) and the porosity of the material. The linear correlations connecting adsorption capacity and physical parameters like surface area and pore volume of activated carbons have been attempted but the results available indicate only limited applicability. It is also to be noted that activated carbons show hydrogen adsorption capacities at cryogenic conditions and this is not very suitable for the applications envisaged for hydrogen economy.

Table 2 Data on hydrogen storage capacities of different activated carbon materials (Data from literature)

| Adsorbent employed | Reported hydrogen storage (wt.%) | Conditions (temperature and pressure) |
|--------------------------------------|----------------------------------|---------------------------------------|
| Activated carbon | 0.67 | 303 K 10 MPa |
| Activated carbon | 1.4 | 77 K 0.1 MPa |
| Activated carbon | 1.6 | 298 K 13 MPa |
| Activated carbon | 4.5 | 77 K |
| Activated carbon | 5.7 | 77 K 3 MPa |
| Activated carbon | 3.2 | 298 K 20 MPa |
| Activated carbon | 6/5 | 298 K 50 MPa |
| Chemically activated carbon | 8.0 | 77 K 4 MPa |
| Activated carbon | 2.3–5.8 | 77 K 4 MPa |
| Activated carbon (treated with KOH) | 6.6 | 4 MPa |
| Activated carbon (activated with Ni) | 1.8 | 77 K 0.1 MPa |
| Activated carbon (activated with Pt) | 2.3 | 298 K 10 MPa |
| Activated carbon (activated with Pd) | 5.5 | 298 K 8 MPa |

3 Graphite

Graphite has Sp^2 hybridized carbon atoms arranged in a hexagonal lattice with a layered structure such that the layers themselves are held together by van der Waals forces of interaction. Graphite can be naturally obtained or can be artificially prepared. It is also widely explored for hydrogen storage applications. Various studies have modified their porosity, chemical bonding, and surface area by using different activation methods as well as doping them with different metals. Ball-milled graphite and intercalated graphite are widely explored for hydrogen storage applications. Ball-milled graphite contains tremendous defect sites and high surface area, which lead to chemisorption resulting in high hydrogen storage capacity. The ball-milling-induced rupture of graphite sheets and the emerging active edges and defects on the fragmented part are also confirmed by neutron scattering and spin resonance studies.

4 Graphene: The Hydrogen Adsorption/Desorption Isotherm

The hydrogen adsorption/desorption isotherm of the nitrogen-doped graphene, Graphitic Oxide and Graphite powder is shown in Ref. [3]. The hydrogen adsorption isotherm has been carried out at 298 K and 90 bar pressure. The nitrogen-doped graphene material showed nearly ~1.5 wt.% hydrogen storage capacity at room temperature and 90 bar pressure. In this context, the graphitic oxide (GO) showed ~0.21 wt.% hydrogen storage capacity at room temperature and 90 bar. This value is less than that of nitrogen-doped graphene material. However, nitrogen doping of graphene materials takes up substitution positions in the carbon lattice, there is transportation of hydrogen atoms on to the graphene surface. Furthermore, these results reveal that the nitrogen doping on graphene materials can extensively modify the catalytic effect of the graphene materials for hydrogen dissociative adsorption, foremost for the improvement of the dissociative hydrogen adsorption. This observation suggests that the nitrogen atoms possibly take part in a role in the hydrogen adsorption capacity at room temperature. A previous study recommended that the presence of nitrogen atoms in graphene sheets increases the enthalpy of hydrogen adsorption [4]. Potentially almost all the adsorbed amount can be desorbed which is an interesting characteristic expected for hydrogen storage materials. Various attempts have been made to modify or adopt different preparation procedures for graphene materials and it has been shown that N and P doping in graphene does not improve the materials' hydrogen storage capacity [5]. It has been proposed that the hydrogen binding energy can be tuned as a function of the graphene local curvature. The adsorption is facilitated by convex sites and desorption is facilitated on concave sites. The corrugation of graphene flakes and its control with large variety of functionalization may make these materials can impact in the search for hydrogen storage [6].

5 Modification of Activated Carbon

For conventional activated carbon materials, the hydrogen uptake is proportional to the surface area and pore volume; and normally the data are fitted well with the Langmuir isotherm model (monolayer adsorption). High adsorption capacity is only obtained at extremely low cryogenic temperatures and high pressures. Hydrogen adsorption on various types of commercial and modified activated carbon products has been extensively studied. Experimental results show that products with micropore volumes greater than 1 mL/g are able to store ca. 2.2 wt.% of hydrogen due to physisorption and it is expected that optimization of the adsorbent and sorption conditions could lead to a storage capacity of 4.5–5.3 wt.%. Agricultural waste materials such as coconut shells, coconut fibers, jute fibers, nut shells, oil seeds, etc., are popular raw materials for producing activated carbon materials. Carbon materials and their activation have been extensively discussed in Ref. [7]. Jin et al. [8] prepared activated carbons with different porosities using chemically activated coconut shells. They reported a maximum hydrogen adsorption capacity of 0.85 wt.% at 100 bar and 298 K. Sharon et al. [9], produced activated carbon fibers (ACF) using soybean and bagasse. The authors measured hydrogen storage capacities of 1.09–2.05 wt.% at a pressure of 11 Pa and room temperature. Another form of AC, the advanced AC monoliths, with good mechanical strength (maximum compression strength of 22 MPa), high volume of micropores (up to 1.04 cm³/g), and high density (up to 0.7 g/cm³) have been shown to adsorb 29.7 g/L of hydrogen at 77 K and 4 MPa [9]. Mechanically milled AC consists of some form of defective nanostructure, which increases the specific surface area. Research findings have revealed that after 10 h of milling, the hydrogen storage capacity increases from 0.90 wt.% to ca. 1.7 wt.%. Studies have shown that the loading of precious metals, e.g., Pt, onto AC, increases the adsorption capacity. The merging of the two adsorption phenomena, i.e. chemisorption (on the Pt surface) and physisorption (on the carbon surface) gives rise to a significant amount of spillover hydrogen.

6 Carbon Nanotubes

Ever since the discovery of carbon nanotubes was reported in 1991, there have been various attempts to use this new type of carbon material for hydrogen storage. These studies have led to some unexpected levels of storage up to nearly 60 wt.% or even more. However, the consensus now is that these reports claiming over 60 wt.% are flawed by experimental aberrations.

Only limited data are given in Table 3. For more extensive compilations, one is directed to references [35]. Various nanotubes like carbon nanotubes, boron nitride nanotubes, silicon carbide nanotubes, carbon nano-scrolls, pillared Graphene, and porous nanotube network materials have been extensively investigated and the final suggestion is that one should design novel materials with the following key

parameters namely high accessible surface area, large free pore volume and strong interactions between the surface-active sites and the substrate hydrogen.

In a recent review, Lyu et al. [36] propose that “a detailed study of the optimum number of metal atoms without aggregation on CNT should be performed. (1) At the same time suitable preparation methods for realizing controllable doping sites and doped configurations should be devised; (2) The material synthesis, purification, and activation methods have to be optimized; (3) Active sites, molecular configurations, effectively accessible surface area, pore size, surface topology, the chemical composition of the surface, applied pressure and temperature, defects, and dopant,

Table 3 Selected data (for comparison) on the storage of hydrogen by carbon nanotubes

| Sample | Temp (K) | P (MPa) | Hydrogen storage (wt.%) | Refs. |
|---|----------|---------|-------------------------|-------|
| Herring bone GNFs | RT | 11–35 | 67.5 | [10] |
| Platelet GNFs | RT | 11–35 | 53.68 | [10] |
| Graphitic nano fibers | RT | 101 | 10 | [11] |
| Graphitic nano fibers | RT | 8–120 | 10 | [12] |
| SWNTs (low purity) | 273 | 0.4 | 5–10 | [13] |
| SWNTs (high purity) | 80 | 70–80 | 8.25 | [14] |
| SWNT (high purity + Ti alloy) | 300–600 | 0.7 | 3.5–4.5 | [15] |
| Li-MWNTs | 473–673 | 1 | 20 | [16] |
| Li-MWNTs (KOMWNTs) | 473–673 | 1 | 2.5 (1.8) | [17] |
| MWNTs | RT | Ele- | <1 | [18] |
| SWNTs | 300–520 | 1–100 | 0.1 | [19] |
| Various CN | RT | 1 | <0.1 | [20] |
| SWNTs (+ Ti alloy) | RT | 35 | 0 | [21] |
| SWCNT | RT | 0/8 | 4.5 | [22] |
| SWCNT | 295 | 10 | 0.93 | [23] |
| SWCNT | RT | 0.1 | 1.2 | [24] |
| SWCNT | 323 | 4.8 | 4.77 | [25] |
| SWCNT | – | – | –0.8 | [26] |
| MWCNT | – | 3 | 2 | [27] |
| MWCNT | 77 | 0.005 | 0.54 | [28] |
| MWCNT | 298 | 0.1 | 0.2 | [29] |
| NWCNT | 425 | 10 | 3.8 | [30] |
| MWCNT | 143 | 3 | 3.5 | [31] |
| MWCNT | RT | 7.5 | 1.5–2.1 | [32] |
| MWCNT | – | – | 2.7–3.8 | [31] |
| Carbon nano onion | 77 | 1.5 | >18.2 | [33] |
| g-C ₃ N ₄ nanotubes | RT | 37 | 0.78 | [34] |

which are some of the important factors that strongly affect the hydrogen absorption in carbon nanotubes” should be elucidated.

In contrast, Lobo et al. [37], propose carbon nanostructures are promising materials for hydrogen storage applications. They emphasize that hydrogen can be physisorbed in carbon nanotube bundles on various sites such as external wall surfaces, grooves, and interstitial channels. Therefore, it can have a large energy density (as required for mobile applications). It is also known that by tuning the adsorption conditions, hydrogen can be either chemisorbed or physisorbed in carbon nanotubes. In a review, Lee et al. [38] and others [39] propose that a more detailed understanding of the interfacial interactions between adsorbent and adsorbate should be evolved and the phenomenon of spill-over can contribute to adsorbent surfaces to achieve the desired levels of hydrogen storage.

7 Impact of Structures on Hydrogen Storage in Different Carbon Materials

Increasing hydrogen storage to the levels advocated by DOE through materials in the nanoscale has been proposed and intensively researched but the success appears to elude us. Among the several options available, various allotropic forms of carbon, like CNTs, graphene, and activated carbons have been considered to be appropriate systems owing to their unique properties like high surface area, (this parameter has limited linear variation with absorbed hydrogen) porous nature (but pore volume is limited for each material) and high thermal and mechanical stability, and all these have been so far considered though questionable, as vital factors for hydrogen storage. Emphasis has been given to the hollow and porous structure of CNTs which is supposed to give the possibility of hydrogen storage both in the inner and outer surfaces that are well investigated by many theoretical as well as experimental studies. These studies though have relevance did not answer the stumbling block in achieving the goal of reaching the DOE standards. CNTs are termed to be one of the promising nanostructures for hydrogen storage however this expectation also has not yielded the desired result.

Moreover, the simultaneous presence of defects, both topological and structural types, and other irregularities affect the activation and adsorption and hence the amount of hydrogen stored in the system. In addition to this, doping also leads to structural and electronic property variations. However, these modifications so far have not shown enormous improvement in hydrogen storage capacity. It is however believed that estimated values of hydrogen storage still show the high impact of structure on the storage capacity. Nanomaterials are also analyzed and found that some of these strongly affect the storage capacity. But still, the DOE target could not be achieved which makes this issue an interesting topic of study even today.

Different types of nanotubes like metallic and semiconductor (also single or multi-walled) with varying structures were considered. It has been observed that the adsorption binding energy values as a function of different orientations of adsorbed species and at different sites of nanostructures are compared and the results show the strong impact of CNT structure on the storage capacity of hydrogen. Hydrogen can be adsorbed on graphene in two different ways: physisorption or chemisorption. While the first one is due to Van Der Waals interaction, the second is by forming a chemical bond with the C atoms. Physisorption usually happens with hydrogen in molecular form and in chemisorption, dissociation of H_2 into atomic hydrogen takes place and is a rather favorable process unlike in CNTs where physisorption is the most preferred way of storage. A single graphene layer is a quasi-2D system, and its VD is not well defined, thus in the evaluation of the potentialities of graphene for hydrogen storage, different forms of graphene such as multilayers, three-dimensional assemblies, or nanostructures of graphene are considered. However, it should be remarked that the standards for the necessary hydrogen storage for the projected applications should be realized at the earliest.

8 Modified Carbon Materials for Hydrogen Storage

Modification of the equipotential surface of carbon materials has been attempted for various reasons. Usually, the activation is aimed at introducing active centers on supported phases. It is usually to disperse active metals so that the exposed metal surface area is maximum. Hydrogen adsorption involves dissociation of molecular hydrogen and any storage medium should have dissociating centers for molecular hydrogen. Recognizing this aspect, heteroatom substitution has been proposed as one of the options. DFT calculations have also shown that molecular hydrogen dissociation energy is considerably reduced on heteroatoms like N, P, or B substituted carbon surfaces (Table 5), however, these studies so far have not led to the levels of storage of hydrogen on these materials.

8.1 Nitrogen Doping in Carbon Materials

Nitrogen is an abundant (80%) element in the terrestrial atmosphere. Molecular nitrogen is stable and has a minor role in the lower atmosphere. N-doped carbon materials are the much-studied area in energy storage. Depending on the type of N bonding within the carbon matrix, nitrogen can share one to two π -electrons with the π -electron system of the carbons. This sharing of electrons causes an n -type doping if N atoms directly substitute the C atoms in the graphitic lattice. N-doping in carbon generally manifests itself in three different forms namely, pyrrolic-N, pyridinic-N, and quaternary-N, and each form alters the carbon electronic band

gap differently. The band gaps of pyrrolic-N, pyridinic-N, and quaternary-N-doped carbons are reported to be 1.20, 1.40, and 1.39 eV, respectively.

Particularly, all materials obtained by these techniques have a nitrogen content lower than 10 atoms % because of the high temperature environment that was used in carbonization. An alternate synthesis method needs to be developed that enables the preparation of carbon material with high nitrogen content and time they should be stable at high temperatures. It will be beneficial if one can adopt a polymerization and low-temperature growth process to create nitrogen-doped carbon materials.

Nitrogen is essentially introduced into the carbon matrix in two ways, either by the carbonization of N-containing precursors or by post-modification methods. The common nitrogen-containing precursors are urea, melamine, cyanide, polyacrylonitrile, and ammonia. Another resourceful approach for the synthesis of N-doped carbon materials is based on naturally (sustainable) nitrogen-containing precursors

Table 4 Bond length and dissociation energy of hydrogen on the CNTs calculated using B3LYP with 6.31G (P,D) basis set on the UFF optimized structures [40]

| Substitution | Total energy (Hartrees) | Bond length H ₁ -H ₂ (Å) | Dissociation energy (eV) |
|------------------------------------|-------------------------|--|--------------------------|
| Hydrogen | -1.175 | 0.708 | 4.76 |
| CNT | -3686.5502 | | ... |
| CNT + H ₂ | -3687.7161 | 0.776 | 4/51 |
| NCNT | -3702.5908 | ... | |
| NCNT + H ₂ | -3703.5989 | 0.815 | 0.22 |
| PCNT | -3989.1694 | | ... |
| PCNT + H ₂ | -3990.2550 | 0/815 | 2.33 |
| SCNT | -4046.0020 | ... | |
| SCNT + H ₂ | -3047.0067 | 0.817 | 0.13 |
| BCNT | -3671.7254 | | |
| BCNT + H ₂ | -3672.9440 | 0.818 | 5.95 |
| 2BCNT (adjacent) | -3658.6666 | | ... |
| 2BCNT (adjacent) + H ₂ | -3659.8092 | 0.813 | 3.88 |
| 2BCNT (Alternate) | -3659.3491 | | |
| 2BCNT (alternate) + H ₂ | -3660.3594 | 0.928 | 0.28 |

Table 5 Technical system targets for on-board hydrogen storage for light-duty fuel cell vehicles

| | 2020 | 2025 | Ultimate |
|---|-------|-------|----------|
| Usable specific energy from H ₂ [kWh/kg] | 1.5 | 1.8 | 2.2 |
| Net usable energy/mass system mass [kg H ₂ /kg system] | 0.045 | 0.055 | 0.065 |
| Usable energy density from H ₂ [kWh/L] | 1.0 | 1.3 | 1.7 |
| Net usable energy/max system volume [kgH ₂ /L system] | 0.030 | 0.040 | 0.050 |
| System cost [USD/kWh net] | 10 | 9 | 8 |

like amino-carbohydrates or other N-enriched polymers, amino acids, proteins, N-ionic liquids, and waste crab shells. Another possible way is to pyrolyze the nitrogen and carbon-containing precursors, such as heterocycles or melamine, by which direct incorporation of nitrogen atoms into the forming of carbon backbone becomes possible. One of the procedures for deriving N-doped carbon is hydrothermal treatment of carbohydrate-rich biomass. Using nitrogen-containing biomass-related precursors and hydrothermally treating them yields nitrogen-containing carbonaceous materials that offer tremendous possibilities for further treatments and energy applications. The application of nitrogen-doped carbon materials has been investigated as a material for hydrogen storage at room temperature and ambient pressure [41]. It has been reported that nitrogen-enriched graphitic carbon material exhibits a hydrogen storage capacity of 0.34 wt.% at 298 K under 100 bars [42]. It has also been reported that the addition of N-species in mesoporous carbons showed hydrogen adsorption capacity of 1.1 wt.% at 298 K and 100 bar pressure [43]. It has also been reported that the microwave plasma CVD process enables the growth of specific nanostructured nitrogen-doped carbons. Nitrogen incorporation into these forms of carbon is approximately 1 at.%. It shows a gravimetric hydrogen storage capacity of 0.7–0.8 wt.% under 300 K and 0.1–7 MPa [44]. Hydrogen adsorption on nitrogen-doped carbon xerogels showed maximum hydrogen uptake of 0.28 wt.% at 308 K [45].

8.2 Phosphorus-Doping in Carbon Materials

The changes in the physical properties of Sp^2 carbon motifs after the addition of phosphorous into their lattice are considered. However, P has a larger atomic radius and higher electron-donating ability, which makes it an option as a dopant. Phosphorus is not a common element in carbons, although it is present in carbons obtained using phosphoric acid activation. Due to the addition of P in the carbon matrix, the density of states near the Fermi level is also found to increase, which increases with the increase in the P-doping level. In these reactions, the formation of phosphate and polyphosphate bridges provokes the expansion and cross-linking of the carbon matrix, driving to an accessible pore structure after the removal of the acid. The chemical state of phosphorus in carbons is a rather controversial issue. Some experimental evidence using different analytical techniques (FTIR and XPS) has shown that the most abundant P species introduced in carbons by phosphoric acid activation are $-C-P-$ or $-C-O-P$ bonds in phosphate and phosphonate-like structures. The XPS analysis further allowed for an insight into the binding states, proving the true incorporation of the phosphorus atoms into the graphite sheets, besides some P-O binding sites, most likely on the surface of the material. The existence of pentavalent phosphorus and elemental phosphorus is very infrequently detected, except when high temperatures are applied. Recent studies have reported that P-containing groups might be significant for the progress of graphitic crystallites which contrasts with far reported role of P as an inhibitor of carbon graphitization. Yang et al. [46] reported that

phosphorous-doped ordered mesoporous carbon was synthesized by co-pyrolyzing a phosphorus-containing source and a carbon source collectively using ordered mesoporous silica (SBA-15) as a template without the use of any metal components. More recent approaches have recognized dissimilar synthetic pathways in the direction of phosphorus-doped carbon materials, proving themselves as promising candidates for energy storage applications. It has been shown in the previous section that carbon materials with substitution by heteroatoms like N, S, and B, show hydrogen sorption capacity. However, the effect of substitution of phosphorus in carbon materials has not been investigated to the same extent.

8.3 Boron-Doping in Carbon Materials

Boron is an element with unique properties. It is thus an interesting candidate for doping of carbon materials, modifying the properties of pure carbons. Several researchers have started focusing not only on basic studies on B-doping, but also on applying the obtained materials and exploiting their favorable properties in energy-related applications. Due to its three valence electrons, B is well thought-out as a good dopant. Substitutional boron enhances the graphitization of carbon. It has been found that boron atoms are favored to be substituted in the graphite lattice. The existence of B–C bonds in the carbon framework can lower the Fermi level of the structure and then tune the properties of oxygen chemisorption and electrochemical redox reactions. The synthetic procedure, in which elemental B and graphite powder served as precursors, yielded a mixture of different B-containing carbon nanostructures, such as thin graphitic sheets, tubes, and filaments. The substitutional doping of carbon atoms in Sp^2 and Sp^3 configurations with boron can modify the electronic and structural properties of the resulting carbon. Over the years boron-doped carbons have been synthesized by standard CVD process using BCl_3 . Substituted boron atoms in the carbon lattice accelerate the graphitization and suppress the oxidation of carbon materials, which seems promising for their use as reinforcement materials in aerospace applications. The positive effect of boron doping on diamond and carbon electrodes and in the field of hydrogen storage has also been reported, although further optimization of the boron doping environment seems yet to be needed.

The storage of hydrogen in carbon nanomaterials requires appropriate chemical activators in suitable geometry. Sankaran et al. reported different types of carbon materials employed for the hydrogen sorption capacity. The storage capacity of 2 wt.% at 298 K and 80 bar pressure is obtained for boron boron-substituted carbon nanotube. However, a maximum storage capacity of 2 wt.% is attained at 80 bar and 300 K for boron-containing carbon nanotubes (BCNT) whereas pure carbon nanotubes (CNT) show only 0.6 wt.% at 300 K and 80 bar and B-doped bulk carbon material (PBC) shows only 0.2 wt.%. Mike Chung et al., reported the microporous boron-substituted carbon (B/C) materials show a significantly higher hydrogen binding energy and reversible hydrogen physisorption capacity of 0.6 and 3.2 wt.%

at 293 and 77 K, under 40 bar of hydrogen pressure [47]. B-containing polymeric precursors and pyrolysis were employed to synthesize microporous B/C materials with a high B content (7.2%) and high surface area (780 m²/g). The substitutional B elements in B/C material serve as internal p-type dopants and polarize the C surface, which exhibits a significantly higher hydrogen binding energy [48]. For efficient hydrogenation and hydrogen storage, these boron atoms should be incorporated geometrically and chemically into the carbon network. Wang et al. reported that B- and N-doped microporous carbon had a hydrogen storage capacity of 0.55 wt.% at 298 K and 10 MPa. By doping 6.0 wt.% Ru metal on the B- and N-doped microporous carbon, the hydrogen uptake at 10 MPa was increased to 1.2 wt.%, i.e. The improvement of hydrogen storage was due to the spillover of atomic hydrogen from the Ru metal particles to the B- and N-doped microporous carbon [49].

9 Perspectives

The standards that one wishes to achieve in the storage of hydrogen are:

- Gravimetric H density in the range of 5–10 wt.% H₂, and energy density of 1.6–3.2 kWh/kg.
- Volumetric H density >50 kg H₂ m⁻³ and energy density >1.6 kWh/L.
- Thermodynamics: T < 85 °C (transport applications) or <200 °C (stationary applications).
- Kinetics (tank level): fill time 3–5 min; H₂ release flow 1.6 g/s.
- Durability: 1500 cycles (1/4 tank to full).

One of the recent specifications and the time to achieve them are assembled in Table 5.

Of all the available hydrogen storage materials, why carbon materials are preferred option? What is the maximum hydrogen storage capacity that can be expected and what will be the limit that can be practically achieved? It may be remembered that nature mostly provides hydrogen source in combined form with carbon and oxygen though other elemental compositions are also possible. If carbon materials can be obtained in an atomic state, then the maximum storage capacity can be expected to be around 25 wt.%. However, since it is not possible to get atomic hydrogen, the carbon materials can be obtained at the limit with one vacant valency in carbon two-dimensional material and the maximum storage can be expected to be 6.25 wt.%. This limit is arrived at assuming that hydrogen is held by the solid by valence forces. If hydrogen is stored or retained by other forces, this limit may not hold good.

If the stored hydrogen were to occupy the interstitial sites in carbon materials, then the energetics of storing and releasing should also be considered for practical application.

Since normally carbon materials are microporous in nature, hydrogen may be held in these pores by condensation forces and hence one can hope for higher storage

capacity, however, the experimental variables for this process namely temperature and pressure have to be different from normal ambient conditions.

10 Conclusion

Hydrogen storage characteristics and treatments for improving the storage capacities of different carbon materials are presented. The following deductions can be stated:

1. The hydrogen storage capacity of carbon materials depends upon surface area, which is affected by micropore size distribution that counts for the presence of narrow micropores.
2. Thermal treatments and metal doping on carbon nanostructures are observed to be useful for improving hydrogen storage capacities but higher storage capacities can be obtained at cryogenic temperature and higher pressure. Further investigations on modified carbon nanostructures may be useful to achieve the target of 7.5 wt.% for automobile applications.
3. Theoretical studies show a strong structural dependence of carbon materials on hydrogen adsorption capacity, especially in CNTs. The defects influence the adsorption capacity.
4. Several theoretical studies predicted amazing storage capacities but were not confirmed experimentally. Also, higher storage capacities like 20 wt.% for metal doped MWCNT and 10 wt.% for CNF measured experimentally are reported in the literature but are to be confirmed.
5. Experimental and theoretical studies on adsorption storage reactors are scarce in the literature. Studies on the design, material, and thermophysical properties of reactors can be done for isotherm measurements, especially for automotive applications. These vital issues will be a good technical contribution in the field of hydrogen-adsorption systems for onboard applications.

Spill-over is one of the phenomena invoked by the transport of hydrogen from the site of impact to other normally inactive sites. This phenomenon has been investigated and is commonly accepted alternate way of surface transport. This transport requires a transporting medium and in the case of hydrogen, it is usually water and its fragments. In the case of carbon, this transporting medium can be either adsorbed water species or the carbon species themselves. The role of spillover in hydrogen sorption and storage needs more information.

References

1. Panella, B., Hirscher, M., Roth, S.: Hydrogen adsorption in different carbon nanostructures. *Carbon* **43**, 2209 (2005)
2. Zhu, Z.H., Hatori, H., Wang, S.B., Lu, G.Q.: New insights into the interaction of hydrogen atoms with boron substituted carbon. *J. Phys. Chem. B* **109**, 16744 (2005)

3. Arjunan, A., Viswanathan, B., Nandhakumar, V.: Nitrogen doped graphene as potential material for hydrogen storage. *Graphene* **6**, 41 (2017)
4. Wang, L., Lee, K., Sun, Y.-Y., Lucking, M., Chen, Z., Zhao, J.J., Zhang, S.B.: Graphene oxide as an ideal substrate for hydrogen storage. *ACS Nano* **3**, 2995 (2009)
5. Ariharan, A., Viswanathan, B., Nandhakumar, V.: Heteroatom doped multi-layered graphene material for hydrogen storage application. *Graphene* **5**, 39 (2016)
6. Tozzini, V., Pellegrini, V.: Prospects for hydrogen storage in Graphene. *Phys. Chem. Chem. Phys.* **15**, 80 (2013)
7. Viswanathan, B., Indraneel, P., Varadarajan, T.K.: A process for the preparation of activated carbon from botanical sources. *Catal. Surv. Asia* **13**, 164 (2008)
8. Jin, H., Lee, Y.S., Hong, I.: Hydrogen adsorption characteristics of activated carbon. *Catal. Today* **120**, 399 (2007)
9. Jorda-Beneyto, M., Lozano-Castello, D., Suarez-Garcia, F., Cazorla-Amoros, D., Linares-Solano, A.: Advanced activated carbon monoliths and activated carbons for hydrogen storage. *Microporous Mesoporous Mater.* **112**, 235 (2008)
10. Chambers, A., Park, C., Baker, R.T.K., Rodriguez, N.M.: Computer simulations of hydrogen adsorption on graphite nanofibers. *J. Phys. Chem. B* **102**, 4253 (1998)
11. Fan, Y.Y., Liao, B., Liu, M., Wei, Y.L., Lu, M.Q., Chang, H.M.: Hydrogen uptake in vapor grown carbon nanofibers. *Carbon* **37**, 1649 (1999)
12. Gupta, B.K., Srivastava, O.N.: Synthesis and hydrogenation behaviour of graphitic nanofibers. *Int. J. Hydrog. Energy* **25**, 825 (2000)
13. Dillon, A.C., Jones, K.H., Bekkedahl, T.A., Klang, C.H., Bethune, D.S., Eben, H.J.: Storage of hydrogen in single-walled carbon nanotubes. *Nature* **386**, 377 (1997)
14. Ye, Y., Ahvi, C.C., Witham, C., Fultz, B., Liu, J., Rinzler, A.G., Colbert, D., Smith, K.A., Smalley, R.E.: Hydrogen adsorption and cohesive energy of single-walled carbon nanotubes. *Appl. Phys. Lett.* **74**, 2307 (1999)
15. Dillon, A.C., Genneth, T., Jones, K.M., Alleman, J.A., Parilla, P.A., Heben, H.J.: A simple and complete purification of single-walled carbon nanotube (SWNT) materials. *Adv. Mater.* **11**, 1354 (1999)
16. Chen, P., Wu, A., Lim, J., Tan, K.L.: High H₂ uptake by alkali doped carbon nanotubes under ambient pressure and moderate temperatures. *Science* **265**, 91 (1999)
17. Yang, R.T.: Hydrogen storage by alkali-doped carbon nanotubes-revisited. *Carbon* **38**, 623 (2000)
18. Elzbeta Fracko Wiak and Francois Bequin: Electrochemical storage of energy in carbon nanotubes and nanostructured carbons. *Carbon* **40**, 1775 (2002)
19. Hirscher, M., Bechner, M., Haluska, M., Quintel, A., Skakalova, V., Choi, Y.-M., Dettlaff-Weglikowska, U., Roth, S., Stepanek, I., Bernier, P., Leonhardt, A., Fink, J.: Hydrogen storage in carbon nanostructures. *J. Alloy. Compd.* **330–332**, 654 (2002)
20. Tirbetti, G.G., Heisner, G.P., Olk, C.H.: Hydrogen storage capacity of carbon nanotubes, filaments, and vapor-grown fibers. *Carbon* **39**, 2291 (2001)
21. Hirscher, M., Becher, M., Haluska, M., Dettlaff-Weglikowska, U., Quintel, A., Duesberg, G.S., Choi, Y.M., Downes, P., Hulman, M., Roth, S., Stepanek, I.: Hydrogen storage in sonicated carbon materials. *Appl Phys A* **72**, 129 (2001)
22. Chambers, A., Park, C., Baker, R.T.K., Rodriguez, N.M.: Hydrogen storage in graphite nanofibers. *J. Phys. Chem. B* **102**(22), 4253–4256 (1998)
23. Nishimiya, N., Ishigaki, K., Takikawa, H., Ikeda, M., Hibi, Y., Sakakibara, T., Matsumoto, A., Tsutsumi, K.: Hydrogen sorption by single-walled carbon nanotubes prepared by a torch arc method. *J. Alloy. Compd.* **339**, 275–282 (2002)
24. Smith, M.R., Bittner, E.W., Shi, W., Johnson, J.K., Bockrath, B.C.: Chemical activation of single-walled carbon nanotubes for hydrogen adsorption. *J. Phys. Chem. B* **107**, 3752–3760 (2003)
25. Silambarasan, D., Surya, V.J., Vasu, V., Iyakutti, K.: Experimental investigation of Hydrogen storage in single walled carbon nanotubes functionalized with borane. *Int. J. Hydrog. Energy* **36**, 3574–3579 (2011)

26. Rashidi, A.M., Nouralishahi, A., Khodadadi, A.A., Mortazavi, Y., Karimi, A., Kashefi, K.: Modification of single wall carbon nanotubes (SWNT) for hydrogen storage. *Int. Hydrog. Energy* **35**, 9489–9495 (2010)
27. Mosquera, E., Diaz-Droguett, D.E., Carvajal, N., Roble, M., Morel, M., Espinoza, R.: Characterization and hydrogen storage in multi-walled carbon nanotubes grown by aerosol assisted CVD method. *Diam. Relat. Mater.* **43**, 66–71 (2014)
28. Lee, S., Park, S.: Influence of the pore size in multi-walled carbon nanotubes on the hydrogen storage behaviors. *J. Solid-State Chem.* **194**, 307–312 (2012)
29. Barghi, S.H., Tsotsis, T.T., Sahimi, M.: Chemisorption, physisorption and hysteresis during hydrogen storage in carbon nanotubes. *Int. J. Hydrog. Energy* **39**, 1390–1397 (2014)
30. Lin, K., Mai, Y., Li, S., Shu, C., Wang, C.: Characterization and hydrogen storage of surface modified multiwalled carbon nanotubes for fuel cell application. *J. Nanomater.* 1–12 (2012)
31. Rakhi, R.B., Sethupathi, K., Ramaprabhu, S.: Synthesis and hydrogen storage properties of carbon nanotubes. *Int. J. Hydrog. Energy* **33**, 381–386 (2008)
32. Rostami, S., Pour, A.N., Izadyar, M.: A review on modified carbon materials as promising agents for hydrogen storage. *Sci. Prog.* **101**, 171 (2018)
33. Sahu, S., Khan, M.S., Gupta, N., Chennakesavulu, K., Sasikumar, C.: The hydrogen storage capacity of carbon nano-onions fabricated by thermal chemical vapour. *Int. J. Hydrog. Energy* **48** (2023). <https://doi.org/10.1016/j.ijhydene.2023.03.156>
34. Guo, R., Teng, Y.-S., Retita, I., BakmanrokJ, G., Arhurst, N., Chan, S.L.I.: A detailed experimental comparison on the hydrogen storage ability of different forms of graphitic carbon nitride bulk, nanotubes and sheets with multiwalled carbon nanotubes. *Mater. Today Chem.* **30**, 101508 (2023)
35. Lyu, J., Kudiiarov, V., Lider, A.: An overview of the recent progress in modifications of carbon nanotubes for hydrogen adsorption. *Nanomaterials*, **10**, 255 (2020)
36. Lyu, J., Kudiiarov, V., Lider, A.: An overview of the recent progress in modifications of carbon nanotubes for hydrogen adsorption. *Nanomaterials* **10**, 255 (2020)
37. Lobo, R., Ribeiro, J., Inok, F.: Hydrogen uptake and release in carbon nanotube electrocatalysts. *Nanomaterials* **11**, 97 (2021)
38. Lee, S.Y., Lee, J.H., Kim, Y.H., Kim, J.W., Lee, K.J., Park, S.J.: Recent progress using solid-state materials for hydrogen storage: a short review. *Processes* **10**, 304 (2022)
39. Lim, K.L., Kazemian, H., Yaakob, Z., Daud, W.W.: Solid-state materials and methods for hydrogen storage: a critical review. *Chem. Eng. Technol.* **33**(2), 213–226 (2010)
40. Sankaran, M.: On the potential of carbon materials for solid state hydrogen storage. Ph.D. thesis, IIT Madras (2007)
41. Yao, Y., Zhang, B., Shi, J., Yang, Q.: Preparation of Nitrogen-doped carbon nanotubes with different morphologies from melamine-formaldehyde resin. *ACS Appl. Mater. Interfaces* **7**, 7413–7420 (2015)
42. Yang, S.J., Cho, J.H., Oh, G.H., Nahm, K.S., Park, C.R.: Easy synthesis of highly nitrogen enriched graphitic carbon with high hydrogen storage capacity at room temperature. *Carbon* **47**, 1585–1591 (2009)
43. Cai, J., Bennici, S., Shen, J., Auroux, A.: The acid-base properties of nitrogen-containing carbon materials. *Mater. Chem. Phys.* **161**, 142–152 (2015)
44. Badzian, A., Badzian, T., Breval, E., Piotrowski, A.: Nanostructured, nitrogen-doped carbon materials for hydrogen storage. *Thin Solid Films* **398**, 170–174 (2001)
45. Kang, K.Y., Lee, B.I., Lee, J.S.: Hydrogen adsorption on nitrogen-doped carbon xerogels. *Carbon* **47**, 1171–1180 (2009)
46. Yang, D.-S., Bhattacharjya, D., Song, M.Y., Yu, J.-S.: High efficient metal-free phosphorus-doped platelet ordered mesoporous carbon for electrocatalytic oxygen reduction. *Carbon* **67**, 736–743 (2014)
47. Chung, T.M., Jeong, Y., Chen, Q., Kleinhammes, A., Wu, Y.: Synthesis of microporous boron-substituted carbon (B/C) materials using polymeric precursors for hydrogen physisorption. *J. Am. Chem. Soc.* **130**, 6668–6669 (2018)

48. Chung, T.M., Jeong, Y., Kleinhammes, A., Wu, Y.: Synthesis of micro-porous boron substituted carbon (BC) materials using polymeric precursors for hydrogen physisorption. *ECS Trans.* **19**, 57–66 (2009)
49. Wang, L., Yang, F.H., Yang, R.T.: Hydrogen storage properties of B- and N-doped microporous carbon. *AIChE J.* **55**, 1823–1833 (2009)

Nanocarbon as Catalyst Support for Fuel Hydrogen Generation by Hydrolysis of Sodium Borohydride



Iterlandes M. Junior, Gabriel H. Sperandio, Renata P. L. Moreira, and Tiago A. Silva

Abstract Climate change-related disasters have occurred worldwide due to the exhaustive use of fossil fuels. One promising fuel alternative is hydrogen (H_2), which has a high energy potential ($1.42 \times 10^8 \text{ J Kg}^{-1}$) and is considered the future fuel. However, its storage processes, such as gas compression or liquefaction are still unfeasible due to its low density and boiling point. Inorganic hydrides such as sodium borohydride ($NaBH_4$) can be used as storage systems, but the hydrolysis reaction needed to release H_2 is slow and requires catalysts. In this sense, several recent research efforts have been made to propose heterogeneous catalysts based on metallic nanoparticles anchored in different support materials for the generation of H_2 . Special emphasis can be given to nanocarbon as a support for nanostructured catalysts, such as carbon nanotubes, graphene, and biochar obtained from biomass, considering the availability of these materials, high surface area, and versatility in terms of functionalization. This book chapter provides a review of recent advances in the use of metallic nanocatalysts supported by nanocarbon to generate fuel hydrogen from $NaBH_4$, detailing aspects related to the synthesis, characterization, and application of the materials. Future perspectives on the use of these catalysis systems are also addressed.

Keywords Energy storage · Hydrogen storage · Supported catalysts · Sustainable fuels · Carbon nanomaterials

1 Introduction

Recently, there has been a global effort to replace the energy matrix based on fossil fuels with renewable sources. These efforts are primarily motivated by the need to address climate change. To support this transition, the United Nations (UN) launched Sustainable Development Goals (SDGs), which include objectives aimed at achieving

I. M. Junior · G. H. Sperandio · R. P. L. Moreira · T. A. Silva (✉)
Department of Chemistry, Federal University of Viçosa, Avenida Peter Henry Rolfs S/N, Viçosa, Minas Gerais 36570-900, Brazil
e-mail: tiago.a.silva@ufv.br

sustainable economic growth and eradicating poverty by 2030. Notably, the goals of ‘Accessible and Clean Energy’ and ‘Combating Climate Change’ stand out among these objectives. Although wind and solar energy are valuable sources of renewable and clean energy, they are intermittent. Therefore, it is crucial to explore other means of producing renewable energy.

Hydrogen possesses significant energy potential, with a high energy content of $1.42 \times 10^8 \text{ J kg}^{-1}$, and its combustion for energy generation results in the production of only water vapor. However, practical challenges arise due to its low density (0.0899 g L^{-1}) and low boiling point (20.37 K), rendering storage methods like gas compression or liquefaction unsuitable for widespread applications. Furthermore, hydrogen is frequently produced through processes such as steam reforming of hydrocarbons or coal gasification, which unfortunately lead to inevitable carbon dioxide emissions, being classified as brown hydrogen [1]. Hydrogen color classification involves a scale that facilitates the identification of the source of hydrogen production, primarily based on its carbon emissions. Green hydrogen is produced by the electrolysis of water using nuclear or renewable energy.

To address the storage and transportation challenges, solid-state storage methods, such as hydrides, have emerged as promising alternatives. This is attributed to their significant hydrogen storage capacity and robust process stability, drawing global attention [2]. This process can be categorized into two main mechanisms: (1) physisorption or physical adsorption, which takes place through Van der Waals forces (dipole–dipole or induced dipole) between the adsorbate and the adsorbent; and (2) chemisorption, where hydrogen gas molecules undergo a chemical reaction with solid-state materials, leading to the formation of stable hydrides. The latter can be categorized into three types: elemental hydrides, intermediate hydrides, and complex hydrides. There are different materials employed for physisorption including metal–organic structures, zeolites, and carbon-based materials (Fig. 1). Nevertheless, these materials are generally considered less effective when compared to Light-weight Solid-state Hydrogen Storage (LSHS) [2]. As examples of these materials, one can mention elemental hydrides, intermetallic hydrides, and complex hydrides.

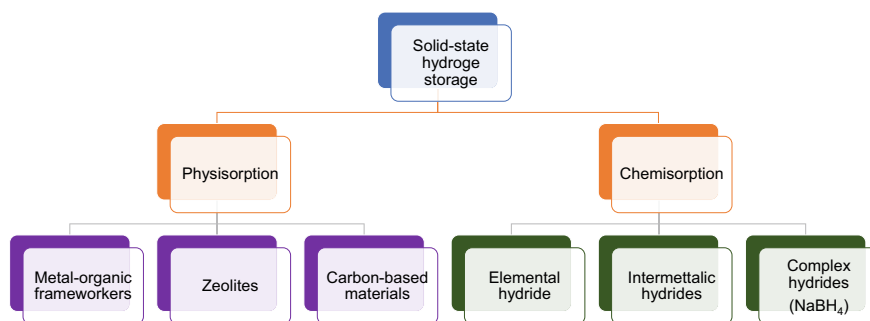


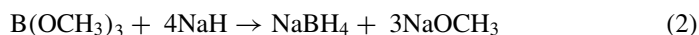
Fig. 1 Different types of solid-state hydrogen storage. Adapted with permission [2], Copyright (2022), Elsevier

Among LSHS materials, the hydrogen evolution from sodium borohydride (NaBH_4) has emerged prominently, primarily owing to its remarkable theoretical storage capacity of 10.8% m/m. Schlesinger and coworkers [3] were pioneers in the utilization of NaBH_4 for hydrogen evolution, and there have been significant recent advancements in this area. The frequency of papers containing the keywords ‘solid-state hydrogen storage’ and ‘hydrogen’ in Web of Science indicates a total of 5,779 publications as of August 15, 2023.

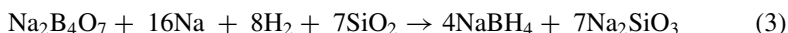
The release of hydrogen from NaBH_4 can occur by hydrolysis, according to Eq. (1). It is important to highlight that the associated high gravimetric hydrogen storage capacity (GHSC) is contingent upon the hydration state of the resulting by-product NaBO_2 (GHSC = 10.8% when $x = 0$; GHSC = 7.3% when $x = 2$; and GHSC = 5.5% when $x = 4$) [4].



NaBH_4 is a chemical hydride with a molar mass of 37.83 g/mol, and it exhibits a tetrahedral structure characterized by a boron atom with sp^3 hybridization. The tetrahedral anion (BH_4^-) interacts in electrostatic interactions with the Na^+ cation along its tetrahedral faces. Notably, NaBH_4 is not a naturally occurring substance. It is synthesized through either the Brown-Schlesinger or Bayer processes [1]. The first method, which is the most employed, involves the reaction of sodium hydride with trimethylborate, resulting in the formation of sodium borohydride and sodium methoxide (Eq. (2)). The reaction yield is close to 100%.



The second method involves the combination of borax, metallic sodium, hydrogen, and silicon oxide at a temperature of 973 K (Eq. (3)). The reaction is conducted in a batch process, yielding NaBH_4 and sodium silicate (Na_2SiO_3). This process, however, has low efficiency due to limitations in mass transfer and water vaporization.



The hydrogen evolution rate (r) (mL min^{-1}) from the alkaline hydrolysis of NaBH_4 , as described in Eq. (4), is thermodynamically favorable, but kinetically slow.

$$r = A e^{\left(-\frac{E}{RT}\right)} [\text{catalyst}]^a [\text{NaBH}_4]^b [\text{NaOH}]^c \quad (4)$$

wherein A represents the pre-exponential factor; E denotes the activation energy; R is the universal gas constant ($0.082 \text{ atm L K}^{-1} \text{ mol}^{-1}$); T is the absolute temperature; and ‘ a ,’ ‘ b ,’ and ‘ c ’ denote the reaction orders with respect to the dose of the catalyst, NaBH_4 , and NaOH , respectively.

Therefore, catalysts based on transition metals are widely used in these processes [5]. In general, decorating a porous substrate with nanoscale catalysts is a viable

way to increase the surface area of the catalysts, in addition to enabling their reuse in different catalytic cycles [6]. Among the supports used for this purpose, carbon-based materials stand out.

2 Nanocarbons as Catalyst Support for Fuel Hydrogen Generation

Carbon is a chemical element found in the second period of Group 14 on the periodic table. It possesses an electron configuration of $1s^2 2s^2 2p^2$ ($2p_x$, $2p_y$, $2p_z$), with 4 electrons in its outermost electron shell. To form a chemical bond, carbon's atomic orbitals undergo hybridization, leading to the creation of molecular orbitals capable of forming sigma and pi bonds. Carbon exhibits different hybridization states, including sp^3 hybridization (an s orbital combines with 3 p orbitals); sp^2 (an s orbital combines with 2 p orbitals) and sp (an s orbital combines with a p orbital). The wide range of atomic orbital combinations enables carbon atoms to create various types of bonds with each other, giving rise to a variety of allotropic forms, including the remarkable substance known as graphene.

2.1 Graphene-Based Catalysts

Graphene was first discovered by Geim and Novoselov in 2004 [7]. It is characterized by a carbon atom structure with sp^2 hybridization, forming hexagonal planar structures that systematically repeat across the xy plane (Fig. 2).

Graphene stands out as the resistant and thinnest material ever discovered [8]. Due to sp^2 hybridization, π electrons are conjugated inside the hexagonal ring, granting the material a high capacity for conducting electricity, along with minimal thermal energy loss. Other properties include high thermal conductivity (5000 W/m K), flexibility and rigidity, lightness, and transparency, being able to absorb only 2.3% of light [9]. These properties make graphene suitable for various applications in the fields of science and engineering. It can be employed as sensors, transistors, capacitors, as a polymeric material, for chemical energy storage, and in catalytic reactions.

While the original structure of graphene consists of just a single carbon sheet, other structural variants are also considered, including materials formed by multiple graphene sheets arranged in an organized manner, as shown in Fig. 2 [10]. Its surface is a highly crystalline containing a plane without defects, making it inert or minimally reactive. Consequently, interactions with other compounds can occur through physisorption [8]. Hence, studies have employed graphene as a solid-state hydrogen storage medium.

According to Tozzini and Pellegrini [11], hydrogen can be adsorbed onto graphene through two mechanisms: physisorption and chemisorption. The process to promote

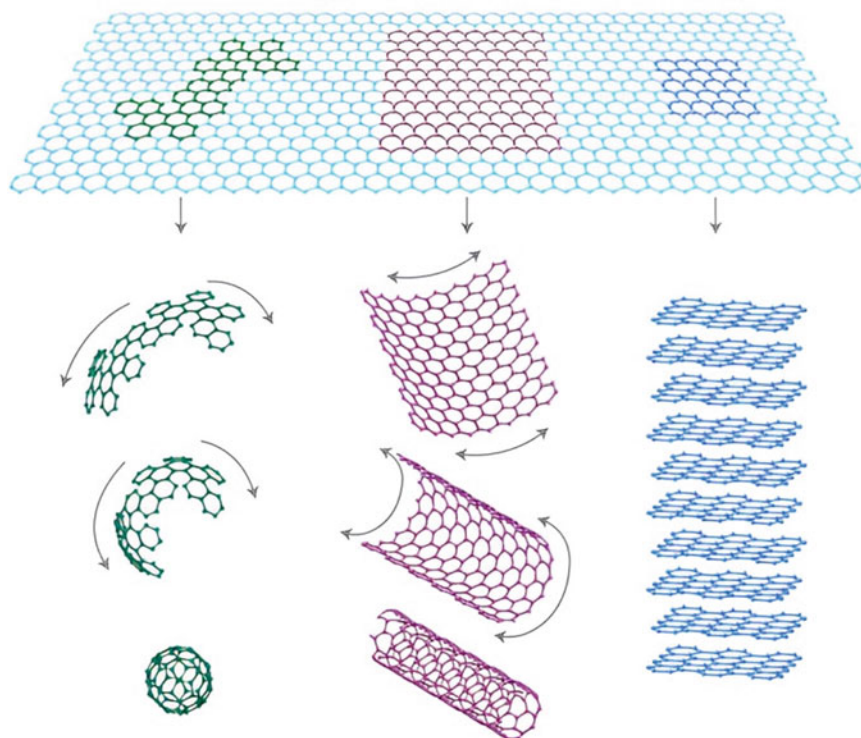


Fig. 2 Structure of graphene and materials produced from it (fullerene, nanotubes, and graphite). Adapted with permission [7], Copyright (2007), Springer Nature

hydrogen physisorption and chemisorption presents different levels of energy involved, and Fig. 3 shows the energy level diagram for the graphene-hydrogen system.

In the case of physisorption, the binding energy of H_2 has been theoretically calculated to fall within the range of 0.01–0.06 eV, typically occurring under high pressure and low temperature conditions. Under these circumstances, H_2 can form a compact and uniform monolayer on the graphene sheet, resulting in a gravimetric density (GD) of 3.3%. This value can be doubled if both sides of the graphene sheet are considered. Conversely, molecular hydrogen chemisorption on graphene presents substantial barriers, estimated at around 1.5 eV, as it necessitates the dissociation of H_2 (dissociative adsorption). In contrast, atomic hydrogen chemisorption is a highly favorable process, characterized by H binding energy and chemisorption barriers on the order of ~ 0.7 eV and ~ 0.3 eV, respectively. Graphene offers distinct advantages for this application, including its high gravimetric density, expansive surface area and remarkable mechanical strength. Moreover, its cost-effective production is facilitated by the readily available raw material, graphite [12].

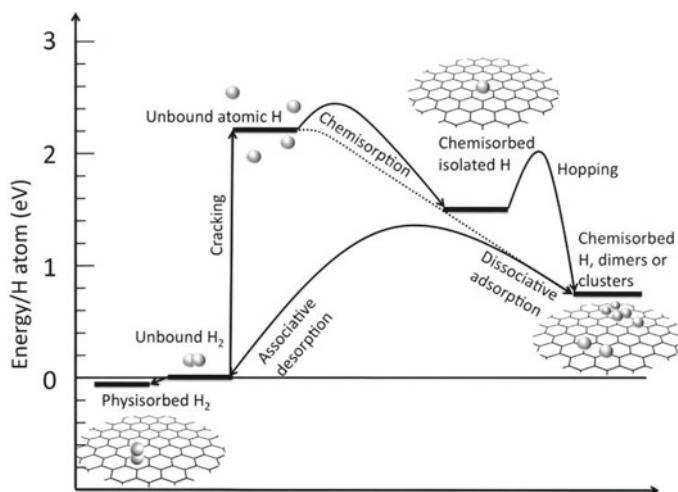


Fig. 3 Energy level diagram for the graphene-hydrogen system. Adapted with permission [11], Copyright (2013), Royal Society of Chemistry

To employ graphene in catalysis reactions, it requires modification. Typically, oxidation reactions are employed to introduce oxygenated groups into its structure, facilitating the creation of interaction sites on the basal carbon plane [13]. Additionally, graphene can be doped with boron or nitrogen atoms, and there's also the possibility of oxidizing the carbon structure, thereby introducing defects on the surface via the incorporation of oxygenated functional groups.

Graphene quantum dots (GQDs) have garnered significant attention due to their outstanding performance and promising applications. GQDs typically exhibit sizes within the range of 2–20 nm and possess surfaces functionalized with various organic groups, including hydroxyl, epoxy, and carboxylic acid [14]. GQDs exhibit excellent hydrophilicity, low biotoxicity and stable photoluminescent (PL) properties [15]. Liu and colleagues synthesized a $\text{CoO}_x\text{@C-rGO}$ core-shell structure using a solvothermal process followed by calcination (Fig. 4) [16].

The $\text{CoO}_x\text{@C-rGO}$ was employed as a catalyst for the hydrolysis of NaBH_4 and NH_3BH_3 , resulting in the production of hydrogen. Additional studies exploring graphene-based catalysts for NaBH_4 hydrolysis catalysis are detailed in Table 1.

2.2 Carbon Nanotubes-Based Catalysts

Carbon nanotubes (CNTs) belong to the fullerene structural family and can be classified into single-walled carbon nanotubes (SWCNTs) and multi-walled carbon nanotubes (MWCNTs) [25]. Both MWCNTs and SWCNTs were discovered by Sumio Iijima in 1991 and 1993, respectively [43, 44]. MWCNTs can reach lengths

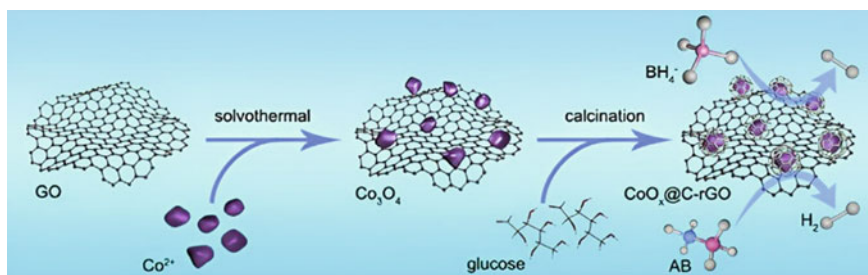


Fig. 4 Synthesis of CoO_x@C-Reduced graphene oxide composite with catalytic activity towards hydrogen generation. Adapted with permission [16], Copyright (2019), Elsevier

of up to 1.0 μm and exhibit external diameters ranging from 4 to 30 nm. They are composed of two or more layers of graphene. SWCNTs typically have diameters within the range of 0.8 to 2.0 nm and are composed of a single layer of graphene. These materials have similar electrical conductivity properties [24]. Various methods have been employed in the synthesis of CNTs, the most common being chemical vapor deposition (CVD), laser ablation, electric arc discharge, and template-based approaches. Additionally, less conventional techniques such as solar furnace, electrolysis, diffusion flame methods, and low-temperature solid pyrolysis have also found application [24].

CNTs possess a substantial surface area and excellent electrical conductivity, making them versatile materials with applications at spanning nanotechnology, electronics, optics, composite materials, and biomedicine [34]. Furthermore, they exhibit a thermal conductivity exceeding 3000 W/m K at room temperature, surpassing that of both graphite and diamond [24]. However, CNTs possess high hydrophobicity, which can lead to limited material dispersion in aqueous reactions [22]. This issue can be addressed by surface functionalization of CNTs through the introduction of functional groups, such as hydroxyl ($-\text{OH}$), carboxyl ($-\text{COOH}$), or amine ($-\text{NH}_2$). CNTs can be suspended and stabilized by incorporating additional conductive polymers to enhance their conductivity, solubility, and chemical properties. Wang et al. [33] synthesized CoPt nanoparticles supported on poly(3,4-ethylenedioxythiophene)/poly(styrenesulfonate) functionalized MWCNTs. This material was successfully used in the hydrogen evolution from NaBH_4 .

The properties of carbon nanotubes can be modulated to meet specific requirements. One approach involves decorating CNTs with metallic nanoparticles, which enhances their conductivity and electron transfer capabilities, thereby improving the catalytic activity of these nanocatalysts [36]. Different researchers describe the use of CNTs for evolution of hydrogen from NaBH_4 , as shown in Table 1.

Table 1 Different carbon-based nanomaterials used as catalysts in the evolution of hydrogen from NaBH₄

| Catalyst | NaBH ₄ hydrolysis conditions | E_a (kJ mol ⁻¹) | HGR (mL min ⁻¹ g ⁻¹) | Ref |
|--|---|----------------------------------|--|------|
| Co-Ni α C | 50 mg of catalyst; 0.1 g NaBH ₄ ; 0.1 g NaOH; 25 °C | 30.3 | 6364 | [17] |
| Ni-Co/r-GO | 5 g of 10 wt% NaBH ₄ ; 5 wt% NaOH; 0.05 g of catalysts; 25 °C | 55.12 | 1280 | [18] |
| Co/PGO | 0.1 g PGO + 6 mL (NaOH 0.25 M, NaBH ₄ 0.25 M) | 55.22 | 5955 | [19] |
| Co _{0.7} Mo _{0.3} /3DGO | 0.25 mM NaBH ₄ and 0.25 mM NaOH + 6 mL ultrapure water + 0.10 g of catalyst | 35.6 | 7023.3 | [20] |
| Pd/MWCNT | 10 mg of catalyst; 835 μ mol of NaBH ₄ ; 22 °C | 62.66 | 23 | [21] |
| Au-MWCNT | 835 μ mol of NaBH ₄ ; pH 7; 30 °C | 21.1 | 29 | [22] |
| Fe ₂ O ₃ @OMWCNTs | 37 mg of material (7.5% wt), 0.5 g of NaBH ₄ ; Room temperature | 15.92 | 264.09 | [23] |
| Co/MWCNTs-20 | 30 mg of catalyst (Co 20% wt); 200 mg of NaBH ₄ ; 35 °C | 51.3 | 410 | [24] |
| Pt _{0.3} -MWCNT | 0.03 g of Pt _{0.3} -MWCNT (30% wt of Pt on MWCNT), 5.03% wt of NaBH ₄ ; 27 °C | 27 | 1107 | [25] |
| Co-Fe ₃ O ₄ -CNT ₁₂ | 0.5 g de NaBH ₄ ; 0.03 g de Co-Fe ₃ O ₄ -CNT ₁₂ , where subscript denotes the starting wt% of the CNT (Co 5% wt); 25 °C | 42.79 | 1213 | [26] |
| PAN/CoCl ₂ /CNTs where PAN is polyacrylonitrile | 0.5 g of NaBH ₄ (1.0 wt. %); PAN/CoCl ₂ /CNTs (4.5 mg of CoCl ₂ and 12.0 wt.% of CNT); 25 °C | 52.857 | 1255.1 | [27] |
| (CNTs-Fe ₃ O ₄) _(1:4) -Co _(10%) | 96 mg of catalyst; 720 mg of NaBH ₄ ; 40 °C under microwave irradiation | 57.639 | 1664.802 | [28] |
| PdRu/MWCNT-GNP where GNP is graphene nano platelet | 0.2 mol L ⁻¹ of NaBH ₄ , 0.2 mol L ⁻¹ of NaOH, 0.02 g of the catalyst; 45 °C | 22.33 | 2065 | [29] |
| Co-B (17.33 wt%) / MWCNT | 20 wt.% of NaBH ₄ ; 3 wt.% of NaOH, 10 mg of catalyst; 30 °C | 44.40 | 5100 | [30] |

(continued)

Table 1 (continued)

| Catalyst | NaBH ₄ hydrolysis conditions | E_a (kJ mol ⁻¹) | HGR (mL min ⁻¹ g ⁻¹) | Ref |
|-----------------------|---|----------------------------------|---|------|
| CoB-LDH-CNT-50 | 1.5 wt.% of NaBH ₄ + 5.0 wt.% of NaOH; 0.1 g of catalyst; 30 °C | 29.93 | 5167.72 | [31] |
| CoB/o-CNTs | 50 mL of alkaline solution containing 0.5 g of NaBH ₄ (1.0% by weight) and 1.875 g of NaOH (3.75% by weight); 25 °C. All catalysts contained 0.0100 g of CoB | 37.63 | 5248 | [32] |
| CoPt-PEDOT:PSS/MWCNT | 150 mmol of NaBH ₄ ; NaOH concentration = 0.4% by weight; 10 mg of catalyst; 25 °C | 47.3 | 6900 | [33] |
| MWCNT-COOH | 50 mg of MWCNT-COOH as the catalyst, 20 mL of NaBH ₄ (500 mmol) in 20 mL of methanol; 25 °C | 20.1 ± 1.4 | 8766 ± 477 | [34] |
| Co-B-10CNTs | 10 mL of solution containing 5% by weight of NaBH ₄ and 5% by weight of NaOH/0.1 g of catalyst; 25 °C | 23.5 | 12,000 | [35] |
| Ru-Co/CNTs | NaBH ₄ (7% by weight), NaOH (1% by weight), 20 mg of catalyst; 25 °C | 34.35 | 21,190 | [36] |
| 3% Ru-Mo (80:20) /CNT | 50 mg of catalyst, 0.26 mol L ⁻¹ of NaBH ₄ ; 30 °C | 35.11 | 82.758,43 | [37] |
| 3% RuW/MWCNT | 10 mL of solution containing 0.26 mol L ⁻¹ NaBH ₄ , 50 mg of catalyst; 30 °C | 16.327 | 95,841.4 | [38] |
| 3% RuCo(80:20)/MWCNT | 50 mg of catalyst, 0.26 mol L ⁻¹ NaBH ₄ ; 30 °C | 35.978 | 123.9385 | [39] |
| Co-PDA@BC | 1.0 wt% NaBH ₄ , 1.0 wt% NaOH; 30 mg of catalyst; 35 °C | 31.3 | 25 | [40] |
| Ru-Co/C | 10 wt% NaBH ₄ , 1.0 wt% NaOH; 20 µg of catalyst; 25 °C | 36.83 | 9360 | [41] |
| Co-B/Carbon Black | 10 wt% NaBH ₄ , 10 wt% NaOH; carbon supporting containing 5 mg of Co; 25 °C | 56.7 | 8033.89 | [42] |

* Hydrogen Generation Rate (HGR)

2.3 Biochar-Based Catalysts

Biochar (BC) is a material more recently defined as the carbon-rich solid product resulting from the thermochemical conversion of biomass under anoxic conditions [45]. In this sense, different sources of biomass can be explored for the BC synthesis process, including residual biomass from agro-industrial processes, such as sugarcane bagasse, malt bagasse, straw, sewage sludge, among others, configuring a great option for waste management [46]. The chemical composition and structure of BC depend on the characteristics of the biomass feedstock (for example, cellulose and lignin content), the working temperature and the type of thermochemical process. In general, the basic elemental composition of BC consists of C, H, O, N, S, P, K, Ca, Mg, Na and Si, and is based on a well-developed pore network that guarantees a high specific surface area [45].

Thermochemical conversion (or carbonization) can be carried out by different processes, such as pyrolysis, gasification, or hydrothermal carbonization (HTC) [46]. Pyrolysis is the thermoconversion of biomass into solid (biochar), liquid (bio-oil) and gaseous (biogas) materials, being carried out in a closed system, with an atmosphere free of oxygen gas and under conditions of high pressure and temperatures (300 to 1000 °C). HTC is similar to the previous process in terms of methodology, but it allows the use of water in the reaction medium and lower temperatures (160 to 350 °C) [47]. In contrast, gasification uses an atmosphere of air, oxygen, or steam to obtain another gas with a high calorific value as a product. Pyrolysis is the most used process to obtain biochar due to its high yield rate, in addition to the possibility of varying and studying different operational parameters, such as temperature, heating rate (divided into slow, intermediate, fast, and flash) and residence time in the reactor, to optimize the process [48].

BCs can be utilized in different ways, such as an adsorbent to remove pollutants from water, including dyes and pharmaceuticals [49], fertilizer [50], and as a support for nanocatalysts [51]. In this sense, an interesting aspect is that the rich surface chemistry of BC makes it highly susceptible to various chemical functionalization strategies. In recent work of our group [52], BC was functionalized by carboxyl groups with triazole groups to improve its characteristics as a support for gold nanoparticles with recognized catalytic activity. Figure 5 shows a schematic representation of the synthetic route of triazole-functionalization. AuNPs anchored on the triazole-functionalized BC surface displayed high catalytic activity towards hydrogen evolution from an aqueous solution of $B_2(OH)_4$, with a maximum H_2 generation of 715 mL $g^{-1} \text{ min}^{-1}$.

Focusing on works using sodium borohydride as a solid H_2 storage, Table 1 lists the recent work of Akti [40], who reported using pistachio shell-derived biochar decorated with cobalt nanoparticles synthesized by the modified impregnation-reduction method. The obtained nanocatalyst (Co-TA@BC) under optimal conditions provided the generation of hydrogen from sodium borohydride with a maximum rate of 25 mL $g^{-1} \text{ min}^{-1}$ and activation energy of 31.3 kJ mol^{-1} .

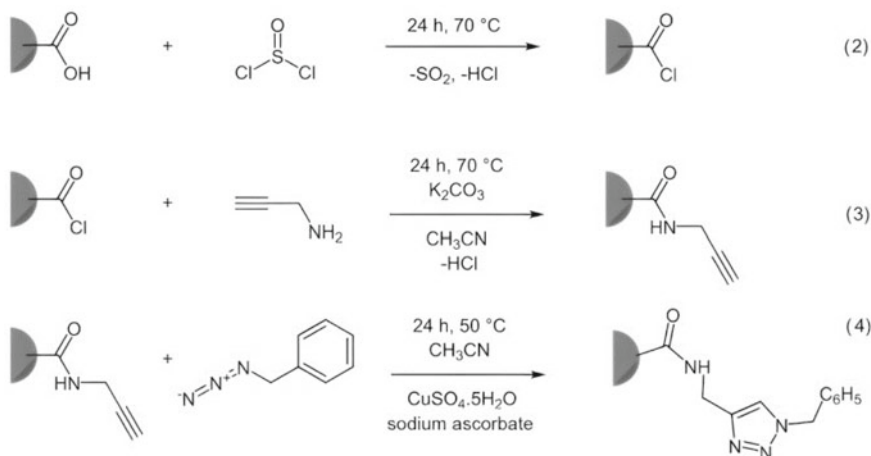


Fig. 5 Scheme for the synthesis of triazole-functionalized biochar. Adapted with permission [52], Copyright (2023), Copyright The Authors, some rights reserved; exclusive licensee PubliSBQ. Distributed under a Creative Commons Attribution License 4.0 (CC BY) <https://creativecommons.org/licenses/by/4.0/>

2.4 Carbon Black-Based Catalysts

Carbon black (CB) is a petrochemical product consisting of finely powdered elemental carbon. It is produced through the incomplete combustion of gaseous or liquid hydrocarbon derivatives under controlled conditions, resulting in various CB grades with specified properties ranges [53, 54]. Carbon black finds application as a black pigment in paints and toners, serves as an antistatic agent, and is primarily used as a filler in the tire industry [55]. It is characterized by spherical graphitic particles ranging in diameter from 10 to 100 nm, with some extending to hundreds of microns (Fig. 6). Carbon black falls within the category of substances known as Industrial Aciniform Aggregates (IAA), resembling grape-like structures [55, 56].

Considering its very low cost, adequate electrical conductivity and high surface area, CB has been extensively explored, for example, as a support for nanostructured electrocatalysts [57]. Furthermore, the use of CB as a support for metallic nanoparticles for the H_2 generation from sodium borohydride has been reported. Table 1 shows some examples in this line of application. For example, Baydaroglu et al. [42] showed that carbon black acted as a better support than activated carbon for Co nanoparticles prepared by the reduction–precipitation method. This was in terms of catalytic activity against the evolution of hydrogen from sodium borohydride, reaching a maximum H_2 generation rate of $23,939.39 \text{ mL g}^{-1} \text{ min}^{-1}$ at 40°C .

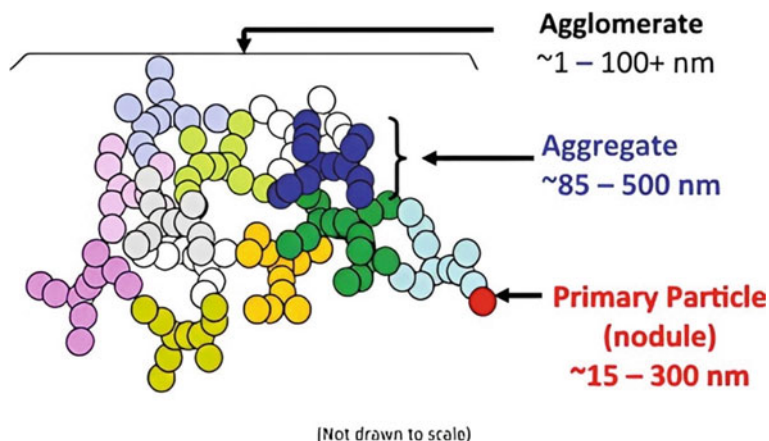


Fig. 6 Carbon black structure. Adapted with permission [54], Copyright (2013), Elsevier

3 Conclusions and Future Perspectives

Over the last few years, there has been a clear increase in the number of research using nanocarbons as support for metallic nanocatalysts to act in the evolution of hydrogen from sodium borohydride. This is a promising technology, considering favorable technical aspects resulting from the use of solid hydrogen storages, such as reduced storage and transportation costs, exponential increase in safety and reduced H_2 gas pressurization costs. Regarding nanocarbon-based catalysts, the chapter review work highlights materials such as graphene, carbon nanotubes, biochar, and carbon black, with carbon nanotubes standing out. The maximum H_2 evolution rates vary greatly, making it difficult to establish a better nanocarbon-nanocatalyst combination, which perhaps creates the need for better standardization of the minimum quality requirements for catalysts. Furthermore, investments must be implemented in the coming years to validate the economic viability of the catalysts developed and carry out production scale-up. Nanocarbon-based support materials from residual biomass should be an important line of work, to add value to agro-industrial waste and reduce catalyst production costs. Without a doubt, the field of nanocarbons as a support for catalysts for hydrogen evolution is vast and promising for countless research and advances soon.

Acknowledgements The authors are grateful to CAPES, CNPq (Grant Number: 405828/2022-5) and FAPEMIG (Grant Number: RED-00144-22) for the financial support.

5. References

1. Dragan, M.: Hydrogen storage in complex metal hydrides NaBH₄: hydrolysis reaction and experimental strategies. *Catalysts* **12**, 356 (2022)
2. Yao, J., Wu, Z., Wang, H., Yang, F., Ren, J., Zhang, Z.: Application-oriented hydrolysis reaction system of solid-state hydrogen storage materials for high energy density target: a review. *J. Energy Chem.* (2022)
3. Schlesinger, H.I., Brown, H.C., Finholt, A.E., Gilbreath, J.R., Hoekstra, H.R., Hyde, E.K.: Sodium borohydride, its hydrolysis and its use as a reducing agent and in the generation of hydrogen. *J. Am. Chem. Soc.* **75**, 215–219 (1953)
4. Marchionni, A., Bevilacqua, M., Filippi, J., Folliero, M.G., Innocenti, M., Lavacchi, A., Miller, H.A., Pagliaro, M.V., Vizza, F.: High volume hydrogen production from the hydrolysis of sodium borohydride using a cobalt catalyst supported on a honeycomb matrix. *J. Power. Sources* **299**, 391–397 (2015)
5. Liu, B.H., Li, Z.P., Suda, S.: Nickel-and cobalt-based catalysts for hydrogen generation by hydrolysis of borohydride. *J. Alloys Compd.* **415**, 288–293 (2006)
6. Zou, Y., Yin, Y., Gao, Y., Xiang, C., Chu, H., Qiu, S., Yan, E., Xu, F., Sun, L.: Chitosan-mediated Co–Ce–B nanoparticles for catalyzing the hydrolysis of sodium borohydride. *Int. J. Hydrogen Energy* **43**, 4912–4921 (2018)
7. Geim, A.K., Novoselov, K.S.: The rise of graphene. *Nat. Mater.* **6**, 183–191 (2007)
8. Segundo, J., Vilar, E.O.: Grafeno: Uma revisão sobre propriedades, mecanismos de produção e potenciais aplicações em sistemas energéticos. *Rev. Eletrônica Mater. e Process.* **11**, 54–57 (2016)
9. Pastrana-Martínez, L., Morales-Torres, S., Gomes, H., Silva, A.: Nanotubos e grafeno: os primos mais jovens na família do carbono! *Química* **128**, 21–27 (2013)
10. Mehl, H., Matos, C.F., Neiva, E.G.C., Domingues, S.H., Zarbin, A.J.G.: The effect of variation of reactional parameters in the preparation of graphene by oxidation and reduction of graphite. *Quim. Nova* **37**, 1639–1645 (2014)
11. Tozzini, V., Pellegrini, V.: Prospects for hydrogen storage in graphene. *Phys. Chem. Chem. Phys.* **15**, 80–89 (2013)
12. Ganji, M.D., Emami, S.N., Khosravi, A., Abbasi, M.: Si-decorated graphene: a promising media for molecular hydrogen storage. *Appl. Surf. Sci.* **332**, 105–111 (2015)
13. Hummers, W.S.J., Offeman, R.E.: Preparation of graphitic oxide. *J. Am. Chem. Soc.* **80**, 1339 (1958). <https://doi.org/10.1021/ja01539a017>
14. Dutra, L.V., de Oliveira Fontoura, C.R., da Cruz, J.C., Nascimento, M.A., de Oliveira, A.F., Lopes, R.P.: Green synthesis optimization of graphene quantum dots by Doehlert design for dye photodegradation application. *Colloids Surfaces A Physicochem. Eng. Asp.* **651** (2022) 129442
15. Shen, J., Chen, W., Lv, G., Yang, Z., Yan, J., Liu, X., Dai, Z.: Hydrolysis of NH₃BH₃ and NaBH₄ by graphene quantum dots-transition metal nanoparticles for highly effective hydrogen evolution. *Int. J. Hydrogen Energy* **46**, 796–805 (2021)
16. Liu, Y., Guo, H., Sun, K., Jiang, J.: Magnetic CoOx@ C-reduced graphene oxide composite with catalytic activity towards hydrogen generation. *Int. J. Hydrogen Energy* **44**, 28163–28172 (2019)
17. Sun, L., Gao, X., Ning, X., Qiu, Z., Xing, L., Yang, H., Li, D., Dou, J., Meng, Y.: Cobalt-nickel bimetal carbon sphere catalysts for efficient hydrolysis of sodium borohydride: the role of synergy and confine effect. *Int. J. Hydrogen Energy* **48**, 3413–3428 (2023)
18. Chou, C.-C., Hsieh, C.-H., Chen, B.-H.: Hydrogen generation from catalytic hydrolysis of sodium borohydride using bimetallic Ni–Co nanoparticles on reduced graphene oxide as catalysts. *Energy* **90**, 1973–1982 (2015)
19. Zhang, H., Feng, X., Cheng, L., Hou, X., Li, Y., Han, S.: Non-noble Co anchored on nanoporous graphene oxide, as an efficient and long-life catalyst for hydrogen generation from sodium borohydride. *Colloids Surfaces A Physicochem. Eng. Asp.* **563**, 112–119 (2019)

20. Li, Y., Hou, X., Wang, J., Feng, X., Cheng, L., Zhang, H., Han, S.: Co-Mo nanoparticles loaded on three-dimensional graphene oxide as efficient catalysts for hydrogen generation from catalytic hydrolysis of sodium borohydride. *Int. J. Hydrogen Energy* **44**, 29075–29082 (2019)
21. Huff, C., Long, J.M., Heyman, A., Abdel-Fattah, T.M.: Palladium nanoparticle multiwalled carbon nanotube composite as catalyst for hydrogen production by the hydrolysis of sodium borohydride. *ACS Appl. Energy Mater.* **1**, 4635–4640 (2018)
22. Huff, C., Dushatinski, T., Abdel-Fattah, T.M.: Gold nanoparticle/multi-walled carbon nanotube composite as novel catalyst for hydrogen evolution reactions. *Int. J. Hydrogen Energy* **42**, 18985–18990 (2017)
23. Prasad, D., Patil, K.N., Sandhya, N., Chaitra, C.R., Bhanushali, J.T., Samal, A.K., Keri, R.S., Jadhav, A.H., Nagaraja, B.M.: Highly efficient hydrogen production by hydrolysis of NaBH₄ using eminently competent recyclable Fe₂O₃ decorated oxidized MWCNTs robust catalyst. *Appl. Surf. Sci.* **489**, 538–551 (2019)
24. Narasimharao, K., Abu-Zied, B.M., Alfaifi, S.Y.: Cobalt oxide supported multi wall carbon nanotube catalysts for hydrogen production via sodium borohydride hydrolysis. *Int. J. Hydrogen Energy* **46**, 6404–6418 (2021)
25. Uzundurukan, A., Devrim, Y.: Hydrogen generation from sodium borohydride hydrolysis by multi-walled carbon nanotube supported platinum catalyst: a kinetic study. *Int. J. Hydrogen Energy* **44**, 17586–17594 (2019)
26. Bandal, H.A., Jadhav, A.R., Kim, H.: Cobalt impregnated magnetite-multiwalled carbon nanotube nanocomposite as magnetically separable efficient catalyst for hydrogen generation by NaBH₄ hydrolysis. *J. Alloys Compd.* **699**, 1057–1067 (2017)
27. Li, F., Arthur, E.E., La, D., Li, Q., Kim, H.: Immobilization of CoCl₂ (cobalt chloride) on PAN (polyacrylonitrile) composite nanofiber mesh filled with carbon nanotubes for hydrogen production from hydrolysis of NaBH₄ (sodium borohydride). *Energy* **71**, 32–39 (2014)
28. Luo, C., Liu, S., Yang, G., Jiang, P., Luo, X., Chen, Y., Xu, M., Lester, E., Wu, T.: Microwave-accelerated hydrolysis for hydrogen production over a cobalt-loaded multi-walled carbon nanotube-magnetite composite catalyst. *Appl. Energy* **333**, 120538 (2023)
29. Al-Msrhad, T.M.H., Devrim, Y., Uzundurukan, A., Budak, Y.: Investigation of hydrogen production from sodium borohydride by carbon nano tube-graphene supported PdRu bimetallic catalyst for PEM fuel cell application. *Int. J. Energy Res.* **46**, 4156–4173 (2022)
30. Huang, Y., Wang, Y., Zhao, R., Shen, P.K., Wei, Z.: Accurately measuring the hydrogen generation rate for hydrolysis of sodium borohydride on multiwalled carbon nanotubes/Co–B catalysts. *Int. J. Hydrogen Energy* **33**, 7110–7115 (2008)
31. Luo, X., Sun, L., Xu, F., Cao, Z., Zeng, J., Bu, Y., Zhang, C., Xia, Y., Zou, Y., Zhang, K., Pan, H.: Metal boride-decorated CoNi layered double hydroxides supported on multi-walled carbon nanotubes as efficient hydrolysis catalysts for sodium borohydride. *J. Alloys Compd.* **930**, 167339 (2023)
32. Li, F., Li, Q., Kim, H.: CoB/open-CNTs catalysts for hydrogen generation from alkaline NaBH₄ solution. *Chem. Eng. J.* **210**, 316–324 (2012)
33. Wang, X., Zhao, Y., Peng, X., Wang, J., Jing, C., Tian, J.: Synthesis and characterizations of CoPt nanoparticles supported on poly (3,4-ethylenedioxythiophene)/poly (styrenesulfonate) functionalized multi-walled carbon nanotubes with superior activity for NaBH₄ hydrolysis. *Mater. Sci. Eng. B* **200**, 99–106 (2015)
34. Sahiner, N.: Modified multi-wall carbon nanotubes as metal free catalyst for application in H₂ production from methanolysis of NaBH₄. *J. Power. Sources* **366**, 178–184 (2017)
35. Shi, L., Chen, Z., Jian, Z., Guo, F., Gao, C.: Carbon nanotubes-promoted Co–B catalysts for rapid hydrogen generation via NaBH₄ hydrolysis. *Int. J. Hydrogen Energy* **44**, 19868–19877 (2019)
36. Kong, L., Yu, T., Zhan, J., Zhang, Y., Li, G., Wang, H., Wang, X., Cheng, L., Wang, F.: Study on the performance of NaBH₄ using Ru-Co/CNTs catalyst to catalyze alcoholysis to produce hydrogen, Fullerenes. *Nanotub. Carbon Nanostruct.* **28**, 891–899 (2020)

37. Avci Hansu, T., Sahin, O., Caglar, A., Kivrak, H.: A remarkable Mo doped Ru catalyst for hydrogen generation from sodium borohydride: the effect of Mo addition and estimation of kinetic parameters, *React. Kinet. Mech. Catal.* **131** (2020) 661–676
38. Hansu, T.A.: A novel and active ruthenium based supported multiwalled carbon nanotube tungsten nanoalloy catalyst for sodium borohydride hydrolysis. *Int. J. Hydrogen Energy* **48**, 6788–6797 (2023)
39. Avci Hansu, T., Sahin, O., Çağlar, Demir Kivrak, H.: Untangling the cobalt promotion role for ruthenium in sodium borohydride dehydrogenation with multiwalled carbon nanotube-supported binary ruthenium cobalt catalyst. *Int. J. Energy Res.* **45** (2021) 6054–6066
40. Akti, F.: Green synthesis of pistachio shell-derived biochar supported cobalt catalysts and their catalytic performance in sodium borohydride hydrolysis. *Int. J. Hydrogen Energy* **47**, 35195–35202 (2022)
41. Wang, F., Wang, Y., Zhang, Y., Luo, Y., Zhu, H.: Highly dispersed RuCo bimetallic nanoparticles supported on carbon black: enhanced catalytic activity for hydrogen generation from NaBH₄ methanolysis. *J. Mater. Sci.* **53**, 6831–6841 (2018)
42. Baydaroglu, F., Özdemir, E., Hasimoglu, A.: An effective synthesis route for improving the catalytic activity of carbon-supported Co–B catalyst for hydrogen generation through hydrolysis of NaBH₄. *Int. J. Hydrogen Energy* **39**, 1516–1522 (2014)
43. Iijima, S.: Helical microtubules of graphitic carbon. *Nature* **354**, 56–58 (1991)
44. Iijima, S., Ichihashi, T.: Single-shell carbon nanotubes of 1-nm diameter. *Nature* **363**, 603–605 (1993)
45. Chen, W., Meng, J., Han, X., Lan, Y., Zhang, W.: Past, present, and future of biochar. *Biochar* **1**, 75–87 (2019)
46. Cha, J.S., Park, S.H., Jung, S.-C., Ryu, C., Jeon, J.-K., Shin, M.-C., Park, Y.-K.: Production and utilization of biochar: a review. *J. Ind. Eng. Chem.* **40**, 1–15 (2016)
47. de Souza, L.Z.M., Pinto, B.C., Alves, A.B., de O. Ribeiro, A.V., Feliciano, D.C.T., da Silva, L.H., Dias, T.T.M., Yilmaz, M., de Oliveira, M.A., da S. Bezerra, A.C., Ecotoxicological effects of biochar obtained from spent coffee grounds. *Mater. Res.* **25** (2022)
48. Kazawadi, D., Ntalikwa, J., Kombe, G.: A review of intermediate pyrolysis as a technology of biomass conversion for coproduction of biooil and adsorption biochar. *J. Renew. Energy* **2021**, 1–10 (2021)
49. de Oliveira Fontoura, C.R., Dutra, L.V., Guezgüan, S.M., Nascimento, M.A., de Oliveira, A.F., Lopes, R.P.: Optimization of one-pot H₃PO₄-activated hydrochar synthesis by Doehlert design: Characterization and application. *J. Anal. Appl. Pyrolysis* **168**, 105775 (2022)
50. Petter, F.A., Madari, B.E., da Silva, M.A.S., Carneiro, M.A.C., de M. Carvalho, M.T., Marimon Júnior, B.H., Pacheco, L.P.: Soil fertility and upland rice yield after biochar application in the Cerrado, Pesqui. *Agropecuária Bras.* **47**, 699–706 (2012)
51. Lopes, R.P., Astruc, D.: Biochar as a support for nanocatalysts and other reagents: recent advances and applications. *Coord. Chem. Rev.* **426**, 213585 (2021)
52. Lopes, R.P., Zhao, Q., Moya, S., Moroc, M.M., Astruc, D.: Gold nanoparticles supported on triazole-functionalized biochar as nanocatalyst for hydrogen evolution from aqueous solution (2023)
53. Ari, B., Ay, M., Sunol, A.K., Sahiner, N.: Surface-modified carbon black derived from used car tires as alternative, reusable, and regenerable catalysts for H₂ release studies from sodium borohydride methanolysis. *Int. J. Energy Res.* **43**, 7159–7172 (2019)
54. Long, C.M., Nascarella, M.A., Valberg, P.A.: Carbon black vs. black carbon and other airborne materials containing elemental carbon: physical and chemical distinctions. *Environ. Pollut.* **181**, 271–286 (2013)
55. Zarbin, A.J.G., Orth, E.S.: Some elemental carbon structures and their importance on the development and sovereignty of Brazil. *Quim. Nova* **42**, 1225–1231 (2020)
56. Gray, C.A., Muranko, H.: Studies of robustness of industrial aciniform aggregates and agglomerates—carbon black and amorphous silicas: a review amplified by new data. *J. Occup. Environ. Med.* **1279–1290** (2006)

57. Bu, Y., Wang, Y., Han, G., Zhao, Y., Ge, X., Li, F., Zhang, Z., Zhong, Q., Baek, J.: Carbon-based electrocatalysts for efficient hydrogen peroxide production. *Adv. Mater.* **33**, 2103266 (2021)

Exploiting the Potential of Carbon Nanotubes and Nanofluids to Boost Efficiency in Solar Applications



Amir M. Alinia and M. Sheikholeslami

Abstract This work comprehensively reviews recent advancements and applications of Carbon Nanotube (CNT) nanofluids, specifically concentrating on their integration into energy harvesting systems, particularly solar collectors. The effectiveness of collectors. Utilizing CNT nanofluids is assessed, accompanied by exploring preparation methods and factors influencing thermal conductivity and optical properties. Also mentioned are the drawbacks and potential directions for using CNT nanofluids in thermal collectors. CNTs, possessing the highest thermal conductivity among known nanoparticles, offer promising potential as heat transfer fluids when dispersed into various base fluids, creating CNT nanofluids. However, maintaining prepared CNT nanofluids' homogeneity and sustained durability poses a significant challenge. The paper provides a detailed study of the preparation techniques and reported stability periods of stationary CNT nanofluids. Various treatment methods, including chemical and physical treatments, are systematically analyzed, offering insights into overcoming stability challenges and future directions. The paper advocates for a balanced combination of techniques to achieve CNT dispersion without excessive treatment. Methods for analyzing nanofluid stability are also surveyed, emphasizing the need for cost-effective and rapid stability prediction methods.

Keywords Carbon nanotubes (CNT) · Nanomaterials · Carbon-based materials nanofluid · Solar collectors · Thermal conductivity · Nanofluid stability · Covalent functionalization surfactant · Energy efficiency

A. M. Alinia · M. Sheikholeslami (✉)
Department of Mechanical Engineering, Babol Noshirvani University of Technology, Babol,
Islamic Republic of Iran
e-mail: mohsen.sheikholeslami@nit.ac.ir

Renewable Energy Systems and Nanofluid Applications in Heat Transfer Laboratory, Babol
Noshirvani University of Technology, Babol, Iran

1 Introduction

In the last several decades, research in nanoscience and nanotechnologies has risen quickly, positioning it at the vanguard of contemporary scientific advancements. Because of their excellent thermal, physical, optical, and electrical qualities, carbon nanotubes (CNTs) have significantly contributed to the nano revolution. These remarkable attributes have propelled CNTs into becoming among the most comprehensive scrutinized Materials at the nanoscale.

The astonishingly high thermal conductivity of CNTs is one of its most noticeable features, which sets them apart from other nanoparticles. The revelation of this remarkable thermal conductivity in nanoparticles has ignited significant interest in research endeavors focusing on heat transfer fluids. The pioneering work of Choi et al. [1] marked the inception of this concept, as they stumbled upon an unexpectedly increased thermal conductivity in nanofluids in contrast to their base fluids. This discovery triggered a flurry of research efforts, documented in the literature, exploring various nanofluids in the context of energy harvesting and cooling systems. Consistent results throughout this research show how incorporating nanoparticles inside the fluid substantially enhances heat transmission. A specific emphasis is placed on the various preparation techniques used to maintain the stability of these nanofluids. While it is worth acknowledging that a few earlier review articles have explored this subject, it is imperative to highlight the burgeoning research trends revealed by the Scopus database. These trends unequivocally indicate a consistent upward trajectory in research activities related to CNT-infused nanofluids, with the past couple of years witnessing an unprecedented surge in interest from researchers worldwide.

Notably, most of the previously mentioned review articles predominantly focused on the thermal aspects of CNT nanofluids. A sizable body of research has recently been devoted to improving heat transfer by altering the thermophysical characteristics of working fluids. Their exceptional strength, electrical conductivity, and thermal conductivity result from their distinctive atomic arrangement. CNTs find applications across materials science, electronics, and nanotechnology, reflecting their potential for diverse technological and scientific progress.

A few reviews delved into the chemical and non-chemical modification of CNTs. It is worth noting that stability analysis presents a significant challenge, often requiring costly equipment and substantial time. In numerous studies, stability was either not addressed or was reported insufficient. Consequently, there is a pressing need to develop an economical and rapid approach to forecasting the stability of CNT nanofluids. Furthermore, it is noted that chemical and material scientists conduct most studies and investigations associated with preparing CNT nanofluids. In contrast, scientists in mechanical, chemical, and thermophysical engineering primarily investigate the thermal applications of nanofluids. Bridging this interdisciplinary gap and fostering knowledge exchange among these fields is essential for advancing the development of stable CNT nanofluids for thermal applications.

Furthermore, surfactants are more accessible to remove than polymers or proteins, and surfactant-attached CNTs can be easily removed by rinsing with deionized water

(DIW). SDS has found extensive application in preparing CNT solutions for various purposes, including nanocomposites, nanofluids, substances with antibacterial properties, and materials for coating applications. Numerous research studies have investigated the influence of SDS surfactants in solutions containing CNTs, considering variables like temperature, SDS concentration, sonication power, and binding energy.

There has been constrained investigation into the optimal Concentration of SDS in solutions containing carbon nanotubes for electrokinetic manipulation systems, specifically in the context of dielectrophoretic deposition multi-walled carbon nanotubes (MWCNTs) involving the use of non-uniform electric fields to manipulate and position CNTs within a solution.

CNTs have emerged as promising reinforcements for high-strength metal matrix composites. Compared to pure metals, a metal matrix composite featuring CNTs boasts a higher strength-to-density ratio, specific modulus, improved fatigue resistance, and a lower coefficient of thermal expansion (CTE). Among MMCs, aluminum-based composites have gained significant attention and found applications across various industrial sectors due to their outstanding strength and a favorable combination of properties. The synergistic effects resulting from the unique properties of CNTs and aluminum alloys have prompted extensive research into manufacturing aluminum/CNT nanocomposites, especially for weight-sensitive applications. Typically, significant enhancements in the strength of aluminum alloys occur with the addition of small concentrations of CNTs. However, a substantial increase in reinforcement content can lead to embrittlement of the composite. Achieving an increase in strength with only a slight reduction in flexibility is possible by incorporating CNTs in small concentrations.

One significant approach that has garnered attention in recent years is using nanofluids. Nanofluids are a class of engineered fluids consisting of a base fluid and solid nanoparticles suspended at nanoscale dimensions within the base fluid. Incorporating nanofluids into various thermal devices has shown promise in modifying their performance. For instance, scientists have evaluated the effectiveness of a pulsating heat pipe when filled with water and a nanofluid consisting of graphene oxide and water, demonstrating a significant lowering of heat resistance when utilizing nanofluid, ascribed to altered thermal conductivity and the presence of nucleation sites. In another study, Ni/water-glycerol nanofluid was used in a thermosyphon, revealing a decrease in overall thermal performance due to the addition of Ni nanoparticles. Nanofluids have also found applications in heat exchangers, where the use of TiO_2 /water nanofluid resulted in a substantial improvement in heat transfer compared to pure water. In addition to these applications, nanofluids have been integrated into clean energy technologies to enhance their efficiency. Geothermal systems, for example, benefit from nanofluids in heat exchangers, leading to size reduction and efficiency improvements. Nanofluids have also found application in fuel cells for thermal management, enhancing the reliability of these systems. However, one area where nanofluids have demonstrated significant potential is in solar technologies. They have been utilized in various solar systems, including solar collectors, ponds, and PVT systems, contributing to increased efficiency. The choice of nanofluid type and solid nanoparticles significantly impacts thermal performance,

as the thermophysical properties depend on the specific materials used. Carbon nanotubes, known for their excellent heat transfer properties, have become a focus of Concern about solar energy devices' utilization of nanofluids.

2 Categories and Arrangement

While carbon is abundant in the natural world, CNTs are a product of human engineering. These methods yield distinct shapes of CNTs, categorized into Single-walled carbon nanotubes (SWCNTs), composed of a mono seamless graphene layer rolled into a cylinder, and MWCNTs, formed from multiple rolled-up graphene sheets. The nearest example we found was a study where researchers used this approach to create nanofluids containing carbon nanoparticles in flake form, which are distinct from carbon nanotubes. Traditional Essential fluids like water and ethylene glycol oil are frequently used as coolants, and primary fluids like water and ethylene glycol oil are commonly used as heat storage mediums. Still, they have limitations regarding their thermal and physical properties. Incorporating nanoparticles into these fluids has demonstrated a notable improvement in their thermophysical characteristics, leading to the emergence of novel terminologies and distinct functions for these nanoparticle-dispersed fluids. These include nano coolants or heat-storage nanofluids, nano lubricants, nano greases, nano refrigerants, and nanofluids. A different class of foundational fluid, an ionic liquid, essentially consists of molten salt and exhibits unique thermal and physical attributes, including a notable heat storage capacity, outstanding thermal resilience, and elevated viscosity. The dispersion of nanoparticles into ionic liquids gives rise to nanofluids. However, the concept of nanofluids was first proposed.

2.1 Carbon Nanotubes

CNTs are truly exceptional formations, representing a significant advancement in nanostructures. They are cylindrical monolayer sheets of carbon atoms and can be synthesized in various ways. Such frameworks are excellent for various applications because of their unique characteristics. SWCNTs, for instance, are constructed by seamlessly rolling a single graphene sheet into a tube, while MWCNTs are formed by rolling multiple graphene sheets. This classification is based on how many layers there are comprising the nanotube and affects their dimensions, density, and specific characteristics. This exceptional thermal conductivity makes CNTs an attractive candidate for improving the thermal properties of various fluids.

To harness the benefits of CNTs in heat transfer applications, researchers have explored the creation of CNT nanofluids. These nanofluids involve dispersing CNTs into different fluids or solvents, such as H₂O, ethylene glycol, or ionic liquids, to enhance their thermal and physical properties. Similarly, adding CNTs to engine oil at a 2% volume concentration results in a 30% conductivity of heat rising.

These improvements in thermal conductivity suggest that CNT-based nanofluids hold promise as heat transfer fluids. Various studies have investigated their impact on heat transfer in different applications. For instance, researchers have used CNT nanofluids in pulsating heat pipes, heat exchangers, and other thermal devices, consistently observing reductions in thermal resistance and enhancements in heat transfer performance. In solar thermal technologies, where the efficiency of systems heavily relies on the heat transfer properties of the operating fluid, the incorporation of CNTs can be transformative. CNTs not only possess superior thermal conductivity but also exhibit favorable optical properties. When dispersed in fluids, they can alter the spectral absorptivity of the fluid across the solar spectrum. By reducing transmittance, CNT-based nanofluids can enhance their performance in solar systems. Studies have demonstrated that nanofluids containing CNTs reduce the transmittance of light, particularly in the visible and long-wavelength ranges. The extent of transmittance reduction is correlated with a specified volume fraction of CNTs in the primary fluid. Additionally, the absorption properties of nanofluids with CNTs significantly improve, making them efficient radiation absorbers. This enhanced absorption is especially beneficial in solar applications, as it allows for the effective utilization of solar energy-based nanofluids and offers exciting prospects for enhancing heat transfer efficiency and solar energy utilization.

2.2 *CNT-Based Nanofluids*

The distinguishing factors between these two types include differences in length, diameter, density, and other intrinsic traits, rendering them suitable for specific applications. The historical development of CNTs reveals that the first CNT was an MWCNT.

Traditional base fluids like water have been conventionally employed for cooling and heat storage, albeit with limited thermal and physical capabilities. The addition of nanoparticles to these fluids enhances their heat transfer capabilities, leading to the emergence of nanofluids with various designations, including nano coolants, heat-storage nanofluids, nano lubricants, nano greases, nano refrigerants, and nanofluids. Intriguingly, some of these nanofluids were first created by introducing CNTs into them, as exemplified by the introduction of “nano grease” by Hong et al. [2]. Their work demonstrated improved thermal conductivity and lubricity in nano lubricants and nano greases containing MWCNTs dispersed in commercial oils. Furthermore, a distinct category of base fluid comprises molten salts characterized by unique physical attributes such as high heat storage capacity, excellent thermal stability, and high viscosity.

Integrating nanoparticles into ionic liquids results in nanofluids, a concept pioneered. Consequently, nanofluids containing these CNTs have become attractive alternatives for thermal medium operating fluids. CNTs possess favorable optical properties, making them well-suited for solar applications. When CNTs are dispersed in different fluids, they modify spectral absorptivity across the solar spectrum.

Studies have indicated that the presence of CNTs in nanofluids reduces transmittance. Notably, the presence of SWCNTs in water at a 0.5% volume fraction significantly increased its absorption, enabling the nanofluid to absorb nearly all emitted light. Increasing the volume fraction of SWCNTs had a relatively minor impact on the absorption characteristics of the nanofluid. It was demonstrated that increasing the nanofluid's temperature led to a reduction in radiation absorption levels. These higher absorption properties of nanofluids containing CNTs make them particularly advantageous for solar applications. Carbon nanotubes (CNTs) boast many enticing qualities, ranging from their remarkable aspect ratio to their outstanding mechanical, thermal, and optical attributes. These characteristics position them as up-and-coming candidates for application in many mediums and devices. Notably, CNTs exhibit an exceptionally high thermal conductivity, typically ranging from 2000 to 6000 $\frac{W}{m.K}$. An enlightening study by Liu et al. [3] provides valuable insights into this enhancement. Numerous investigations have delved into the influence of employing nanofluids that include solid-phase carbon-based particles in thermal devices. Tanshen et al. [4] implemented a pulsating heat pipe charged with water functionalized with multi-walled carbon nanotubes at various concentrations, spanning from 0 to 0.3% wt. This caused a significant decrease in thermal resistance.

Qu et al. [5] examined how adding MWCNTs to water affected transmittance. They observed that the tiny increase in MWCNTs resulted in a considerable decrease in transmittance. For instance, compared to pure water, a nanofluid containing 0.0015% weight of MWCNTs in water had a 40% lower transmittance throughout wavelengths between 200 and 880 nm. The concentration of nanostructures in the water was increased to reduce transmission further. Additionally, a study found that the 0.5% volume fraction of SWCNTs in water caused a noticeably higher absorption rate. This led to the nanofluid absorbing almost all the light being released. Contrary to expectations, additional increases in the volume fraction of SWCNTs did not appreciably change its absorption rate.

3 Durability of CNT Nanofluid

Mechanical treatment involves physically mixing nanoparticles in a solvent through ultrasonication, irrespective of whether the CNTs have been functionalized. Qualitative observation of nanofluids in static conditions and quantitative measurements like zeta potential provide insights into colloidal stability. Zeta potential, representing the degree of repulsion between charged particles on CNTs and the base fluid, is a crucial parameter. Positive or negative values indicate repulsion, with higher values signifying better stability. Both functionalization and the addition of surfactants can alter the iso-electric point, where nanoparticles carry no net electrical charge, impacting stability. Regarding the electrostatic charge on particle surfaces, pH measurement is critical in determining stability.

The interplay of these forces determines the stability of the nanofluid. High attractive forces, dependent on interparticle distances and nanoparticle shape, lead to aggregation. The shape of nanoparticles impacts the attractive forces, with larger contact areas favoring stronger attraction and aggregate formation aggregation, resulting in increased particle size, promoting settling, and affecting dispersive behavior. Conversely, high repulsive forces maintain suspension stability.

Nanofluids subjected to repeated heating and cooling cycles in heat exchangers suffer processes that promote nanoparticle aggregation. Brownian motion is accelerated by high temperatures, which increases the likelihood of nanoparticle collisions and encourages aggregation formation. A dragging force and a reduced fluid viscosity also support aggregation. The coordinated, directed movement of nanoparticles encourages aggregation and interferes with homogenous dispersion due to CNTs' proclivity for irreversible aggregation over time, fueled by strong-interactions; CNT nanofluids, particularly, encounter difficulties.

Depending on interparticle distances and nanoparticle shape, high attractive forces lead to aggregation. Aggregation results in increased particle size, promoting settling and affecting dispersive behavior. Conversely, high repulsive forces maintain suspension stability.

In heat exchangers, nanofluids undergoing repeated heating and cooling cycles experience phenomena that enhance nanoparticle aggregation. Elevated temperatures accelerate Brownian motion, increasing nanoparticle collision probability and favoring aggregate formation. Reduced fluid viscosity and dragging force further support aggregation. The collective directional movement of nanoparticles disrupts homogeneous dispersion and promotes aggregation. The quest for harnessing the full potential of CNT nanofluids requires addressing challenges related to dispersion and stability. Chemical and mechanical treatments offer promising avenues, and researchers continue to explore novel functionalization techniques and stability assessment methods.

4 Heat-Conducting Properties of CNT Nanofluids

A distinguishing quality of carbon nanotube CNT-nanofluids over base fluids is their excellent conductivity. The transient hot-wire method is one of several methods that can be used to evaluate the conductivity of nanofluids. The thermal conductivity enhancement observed in nanofluids varies depending on factors. A dual-phase procedure is typically utilized for synthesizing CNT nanofluids, involving the dispersion of CNTs in a base fluid followed by stabilization through chemical and physical treatments. One of the most straightforward techniques for stabilizing CNT nanofluids is homogenization using an ultrasonication device. An effective procedure commonly used involves chemicals. They are altering the surfaces of CNTs by treating them with acids before achieving homogeneous dispersion in base fluids through ultrasonication. Another way involves dispersing CNTs into the foundational fluid and adding a surfactant before homogenization using ultrasonication.

Covalent functionalization, which utilizes a combination of acids, constitutes one of the chemical treatments applied to CNTs to enhance their thermal conductivity.

In a study conducted in 2009, investigating the consequences of covalently functionalizing multi-walled carbon nanotubes using nitric and sulfuric acids on the thermal conductive characteristics of water-based nanofluids were examined. Specifically, a 16% enhancement was recorded for f-MWCNT nanofluids at 0.5% of MWCNTs, compared to a 4.6% enhancement for pristine MWCNT nanofluids. A similar outcome was observed in another study involving water-based nanofluids.

Non-covalent alteration, in contrast to covalent functionalization, involves using surfactants to modify the surface of CNTs. This process aims to make the CNTs hydrophilic, allowing them to interact favorably in conjunction with the foundational fluid and repel alternative CNTs, thus preventing aggregation. Researchers have conducted studies to identify the most effective concentration of different surfactants for achieving the most stability and the highest thermal conductivity of nanofluids. The outcomes revealed that all surfactants enhanced thermal conductivity generally rise in higher surfactant concentrations, except in the case of SDS (sodium dodecyl sulfate), which led to a decrease in thermal conductivity enhancement. Maintaining the homogeneity of nanoparticles in the solvent is crucial for achieving high thermal conductivity in nanofluid suspensions. Ultrasonication, especially at elevated power levels, supplies ample energy to disperse particle clusters, fostering the creation of uniform suspensions. Moreover, the duration of ultrasonication was found to significantly impact thermal conductivity, with longer ultrasonication times leading to increased thermal conductivity, especially at higher concentrations of nanoparticles.

Han et al. [6] conducted experiments on water-based SWCNT nanofluids with varying SWCNT concentrations (0.05–0.25 vol%) in the presence of SDS surface-active agents at temperatures ranging from 40 °C.

Furthermore, higher temperatures provide the suspended nanoparticles with increased energy, enhancing their random movement and collision frequency, which is essential to the mechanics of heat conduction.

The diameter and length of CNTs have been investigated for their impact on CNT nanofluids' thermal conductivity. The diameter of CNTs is mainly associated with the number of layers and affects their thermal properties. In a work by Lee et al. [7], the minor Functionalized Multi-Walled Carbon Nanotubes (f-MWCNT) diameter, 10 nm, was found to boost thermal conductivity in a water-based nanofluid by up to 16% when compared to larger f-MWCNT width sizes at a concentration of 0.5 vol%. Wu et al. [8] investigated the thermal conductivity of nanofluids based on water, incorporating distinct types of CNTs, such as SWCNTs measuring 1–2 nm in diameter and MWCNTs with an 8 nm diameter.

They found that SWCNTs exhibited a more substantial enhancement in thermal conductivity, reaching approximately 40%, while MWCNTs showed a lower enhancement of only 10% at a concentration of 0.38 vol%. This suggests that SWCNTs, with their smaller diameter, are more effective in enhancing thermal conductivity in this study. Glory et al. [9] investigated the effect of ultrasonication time on conductivity enhancement. They found that longer CNTs (5 μm in length) led to a noticeable increase in thermal conductivity enhancement to 45% compared

to shorter CNTs (0.5 μm in length) when the sonication time was reduced from 700 to 50 min. The diameter and length of CNTs can impact the thermal conductivity enhancement of CNT nanofluids, with smaller-diameter CNTs and longer CNTs generally leading to higher enhancements. However, the relationship between CNT properties and thermal conductivity can be influenced by various factors, including the type of base fluid and experimental conditions.

The adjustment of MWCNT lengths was achieved through a controlled process of ball milling, yielding a noteworthy enhancement in thermal conductivity of approximately 29.5% and a temperature of 63.9 °C. In a parallel investigation, the same research group, Chen and Xie [10], delved deeper into the impact of varying CNT lengths achieved through ball milling on the silicon oil-based nanofluids thermal conductivity, which incorporated functionalized MWCNTs (f-MWCNTs). Notably, at a concentration of 0.05 vol% and a temperature of 65 °C, they recorded a peak enhancement of 27.5% after 20 h of ball milling. However, the enhancement began diminishing as the ball milling treatment extended beyond this point. Regarding the impact of CNT length, they discerned no significant alterations in thermal conductivity when the temperature was near room temperature. However, beyond 310 K, nanofluids with shorter MWCNTs exhibited higher thermal conductivity than those with longer counterparts. This observation led to the hypothesis that shorter MWCNTs are more mobile and capable of faster movement at elevated temperatures. In contrast, longer MWCNTs may tend to entangle to a greater extent. Numerous studies have highlighted the potential for achieving more excellent thermal conductivity enhancements in CNT nanofluids when employing lower inherent thermal conductivity base fluids. For instance, A notable 46% improvement in thermal conductivity was observed by Jiang et al. [11] for a nano-refrigerant containing MWCNTs distributed in R113. The 13% improvement attained in a water-based nanofluid at an analogous nanoparticle volume fraction of 0.2% was significantly outperformed by this improvement. In contrast, hybrid nanofluids featuring CNTs yielded opposing effects compared to their base fluids regarding thermal conductivity enhancement. In some instances, water-based hybrid nanofluids exhibited more remarkable thermal conductivity enhancements than their EG-based counterparts despite EG having lower inherent thermal conductivity than water [12, 13].

5 Utilization of CNT Nanofluids in Solar Applications

Over the past decade, substantial research efforts have been directed toward understanding nanofluids' fundamental principles and practicality, explicitly focusing on carbon nanotube (CNT) nanofluids within solar collector applications. This discussion will provide an extensive overview of solar thermal technology, emphasizing the potential enhancements achieved by employing CNT nanofluids as heat-absorbing fluid. Solar collectors, designed to harness solar energy, have a rich history dating back centuries.

Research efforts have also extended to evaluating the evacuated tube's thermal performance using nanofluids. Sabiha et al. [14] conducted experiments to assess the improved heat transfer by employing water-based nanofluids, including SWCNTs, as capturing media. Their study considered varying nanoparticle concentrations and mass flow. They reported that both nanoparticle concentration and mass flow significantly contributed to the application of evacuated tube solar collectors. Notably, they achieved a peak collector 93.43% efficiency with 0.2 vol% Nanofluid of SWCNT and a flow rate of 0.025 kg/s, representing a remarkable 71.84% improvement over pure water. Moreover, they observed that on cloudy days, the collector's efficiency utilizing 0.2 vol% SWCNT nanofluid surpassed water on sunny days, underlining the advantages of nanofluid-based systems in diverse weather conditions.

Theoretical investigations have also delved into the application of enclosed-type, nanofluid-using evacuated U-tube collectors. Tong et al. [15] performed a comprehensive review of U-tube collectors equipped in the U-tube with a copper fin, analyzing varying Reynold's ratios (ranging from 400 to 2000) with constant heat flux and utilizing MWCNT/water nanofluids with varying MWCNT concentrations (up to 0.24 vol%). Their results revealed an average 8% relative rise in pure water's heat transfer coefficient ratio.

Collector efficiency rapidly increased with rising radiation levels under low-radiation conditions, leveling off under high-radiation exposure. In recent research, the heating capacity and energy efficiency potential of a U-tube collector for sunlight using nanofluids have been studied by Kim et al. [16]. They investigated nanofluids containing MWCNTs spread among a combination of 20% propylene glycol and water. They also emphasized the environmental and economic benefits, estimating a reduction of coal usage by up to 131.3 kg annually and a savings of about 0.64 MW/h of electricity annually when 50 solar collectors employing nanofluids as the absorbed substance were deployed. While evacuated tubes and flat plates have played a vital role in harnessing solar energy, they are not without limitations, particularly in terms of efficiency due to the conductive and convective absorbent surface and its impedance and the working fluid, resulting in significant heat losses. To address these challenges, a novel concept emerged in the 1970s aimed at minimizing heat losses while efficiently absorbing solar energy. This innovation led to the development of direct absorption solar collectors (DASCs), a unique category of solar collectors. DASCs directly absorb solar radiation and convert it into heat, offering a promising alternative to traditional collectors. Researchers have made significant strides in understanding the complex interplay of factors affecting nanofluid behavior within various collectors, including flat-plate, evacuated tube, and direct Absorption solar collectors. From pH adjustments to the addition of surfactants and careful consideration of nanoparticle concentrations and flow rates, these studies have provided valuable insights into optimizing nanofluid-based solar collector systems. Furthermore, theoretical analyses have underscored the advantages of CNT nanofluids, particularly SWCNT-based nanofluids, over other nanofluid types and pure water in terms of energy and exergy efficiencies, as well as reductions in entropy generation and enhancements in heat transfer coefficients. These findings can potentially

revolutionize the field of solar thermal technology, offering more efficient and environmentally friendly solutions for harnessing solar energy. In particular, the remarkable performance enhancements achieved in evacuated tube solar collectors and U-tube solar collectors using CNT nanofluids have significant implications. The capability of carbon nanotube (CNT) nanofluids as absorbent media in direct absorption solar collectors offers an exciting avenue for further research and innovation in solar energy capture. As researchers continue to delve into optical characteristics and the long-term consistency of CNT with nanofluids within DASCs, the future of solar collector systems appears increasingly promising by harnessing the sun's energy more efficiently and sustainably. These developments open the door for a brighter and greener future powered by nanofluid-enhanced solar technology. The researchers prepared a nanofluid based on water with varying concentrations of MWCNTs, ranging from 0.0005 to 0.005 volume percent. They used Cetyltrimethylammonium Bromide (CTAB) as a surfactant and employed a self-assembled apparatus based on the Lambert–Beer law to measure the extinction coefficient. Surprisingly, they discovered that nanofluids with a volume fraction of 0.0005 and exceedingly low percent could completely absorb solar energy up to a depth of 10 cm. They conducted an analytical investigation to explore the impact of varying wavelengths from 200 to 2000 nm. Their findings highlighted the crucial role of MWCNT nanofluids in absorbing sunlight within the visible and near-infrared wavelength ranges, specifically from 200 to 1400 nm, a feat not achievable with pure water alone.

5.1 Photovoltaic-Thermal (PVT) Systems

Applying photovoltaic (PV) solar cells for electricity generation has seen significant growth. While PV cells are known for their low greenhouse gas emissions during electricity production, the commercial versions often suffer from relatively modest efficiencies. Moreover, these efficiencies tend to decrease as the operating temperature of the cells rises. To address this challenge, substantial efforts have been devoted to managing the thermal conditions of PV cells, ensuring they operate at optimal temperatures for peak performance. Various advanced techniques, such as Heat pipes, PCM, and active cooling techniques, have tackled this thermal management issue. One efficient approach in this sector is PV/T (Photovoltaic/Thermal) systems.

The heat produced by the PV cells in PV/T systems is used for focused thermal functions, such as heating water or air. Nanofluids have been used as the operating liquids in PV/T systems to increase their efficiency further their efficiency.

Alous et al. [17] conducted an experimental study on a Photovoltaic/Thermal (PV/T) system. This system incorporated a sheet and tube heat exchanger connected to the rear of a monocrystalline PV cell. Three different coolants were employed: water, graphene nanoplatelet/water, and MWCNT/water nanofluids, all at a concentration of 0.5% by weight. The results demonstrated energy efficiency enhancements of

53.4%, 57.2%, and 63.1% when using water, MWCNT/water, and graphene/water nanofluids, respectively. Researchers monitored PV cell temperatures at different times of the day. It was shown that using nanofluids during hours of higher solar irradiation was more advantageous since the temperature differential between the cooling conditions and the reference condition grew during these hours. Compared to water, the entropy generation in the system was reduced by 0.82%, 1.23%, and 2.88% when these nanofluids were used as coolants.

The efficiency of PVT systems, particularly in comparison to standalone PV systems, is a multifaceted aspect influenced by various factors. Beyond the intrinsic nature of the nanofluid used, the operational conditions play a pivotal role in determining the enhancement rate in PV/T systems, especially when juxtaposed with standalone PV systems. This intricate relationship was investigated by Sangeetha et al. [18], who explored the impact of three different nanofluids—CuO/water, Al₂O₃/water, and MWCNT/water—on a PV/T system. The study revealed that the highest efficiency improvement occurred around mid-day, aligning with peak solar irradiance. This finding underscores the significance of effective cooling mechanisms for PV panels, particularly in regions characterized by intense sunlight and elevated temperatures.

MWCNT/water nanofluids with concentrations ranging from 0% to 0.3% by volume were used in an inquiry by Abdallah et al. [19] in a PV/T system. Intriguingly, the study identified the concentration of 0.075% by volume as the maximum average efficiency enhancement point. This shows that there may be an ideal concentration where changes in specific heat, thermal conductivity, and viscosity change combine to produce the best outcomes. The study underscores the nuanced interplay between nanofluid composition and concentration in achieving optimal PV/T system efficiency. Moving beyond active cooling methods, passive thermal management strategies have garnered attention, particularly in the context of PV cell temperature control. Among these, using phase change materials (PCMs) is noteworthy. This suggests the promising potential of MWCNT-based nanofluids in passive thermal management strategies, presenting an avenue for improving the overall efficiency and longevity of PV/T systems.

In conclusion, the efficiency of PV/T systems is intricately linked to the interplay of nanofluid characteristics, operating conditions, and cooling strategies. As research in this field progresses, a comprehensive understanding of these factors will be crucial for advancing the efficiency and applicability of PV/T systems in diverse environmental contexts.

5.2 Solar Collector

To transform solar irradiance into helpful heat energy, solar collectors are essential. The thermophysical characteristics of the fluid being significantly used impact how well these collectors perform. Different nanofluids, including those comprising metallic, metal oxide, hybrid, and carbon-based nanoparticles, have been used to

increase the efficiency of solar collectors. Carbon-based nanofluids have garnered considerable interest due to their exceptional heat transfer properties, making them popular for improving solar collector efficiency. Using MWCNT/water nanofluids in a U-tube solar collector was the subject of a significant study that tested different concentrations of MWCNTs in water, ranging from 0.06% to 0.24% by volume. It found that the highest enhancement in efficiency was achieved with a 0.24% concentration. Compared to using water as the operating fluid, employing the nanofluid resulted in an average heat transfer enhancement of 8% across various Reynolds numbers. Importantly, this transition to nanofluid usage also had positive environmental implications. A thorough environmental analysis revealed that when 50 such collectors were employed, replacing water with nanofluid led to annual reductions of 1600 kg and 5.3 kg in Carbon Dioxide and Sulfur Dioxide emissions, respectively. As previously mentioned, carbon-based nanofluids, particularly those containing Carbon Nanotubes (CNTs), exhibit superior optical properties compared to pure fluids. This makes them ideal for use in direct-absorption solar collectors.

However, it is worth noting that higher nanofluid concentrations result in more excellent Absorption of solar radiation at the collector's top, and the subsequent temperature rise can lead to higher heat losses. Interestingly, it has been observed that SWCNTs offer even more significant improvements in thermal conductivity compared to MWCNTs. Said et al. [20] used volume fractions of 0.1% to 0.3% of SWCNT/water nanofluid in a flat plate solar collector. The energy effectiveness of the collector was found to be 89.26% and 95.12%, respectively, when employing nanofluids with concentrations of 0.1% and 0.3% at a mass flow rate of 0.5 kg/min, compared to just 42.07% when using water. The effectiveness of an evacuated tube using SWCNT/water nanofluid at three distinct concentrations and varied mass flow rates was investigated by Sabiha et al. [21]. The highest collector efficiency observed was 93.43%, achieved at a mass flow rate of 0.025 kg/s and a volumetric nanofluid concentration of 0.2%.

A further inquiry by Mahbulul et al. [22] demonstrated the potential of SWCNT/water nanofluid in improving evacuated tube solar collecting' efficiency. Carbon nanotube-containing nanofluids have shown promise in high-temperature collectors. A linear Fresnel collector was numerically studied by Ghodbane et al. [23], employing MWCNT/diathermic oil (DW) nanofluid as the working fluid.

5.3 Solar Pond

Solar ponds featuring a layered salt solution structure are innovative systems that capture and preserve solar energy. These ponds typically consist of layers with varying salt concentrations, reaching saturation at 1–2 m. The Non-Convicting Zone (NCZ)'s upper layer contains water with lower salinity and density than the Lower Convicting Zone (LCZ) beneath it. The increased salt concentration in the LCZ inhibits free convection, effectively trapping and storing the energy from the sunlight hits over here. The ratio of the total energy collected from a solar pond to its

predicted capacity is known as its efficiency, and it depends on several variables, including the heat recovery temperature and the specific layers from which energy is extracted. By harnessing nanofluids in solar pond tubes, it becomes possible to significantly enhance heat extraction efficiency from these innovative solar energy storage systems, thereby increasing their practicality and effectiveness in various applications.

5.4 Generation of Solar Steam

Solar energy holds great potential for various applications, including generating steam required for seawater desalination, waste sterilization, and power generation. Nanotechnology has played a pivotal role in significantly enhancing the performance of these solar steam generation systems. Using appropriate nanofluids in these systems can lead to substantial improvements in efficiency. Research findings from a study have demonstrated that using plasmonic nanofluids containing gold particles can result in an approximate 300% increase in system efficiency. Regarding solar steam generation, nanofluids containing Carbon Nanotubes (CNTs) are particularly promising choices. Wang et al. [24] conducted a study where they employed SWCNT-based nanofluids in direct gas creation from a solar energy setup. For instance, when using a nanofluid with a concentration of 19.04×10^{-4} vol% and solar power for lighting 10 Suns, this system achieved an impressive efficiency of 46.8%. In contrast, if pure water were employed in the system, the efficiency would not exceed 7.8%. This substantial improvement underscores the remarkable potential of nanofluids containing CNTs in enhancing the performance of solar power systems. The study concentrated on applying nanofluids with CNTs in solar energy systems, which has yielded significant modifications in system performance. The extent of enhancement depends on several elements, including the kind and concentration of CNTs used, the specific system under investigation, and the operating conditions employed.

6 Conclusion

According to our in-depth literature research, preserving a uniform dispersion and long-term stability are essential for the CNT nanofluids to keep their superior thermal characteristics. The goal of maintaining the conditions mentioned above is challenging due to the hydrophobic nature of the CNT against most fluids and the potent van der Waals interaction among CNT nanoparticles. Nevertheless, many scholars have made countless attempts to meet those requirements.

However, it should be highlighted that numerous obstacles must be found and overcome for various CNT nanofluid applications, particularly solar devices. Two significant barriers to its commercialization are the stability and production cost.

Because of this, it is necessary to redesign the majority of solar collectors to accommodate the practical usage of nanofluid in water heating systems used in home and industrial settings. By overcoming these obstacles, it is anticipated that nanofluids will have a significant impact on both the engineering and industrial sectors, as well as improve people's quality of life.

To attain good thermal characteristics of the CNT nanofluids for an extended period, homogeneous dispersion and long-term stability must be maintained. It isn't easy to uphold the criterion above because of the CNTs' hydrophobicity toward most fluids and their robust van der Waals interaction. Chemical treatments (covalent and non-covalent functionalization) and physical treatments are the two main ways to stabilize CNTs in any base fluid.

Depending on the base fluids, CNT concentrations, and CNT kinds utilized, each treatment results in varying stability periods, according to prior studies' findings. For comparing covalent functionalization to non-covalent functionalization, it was discovered that covalent functionalization was more effective at maintaining the stability of CNT nanofluids. Physical treatment is frequently applied following chemical treatment to produce homogeneous solutions. In this regard, deagglomerating CNTs in suspensions using ultrasonication was a successful technique. The long-term stability and homogeneity of CNT nanofluids were shown to be maintained by covalent functionalization and ultrasonication, respectively. Still, the effects of each method's prolonged treatment on these properties were adverse.

References

1. Choi, S. U.S., Eastman, J. A.: Enhancing Thermal Conductivity of Fluids with Nanoparticles. No. ANL/MSD/CP-84938; CONF-951135-29. Argonne National Lab. (ANL), Argonne, IL (United States) (1995)
2. Hong, H., Wensel, J., Roy, W.: Heat transfer nano lubricant and nano grease based on carbon nanotube. *ECS Trans.* **2**(12), 133 (2007)
3. Liu, MinSheng, Lin, M.C., Wang, ChiChuan: Enhancements of thermal conductivities with Cu, CuO, and carbon nanotube nanofluids and application of MWNT/water nanofluid on a water chiller system. *Nanoscale Res. Lett.* **6**, 1–13 (2011)
4. Tanshen, M.R., et al.: Effect of functionalized MWCNTs/water nanofluids on thermal resistance and pressure fluctuation characteristics in oscillating heat pipe. *Int. Commun. Heat Mass Transfer* **48**, 93–98 (2013)
5. Qu, J., et al.: Photo-thermal conversion characteristics of MWCNT-H₂O nanofluids for direct solar thermal energy absorption applications. *Appl. Therm. Eng.* **124**, 486–493 (2017)
6. Han, Z.H., et al.: Application of hybrid sphere/carbon nanotube particles in nanofluids. *Nanotechnology* **18**(10), 105701 (2007)
7. Lee, K.J., Yoon, S.H., Jang, J.: Carbon nanofibers: a novel nanofiller for nanofluid applications. *Small* **3**(7), 1209–1213 (2007)
8. Wu, G.S., et al.: Thermal conductivity measurement for carbon-nanotube suspensions with 3 ω method. *Adv. Mater. Res.* **60**, 394–398 (2009)
9. Glory, J., Bonetti, M., Helezen, M., Mayne-L'Hermite, M., & Reynaud, C.: Thermal and electrical conductivities of water-based nanofluids prepared with long multiwalled carbon nanotubes. *J. Appl. Phys.* **103**(9) (2008)

10. Chen, L., Xie, H.: Silicon oil based multiwalled carbon nanotubes nanofluid with optimized thermal conductivity enhancement. *Colloids Surf. A* **352**, 136–140 (2009)
11. Jiang, W., Ding, G., Peng, H.: Measurement and model on thermal conductivities of carbon nanotube nano refrigerants. *Int. J. Therm. Sci.* **48**, 1108–1115 (2009)
12. Zubir, M.N.M., Badarudin, A., Kazi, S., Huang, N.M., Misran, M., Sadeghinezhad, E., et al.: Experimental investigation on the use of reduced graphene oxide and its hybrid complexes in improving closed conduit turbulent forced convective heat transfer. *Exp. Therm. Fluid Sci.* **66**, 290–303 (2015)
13. Hong, H., Wright, B., Wensel, J., Jin, S., Ye, X.R., Roy, W.: Enhanced thermal conductivity by the magnetic field in heat transfer nanofluids containing carbon nanotube. *Synth. Met.* **157**, 437–440 (2007)
14. Sabiha, M., Saidur, R., Hassani, S., Said, Z., Mekhilef, S.: Energy performance of an evacuated tube solar collector using single-walled carbon nanotubes nanofluids. *Energy Convers. Manage.* **105**, 1377–1388 (2015)
15. Tong, Y., Kim, J., Cho, H.: Effects of thermal performance of enclosed-type evacuated U-tube solar collector with multi-walled carbon nanotube/water nanofluid. *Renew. Energy* **83**, 463–473 (2015)
16. Kim, H., Ham, J., Park, C., Cho, H.: Theoretical investigation of the efficiency of a U-tube solar collector using various nanofluids. *Energy* **94**, 497–507 (2016)
17. Alous, S., Kayfeci, M., Uysal, A.: Experimental investigations of using MWCNTs and graphene nanoplatelets water-based nanofluids as coolants in PVT systems. *Appl. Therm. Eng.* **162**, 114265 (2019)
18. Sangeetha, M., Manigandan, S., Chaichan, M.T., Kumar, V.: Progress of MWCNT, Al₂O₃, and CuO with water enhance the photovoltaic thermal system. *Int. J. Energy Res.* **44**, 821–832 (2020)
19. Abdallah, S.R., Saidani-Scott, H., Abdellatif, O.E.: Performance analysis for hybrid PV/T system using low concentration MWCNT (water-based) nanofluid. *Sol. Energy* **181**, 108–115 (2019)
20. Said, Z., Saidur, R., Sabiha, M.A., Rahim, N.A., Anisur, M.R.: Thermophysical properties of Single Wall carbon nanotubes and its effect on exergy efficiency of a flat plate solar collector. *Sol. Energy* **115**, 757–769 (2015). <https://doi.org/10.1016/j.solener.2015.02.037>
21. Sabiha, M.A., Saidur, R., Hassani, S., Said, Z., Mekhilef, S.: Energy performance of an evacuated tube solar collector using single-walled carbon nanotubes nanofluids. *Energy Convers. Manag.* **105**, 1377–1388 (2015)
22. Mahbubul, I.M., Khan, M.M.A., Ibrahim, N.I., Ali, H.M., Al-Sulaiman, F.A., Saidur, R.: Carbon nanotube nanofluid enhances the efficiency of evacuated tube solar collector. *Renew. Energy* **121**, 36–44 (2018)
23. Ghodbane, M., Said, Z., Hachicha, A.A., Boumeddane, B.: Performance assessment of linear Fresnel solar reflector using MWCNTs/DW nanofluids. *Renew. Energy* **151**, 43–56 (2020)
24. Wang, X., He, Y., Cheng, G., Shi, L., Liu, X., Zhu, J.: Direct vapor generation through localized solar heating via carbon-nanotube nanofluid. *Energy Convers. Manag.* **130**, 176–183 (2016)

Recent Advancements in Conducting Polymers for Biomedical Sensors



Aniruddh Mehra, Mayankkumar Chaudhary, Filipe De Souza,
and Ram K. Gupta

Abstract The healthcare system heavily relies on quantitative analyses of samples, including blood work, laboratory tests, vitals, imaging, health risk assessments, and health records. However, trends in point-of-care diagnostics and accurate, real-time monitoring of patient's physiological parameters must meet demands to cut healthcare expenditures, optimize treatment efficiency, and ameliorate patient outcomes. One revolutionary solution in biomedical technology and diagnostic bio-instrumentation is the biomedical sensor, an analytical device capable of transducing biological signals into electrical signals to detect and quantify chemical substances or biological molecules with robust sensitivity. Conducting polymers (CPs) are a pivotal advancement in biosensor design due to their biocompatibility, inherent and tunable electroactivity, selectivity, and inexpensive synthesis. CP-based biosensors pave the way for minimally invasive, continuous patient monitoring, wearable, flexible, and implantable applications, personalized diagnoses, point-of-care treatments, early disease interventions, and affordable devices for underserved populations. This comprehensive review will cover different types, and characterization of conducting polymers commonly used in biosensors, followed by an introduction to types of biosensors, the requirements and challenges of biomedical sensor design, and recent advancements in the field, the lattermost focusing on the benefits of employing conducting polymers. Finally, CP-based biosensors for pathogen, DNA, protein, and early disease detection are reviewed.

Keywords Conducting polymers · Biosensor · Detection · Biomedical · Application

A. Mehra
Nova Southeastern University, Fort Lauderdale, FL 33328, USA

A. Mehra · M. Chaudhary · R. K. Gupta (✉)
Department of Chemistry, Pittsburg State University, Pittsburg, KS 66762, USA
e-mail: ramguptamsu@gmail.com

M. Chaudhary · F. De Souza · R. K. Gupta
National Institute for Materials Advancement, Pittsburg State University, Pittsburg, KS 66762,
USA

1 Introduction

New technological developments in biomedical sensing are rapidly taking over the healthcare industry. By definition, a biomedical sensor is a device made for measuring chemical, physical, and biological processes, predominantly biomolecules, known as (bio)analytes, and translating their detection into electrical signals that provide crucial monitoring data for medical applications. Biomedical sensors are generally utilized to detect specific physical or chemical qualities, such as temperature, pH, blood glucose levels, etc., while biosensors strictly detect bioanalytes. To this extent, a biomedical sensor can also be a biosensor, and this review will use the terms interchangeably. Nonetheless, a biosensor is generally made up of three main components: (i) a substrate with high mechanical flexibility to act as the backbone for the system; (ii) electrodes for exporting the electronic signals; and (iii) sensing elements/bioreceptors to capture and recognize analytes [1–3]. Figure 1 depicts the underlying fundamentals of a biomedical sensor. The benefit of biomedical sensors is their analytical versatility, as they can also report data on electrolytic levels, namely Na^+ , K^+ , NH_4^+ , Ca^{2+} , H^+ (pH), uric acid, lactate, ascorbic acid, and urea metabolites. In addition, biomedical sensors can supply real-time and long-term health data monitoring through wearable applications, allowing healthcare workers to formulate early-stage diagnoses for potential diseases and patients to employ preventative measures and observe their health and lifestyle holistically [4–6].

Several key aspects are considered for a biosensor to display a satisfactory performance which are sensitivity, selectivity, speed, stability, reproducibility, detection limit, biocompatibility, portability, integration easiness, durability, and cost-effectiveness. Sensitivity is related to the biosensor's capability to detect an analyte in small concentrations, all while providing outstanding accuracy. Selectivity lies in the biosensor's ability to identify a specific analyte with negligible interference from other components in the media. The speed of the measurement is an essential aspect of a quick diagnosis to enable a fast treatment response. Stability and reproducibility lie in the biosensor's consistency in providing accurate results over time which is a core aspect of long-term analysis and data reliability. The detection limit is the lowest concentration of a given analyte that can be accurately detected. Hence, a biosensor is desired to present a low detection limit as it enables it to measure trace

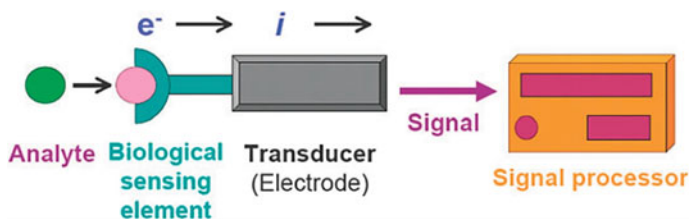


Fig. 1 A basic principle of how a biosensor transduces biological signals into electrical signals. Adapted with permission [4]. Copyright 2021, American Chemical Society

concentrations of an analyte. To avoid triggering an allergic reaction or inflammation, a biosensor should also be biocompatible with the tissue or biological sample with which it enters contact. Thus, there are multitudes of materials used in biomedical sensors, but most fall into the categories of either nanomaterials or polymers. Nanomaterials, through their quantum size effect, can enhance molecule adsorption, signal response speed, and electrode stability and come in different structures, such as nanospheres, nonporous structures, nanotubes, nanowires, or combined with other nanomaterials to form nanocomposites. Specifically, metallic nanomaterials consist of gold nanoparticles (AuNPs), metal-oxide derivatives, noble metals, and alloys, all with different properties and roles. By the same token, bimetallic nanocrystals possess stability and hefty catalytic properties, while microporous nanomaterials can supplement interfaces with their sizeable effective area and capacitive properties.

Regarding polymeric materials in biosensors, there are three most common types of polymers are chitosan, cellulose membrane, and conducting polymers (CPs). Chitosan offers biocompatibility, adhesive forces, film-formability, and, thus, a powerful force to bind proteins and enzymes. The glucose-based cellulose polymer is highly transparent, dimensionally stable, easily modifiable, and suitable for covalent bonding, physical adsorption, and immobilization. Moreover, since plant cell walls are made of cellulose, it displays excellent biocompatibility and can easily interact and detect biological substances such as urea, lactic acid, glucose, ribonucleic acids (RNAs), deoxyribonucleic acids (DNAs), amino acids, cholesterol, and proteins. Finally, conductive polymers, covered in depth later, are materials whose inherent properties permit them to transmit electrical signals dependent on responses from biological stimuli. Though both types of materials have their roles, a combination of nanomaterials and polymers provides greater biosensor efficiency, sensitivity, and stability than either alone, often referred to as a synergy effect [7]. Conductive metals have often been used to power analytical devices such as biomedical sensors because of their widespread accessibility. However, they can incite an immunological response through corrosion and imminent contact with some proteins in the skin, blood, and connective tissue [8]. CPs has grown as its features not only mimic semiconductors and metals in their electric, electronic, magnetic, and optical properties through delocalization of π -electrons in polymer double bonds (Fig. 2a) but, in some cases, can also include providing biodegradability and biocompatibility in vivo and in vitro. Molecularly, CPs present multiple functional groups that can augment the loading quantity of an enzyme, a trait favorable for biosensor production. Another advantage of CPs is their increased sensitivity and versatile nature. CPs can be covalently or physically modified by multiple biomaterials, such as proteins, nucleic acids, or neurotransmitters, or doped/hybridized with carbon nanotubes, graphene, metal nanoparticles, or metal oxide nanoparticles to produce a desired biosensor with improved catalytic activity, adsorbent, and interactive properties. Moreover, the polymers' adaptability with nanomaterials and hydrogels allows for the enhancement of surface area and electrical conductivity, providing better sensitivity and response times. Such attributes, combined with low cost, stability, and ease of preparation, have enabled CPs to be applied as biosensors in the fields of

healthcare, DNA sensors, immunosensors, food analysis, and environmental monitoring. Ongoing projects in the biomedical industry involving CPs include tissue engineering and regeneration, drug delivery, biosensing, and bioimaging. The most used CPs are polyacetylene (PA), polypyrrole (PPy), polyaniline (PANI), polythiophene (PTh), poly(3,4-ethylene dioxythiophene) (PEDOT), polyfluorenes (PF), poly(*p*-phenylene) (PPP), poly(*p*-phenylenevinylene) (PPV), and poly(*p*-phenylene ethynylene) (PPE) (Fig. 2b) [9–11].

This chapter covers CPs, biomedical sensors, and the role of CPs in the procurement of biomedical sensors. First, the basics of CPs are discussed, followed by their

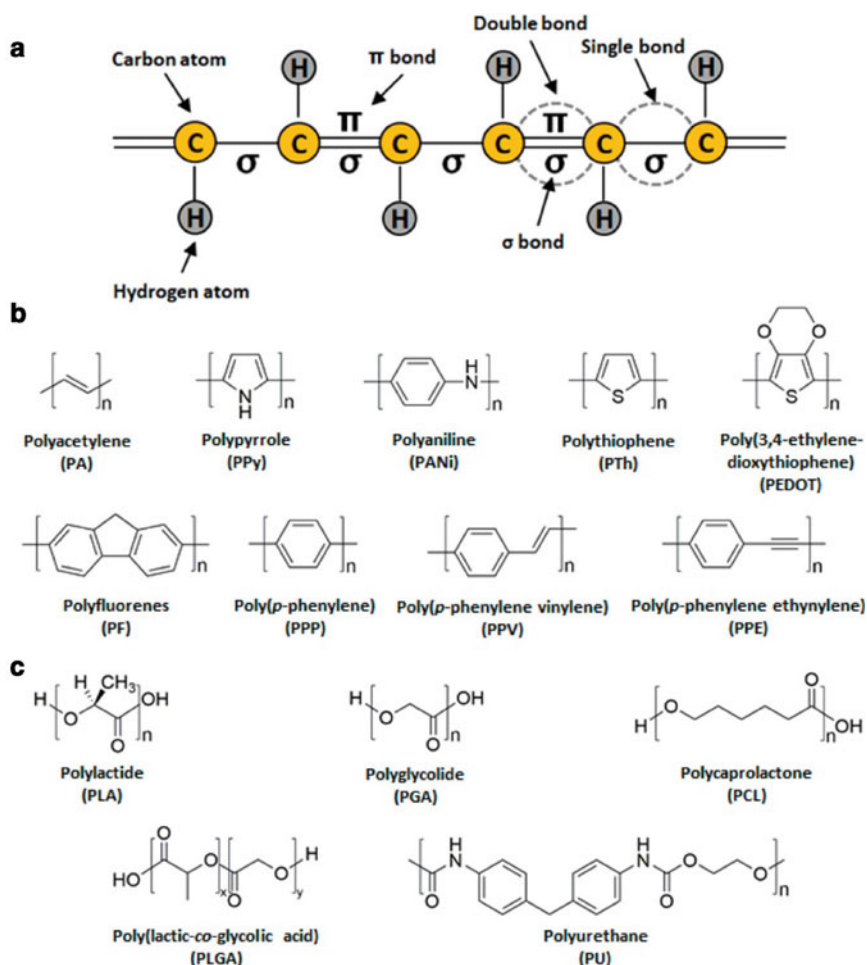


Fig. 2 Molecular structure for general and most common CPs. **a** Molecular structure depicting the process of electron delocalization on CPs, which accounts for the flow of electrons and, thus, electrical conductivity. **b** Chemical structures for some of the most common CPs. Adapted with permission [11]. Copyright 2018, American Chemical Society

general and specific characteristics of various known CPs, developing an understanding of why they are favorable materials in current scientific research. The succeeding section dives into detail about biomedical sensors, mainly analyzing types of biosensors, requirements and challenges in biomedical sensor design, and advancement, outlook, and obstacles. Finally, this newfound knowledge is accumulated to explore real-world applications of CP-based biomedical sensors, i.e., biosensors specific for the detection of pathogens, DNA, proteins, and early stages of disease.

2 Basics of Conducting Polymers

A polymer is a chain of identical monomers, building blocks of a particular substance. Thus, a conducting polymer is a chain of electrically potent monomers that resemble inorganic semiconductors in their electrical and optical properties yet retain their lightweight and corrosion-resistant polymeric properties [12–14]. Other advantages of conducting polymers are their easily modifiable chemical and charge transfer properties to match a desired function, relatively straightforward and inexpensive production procedures, thermal and environmental stability, electromagnetic shielding, microwave absorption, and ability to capture and release biomolecules. These characteristics give them preference in applications such as (bio)sensor designing, electronics, solar cells, transducers, plastic batteries, light emitting devices (LEDs), supercapacitors/conductors, etc. [15]. In terms of the molecular structure that confers these advantages, CPs comprise conjugated carbon chains with alternating single and double bonds of polyenes or aromatic rings, giving the backbone the conjugated status and the mechanical property of a polymer [5]. While solubility and processability are dependent on attached side chains, the electrical/charge-carrying and optical behaviors that mimic semiconductors/metals come from the delocalized, polarized, and electron-dense π bonds in the main chains. Apart from these electrical properties, CPs also possess optical and electrochemical properties. The optical properties include electroluminescence, electrochromic and photochromic effects. Electroluminescence is an organic and inorganic semiconductors process that generates light via electrical excitation. The electrochromic aspect is the visible color change through reversible redox procedures, generally affected by excitation/ionization impurities, presence of phonons, strain factor, recombination excitons, degree of anisotropy, conjugation length, and topochemical reaction (UV, Gamma, X-ray radiation). Polyaniline, polypyrrole, PEDOT, and PEDOT: PSS, polymers all display photochromic effects [16]. On the other hand, the electrochemical properties of CPs include reversible oxidation and reduction, pseudo capacitance, swelling/deswelling, and electrochromism. Reversible oxidation and reduction reactions (redox) essentially modify polymers into either their conductive or pristine/undoped states through the loss of electrons (oxidation) or gain of electrons (reduction). This mechanism provides the underlying functionality for polymer-based sensors and capacitors. Pseudo capacitance is the process of storing charge in electrodes through oxidation/

reduction reactions rather than absorption of electrolyte ions on electrodes. Thus, this method can increase the specific capacitance and energy density for applications compared to the traditional electrochemical double-layer capacitors. Finally, the swelling/de-swelling of a conducting polymer can be attributed to the notion that CPs can change these volumetric dimensions based on different redox states. As a result, such a process can be used to make actuators from CPs that drive mechanisms in systems such as sensors [16].

When discussing conducting polymers, the term “doping” is almost always referred to. Doping stabilizes the conjugation of the double bonds in polymer chains and either reduces or oxidizes the main chain through Lewis’s acids or bases, known as doping agents or dopants. Since the organic state of conducting polymers is not sufficiently conductive, doping allows the π -electrons of the double bonds to get ousted and flow through the polymer chain. This results in the procurement of charge carriers like polarons, bipolarons, and solitons; augmentation of the solubility, processability, stability, and, most importantly, electrical conductivity of a polymer; and transition from an insulative state to a metallic state. The techniques to apply doping include electrochemical, chemical, in-situ, radiation-induced, or charge-injection, but electrochemical and chemical methods are the most common due to low cost and feasibility. Doping, or even de-doping, can be acted on conducting polymers through either positive-doping or negative-doping. The p-doping method enables oxidation and movement of electrons from the polymer’s highest occupied molecular orbital (HOMO) to the doping agent, hence the loss of electrons. The n-doping method is the reverse, as it transfers electrons from the doping agent to the lowest unoccupied molecular orbital (LUMO), hence the addition of electrons and improved electrical conductivity. Therefore, the molecular/monomer arrangement, length of a polymer chain, type of dopant, concentration of dopant, as well as environmental conditions can all be tuned to determine the level of conductivity for a conducting polymer [12–15]. To appreciate the importance and impact, conducting polymers have had in countless industries since their discovery, Heeger, MacDiarmid, and Shirakawa, who established the effects of CPs and doping, were esteemed the Nobel Prize in the year 2000 [12].

2.1 Types of Conducting Polymers

The following are the most common types of conducting polymers, and a brief overview of these polymers and their properties is depicted in Fig. 3. Such CPs can exist as functionalized CPs, CP nanostructures (nanowires, nanotubes, microspheres), porous CPs, CP nanocomposites (carbon composites, metal oxide nanoparticle composites), conducting copolymers, and CP hydrogels [3].


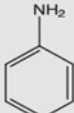
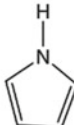
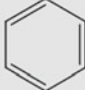
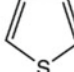


| CPs | Monomer unit | Synthesis techniques | Properties | Morphology | Applications |
|-------|--|---|--|---|---|
| PA |  | Chemical, metathesis, high pressure polymerization and electrochemical method | Electrical conducting, optical and magnetic property | Exists as foam, film, crystalline, powder | Electrical conductors, semiconducting devices, rechargeable batteries, solar cells, battery electrodes. |
| PANI |  | Chemical, plasma polymerization and electrochemical method | Wettability, thermal and environmental stability, Electrical conducting, Optical, mechanical and magnetic property | Exists as Film, Globules, fibrils, nanotubes, nanospheres, nanofibers, nanowires, microtubes, nanoparticles | Electrochromic glass, super capacitors, Flexible electrode, LEDs, sensors, flexible electrode and conductive fibers |
| PPy |  | Chemical and electrochemical method | Electrical conducting, Mechanical, optical, microwave absorbing property, thermal & environmental stability | Exists as Films, nanowires, nanospheres, nanoribbons & nanoplates | Medical diagnosis, fertilizer industries, microwave shielding, batteries, super capacitors and corrosion protection |
| PPP |  | Chemical method, metal catalyzed coupling reaction | Electrical conducting property, electroluminescent behavior | Exists as wires and fibers. | LEDs, energy storage, catalyst and sensors |
| PT |  | Chemical and electrochemical method | Electrical conducting property, electrochromic, optical property, thermal & environmental stability | Exists as film, Nanofibers, nanospheres, nanoparticles & nanoribbons | Super capacitor, antistatic coating, electromagnetic shielding, LEDs, memory devices, energy storage, sensors |
| PPV |  | Chemical, electrochemical and metathesis method | Electrical conducting property, optical property, photoluminescence, environmental stability, | Exists as Film and fibers | Photodiodes, LED, transistors, photovoltaic cell and electro photography |
| PEDOT |  | Chemical and electrochemical method | Electrical conducting, optical property, thermal stability, optoelectronic property | Exists as film, nano-hybrid, Nanowires, nanofibers & nanotubes | Sensors, antistatic layers coating, electroluminescent lamps, energy storage, capacitors, food & drug analysis |

Fig. 3 A comprehensive review of types of conducting polymers, molecular units for visualization, synthesis technique, properties, state of existence, and application. Adapted with permission [15]. Copyright 2021, John Wiley and Sons

2.1.1 I. Polyaniline

Polyaniline (PANI) is one of the most studied conducting polymers with immense environmental, chemical, and thermal stability, high tunable conductivity, and is comparatively simple and inexpensive to synthesize. PANI is found in the four states of leucoemeraldine base, pernigraniline base, emeraldine base, and emeraldine salt, the first two of which are insulating states and the second two are conducting states through doping/de-doping. With an electrical conductivity of 10–100 S/cm (Siemens per centimeter, the unit for measuring conductivity), raw PANI has been widely used in corrosion protection, circuit board manufacturing, and pH sensors. In contrast,

doped PANI has been used in conducting material, electromagnetic shielding, electrochromic glass, supercapacitors, flexible electrodes, LEDs, sensors, and conductive fibers. It can be synthesized through either electropolymerization, (oxidative) chemical polymerization, or the plasma polymerization method, with chemical oxidation the most common [13–15].

2.1.2 II. Polypyrrole

Polypyrrole (PPy) is a CP with a conductivity near 10–1000 (average: 300) S/cm (depending on dopant and forms) and presents strong redox properties, towering conductivity, electrical and optical properties, water solubility, environmental, thermal, and oxidized stability, biocompatibility, nontoxicity, and is commercially accessible. These properties not only make it suitable for supercapacitors, semiconductors, electrochemical sensors, batteries, microwave shielding, and corrosion protection but also allow for combination with other polymers to be used as efficient wearable and non-wearable sensors to detect organic compounds, gasses, disease, and bioanalytes like cholesterol, bilirubin, and glucose. PPy is synthesized through either the electrochemical method, which is most often used to produce highly conductive PPy, or chemical oxidative polymerization. Polypyrrole can also be prepared by the chemical oxidation of a pyrrole monomer with hydrogen peroxide [14, 15].

2.1.3 III. Poly (3,4-Ethylene Dioxythiophene) (PEDOT)

PEDOT, a 3,4-ethylene dioxy thiophene polymer, confers transparency in thin, oxidized films, increased stability, biocompatibility, large surface area, and a fast electron transfer rate. Thus, PEDOT displays a high conductivity for thin films at 6,259 S/cm and 8,797 S/cm for a single-crystal nanowire. Although PEDOT itself is not soluble in water, combining it with a polyelectrolyte, namely polysulfonates (PSS), drives the matrix to be more soluble in aqueous environments, conductible, mechanically flexible, and thermally stable in the long term. PEDOT can be used in antistatic coating, conductive shells, organic LEDs, nano-fiber electrodes, solar cells, cathodes, transparent electrodes, and semiconductors. Due to the enhanced biocompatibility, it also has applications in bone, cardiac, and neural tissue engineering, drug delivery, biosensors, and bioelectronics. PEDOT is synthesized through one of 3 methods: electrochemical polymerization (electropolymerization), oxidative chemical polymerization, or transition metal-mediated coupling [14, 15].

2.1.4 IV. Polyacetylene

Polyacetylene (PA), a polymer created through the polymerization of acetylene, offers efficient electrical conductivity, photoconductivity, liquid crystal properties, chiral recognition, and optical and magnetic properties (through higher doping

concentrations), making it one of the core structures found in many conducting polymers. Doping is necessary for PA as its conductivity is 10^{-5} S/cm without any doping and in the magnitude of 10^2 – 10^3 S/cm with doping. PA in both its doped and undoped form has been applied for electrical conductors, semiconductors, rechargeable batteries, solar cells, and battery electrodes. The synthesis of polyacetylene can be achieved through many methods, including catalytic polymerization, non-catalytic polymerization, catalytic polymerization through other polymers, pre-cursor assisted synthesis, and interfacial polymerization, which is the most common polymerization method, along with chemical polymerization. Both catalytic and interfacial polymerization utilize Ziegler–Natta catalysts as it is highly soluble in organic solvents and is quite selective. PA can also be synthesized through metathesis polymerization, electrochemical polymerization, and high-pressure polymerization, which, along with reaction mediums and type of catalyst, determine the attributes of PA [14, 15].

2.1.5 V. Polythiophene

Polythiophene (PT) is a conducting polymer with thermal and environmental stability and relatively high optical properties. Nanosized PT is used for its great surface area and consistent porosity. The applications of this polymer often include electrical supercapacitors, polymer LEDs, electrochromics, photoresists, antistatic coatings, non-linear optics, sensors, batteries, electromagnetic shields, solar cells, transistors, and imaging materials. Polythiophene can be synthesized through green synthesis, microfluid system synthesis, chemical polymerization, or electrochemical polymerization; however, electrochemical synthesis is the most common as the conductivity of PT rises to 100 S/cm with this method compared to conductivity with a magnitude of 10^{-2} S/cm via (oxidative) chemical polymerization [14, 15].

2.2 *Characterization of Conducting Polymers*

As displayed in Fig. 3, there are many types of conducting polymers used. Therefore, there are numerous techniques used to characterize CPs. The first method of dielectric relaxation spectroscopy and electron paramagnetic resonance is used to analyze the electric properties of CPs, namely PANI and its composites. The analysis is done by compressing the powder form of such polymers into pellets. Next, Fourier Transform Infra-Red Spectroscopy (FT-IR) and UV–vis are employed to determine which functional groups a polymer exhibits [15]. The mechanism behind FT-IR involves molecules absorbing infrared radiation at specific wavelengths from a spectrometer to reach an excited molecular state from the ground state. The vibrational energy gap between these states affects the frequency of the absorption peak, while the intensity of the peaks reflects changes in the molecule's dipole moment. Thus, an FT-IR graph can analyze the structural information of a molecule, specifically during the processing of conducting polymers. UV–vis utilizes visible light rather than infrared

radiation for the excitation of molecules. Third, the analyses which measure properties as a function of temperature include differential scanning calorimetry (DSC) and thermo-gravimetric analysis (TGA); DSC displays the change in heat capacity as a function of temperature while TGA shows material weight as a function of temperature [15]. In addition, X-ray diffraction (XRD) techniques are used not only for quantitative and qualitative analyses of crystalline structures but also for polymer nanocomposites. XRD can relay amorphous nanocomposite crystalline arrangement, bond nature, and changes in microstructure and interlayer spacing [17]. Likewise, the morphological techniques of scanning electron microscopy (SEM) and transmission electron microscopy (TEM) can be implemented. SEM produces images of the surface of a material, but TEM gives information on the topography, internal structure, spatial distribution, and defect visualization of a material. Finally, the last characterization technique most often used is electrical resistivity. Using a probe station, a direct-current source, an ammeter, and a voltmeter, two of the four probes produce a current, while the other two measure the voltage of a material.

Some other useful characterization techniques include cyclic voltammetry (CV), optical characterization of conducting polymers, nuclear magnetic resonance (NMR), gel permeation chromatography, Raman Analysis, temperature, electric field and magnetic susceptibility, and electroluminescence. Markedly, CV is used in the oxidation and reduction processes in conducting polymer development; NMR provides chain orientation, molecular motion, and structure confirmation; gel permeation chromatography determines molecular weight; Raman Analysis displays vibrational assignments; temperature, electric field, and magnetic susceptibility analyze conducting mechanisms; and electroluminescence has applications in LEDs [18].

3 Introduction to Biomedical Sensor

3.1 Types of Biomedical Sensors

Biomedical sensors are defined as a device that can detect chemical, physical, and biological processes and employ the data from these signals in medical devices and applications for healthcare². The types of biosensors are generally grouped into the category they identify; thus, there are three types of biosensors: physical, chemical, and biological. Physical sensors consist of geometric, mechanical, thermal, hydraulic, electrical, and optical sensors and measure pressure, body temperature, blood flux, blood viscosity, and the biological magnetic field. Chemical sensors consist of gas, electrochemical, and photometric and can identify ingredients and concentrations of body liquids, like pH value, Ca⁺ concentration, and glucose concentration. Finally, biosensors consist of sensors that detect enzymes, antigens, proteins, ligands, cells, antibodies, hormones, DNA, RNA, and microbes [19].

Biomedical sensors can also be grouped as implantable, wearable and amperometric flexible. Implantable biosensors are devices used in vivo, or inside a living

organism, that continuously monitor metabolites or read the organism's electrophysiological signals. Furthermore, this advantage of being in vivo enables implantable biosensors to provide health trends to patients for their observation without needing a visit to a healthcare professional [20]. Wearable sensors are defined as devices that present mobility, wearability, sustainability, simple operation, and interactivity and assume various forms, such as smart glasses, watches, wristbands, helmets, belts, armbands, rings, running shoes, and buttons. Their proximity to the body allows them to wire or wirelessly relay information through biocompatible and highly sensitive sensors to the user or other medical staff to prevent and manage health conditions. Most of their applications are as physical and chemical sensors as they mostly measure body temperature, pulse rate, blood pressure, respiratory rate, and blood sugar [2]. Amperometric flexible sensors function by applying a constant potential through the electrochemical cell's working electrode and reference electrode. The level of current going via the working electrode can be measured to specify a reaction, and, as the working electrode undergoes electrochemical redox reactions with biomolecules in electrolytic solutions, fluctuations in current are mapped as a function of time while potential remains constant. As a result of this mechanism, ease of configuration, and low detection limit, amperometric sensors are highly applicable as biosensors in biocatalytic and affinity-sensing situations. On the other hand, biosensors utilizing potentiometry measure change in potential as opposed to the current through the working electrode and reference electrode while keeping the current constant. Modification of the working electrode with a biological recognition element and materials like graphene or carbon nanotubes allows the sought-after bioanalyte in an electrolytic solution to interact with the biological recognition element, producing a biochemical signal that resultingly induces a potential change for measurement and detection by an external meter [4].

3.2 Requirements and Challenges in Biomedical Sensor Design

As biomedical sensors are complex devices and must be foolproof in their applications, especially inside the human body, they require strict protocols for design and functioning. Thus, many requirements must be met to achieve an appropriate and applicable biosensor. The most basic requirements for a sensor are defined as follows: range of measurement, sensitivity, accuracy, precision, resolution, reproducibility, offset, linearity, response time, drift, and hysteresis. First, the range of measurement is the minimum and maximum threshold that a sensor can accurately read measurements within. Sensitivity, defined mathematically, is the ratio of the change in output to the change in input, or the slope of a calibration line. For instance, a high sensitivity indicates a higher change in the output compared to the input values. Next, accuracy is the difference between the value measured by the sensor and the actual/true value and is presented as a percentage of how close the determined value

is to the actual value. Precision, on the other hand, is how repeatable the detection of a measurand is (i.e., high precision detections indicate that the sensor measures a similar value for the same conditions). Resolution refers to the minimum value for an input until which a detectable output is produced or the slightest change in input that can be measured. Reproducibility is defined as the proximity of measurements detected by the sensor at the same input under the same conditions. It relates to the range of measurement as a smaller range establishes greater reproducibility. Offset is the output value for a sensor when the input is zero. Next, the linearity of a sensor is described as the most significant difference between the calibration curve, which indicates the performance of the sensor, and the best fit/linear regression line. Response time is the time a sensor requires to reach its maximum value when the input value is changed. Shorter response times mean the sensor needs less time to detect a change in the input. Drift is the change in the output of a sensor reading when the input is kept constant. Ideally, drift should be as low as possible to promise accuracy and precision for detection. Hysteresis is the lag between the input and output values when there is a change in measurements, such as reversing the input from its maximum value back to zero. In conclusion, these are the requirements for which sensors should demonstrate [19].

Biosensors, specifically, share similar requirements but have additional specifications. Primarily, sensors must be able to immobilize metabolites, and reagents should be available for reuse in the repeated detection of similar biological parameters. Next, biosensors must present extreme sensitivity in that they only detect the desired material and are not distracted by non-desired particles in the solution. Such sensors should also provide a fast response time with immense accuracy, preferably within a 1% margin of error. The final must-haves include a non-complex design and inexpensive cost. However, this is not all; since biomedical sensors have applications in and on the human body, they must be comfortable, reliable, and safe for interaction with human skin and organs [19]. Figure 4 provides an overarching visual of some of the most essential required characteristics of a viable biosensor, combining specific aspects of the biosensor with the general needs of any sensor.

3.3 Advancement and Challenges

Due to advancements in research and the discovery of suitable materials for the design of sensors, many upgrades have come to light, improving the overall viability, performance, and capabilities of sensors, especially biomedical sensors. Therefore, such sensors enable increased access to point-of-care treatments by bringing the diagnosis, treatment, and management solutions to the patient rather than vice versa to avoid a backlogging or overflowing of the medical system. The main advancements receiving the most attention in today's biomedical sensor research is the Internet of Things, wearable sensor technology (smart textiles), and the use of novel materials.

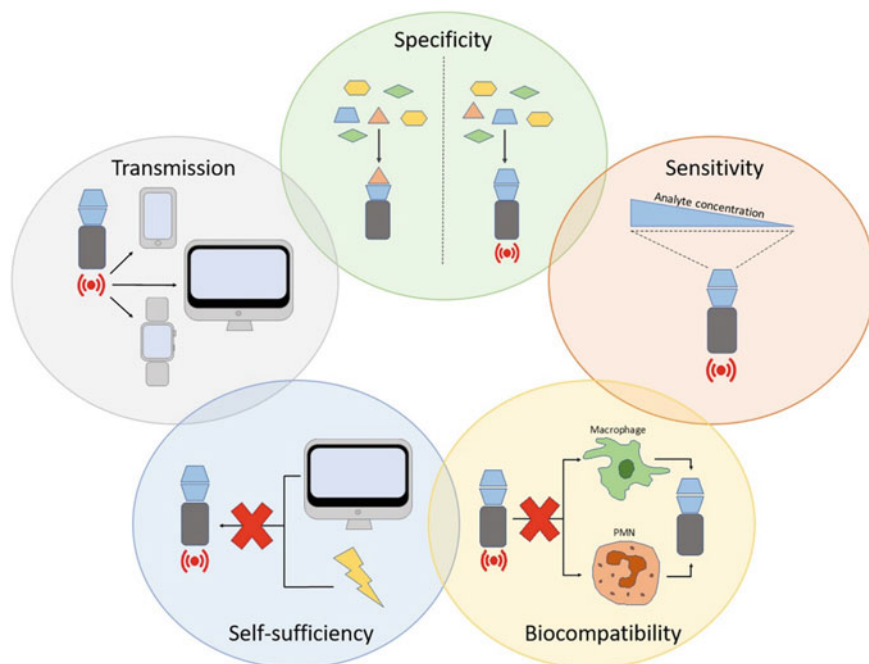


Fig. 4 Five most important qualities of a biosensor. Adapted with permission [20]. Copyright 2018 The Authors. Published by Elsevier Ltd. This is an open access article under the CC BY license (<http://creativecommons.org/licenses/by/4.0/>)

However, as these breakthroughs are quite recent, there continue to be various obstacles that need to be conquered before they can be considered safe in the industry of biosensing.

The Internet-of-Things (IoT) is a “smart” network of interconnected devices consisting of electronic equipment, sensors, and connectivity to gather and communicate data efficiently. The challenge with IoT is mostly maintaining and exchanging real-time communication of data between itself and other devices to keep observation of parameters, such as vitals, on a live loop. The other challenge is the interpretation of such large amounts of data from various origins since it requires training artificial intelligence and machine-learning software first to gather the data, analyze it, and finally return its investigations to the user for a real-time report; however, this problem which involves “big data” goes beyond IoT-sensors and is a significant roadblock to smooth streaming of biosensing data [21, 22].

The advancement in the world of smart textiles—precisely what they sound like—materials that can sense and respond to environmental stimuli. Essentially, the background is textile-based but with an additional component serving various functions, especially sensing. By the same token, they are produced by combining traditional textile production methods of weaving, knitting, and embroidery with novel techniques like coating, lithography, and ink-jet printing, producing textiles as small as

fibers to complete clothing materials. Textiles are preferred for their lightweight properties, flexibility, dimensional variability, and modifiability of structure and surface properties to reach a desired sensing mechanism. The *in vitro* biosensing applications of smart textiles in healthcare include bandages, medical personnel uniforms, plasters, monitoring cardiovascular, hemodynamic, neural, muscle kinematics, respiratory, and thermoregulation activity, and electrical stimulation therapy and physiotherapy. *In vivo*, applications include sutures, soft tissues, and cardiovascular and orthopedic implants. In surgery, textile technology has granted 2-D and 3-D implantable structure development that promotes cell distribution and adhesion in the body, while non-implantable miniature fiber textile-based biosensors can oversee and augment healing [21, 23]. The challenges with smart textiles include their complex manufacturing process that must combine old and new synthesis techniques; mechanical and tensile duress/stability; bulky, insufficient, and lack of integrable power sources; struggles to employ smart textiles due to imbalance between fashion and electronic industries; inefficient software reliability; obtrusiveness; balancing user needs with privacy; cost; ethics; technological, acceptance, and dependence barriers, especially with the elderly population; legislation; and interoperability [24, 25]. Finally, yet importantly, in the list of advancements is the most impactful advancement yet: novel materials, namely conducting polymers. The first type of material is graphene quantum dots (GQD). GQDs prove to be likable for biomedical fluorescent sensors because of their strong optical properties, a high specific surface area, a sufficient π -conjugated system, and modifiable edge groups, which allow them to be tweaked through physical and chemical methods to detect a certain bioanalyte *in vivo*. GQDs can also work in tandem with fluorescence imaging technology to observe *in vivo* targets in real time. Other applications with fluorescence technology include loading GQD-based fluorescent sensors with drugs for drug release mechanisms, drug targeting, dynamic monitoring, analysis, and diagnosis. A current and tested application of the GQD fluorescent sensor could detect glutathione reductase in human body fluids, such as blood, urine, sweat, and tears, for early-stage disease analysis and diagnosis by combining GQDs with gold nanoparticles (AuNPs) [26]. CPs have advanced biomedical sensors not only by keeping their metallic/semiconductor properties but also displaying flexibility, ease in synthesis, large surface area, modifiability with nanoparticles, hydrogels, and other novel materials, immobilization of metabolites, functionalization with many biorecognition molecules, and biocompatibility in neutral aqueous solutions. Taking a deeper dive, the inherent characteristic of CPs to transfer electrons from biochemical reactions allows them to act as transducers in the intermediate layers of biosensors between the biological sample and electronic parts that produce a readable signal. The most common CPs used are PANI, PPy, and PEDOT. For example, PANI has been commonly used in sensors that can detect pH, creatinine, cancer markers, prostate-specific antigens in blood samples, tumor necrosis factor- α antibodies, and, due to its structure. Similarly, PPy showed how its administrative capabilities as it could be polymerized onto the surface of a leather band to produce a wearable electrocardiogram (ECG) electrode, supplementing the conductivity and antimicrobial properties of the surface, boosting the stability beyond gel-assisted electrodes, and multiplying the

detection level compared to commercially available electrodes. The biocompatibility and conductivity of these two materials proved to be not only ideal for the growth and differentiation of myoblast and neuronal cells but also desirable for tissue engineering scaffolds, implantable electrodes, and other low-cost point-of-care/wearable devices. Finally, due to their biocompatibility and electrical properties, PEDOT:PSS matrices have been arguably the most often used in biomedical sensors. Primarily, they can integrate with graphene oxide to immobilize glucose oxidase for enzyme-based glucose sensors or be deposited on gold microelectrodes for neural implants. Lastly, PEDOT has been applied in organic implantable applications, such as for producing the electrode in neural probes that were later grafted into the visual cortex of mice. It should be mentioned that the electrode formed a looser glial scar and was functioning well even several months after implantation compared to similar electrodes of its nature.

Within CPs-based biosensing, conducting polymer hydrogels (CPHs) have shown immense advancement and contribution to the field within the last five years. Examples of applications using CPH-based biosensors are shown in Fig. 5 [5]. Part of this growth is due to the healthcare industry shifting its focus towards less invasive, non-surgical procedures, such as the implantation of bioresorbable sensors that can monitor real-time biophysical and biochemical conditions *in vivo* and do not require a second surgery for removal. Moreover, CPHs can respond to environmental stimuli, such as changes in temperature, pressure, light, pH, humidity, or the presence of compounds, and accordingly experience physical and chemical transitions. These unitive properties of biopolymers' biocompatibility and biodegradability and the electroactivity of conductive hydrogels make CPHs preferable in biocompatible and biodegradable sensor synthesis. Regardless, as the industry develops to overcome these limitations, the potential effects for conducting polymers through biosensing can have profound worldwide implications in today's healthcare system as both patients and clinicians can transition from off-site and lengthy laboratory analysis methods to on-site detection/quantification, supervise treatment efficacy and disease recurrence, and apply biomarker-based screening for early disease detection, preventative measures, and personalization of medicine to the unique biomolecular fingerprint of the patient and their physiology [27, 28].

4 Conducting Polymer-Based Biomedical Sensors

4.1 Biosensors for Pathogen Detection

Pathogens are agents of infectious diseases, usually in the forms of viruses—such as norovirus, influenza virus—bacteria, like *E. coli*, fungi, protozoa, or prions. Detection of pathogens occurs either through immunoassays, in which the antibodies produced during or after infection are measured, or through toxin-producing genes or viral-producing DNA. Compared to enzyme-linked immunosorbent assays (ELISA)

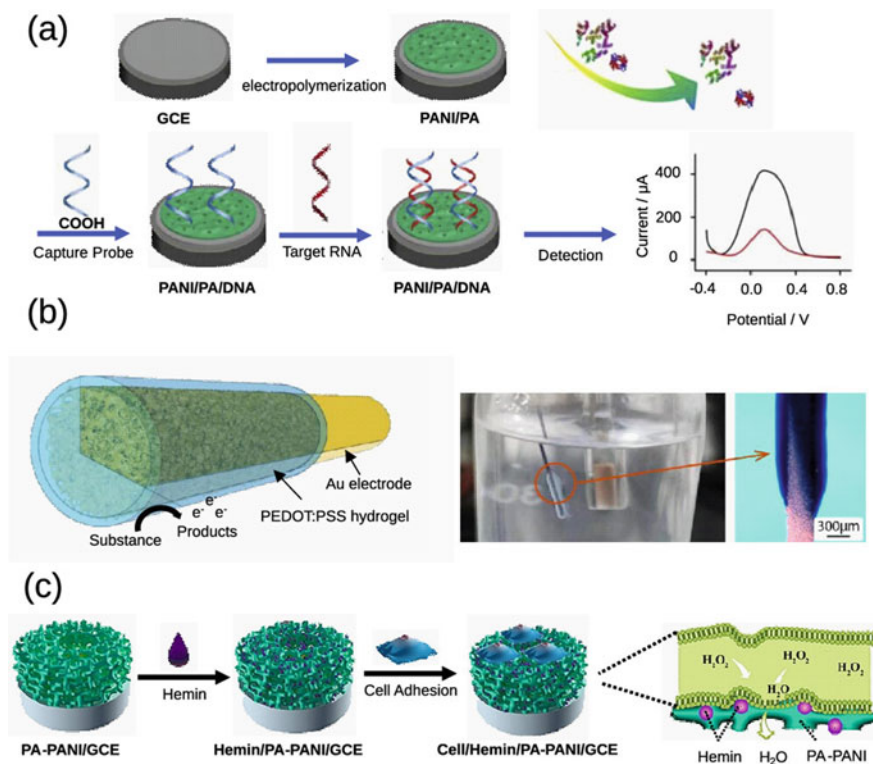


Fig. 5 Examples of applications using CPH-based biosensors. **a** PANI/PA hydrogel microRNA detector. **b** PEDOT:PSS hydrogel-coated gold electrodes used as glucose, hydrogen peroxide, DA, and L-DOPA sensor. **c** PA and hemin-doped PANI hydrogel used as a sensor for hydrogen peroxide from living cells. Adapted with permission [5]. Copyright 2023 The Authors. Published by American Chemical Society. This is an open access article under the CC BY license (<http://creativecommons.org/licenses/by/4.0/>)

and polymerase chain reactions (PCR), which take extensive steps and increase the time-to-results (TTR), conducting polymer-based electrochemical biosensors offer a lower TTR, cost-efficiency, robustness, high sensitivity and selectivity, on-site detection, lower required sample volumes, miniaturization capabilities, and, thus, point-of-care sensing. Furthermore, using pathogen-detecting biosensors can reduce the chance and duration of hospitalization, antimicrobial use, and mortality rate [29, 30]. CPs are used in such biosensors for their high sensitivity, simple production mechanisms, high porosity, electrical conductivity, signal conversion from a binding/adsorption event, ease and variety in immobilization, organic and sustainable biomolecular environment, and, specifically for pathogen biosensors, ability to produce array sensing devices. The most common use of CPs is either on electrodes or nanowires, known as electrically conducting polymer nanowires (ECPNWs), and include PANI, PPy, and PEDOT [31, 32]. The CP electrodes display thin-film form

factors and are deposited on the insulating substrates through layer-by-layer methods, spin-coating, or electrochemical polymerization, and are dispersed throughout most of the polymer layer rather than just the surface [30]. An ECPNW-based biosensor involves, primarily, manufacturing of the ECPNWs through either chemical or electrochemical polymerization, template-assisted synthesis, ink-jet printing, nanoimprinting, or dip-pen lithography (scanning probe nanopatterning/nanowire production technique in which an atomic force microscope tip delivers molecules to a surface via a solvent meniscus). The general process for producing a general biosensor for pathogenic detection begins with a transducing element, an electrochemical cell in which the main component is an electrode. For CP-based biosensing, the electrodes are polymeric materials—conducting polymers or polymer composites—because of their tunable electrical conductivity, biocompatibility, environmental stability, and capability to implement various biorecognition element immobilization approaches. The most common CPs for pathogen biosensors are PANI and PPy since they are highly conductive in their doped state. The next part is to determine the type of biorecognition element. The most common biocatalytic elements include enzymes, whole cells, and tissues. Bio complexing elements produce a response in the sensor system by facilitating reactions between analytes and macromolecules or molecular assemblies. The most common bio complexing elements in pathogen detection sensors include antibodies, peptides, phages, and imprinted polymers. Antibodies are the most frequent element and comprise immunosensors due to their strong selectivity, binding affinity for target analytes, and broad production range for many pathogens. Further, antibodies can bind to antigens at specific recognition sites known as epitopes and come in either monoclonal or polyclonal forms in which the former is produced via hybridoma technology, highly selective, capable of binding to one epitope, more expensive, and lengthier in production. On the other hand, polyclonal antibodies are developed by separating immunoglobulin proteins from the blood of an infected host, and they target various epitopes on one antigen, have more robust measurement levels, and are less expensive [33]. As the field of pathogen biosensors grows along with advancements in biomedical engineering, conducting polymers, and other novel materials, the industry will expand to fit more niches in the medical sectors and beyond.

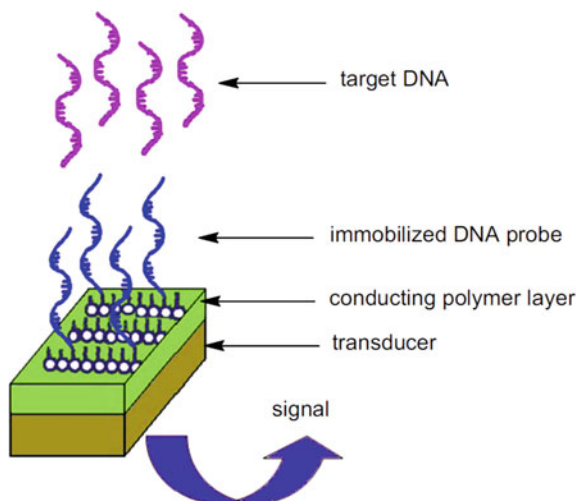
4.2 Biosensors for DNA Detection

Deoxyribonucleic acid (DNA), is the genetic sequence that allows our cells, tissues, and organs to function, making each organism immensely unique. Biosensors for DNA detection are sensors that can recognize strands of complementary DNA on its surface, producing a readable electrical signal for analysis. Specifically, electrochemical biosensors are the leading choice due to their ability to convert the hybridization of DNA directly and quickly into an electrical signal. As such, these biosensors, also known as genosensors, do not require elaborate signal transduction equipment but rather other affordable electrochemical analyzers. Conducting polymers are used in

DNA biosensors to immobilize/bond the DNA probes as per a desired orientation and recognize target DNA via the Watson–Crick complementary base-pairing rules that adenine and guanine are base pairs, and cytosine and thymine are base pairs. Furthermore, sensors not only rely on CPs for the recognition process of target DNA but also the transmission of the generated signal. Multiple CPs are used, including polypyrrole, polyaniline, and polythiophene. Using DNA as a recognition element in biosensors is common practice in many industries since DNA analysis influences the diagnosis of infectious diseases, personal identification, toxicology, genetic mutations, drug discovery/pharmacology, forensics, and food technology. Similarly, the specificity of DNA sequences, namely single-stranded DNA sequences, to each organism allows for unique detection of micro-organisms. DNA biosensors and other biosensors are made first by immobilizing the probe, an oligonucleotide complimentary copy of the target DNA in the case of DNA biosensors, onto the biosensor transducer through physical adsorption, electrochemical adsorption, covalent attachment (most often used), or avidin–biotin. The selection of electrodes—which, defined in the context of biosensors, are electronic conductors through which charge is transported by the movement of electrons and holes— for DNA immobilization, route of immobilization, and procurement of linkers for DNA coupling must also be decided, specifically to produce an immobilization method that confers high DNA density, amplifies the output signal, efficiently hybridizes with the target, is reproducible, sensitive, and stable, and has minimal background noise. Furthermore, for immobilization of a biomaterial, especially for DNA biosensors, there are numerous requirements: (i) the biological recognition/catalytic properties of the biomaterial should endure the immobilization process; (ii) the biomaterial should be fixed on or within the substrate, otherwise the biosensor can lose its activity; (iii) improvement or, minimally, decreasing selectivity of the constructed biosensor; (iv) improvement of electron transfer if amperometric measurements are applied as the signal transducer. A signal is then produced when the probe is hybridized by the target sequence by optical, electrochemical, or piezoelectrical routes. Electrochemical transduction is preferable for most applications as biorecognition events result in direct electrochemical signals and possible miniaturization capabilities of the sensor. The signal can be read via amperometry, conductometry, impedimetry, or potentiometry. A recapitulation of a conducting polymer-based DNA biosensor design is shown in Fig. 6 [35–37].

Biosensors made from CPs that detect DNA have multiple varied applications. For instance, a PPy film-based DNA biosensor has been used to detect *Escherichia coli* bacteria, while another can detect the *Variola major* pathogen. Furthermore, a poly(pyrrole-NHS) material was used to covalently immobilize a probe that could detect complementary DNA sequences from the West Nile Virus through amperometry. One such revelation involves introducing a variety of bioreceptors to the clustered regularly interspaced short palindromic repeats (CRISPR)-based biosensors for nucleic and non-nucleic acid target detection [36, 38].

Fig. 6 Basic principle behind conducting polymer-based DNA biosensors. Adapted with permission [36]. Copyright 2009, Elsevier



4.3 Biosensors for Protein Detection

Proteins are crucial organic compounds to the human body and comprise a considerable quotient of the macromolecules housed in the organs. Molecularly, they form the enzymes that accelerate all biochemical reactions in the body, antibodies necessary for fending off infection, biomarkers for identifying various diseases like tumor formation, and are found within cellular structures, which make tissues, organs, and organ systems; in other words, they are vital for life [39]. Although traditional techniques of detecting proteins, such as enzyme-linked immunosorbent assay (ELISA), offer low limits of detection and strong specificity, they cannot be used for point-of-care treatments due to extensive assay times, lack of multiplex sensing capabilities, low cost-effectiveness, and lack in portability [40]. Thus, detecting proteins by biosensors in a timely, sensitive, and accurate manner is essential. For the synthesis of such a sensor, there should be an interfacial protein-surface interaction and a resulting electronic or optical signal dependent on protein detection. Unlike some other sensors, such as immunosensors in which the biorecognition element is different from the target element (antibody vs. antigen), biosensors for protein detection often contain proteins themselves as biorecognition elements to detect other protein target elements and transform them for signal transduction. To exemplify this concept, a previous study immobilized glucose oxidase—an enzyme and, thus, a protein—to a polymer matrix to transfer glucose to gluconic acid and H_2O_2 , of which H_2O_2 could be detected via the polymer's electroactive properties. Glucose oxidase, specifically within PPy films, has often been used in studies involving biosensors for protein detection, paving the way for advances in multilayer and multienzyme biosensors. It should be noted that the process of transduction to produce the signal based on the recognition event is like previously discussed biosensors. The most popular conducting polymers for biosensors for protein detection are PPy, PEDOT, and PANI,

and are often come in the form of nanomaterials [41]. Label-free options exist for such biosensors as well [42].

Due to the extensive presence of proteins in the human body, there are multiple applications for biosensors detecting proteins, including cancer biomarkers like antigens, thrombin, human serum albumin (HSA), and antigens belonging to bacteriophages/viruses [43]. One study fabricated a CP-based biosensor for detecting vascular endothelial growth factor (VEGF), a protein regulator for blood vessels, namely the processes of angiogenesis, vasculogenesis, endothelial cell growth, and is a role player in tumor formation, and metastasis of cancer cells. The flexible biosensor, shown in Fig. 7, was produced through silk protein photolithography, while the sensing was carried out by photolithographically micropatterned electrodes made from conductive ink with PEDOT: PSS. VEGF₁₆₅ was detected by integrating anti-VEGF₁₆₅ antibodies into the conductive ink, establishing an electrode mechanism for the sensor. Electrochemical impedance spectroscopy (EIS) allowed for the rapid and label-free detection of low concentrations of VEGF, which has been done in this study through buffer, human serum, and simulated urine with and without urine [40]. The challenges associated with CP-based and traditional biosensors for protein detection mainly involve immobilizing biorecognition elements, such as antibodies and aptamers, and signal transduction. These issues are the root causes for large molecule biomarkers, namely proteins, due to their electrochemical inactive nature, not being viable targets, hindering the use of protein sensing biosensors as point-of-care tools and wearable devices that could detect protein biomarkers like VEGF on bio-interfaces/biofluids [40]. Another challenge involving CPs is their lack of biodegradability and, thus, a lack of regenerative biosensing devices [41].

4.4 Biosensors for Early Disease Detection

Early disease detection, also known as screening, is a medical testing process done on asymptomatic patients to evaluate qualitative and quantitative signs of preclinical disease, often utilizing biomarkers, which are defined as indicators of biological or pathogenic processes. Additionally, screening aims to prevent by means of discovering signs of illness and treating them before they develop into serious health complications leading to disability and disease [44]. For instance, considering the recent COVID-19 pandemic, several screening methods, namely polymerase chain reaction (PCR) tests and antigen tests, were employed to halt the rapid, contagious outbreak and, thus, limit the morbidity and mortality rate of the disease: the earlier one gains the knowledge that they may develop the infection, the earlier they can quarantine themselves and prevent contagion [45].

The discussions on biosensors in this section have had applications in which detection of the target element played a role in discovering components of disease, such as the CP-based DNA biosensor identifying HIV. However, the following applications focus on the early detection of disease rather than the detection of disease when it gains symptomatic status. A biosensor composed of nanocomposites from graphene

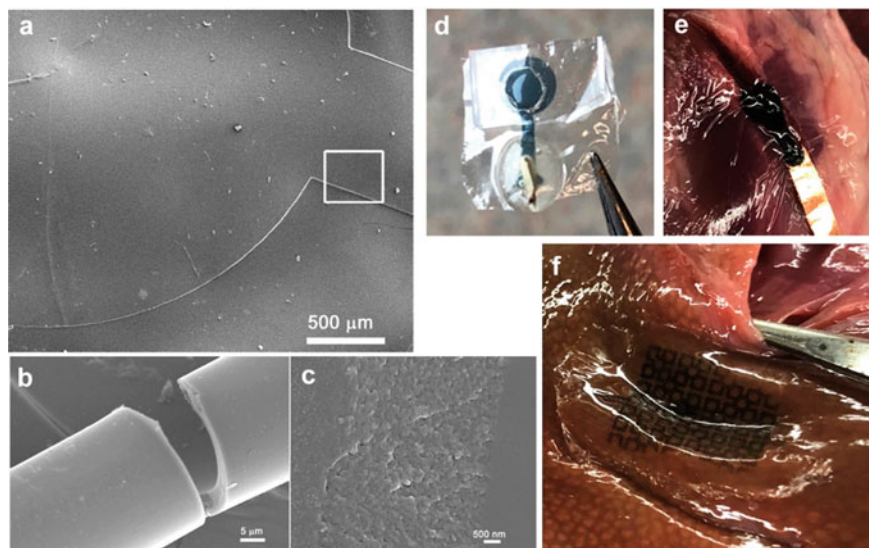


Fig. 7 **a** SEM image of the PEDOT: PSS-based conductive ink micropatterned electrodes, **b** close-up SEM image of the rolled-up electrode, **c** image of electrode surface, **d** VEGF-biosensor demonstrating flexibility and conformability to tissue interfaces for in situ detection applications of biomarkers as shown in panels **e** and **f**. Adapted with permission [40]. Copyright 2019, American Chemical Society

oxide, zinc oxide, PPy, and PANI displayed comparable selectivity and enhanced sensitivity for detecting cholesterol and bilirubin while lowering detection and quantification limits. As cholesterol is the principal agent in atherosclerosis and cerebral thrombosis (both leading to angina, heart attack, and stroke) and bilirubin is a critical analyte for measuring liver complications, premature detection of these biomarkers is vital for healthy and disease-free cardiovascular and liver operation [46]. By the same token, a biosensor was developed using PANI nanostructures and immobilization of horseradish peroxidase and glucose oxidase to detect hydrogen peroxide and glucose. The purpose of this device was for the early, accurate, and quick detection of diabetes mellitus, a disease affecting nearly 422 million people worldwide and claiming the lives of 1.5 million annually [10]. One recent study from 2021 attempts to form a CP-based biosensor to detect COVID-19 as the infectious disease resulting from exposure to the severe acute respiratory syndrome coronavirus 2 (SARS-CoV-2) virus. Modern research has shed light on multiple approaches to overcome the above challenges: (i) improving the stability of CPs via functionalization with various functional groups or blending with other nanomaterials (graphene, CNTs, metals, metal oxides, or insulator polymers); (ii) enhancing electrochemical and charge transport properties of CPs by implanting them as nanostructures (nanotubes, nanowires, and microspheres); (iii) increasing CP surface area and thus facilitating interactions between CP surfaces and biomarkers through microporous structures; and (iv) fabricating CP structures with high flexibility, such as CP hydrogels, as they are preferred in the

design of wearable biosensors [3]. To evince the recent advancements of CP-based biosensors for early disease detection that have implemented these approaches, a report synthesized a sensor to detect varying concentrations of cancer antigen 125 (CA125), a 19-base pair-long breast cancer gene sequence, plaque-forming T7 and MS2 bacteriophages, and a colony of *Bacillus globigii* in the presence of non-target bacteria *Escherichia coli*. The remarkable versatility of this chemiresistive biosensor was single-handedly achieved through PPy nanowires.[47] With growing attention towards conducting polymers and their multiplex capabilities, vast possibilities arise in the field of biosensing, especially with the advent of the IoT, for the early detection of disease and improved patient outcomes.

5 Conclusion

This review accentuates the importance of biomedical sensors along with the chief role of conducting polymers in the functioning of these devices. As discussed previously, conducting polymers are materials whose principal property is an inherent electroactivity state, mimicking metals, and semiconductors, hence the name. These characteristics can be attributed to delocalized, polarized, and electron-dense π bonds in the main chains of the polymers. The most widely used CPs in biosensing include PPy, PANI, and PEDOT: PSS, among others, as they either offer strong biocompatibility, ease in synthesis, high conductivity, stability, or combinations of these. Oxidative chemical polymerization and electrochemical polymerization are the most common synthesis routes for the polymers. Biomedical sensors are pivotal agents in the healthcare system because of their high order of sensitivity, versatility in detecting a wide range of bioanalytes, and accurate, real-time monitoring of patient parameters. These sensors fall into the categories of chemical, physical, and biological, in which they are commonly recognized by their target element (i.e., immunosensors detect antigens and genosensors detect DNA, while blood pressure sensors and glucose sensors detect blood pressure and glucose, respectively). Further, requirements for a successful biosensor include identifying and optimizing the range of measurement, sensitivity, accuracy, precision, resolution, reproducibility, offset, linearity, response time, drift, and hysteresis. On the other hand, challenges in biomedical sensor design pertain to biocompatibility, sensitivity, specificity, miniaturization, and battery life. The most notable advancement in biomedical sensors has been the advent of CPs. Still, other notable upgrades that will take the CP-based biosensor to a step above principally involve the Internet of Things (IoT). Biosensors for pathogens, DNA, and proteins all involve notions for early disease detection, but improving multiplex capacities will promote accuracy and rapid response in disease detection.

Despite the recency in development and research on biosensors, the current and potential applications, as well as the possibilities in combining newer materials and technological advancements, will be deemed vital for any patient interaction within healthcare. This is evident as biosensors become the sought-after choice in point-of-care diagnostics in which tests are brought to the patient for rapid and accurate

diagnostic results rather than being sent to a clinical laboratory where they experience delays. Additionally, with enhancements to CP synthesis and their specificity properties, personalized medicine will no longer be of the future; healthcare professionals could take advantage of real-time, CP-based parameter monitoring to contrive diagnostic and treatment procedures specifically for a patient to reduce side effects and improve patient outcomes. Continuous monitoring, which can be enhanced to remote monitoring via IoT, can allow rapid response teams to act quickly to severe fluctuations in physiological parameters before they prove to be injurious or fatal. Even outside of a healthcare facility, wearable health monitoring by CP-based sensors woven into smart textiles can bestow patients with portable and accurate detection for fitness, management of chronic diseases, and early disease detection/prevention. This review sheds light on such beneficial applications and the profound potential for CP-based biosensors and biotechnology to introduce reliability, rigor, and uninterrupted flow through the healthcare system.

Before biosensing technology can have its impact on medicine, multiple kinks in sensor design and functioning must be straightened out. The first and possibly most pressing is the stability of conducting polymers for their applications within biosensors. The long-term electro stability of CPs currently needs to be improved for many sensors due to degradation and exposure to oxidation, resulting in diminished sensor performance. The second most crucial issue is biocompatibility since any lingering toxicity within a sensor can lead to more harm than good—a violation of the Hippocratic Oath. The methods to increase the signal-to-noise ratio to augment sensitivity and specificity in biomolecular/biomarker detection must be explored before CPs can replace other metal and semiconducting materials. Finally, poor regenerative capabilities, lack of reproducibility, fabrication complications, and cost-effectiveness are all obstacles needing further research. Current and future research seems promising in the face of these drawbacks, especially given the dawn of the IoT and integration with propitious materials such as nanomaterials and smart textiles. Future directions for CP-based biomedical sensors should focus on multiplex sensing of various bioanalytes from a single solution, implementation of nanostructures, more significant presence of implantable and wearable applications, affordable commercialization, and embracing machine learning/artificial intelligence to improve patient outcomes. Nonetheless, the present-day viability of conducting polymers in biomedical sensors outlined in this review alone is a sufficient reason to be optimistic for the future of medicine and healthcare.

References

1. Wiriyaichai, N., Leelawattanachai, J., Muangnapoh, K., Bamrungsap, S., Maneeprakorn, W., Japrun, D.: Chapter 25—Biomedical sensor, In: Lau, W.J., Faungnawakij, K., Piya-chomkwan, K., U.R.B.T.-H. of Ruktanonchai N.A. (eds.) *Micro Nano Technol.*, pp. 657–681. Elsevier (2021)
2. Wan, H., Zhuang, L., Pan, Y., Gao, F., Tu, J., Zhang, B., Wang, P.: *Biomedical Sensors*, Elsevier Inc. (2019)

3. Van Tran, V., Tran, N.H.T., Hwang, H.S., Chang, M.: Development strategies of conducting polymer-based electrochemical biosensors for virus biomarkers: Potential for rapid COVID-19 detection. *Biosens. Bioelectron.* **182**, 113192 (2021)
4. Yang, A., Yan, F.: Flexible electrochemical biosensors for health monitoring. *ACS Appl. Electron. Mater.* **3**, 53–67 (2021)
5. Gamboa, J., Paulo-Mirasol, S., Estrany, F., Torras, J.: Recent progress in biomedical sensors based on conducting polymer hydrogels. *ACS Appl. Bio Mater.* **6**, 1720–1741 (2023)
6. Srichan, C., Srichan, W., Danvirutai, P., Ritsongmuang, C., Sharma, A., Anutrakulchai, S.: Non-invasively accuracy enhanced blood glucose sensor using shallow dense neural networks with NIR monitoring and medical features. *Sci. Rep.* **12**, 1–9 (2022)
7. Rohaizad, N., Mayorga-Martinez, C.C., Fojtů, M., Latiff, N.M., Pumera, M.: Two-dimensional materials in biomedical, biosensing and sensing applications. *Chem. Soc. Rev.* **50**, 619–657 (2021)
8. Eliaz, N.: Corrosion of metallic biomaterials: A review. *Materials (Basel)* **12** (2019)
9. Ates, M.: A review study of (bio)sensor systems based on conducting polymers. *Mater. Sci. Eng. C* **33**, 1853–1859 (2013)
10. El-Said, W.A., Abdelshakour, M., Choi, J.H., Choi, J.W.: Application of conducting polymer nanostructures to electrochemical biosensors. *Molecules* **25**, 1–11 (2020)
11. Kenry, B.: Liu, recent advances in biodegradable conducting polymers and their biomedical applications. *Biomacromol* **19**, 1783–1803 (2018)
12. Almeida, L.C.P.: Conducting polymers: Synthesis, properties and applications, *Conduct. Polym. Synth. Prop. Appl.*, 1–358 (2013)
13. Yi, N., Abidian, M.R.: *Conducting polymers and their biomedical applications* (2016)
14. Namsheer, K., Rout, C.S.: *Conducting polymers: A comprehensive review on recent advances in synthesis, properties and applications*. *RSC Adv.* **11**, 5659–5697 (2021)
15. Poddar, A.K., Patel, S.S., Patel, H.D.: Synthesis, characterization and applications of conductive polymers: A brief review. *Polym. Adv. Technol.* **32**, 4616–4641 (2021)
16. Le, T.H., Kim, Y., Yoon, H.: Electrical and electrochemical properties of conducting polymers. *Polymers (Basel)*. **9**, 150 (2017)
17. Assad, H., Sharma, S., Kaya, S., Sharma, P.K., Kumar, A.: Overview and fundamentals of polymer nanocomposites. In: *Nanocomposites-Adv. Mater. Energy Environ. Asp.*, pp. 41–66. Elsevier (2023)
18. Kumar, S.: Conducting polymers and their characterization. *Int. Res. J. Eng. Technol.* **3**, 479–482 (2016)
19. Zhou, G., Wang, Y., Cui, L.: Biomedical sensor, device and measurement systems. *Adv. Bioeng.* (2015)
20. Gray, M., Meehan, J., Ward, C., Langdon, S.P., Kunkler, I.H., Murray, A., Argyle, D.: Implantable biosensors and their contribution to the future of precision medicine. *Vet. J.* **239**, 21–29 (2018)
21. Comini, E.: Achievements and challenges in sensor devices. *Front. Sensors* **1**, 607063 (2021)
22. Javaid, M., Khan, I.H.: Internet of Things (IoT) enabled healthcare helps to take the challenges of COVID-19 Pandemic. *J. Oral Biol. Craniofacial Res.* **11**, 209–214 (2021)
23. Mečņika, V., Hoerr, M., Krieviņš, I., Schwarz, A.: Smart textiles for healthcare: Applications and technologies. *Rural Environ. Educ. Personal.* **7**, 150–161 (2014)
24. Cherenack, K., Van Pieterse, L.: Smart textiles: Challenges and opportunities. *J. Appl. Phys.* **112** (2012)
25. Chan, M., Estève, D., Fourniols, J.Y., Escriba, C., Campo, E.: Smart wearable systems: Current status and future challenges. *Artif. Intell. Med.* **56**, 137–156 (2012)
26. Li, G., Liu, Z., Gao, W., Tang, B.: Recent advancement in graphene quantum dots based fluorescent sensor: Design, construction and bio-medical applications. *Coord. Chem. Rev.* **478**, 214966 (2023)
27. Nambiar, S., Yeow, J.T.W.: Conductive polymer-based sensors for biomedical applications. *Biosens. Bioelectron.* **26**, 1825–1832 (2011)

28. Runsewe, D., Betancourt, T., Irvin, J.A.: Biomedical application of electroactive polymers in electrochemical sensors: A review. *Materials (Basel)* **12** (2019)
29. Vidic, J., Manzano, M.: Electrochemical biosensors for rapid pathogen detection. *Curr. Opin. Electrochem.* **29**, 100750 (2021)
30. Cesewski, E., Johnson, B.N.: Electrochemical biosensors for pathogen detection. *Biosens. Bioelectron.* **159**, 112214 (2020)
31. Travas-Sejdic, J., Aydemir, N., Kannan, B., Williams, D.E., Malmström, J.: Intrinsically conducting polymer nanowires for biosensing. *J. Mater. Chem. B.* **2**, 4593–4609 (2014)
32. Aravinda, C.L., Cosnier, S., Chen, W., Myung, N.V., Mulchandani, A.: Label-free detection of cupric ions and histidine-tagged proteins using single poly(pyrrrole)-NTA chelator conducting polymer nanotube chemiresistive sensor. *Biosens. Bioelectron.* **24**, 1451–1455 (2009)
33. Magar, H.S., Hassan, R.Y.A., Mulchandani, A.: Electrochemical impedance spectroscopy (Eis): Principles, construction, and biosensing applications. *Sensors* **21** (2021)
34. Wang, R., Wang, L., Yan, J., Luan, D., Tao sun, Wu, J., Bian, X.: Rapid, sensitive and label-free detection of pathogenic bacteria using a bacteria-imprinted conducting polymer film-based electrochemical sensor. *Talanta* **226** 122135 (2021)
35. Velusamy, V., Arshak, K., Korostynska, O., Oliwa, K., Adley, C.: Conducting polymer based DNA biosensor for the detection of the *Bacillus cereus* group species. *Sens. Agric. Food Qual. Saf.* **7315**, 731504 (2009)
36. Peng, H., Zhang, L., Soeller, C., Travas-Sejdic, J.: Conducting polymers for electrochemical DNA sensing. *Biomaterials* **30**, 2132–2148 (2009)
37. Ramanavičius, A., Ramanavičiene, A., Malinauskas, A.: Electrochemical sensors based on conducting polymer-polypyrrole. *Electrochim. Acta* **51**, 6025–6037 (2006)
38. Kim, E.R., Joe, C., Mitchell, R.J., Gu, M.B.: Biosensors for healthcare: Current and future perspectives. *Trends Biotechnol.* (2022)
39. Valastyan, J.S., Lindquist, S.: Mechanisms of protein-folding diseases at a glance. *DMM Dis. Model. Mech.* **7**, 9–14 (2014)
40. Xu, M., Yadavalli, V.K.: Flexible biosensors for the impedimetric detection of protein targets using silk-conductive polymer biocomposites. *ACS Sensors* **4**, 1040–1047 (2019)
41. Higgins, M.J., Molino, P.J., Yue, Z., Wallace, G.G.: Organic conducting polymer-protein interactions. *Chem. Mater.* **24**, 828–839 (2012)
42. Yoon, H., Kin, J.H., Lee, N., Kim, B.G., Jang, J.: A novel sensor platform based on aptamer-conjugated polypyrrole nanotubes for label-free electrochemical protein detection. *ChemBioChem* **9**, 634–641 (2008)
43. Mulchandani, A., Myung, N.V.: Conducting polymer nanowires-based label-free biosensors. *Curr. Opin. Biotechnol.* **22**, 502–508 (2011)
44. Califf, R.M.: Biomarker definitions and their applications. *Exp. Biol. Med.* **243**, 213–221 (2018)
45. Steele, L., Orefuwa, E., Dickmann, P.: Drivers of earlier infectious disease outbreak detection: a systematic literature review. *Int. J. Infect. Dis.* **53**, 15–20 (2016)
46. Kumar, A., Gupta, G.H., Singh, G., More, N., Keerthana, M., Sharma, A., Jawade, D., Balu, A., Kapusetti, G.: Ultrahigh sensitive graphene oxide/conducting polymer composite based biosensor for cholesterol and bilirubin detection. *Biosens. Bioelectron. X.* **13**, 100290 (2023)
47. Li, Y., Han, R., Chen, M., Yang, X., Zhan, Y., Wang, L., Luo, X.: Electrochemical biosensor with enhanced antifouling capability based on amyloid-like bovine serum albumin and a conducting polymer for ultrasensitive detection of proteins in human serum. *Anal. Chem.* **93**, 14351–14357 (2021)